PRINCIPLES OF ADSORPTION AND ADSORPTION PROCESSES

DOUGLAS M. RUTHVEN

University of New Brunswick, Fredericton

ACKNOWLEDGMENTS

PREFACE

Adsorption separation processes are in widespread industrial use, particularly in the petroleum refining and petrochemical industries, and the underlying physical and chemical principles on which such processes are based are reasonably well understood. However, apart from the pioneering but now outdated work of Mantell (*Adsorption*, McGraw-Hill, New York, 1951), there has been no attempt, at least in the Western literature, to present a consolidated summary and review of the subject. This is the objective of the present volume which is intended to cover both fundamental principles and industrial practice. The main emphasis is on the understanding of adsorption column dynamics and the modeling of adsorption systems, but some of the more fundamental aspects of sorption kinetics and equilibria are covered in greater detail than is required simply for the understanding of adsorption column dynamics. These subjects are central to an understanding of adsorption phenomena and provide the theoretical framework for the analysis and interpretation of experimental data. Because of their practical importance, the correlation and analysis of multicomponent equilibrium data are considered in detail, with emphasis on available methods for predicting the behavior of binary and multicomponent systems from the single component isotherms.

Industrial practice is covered mainly in Chapter 11, which deals with cyclic batch systems, and Chapter 12, which deals with continuous countercurrent processes. Representative processes are described, but no attempt has been made to provide a comprehensive review of all important adsorption separation processes; areas such as solvent drying and wastewater purification have not been considered. These chapters proved difficult to write because, although a great deal of design and operating data have been accumulated, such information is generally not publicly available. In some cases inferences concerning probable industrial practice have been drawn from the patent literature. Even when detailed information was available, considerations of proprietary rights sometimes made it difficult to present more than a somewhat general account.

In the selection of material for a book of this kind it is inevitable that the areas with which the author is most familiar will be emphasized, while other

areas of equal or even greater importance are ignored or treated only briefly. Thus, although this book treats adsorption in a general way, the emphasis is on molecular sieve adsorbents which have, for some years, been my own area of special interest. The fundamental aspects of adsorption have been elaborated in various ways by many different authors. In reviewing this information the choice between alternative treatments has been made largely on a subjective basis. The intention has not been to produce a comprehensive review but rather to provide the reader with a concise survey which may serve as a useful summary of the scientific principles underlying the design and optimal operation of adsorption processes and as an introduction to the more detailed information available in the scientific literature.

Douglas M. Ruthven

Fredericton, New Brunswick
March 1984

CONTENTS

LIST OF SYMBOLS[†]

$A, (A_s)$	Helmholtz free energy (of adsorbed phase) (3)
$A_1, A_2, \ldots$	dispersion force constants (2)
$A_2, A_3, \ldots, A_s$	virial coefficients, coefficients in Eq. (3.105) (3, 4); constants in Eq. (8.28) (8); coefficients of the van Deemter equation [Eq. (8.50)] (8)
$\mathscr{A}$	surface area (2, 3)
$a, (a^\circ)$	sorbate activity (in standard state) (3); external surface area per unit particle volume (6, 7)
a	lattice parameter (5)
B	repulsion force constant (2); mobility of sorbate (5)
$B_1, B_2, \ldots$	constants in Eq. (8.29) (8)
b, b_i	Langmuir equilibrium constant; van der Waals co-volume [Eq. (2.5)]
b_0	pre-exponential factor in $b = b_0 \exp(-\Delta H / RT)$
C	total fluid phase concentration (all species) (9, 12)
$C_0, C_1, C_2 \ldots$	constants in Eq. (8.29)
C_0', C_0, C_∞	fluid phase concentration of sorbate at $t < 0$, $t = 0$ and $t \to \infty$. (For negligible uptake $C_0 \approx C_\infty$) (6)
C_f, C_s	volumetric heat capacity of fluid and solid phases, respectively (6, 7, 8, 9)
$\overline{C}_s$	partial molar heat capacity of adsorbed phase (4)
$c, (c_i)$	sorbate concentration (of component i) in fluid phase, local concentration of species in fluid phase within the macropores (6)
c_0', c_0	initial ($t < 0$) and final ($t \geqslant 0$) steady state values of c

---

[†]Numbers in parentheses refer to the chapter in which the symbol is used. Where no chapter reference is given, symbols are common to several chapters.

c_0, c_L	fluid concentrations at inlet and outlet of countercurrent adsorber under steady-state conditions (12)
D	molar flow rate of desorbent per unit column cross section (12)
D	diffusivity
D_0	corrected diffusivity
D_*	pre-exponential factor in $D = D_* \exp(-E/RT)$
D_c	intracrystalline diffusivity
D_e	effective diffusivity
D_K	Knudsen diffusivity
D_L	axial dispersion coefficient
D_{LH}, D_{LL}	values of D_L for high- and low-pressure steps in PSA system (9)
D_m	molecular diffusivity
D_p	pore diffusivity
D_s	surface diffusivity
$\mathscr{D}$	self-diffusivity (tracer or NMR)
d	internal diameter of adsorbent bed (7)
d_e	external diameter of adsorption column (7)
d_{lm}	log mean value of d (7)
E	electric field (2); diffusional activation energy (5, 6); molar flow rate of extract per unit column cross section (12)
F	molar feed rate per unit cross-sectional area of column (12)
F_s	free energy of adsorbed phase defined by Eq. (3.26) (3)
$\mathscr{F}$	canonical partition function
f	friction factor defined by Eq. (7.1) (7)
f_s	partition function of adsorbed molecule
f_g	partition function of gaseous molecule
f_g', f_s'	partition function per unit volume for gaseous molecule
$\mathscr{f}$	fugacity (3)
G_g, G_s	molar Gibbs free energy of gaseous and adsorbed phases (3)
g	acceleration due to gravity (8)
H	HETP for a chromatographic column (8, 10, 12)
H'	HETP for a countercurrent system (12)
H, H_g, H_s	molar enthalpy of gaseous and adsorbed phases (3)
$-\Delta H$	heat of adsorption
$-\Delta H_0$	limiting heat of adsorption at low coverage
h	overall heat transfer coefficient between adsorbent particle and ambient fluid (7, 9)

h_e	external heat transfer coefficient from column wall to surroundings (7)
h_i	internal heat transfer coefficient at column wall (7)
h_w	overall heat transfer coefficient at column wall (7, 9)
J	flux (5, 6)
$K, (K_c)$	dimensionless Henry's law adsorption equilibrium constant defined as a concentration ratio based on particle volume (for zeolite crystal); combined effective equilibrium constant in Eq. (8.28) (8)
K'	Henry's law adsorption equilibrium constant defined in terms of sorbate pressure
K_0, K_0'	pre-exponential factors in $K = K_0 \exp(-\Delta U_0 / RT)$ and $K' = K_0' \exp(-\Delta H_0 / RT)$
K_{ads}, K_{des}	values of K for adsorption and desorption sections of countercurrent unit (12)
k	Boltzmann's constant (2); overall effective mass transfer coefficient (s^{-1}); constant in Eq. (3.107)
k_a, k_d	adsorption and desorption rate constants (2)
k_f	external fluid film mass transfer coefficient (7, 8)
k, k_1, k_2	constants in Eq. (3.107) (3)
k'	effective rate coefficient defined by Eq. (8.42) (8)
L	adsorbent bed length
L_{AA}, L_{AA^*}	straight and cross coefficients in Eq. (5.7) (5)
l	length of pore (2); depth of adsorbent sample (6); length of mixing element (8)
M	number of sites or subsystems (2); molecular weight (5)
$m, (m_t, m_\infty)$	mass adsorbed (at time t and as $t \to \infty$) (6)
m_1, m_2	roots of auxiliary equation (7)
N	Avogadro's number (2); number of molecules (3); number of theoretical plates in chromatographic system
N'	number of theoretical stages in countercurrent system
n	difference in number of degrees of freedom between vapor and adsorbed phases; number of moles (2)
n_1, n_2	exponents in Eq. (4.16) (6)
n_s	number of molecules or surface concentration (3)
P	total pressure
P_H, P_L	high and low pressures for PSA system
p, p_1, p_2	sorbate partial pressure
p_1, p_2	$b_1 b_2 c_1 (b_2 - b_1)^{-1}$ and $b_1 b_2 c_2 (b_2 - b_3)^{-1}$ (9)
p°	sorbate pressure in single-component system at defined spreading pressure (4) reference pressure (3)

p_s	saturation vapor pressure of liquid sorbate
Q	quadrupole moment (2)
$q, (q_1, q_2, q_i)$	sorbate concentration (of species 1, 2, and i)
q_0', q_0, q'	initial, final, and surface values of q (q_0 is in equilibrium with c_0, q_0' is in equilibrium with c_0')
$\bar{q}, \bar{\bar{q}}$	value of q averaged over crystal and pellet
q_s, q_m	saturation limit, monolayer coverage (2)
q_L	value of $\bar{q}$ at $z = L$ in countercurrent system (12)
q^*	equilibrium value of q
R	gas constant; radial coordinate for macroparticle or pellet; molar flow rate of raffinate per unit cross-sectional area of column (12)
R_f	radius of front (6)
R_p	adsorbent pellet radius
$\boldsymbol{r}$	radius vector (2)
r	radial coordinate for microparticle or crystal
r_{12}, r	distance between centers of molecules (2)
r_0	equilibrium separation between two molecules (2)
r_c	crystal or microparticle radius
$\bar{r}$	macropore radius (2); average macropore radius (5)
$S, (S_g, S_s)$	molar entropy (of gas and adsorbed phases); molar flow rate of adsorbed phase per unit column cross-sectional area (12) [$S = (1 - \epsilon)uK$ for linear systems]
ΔS	change in entropy on adsorption
T	absolute temperature
T_0', T_0	initial and final steady-state temperatures
T_s	temperature of solid (7)
T_f	temperature of fluid (7)
T_w	wall temperature (7)
$\Delta T_x, \Delta T_0$	temperature difference between bulk fluid and particle surface and between bulk fluid and center of adsorbent particle (7)
t	time
t_c	cycle time (11)
$\hat{t}$	adjusted time variable $\hat{t} = t - z/v$ (9)
$\bar{t}_A, \bar{t}_B$	mean retention times of components A and B
$U, (U_g, U_s)$	molar internal energy (of gaseous and adsorbed phases)
U_0	limiting value of U at low coverage (2)
u	linear velocity of solid in countercurrent system (12)
V	volume

V_m	molar volume of sorbate (2)
$\bar{V}_1, \bar{V}_2$	partial molar volumes of components 1 and 2
V_0	amplitude of potential variation in Eq. (5.23) (5)
$\mathscr{V}$	micropore volume
v	interstitial velocity of fluid; free volume of zeolite cage (2, 3, 4)
v_0	initial value of v at column inlet (8)
v_H, v_L	values of v for high- and low-pressure steps in PSA system (11)
v_{mf}	minimum fluidization velocity (7)
v_{max}	maximum allowable interstitial velocity (upflow) (7)
W	volume adsorbed (3)
W_0	specific micropore volume of adsorbent (3)
w	interaction energy (3, 4)
$w, (w_i)$	wave velocity (for component i) (8)
$\hat{w}$	adjusted wave velocity (9)
w'	shock wave (or constant-pattern) velocity (8)
$\hat{w}'$	adjusted shock velocity (9)
w_c, w_t	wave velocities for concentration and temperature fronts (9)
$X, (X_i)$	mole fraction (of component i) in adsorbed phase
x	coordinate [Eq. (5.23), and (6)]; wall thickness (7)
$Y, (Y_i)$	mole fraction (of component i) in fluid phase
y	coordinate [Eq. (5.23)]
Z	configuration integral (2, 3, 4); dimensionless distance z/L (12)
z	distance measured from column inlet; coordinate [Eq. (5.23)]
z'	modified distance coordinate $z - wt$

GREEK LETTERS

α	polarizability (2); van der Waals attraction constant (3); ratio of diffusional time constants $(D_c/r_c^2)/(D_p/R_p^2)$ or $(D_c/r_c^2)/(D_e/l^2)$ (6)
α, α_{ij}	separation factor $(X_i Y_j / X_j Y_i = \alpha_{ij})$
α'	ratio of time constants for heat transfer and diffusion $(ha/C_s)/(D_c/r_c^2)$ or $(ha/C_s)/(D_e/l^2)$ (6)
β	effective molecular area or volume (3, 4); $3\alpha(1 - \epsilon_p)q_0/\epsilon_p c_0$ (intraparticle diffusion) or $3\alpha(1 - \epsilon)q_0/\epsilon c_0$ (diffusion in a bed of particles) (6); constant (7)
β, β_{ij}	equilibrium factor [Eq. (8.3)]; $\beta_{ij} = 1/\alpha_{ji}$ [Eq. (9.5)]

β'	modified separation factor [Eq. (11.9)]; $(\Delta H/C_s)(\partial q^*/\partial T)_p$ (6)
γ	$\beta \Lambda/[\beta + 3\alpha(1 - \Lambda)]$ (6); ratio of external film and diffusional time constants $(15\epsilon_p D_p/R_p^2)/(3k_f/R_p)$ (8); $q_0 C_f/c_0 C_s$ (9); λ^d/λ^a (11); ratio of downflow to upflow rates in countercurrent system $= (1 - \epsilon)Ku/\epsilon v$ (12)
$\gamma, (\gamma_1, \gamma_2)$	activity coefficient (of components 1, 2) (3, 4)
γ_1, γ_2	constants in Eq. (7.6)
δ	ratio defined in Eq. (6.79) (6); ratio of external film resistance and axial dispersion $[kKD_L(1 - \epsilon)/\epsilon v^2$ or $3k_f D_L(1 - \epsilon)/\epsilon R_p v^2]$ (8)
$\epsilon, \epsilon_1, \epsilon_2$	attractive force constants in Lennard-Jones potential (2)
ϵ	voidage of adsorbent bed; adsorption potential defined by Eq. (3.106) (3)
ϵ_p	porosity of adsorbent particle
Θ	fractional saturation $= q/q_m$ or q/q_s (2, 3, 4)
θ	contact angle (2); $(\Delta H/RT_0^2)(T - T_0)$ (8); $(T - T_0)C_s/T_0(-\Delta H)q_0$ (9)
Λ	$(C_0 - C_\infty)/C_0 =$ fraction of sorbate taken up by adsorbent (6)
$\Lambda_1, \Lambda_1', \Lambda_2, \Lambda_2'$	constants in Wilson equation (3, 4)
λ	absolute activity $= e^{\mu/kT}$ (3); nonlinearity parameter $\lambda = 1 - \beta = q_0/q_s$ (8, 9); parameter in Eq. (9.26) (9)
$\lambda_f, (\lambda_g)$	thermal conductivity of fluid (gas) (7)
λ_s	thermal conductivity of solid (7)
λ_w	thermal conductivity of column wall (7)
λ_L	effective axial thermal conductivity
λ^a	q_0/q_s for adsorption (11)
λ^d	q_0/q_s for desorption (11)
μ	$(C_s/q_0 - C_f/c_0)/R(-\Delta H/RT_0)^2$ (8)
μ	dipole moment (2); chemical potential (3); viscosity (7); mean retention time (8); parameter in Eq. (9.27) (9)
μ°	standard chemical potential parameter in Eq. (9.30)
ν	vibration frequency (Appendix A)
χ	parameter in Eq. (9.31)
Ξ	grand partition function (3, Appendix A)
ξ	defined by Eq. (3.90) (3); dimensionless column length $(kKz/v)(1 - \epsilon)/\epsilon$ or $(15D/R^2)(Kz/v)(1 - \epsilon)/\epsilon$. In nonlinear case K is replaced by q_0/c_0 (8, 9)
ξ^a, ξ^d	values of ξ for adsorption and desorption cycle (11)
ξ'	$(k'Kz/v)(1 - \epsilon)/\epsilon$ (7); $\xi - \gamma\tau$ (9)

ξ''	$(kz/v)(1-\epsilon)/\epsilon$ or $(15D/R^2)(z/v)(1-\epsilon)/\epsilon$ (8)
ξ	extent of separation (12)
π	spreading pressure (2, 3, 4)
ρ	density of adsorbent (6)
ρ_l	density of liquid sorbate (2)
ρ_f	density of fluid (7)
ρ_s	density of solid (7)
$\sigma, \sigma_1, \sigma_2$	repulsive force constants in Lennard-Jones potential (2); surface tension [Eq. (2.33)–(2.35)] (2); average area per molecule (4); standard deviation of chromatographic response peak (8)
σ_i	standard deviation of injection peak (10)
σ_A, σ_B	standard deviation of response peaks for components A and B
σ_0	van der Waals radius (2)
τ	dimensionless time variable Dt/R^2, $D_c t/r_c^2$; stoichiometric time in Eq. (6.28) (6); dimensionless time $k(t-z/v)$ or $(15D/R^2)(t-z/v)$ (8, 9, 12); tortuosity factor (5, 7, 10)
τ'	modified dimensionless time variable (8); $D_e t/l^2$ (6)
τ_c	correlation time (5); cyclic time (11)
Φ	surface potential $= \mu_{0a} - \mu_a$ (3, 4)
ϕ	three-dimensional spreading pressure (3); potential energy (subscripts D, R, P, Q, μ denote contributions from dispersion, repulsion, polarization, quadrupole, and dipole interactions) (2); ϕ_0 is zero point energy of sorbate (2)
ϕ, ϕ_i	dimensionless fluid phase concentration (8, 9)
$\bar{\phi}$	value of ϕ averaged over a zeolite cage (2, 5)
ψ, ψ_i	dimensionless concentration in adsorbed phase q/q_0 (8, 9)
$\bar{\psi}$	value of ψ averaged over adsorbent bed (11)
χ	$4h_w/kq_0 d(1-\epsilon)R(-\Delta H/RT_0)^2$ (8); magnetic susceptibility (2)
Ω	$(-\Delta H)c_0/C_f T_0$ (9)

COMMON DIMENSIONLESS GROUPS

$(\text{Bi})_h$	$hR_p/3\lambda_s$	Biot Number for heat transfer
$(\text{Bi})_m$	$k_f R_p/3\epsilon_p D_p$	Biot Number for mass transfer
Nu	$h(2R_p)/\lambda_f$	Nusselt Number
Pe'	$v(2R_p)/D_L$	Peclet Number for particle (7)
Pe'_∞	Limiting value of Pe' as $\text{Re} \to \infty$ (11)	

Pe	vL/D_L	Axial Peclet Number for column (8, 12)
Pr	$C_f\mu/\lambda_f\rho_f$	Prandtl Number
Re	$\rho_f v\epsilon(2R_p)/\mu$	Reynolds Number
Sc	$\mu/\rho_f D_m$	Schmidt Number
Sh	$k(2R_p)/D_m$	Sherwood Number
St	kL/v or kL/u	Stanton Number (8, 12)

1

MICROPOROUS ADSORBENTS

The ability of porous solids to reversibly adsorb large volumes of vapor was recognized in the eighteenth century and early experiments were carried out by Scheele and Fontana[1] but the practical application of this property to the large-scale separation and purification of industrial process streams is relatively recent. Perhaps the most familiar example of such a process is the use of an adsorbent column, packed with a suitable hydrophilic adsorbent, as a drier for the removal of traces of moisture from either gas or liquid streams. Similar processes are also in common use on a large scale for the removal of undesirable impurities such as H_2S and mercaptans from natural gas and organic pollutants from water. Such processes are conveniently classified as purification processes since the components which are adsorbed are present only at low concentration, have little or no economic value, and are frequently not recovered. The economic benefit of the process is derived entirely from the increase in the purity and hence the value of the stream containing the major component.

The application of adsorption as a means of separating mixtures into two or more streams, each enriched in a valuable component which is to be recovered, is a more recent development. Early examples include the Arosorb process for recovery of aromatic hydrocarbons[2] which was introduced in the early 1950s and a variety of processes, first introduced in the early 1960s, for the separation of linear paraffins from branched and cyclic isomers. During the 1970s there has been a significant increase in both the range and scale of such processes. The economic incentive has been the escalation of energy prices, which has made the separation of close boiling components by distillation a costly and uneconomic process. For such mixtures it is generally possible to find an adsorbent for which the adsorption separation factor is much greater than the relative volatility, so that a more economic adsorptive separation is in principle possible. However for an adsorption process to be developed on a commercial scale requires the availability of a suitable

1

adsorbent in tonnage quantities at economic cost. This has stimulated funda-mental research in adsorption and led to the development of new adsorbents.

The earlier adsorption processes used either activated carbon or silica gel adsorbents but the potential of adsorption as a separation process was greatly enhanced by the development of molecular sieve adsorbents, especially the synthetic zeolites, which first became available on a commercial scale in the late 1950s. Since then a wide range of zeolite structures have been synthesized, several of which have proved to be useful adsorbents and are now available commercially.

1.1. ADSORPTION VS DISTILLATION

Because of its simplicity and near universal applicability, distillation has assumed a dominant role in separations technology and is the standard against which other potential processes are generally measured. However, distillation is not an energy efficient process and with the rising cost of energy alternative separation processes have attracted increasing attention.
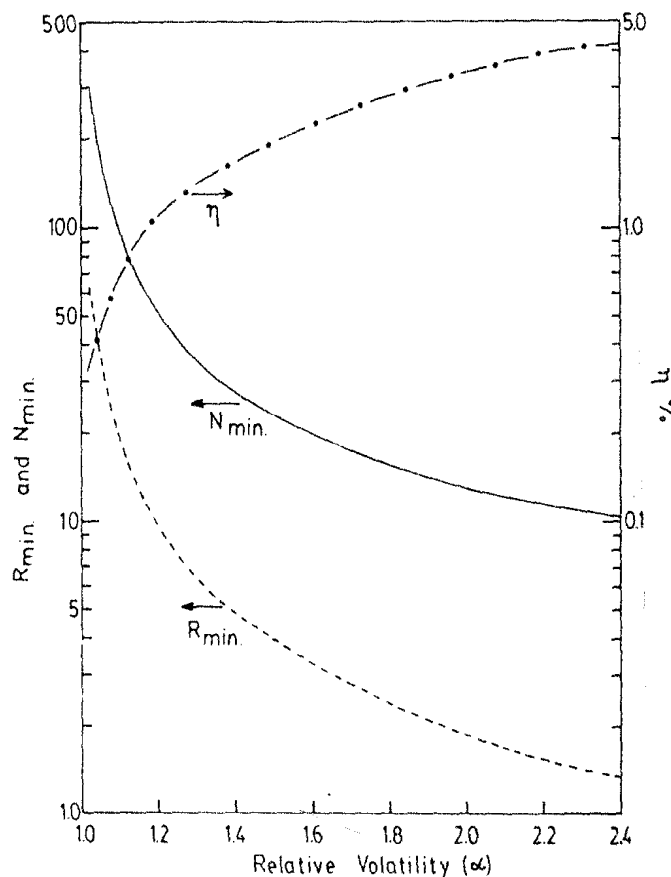
FIGURE 1.1. Variation of thermal efficiency (η), minimum number of theoretical stages (N), and minimum reflux ratio (R) with relative volatility (α) for separation of a 50–50 molar mixture into top and bottom products each of 99% purity.

Figure 1.1 shows a plot of the thermal efficiency and minimum reflux requirement against relative volatility (α) for the separation, by distillation, of a hypothetical 50–50 mixture of two aromatic hydrocarbons (A and B) into two streams, one containing 99% A + 1% B and the other containing 99% B + 1% A. Thermal efficiency is calculated as the ratio of the free energy of mixing to the reboiler heat load at minimum reflux. The heat of evaporation has been taken as 8070 cal/mole, corresponding to toluene. For separation of a mixture of benzene and toluene ($\alpha \sim 2.4$) the thermal efficiency is about 4.2%. As the relative volatility is decreased the thermal efficiency falls rapidly due to the increasing reflux requirement.

Also shown in Figure 1.1 is a plot of the minimum number of theoretical stages required to effect the specified separation at total reflux. This number increases rapidly with decreasing α, and it is evident that for systems in which α is less than about 1.2 distillation is very inefficient.

Although the cost of an adsorption separation process is generally higher than that of a distillation unit with an equivalent number of theoretical stages, much higher separation factors are commonly attainable in an adsorption system. Thus, as the relative volatility decreases, an adsorption process eventually becomes the more economic option. The break-even point, of course, depends to a considerable extent on the particular system as well as on the cost of energy, but as a rough guide it appears that, with present technology, adsorption becomes competitive with distillation for bulk separations when the relative volatility is less than about 1.25. For purification processes involving light gases, where the alternative is cryogenic distillation, the cost comparison is generally more favorable to adsorption so that adsorption is commonly the preferred route even when the relative volatility is high.

1.2. SELECTIVITY

The primary requirement for an economic separation process is an adsorbent with sufficiently high selectivity, capacity, and life. The selectivity may depend on a difference in either adsorption kinetics or adsorption equilibrium. Examples of processes of both kinds are noted in Chapter 11 but most of the adsorption processes in current use depend on equilibrium selectivity. In considering such processes it is convenient to define a separation factor:

$$\alpha_{AB} = \frac{X_A/X_B}{Y_A/Y_B} \tag{1.1}$$

where X_A and Y_A are, respectively, the mole fractions of component A in adsorbed and fluid phases at equilibrium. The separation factor defined in this way is precisely analogous to the relative volatility, which measures the ease with which the components may be separated by distillation. The analogy is, however, purely formal and there is no quantitative relationship between the separation factor and relative volatility. For two given components the relative

volatility is fixed whereas the separation factor varies widely depending on the adsorbent.

The search for a suitable adsorbent is generally the first step in the development of an adsorption separation process. Since the separation factor generally varies with temperature and often also with composition, the choice of suitable conditions to maximize the separation factor is a major consideration in process design. For an ideal Langmuir system the separation factor is independent of composition and equal to the ratio of the Henry's law constants of the two relevant components. Preliminary selection of suitable adsorbents can therefore sometimes be made directly from available Henry constants. More commonly it is necessary to screen a range of possible adsorbents, which may be conveniently accomplished by the measurement of chromatographic retention times. In addition to providing a quick and reliable method of estimating separation factors the chromatographic method has the advantage that it also provides information on the adsorption kinetics.

Kinetic separations are in general possible only with molecular sieve adsorbents such as zeolites or carbon sieves. The kinetic selectivity is measured by the ratio of the micropore or intracrystalline diffusivities for the components considered. Differences in diffusion rates between molecules of comparable molecular weight become large enough to provide a useful separation only when diffusion is hindered by steric effects. This requires that the diameter of the micropore be comparable with the dimensions of the diffusing molecule. Molecular sieve separations, which depend on the virtually complete exclusion of the larger molecule from the micropores, as in the separation of linear from branched and cyclic hydrocarbons on 5A zeolite, may be regarded as the extreme limit of a kinetic separation in which the rate of adsorption of one component is essentially zero. Because the geometric requirements for a molecular sieve separation are stringent, such separations are less common than separations based on differences in adsorption equilibrium or on moderate differences in intracrystalline diffusivity.

1.3. PRACTICAL ADSORBENTS

The requirement for adequate adsorptive capacity restricts the choice of adsorbents for practical separation processes to microporous adsorbents with pore diameters ranging from a few Ångstroms to a few tens of Ångstroms. This includes both the traditional microporous adsorbents such as silica gel, activated alumina, and activated carbon as well as the more recently developed crystalline aluminosilicates or zeolites. There is however a fundamental difference between these materials. In the traditional adsorbents there is a distribution of micropore size, and both the mean micropore diameter and the width of the distribution about this mean are controlled by the manufacturing process. By contrast, the micropore size of a zeolitic adsorbent is controlled by the crystal structure and there is virtually no distribution of pore size. This

leads to significant differences in the adsorptive properties, and it is therefore convenient to consider the zeolites and other crystalline adsorbents such as the aluminum phosphate molecular sieves as a separate class of adsorbents.

Silica Gel

Silica gel is a partially dehydrated form of polymeric colloidal silicic acid. The chemical composition can be expressed as $SiO_2 \cdot nH_2O$. The water content, which is present mainly in the form of chemically bound hydroxyl groups, amounts typically to about 5 wt. %. The material appears first to have been developed during the First World War for use in gas masks although in this service it proved inferior to activated carbon.

A variety of methods for the manufacture of silica gel have been described including the hydrolysis of soluble alkali metal silicates with acid[3] and the direct removal of sodium from sodium silicate solutions by ion exchange.[4] The silicic acid liberated polymerizes and condenses in the aqueous solution to form chains and nets of linked SiO_4 tetrahedra which aggregate to form approximately spherical particles of 20–200 Å diameter. On drying, the particles agglomerate to form a microporous structure in which the pore size is determined mainly by the size of the original microparticles. Bond formation between adjacent particles occurs with the elimination of water between neighboring hydroxyl groups and the final structure is therefore physically robust. The size of the original microparticles and consequently the size of the
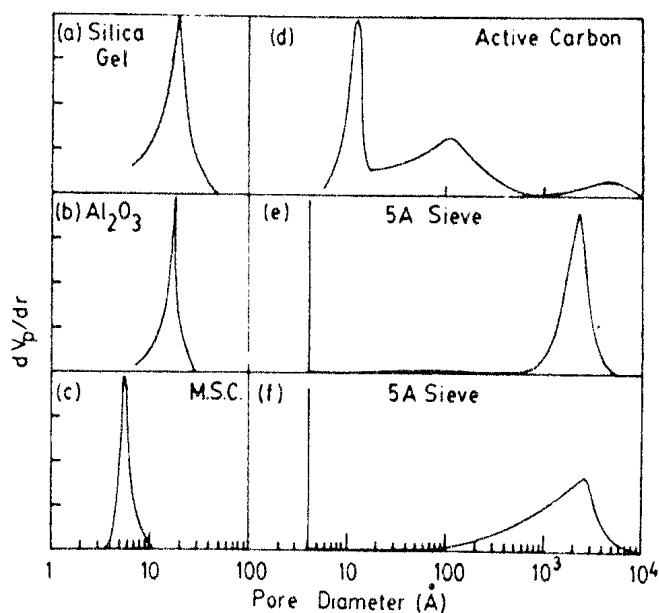
FIGURE 1.2. Pore size distribution for (a) silica gel ($V_p = 0.82$ cm³/g)[5]; (b) porous alumina ($V_p = 0.37$ cm³/g)[7]; (c) molecular sieve carbon ($V_p = 0.25$ cm³/g)[9]; (d) activated carbon ($V_p = 0.95$ cm³/g)[8]; (e) Davison binderless 5A molecular sieve type 625 ($V_p = 0.25$ cm³/g)[10]; (f) Davison 5A molecular sieve type 525 ($V_p = 0.28$ cm³/g)[10]. (Ordinate scale is in arbitrary units.)
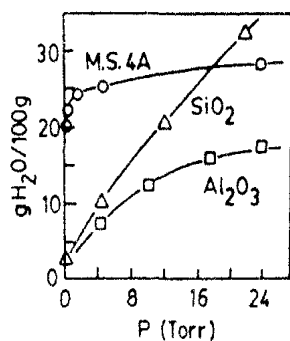
FIGURE 1.3. Equilibrium isotherms for sorption of water vapor at 25°C on 4A molecular sieve, activated alumina, and silica gel. (From ref. 19, copyright John Wiley & Sons, Inc., 1974; reprinted with permission.)

micropores in the final dried gel is sensitive to pH[5] and to the presence of other cations in the solution[6] during precipitation. By careful control of the synthesis conditions it is therefore possible to control the pore size, which generally shows a unimodal distribution, as illustrated in Figure 1.2.

The presence of hydroxyl groups imparts a degree of polarity to the surface so that molecules such as water, alcohols, phenols, and amines (which can form hydrogen bonds) and unsaturated hydrocarbons (which can form π-complexes) are adsorbed in preference to nonpolar molecules such as saturated hydrocarbons. Because of its selectivity for aromatics silica gel was used as the adsorbent in the Arosorb process for separation of aromatics from paraffins and naphthenes[2] but by far the most important current application is as a desiccant.

Equilibrium isotherms for adsorption of water on 4A zeolite, silica gel, and alumina are compared in Figure 1.3.[11] The water isotherms for all zeolites are similar, with a well-defined saturation plateau corresponding to complete filling of the intracrystalline micropore volume. By contrast, the isotherms for silica gel and alumina show a continuous increase in loading with water vapor pressure as a result of the distribution of micropore size. As the water vapor pressure increases the regime of multilayer surface adsorption merges into capillary condensation, which occurs in pores of ever increasing diameter as the pressure is raised. Thus, preliminary information concerning the distribution of pore size can often be deduced directly from the form of the

TABLE 1.1. Properties of Commercial Silica Gels (W. R. Grace)[12]

	High Area	Low Area
Specific pore vol. (cm³/g)	0.43	1.15
Average pore diameter (Å)	22	140
Specific surface Area (m² g⁻¹)	800	340
Particle density (g cm⁻³)	1.09	0.62

equilibrium isotherm. Although water is adsorbed more strongly on molecular sieves than on alumina or silica gel, as may be judged from the initial slopes of the isotherms, the ultimate capacity of silica gel, at least at low temperatures, is generally higher. Silica gel is therefore a useful desiccant where high capacity is required at low temperature and moderate vapor pressures.

Some properties of two representative commercial silica gels are summarized in Table 1.1.

Activated Alumina

Activated alumina is a porous high-area form of aluminum oxide, prepared either directly from bauxite ($Al_2O_3 \cdot 3H_2O$) or from the monohydrate by dehydration and recrystallization at elevated temperature. The surface is more strongly polar than that of silica gel and has both acidic and basic character, reflecting the amphoteric nature of the metal.

As may be seen from Figure 1.3, at room temperature the affinity of activated alumina for water is comparable with that of silica gel but the capacity is lower. At elevated temperatures the capacity of activated alumina is higher than silica gel and it was therefore commonly used as a desiccant for drying warm air or gas streams. However, for this application it has been largely replaced by molecular sieve adsorbents which exhibit both a higher capacity and a lower equilibrium vapor pressure under most conditions of practical importance.

Activated Carbon

Activated carbon is normally made by thermal decomposition of carbonaceous material followed by activation with steam or carbon dioxide at elevated temperature (700–1100°C).[4] The activation process involves essentially the removal of tarry carbonization products formed during the pyrolisis, thereby opening the pores.

The structure of activated carbon consists of elementary microcrystallites of graphite, but these microcrystallites are stacked together in random orientation and it is the spaces between the crystals which form the micropores. The pore size distribution is typically trimodal as illustrated in Figure 1.2.[8] The actual distribution and the total pore volume associated with each pore size range are however sensitive to the conditions of the initial pyrolisis and activation procedures. Typical ranges are given in Table 1.2, but by special procedures it is possible to prepare activated carbons with even higher porosity, surface area, and adsorptive capacity.

The surface of carbon is essentially nonpolar although a slight polarity may arise from surface oxidation. As a result, carbon adsorbents tend to be hydrophobic and organophilic. They are therefore widely used for the adsorption of organics in decolorizing sugar, water purification, and solvent recovery systems as well as for the adsorption of gasoline vapors in automobiles and as

TABLE 1.2.   Pore Sizes in Typical Activated Carbons

	Micropore	Mesopores or Transitional Pores	Macropores
Diameter (Å)	< 20	20–500	> 500
Pore volume (cm³/g)	0.15–0.5	0.02–0.1	0.2–0.5
Surface area (m²/g)	100–1000	10–100	0.5–2
(Particle density 0.6–0.9 g/cm³; porosity 0.4–0.6)			

a general purpose adsorbent in range hoods and other air purification systems. In order to decrease the mass transfer resistance, the activated carbons used for adsorption from the liquid phase generally have somewhat larger pore diameters than those used for adsorption from the gas phase.

Carbon Molecular Sieves

Activated carbon adsorbents generally show very little selectivity in the adsorption of molecules of different size. However, by special activation procedures it is possible to prepare carbon adsorbents with a very narrow distribution of micropore size and which therefore behave as molecular sieves. The earliest examples of carbon molecular sieves appear to have been prepared by decomposition of polyvinylidene dichloride (Saran) but more recently a wide variety of starting materials have been used.[13,14] Most commercial carbon sieves are prepared from anthracite or hard coal by controlled oxidation and subsequent thermal treatment.[15] The pore structure may be modified to some extent by subsequent treatment including controlled cracking of hydrocarbons within the micropore system and partial gasification under carefully regulated conditions.[16,17]

By these means it is possible to prepare carbon sieves with effective micropore diameters ranging from about 4 to 9 Å. The micropore size distribution of such sieves is much narrower than in a typical activated carbon and the porosity and therefore the adsorptive capacity are generally very much smaller, as may be seen from Figure 1.2. The ability to modify the effective pore size by adjusting the conditions of the manufacturing process makes it relatively easy to tailor a carbon sieve to achieve a particular separation. However, it is difficult to achieve absolute reproducibility between different batches,[14] and the existence of a distribution of pore size, even if narrow, means that the molecular sieving selectivity of a carbon sieve seldom approaches the almost perfect separation achievable under favorable circumstances with a zeolite sieve. Nevertheless, the kinetic selectivities which may be attained with a well-prepared carbon sieve are remarkably high.

A review of current and proposed applications of carbon sieves has been given by Jüntgen.[9] At present the most important large-scale application is in air separation. Surprisingly, deterioration of the sieve due to oxidation appears not to have proved a significant problem. Other potential areas of application include the clean-up of the off-gases from nuclear facilities and the production of pure hydrogen from gas streams containing small amounts of hydrocarbons. However, in the former application considerations of safety make the use of a combustible adsorbent highly undesirable[18] and in the latter application hydrogen purification processes based on zeolite molecular sieves are well established. A wider range of process applications seems likely to emerge as the technology of producing carbon sieves develops further.

1.4. ZEOLITES

Zeolites are porous crystalline aluminosilicates. The zeolite framework consists of an assemblage of SiO_4 and AlO_4 tetrahedra,[†] joined together in various regular arrangements through shared oxygen atoms, to form an open crystal lattice containing pores of molecular dimensions into which guest molecules can penetrate. Since the micropore structure is determined by the crystal lattice it is precisely uniform with no distribution of pore size. It is this feature which distinguishes the zeolites from the traditional microporous adsorbents.

About 38 different zeolite framework structures have been identified, including both natural and synthetic forms. Detailed reviews have been given by Breck,[19] Barrer,[20] Meier,[21] and Smith.[22,23] The "Atlas of Zeolite Structures" prepared by Meier and Olson[24] contains numerous stereoscan pictures and is especially useful for quick reference. The present discussion is therefore limited to a brief review of the structures of some of the more important commercial zeolite adsorbents.

In considering zeolite frameworks it is convenient to regard the structures as built up from assemblages of secondary building units, which are themselves polyhedra made up of several SiO_4 and AlO_4 tetrahedra. The secondary building units and some of the commonly occurring polyhedra are shown schematically in Figure 1.4. In these diagrams each vertex represents the location of a Si or Al atom while the lines represent, approximately, the diameters of the oxygen atoms or ions which are very much larger than the tetrahedral Si or Al atoms.

Each aluminum atom introduces one negative charge on the framework which must be balanced by an exchangeable cation. The exchangeable cations are located at preferred sites within the framework and play a very important role in determining the adsorptive properties. Available information on cation

---

[†] Since each oxygen is shared between two tetrahedral Al or Si atoms the stoichiometric composition of each tetrahedral unit is SiO_2 or AlO_2.

(a)

S4R   S6R   S8R

T_8O_{16} (5-1)   D5R
(Mordenite)   (Silicalite/ZSM-5)

(b)

α   β   D8R   D6R

γ   ε
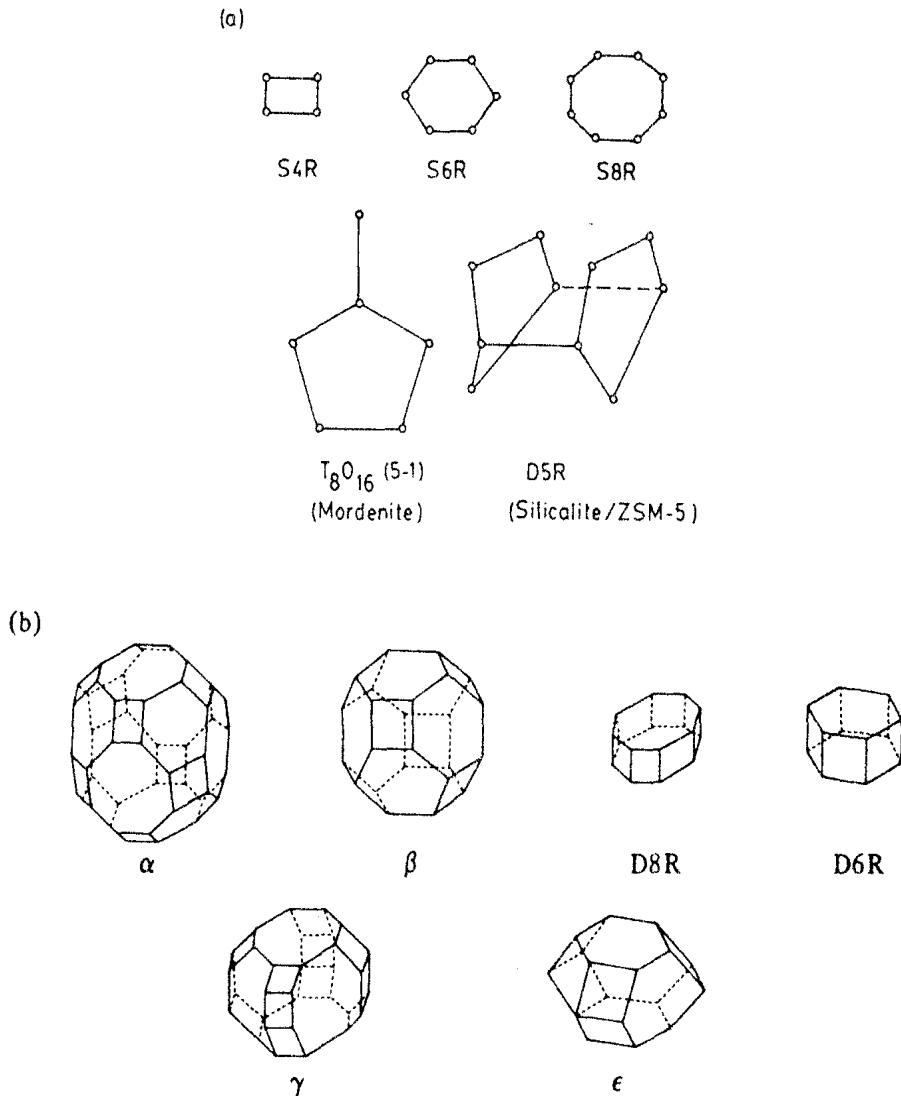
FIGURE 1.4. (a) Secondary building units and (b) commonly occurring polyhedral units in zeolite framework structures. (From ref. 19, copyright John Wiley & Sons, Inc., 1974; reprinted with permission.)

locations has been recently summarized by Mortier.[25] Changing the exchangeable cation by ion exchange provides a useful and widely exploited means of modifying the adsorptive properties.

The Si/Al ratio in a zeolite is never less than 1.0 but there is no upper limit and pure silica analogs of some of the zeolite structures have been prepared. The adsorptive properties show a systematic transition from the aluminum-rich sieves, which have very high affinities for water and other polar molecules, to the microporous silicas such as silicalite which are essentially hydrophobic and adsorb n-paraffins in preference to water. The transition from hydrophilic to hydrophobic normally occurs at a Si/Al ratio of between 8 and 10. By appropriate choice of framework structure, Si/Al ratio and cationic
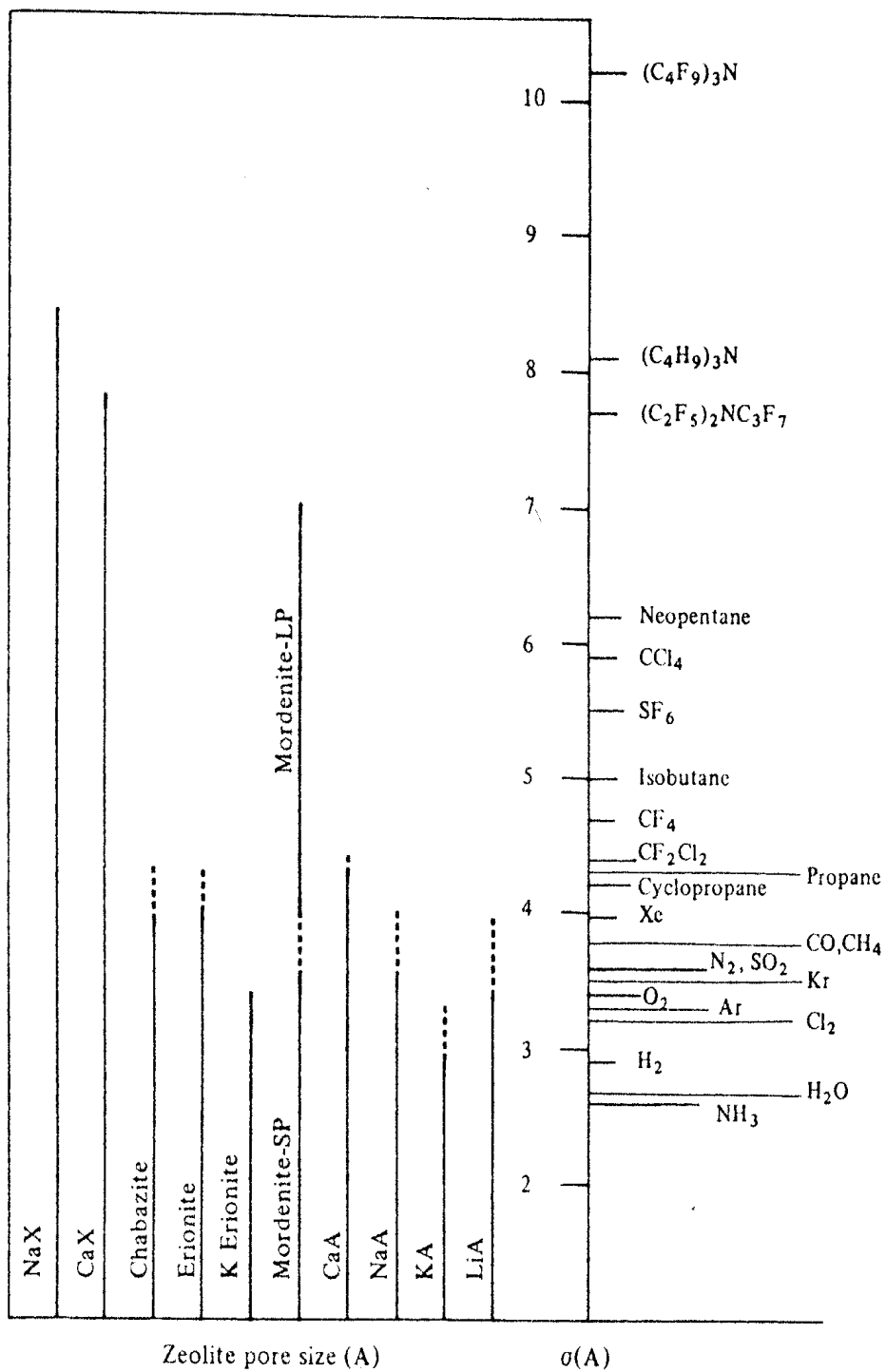
FIGURE 1.5. Chart showing correlation between effective pore size of various zeolites and Lennard–Jones kinetic diameter. The dotted portions indicate the range over which the cut-off occurs between low and high temperatures (77–420 K). (From ref. 19, copyright John Wiley & Sons, Inc., reprinted with permission.)

form, adsorbents with widely different adsorptive properties may be prepared. It is therefore possible, in certain cases, to tailor the adsorptive properties to achieve the selectivity required for a particular separation.

The intracrystalline diffusivity and hence the kinetic selectivity and, in extreme cases, the molecular sieve properties are determined mainly by the free diameters of the windows in the intracrystalline channel structure. In zeolites such as a sodalite the channels are constricted by six-membered oxygen rings with free diameter of about 2.8 Å. These pores are so small that only small polar molecules such as H_2O and NH_3 can penetrate. In the "small-port" zeolites such as type A, chabazite, and erionite, the limiting constrictions are eight-membered oxygen rings with free diameter of 4.2 Å while in the "large-port" zeolites, X and Y and mordenite access is through twelve membered oxygen rings which have free diameters of 7–7.4 Å. The pentasil zeolites, which include ZSM-5, ZSM-11, and silicalite, are characterized by an intermediate channel size (5.7 Å) formed by 10-membered oxygen rings.

The window apertures quoted here are the free diameters calculated from structural models assuming a diameter of 1.4 Å for the oxygens. Due to the effects of vibration of both the diffusing molecule and the crystal lattice, these windows may be penetrated by molecules with critical kinetic diameters which are somewhat greater than the nominal aperture. The effective diameters of the unobstructed 8-, 10-, and 12-ring sieves are therefore approximately 4.5, 6.0, and 8.5 Å.

The reduction in the free diameter of the windows by blocking cations causes a dramatic reduction in the diffusivity of the guest molecules. The extent to which the windows are obstructed depends on the number and nature of the cations since different cations show differing affinities for the window sites. By appropriate choice of cationic form it is sometimes possible to develop kinetic selectivity and even, in certain cases, to obtain a molecular sieve separation between species which can both diffuse easily in an unobstructed sieve. A schematic representation showing the effective apertures for some cationic forms of A and X zeolites, as well as in some other sieves, is shown in Figure 1.5.

Zeolite A

The structure of zeolite A[11] is shown schematically in Figure 1.6. The pseudo cell consists of eight β cages (or sodalite cages) located at the corners of a cube and joined through four-membered oxygen rings (S4R). This arrangement forms a large polyhedral α cage of free diameter about 11.4 Å accessible through eight-membered oxygen windows. Stacking these units in a cubic lattice gives a three-dimensional isotropic channel structure, constricted by eight-membered oxygen rings.

Each pseudo cell contains 24 tetrahedral (AlO_2 or SiO_2) units and as the
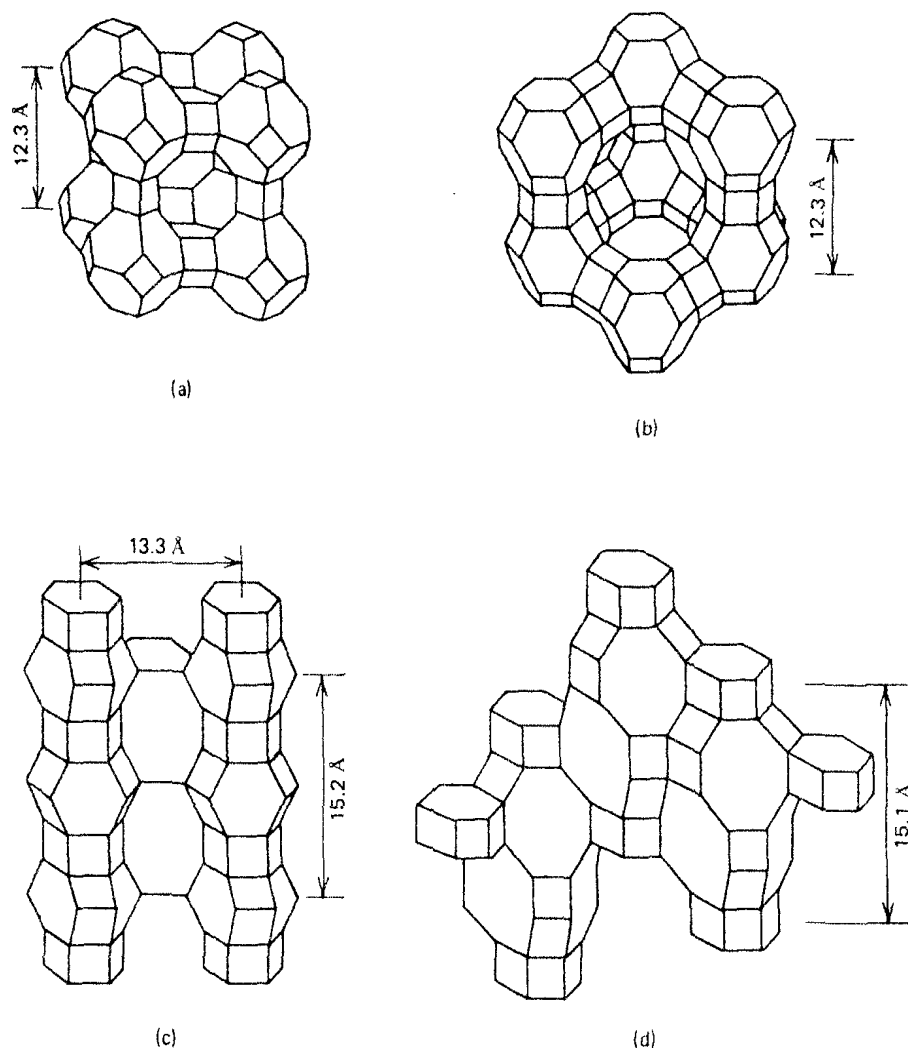
FIGURE 1.6. Schematic representation showing framework structures of (a) zeolite A, (b) zeolites X and Y, (c) erionite and (d) chabazite. (To translate these schematic diagrams into the actual structure, a Si or Al is placed at each vertex and an O at or near the center of each line.)

Si/Al ratio in zeolite A is always close to 1.0 there are 12 univalent exchangeable cations per cell. Three distinct cation sites have been identified; near the centers of the six-rings in the eight corners of the central cavity (type I), in the eight-rings (type II), and on the cage wall in close proximity to a four-ring (type III). With most cations the type I sites are preferentially occupied, followed by the type II sites, and the type III sites are filled only after all sites of types I and II have been occupied. In the sodium form (4A) there are 12 cations per cage. These are accommodated in the eight type I sites and the three type II sites (the six eight-rings are each shared between two cages) with one cation in a type III site. All windows are therefore partially obstructed by a sodium cation and the effective aperture of the sieve is therefore reduced from about 4.4 to 3.8 Å. If the Na^+ cations are exchanged for Ca^{2+} or Mg^{2+}

the number of cations per cell decreases. At 67% exchange there are only eight cations per cell and all these can be accommodated in the type I sites. Thus in Ca^{2+} or Mg^{2+} form (5A) the effective aperture is increased and somewhat larger molecules can penetrate.

Since the diameter of the potassium ion is greater than that of sodium, a sieve with a smaller effective aperture (3A sieve) is obtained by potassium exchange. The 3A sieve is widely used for drying reactive hydrocarbons such as olefins since the small pore size prevents penetration of the lattice and thus the possibility of reaction.

Zeolites X and Y

The synthetic zeolites X and Y and the natural zeolite faujasite all have the same framework structure which is sketched in Figure 1.6. The crystallographic unit cell consists of an array of eight cages containing a total of 192 AlO_2 and SiO_2 tetrahedral units. The framework may be thought of as a tetrahedral lattice of sodalite units connected through six-membered oxygen bridges, or equivalently as a tetrahedral arrangement of double six-ring units. The resulting channel structure is very open with each cage connected to four other cages through twelve-membered oxygen rings of free diameter ~ 7.4 Å. Quite large molecules such as neopentane and tertiary butyl amine can penetrate these pores.

The difference between the X and Y sieves lies in the Si/Al ratio which is within the range 1–1.5 for X and 1.5–3.0 for Y. There is a corresponding difference in the number of exchangeable univalent cations, which varies from about 10–12 per cage for X to as low as 6 for high silica Y. Five different cation sites have been identified as indicated in Figure 1.7. The cation distribution, which is much more complex than in zeolite A has been discussed by Breck[19] and Smith[22,23] and a comprehensive summary, including 69 references giving information on cation locations for a wide variety of different cationic forms of X and Y, is included in Mortier's compilation of extra-framework cation sites.[25]

The distribution of the cations between the various sites depends both on the nature and number of the cations and is affected by the presence of traces of moisture. There is even some tentative evidence that the equilibrium

---

FIGURE 1.7.   Schematic diagrams showing disposition of the cation sites in zeolites X and Y in two different representations. Starting at the center of symmetry and proceeding along the threefold axis toward the center of the unit cell, site I is the 16-fold site located in the center of the double six-ring (hexagonal prism). Site I' is on the inside of the β-cage adjacent to the D6R. Site II' is on the inside of the sodalite unit adjacent to the single six-ring. Site II approaches the single six-ring outside the β-cage and lies within the large cavity opposite site II'. Site III refers to positions in the wall of the large cavity, on the fourfold axis in the large 12-ring aperture. The four different types of oxygens, O(1), O(2), O(3), and O(4), are also indicated in their relative positions. (Reprinted with permission from ref. 22. Copyright 1971 American Chemical Society and from ref. 19, copyright John Wiley & Sons, Inc., 1974.)

bridging 4-ring
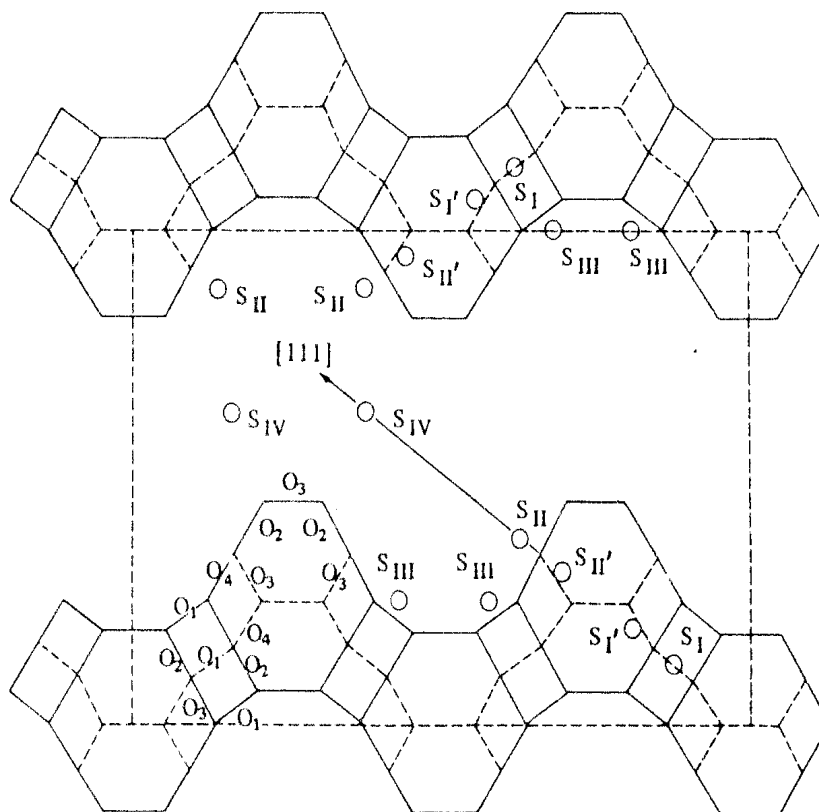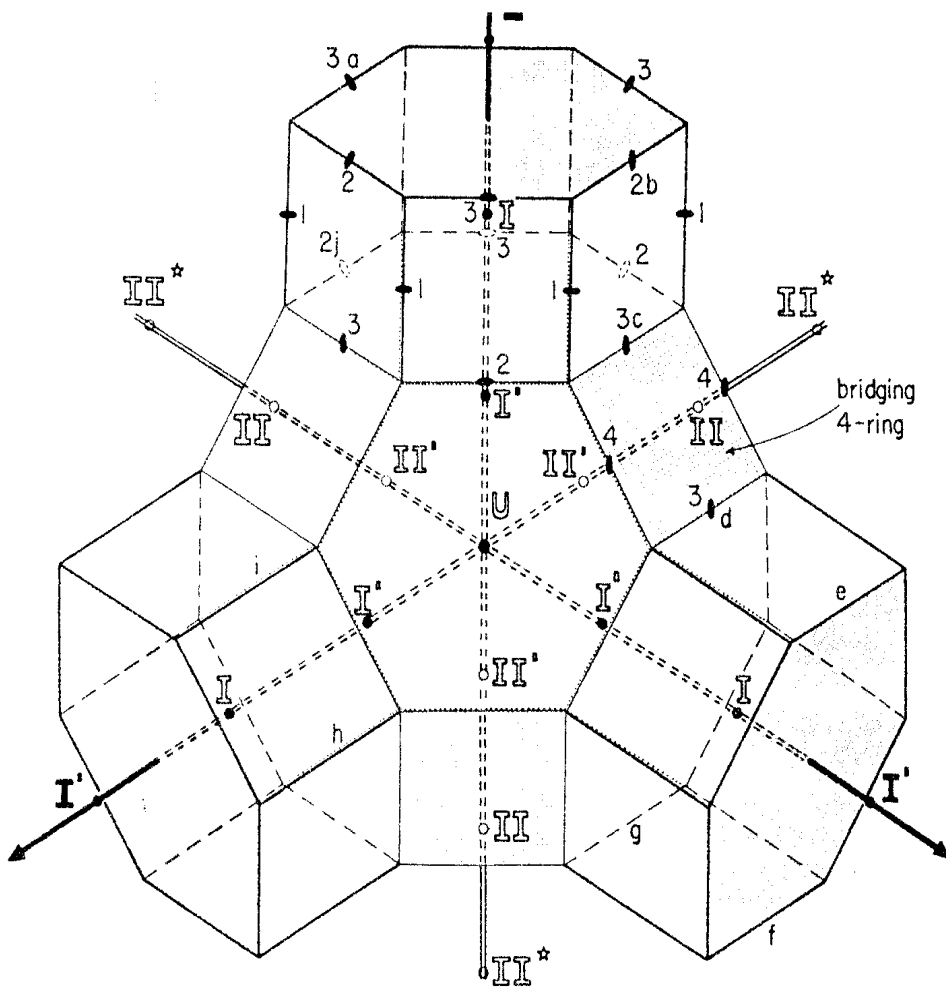
distribution may change when the sieve is loaded with adsorbent. The adsorptive properties of X and Y sieves may therefore be greatly modified by ion exchange and improvements in selectivity can sometimes be obtained by using mixed cationic forms. While it is evident that the variation in adsorptive properties is probably related to a redistribution of the cations among the possible sites, the precise relationship between the adsorptive properties and the cation distribution is still not fully understood. Adsorbent development has generally been based on empirical screening studies, guided by a few simple general principles.

Mordenite

The framework structure of mordenite, which can be considered as built up from stacked T_8O_{16} units, as shown schematically in Figure 1.8. The Si/Al ratio in both natural and synthetic forms is generally close to 5.0 but the aluminum content of the framework may be decreased substantially by acid leaching without significant loss of crystallinity. Unlike the other zeolites considered in this chapter, the channel structure of mordenite is unidimensional with blind side pockets. The main channel, which is formed from twelve-membered oxygen rings, has a nominal free diameter of 6.7–7.0 Å. However, natural mordenite behaves as a small-port zeolite and even small molecules such as methane and ethane are only slowly adsorbed. This appears to be due to blocking of the main channels by extraneous material. The sieve may be opened by controlled acid leaching which evidently removes some of the detrital material from the channels. It is possible to prepare synthetically the large-port form of mordenite in which the channels are substantially free from blockage and which shows the expected diffusional properties for a 12-ring sieve.

The effects of pore blocking may be expected to be more serious in a one-dimensional channel system than in a three-dimensional pore structure since comparatively few blocks are required to seal off access to the interior of
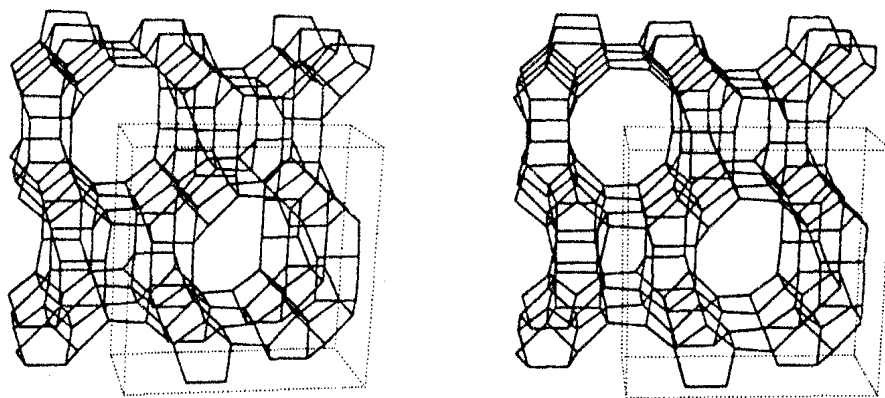
FIGURE 1.8.   Schematic representation of the mordenite structure. (From ref. 24, reprinted with permission.)

the crystal. Thus the presence of a small amount of extraneous material within the crystal has a pronounced effect on the adsorptive properties of mordenite, whereas the same quantity of residual material in zeolites A, X, or Y would have little effect. For similar reasons the one-dimensional structure makes mordenite unsuitable for use as an adsorbent in applications involving sorption of hydrocarbons where there is always a possibility of intracrystalline coke formation. The practical application of mordenite as an adsorbent is therefore limited to relatively clean nonhydrocarbon gases.

Pentasil Zeolites

The pentasil zeolites comprise a family of silica-rich zeolite with structures based on the double five-ring unit shown in Figure 1.4. The structure of a characteristic layer of a pentasil zeolite is shown schematically in Figure 1.9. By stacking such layers in different sequences a variety of related structures may be obtained. More detailed descriptions have been given by Kokatailo, Meier, Olson, and co-workers.[27,29]

The channel systems of the two end members, ZSM-5 and ZSM-11, are sketched in Figure 1.10. The channels are characterized by a ten-membered oxygen ring of free diameter about 6 Å, which is intermediate between the small-port sieves with 8-ring channels and the large-port sieves with 12-ring channels. The Si/Al ratio is typically about 30 but wide variation is possible
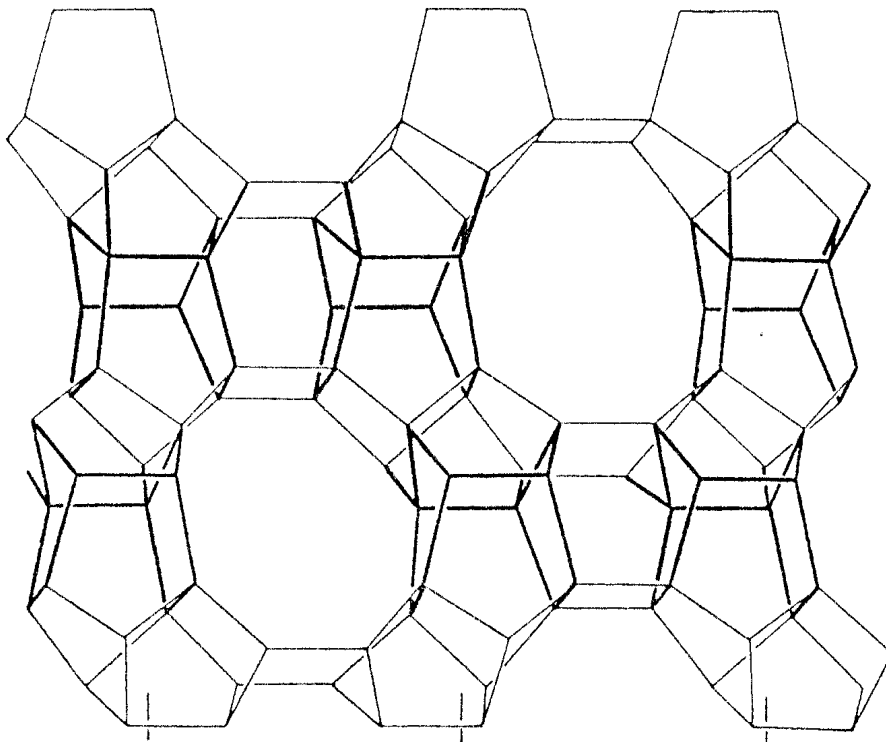
FIGURE 1.9. Schematic diagram of one layer of a pentasil zeolite structure showing how the framework is built up from the D5R units. (From ref. 27, reprinted with permission.)
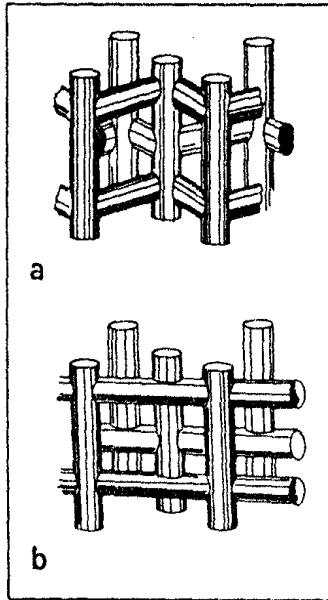
FIGURE 1.10. Diagrammatic representation of the channel structures of (a) ZSM-5 (or silicalite) and (b) ZSM-11. (From ref. 27, reprinted with permission.)
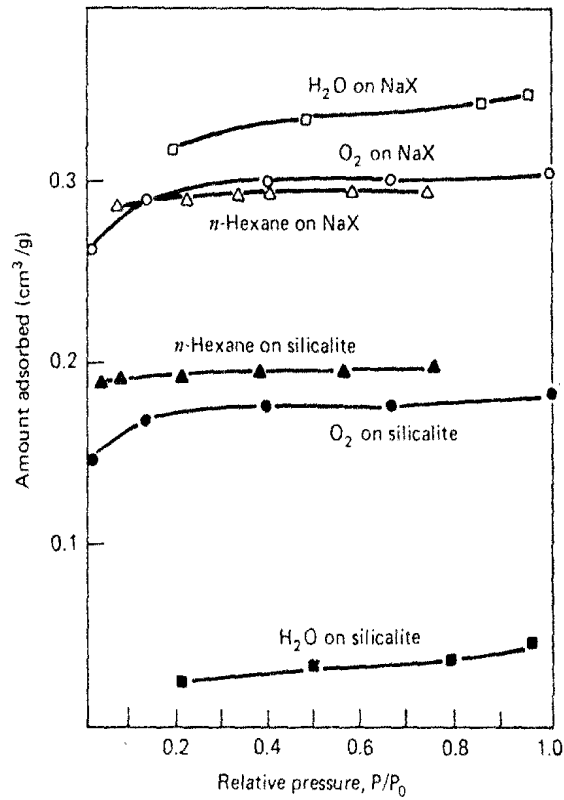
FIGURE 1.11. Comparison of adsorption equilibrium isotherms for water, oxygen, and n-hexane on NaX zeolite and silicalite. (From ref. 26, reprinted by permission from *Nature*, **271**, 512. Copyright © 1978 Macmillan Journals Limited.)

18

and the structures may be prepared in essentially aluminum-free form. The aluminum-free form of ZSM-5 is often referred to as silicalite.

These materials are characterized by great thermal and hydrothermal stability and show a number of useful catalytic properties, including the ability to catalyze the conversion of methanol to gasoline range hydrocarbons without excessive coke formation.

Equilibrium isotherms for sorption of oxygen, water, and n-hexane on silicalite and NaX zeolite are compared in Figure 1.11. The affinity for water is low while the affinity for linear paraffins and para-substituted aromatic hydrocarbons is surprisingly high. These adsorbents are therefore potentially useful as an alternative to activated carbon for removal of organics from aqueous streams.

1.5. COMMERCIAL MOLECULAR SIEVE ADSORBENTS

Synthesis

The manufacture of molecular sieve adsorbents has been reviewed by Breck[19] and more recently by Roberts.[28] The steps in the process are shown schematically in Figure 1.12. A variety of different starting materials may be used. In the hydrogel process the reagents are added in soluble form as sodium silicate and sodium aluminate, whereas in the clay conversion process the alumina is added as a clay mineral, usually metakaolin. Formation of the desired zeolite depends on maintenance of the correct conditions of pH, temperature, and concentration. Seeding may be used to promote crystalliza-
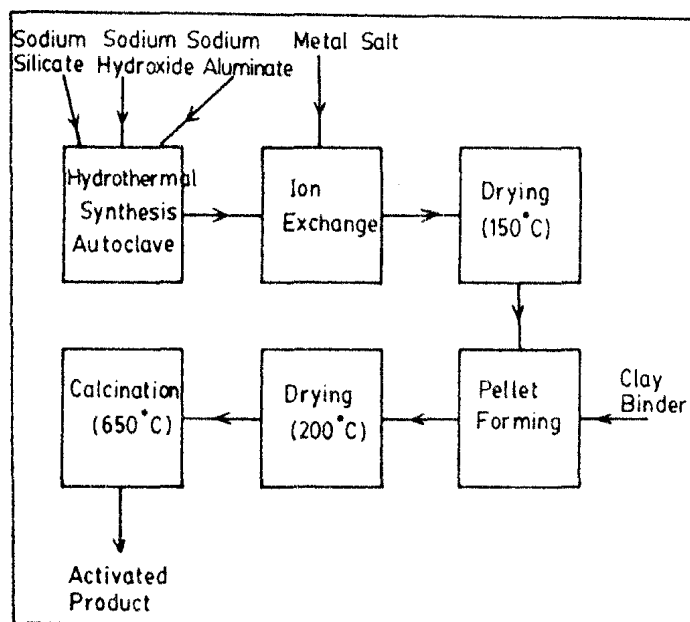
FIGURE 1.12. Steps in the manufacture of a pelleted molecular sieve adsorbent.

tion. Since the required temperature is often above the boiling point of the solution, high-pressure operation may be required. Zeolites A, X, and Y and mordenite may be crystallized directly in the sodium form but the formation of some other zeolites, notably the pentasil zeolites, depends on the addition of a quaternary amine which acts as a template. Following filtration to remove the zeolite crystals from the synthesis liquor, the required ionic form is prepared by cation exchange in aqueous solution.

Pelletization

As synthesized, commercial molecular sieve zeolite crystals are quite small (typically 1–10 μm) and to prepare a practically useful adsorbent these crystals must be formed into a macroporous pellet of suitable dimensions, porosity, and mechanical strength. Scanning electron micrographs of two representative commercial pelletized adsorbents are shown in Figure 1.13. The optimal pellet generally represents a compromise between various conflicting requirements and may therefore be different for different process applications.

A composite pellet offers two distinct diffusional resistances to mass transfer: the micropore diffusional resistance of the individual zeolite crystals and the macropore diffusional resistance of the extracrystalline pores. A low resistance to mass transfer is normally desirable and this requires a small crystal size to minimize intracrystalline diffusional resistance. However, the diameter of the intercrystalline macropores is also determined by the crystal size and if the crystals are too small the macropore diffusivity may be reduced to an unacceptable level. The macropore resistance may of course be reduced by reducing the gross particle size but the extent to which this is possible is limited by pressure drop considerations. The optimal choice of crystal size and particle size thus depends on the ratio of inter- and intracrystalline diffusivities which varies widely from system to system.

At least three different pellet-forming processes are in common use: extrusion to form cylindrical pellets, granulation to form spherical particles, and combined processes involving extrusion followed by rolling to form spheres. Generally, a clay binder is added to help cement the crystals together in order to achieve satisfactory physical strength. The proportion of binder commonly amounts to 10–20% in the final product but in the so-called binderless sieves some of the binder is converted to zeolite during the forming process, and the proportion of amorphous clay in the final product is therefore very much smaller.

The commonly used binders consist of mixtures, in various proportions, of sepiolite, kaolinite, attapulgite, and montmorillonite, often with added silica or alumina. Since these materials also show adsorptive properties, there is commonly some loss in selectivity in the pelleted material relative to the unaggregated crystals. Such effects tend to be more serious with attapulgite and sepiolite which are high-area clays and must be balanced against any advantage in the physical strength which may be gained from using these materials.
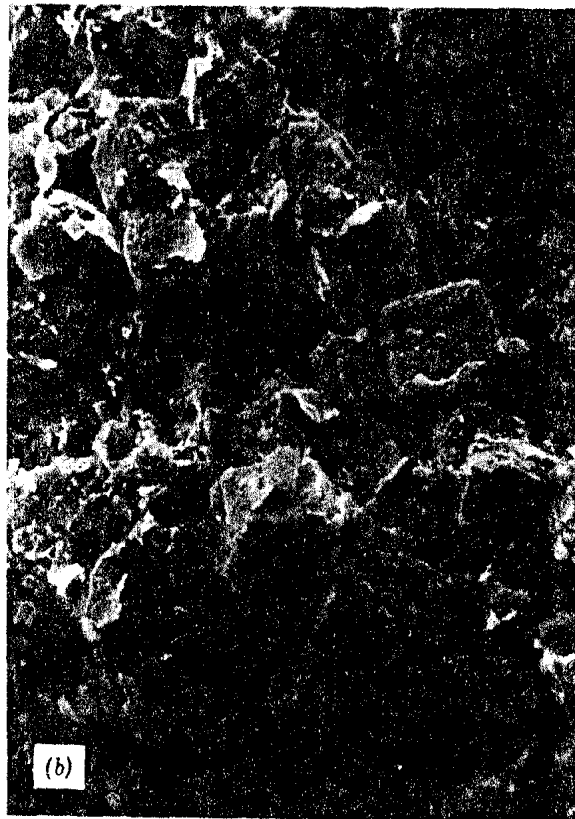
FIGURE 1.13. Scanning electron micrographs of pelleted molecular sieve adsorbents. (*a*) 5A with 12% sepiolite binder and (*b*) 3A with 20% kaolinite binder. Crystal size is about 2 μm. (Photographs kindly provided C. W. Roberts of Laporte Industries Ltd.)
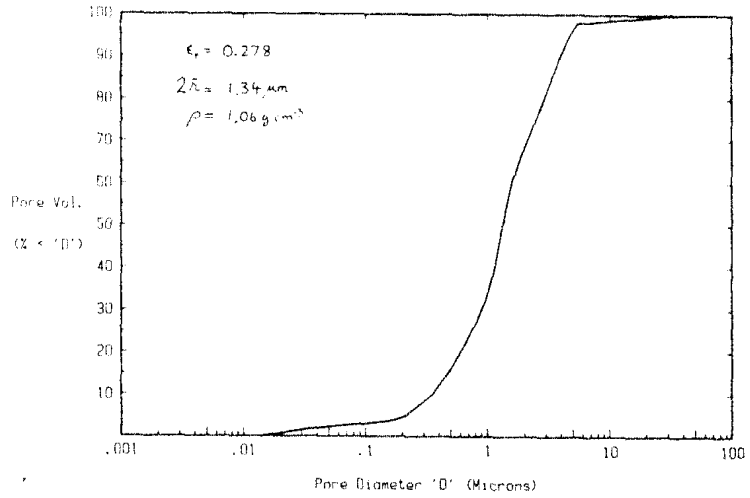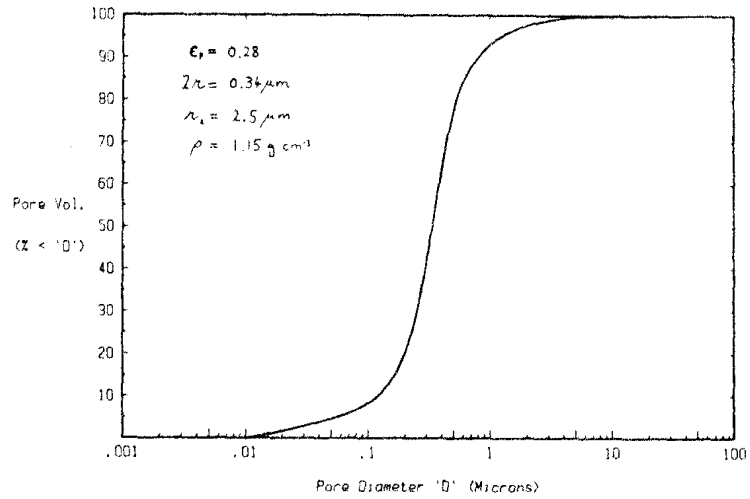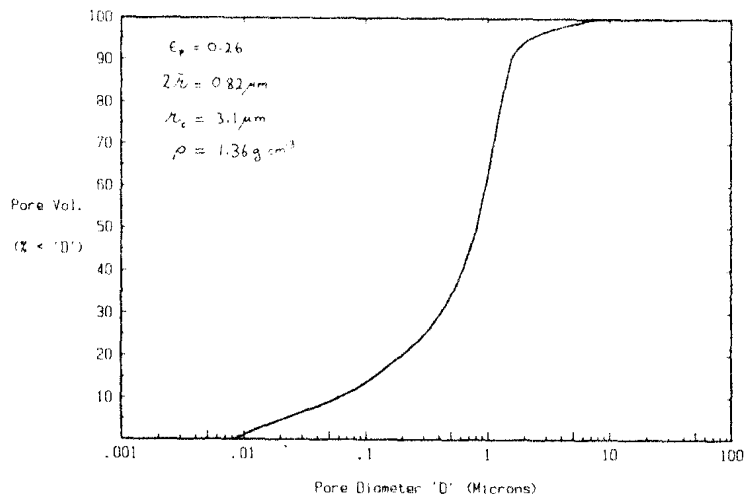
FIGURE 1.14. Macropore size distribution determined from mercury penetration measurements for (a) carbon molecular sieve, (b) Linde 5A (extrudates), and (c) H-Zeolon (H-mordenite).

Other problems which can arise as a result of a poor choice of binder and/or conditions for the pelletization process include blinding of the crystal surface, leading to low mass transfer rates, and coking due to the catalytic activity of the binder.

The macroporosity and pore size distribution are commonly determined by mercury porosimetry as discussed in Section 2.6. The results of such measurements are commonly displayed either as a frequency distribution showing dV_p/d_r plotted against pore radius r as in Figure 1.2 or as a cumulative distribution shown as V_p versus r. Pore size distribution data for a carbon molecular sieve and for two different commercial zeolite sieves are shown in Figure 1.14.

Dehydration and Calcination

Most zeolites, particularly the aluminum-rich members, show only limited hydrothermal stability. Thus care must be taken in the selection of processing conditions for dehydration and calcination of the pellets. Under anhydrous conditions many zeolites are stable to temperatures even exceeding 700°C, at least for limited periods, but in the presence of water, loss of crystallinity may occur quite rapidly even at much lower temperatures. Conditions involving a combination of high temperature and high humidity should generally be avoided and this may mean dehydrating the sieve relatively slowly at a moderate temperature and under good purge. Since thermal stability also depends on the ionic form, it is sometimes necessary to prepare the formed sieve before exchanging to the required ionic form, rather than forming the pellets from the pre-exchanged crystals.

Hydrothermal treatment can however be used constructively to modify the properties of an adsorbent. Perhaps the best example is the formation of ultrastable Y by hydrothermal treatment of sodium ammonium Y zeolite. The change is accompanied by a contraction in the unit cell parameter and an increase in the Si/Al ratio due to elimination of aluminum from the lattice. The resulting product shows greater thermal stability than Y zeolites of similar composition which have not been subjected to the hydrothermal treatment. However, with X zeolite the usual result is a loss of crystallinity with attendant deterioration of the adsorptive properties while with A zeolite a more subtle effect referred to as pore closure occurs. Hydrothermally treated 4A zeolite behaves as if the window aperture is somewhat smaller than in normal 4A sieve. This effect can be useful since a pore-closed 4A does not admit chlorinated hydrocarbons and is therefore useful for drying freon refrigerants.[19] If a wider pore sieve is used for this purpose premature breakdown and loss of capacity may occur due to formation of HF and/or HCl by hydrolysis. The precise mechanism of pore closure has not yet been established and it remains uncertain whether it involves a true modification of the crystal structure or merely a rearrangement of the surface layers.

Applications

A brief list of some important separations which are carried out with zeolite adsorbents is given in Table 1.3. A much more comprehensive list has been given by Collins[30] and reprinted by Breck.[19] The large majority of these applications are purification processes in which the zeolite is used as a selective adsorbent to remove an undesirable impurity such as water, H_2S, or radioactive Kr. Important examples of true separation processes include the linear/branched chain hydrocarbon separation, carried out with zeolite A and the separation of xylene isomers which utilizes various cationic forms of the X and Y zeolites. Some of these processes are considered in greater detail in Chapters 10–12.

Deactivation

Deactivation of an adsorbent, involving either a loss of equilibrium capacity or an increase in mass transfer resistance, commonly occurs during service as a result of either coke formation or slow loss of crystallinity. The latter is a common problem in thermal swing cycles where the sieve is used as a desiccant or even when water is present as an impurity in the feed which is adsorbed in the first few layers of the adsorbent bed. During thermal regeneration the sieve is exposed to a combination of high temperature and high humidity and under these conditions a slow and irreversible breakdown of the crystal structure may occur. Such effects tend to be most serious with zeolite X on account of its limited hydrothermal stability. However, with zeolite A under similar conditions partial pore closure may occur leading to a reduction in the intracrystalline diffusivity and an undesirable broadening of the mass transfer zone.

Results from an accelerated aging study of several different commercial samples of 4A and 13X sieves are shown in Figure 1.15. The differences in initial capacity are probably due to differences in binder content. Each sample was subjected to 725 two-hour cycles during which it was repeatedly saturated with water at room temperature and dehydrated at 260°C. It may be seen that even under these comparatively mild conditions there was some deterioration with four of the six sieves tested. The deterioration appears to be generally more severe for the 13X sieves, although one of the 13X sieves showed essentially no deterioration over the duration of the test.

When reactive hydrocarbons such as olefins are present, slow formation of polymeric species may occur within the zeolite crystals. On thermal regeneration these species are converted to coke, leading to a decline in the useful capacity of the adsorbent and in some cases also a decline in intracrystalline diffusivity. In the drying of cracked gas this problem may be avoided by using

TABLE 1.3. Some Important Applications of Zeolite Adsorbents

Framework	Cationic Form	Formula of Typical Unit Cell	Window	Effective Channel Diameter (Å)	Application
A	Na	$Na_{12}[(AlO_2)_{12}(SiO_2)_{12}]$	8-ring (obstructed)	3.8	Desiccant. CO_2 removal from natural gas
	Ca	$Ca_5Na_2[(AlO_2)_{12}(SiO_2)_{12}]$	8-ring (free)	4.4	Linear paraffin separation. Air separation
	K	$K_{12}[(AlO_2)_{12}(SiO_2)_{12}]$	8-ring (obstructed)	2.9	Drying of cracked gas containing C_2H_4, etc.
X	Na	$Na_{86}[(AlO_2)_{86}(SiO_2)_{106}]$	12-ring	8.4	Pressure swing H_2 purification
	Ca	$Ca_{40}Na_6[(AlO_2)_{86}(SiO_2)_{106}]$	12-ring	8.0	Removal of mercaptans from natural gas
	Sr, Ba[a]	$Sr_{21}Ba_{22}[(AlO_2)_{86}(SiO_2)_{106}]$	12-ring	8.0	Xylene separation
Y	Na	$Na_{56}[(AlO_2)_{56}(SiO_2)_{136}]$	12-ring	8.0	Xylene separation
	K	$K_{56}[(AlO_2)_{56}(SiO_2)_{136}]$	12-ring	8.0	Xylene separation
Mordenite	Ag	$Ag_8[(AlO_2)_8(SiO_2)_{40}]$	12-ring	7.0	I and Kr removal from nuclear off-gases[32–34]
	H	$H_8[(AlO_2)_8(SiO_2)_{40}]$			
Silicalite	—	$(SiO_2)_{96}$	10-ring	6.0	Removal of organics from water
ZSM-5	Na	$Na_3[(AlO_2)_3(SiO_2)_{93}]$	10-ring	6.0	Xylene separation[31]

[a] Also K-BaX.
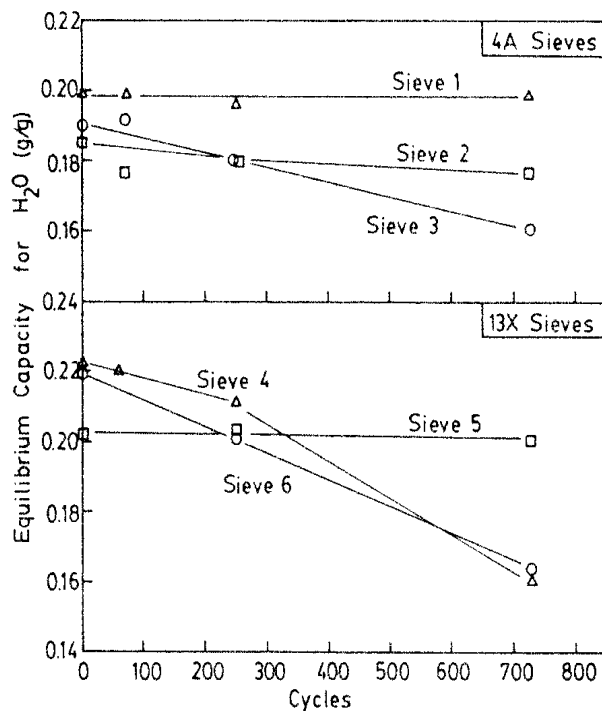
FIGURE 1.15. Results of accelerated aging tests carried out with six different commercial molecular sieve adsorbents (4A and 13X).

a 3A sieve in which the micropores are too small to permit penetration by the olefinic species. Such a solution is not possible in olefin separation processes and in such cases it is usual to avoid high temperatures and regenerate the adsorbent by either pressure swing or displacement (see Chapter II).

Extracrystalline coke formation may also occur with similar adverse effects, but such problems can generally be eliminated by proper choice of binder material and regeneration conditions. Since the catalytic activity of both clays and zeolites is greatly increased by the presence of trace amounts of moisture, rigorous predrying may help to reduce coke formation.

Rejuvenation

Where deactivation has occurred by steam damage or other irreversible chemical reactions the sieve must usually be replaced, but a coked sieve can sometimes be rejuvenated by controlled burn-off of the carbon deposits. This may sometimes be achieved directly without removing the sieve from the process vessel, but clearly the control of oxygen concentration during such a process is crucial, otherwise the temperature may rise to the point where irreversible structural damage occurs. Although such procedures are common industrial practice, very little information has been published.

REFERENCES

1. J. W. McBain, *The Sorption of Gases and Vapours by Solids*. Routledge, London, 1932, Chap. 5.

2. W. H. Davis, J. I. Harper, and E. R. Weatherly, *Petroleum Refiner* **31**, 109 (1952).

3. C. L. Mantell, *Adsorption*. McGraw-Hill, New York, 1951, Chap. 9.

4. V. Ponec, Z. Knor, and S. Cerny, *Adsorption on Solids*. Butterworth and Co., London, 1974, Chap. 14.

5. A. Graham Foster and J. M. Thorp, in *Structure and Properties of Porous Materials*, D. H. Everett and F. S. Stone (eds.). Butterworths, London, 1958, p. 227.

6. G. Mougey, J. Francois-Rossetti, and B. Imelik, in *Structure and Properties of Porous Materials*, D. H. Everett and F. S. Stone (eds.). Butterworths, London, 1958, p. 266.

7. S. J. Gregg and K. S. W. Sing, *Adsorption Surface Area and Porosity*. Academic Press, London and New York, 1967, p. 169.

8. J. J. F. Scholten, in *Porous Carbon Solids*, R. L. Bond (ed.). Academic Press, London and New York, 1967, p. 237.

9. H. Jüntgen, *Carbon* **15**, 273 (1977).

10. C. W. Chi and H. Lee, *AIChE Symp. Ser* **65** (96), 68 (1969).

11. D. W. Breck, W. G. Eversole, R. M. Milton, T. B. Reed, and T. L. Thomas, *J. Am. Chem. Soc.* **78**, 5963 (1956).

12. J. L. Kovach, "Gas Phase Adsorption," in *Handbook on Separation Techniques for Engineers*, P. A. Schweitzer (ed.). McGraw-Hill, New York, 1979.

13. S. P. Nandi and R. L. Walker, *Fuel* **54**, 169 (1975).

14. J. Koresh and A. Soffer, *J. Chem. Soc. Faraday Trans. 1* **76**, 2457 and 2472 (1980).

15. R. L. Patel, S. P. Nandi, and P. L. Walker, *Fuel* **51**, 47 (1972).

16. H. Jüntgen, *Ber. Bunsenges. Physik. Chem.* **79**, 747 (1975).

17. D. L. Trimm, *Carbon* **15**, 273 (1977).

18. T. S. Sridhar, Atomic Energy of Canada Ltd, private communication.

19. D. W. Breck, *Zeolite Molecular Sieves*. Wiley, New York, 1974, p. 95.

20. R. M. Barrer, *Zeolites and Clay Minerals*. Academic Press, London, 1978, Chap. II.

21. W. Meier, in *Molecular Sieves*, Proceedings of the First International Conference on Zeolites. Society of Chemical Industry, London, 1968, p. 10.

22. J. V. Smith, *Adv. Chem* **101**, 171 (1971).

23. J. V. Smith, in *Zeolite Chemistry and Catalysis*, J. Rabo (ed.), A.C.S. Monograph No. 171. American Chem. Soc., Washington, D.C., 1976, p. 1.

24. W. M. Meier and D. H. Olson, *Atlas of Zeolite Structure Types*. Juris Druck und Verlag AG, Zurich, 1978.

25. W. Mortier, *Compilation of Extra Framework Sites in Zeolites*. Butterworths, Guildford, England, 1982.

26. E. Flanigen, J. M. Bennett, R. W. Grose, J. P. Cohen, R. L. Patton, R. M. Kirchner, and J. V. Smith, *Nature* **271**, 512 (1978).

27. G. T. Kokotailo and W. M. Meier, in *Properties and Applications of Zeolites*, R. P. Townsend (ed.), Special Publ. No. 33. Chemical Society, London, 1979, p. 133.

28. C. W. Roberts, in *Properties and Applications of Zeolites*, R. P. Townsend (ed.), Special Publ. No. 33. Chemical Society, London, 1979, p. 103.

29. D. H. Olson, G. T. Kokotailo, S. L. Lawton, and W. M. Meier, *J. Phys. Chem.* **85**, 2238 (1981).

30. J. J. Collins, *Chem. Eng. Prog.* **64**, 66 (1968).

31. B. M. Drinkard, P. T. Allen, and E. H. Unger, U.S. Patent 3, 656, 278, June 8, 1970.

32. P. R. Monson, Paper 19-7, 16th D.O.E. Nuclear Air Cleaning Conference, San Diego, 1980.

33. D. M. Ruthven, J. S. Devgun, F. H. Tezel, and T. S. Sridhar, Paper 3-3, 16th D.O.E. Nuclear Air Cleaning Conference, San Diego, 1980; also issued by AECL as Report No. 7004 (1980).

34. P. R. Monson, *Energy Res. Abstracts* 7(17) No. 42509 (1982).

2

PHYSICAL ADSORPTION AND THE CHARACTERIZATION OF POROUS ADSORBENTS

In discussing the fundamentals of adsorption it is useful to distinguish between physical adsorption, involving only relatively weak intermolecular forces, and chemisorption which involves, essentially, the formation of a chemical bond between the sorbate molecule and the surface of the adsorbent. Although this distinction is conceptually useful there are many intermediate cases and it is not always possible to categorize a particular system unequivocally. The general features which distinguish physical adsorption chemisorption are as follows:

Physical Adsorption	Chemisorption
Low heat of adsorption ($<$ 2 or 3 times latent heat of evaporation.)	High heat of adsorption ($>$ 2 or 3 times latent heat of evaporation.)
Non specific.	Highly specific.
Monolayer or multilayer. No dissociation of adsorbed species. Only significant at relatively low temperatures.	Monolayer only. May involve dissociation. Possible over a wide range of temperature.
Rapid, non-activated, reversible. No electron transfer although polarization of sorbate may occur.	Activated, may be slow and irreversible. Electron transfer leading to bond formation between sorbate and surface.

Almost all adsorptive separation processes depend on physical adsorption rather than chemisorption and this is therefore the focus of the present review. The heat of adsorption provides a direct measure of the strength of the bonding between sorbate and surface. Physical adsorption from the gas phase is invariably exothermic, as may be shown by a simple thermodynamic argument. Since the adsorbed molecule has at most two degrees of translational freedom on the surface and since the rotational freedom of the adsorbed species must always be less than that of the gas phase molecule, the entropy change on adsorption ($\Delta S = S_{ads} - S_{gas}$) is necessarily negative. In order for significant adsorption to occur, the free energy change on adsorption (ΔG) must also be negative and since $\Delta G = \Delta H - T\Delta S$ this requires ΔH negative, or exothermic adsorption. This is generally true also for adsorption from the liquid phase, although the argument is in that case less cogent and exceptions are possible.

2.1. FORCES AND ENERGIES OF ADSORPTION

The forces involved in physical adsorption include both van der Waals forces (dispersion–repulsion) and electrostatic interactions comprising polarization, dipole, and quadrupole interactions. The van der Waals contribution is always present while the electrostatic contributions are significant only in the case of adsorbents such as zeolites which have an ionic structure. However, for the sorption of small dipolar molecules such as H_2O and NH_3 on zeolite adsorbents the electrostatic contribution may be very large, giving rise to unusually high heats of adsorption (25–30 kcal/mole). Thus, although such interactions are properly regarded as physical adsorption, the heat of adsorption may well be of a magnitude generally associated with chemisorption. Furthermore, in such systems the adsorption is quite specific and the rate is often controlled by an activated diffusion process, giving the appearance of a slow activated chemisorption, even though the actual surface adsorption may be rapid. Thus such systems may appear to exhibit many of the characteristic features generally associated with chemisorption.

Dispersion–Repulsion Energy[1-3]

The attractive potential arising from dispersion forces between two isolated molecules may be written in the form

$$\phi_D = -\frac{A_1}{r_{12}^6} - \frac{A_2}{r_{12}^8} - \frac{A_3}{r_{12}^{10}} \tag{2.1}$$

where r_{12} is the distance between the centers of the interacting molecules and A_1, A_2, A_3 are constants. The first term in this expression, which is always dominant, arises from the coupling between instantaneous induced dipoles. The second and third terms represent respectively induced dipole-induced
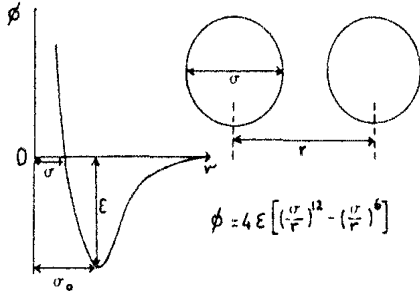
FIGURE 2.1. The Lennard–Jones potential.

quadrupole and induced quadrupole-induced quadrupole interactions. The short-range repulsive energy arising from the finite size of the molecules is generally represented semiempirically by a twelfth-order inverse power expression:

$$\phi_R = \frac{B}{r_{12}^{12}} \tag{2.2}$$

Neglecting the higher order contributions to the dispersion energy and combining the inverse sixth-power attraction with the inverse twelfth-power repulsion leads to the familiar Lennard-Jones potential function:

$$\phi = 4\epsilon\left[\left(\frac{\sigma}{r}\right)^{12} - \left(\frac{\sigma}{r}\right)^{6}\right] \tag{2.3}$$

which is sketched in Figure 2.1. The force constants ϵ and σ are characteristics of the particular molecular species and tabulated values for many common molecules are available.[2] These values may be determined either from transport properties (viscosity, thermal conductivity) or from detailed measurements of the deviations from the ideal gas law (second virial coefficients). For most small molecules the values obtained in both ways are consistent.

The interaction between two different molecules are generally represented by the arithmetic mean of σ and the geometric mean of ϵ:

$$\sigma_{12} = \tfrac{1}{2}(\sigma_1 + \sigma_2), \qquad \epsilon_{12} = \sqrt{\epsilon_1\epsilon_2} \tag{2.4}$$

Setting $d\phi/dr = 0$ in Eq. (2.3) gives, for the equilibrium separation between centers of an isolated pair of molecules, $\sigma_0 = 2^{1/6}\sigma$. Thus, the excluded volume (the van der Waals co-volume b) may be seen to be four times the actual volume of the molecules:

$$b = \frac{4}{3}\pi\frac{\sigma_0^3}{2} = \frac{4}{3}\pi\left(\frac{\sigma_0}{2}\right)^3 \times 4 \tag{2.5}$$

To estimate the dispersion–repulsion forces for larger molecules for which Lennard-Jones force constants are not available it is customary to retain the general form of Eq. (2.3) but to replace the attractive and repulsive constants $(4\epsilon\sigma^6$ and $4\epsilon\sigma^{12})$ by the semiempirical constants A and B:

$$\phi = -\frac{A}{r^6} + \frac{B}{r^{12}} \tag{2.6}$$

There are three commonly used expressions available for the estimation of the attractive constant[3]:

London[4,5]

$$A_L = \frac{3}{2}\alpha_1\alpha_2 I, \qquad \frac{1}{I} = \frac{1}{I_1} + \frac{1}{I_2} \qquad (2.7)$$

Slater–Kirkwood[6]

$$A_{S-K} = \frac{3eh}{4\pi\sqrt{m}} \frac{\alpha_1\alpha_2}{\left(\sqrt{\alpha_1/N_1} + \sqrt{\alpha_2/N_2}\right)} \qquad (2.8)$$

Kirkwood–Müller[7,8]

$$A_{K-M} = 6mc^2 \frac{\alpha_1\alpha_2}{(\alpha_1/\chi_1) + (\alpha_2/\chi_2)} \qquad (2.9)$$

In these expressions the following notation is used:

$$c = \text{velocity of light}$$

$$e = \text{charge on electron}$$

$$m = \text{mass of electron}$$

$$h = \text{Planck's constant}$$

$$I_1, I_2 = \text{ionization potentials}$$

$$\alpha_1, \alpha_2 = \text{polarizability of molecules 1 and 2}$$

$$\chi_1, \chi_2 = \text{magnetic susceptibilities of molecules 1 and 2}$$

$$N_1, N_2 = \text{number of electrons in outer shells}$$

At the equilibrium separation (r_0) $d\phi/dr$ is zero:

$$\therefore \frac{d\phi}{dr} = \frac{6A}{r_0^7} - \frac{12B}{r_0^{13}} = 0, \qquad B = \frac{Ar_0^6}{2} \qquad (2.10)$$

The value of the repulsion constant B may therefore be estimated by setting r_0 equal to the mean of the van der Waals radii.

Unfortunately, as may be seen from Table 2.1, the values of the dispersion constant estimated from Eqs. (2.7)–(2.9) do not agree well even for simple molecules such as the rare gases, although all three expressions give values of the correct order of magnitude. The Slater–Kirkwood expression gives the best estimate for Ne, Kr, and Xe, while the Kirkwood–Muller expression appears to be superior for Ar and CH_4. The inadequacy of the expressions available for the estimation of force constants is a serious barrier to the development of a quantitative theoretical approach to the *a priori* calculation of adsorption energies. Nevertheless, the problem is not quite as severe as it may at first appear since the calculation of repulsion constants according to Eq. (2.10)

TABLE 2.1. Comparison of Dispersion Constants for Inert Gases and Methane Calculated According to Eqs. (2.7)–(2.9) and from Lennard-Jones Force Constants (erg cm^6/molecule)

	$A_L \times 10^{60}$	$A_{K-M} \times 10^{60}$	$A_{S-K} \times 10^{60}$	$A_{L-J} = 4\epsilon\sigma^6 \times 10^{60}$
Ne	4	11	8.7	10
Ar	50	125	73	111
Kr	102	289	205	191
Xe	233	698	422	496
CH$_4$	105	188	145	231

means that to a significant extent errors in A and B will compensate provided that the value used for r_0 is not grossly in error.

Dispersion forces are additive and it is therefore possible, in principle, to calculate the energy of interaction for an adsorbed molecule by summing the pairwise interaction energies arising from the sorbate molecules with each atom of the adsorbent. This approach has been widely used and examples of such calculations are given in Section 2.2. It should be noted that while the additivity of the dispersion energies is strictly valid it does not necessarily follow that the repulsive contributions are additive, although such an assumption is generally made in theoretical calculations of this kind.

Electrostatic Energies

In ionic adsorbents such as zeolites where there is a significant electric field in the region of the surface, additional contributions to the energy of adsorption may arise from polarization (ϕ_P), field-dipole (ϕ_μ), and field gradient-quadrupole (ϕ_Q) interactions. These are given by the following expressions:

$$\phi_P = -\tfrac{1}{2}\alpha E^2$$

$$\phi_\mu = -\mu E \tag{2.11}$$

$$\phi_Q = \frac{1}{2} Q \frac{\partial E}{\partial r}$$

where E is the electric field, α the polarizability, μ the dipole, and Q the quadrupole moment, defined by

$$Q = \frac{1}{2} \int q(\rho,\theta)(3\cos^2\theta - 1)\rho^2 dV \tag{2.12}$$

$q(\rho,\theta)$ is the local charge density at the point (ρ,θ) with the origin at the center of the molecule, and the integration is carried out over the entire volume of the molecule. Thus, for an ionic adsorbent the overall potential is given by the sum of the six terms:

$$\phi = \phi_D + \phi_R + \phi_P + \phi_\mu + \phi_Q + \phi_s \tag{2.13}$$

where ϕ_s represents the contribution from sorbate-sorbate interaction.

Heat of Adsorption at Low Coverage

At low coverage any effects of interaction between neighboring adsorbed molecules can be neglected. Under these conditions there is a simple relationship between the average potential energy ($\bar{\phi}$) and the heat of sorption which may be derived as follows:

Internal energy for 1 mole of sorbate

$$\text{in the vapor phase} = U_g$$

Molar enthalpy of sorbate in the vapor phase

$$(\text{assumed ideal}) = U_g + RT$$

$$\text{Partial molar enthalpy for adsorbed phase} = U_s + \bar{\phi}$$

$$\text{Isoteric heat of sorption } -\Delta H_0 = U_g - U_s + RT - \bar{\phi}$$

$U_g - U_s$ is the difference in kinetic energy between a sorbate molecule in the gaseous and adsorbed states and as such depends on the nature of the adsorbed phase. Using the principle of equipartition of energy

$$U_g - U_s = \frac{nRT}{2}$$

$$-\Delta H_0 = -\bar{\phi} + RT(1 + n/2) \qquad (2.14)$$

where n is the difference in the number of degrees of freedom ("squared terms") between the vapor and adsorbed phases. For example, if the internal degrees of freedom are not affected by sorption and the adsorbed phase behaves as a set of localized three-dimensional oscillators; $n = 3 - 6 = -3$, $U_g - U_s = -3kT/2$, $-\Delta H_0 = -\bar{\phi} - RT/2$. If the adsorbed phase has translational freedom in two dimensions (in the plane of the surface) with one degree of vibrational freedom (perpendicular to the surface); $n = 3 - 4 = -1$, $U_g - U_s = -RT/2$, $-\Delta H_0 = -\bar{\phi} + RT/2$. In most cases the small correction arising from differences in kinetic energy can be ignored and to this approximation $\bar{\phi} \approx \Delta H$.

The value of $\bar{\phi}$ in these equations should really be the average value of ϕ, calculated by integration over all possible positions of the sorbate molecule, weighted according to a Boltzmann factor. In practice, except at very high temperatures the molecules are for the most part located close to the potential minima so it is a good approximation to take:

$$\bar{\phi} \approx \phi_{min} \approx \Delta H_0 \qquad (2.15)$$

2.2. THEORETICAL CALCULATION OF HEAT OF ADSORPTION

Nonpolar Adsorbents[3,9]

For a nonpolar adsorbent there are no dipole or quadrupole contributions to the adsorption energy and if the small contribution from polarization

energy is neglected, the potential, and hence the heat of adsorption, may be calculated by summing the dispersion and repulsion contributions from each atom in the adsorbent. As a first approximation one may neglect the higher order terms in Eq. (2.1) and consider the potential to be represented by a sixth-power attraction and twelfth-power repulsion. The repulsion constant is estimated, according to Eq. (2.10), from the equilibrium separation (r_0) for a sorbate molecule and an isolated atom of the adsorbent; r_0 is in turn determined as the mean of the van der Waals radii or directly from the Lennard-Jones parameters. The resulting expression for the potential is

$$\phi = -A\left(\frac{1}{r^6} - \frac{r_0^6}{2r^{12}} \right)$$ (2.16)

The constant A may be estimated according to Eqs. (2.7)–(2.9).

To calculate the potential profile normal to the surface of the adsorbent, a probe molecule of sorbate is considered located at a fixed distance from the surface and the contributions to the potential arising from each atom in the solid are then calculated according to Eq. (2.16) and summed. In carrying out this summation a number of approximations may be used to simplify the calculation. The simplest approximation is to consider the solid as homogeneous, with a certain number density of atoms, thus replacing the discrete summation by an integration. This turns out to be a rather poor approximation since it underweights the very large contribution to the potential arising from the atoms in the surface layer. A considerable improvement in accuracy is obtained by treating the layers of atoms in the solid separately but it is permissible to treat each layer as having a certain density of atoms per unit area and thus to replace the summation for each layer by an integral, as indicated in Figure 2.2. To obtain the potential profile normal to the surface the calculation is repeated with the probe molecule placed at difference distances (z). The profile shows a minimum at a distance from the surface which is rather smaller than r_0 and the value of the potential at this minimum gives a good approximation to the limiting heat of adsorption [Eq. (2.15)].

Such calculations for the rare gases on graphite have been carried out by many authors. A good review has been given by Ross and Olivier.[9] The results of calculations carried out according to several different approximations are summarized in Table 2.3. It is clear that the more accurate calcula-
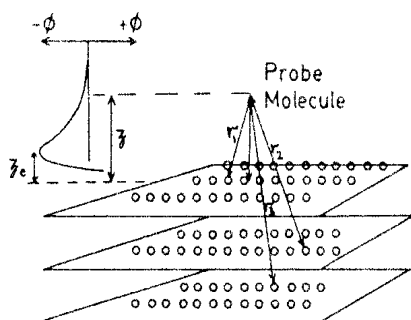
FIGURE 2.2. Schematic diagram showing the potential for a probe molecule approaching the surface of a regular crystalline solid. To calculate the profile it is necessary to sum the pairwise interactions of the probe molecule with each atom of the solid. (Only the first three atomic layers of the solid are indicated.)

TABLE 2.2. Parameters used in Calculation of Dispersion–Repulsion Potentials of Inert Gases on Graphite[9]

	C	Ne	Ar	Kr	Xe
σ_0 (Å)	1.7	1.59	1.91	2.01	2.25
z_c (Å)	—	3.29	3.61	3.71	3.95
$\chi \times 10^3$ (cm³)	10.5	12.0	32.2	46.5	71.5
$\alpha \times 10^{24}$ (cm³)	0.94	0.4	1.63	2.48	4.0
$A_1 \times 10^{45}$ (kcal mole^{-1} cm⁶)	—	0.214	0.77	1.15	1.82
$A_2 \times 10^{60}$ (kcal mole^{-1} cm⁸)	—	0.026	0.104	0.157	0.25
$A_3 \times 10^{76}$ (kcal mole^{-1} cm¹⁰)	—	0.04	0.17	0.31	0.43

TABLE 2.3. Comparison of Experimental Heat of Sorption (kcal/mole) for the Inert Gases on Graphite with Dispersion Potentials Calculated According to Different Approximations[9]

		Ne	Ar	Kr	Xe
	Experimental heat of sorption	0.74	2.12	2.8	3.7
	Theoretical ϕ_{min} from:				
(i)	Layerwise integration of 6–8–10–12 potential	0.76	1.92	2.6	3.2
(ii)	Layerwise integration of 6–12 potential	0.73	1.84	2.48	3.1
(iii)	Direct lattice summation	0.91	2.22	2.95	—
(iv)	Integration treating solid as continuum	0.23	0.64	0.88	1.2

Parameters used in calculations are given in Table 2.2.

tions (direct lattice summation or layerwise integration) give good approximations to the experimental heats of sorption.

Similar calculations may be carried out for the sorption of more complex molecules although it becomes increasingly difficult to estimate reliable force constants. Such calculations confirm the validity of the basic theory of physical adsorption but are of limited quantitative or predictive value since it is generally not possible to estimate the dispersion constants with a sufficiently high accuracy for the results to be practically useful.

Zeolites[10]

Heats of sorption for the rare gases on zeolitic sorbents may be calculated in essentially the same way as for sorption on graphite but the calculation is

TABLE 2.4. Comparison of Experimental Limiting Heat of Sorption (kcal/mole) with Theoretical Values from Potential Calculations

Sorbate	$(-\Delta H)_s$	Theoretical Values of $-\bar{\phi}$		
		London [Eq. (2.7)]	S–K [Eq. (2.8)]	K–M [Eq. (2.9)]
Inert Gases on 5A Zeolite—Derrah and Ruthven[14]				
Ar	3.36	2.9	4.25	5.21
Kr	4.24	3.52	4.3	6.06
Xe	5.4	3.62	5.05	7.8

Sorbate	Zeolite	Experimental $(-\Delta H)_s$	Theoretical $-\bar{\phi}(K-M)$
Inert Gases on Various Forms of Zeolite X–Broier et al.[12]			
	LiX	3.3	3.4
	NaX	2.8	3.04
Ar	KX	3.0	3.2
	CaX	5.0	4.7
	SrX	3.8	3.9
	BaX	3.3	3.2
	LiX	3.8	4.75
Kr	NaX	4.4	4.42
	KX	4.7	4.57
	LiX	4.9–5.4	7.86
Xe	NaX	5.5–5.7	7.67
	KX	5.4–5.9	7.95

more difficult because the interactions with several different types of lattice ions must be considered. Furthermore, as a result of the strong electric field the contribution from polarization energy is of the same order as the dispersion energy and cannot reasonably be ignored. This means that as well as calculating the dispersion–repulsion contributions for a probe molecule it is necessary to calculate the electric field at each point and then estimate the polarization energy from Eq. (2.11).

Such calculations have been carried out by several authors[11–14] and representative results are given in Table 2.4. Derrah and Ruthven[14] carried out their calculations for 5A zeolite using the simple 6–12 potential for dispersion energy and assuming a symmetrical tetrahedral arrangement of $4Ca^{2+}$ and $4Na^{2+}$ in the eight type I cation sites. Representative profiles are shown in Figure 2.3. The potentials calculated according to the three commonly used expressions are significantly different, although all are of similar order of magnitude. For Ar the London formula gives the best prediction of ΔH_s while for Kr and Xe the Slater–Kirkwood formula appears best. The values estimated from the Kirkwood–Muller formula are in all cases too high.
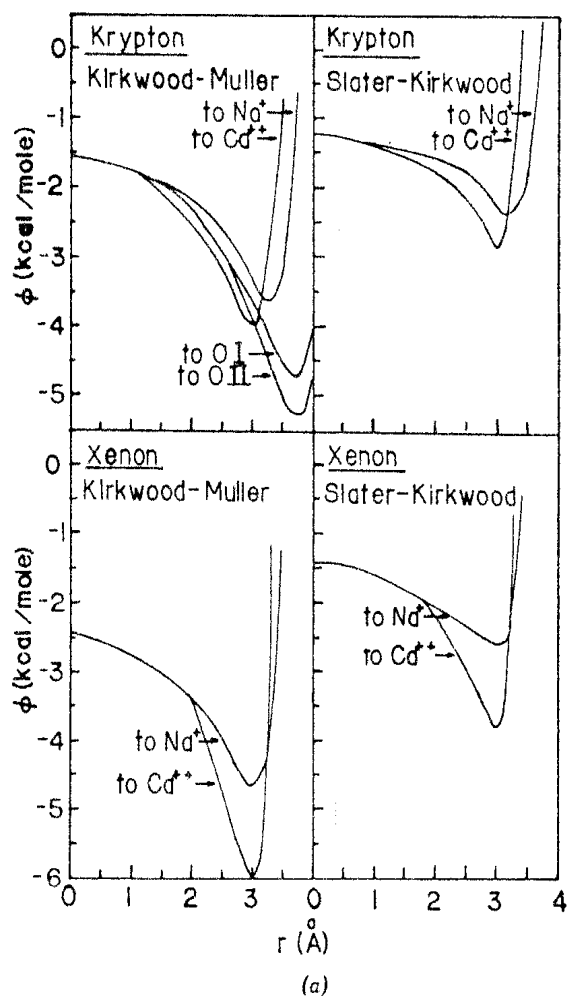
FIGURE 2.3(a). Theoretical potential profiles along the diagonal of the cage to the site I cation, calculated according to Eqs. (2.7)–(2.9) for rare gases in 5A zeolite. (From ref. 14; reproduced by permission of the National Research Council of Canada from the *Canadian Journal of Chemistry*, Volume 53, 1975.)

Somewhat closer agreement between theory and experiment for the rare gases in various forms of zeolite X was obtained by Broier et al.[12] who used the Kirkwood–Muller expression. The calculated values are however quite sensitive to the choice of equilibrium radii, which determine the repulsion constants. The choice of radii is not clearly specified by Broier et al. and it seems likely that the values selected may have been adjusted, within physically reasonable limits, to improve the fit. There is also some uncertainty in the choice of physical parameter values for the estimation of the dispersion constants as well as in the charge distribution.

Relative Importance of Electrostatic and Dispersion Energies

The following procedure was suggested by Barrer[26] as a means of determining the electrostatic contribution to the adsorption potential directly from experimental data. For nonpolar molecules such as the inert gases or paraffin hydrocarbons, only the nonspecific terms $\phi_D + \phi_R + \phi_P$ can contribute to the
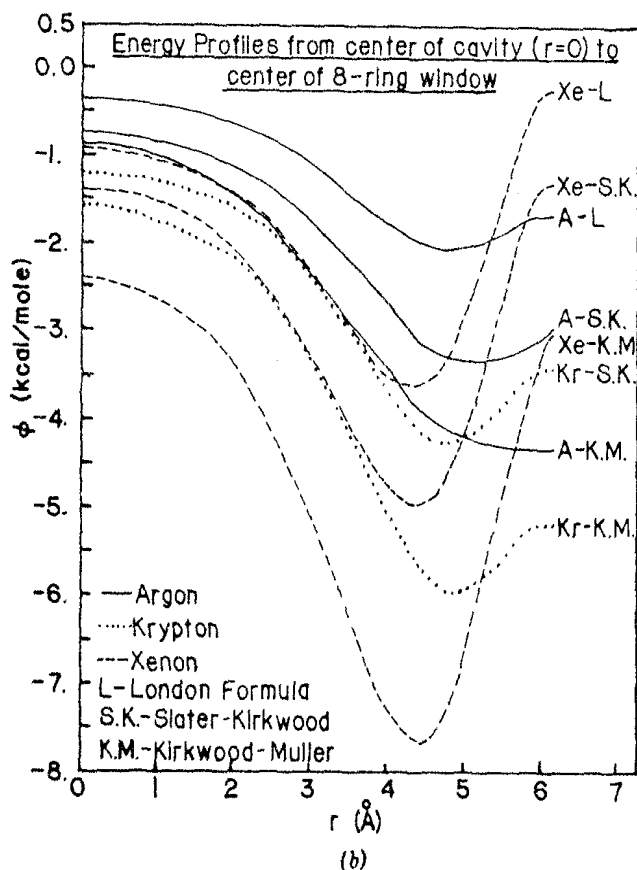
FIGURE 2.3(b). Theoretical potential profiles from center of cage to center of eight-ring, calculated according to Eqs. (2.7)–(2.9) for rare gases in 5A zeolite. (From ref. 14; reproduced by permission of the National Research Council of Canada from the *Canadian Journal of Chemistry*, Volume 53, 1975.)

potential energy and, for a given adsorbent, the magnitude of these contributions is largely determined by the polarizability of the sorbate. Thus, if the initial heats of sorption for a series of different nonpolar molecules in a given adsorbent are plotted against polarizability, as in Figure 2.4, a characteristic reference curve is obtained which defines the total nonspecific potential. The heats of sorption of polar molecules all lie above this curve and the contribution from dipole and quadrupole interactions may be estimated by difference. The curves for three adsorbents are shown in Figure 2.4 and the specific and nonspecific contributions, for several sorbates, are given in Table 2.5.

A somewhat similar approach was followed by Kiselev[13] for NaX zeolite and by Schirmer et al.[16] for CaA zeolite. Representative data from these studies are summarized in Tables 2.6 and 2.7. The effect of specific interactions is clearly evident and for small polar molecules such as H_2O, NH_3, and CH_3OH the electrostatic contribution is in fact dominant. Even for N_2, which has only a relatively small quadrupole moment and no dipole, the specific contribution to the adsorption energy amounts to between 25 and 50%.

A theoretical calculation of the heat of sorption for CO_2 in various cationic forms of zeolite X and has been carried out by Barrer and Gibbons.[17] The
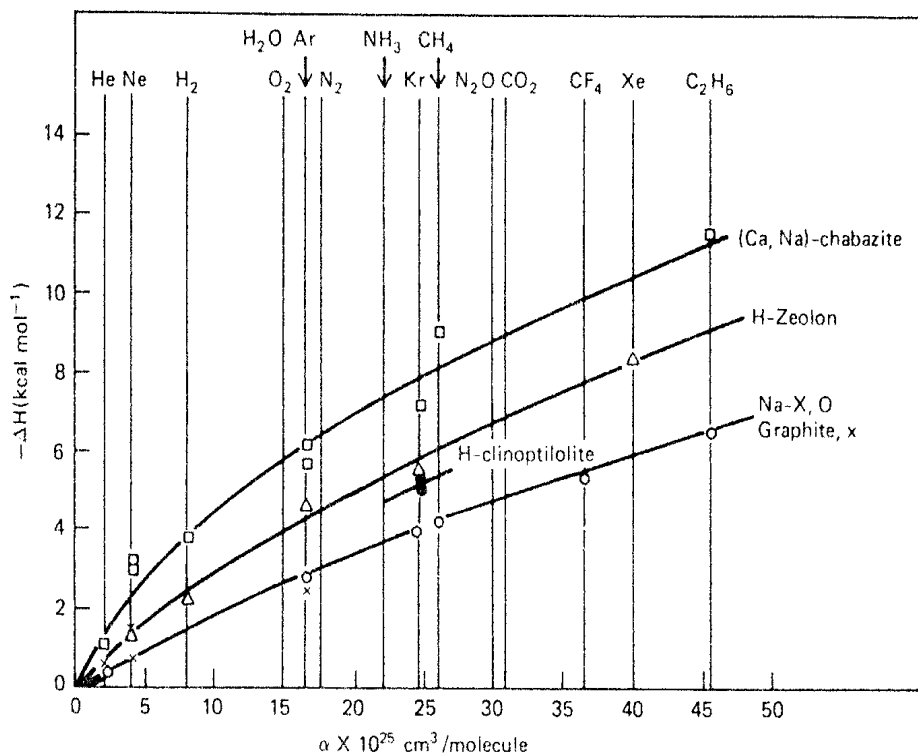
FIGURE 2.4. Characteristic curves of limiting heat of sorption versus polarizability for small symmetric adsorbed species in: □, Ca rich chabazite; △, H-mordenite; +, Na-mordenite; O, 13X; ×, graphitized carbon. (From ref. 15, reprinted with permission.)

TABLE 2.5. Division of Initial Heats of Sorption into Specific (Dipole + Quadrupole) and Nonspecific (Dispersion + Repulsion + Polarization) Contributions

Zeolite	Outgassed at °C	Sorbate	$-\Delta H$ (cal/mole)		
			Total	Dispersion + Repulsion + Polarization	Dipole + Quadrupole Energy
Chabazite	480	N_2	9,000	6,450	2,550
	450	N_2O	15,300	9,100	6,200
	480	NH_3	31,500	7,500	24,000
H-mordenite	350	N_2	6,200	4,500	1,700
		CO_2	11,100	6,750	4,350
Na-mordenite	350	N_2	7,000	4,500[a]	2,500
		CO_2	15,700	6,750[a]	8,950
Na-faujasite (Sieve 13X)	350	N_2	6,500	3,100	3,400
		CO_2	12,200	4,200	8,000
		NH_3	18,000	3,750	14,250
		H_2O	~34,000	2,650	~31,350
Na-faujasite (Sieve Y)	350	CO_2	8,200	4,850[b]	3,350

Source: Barrer.[15]

[a] Assuming dispersion + repulsion + polarization energy does not differ between Na- and H-mordenites.

[b] Assuming dispersion + repulsion + polarization energy does not differ between Sieves X and Y in the Na-forms.

TABLE 2.6. Heats of Adsorption and Specific Interaction Energies (kcal/mole) for Sorption of Various Species on NaX Zeolite

Properties that Determine the Specific Nature of Adsorption	Adsorbate	$-\Delta H$	$-\Delta H_{sp}$	$\dfrac{\Delta H_{sp}}{\Delta H}$
		Molecules of Group B		
π-bonds, quadrupole moment	C_2H_4	8.9	3.0	0.34
	C_6H_6	18.0	4.5	0.25
	N_2	5.0	2.3	0.46
	CO_2	10.0	6.0	0.55
Dipole moment, ability to form hydrogen bonds through oxygen and nitrogen atoms only	$(CH_3)_2O$	21.0	7.6	0.36
	$(C_2H_5)_2O$	16.4	7.6	0.46
	CH_3NO_2	19.9	10.0	0.50
	CH_3CN	10.0	11.0	0.58
		Molecules of Group D		
Dipole moment, ability to form hydrogen bonds through oxygen or nitrogen atoms, as well as through OH or NH hydrogen atoms	H_2O	18.5	(15.5)	(0.8)
	CH_3OH	18.4	13.2	0.72
	C_2H_5OH	20.9	13.2	0.63
	C_3H_7OH	23.2	13.2	0.57
	nC_4H_9OH	26.0	13.2	0.51
	NH_3	16.0	(12.5)	(0.8)
	CH_3NH_2	18.0	11.5	0.64

Source: From Kiselev.[13]

TABLE 2.7. Limiting Heats of Sorption on 5A Zeolite Showing Specific (Dipole + Quadrupole) and Nonspecific (Dispersion − Repulsion + Polarization) Contributions (kcal/mole)

Sorbate	μ (Debye)	Polarizability $\times 10^{25}$ cm^3/ molecule	Nonspecific $(-\phi_D + \phi_R + \phi_P)$	Specific $-(\phi_\mu + \phi_Q)$	$(-\Delta H_0)$
C_2H_6	0	44.7	5.9	0	5.9
C_3H_8	0	62.9	8.4	0	8.4
nC_4H_{10}	0	81.2	10.4	0	10.4
C_3H_6	0.35	60.8	8.1	3.2	11.3
$CH_3 \cdot NH_2$	1.33	53.1	7.1	11.9	19.0
$nC_3H_7 \cdot NH_2$	1.39	89.7	12.0	14.0	26.0
NH_3	1.46	22.2	3.0	22.0	25.0
CH_3OH	1.68	32.3	4.3	15.2	19.5

Source: After Schirmer.[16]

TABLE 2.8. The Components ϕ_D, ϕ_P, ϕ_Q, and ϕ_0 (kcal/mole) for Sorption of CO_2 in Zeolite X

Component of Interaction with CO_2	Cationic Form of Zeolite				
	Li	Na	K	Rb	Cs
ϕ_D^* (oxygen)	− 3.8	− 3.1	− 1.7	− 1.1	− 1.1
ϕ_D^* (cations)	− 0.1	− 0.2	− 0.8	− 1.1	− 2.2
$\phi_P^\dagger$	− 2.3	− 1.2	− 0.5	− 0.2	− 0.0
ϕ_{FQ}^*	− 7.4	− 5.1	− 4.2	− 3.5	− 2.3
ϕ_0	+ 0.4	+ 0.3	+ 0.3	+ 0.3	+ 0.3
$\Sigma\phi$	− 13.2	− 9.3	− 6.9	− 5.6	− 5.3

Source: From Barrer and Gibbons.[17]

dispersion, repulsion, and polarization contributions were estimated in the same way as for the inert gases and the quadrupole contribution was estimated from Eqs. (2.11) and (2.12). Three situations were considered: a freely rotating CO_2 molecule, a CO_2 molecule oriented along the (1, 1, 1) axis from the center of the 12-ring to the type II cation site at the center of the 6-ring, and a molecule with its axis perpendicular to this direction. The results of these calculations, which are summarized in Tables 2.8 and 2.9, suggest that the CO_2 molecule tends to orient along the (1, 1, 1) axis. The variation of ϕ_D, ϕ_P, and ϕ_Q in the different cationic forms shows clearly the increase of the electrostatic contribution ($\phi_P + \phi_Q$) with decreasing cation size.

Similar calculations were carried out for NH_3 in zeolite X by Barrer and Gibbons,[17] but except in the case of LiX, agreement between predicted and experimental heats of sorption was poor.

TABLE 2.9. Comparison of Calculated and Experimental Values of ΔU_0 (kcal/mole)

Energy Values	Cationic Form of Zeolite				
	Li	Na	K	Rb	Cs
− ΔE	12.3	10.8	10.5	10.1	8.8
− $\Sigma\phi$ Eq. (2.9) Axis of CO_2 in ppp axis	13.2	9.3	6.9	5.6	5.3
− $\Sigma\phi$ Eq. (2.7) Axis of CO_2 in ppp axis	11.7	7.9	5.5	4.6	3.7
− $\Sigma\phi$ Eq. (2.9) Axis of CO_2 ⊥ ppp axis	1.7	2.3	0.6	2.1	3.9
− $\Sigma\phi$ Eq. (2.9) Kinetic radius, CO_2 rotating	29.5	15.0	13.3	10.4	9.2\

Source: From Barrer and Gibbons.[17]

2.3. ADSORPTION AT LOW COVERAGE: HENRY'S LAW

For physical adsorption there is no change in molecular state on adsorption (i.e., no association or dissociation). It follows that for adsorption on a uniform surface at sufficiently low concentrations such that all molecules are isolated from their nearest neighbors, the equilibrium relationship between fluid phase and adsorbed phase concentrations will be linear. This linear relationship is commonly referred to as Henry's law by analogy with the limiting behavior of solutions of gases in liquids and the constant of proportionality, which is simply the adsorption equilibrium constant and is referred to as the Henry constant. The Henry constant may be expressed in terms of either pressure or concentration:

$$q = Kc \quad \text{or} \quad q = K'p \tag{2.17}$$

where q and c are expressed as molecules or moles per unit volume in the adsorbed and fluid phases. From the ideal gas law it follows that $K = K'RT$. Alternatively, in terms of surface concentration (n_s) one has

$$n_s = \frac{K}{\mathscr{A}}c = \frac{K'}{\mathscr{A}}P \tag{2.18}$$

where $\mathscr{A}$ is the specific surface area per unit volume of the adsorbent.
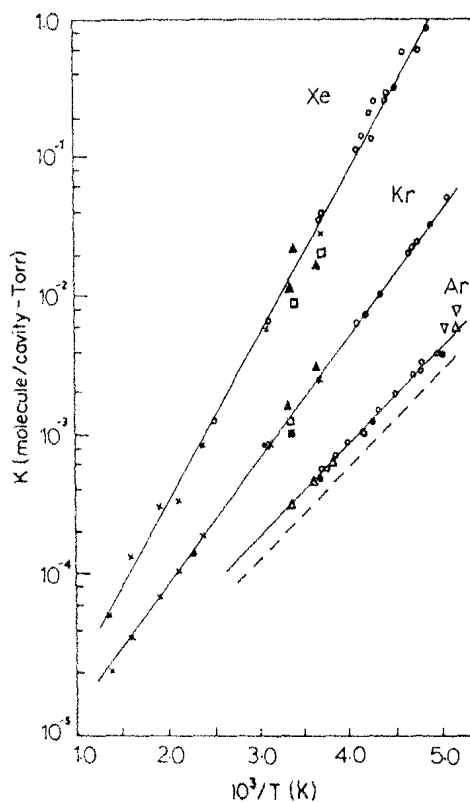
FIGURE 2.5. vant Hoff plots showing temperature dependence of experimental Henry constants for Ar, Kr, and Xe in Linde 5A zeolite crystals. The dotted line represents data for Ar in Linde 4A. (From ref. 14; reproduced by permission of the National Research Council of Canada from the *Canadian Journal of Chemistry*, Volume 53, 1975.)

The temperature dependence of the Henry constant obeys the vant Hoff equation:

$$\frac{d\ln K'}{dT} = \frac{\Delta H_0}{RT^2}, \qquad \frac{d\ln K}{dT} = \frac{\Delta U_0}{RT^2} \qquad (2.19)$$

where ΔH_0 and ΔU_0 represent, respectively, the differences in enthalpy and internal energy between adsorbed and gaseous states. Neglecting differences in heat capacity between the phases Eq. (2.19) may be integrated to yield

$$K' = K_0' e^{-\Delta H_0/RT}, \qquad K = K_0 e^{-\Delta U_0/RT} \qquad (2.20)$$

In accordance with Eq. (2.20), plots of $\ln K$ versus $1/T$ are often found to be essentially linear over a wide range of temperature (Figure 2.5). A more complete thermodynamic discussion is given in Chapter 3.

Theoretical Calculation of Henry Constants

In the statistical thermodynamic formulation (see Appendix A) the Henry constant is given by the ratio of the partition functions per unit volume for the adsorbed and vapor phases, with due correction for the difference in potential energy (f_s'/f_g'). For an inert gas there are no internal degrees of freedom so, assuming classical behavior, this ratio of partition functions is equivalent to the configuration integral[2] and one has the simple result

$$K = \frac{f_s'}{f_g'} = Z = \int_v \exp\left[-\frac{\phi(\mathbf{r})}{kT} \right] d\mathbf{r} \approx K_0 e^{-\bar{\phi}/kT} \qquad (2.21)$$

It is therefore possible in principle to predict the Henry constant theoretically by evaluation of the configuration integral, provided that the potential ϕ is known as a function of position throughout the adsorption space. The evaluation of the integral is straightforward and the main problem is the estimation of the potential profile with sufficient accuracy. The results of calculations of this kind for the inert gases in 5A zeolite are summarized in Figure 2.6. For argon the potentials calculated from the London expression give the best approximation to the experimental data, whereas for xenon the Slater–Kirkwood expression provides the best representation. The experimental values for krypton lie between the predictions of the Slater–Kirkwood and Kirkwood–Muller expressions.

Recognizing the limited accuracy of available methods of predicting dispersion constants, Myers and co-workers[19] proceeded in a somewhat different manner. They calculated the electric field and polarization energy in the usual way but approximated the sum for the dispersion-repulsion potential by an integral in which the average dispersion constant was retained as an unknown parameter. The configuration integral was then evaluated and the value for the mean dispersion coefficient was found by matching theoretical and experimental Henry constants. In that way, with one adjustable parameter for
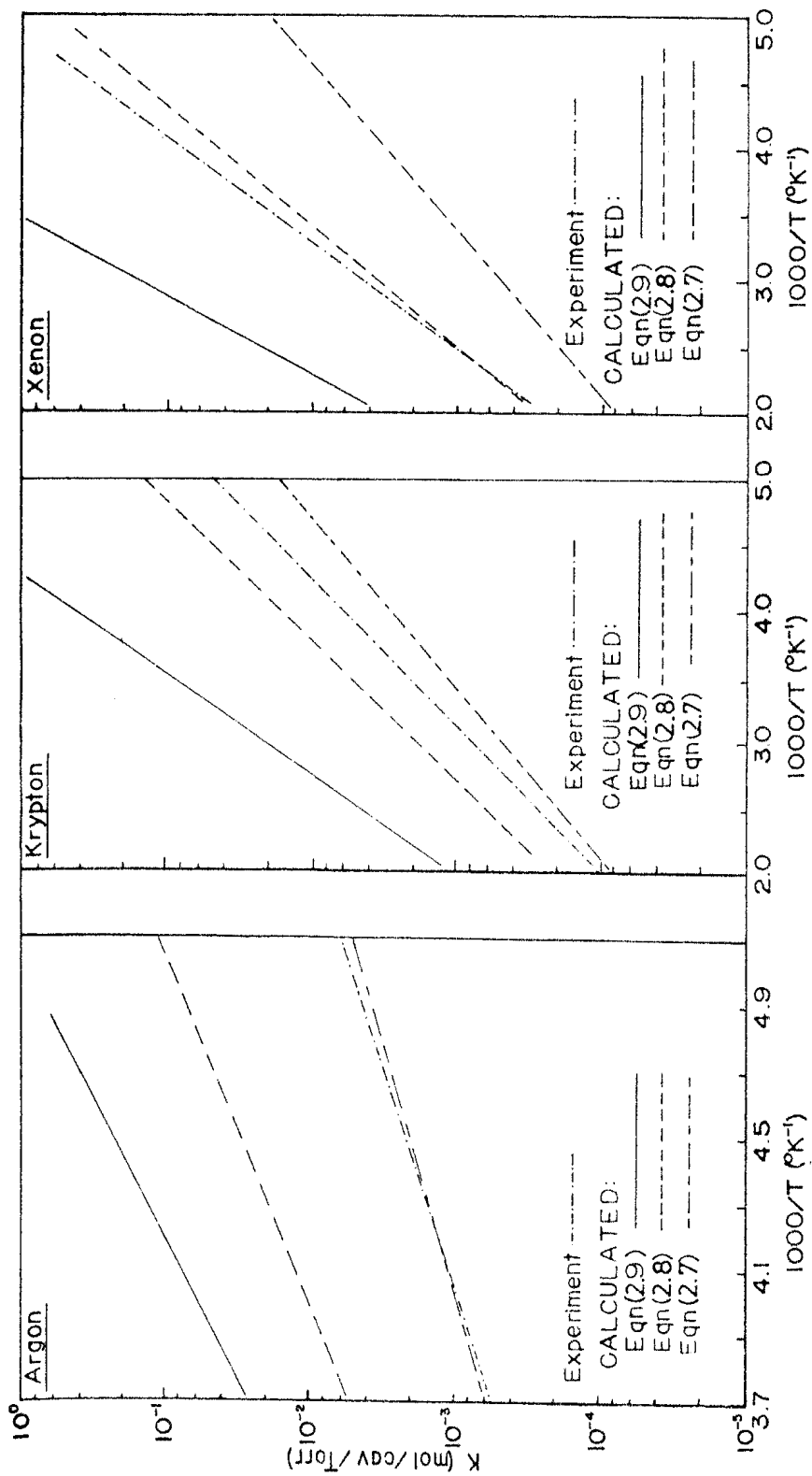
FIGURE 2.6. Comparison of experimental and theoretical Henry constants for Ar, Kr, and Xe in 5A zeolite, calculated from the potential profiles derived from the London, Slater–Kirkwood and Kirkwood–Muller equations [Eqs. (2.7)–(2.9)]. (From ref. 14; reproduced by permission of the National Research Council of Canada from the *Canadian Journal of Chemistry*, Volume 53, 1975.)

TABLE 2.10. Comparison of Theoretical Dispersion Coefficients
for Inert Gases in 5A Zeolite with Values derived from
Henry Constant Data[19]

	$A_{S-K} \times 10^{43}$	$A_{K-M} \times 10^{43}$	$\bar{A} \times 10^{43}$
Ar	8.9	11.9	9.8
Kr	12.0	17.5	13.7
Xe	16.9	27.6	22.0

Units are cal cm^6 mole^{-1}. Average values are calculated assuming $48O^{-1/4}$, $4Ca^{2+}$, and $4Na^+$ per cage.

each gas, excellent agreement was obtained over a wide range of temperature. In Table 2.10 average dispersion coefficients for Ar, Kr, and Xe in 5A sieve, calculated from the values given by Myers et al.,[19] are compared with the theoretical values from the Slater–Kirkwood and Kirkwood–Muller expressions. The values required to match the Henry constants appear eminently reasonable, being close to the average of the estimates from these two theoretical expressions.

For zeolitic adsorbents consisting of discrete cages interconnected through relatively small windows, Eq. (2.21) assumes a very simple form if the adsorbed species can be regarded as retaining complete translational, rotational, and internal freedom within the free volume of the cage[20]:

$$\frac{-\Delta H_0}{N} = -\bar{\phi} + kT$$

$$K = K'kT = \frac{v}{e} e^{-\bar{\phi}/kT} = \frac{v}{e^2} e^{-\Delta H_0/RT}, \qquad K'_0 = \frac{v}{e^2 kT} \tag{2.22}$$

The free volume of the cage (v) is smaller than the actual cage volume, since as a result of its finite size the sorbate molecule cannot approach the cage wall. As a rough approximation we may take the free volume as the volume of a sphere of diameter equal to the actual diameter minus the van der Waals diameter of the sorbate molecule. Values of v and K'_0, estimated on this basis, are summarized in Table 2.11. It is evident that for the nonpolar species the estimated values of K'_0 are quite close to the experimental values. For N_2 and CO_2 the experimental values are much smaller, however, than the values predicted in this way. This is to be expected since, as noted in Section 2.2, a significant degree of localization and possibly some loss of rotational freedom may occur with these sorbates as a result of electrostatic (quadrupole) interaction energy. Considering the very great simplifications involved in this model, the extent to which it gives a correct estimate of the value of K'_0 is remarkable.

It is in principle possible to extend the theoretical calculation of Henry constants to more complex molecules where other contributions to the potential such as dipole and quadrupole energies, as well as restricted rotational freedom, must be considered. Such calculations have been attempted by

TABLE 2.11. Values of K_0' and $-\Delta H$ Giving Temperature Dependence of Henry Constants for Light Gases in 5A Zeolite According to Eq. (2.20)[a]

Sorbate	Theoretical Values[b]		Experimental Values	
	v (Å)^3	$K_0' \times 10^8$	$K_0' \times 10^8$	$-\Delta H_0$
CH_4	285	137	190	4.54
C_2H_6	239	95	77	6.6
C_3H_8	206	80	124	8.1
nC_4H_{10}	167	53	86	10.2
C_2H_4	256	113	109	8.0
C_3H_6	213	77	79	10.0
CF_4	157	51	38	5.9
N_2	293	138	10	5.7
CO_2	284	123	9.2	10.8

Source: Ruthven et al.[20]

[a] K_0' is in molecule/cage torr and $-\Delta H$ in kcal/mole.

[b] Theoretical values of v and K_0' calculated from Eq. (2.22) are given for comparison.

Sargent and Whitford[21] for the CO_2-5A system but the results obtained were not promising.

Restricted Rotation

For a polyatomic molecule the possibility of restricted rotational freedom in the adsorbed phase must be considered so that in place of Eq. (2.21) we have

$$K_{\text{poly}} = \frac{Z(f_{\text{rot}})_s}{(f_{\text{rot}})_g} \qquad (2.23)$$

where $(f_{\text{rot}})_s/(f_{\text{rot}})_g$ represents the ratio of the rotational partition functions for the adsorbed and gaseous molecules. The configuration integral is determined mainly by the size and polarizability of the molecule. For the adsorption of pairs of monatomic and polyatomic molecules of similar size and polarizability on the same adsorbent, the configuration integrals should be essentially the same, so that

$$K_{\text{poly}} \approx \left(K_0 e^{-\bar{\phi}/kT} \right)_{\text{mono}} \frac{(f_{\text{rot}})_s}{(f_{\text{rot}})_g} \qquad (2.24)$$

or

$$\frac{(K_0)_{\text{poly}}}{(K_0)_{\text{mono}}} \approx \frac{(f_{\text{rot}})_s}{(f_{\text{rot}})_g} \qquad (2.25)$$

where K_0 represents the pre-exponential factor in the vant Hoff correlation of

TABLE 2.12. Comparison of Radius, Polarizability, and Henry Constants for O_2-Ar and CH_4-Kr in 5A Zeolite

		Kr		CH_4	Ar	O_2
σ (Å)		3.6		3.8	3.44	3.5
$10^{25} \times \alpha$ (cm^3/molecule)		25		26	16.3	16.0
5A^a Zeolite	ΔH_0 (kcal/mole)	4.25		5.1	3.28	3.3
	K'_0 (molecule/	1.26		0.6	1.2	1.48
	cavity torr) $\times$ 10^6					
	$(K_0)_{poly}/(K_0)_{mono}$		0.5		1.2	
MSC$^{(22)}$	$-\Delta H_0$ (kcal/mole)	5.6		5.7	—	—
	K_0 (cm^3/g at 298 K) $\times$ 10^3	3.28		4.47	—	—
	$(K_0)_{poly}/(K_0)_{mono}$		0.73		—	—

^{a}Data from the University of New Brunswick.

the Henry constants ($K = K_0 e^{-\Delta H/RT}$). Data for the pairs of molecules O_2-Ar and CH_4-Kr which fulfil approximately the requirements of equal size and polarizability are compared in Table 2.12. The experimental Henry constants for sorption on both 5A zeolites and carbon molecular sieve suggest that oxygen retains essentially complete rotational freedom in the adsorbed phase. The values of $(f_{rot})_s/(f_{rot})_g$ for methane are somewhat less than unity which may suggest some restriction of rotational freedom. However, since $(f_s)_{rot}/(f_{rot})_g$ is considerably greater than $1/(f_{rot})_g$, the limiting value for a nonrotating sorbate molecule, one many conclude that considerable rotational freedom is retained. In view of the approximate nature of this argument any such conclusion is obviously tentative. The same conclusion has however been reached from independent spectroscopic evidence which also suggests that adsorbed methane retains some, but not all, of its rotational freedom.[23,24]

Restriction of rotational feedom in the adsorbed phase is much more important with polar and quadrupolar molecules such as CO_2 and NH_3 in polar adsorbents, but unfortunately such systems are not amenable to the simple analysis developed here.

2.4. MONOLAYER AND MULTILAYER ADSORPTION

Brunauer et al.[25] have divided the isotherms for physical adsorption into five classes, as illustrated in Figure 2.7. The isotherms for true microporous adsorbents, in which the pore size is not very much greater than the molecular diameter of the sorbate molecule, are normally of type I. This is because with
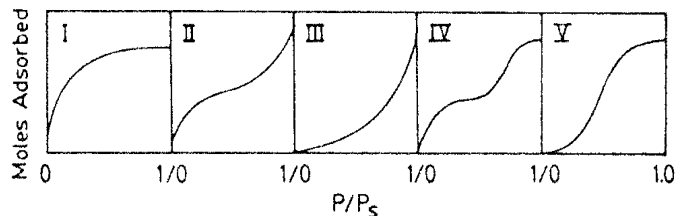
FIGURE 2.7. The Brunauer classification of isotherms.

such adsorbents there is a definite saturation limit corresponding to complete filling of the micropores. Occasionally if intermolecular attraction effects are large an isotherm of type V is observed, as for example in the sorption of phosphorous vapor on NaX.[36] An isotherm of type IV suggests the formation of two surface layers either on a plane surface or on the wall of a pore very much wider than the molecular diameter of the sorbate. Isotherms of types II and III are generally observed only in adsorbents in which there is a wide range of pore sizes. In such systems there is a continuous progression with increasing loading from monolayer to multilayer adsorption and then to capillary condensation. The increase in capacity at high pressures is due to capillary condensation occurring in pores of increasing diameter as the pressure is raised.

The Langmuir Isotherm

The simplest theoretical model for monolayer adsorption is due to Langmuir.[26] The Langmuir model was originally developed to represent chemisorption on a set of distinct localized adsorption sites. A simple kinetic derivation is given below and a more refined thermodynamic derivation, which has the advantage of showing more clearly the precise significance of the Langmuir equilibrium constant, is given in Chapter 3.

The basic assumptions on which the model is based are:

1. Molecules are adsorbed at a fixed number of well-defined localized sites.

2. Each site can hold one adsorbate molecule.

3. All sites are energetically equivalent.

4. There is no interaction between molecules adsorbed on neighboring sites.

Considering the exchange of molecules between adsorbed and gaseous phases

$$\text{Rate of adsorption} \quad k_a p(1 - \Theta)$$

$$\text{Rate of desorption} \quad k_d \Theta$$

(2.26)

where q_s is the total number of sites per unit weight or volume of adsorbent and $\theta = q/q_s$ is the fractional coverage. At equilibrium the rates of adsorption and desorption are equal:

$$\frac{\Theta}{1 - \Theta} = \frac{k_a}{k_d} p = bp \qquad (2.27)$$

where $b = k_a/k_d$ is the adsorption equilibrium constant. Equation (2.27) may be rearranged to the commonly quoted form

$$\Theta = \frac{q}{q_s} = \frac{bp}{1 + bp} \qquad (2.28)$$

This expression shows the correct asymptotic behavior for monolayer adsorption since at saturation $p \to \infty$, $q \to q_s$, and $\Theta \to 1.0$ while at low sorbate concentrations Henry's law is approached:

$$\lim_{p \to 0} \left(\frac{q}{p} \right) = bq_s = K' \qquad (2.29)$$

q_s is supposed to represent a fixed number of surface sites and it should therefore be a temperature-independent constant while the temperature dependence of the equilibrium constant should follow a vant Hoff equation:

$$b = b_0 \exp\left(\frac{-\Delta H_0}{RT} \right) \qquad (2.30)$$

Since adsorption is exothermic (ΔH negative) b should decrease with increasing temperature.

The assumptions of identical sites with no interaction between adsorbed molecules imply that the heat of adsorption is independent of coverage. It follows by differentiation of Eq. (2.27) that the isosteric heat of sorption ($-\Delta H_s$) is the same as the limiting heat of sorption ($-\Delta H_0$):

$$\left(\frac{\partial \ln p}{\partial T} \right)_q = \frac{\Delta H_s}{RT^2} = \frac{d \ln b}{dT} = \frac{d \ln K'}{dT} = \frac{\Delta H_0}{RT^2} \qquad (2.31)$$

Commonly suggested procedures for testing the fit of the Langmuir model to experimental data involve plotting either p/q against p or $1/q$ against $1/p$. Equation (2.28) may be rearranged to yield

$$\frac{p}{q} = \frac{1}{bq_s} + \frac{p}{q_s} \quad \text{or} \quad \frac{1}{q} = \frac{1}{q_s} + \frac{1}{bq_s}\frac{1}{p} \qquad (2.32)$$

so it is evident that the model parameters b and q_s may be easily obtained from the slopes and intercepts of such plots. The plot of p/q and p is somewhat insensitive to small deviations from the model since the pressure occurs in both variables. Since the Langmuir model is of the correct qualitative form to represent a type I isotherm, a reasonably good fit of many experimental isotherms may often be obtained over quite wide concentration
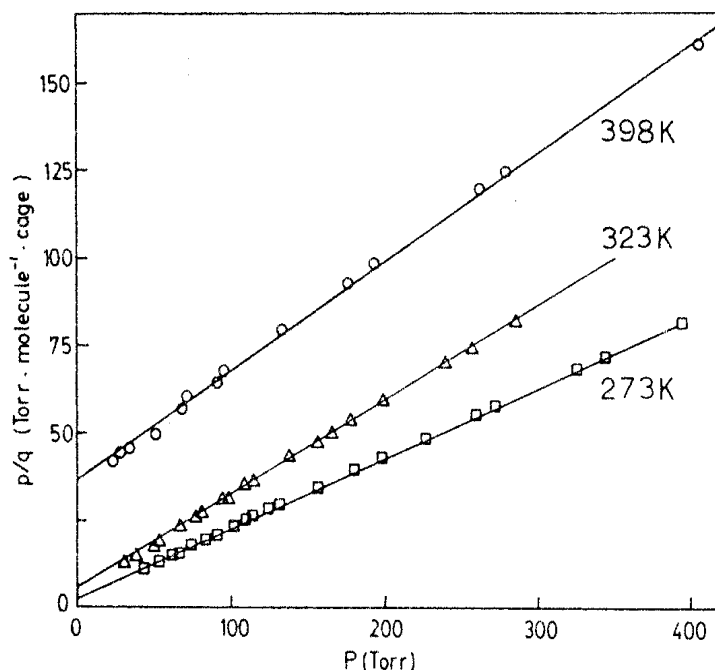
FIGURE 2.8. Langmuir plots showing apparent conformity with the Langmuir equation [Eq. (2.32)] of equilibrium data for propane in 5A zeolite. (From ref. 27.)

ranges by appropriate choice of the constants b and q_s. However, unless the experimental data extend over the entire concentration range from the Henry's law region to near saturation, the constants derived by matching the experimental data to the model may lack physical significance. This is illustrated in Figure 2.8 and Table 2.13[27] which show experimental equilibrium data for propane in 5A zeolite analyzed according to Eq. (2.32). At all temperatures the plots show little deviation from linearity, suggesting that the Langmuir model is a valid representation. At the highest temperature the data extend only up to about 50% of the saturation capacity and the Henry constant derived from the Langmuir plot is reasonably close to the value

TABLE 2.13. Sorption of Propane on 5A Zeolite.
Comparison of Parameters Calculated from the Langmuir Model with Values derived from More Detailed Analysis[27]

Temp (K)	Henry Constant K or bq_s (molecule/cavity torr)		Saturation Limit q_s (molecule/cavity)	
	Detailed Analysis	Langmuir Plot	Detailed Analysis	Langmuir Plot
273	3.96	0.4	~5	5.0
323	0.321	0.182	~5	3.7
398	0.033	0.028	~5	3.18

determined from a more detailed analysis of the low concentration data. The apparent value of q_s is however very much lower than the true saturation limit. Conversely, at the lowest temperature the experimental data cover only the high-concentration region. The value of q_s from the linearized plot is then essentially correct while the Henry constant is grossly in error.

The model of adsorption at a set of distinct localized sites is in general more appropriate to chemisorption than to physical adsorption since in many cases a physically adsorbed layer is highly mobile and resembles more closely a two-dimensional gas. The Langmuir equation may however be derived from the Gibbs adsorption isotherm as an approximation for mobile physical adsorption at relatively low coverage (see Chapter 3), and the application of this model to physical adsorption is therefore not without theoretical justification. Furthermore, there are a number of zeolitic systems such as argon in sodalite for which the basic assumptions of the localized model are accurately fulfilled since each cage can accommodate only one sorbate molecule. The deviations from the Langmuir model which are observed for most real systems are discussed more fully in Chapter 4.

The BET Isotherm

Since almost all practically important adsorbents are porous solids a key parameter which is required to characterize an adsorbent is the specific surface area. The specific areas of microporous solids are very large, and values of several hundred square meters/gram are not uncommon. Accurate measurement of the surface area of a microporous solid presented a significant problem in early studies of adsorption and catalysis.

It is evident that if the physical adsorption capacity were limited to a close-packed monolayer, determination of the saturation limit from an experimental isotherm with a molecule of known size would provide a simple and straightforward method of estimating the specific area. The main difficulty is that in chemisorption the sites are usually widely spaced so that the saturation limit bears no obvious relationship to specific surface area while physical adsorption generally involves multilayer adsorption. The formation of the second and subsequent molecular layers commences at pressures well below that required for completion of the monolayer so it is not immediately obvious how to extract the monolayer capacity from the experimental isotherm. This problem was first solved by Brunauer, Emmett, and Teller[28] (BET) who developed a simple model isotherm to account for multilayer adsorption and used this model to extract the monolayer capacity and hence the specific surface area. A number of refinements to the BET model and to the experimental method have been developed more recently but the basic BET method remains the most widely used technique for measurement of specific surface area.[29]

An exact theoretical treatment of multilayer adsorption presents formidable

problems since it is necessary to take account not only of the interactions between sorbate molecules and the adsorbent surface but also of the sorbate-sorbate interactions which are often of comparable magnitude. The BET model is based on a number of rather serious idealizations which can at best be no more than a first approximation. Each molecule in the first adsorbed layer is considered to provide one "site" for the second and subsequent layers. The molecules in the second and subsequent layers, which are in contact with other sorbate molecules rather than with the surface of the adsorbent, are considered to behave essentially as the saturated liquid while the equilibrium constant for the first layer of molecules in contact with the surface of the adsorbent is different. The expression for the BET isotherm may be derived from these assumptions, either by an extension of the simple kinetic argument put forward above for the monolayer case or by a more refined thermodynamic argument, as outlined in Chapter 3. The resulting equation for the BET equilibrium isotherm is

$$\frac{q}{q_m} = \frac{b(p/p_s)}{(1 - p/p_s)(1 - p/p_s + bp/p_s)} \tag{2.33}$$

in which p_s represents the saturation vapor pressure of the saturated liquid sorbate at the relevant temperature. This expression, which has the general form of a type II isotherm in Brunauer's classification, has been found to provide a good representation of experimental physical adsorption isotherms provided that the range of reduced pressure is restricted to $0.05 < p/p_s < 0.35$.

Knowing the saturation vapor pressure and the equilibrium uptake at several pressures within the prescribed range, q_s, the sorbate concentration corresponding to a close-packed monolayer, may be easily found from a plot of $p/q(p_s - p)$ versus p/p_s. Representative experimental data plotted in this way are shown in Figure 2.9. In order to translate the monolayer coverage into a specific area, knowledge of the size of the sorbate molecule is required. Close packing of spherical molecules of diameter equal to the van der Waals diameter is generally assumed.

It is evident that in order to make measurements within the required range of relative pressures at conveniently measurable absolute pressures, the temperature of the measurements should be carefully selected. Measurements are commonly made using nitrogen as the sorbate at liquid N_2 temperatures but other small molecules may also be employed. Some indication of the accuracy of the BET model as a method for the determination of surface area may be obtained from a comparison of data obtained with different sorbates on the same porous material. Some representative data obtained with a microporous NH_3 synthesis catalyst are summarized in Table 2.14. These data suggest that the absolute area may be determined to within about 20–25% by this method. Relative areas may be determined with somewhat greater accuracy by comparing the uptake by different adsorbents over the same relative pressure range.
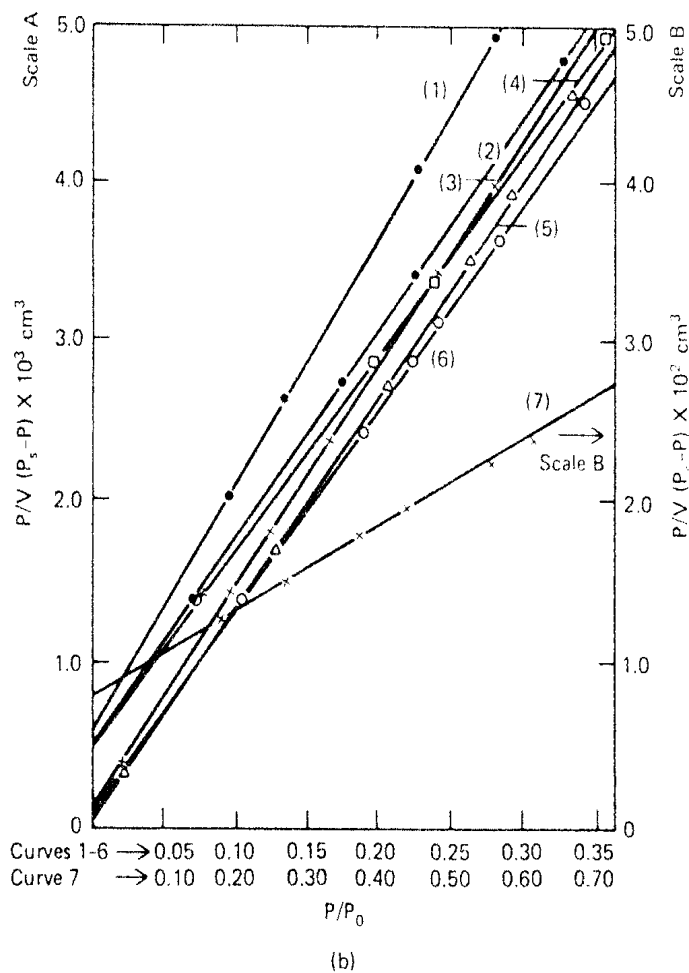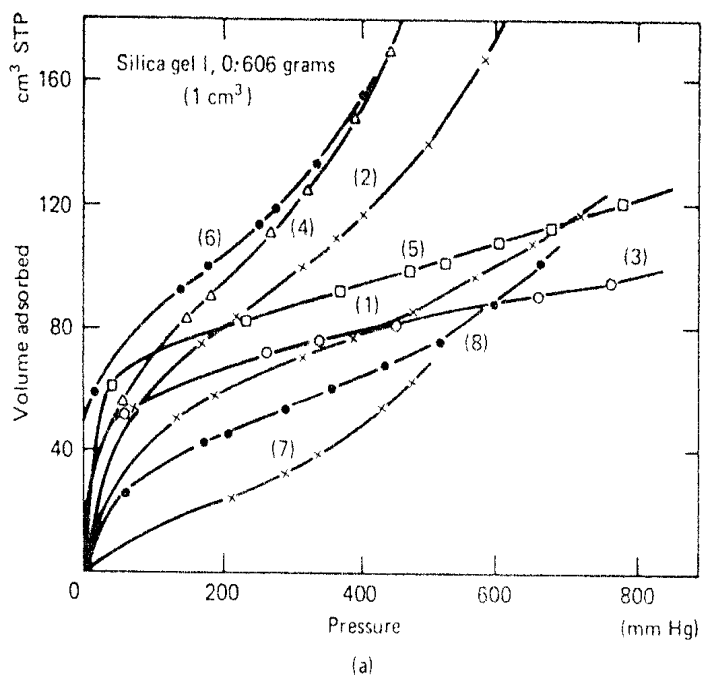
FIGURE 2.9. (a) Experimental isotherms and (b) BET plots for sorption on silica gel of (1) CO_2 at $-78°C$; (2) Ar at $-183°C$; (3) N_2 at $-183°C$; (4) O_2 at $-183°C$; (5) CO at $-183°C$; (6) N_2 at $-195.8°C$; (7) C_4H_{10} at $0°C$; and (8) SO_2 at $0°C$. (From ref. 28.)

TABLE 2.14. Comparison of BET Area of
NH$_3$ Synthesis Catalyst Determined with
Different Sorbates[28]

Sorbate	T (K)	Area (m^2/g)
N$_2$	77	580
Br$_2$	352	470
CO$_2$	195	460
CO	90	550

2.5. CAPILLARY CONDENSATION: THE KELVIN EQUATION

In a porous adsorbent there is a continuous progression from multilayer adsorption to capillary condensation in which the smaller pores become completely filled with liquid sorbate. This occurs because the saturation vapor pressure in a small pore is reduced, in accordance with the Kelvin equation,[30] by the effect of surface tension.

The Kelvin equation may be derived from simple thermodynamic considerations. We consider a straight cylindrical pore (radius r) containing liquid adsorbate, as sketched in Figure 2.10. Suppose that n moles of liquid ($n = \pi r^2 \, dl / V_m$) are evaporated from the pore under the equilibrium vapor pressure p and condensed to liquid on a plane surface over which the vapor pressure is p_s, the saturation vapor pressure for the pure liquid at the same temperature. The work done against surface tension is exactly equal to the free energy difference:

$$n\Delta G = (2\pi r \, dl)\sigma \cos\theta = nRT \ln\left(\frac{p_s}{p}\right) = \frac{\pi r^2 dl \, RT}{V_m} \ln\left(\frac{p_s}{p}\right) \quad (2.34)$$

$$\frac{p}{p_s} = \exp\left(\frac{-2\sigma V_m \cos\theta}{rRT}\right) \quad \text{(Kelvin equation)} \quad (2.35)$$

If the restriction to cylindrical pore geometry is relaxed, the same argument leads to the more general relationship:

$$\frac{dV}{d\mathscr{A}} = -\frac{V_m \sigma \cos\theta}{RT \ln(p/p_s)} \quad (2.36)$$

FIGURE 2.10. Derivation of Kelvin equation.
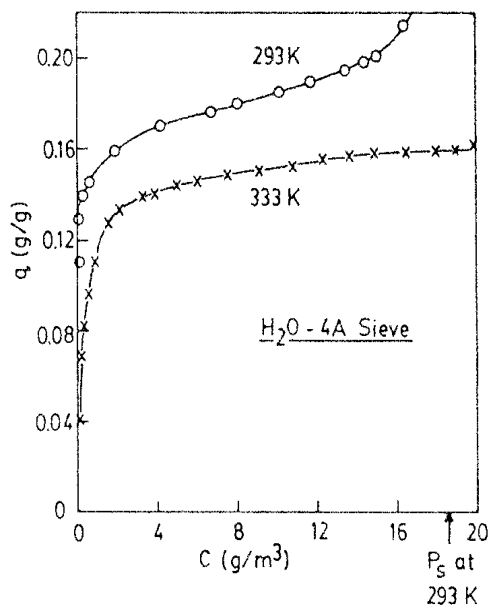
FIGURE 2.11. Experimental isotherms for sorption of water on 4A molecular sieve pellets showing capillary condensation at 293 K. (Experimental data of Kyte[35] for Laporte 4A sieve.)

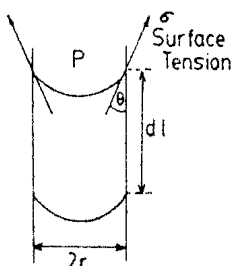where $dV/d\mathscr{A}$ is simply the rate of change of pore volume with surface area which, for a cylindrical pore, corresponds to $r/2$.

Taking benzene at 20°C as an example ($\sigma \approx 29$ dyne/cm, $V_m \approx 89$ cm^3/mole, $\theta \approx 0$) we note that in cylindrical pores of 50 Å capillary condensation will occur at a relative pressure of $p/p_s \approx 0.67$ whereas in pores of 500 Å the relative pressure will be 0.96. It is evident that the capillary effect is significant only in quite small pores.

The onset of capillary condensation generally coincides with an inflection in the equilibrium isotherm, that is, a type 4 isotherm of Brunauer's classification. A typical example is shown in Figure 2.11.

In the capillary condensation region the isotherm generally shows hysteresis so that the apparent equilibrium pressures observed in adsorption and desorption experiments are different. Several plausible explanations for this effect have been put forward. Foster[31] suggested that during adsorption multilayers build up on the capillary walls but a complete meniscus is not formed until saturation is reached at which all pores are filled. The relationship between pressure and adsorbed phase concentration along the adsorption branch of the isotherm will therefore be governed by an appropriate multilayer isotherm analogous to the BET equation. (Note that the BET equation itself is not applicable in this region since its range of validity is limited to relative pressures of less than about 0.35.) Once the saturation limit for capillaries of a particular size has been reached desorption will occur from a curved meniscus and the equilibrium pressure will be governed by the Kelvin equation. According to this theory the adsorbed film formed during adsorption is in a metastable state, the true equilibrium state being represented by the capillary condensed liquid. The apparent stability of the multilayer film depends on the absence of nuclei to allow condensation to the bulk liquid.

(a)   (b)

FIGURE 2.12. (a) Radial filling of pores during adsorption and (b) evaporation from filled pores with hemispherical meniscus during desorption.
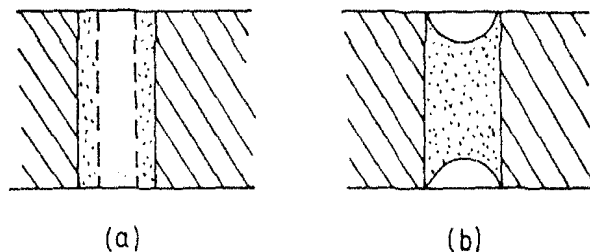
An alternative view was suggested by Cohan[32] who suggested that capillary condensation occurs along both adsorption and desorption branches of the isotherm, the difference being due to a difference in the shape of the meniscus. During adsorption the pore fills radially and a cylindrical meniscus is formed as sketched in Figure 2.12a. Under these conditions $dv/ds = r$ (rather than $r/2$ as assumed in the Kelvin equation) and with $\theta = 0$:

$$\frac{p}{p_s} = \exp\left(\frac{-\sigma V_m}{rRT}\right) \qquad (2.37)$$

During desorption the meniscus is hemispherical and the Kelvin equation [Eq. (2.35)] applies. It follows that

$$\left(\frac{p_a}{p_s}\right)^2 = \frac{p_d}{p_s} \qquad (2.38)$$

where p_a and p_d represent the apparent equilibrium pressures on the adsorption and desorption branches of the isotherm at a given loading. Many experimental isotherms show approximate agreement with this equation but the agreement is by no means quantitative and universal. Deviations may be explained as arising from deviations in the shape of the pores from simple cylindrical geometry or alternatively such deviations can be taken as evidence against Cohan's mechanism.

Measurement of an isotherm under conditions of capillary condensation provides a simple means of determining the pore size distribution of the adsorbent. Applying the Kelvin equation to the desorption branch of the isotherm gives the value of r' corresponding to a known relative pressure (p'/p_0) and the corresponding adsorption loading (q'). If adsorption on the pore walls is neglected, q'/ρ would correspond to the total pore volume made up of pores of radius less than or equal to r'. A plot of q'/ρ versus r thus gives the cumulative pore size distribution from which the frequency distribution may be readily determined by differentiation. If an accurate determination of the pore size distribution is required it is necessary to correct for adsorption on the pore walls. This correction may be found from measurement of the equilibrium isotherm for the same sorbate on a large pore adsorbent under conditions such that there is no capillary condensation. Full details of the method of calculation have been given by Gregg and Sing.[30] A representa-
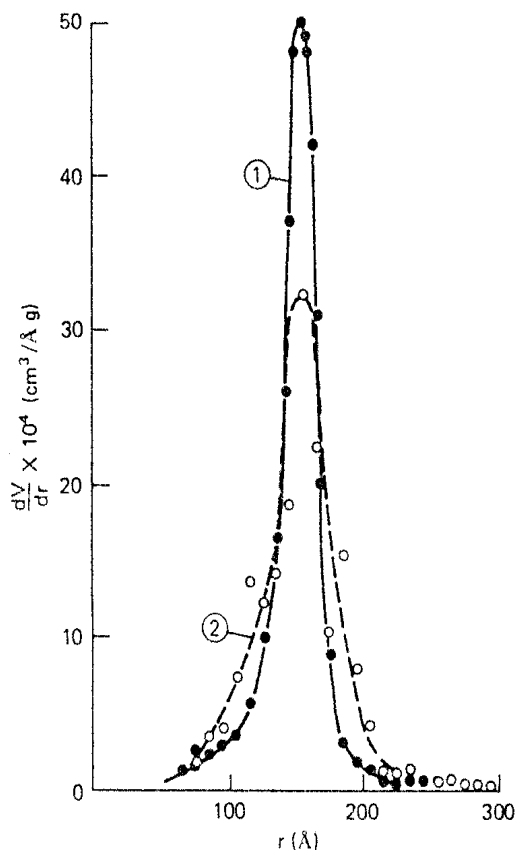
FIGURE 2.13. Comparison of pore size distribution for Cr_2O_3-Fe_2O_3 catalyst measured by mercury penetration and from the nitrogen desorption isotherm. (1) Pore size distribution from N_2 desorption isotherm. (2) Pore size distribution from mercury penetration. (From ref. 33, reprinted with permission.)

tive example of a pore size distribution calculated in this way is shown in Figure 2.13.

2.6. MERCURY POROSIMETRY

If the contact angle between liquid and solid is greater than 90°, then at equilibrium the pressure on the convex side of the meniscus must be greater than on the concave side. Thus if a porous solid is immersed in a nonwetting liquid such as mercury there will be no penetration of the pores until the
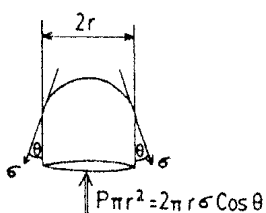
FIGURE 2.14. Force balance for mercury penetrometer.

TABLE 2.15. Pore Radius
for Mercury Penetration as
Function of Pressure

P (atm)	r (Å)
10	2.2×10^4
100	2200
10^3	220
10^4	22

applied pressure reaches the equilibrium value. The equilibrium pressure and pore radius are related through a simple force balance as illustrated in Figure 2.14.

Some values of P and r for mercury ($\theta \approx 40°$, $\sigma \sim 480$ dyne/cm) are summarized in Table 2.15. It is evident that penetration of the smaller pores characteristic of microporous adsorbents is achieved only at very high pressures.

The mercury porosimeter is simply an instrument designed to apply a controlled mercury pressure to the adsorbent and record the volume of mercury penetrating the pore structure. Because of practical limitations on the maximum pressure, the minimum pore radius which can be measured by this method is about 50–100 Å. The method is however more suitable for measurement of larger pores in the range 1000–10,000 Å. Some examples of pore size distribution curves measured by mercury penetration are given in Figure 1.14.

Since pore size distribution may also be measured by gas adsorption, as discussed above, a comparison of the two methods is possible. Such a comparison was made by Zwietering[33] for a Cr_2O_3-Fe_2O_3 catalyst with a mean pore radius of about 150 Å. The results of the two methods showed good agreement as may be seen from Figure 2.13. However, since mercury penetration measures in effect the pore volume accessible through openings of a given diameter, agreement with the results of gas adsorption measurements can be expected only when the pore shape is reasonably regular. If the pore mouths are constricted ("ink bottle pores") the apparent pore diameters derived from mercury penetration will be too low. It is therefore possible, in principle, to obtain some information about the macropore structure from a comparison of results obtained by the two methods. Other methods of characterizing in detail the structure of porous materials have been discussed by Dullien.[34]

2.7. CHARACTERIZATION OF ZEOLITES

The micropores of zeolitic adsorbents are too small to be characterized by normal porosimetry and other physical methods are therefore required. One of

the simplest but most effective methods is the measurement of sorption rates and capacities using a series of sorbates of progressively increasing molecular diameter. Since the sorption cutoff is very sharp when the free diameter of the aperture is exceeded, a good estimate of the effective pore size may often be obtained in this way. Other more sophisticated methods of characterization involve determination of the crystal structure by X-ray diffraction, detailed analysis of the infrared spectrum of the framework, and NMR methods. An excellent general review has been given by Lechert.[37]

REFERENCES

1. E. A. Moelwyn-Hughes, *Physical Chemistry*, 2nd ed. Pergamon Press, Oxford, 1961.

2. J. O. Hirschfelder, C. F. Curtis, and R. B. Bird, *Molecular Theory of Gases and Liquids*. Wiley, New York, 1954.

3. D. M. Young and A. D. Crowell, *Physical Adsorption of Gases*. Butterworths, London, 1962.

4. F. London, *Zeit. Phys.* **63**, 245 (1930).

5. F. London, *Zeit. Phys. Chem.* **B11**, 222 (1940).

6. J. C. Slater and J. G. Kirkwood, *Phys. Rev.* **37**, 682 (1931).

7. J. G. Kirkwood, *Phys. Zeit.* **33**, 57 (1932).

8. A. Muller, *Proc. Roy. Soc.* **A154**, 624 (1936).

9. S. Ross and J. P. Olivier, *On Physical Adsorption*. Wiley, New York, 1964, p. 267.

10. R. M. Barrer, *Zeolites and Clay Minerals*. Academic Press, London, 1978.

11. P. Broier, A. V. Kiselev, E. A. Lesnik, and A. A. Lopatkin, *Russ. J. Phys. Chem.* **42**(10), 135 (1968).

12. P. Broier, A. V. Kiselev, A. A. Lopatkin, and S. Shpigil, *Doklady Akad. Nauk. SSSR* **161**(4), 853–856 (1965).

13. A. V. Kiselev, *Adv. Chem.* **102**, 37 (1971).

14. R. I. Derrah and D. M. Ruthven, *Can. J. Chem.* **53**, 996 (1975).

15. R. M. Barrer, *J. Coll. Interface Sci.* **21**, 415 (1966).

16. W. Schirmer, G. Meinert, and A. V. Grossmann, *Monatsberichte* **11**, 886 (1969).

17. R. M. Barrer and R. M. Gibbons, *Trans. Faraday Soc.* **59**, 2569 (1963) and **61**, 948 (1965).

18. A. V. Kiselev and P. Q. Du, *J. Chem. Soc. Faraday Trans. II* **74**, 367 (1978); **77**, 1 (1981); and **77**, 17 (1981).

19. J. L. Soto, P. W. Fisher, A. J. Glessner, and A. L. Myers, *J. Chem. Soc. Faraday Trans. I* **77**, 157 (1981).

20. D. M. Ruthven, K. F. Loughlin, and R. I. Derrah, *Adv. Chem.* **121**, 330 (1973).

21. R. W. Sargent and C. J. Whitford, *Adv. Chem.* **102**, 144 (1971).

22. K. Chihara, M. Suzuki, and K. Kawazoe, *AIChE Jl* **24**, 237 (1978).

23. E. Cohen de Lara, *Proceedings of the Fifth International Conference on Zeolites, Naples, June 1980*. Heyden, London, 1980, p. 414.

24. E. Cohen de Lara and Y. DeLaval, *J. Phys. Chem.* **78**, 2180 (1974).

25. S. Brunauer, L. S. Deming, W. E. Deming, and E. J. Teller, *J. Am. Chem. Soc.* **62**, 1723 (1940).

26. I. Langmuir, *J. Chem. Soc.* **40**, 1361 (1918).

27. D. M. Ruthven and K. F. Loughlin, *J. Chem. Soc. Faraday Trans. I* **68**, 696 (1972).

28. S. Brunauer, P. H. Emmett, and E. Teller, *J. Am. Chem. Soc.* **60**, 309 (1938).

29. D. M. Young and A. D. Crowell, *Physical Adsorption of Gases.* Butterworths, London, 1962, p. 190.

30. S. J. Gregg and K. S. W. Sing, *Adsorption Surface and Porosity.* Academic Press, London, 1967, p. 160.

31. A. G. Foster, *J. Chem. Soc.* (London), 1806 (1952).

32. L. H. Cohan, *J. Am. Chem. Soc.* **60**, 433 (1938).

33. P. Zwietering, in *The Structure and Properties of Porous Solids.* Butterworths, London, 1958, p. 287.

34. F. A. L. Dullien, *Porous Media.* Academic Press, New York, 1979, Chap. III.

35. W. S. Kyte, Ph.D. thesis, University of Cambridge, 1970.

36. R. M. Barrer and J. L. Whiteman, *J. Chem. Soc. A*, 13 (1967).

37. H. Lechert, *Physical Characterization of Zeolites*, in Proceedings of NATO ASI, Sintra-Estoril, Portugal, May 1983. Martinus Nijhoff, the Hague, Holland, (to be published).

3

THERMODYNAMICS OF ADSORPTION

The thermodynamic approach to the study of equilibrium is quite general and may be applied to adsorption just as to any other phase equilibrium. The only general assumption which is implicit in such an approach is that the adsorbed layer can be treated as a distinguishable phase in the thermodynamic sense. This is in general correct, even though the precise location of the phase boundary may be somewhat uncertain. Our present understanding of the classical thermodynamics of adsorption is due largely to the work of Hill[1-4] and Everett.[5] The subject has been well reviewed by Young and Crowell.[6]

It is possible to adopt two somewhat different but entirely consistent perspectives in applying thermodynamic principles to adsorption equilibrium. The surface layer, consisting of adsorbent plus adsorbate, may be considered as a single phase having the general properties of a solution. Alternatively, if the thermodynamic and geometric properties of the adsorbent can be regarded as independent of the temperature and pressure of the surrounding gas and the concentration of adsorbed molecules, the adsorbent may be considered as thermodynamically inert. Under these conditions the adsorbed molecules themselves may be regarded as a distinct phase and the effect of the adsorbent is limited to the creation of a force field, the detailed nature of which need not be specified. This view was originally formulated and applied by Gibbs.[7] The former view is somewhat more general but more detailed information can be obtained from the Gibbsian formulation.

3.1. CLASSICAL EQUILIBRIUM RELATIONSHIPS

Whichever view of the adsorbed phase is adopted, the condition for equilibrium between the adsorbed phase and the ambient gas phase is simply

$$\mu_s = \mu_g \qquad (3.1)$$

This relationship is still applicable even when adsorption occurs from the liquid phase since at equilibrium the chemical potentials of the adsorbed species in all three phases must be equal. Assuming an ideal vapor phase we may write

$$\mu_s = \mu_g = \mu_g^o + RT\ln\left(\frac{p}{p^o}\right) \tag{3.2}$$

where μ_g^o is the standard chemical potential of the vapor phase, that is, the chemical potential at the reference pressure p^o. Differentiating at constant adsorbed phase concentration (q) and applying the Gibbs–Helmholtz relation $[\partial(\mu/T)/\partial T = -\bar{H}/T^2]$ we obtain

$$\frac{-\bar{H}_s}{T^2} = \frac{-\bar{H}_g^o}{T^2} + R\left(\frac{\partial \ln p}{\partial T}\right)_q \tag{3.3}$$

$$\left(\frac{\partial \ln p}{\partial T}\right)_q = \frac{\bar{H}_g^o - \bar{H}_s}{RT^2} = \frac{H_g - \bar{H}_s}{RT^2} = \frac{-\Delta H_s}{RT^2} \tag{3.4}$$

since for an ideal vapor phase the partial molar enthalpy $\bar{H}_g^o$ is independent of composition and identical to the molar enthalpy H_g. ΔH_s $(\equiv \bar{H}_s - H_g)$ is the enthalpy change on adsorption and $-\Delta H_s = H_g - \bar{H}_s$ is commonly referred to as the isosteric heat of adsorption. $\bar{H}_s$ and therefore ΔH_s are in general functions of the adsorbed phase concentration q.

If the difference in the heat capacity of the sorbate in adsorbed and vapor phases can be neglected, ΔH_s is independent of temperature and Eq. (3.4) may be integrated directly to yield

$$\ln p = \text{constant} - \frac{\Delta H_s}{RT} \tag{3.5}$$

Assuming that the above approximation concerning the heat capacity is valid, a plot of $\ln p$ versus $1/T$ should yield a linear isostere of slope $(-\Delta H_s)$. This provides a simple and practically useful method for determination of the isosteric heat. (A set of isosteres for H$_2$O-4A sieve is given in Figure 11.2.)

The isosteric heat is also the heat which would be transferred to the surroundings in the transfer of a differential quantity of sorbate from the vapor phase to the adsorbed phase under isothermal and isobaric conditions. In a similar differential calorimetric measurement carried out at constant volume, the heat released to the heat bath would be $H_g - \bar{U}_s$. This quantity is sometimes referred to as the differential heat of sorption, but the term is redundant and it is probably better to consider this quantity simply as the difference in partial molar internal energy.

From the definition of enthalpy we have, for an ideal vapor phase,

$$H_g = U_g + PV = U_g + RT \tag{3.6}$$

and since the volume of the adsorbed phase is negligible in comparison with

the vapor

$$\overline{U}_s \approx \overline{H}_s, \qquad -\Delta H_s = U_g - \overline{U}_s + RT \qquad (3.7)$$

Since $\mu = \overline{H} - T\overline{S}$ it follows from Eq. (3.1) that at equilibrium

$$\overline{S}_s - \overline{S}_g = \frac{\overline{H}_s - H_g}{T} \qquad (3.8)$$

The partial molar entropy of the ideal vapor phase is given by

$$\overline{S}_g = S_g^\circ - R \ln \frac{p}{p^\circ} \qquad (3.9)$$

where S_g° is the molar entropy of the vapor in the standard state at pressure p°. The partial molar entropy of the adsorbed phase may therefore be calculated directly from an experimental equilibrium isotherm once the concentration dependence of the isosteric heat has been determined:

$$\overline{S}_s - S_g^\circ = \frac{\overline{H}_s - H_g}{T} - R \ln \frac{p}{p^\circ} \qquad (3.10)$$

It is also convenient to define a standard state for the adsorbed phase and a corresponding adsorption equilibrium constant:

$$\mu_s = \mu_s^* + RT \ln \left(\frac{a_s}{a_s^\circ} \right) \qquad (3.11)$$

where a_s is the activity of the adsorbed phase and μ_s^* is the standard chemical potential at activity a_s°. It follows from Eq. (3.2) that

$$\mu_s^* - \mu_g^\circ = RT \ln \left(\frac{p}{p^\circ} \frac{a_s^\circ}{a_s} \right) \qquad (3.12)$$

whence it may be seen that the adsorption equilibrium constant is given by

$$K'' = \frac{p^\circ a_s}{p a_s^\circ} \qquad (3.13)$$

If the standard state is taken as an infinitely dilute ideal adsorbed phase Eq. (3.13) reduces simply to Henry's law in the low concentration limit and at higher concentrations to a definition of the activity coefficient of the adsorbed phase (γ):

$$\lim_{p \to 0} \frac{q}{p} = \frac{K'' a_s^\circ}{p^\circ} \equiv K', \qquad \gamma = \frac{K' p}{q} \qquad (3.14)$$

The temperature dependence of K' follows the usual van't Hoff equation [Eq. (2.19)].

3.2. THERMODYNAMICS OF AN ADSORBED PHASE

Spreading Pressure

In the thermodynamic discussion of bulk phases the fundamental differential equation which summarizes the first and second law of thermodynamics may be written

$$dU = T\,dS - P\,dV + \sum \mu_i dn_i \qquad (3.15)$$

Integration of this equation, holding the intensive variables T, P, and μ constant yields

$$U = TS - PV + \sum \mu_i n_i \qquad (3.16)$$

If we consider the adsorbed phase as a solution of n_s moles of sorbate and n_a moles of nonvolatile adsorbent, Eq. (3.15) becomes

$$dU = T\,dS - P\,dV + \mu_a dn_a + \mu_s dn_s \qquad (3.17)$$

We may also write for the adsorbent in the absence of sorbate:

$$dU_{0a} = T\,dS_{0a} - P\,dV_{0a} + \mu_{0a} dn_a \qquad (3.18)$$

and by subtraction we obtain

$$dU_s = T\,dS_s - P\,dV_s - \Phi\,dn_a + \mu_s dn_s \qquad (3.19)$$

where $U_s \equiv U - U_{0a}$, $V_s \equiv V - V_{0a}$, $S_s \equiv S - S_{0a}$, $-\Phi \equiv \mu_a - \mu_{0a}$. So far these quantities have no special significance, but if we now adopt the Gibbsian view and consider the n_a moles of adsorbent to be thermodynamically inert, these quantities, defined by difference, become simply the thermodynamic properties of the adsorbed phase since any contribution from the adsorbent is eliminated in the subtraction. For example, U_s now refers to the internal energy of the n_s moles of sorbate in the potential field of the absorbent.

The meaning of the variable Φ requires further consideration:

$$\Phi \equiv \mu_{0a} - \mu_a = \left(\frac{\partial U_{0a}}{\partial n_a}\right)_{S_0,V_{0a}} - \left(\frac{\partial U}{\partial n_a}\right)_{S,V,n_s} = -\left(\frac{\partial U_s}{\partial n_a}\right)_{S_s,V_s,n_s} \qquad (3.20)$$

It is evident that Φ represents the change in internal energy per unit of adsorbent due to the spreading of the adsorbate over the surface or through the micropore volume of the adsorbent. For adsorption on a two-dimensional surface, the surface area $\mathscr{A}$ is directly proportional to n_a while for adsorption in a three-dimensional microporous adsorbent the micropore volume $\mathscr{V}$ is proportional to n_a. We may therefore write

$$\Phi\,dn_a = \pi\,d\mathscr{A} = \phi\,d\mathscr{V} \qquad (3.21)$$

where π and ϕ are respectively the two-dimensional or three-dimensional

spreading pressures defined by

$$\pi = -\left(\frac{\partial U_s}{\partial \mathscr{A}}\right)_{S_s,V_s,n_s}, \qquad \phi = -\left(\frac{\partial U_s}{\partial \mathscr{V}}\right)_{S_s,V_s,n_s} \tag{3.22}$$

Defined in this way π corresponds to the difference in surface tension between a clean surface and a surface covered with adsorbate.

The concept of the spreading pressure as the appropriate intensive variable for the discussion of surface adsorption was first introduced by Gibbs. However, the Gibbs formulation implies a two-dimensional adsorbed phase which is unnecessarily restrictive. Essentially the same thermodynamic relations may be developed in terms of the surface energy, and this approach has the advantage that it is equally applicable to two-dimensional adsorption on a surface or three-dimensional adsorption in a microporous solid.

Just as with a bulk phase, the fundamental thermodynamic equations representing the combined first and second laws may be written in four equivalent ways in terms of the internal energy, enthalpy, Helmholtz free energy, or Gibbs free energy. For an adsorbed phase

$$dU_s = T\,dS_s - P\,dV_s - \Phi\,dn_a + \mu_s dn_s$$
$$dH_s = T\,dS_s + V_s dP - \Phi\,dn_a + \mu_s dn_s$$
$$dA_s = -S_s dT - P\,dV_s - \Phi\,dn_a + \mu_s dn_s \tag{3.23}$$
$$dG_s = -S_s dT + V_s dP - \Phi\,dn_a + \mu_s dn_s$$

Since the volume of the adsorbed phase is negligible in comparison with the volume of the vapor phase the term $P\,dV_s$ can be neglected. These equations may therefore be integrated with all intensive variables held constant to yield

$$U_s = U_s(S_s,V_s,n_a,n_s) = TS_s - \Phi n_a + \mu_s n_s$$
$$H_s = H_s(S_s,P,n_a,n_s) = TS_s - \Phi n_a + \mu_s n_s$$
$$A_s = A_s(T,V_s,n_a,n_s) = -\Phi n_a + \mu_s n_s \tag{3.24}$$
$$G_s = G_s(T,P,n_a,n_s) = -\Phi n_a + \mu_s n_s$$

The four equivalent definitions of Φ and μ_s follow naturally:

$$\Phi \equiv -\left(\frac{\partial U_s}{\partial n_a}\right)_{S_s,V_s,n_s} = -\left(\frac{\partial H_s}{\partial n_a}\right)_{S_s,P,n_s} = -\left(\frac{\partial A_s}{\partial n_a}\right)_{T,V_s,n_s} = -\left(\frac{\partial G_s}{\partial n_a}\right)_{T,P,n_a}$$

$$\mu_s \equiv \left(\frac{\partial U_s}{\partial n_s}\right)_{S_s,V_s,n_a} = \left(\frac{\partial H_s}{\partial n_s}\right)_{S_s,P,n_a} = -\left(\frac{\partial A_s}{\partial n_s}\right)_{T,V_s,n_a} = \left(\frac{\partial G_s}{\partial n_s}\right)_{T,P,n_a} \tag{3.25}$$

From these equations it may be seen that four independent variables are required to define each extensive thermodynamic property, whereas in normal three-dimensional thermodynamics only three variables are required for a single-component system. The additional variable is of course the total surface area or quantity of adsorbent over which the n_s moles of sorbate are distributed.

In the thermodynamic analysis of bulk phases, P and T are the most convenient intensive variables, and since the criterion for equilibrium at constant P and T is minimum Gibbs-free energy, equilibrium relationships are generally developed in terms of G. For an adsorbed phase, pressure is not a significant intensive variable; the thermodynamic properties are determined by T and Φ (or π) rather than T and P. Following Hill[1,3] and Everett[5] it is therefore logical to introduce a new free energy (F_s) defined in analogy with $G = A + PV$ by

$$F_s = A_s + \Phi n_a = A_s + \pi \mathscr{A} \approx G_s + \pi \mathscr{A} \qquad (3.26)$$

With this definition the condition of equilibrium at constant T and Φ (or T and π) is minimum F_s. All thermodynamic relations developed for a bulk phase in terms of G apply to the adsorbed phase with G, P, and V replaced by F_s, Φ, and n_a or equivalently F_s, π, and $\mathscr{A}$. In particular

$$dF_s = dA_s + \Phi \, dn_a + n_a d\Phi = dA_s + \pi \, d\mathscr{A} + \mathscr{A} \, d\pi$$

$$= -S_s dT + n_a d\Phi + \mu_s dn_s = -S_s dT + \mathscr{A} \, d\pi + \mu_s dn_s \qquad (3.27)$$

Gibbs Adsorption Isotherm

The derivation of the Gibbs adsorption isotherm from Eqs. (3.23) and (3.24) follows essentially the same logic as the derivation of the Gibbs–Duhem equation. At constant temperature and neglecting the term $P\,dV_s$, Eq. (3.23) becomes

$$dA_s = -\Phi \, dn_a + \mu_s dn_s = -\pi \, d\mathscr{A} + \mu_s dn_s \qquad (3.28)$$

Differentiation of Eq. (3.24) yields

$$dA_s = -\Phi \, dn_a - n_a d\Phi + \mu_s dn_s + n_s d\mu_s \qquad (3.29)$$

and on subtracting Eq. (3.28)

$$n_a d\Phi = \mathscr{A} \, d\pi = \mathscr{V} \, d\phi = n_s d\mu_s \qquad (3.30)$$

Considering equilibrium between the adsorbed phase and an ideal vapor phase, we have, by differentiation of Eq. (3.2),

$$d\mu_s = \frac{RT \, dp}{p} \qquad (3.31)$$

and hence

$$n_a \left(\frac{\partial \Phi}{\partial p} \right)_T = \frac{RT}{p} n_s \quad \text{or} \quad \mathscr{A} \left(\frac{\partial \pi}{\partial p} \right)_T = \frac{RT}{p} n_s \qquad (3.32)$$

which is the Gibbs adsorption isotherm.

As noted in Eq. (3.21) the variables (Φ, n_a), $(\pi, \mathscr{A})$, and $(\phi, \mathscr{V})$ are equivalent and relations such as Eqs. (3.26) and (3.27) have been written in two equivalent ways. For economy of space and to conform with conventional notation subsequent relations are written only in terms of π and $\mathscr{A}$ but

equivalent expressions may of course be written in terms of $\phi, \mathcal{V}$ or Φ, n_a if desired.

3.3. DERIVATION OF ISOTHERM EQUATIONS FROM THE GIBBS EQUATION

The Gibbs adsorption isotherm[8] provides a general relation between spreading pressure (or energy) and adsorbed phase concentration. However, neither the spreading pressure nor the energy Φ_s are amenable to direct experimental measurement and, from the practical point of view, we are therefore more interested in the relation between adsorbed phase concentration and the equilibrium vapor pressure. In a single-component vapor phase system the concentration is determined by temperature and pressure. Similarly, in a single-component adsorbed phase, the concentration is determined by temperature and spreading pressure. Just as the vapor phase system may be characterized by an equation of state $V(P, T)$ so the adsorbed phase may be characterized by an equation of state in the spreading pressure $\mathcal{A}(\pi, T)$ or $\mathcal{V}(\phi, T)$.

Henry's Law

If the equation of state for the adsorbed phase corresponds to the ideal gas law

$$\pi \mathcal{A} = n_s RT \tag{3.33}$$

then from the Gibbs isotherm [Eq. (3.32)]

$$\left(\frac{\partial \pi}{\partial p} \right)_T = \frac{\pi}{p}$$

$$\pi = K'p \tag{3.34}$$

$$q = \frac{n_s}{\mathcal{A}} = \frac{K'p}{RT} = Kc$$

Thus a linear relationship between pressure and adsorbed phase concentration (Henry's law) is equivalent to an ideal gas type of equation of state for the adsorbed layer in terms of spreading pressure.

Langmuir Isotherm

At somewhat higher concentrations one may postulate an equation of state of the form

$$\pi(\mathcal{A} - \beta) = n_s RT \tag{3.35}$$

in analogy with $P(V - b) = nRT$;

$$\left(\frac{\partial \pi}{\partial \mathcal{A}} \right)_T = \frac{- n_s RT}{(\mathcal{A} - \beta)^2} \tag{3.36}$$

and with the Gibbs isotherm [Eq. (3.32)]

$$\frac{dp}{p} = - \frac{\mathscr{A}\, d\mathscr{A}}{(\mathscr{A} - \beta)^2}$$ (3.37)

If we assume $\beta \ll 2\mathscr{A}$, which is a reasonable assumption at low concentrations, and neglect the term in β^2 in the denominator of Eq. (3.37), this expression integrates to

$$bp = \frac{2\beta/\mathscr{A}}{1 - 2\beta/\mathscr{A}} = \left(\frac{\Theta}{1 - \Theta} \right)$$ (3.38)

which becomes identical with the Langmuir isotherm [Eq. (2.28)] provided we take $\Theta = 2\beta/\mathscr{A}$.

Volmer Isotherm

If we make no approximation concerning the relative magnitude of $\beta/\mathscr{A}$ and integrate Eq. (3.37) directly, setting $\Theta = \beta/\mathscr{A}$, we obtain the Volmer isotherm equation:

$$bp = \left(\frac{\Theta}{1 - \Theta} \right) \exp\left(\frac{\Theta}{1 - \Theta} \right)$$ (3.39)

Van der Waals Isotherm

The assumption of a van der Waals equation of state for the adsorbed phase:

$$\left(\pi + \frac{\alpha}{\mathscr{A}^2} \right)(\mathscr{A} - \beta) = n_s RT$$ (3.40)

leads by the same logic to the isotherm equation:

$$bp = \left(\frac{\Theta}{1 - \Theta} \right) \exp\left(\frac{\Theta}{1 - \Theta} \right) \exp\left(- \frac{\alpha'\Theta}{RT} \right)$$ (3.41)

where $\alpha' = 2\alpha q_m$.

Virial Isotherm

Finally we may consider the adsorbed layer to obey a general equation of state of the virial form

$$\frac{\pi}{n_s RT} = 1 + A_1 n_s + A_2 n_s^2 + A_3 n_s^3 \cdots$$ (3.42)

Proceeding through the Gibbs equation in the same way leads to the virial isotherm equation

$$\frac{bp}{n_s} = \exp\left(2A_1 n_s + \frac{3}{2} A_2 n_s^2 + \cdots \right)$$ (3.43)

This expression provides the basis of a very useful means of evaluating Henry
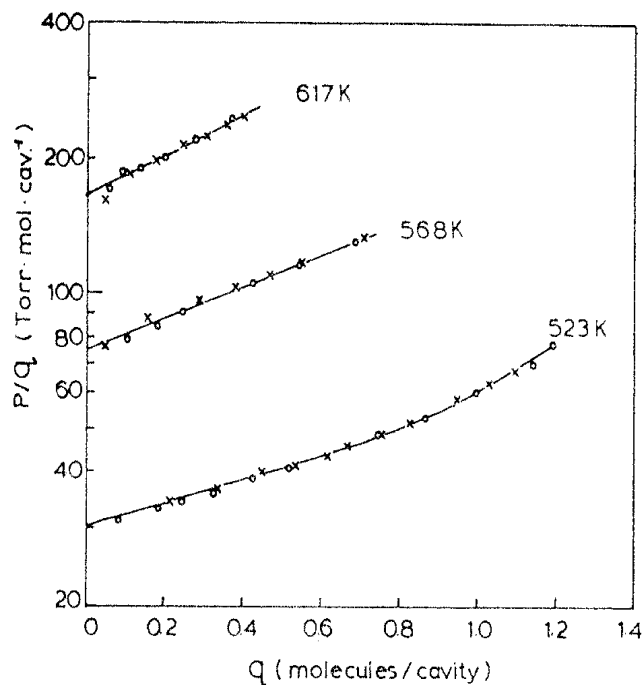
FIGURE 3.1.   Virial plot of $\log(p/q)$ versus q for pentane in 5A zeolite showing extrapolation to determine the Henry constant. (From ref. 10, reprinted by permission from *J. Colloid Interface Soc.* **84**, 526. Copyright © 1981 Academic Press.)

constants from experimental isotherms.[9] With strongly adsorbed components it may be difficult to make reliable experimental measurements at sufficiently low pressure to permit the Henry's law constant to be determined directly from the limiting slope of the isotherm. According to Eq. (3.43), a plot of $\ln(p/n_s)$ versus n_s should be linear at concentrations well above the Henry's law limit so that extrapolation of such a plot to zero-adsorbed phase concentration provides a simple method of determining the Henry constant. The application of this method is illustrated in Figure 3.1.[10]

3.4. ADSORPTION OF MIXTURES

Treatment of Myers and Prausnitz[11]

The activity coefficient for component i in a bulk phase is defined by

$$\Delta G^m = G(T, P, X_1, X_2, \ldots) - \sum X_i G_i^\circ(T, P) = RT \sum X_i \ln(\gamma_i X_i) \quad (3.44)$$

where $G(T, P, X_1, X_2, \ldots)$ is the molar free energy of the mixture and $G_i^\circ(T, P)$ is the molar free energy of the pure components at the same temperature and pressure. For a liquid or solid phase the specification of constant pressure is of minor importance since the free energy of a bulk liquid or solid is almost independent of pressure. Recalling that the relevant intensive variables for an adsorbed phase are T and π it is logical to define the

activity coefficients for an adsorbed mixture by

$$\Delta F_s^m = F_s(T, \pi, X_1, X_2, \dots) - \sum X_i F_i^\circ(T, \pi) = RT \sum X_i \ln(\gamma_i X_i) \quad (3.45)$$

Defined in this way ΔF_s^m is the difference in molar free energy between the mixed adsorbed phase and the corresponding quantities for the pure components in a single-component adsorbed phase at the same temperature and spreading pressure (i.e., the standard state is taken as the pure adsorbed species at the same temperature and spreading pressure as the mixture). Since the free energy of the adsorbed phase is much more sensitive to π than is a bulk liquid or solid phase to P, the specification of constant spreading pressure in the definition of the standard state is important.

The expression for the chemical potential follows by differentiation of Eq. (3.45) at constant temperature and spreading pressure:

$$\mu_i(T, \pi, X_1, X_2, \dots) = F_i^\circ(T, \pi) + RT \ln(\gamma_i X_i) \quad (3.46)$$

Considering equilibrium with the vapor phase (assumed ideal) we have for the pure component

$$F_i^\circ(T, \pi) = \mu_i^\circ(T) + RT \ln\left[p_i^\circ(\pi) \right] \quad (3.47)$$

and for the mixture

$$\mu_i(T, \pi, X_1, X_2, \dots) = \mu_i^\circ(T) + RT \ln\left[p_i^\circ(\pi) \right] + RT \ln(\gamma_i X_i)$$
$$= \mu_i^\circ(T) + RT \ln p_i \quad (3.48)$$

where $\mu_i^\circ(T)$ is the standard chemical potential for component i in the vapor phase at unit pressure. It follows that

$$p_i = p_i^\circ(\pi) \gamma_i X_i \quad (3.49)$$

For a single-component system the relationship between spreading pressure and adsorbed phase concentration may be obtained directly by integration of the Gibbs adsorption isotherm [Eq. (3.32)]:

$$\frac{\pi \mathscr{A}}{RT} = \int_0^{p_i^\circ} q^\circ(p) \frac{dp}{p} \quad (3.50)$$

where $q^\circ(p)$ represents the equilibrium isotherm for the pure component. From Eq. (3.30) the Gibbs isotherm for a binary mixture may be written

$$\mathscr{A} \, d\pi = q_1 d\mu_1 + q_2 d\mu_2 \quad (3.51)$$

and considering equilibrium with the (ideal) vapor phase

$$\frac{\mathscr{A} \, d\pi}{RT} = q_1 d \ln p_1 + q_2 d \ln p_2 \quad (3.52)$$

or at constant total pressure P

$$\frac{\mathscr{A} \, d\pi}{RT} = q_1 d \ln Y_1 + q_2 d \ln Y_2 \quad (3.53)$$

To calculate the spreading pressure for an adsorbed mixture at a specified temperature total pressure and vapor composition thus requires equilibrium

data at that total pressure and temperature over the entire range of vapor composition in order to permit the integration of Eq. (3.53). Knowing the spreading pressure for the mixture and the relationship between spreading pressure and p_i° from Eq. (3.50) the activity coefficient for the adsorbed phase may be calculated directly from Eq. (3.49). However, there is no obvious way of predicting the activity coefficients for a mixed adsorbed phase from single-component isotherm data. This approach therefore provides a means of predicting mixture equilibrium only in the special case of an ideal adsorbed phase.

At constant temperature and spreading pressure we have [Eq. (3.30) or (3.51)]

$$\sum X_i d\mu_i = 0 \tag{3.54}$$

and with Eq. (3.48)

$$\sum X_i d\ln\gamma_i = 0 \quad \text{(constant } \pi, T) \tag{3.55}$$

which is the analog of the Gibbs–Duhem equation for an adsorbed phase and provides a means of checking the thermodynamic consistency of binary (and multicomponent) equilibrium data.

A somewhat different definition was introduced by Broughton[12] who defined the activity coefficient (γ_i') as the ratio of the equilibrium pressure of component i in the mixture to the equilibrium pressure for the pure adsorbed species at the same temperature and at a concentration equal to the total adsorbed phase concentration for the mixture:

$$\gamma_i' = \frac{p_i(n_i, n_j, \ldots)}{p_i^0(n_i^0 = \sum n_i)} \tag{3.56}$$

If the spreading pressure depends only on the total adsorbed phase concentration, which may be a reasonable approximation for many systems, this definition is equivalent to the Myers and Prausnitz definition [Eq. (3.49)]. The condition for thermodynamic consistency with this definition of activity coefficients is[12]

$$\int_0^1 \ln\gamma_1' dX_1 = \int_0^1 \ln\gamma_2' dX_2 \quad \text{(constant } P, T) \tag{3.57}$$

Vacancy Solution Theory

The vacancy solution theory was developed by Suwanayuen and Danner[13] as a method of predicting multicomponent adsorption equilibria from single-component isotherms without the assumption of an ideal adsorbed phase. A somewhat different analysis is given here although the essential features of the model are retained.

Instead of incorporating the surface work term $\pi\mathscr{A}$ directly into the definition of the free energy of the adsorbed phase [Eq. (3.26)] one may

choose to proceed directly from Eq. (3.24) which, when written in terms of spreading pressure, becomes

$$G_s = \mu_s(T,\pi)n_s - \pi\mathscr{A} \tag{3.58}$$

Differentiating at constant temperature and spreading pressure we may define a partial molar free energy or chemical potential by the relation

$$\mu_s'(T,\overline{\mathscr{A}}) = \left(\frac{\partial G_s}{\partial n_s}\right)_{T,\pi} = \mu_s(T,\pi) - \pi\overline{\mathscr{A}} \tag{3.59}$$

where $\overline{\mathscr{A}} = (\partial\mathscr{A}/\partial n_s)_{T,\pi}$ is the partial molar area. If, following Suwanayuen and Danner, the adsorbed phase is considered as a mixture of sorbate and vacancies, we may express this chemical potential in the usual manner in terms of a standard chemical potential and an activity:

$$\begin{aligned}
\mu_s' &= \mu_s^\circ(T) + RT\ln(\gamma_v X_v) \\
\mu_s &= \mu_s^\circ(T) + RT\ln(\gamma_v X_v) + \pi\overline{\mathscr{A}}
\end{aligned} \tag{3.60}$$

where $\gamma_v X_v$ is the activity of the vacancies. The standard state is taken as an infinitely dilute adsorbed phase for which $\gamma_v \to 1.0$, $X_v \to 1.0$, and $\pi \to 0$. The equation of state of the adsorbed phase is then seen to be

$$\frac{\pi\overline{\mathscr{A}}}{RT} = -\ln(\gamma_v X_v) = -\ln\left[\gamma_v(1-\Theta)\right] \tag{3.61}$$

where Θ is the fraction of saturation coverage. The equation for the equilibrium isotherm may be obtained from the Gibbs adsorption isotherm [Eq. (3.32)] once an expression for the concentration dependence of the activity coefficient of the vacancies is specified.

If we suppose the vacancy solution to be ideal ($\gamma_v = 1.0$) we obtain from Eqs. (3.32) and (3.61)

$$\frac{\overline{\mathscr{A}}}{RT}\left(\frac{\partial\pi}{\partial p}\right)_T = \frac{1}{(1-\Theta)}\left(\frac{\partial\Theta}{\partial p}\right)_T = \frac{\Theta}{p} \tag{3.62}$$

which may be integrated at constant temperature to obtain the Langmuir isotherm:

$$\int\frac{d\Theta}{\Theta(1-\Theta)} = \int\frac{dp}{p}, \qquad \frac{\Theta}{1-\Theta} = bp \tag{3.63}$$

As a first-order deviation from ideal behavior one may assume that the adsorbed phase obeys the regular solution model:

$$RT\ln\gamma_v = w(1 - X_v)^2 = w\Theta^2 \tag{3.64}$$

$$\frac{\pi\overline{\mathscr{A}}}{RT} = -\frac{w}{RT}\Theta^2 - \ln(1-\Theta) \tag{3.65}$$

Proceeding in the same manner through the Gibbs isotherm Eq. (3.65) leads to

the isotherm equation

$$bp = \frac{\Theta}{1 - \Theta} \exp\left(- \frac{2w\Theta}{RT} \right)$$ (3.66)

The same expression was derived statistically by Fowler[14] for small deviations from ideal localized adsorption in which sorbate–sorbate interaction effects are significant but not large enough to interfere with the random distribution of adsorbate over the surface sites.

In this formulation the concentration dependence of the activity coefficient is described by a one-parameter expression [Eq. (3.64)]. To extend the analysis to allow for more pronounced deviations from ideal Langmuir behavior it is only necessary to use a two-parameter expression for the activity coefficient. Danner and Suwanayuen used the Wilson expression[15,16]:

$$\ln \gamma_v = -\ln\left[(1 - \Theta) + \Lambda_1\Theta \right] - \Theta\left(\frac{\Lambda_1'}{\Theta + \Lambda_1'(1 - \Theta)} - \frac{\Lambda_1}{1 - \Theta + \Lambda_1'} \right)$$ (3.67)

which leads by the same argument to the isotherm equation

$$bp = \frac{\Theta}{1 - \Theta} \Lambda_1'\left(\frac{1 - (1 - \Lambda_1)\Theta}{\Lambda_1' + (1 - \Lambda_1')\Theta} \right)\exp\left(- \frac{\Lambda_1(1 - \Lambda_1)\Theta}{1 - (1 - \Lambda_1)\Theta} - \frac{(1 - \Lambda_1')\Theta}{\Lambda_1' + (1 - \Lambda_1')\Theta} \right)$$

(3.68)

but other expressions for the activity coefficient such as the van Laar equations could also be used. Equation (3.68) contains four parameters (b, Λ_1, Λ_1', and n_∞ which is contained in Θ) and is capable of fitting virtually all single-component isotherms.*

The extension to an adsorbed mixture follows naturally although the calculations are somewhat tedious. For each adsorbed species, assuming an ideal vapor phase,

$$\mu_i = \mu_{is}^0(T) + RT\ln(\gamma_i X_i') + \pi \overline{\mathscr{A}}_i = \mu_{ig}^0(T) + RT\ln p_i$$

$$p_i = \gamma_i X_i' \exp\left(\frac{\Delta G_i^0}{RT} + \frac{\pi \overline{\mathscr{A}}}{RT} \right)$$ (3.69)

where $\Delta G_i^0 = \mu_{is}^0 - \mu_{ig}^0$ and $X_i' = X_i\Theta$ is the mole fraction of component i in the adsorbed phase, including the vacancies as a hypothetical species, X_i is the actual mole fraction in the adsorbed phase, and $\Theta = n_m/n_{m\infty}$ is the total fractional coverage calculated relative to the saturation limit for a mixture of the specified composition. $\Delta G_i^0/RT$ and $\pi \overline{\mathscr{A}}_i/RT$ may be derived from the single-component isotherms while the activity coefficient for the mixed phase may be derived in terms of the Wilson parameters Λ_1, Λ_1', Λ_2, and Λ_2' and the

*In the latest version of the theory the three-parameter Flory–Huggins equation is used. This provides an equally good correlation of the single-component isotherms and a somewhat better prediction of the binary isotherms than the Wilson equation (T. W. Cochran, R. L. Kabel, and R. P. Danner, A.I.Ch.E.J., in press.)

cross coefficients Λ_{12} and Λ'_{12} according to the combining formula given by Prausnitz[16]:

$$\ln \gamma_k = 1 - \ln\left(\sum_{j=1}^{n} X_j \Lambda_{kj} \right) - \sum_{i=1}^{n} \left(\frac{X_i \Lambda_{ik}}{\sum_{j=1}^{n} X_j \Lambda_{ij}} \right) \qquad (3.70)$$

The parameters Λ_1, Λ'_1, Λ_2, and Λ'_2 are known from the fit of the single-component isotherms but additional assumptions are required in order to estimate the cross coefficients Λ_{ik}.

For many systems it has been found that the cross coefficients are related by

$$\frac{\Lambda_{12}}{\Lambda_{21}} = \frac{\Lambda_1}{\Lambda'_1} \frac{\Lambda'_2}{\Lambda_2}$$

so only one parameter, in addition to those obtained from the single-component isotherms, is required.[35]

In order to show the relationship with the Myers and Prausnitz treatment we ignore the vacancies and consider the adsorbed phase simply as a mixture of the adsorbed species. Equation (3.69) becomes

$$p_i = \gamma_i X_i \exp\left(\frac{\mu_{is}^\circ - \mu_{ig}^\circ + \pi \mathscr{A}_i}{RT} \right) \qquad (3.71)$$

and for adsorption of component i alone:

$$p_i^\circ = \exp\left(\frac{\mu_{is}^\circ - \mu_{ig}^\circ + \pi^\circ \mathscr{A}_i^\circ}{RT} \right) \qquad (3.72)$$

so that

$$p_i = \gamma_i X_i p_i^\circ \exp\left(\frac{\pi \mathscr{A}_i - \pi^\circ \mathscr{A}_i^\circ}{RT} \right) \qquad (3.73)$$

If we choose the standard state such that $\pi = \pi^\circ$, $\mathscr{A}_i = \mathscr{A}_i^\circ$ we recover Eq. (3.49). The difference between the vacancy solution and the Myers and Prausnitz formulations is seen to lie in the choice of standard state and the way in which adsorbed phase concentrations are expressed.

3.5. STATISTICAL THERMODYNAMIC APPROACH

The approach to the modeling of adsorption equilibria outlined in Section 3.3 depends on the implicit assumption of a mobile adsorbed phase, the thermodynamic behavior of which can be represented by an equation of state. An alternative view is to consider the adsorbed molecules as localized at distinct surface sites, with only relatively infrequent movement of the molecules between sites. Each site may then be regarded as a separate subsystem and the equilibrium behavior may be deduced by the methods of statistical

thermodynamics. It may be shown that in the limit where one allows rapid interchange of molecules between sites this approach leads to the same results as the classical approach based on the Gibbs adsorption isotherm.

The statistical approach to adsorption, which was developed largely by Fowler and Guggenheim[14] and Hill,[4] depends on representing the adsorbed species in terms of a simplified physical model for which the appropriate expression for the partition function may be derived. The thermodynamic properties are then obtained using the established relationships between the partition functions and the classical thermodynamic properties. A brief summary of some of the more important relationships is given in Appendix A.

Elementary Statistical Derivation of the Langmuir Isotherm

As an illustration of the statistical method at its simplest we may consider the derivation of the Langmuir isotherm. The Langmuir model (see Section 2.4) is based on the assumption of a fixed number of identical sites with no interaction between adsorbed molecules. We consider a set of M equivalent sites on which N molecules $(N < M)$ are adsorbed. The canonical partition function for the system is given simply by

$$\mathscr{F} = f^N \frac{M!}{N!(M-N)!} \tag{3.74}$$

In this expression f is the molecular partition function for an individual adsorbed molecule while the factor $M!/N!(M-N)!$ is simply the degeneracy factor or the number of ways in which the N identical molecules can be arranged on the M equivalent but physically distinguishable sites. Since both M and N are large numbers we may use Stirling's theorem $(\ln N! = N \ln N - N)$ and write

$$\ln \mathscr{F} = M \ln M - N \ln N - (M-N)\ln(M-N) + N \ln f \tag{3.75}$$

Using Eq. (A17)

$$\frac{\mu}{kT} = -\left(\frac{\partial \ln \mathscr{F}}{\partial N}\right)_{M,T} = \ln\left(\frac{N}{M-N}\right) - \ln f$$

$$= \ln\left[\frac{\Theta}{(1-\Theta)f}\right] \quad \text{where } \Theta = N/M \tag{3.76}$$

and considering equilibrium between adsorbed and gas phases:

$$\frac{\mu}{kT} = \frac{\mu^\circ}{kT} + \ln p = \ln\left[\frac{\Theta}{(1-\Theta)f}\right] \tag{3.77}$$

$$bp = \frac{\Theta}{1-\Theta} \quad \text{or} \quad \Theta = \frac{bp}{1+bp} \tag{3.78}$$

where $b(T) = f(T)e^{\mu^\circ/kT}$ is an equilibrium constant.

The advantage of this derivation over the simpler kinetic derivation given in Section 2.4 is that the physical significance of the constant b is more clearly defined.

Application of the "Grand Partition Function"

In the above derivation of the Langmuir equation we were able to proceed directly from the canonical partition function, but in more complex systems such as those which involve interactions between molecules on adjacent sites this approach is not possible. Instead it is necessary to proceed through the "grand partition function." The grand partition function (Ξ) is simply the sum of all canonical partition functions for the system weighted according to $e^{N\mu/kT}$. It is shown in Appendix A [Eq. (A22)] that the average number of molecules per subsystem is given by

$$\bar{N} = \lambda \frac{\partial \ln \Xi}{\partial \lambda} \tag{3.79}$$

where $\lambda = \exp(\mu/kT)$, $\Xi = \sum \mathscr{F} e^{N\mu/kT}$.

As a simple example of the application of this method we again derive the Langmuir equation.

For ideal Langmuir adsorption

$$\mathscr{F} = \frac{M!}{N!(M-N)!} f^N \tag{3.80}$$

$$\Xi = \sum \frac{M!}{N!(M-N)!} (f\lambda)^N = (1+f\lambda)^M \tag{3.81}$$

The last equation above follows directly from the binomial theorem.

$$\ln \Xi = M \ln(1 + f\lambda) \tag{3.82}$$

$$\bar{N} = \lambda \frac{\partial \ln \Xi}{\partial \lambda} = \frac{\lambda M f}{1 + f\lambda} \tag{3.83}$$

or

$$\Theta = \frac{N}{M} = \frac{f\lambda}{1 + f\lambda} = \frac{bp}{1 + bp} \tag{3.84}$$

Many modifications to the simple Langmuir model are amenable to analysis in this way. For example, consider adsorption on a set of M independent *pairs* of identical sites such that there is an interaction energy ($2w$) when both sites of a given pair are occupied. The expression for the grand partition function for such a system is

$$\Xi = 1 + 2f\lambda + f^2 e^{-2w/kT} \lambda^2 \tag{3.85}$$

whence

$$\Theta = \frac{\bar{N}}{M} = \frac{2f\lambda + 2f^2 e^{-2w/kT} \lambda^2}{1 + 2f\lambda + f^2 e^{-2w/kT} \lambda^2} \tag{3.86}$$

The BET isotherm may also be easily derived via the grand partition function. As with the Langmuir model we consider a system of M independent sites with no interaction between adsorbed molecules. However, in the BET model each site in the first adsorbed layer is considered to provide a site for the second layer of adsorbed molecules and similarly for the third layer,

and so on. The partition function for a molecule in the first adsorbed layer is f_1 and for a molecule in the second or subsequent layers, f_2. The grand partition function for such a system is given by

$$\Xi = 1 + f_1\lambda + f_1 f_2\lambda^2 + f_1 f_2^2\lambda^2 + \cdots \qquad (3.87)$$

$$\Theta = \frac{\overline{N}}{M} = \frac{f_1\lambda(1 + 2f_2\lambda + 3f_2^2\lambda^2 + \cdots)}{1 + f_1\lambda(1 + f_2\lambda + f_2^2\lambda^2 + \cdots)} \qquad (3.88)$$

Summing the terms in parentheses as geometric series, we obtain

$$\frac{\overline{N}}{M} = \frac{f_1\lambda}{(1 - f_2\lambda)(1 - f_2\lambda + f_1\lambda)} \qquad (3.89)$$

where $\lambda = e^{\mu/kT} = e^{\mu_0/kT}p$ which is of the form of the BET equation [Eq. (2.32)].

The surface potential Φ is given by

$$\Xi = e^{\Phi M/kT} = \xi^M \qquad (3.90)$$

and for a BET system

$$\frac{\Phi}{kT} = \ln \xi = \ln\left(\frac{1 - f_2\lambda + f_1\lambda}{1 - f_2\lambda}\right) \qquad (3.91)$$

Hill[4] has pointed out that this equation implies $\Phi \to \infty$ as $f_2\lambda \to 1.0$ whereas thermodynamically Φ is necessarily finite at $f_2\lambda = 1$. This is a serious deficiency of the BET theory.

Simple Statistical Model Isotherms for Zeolites

The regularity of the zeolite pore structure makes these adsorbents especially convenient for application of the methods of statistical thermodynamics. This approach has been followed by several authors including Riekert,[17] Bakaev,[18] Brauer,[19] and Ruthven.[20-23] The method is best suited to those zeolites where the structure consists of more or less discrete cages interconnected through relatively small windows. Under these conditions each cage can be considered as an independent site or subsystem and, to a first approximation, interactions between molecules in neighboring cages may be neglected. Sodalite is an extreme example of such a system since each cage can contain only one molecule of gases such as argon or methane and passage through the six-ring is slow so that, except at very high temperatures, transitions between cages occur only infrequently. It is therefore not surprising to find that at moderate temperatures the isotherms for such systems conform closely to the ideal Langmuir model since the basic assumptions of the model are accurately fulfilled.[24]

The cages of A and X zeolites are larger and can accommodate several molecules. The rate of interchange of molecules between cages, particularly in the X zeolites, may be rapid but as a first approximation it is still reasonable

to treat the cages as independent subsystems. If we consider M cages and suppose that each cage can contain up to m molecules, the canonical ensemble partition function is given by

$$\mathscr{F}(N,M,T) = \sum \frac{M!\, f(1)^{n_1} f(2)^{n_2} \cdots}{n_0!\, n_1! \cdots n_m!} \tag{3.92}$$

where $f(s)$ represents the partition function for a cage containing s sorbate molecules. The grand partition function for the system is given by

$$\Xi = \left[f(0) + f(1)\lambda + f(2)\lambda^2 + \cdots + f(m)\lambda^m \right]^M \tag{3.93}$$

This result may be expressed in terms of the configuration integrals $Z(s)$ for cages containing $0, 1, \ldots$ molecules since $f(s)\lambda^s = Z(s)a^s$.

$$\Xi = \left[1 + Z(1)a + Z(2)a^2 + \cdots + Z(m)a^m \right]^M \tag{3.94}$$

where, for an ideal vapor phase, the activity a is given by p/kT.

The average number of molecules per cage is given by

$$\bar{s} = \frac{\bar{N}}{M} = \frac{a\partial \ln \Xi}{\partial a} = \frac{\sum_{s=0}^{m} sZ(s)a^s}{\sum_{s=0}^{m} Z(s)a^s} \tag{3.95}$$

The assumption that the molecules within a given cage are freely mobile and have no interaction with each other leads to

$$Z(s) = \frac{Z(1)^s}{s!} \tag{3.96}$$

Since $Z(1)a = K'p$ we have

$$Z(s)a^s = \frac{(K'p)^s}{s!} \tag{3.97}$$

and if each cage can contain a maximum of m molecules the expression for the isotherm becomes

$$\bar{s} = \frac{\bar{N}}{M} = \frac{K'p + (K'p)^2 + (K'p)^3/2! + \cdots + (K'p)^m/(m-1)!}{1 + K'p + (K'p)^2/2! + \cdots + (K'p)^m/m!} \tag{3.98}$$

as obtained by Riekert.[17] The form of Eq. (3.98) for various values of m is illustrated in Figure 3.2.
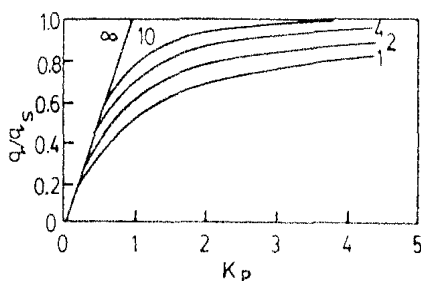

FIGURE 3.2. Theoretical isotherms calculated according to Eq. (3.98). (From ref. 17, reprinted by permission from *Adv. Catalysis* 21, 287. Copyright © 1970 Academic Press.)

The assumption of no interaction between adsorbed molecules is clearly unrealistic since, quite apart from any possible forces of attraction, the space available within the cage is reduced when more than one molecule is present. Equation (3.97) should therefore be replaced by

$$Z(s)a^s = \frac{(K'p)^s}{s!} A_s \tag{3.99}$$

where A_s ($s = 2, 3, \ldots$) are coefficients which account for the interaction between molecules. The idealized case of Eq. (3.98) corresponds to $A_s = 1.0$. If the reduction in free volume is the dominant interaction effect one may assume as a first approximation

$$A_s = \left(\frac{v - s\beta}{v} \right)^s \tag{3.100}$$

where v is the volume of the cage and β the effective volume of a molecule. This leads to the isotherm equation[20]:

$$\frac{\bar{N}}{M} = \frac{K'p + (K'p)^2(1 - 2\beta/v)^2 + \cdots + \left((K'p)^m/(m-1)! \right)(1 - s\beta/v)^m}{1 + K'p + \frac{1}{2}(K'p)^2 + \cdots + (1/m!)(K'p)^m(1 - s\beta/v)^m} \tag{3.101}$$

where m is an integer such that $m \leqslant v/\beta$. This expression has proved to be a useful approximation for the isotherms of several small nonpolar molecules in type A zeolites as well as for some other systems (see Section 4.2). The extension to mixtures follows naturally.[22] For a binary mixture of components 1 and 2

$$q_1 = \frac{\bar{N}_1}{M} = \frac{K_1'p_1 + \sum_j \sum_i \left[(K_1'p_1)^i (K_2'p_2)^j (1 - i\beta_1/v - j\beta_2/v)^{i+j} \right]/(i-1)!\, j!}{1 + K_1'p_1 + K_2'p_2 + \sum_j \sum_i \left[(K_1'p_1)^i (K_2'p_2)^j (1 - i\beta_1/v)^{i+j} \right]/i!\, j!} \tag{3.102}$$

with a similar expression for component 2. In these expressions the summations are carried out over all values of i and j satisfying both the restrictions $i + j \geqslant 2$; $i\beta_1 + j\beta_2 \leqslant v$.

In this formulation no allowance is made for the reduction in free volume when the cage contains only one adsorbate molecule. It is somewhat more logical and consistent to write the Henry constant as the product of a hypothetical constant for a point molecule (K^*) and a free volume reduction factor reflecting the size of the actual molecule so that in place of Eq. (3.100) we have

$$K' = K^*(1 - \beta/v), \qquad A_s = \left[\frac{(1 - s\beta/v)}{(1 - \beta/v)} \right]^s \tag{3.103}$$

This leads to the slightly modified isotherm equation[24]:

$$q = \frac{\bar{N}}{M} = \frac{K'p + (K'p)^2 \left(\frac{1 - 2\beta/v}{1 - \beta/v} \right)^2 + \cdots + \frac{(K'p)^m}{(m-1)!} \left(\frac{1 - m\beta/v}{1 - \beta/v} \right)^m}{1 + K'p + \cdots + \frac{(K'p)^m}{m!} \left(\frac{1 - m\beta/v}{1 - \beta/v} \right)^m}$$

(3.104)

There is little numerical difference between Eqs. (3.101) and (3.104) except when m is small. In both equations the saturation limit is given by $q_s = m - 1$. For $v/\beta \leqslant 2$, the saturation limit becomes 1 molecule/cage and both expressions reduce to the Langmuir form. If the isotherms are plotted as q/q_s versus $K'p/q_s$ (Figure 3.3) we obtain a family of curves which show a smooth transition from the Langmuir form (for $v/\beta \leqslant 2$) to the Volmer form [Eq. (3.39)] when v/β is large. This is physically reasonable since $v/\beta \to \infty$ corresponds to free mobility throughout the micropore volume of the adsorbent which is the basis of the Volmer model.

A more general form of expression for the equilibrium isotherm may be obtained by retaining the coefficients A_s [Eq. (3.99)] as parameters:

$$q = \frac{\bar{N}}{M}$$

$$= \frac{1 + K'p + A_2(K'p)^2 + (A_3/2!)(K'p)^3 + \cdots + (A_m/(m-1)!)(K'p)^m}{1 + K'p + A_2(K'p)^2/2! + A_3(K'p)^3/3! + \cdots + A_m(K'p)^m/m!}$$

(3.105)
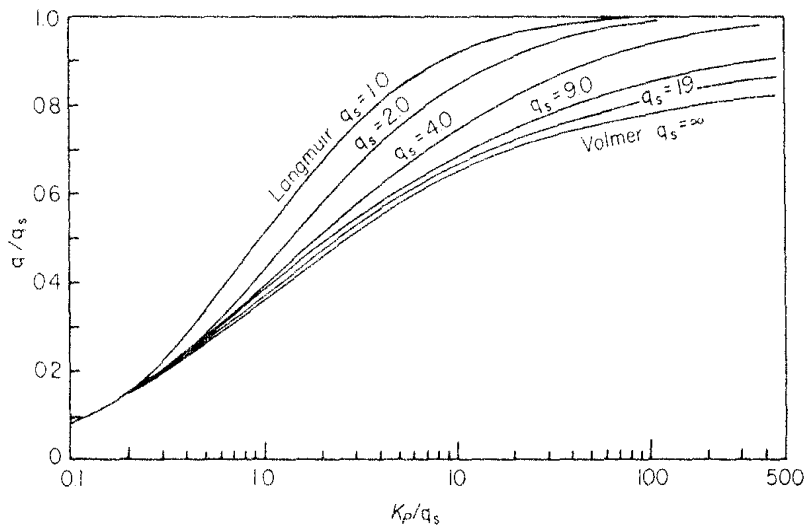
FIGURE 3.3. Theoretical isotherms calculated according to Eq. (3.104) showing transition from Langmuir to Volmer form with increasing m. [Reproduced from ref. 25 by permission of the publishers, Butterworth & Co (Publishers) Ltd. ©.]

The values of these coefficients may be deduced directly by matching experimental isotherm data. Equation (3.105) thus provides a useful semiempirical correlation in which the parameters have a simple and well-defined physical significance. In that sense Eq. (3.105) is comparable with the virial isotherm [Eq. (3.43)]. In general the coefficients A_s are temperature dependent but we have found that for many nonpolar sorbates the temperature dependence is modest. For such systems an approximate correlation of equilibrium data over a wide range of temperatures may therefore be obtained with a single set of constant coefficients, considering the Henry constant as the only temperature-dependent parameter (see Figure 4.9).

3.6. DUBININ-POLANYI THEORY

A third general approach to the correlation of adsorption equilibria for microporous adsorbents has been developed by Dubinin and his co-workers[26-30] from ideas originally put forward by Polanyi[31,32] and Berenyi.[33] The adsorbed species within the micropores is considered to behave as a liquid although, due to the effect of the force field of the adsorbent, the properties of this liquid phase may differ from the properties of the bulk liquid at the same temperature. The difference in free energy between the adsorbed phase and the saturated liquid sorbate at the same temperature, which may be calculated directly from the ratio of the equilibrium pressure and the saturation vapor pressure, is referred to as the adsorption potential ϵ:

$$\epsilon = -RT\ln\left(\frac{f}{f_s}\right) = -RT\ln\left(\frac{p}{p_s}\right) \tag{3.106}$$

where f_s and p_s refer to the saturation fugacity and pressure for the liquid sorbate and f and p are the corresponding equilibrium quantities for the adsorbed phase. It should be pointed out that the adsorption potential defined in this way includes both an energy and an entropy term and should not be confused with the potentials discussed in Chapter 2.

For a given adsorbent-adsorbate system there is a unique temperature-independent relation between the adsorption potential and the *volume* of fluid adsorbed. This relation which is referred to as the characteristic curve, provides a concise means of summarizing equilibrium data over a wide range of temperatures and concentrations. The volume of the adsorbed liquid phase is calculated from the molar concentration and the molar volume. Various semiempirical methods of estimating the molar volume, which is temperature dependent, from the density of the liquid sorbate have been proposed.[27,34] At temperatures below the normal boiling point the molar volume of the adsorbed fluid is taken to be the same as that of the saturated liquid. At temperatures above the boiling point either an extrapolation along the tangent to the molar volume-temperature curve at the normal boiling point or an interpolation between the molar volume at the boiling point and the van der Waals co-volume at the critical temperature have been recommended.

The experimental adsorption isotherms for many systems can indeed be correlated by a single temperature-independent characteristic curve. In the case of nonpolar systems in which the energy of adsorption arises entirely from temperature-independent van der Waals forces, there is some theoretical justification for the assumption of a temperature-independent characteristic curve although this requires the additional assumption that the contribution of the entropy term to the adsorption potential is negligibly small; that is, the entropy of the adsorbed phase is similar to that of the saturated liquid sorbate at the same temperature. In the case of polar systems in which electrostatic energy makes a significant contribution to the adsorption potential, a temperature-independent characteristic curve would not be generally expected and will occur only when there is a high degree of compensation between the enthalpy and entropy terms.

The theory has been tested experimentally for a wide variety of systems and is at its most useful for the correlation of adsorption equilibrium data for activated carbon adsorbents. For such systems the form of the characteristic curve can often be approximated by a Gaussian expression:

$$W = W_0 e^{-k\epsilon^2} \qquad (3.107)$$

where $W = qV_m$ and $W_0 = q_s V_m$. The saturation limit (W_0) may be considered to represent the total specific micropore volume of the adsorbent and it is evident that if Eq. (3.107) is obeyed a semilogarithmic plot of $\ln W$ versus ϵ^2 (or $[\ln(p/p_s)]^2$) provides a simple method of extrapolation to determine this quantity. This appears to be a useful procedure even for systems in which the requirement of a temperature-independent characteristic curve is not precisely fulfilled.

If the form of the characteristic curve is given by Eq. (3.107) then for two different adsorbates at the same value of W/W_0, $k_1/k_2 = (\epsilon_1/\epsilon_2)^2$. For a given adsorbent the ratio k_1/k_2 and hence the characteristic curve for the second adsorbate may therefore be found, in principle, from a single equilibrium point. Berenyi[33] has shown that for a number of nonpolar systems the ratio k_1/k_2 corresponds approximately to the ratio of the van der Waals attraction constants allowing an approximate *a priori* prediction of the equilibrium behavior for different adsorbates once the characteristic curve for one adsorbate has been established. Dubinin[27] has suggested using the ratio of the parachors rather than the van der Waals attraction constants.

The main advantage of this approach is that the determination of a characteristic curve requires, in principle, only a single experimental isotherm covering a wide range of concentration. Once determined, the characteristic curve provides a concise correlation of equilibrium data and a simple means of extrapolation and interpolation. As such it is useful for engineering design. The approach however suffers from three major disadvantages:

1. The expression for the characteristic curve does not reduce automatically to Henry's law in the low concentration limit. This is a theoretical requirement for any thermodynamically consistent physical isotherm

equation, although the practical consequences of this deficiency may not be important if the equation is applied only in the high-concentration region.

2. The methods of estimating the molar volume of the adsorbed phase are subject to considerable uncertainty.

3. The assumption of a temperature-independent characteristic curve is not a good approximation for many systems, particularly when polar sorbates are involved.

. REFERENCES

1. T. L. Hill, *J. Chem. Phys.* **17**, 507 and 520 (1949).

2. T. L. Hill, *Advances in Catalysis* **4**, 211 (1952).

3. T. L. Hill, *J. Chem. Phys.* **18**, 246 (1950).

4. T. L. Hill, *Introduction to Statistical Thermodynamics.* Addison-Wesley, Reading, Mass., 1960.

5. D. H. Everett, *Trans. Faraday Soc.* **46**, 453, 942, and 957 (1950).

6. D. M. Young and A. D. Crowell, *Physical Adsorption of Gases.* Butterworths, London, 1962.

7. J. W. Gibbs, *Collected Works.* Yale University Press, New Haven, Conn., 1928.

8. J. H. DeBoer, *The Dynamical Character of Adsorption*, 2nd ed. Oxford Press, London, 1968.

9. R. M. Barrer and J. A. Davies, *Proc. Roy. Soc. London* **A320**, 289 (1970).

10. A. P. Vavlitis, D. M. Ruthven, and K. F. Loughlin, *J. Colloid Interface Sci.* **84**, 526 (1981).

11. A. L. Myers and J. M. Prausnitz, *AIChE Jl* **11**, 121, (1965).

12. D. B. Broughton, *Ind. Eng. Chem.* **40**, 1506, (1948).

13. S. Suwanayuen and R. P. Danner, *AIChE Jl* **26**, 68 and 76 (1980).

14. R. H. Fowler and E. A. Guggenheim, *Statistical Thermodynamics.* Cambridge University Press, Cambridge, 1939.

15. G. M. Wilson, *J. Am. Chem. Soc.* **88**, 127 (1964).

16. J. M. Prausnitz, *Molecular Thermodynamics of Fluid Phase Equilibria.* Prentice Hall, Englewood Cliffs, NJ, 1969.

17. L. Riekert, *Adv. Catalysis* **21**, 287 (1970).

18. V. A. Bakaev, *Dokl. Akad. Nauk SSSR* **167**, 369 (1967).

19. P. Brauer, A. A. Lopatkin, and G. Ph. Stepanez, *Adv. Chem.* **102**, 97 (1971).

20. D. M. Ruthven, *Nature Phys. Sci.* **232**(29), 70 (1971).

21. D. M. Ruthven and K. F. Loughlin, *J. Chem. Soc. Faraday Trans. 1* **68**, 696 (1972).

22. D. M. Ruthven, *AIChE Jl* **22**, 753 (1976).

23. D. M. Ruthven, K. F. Loughlin, and K. A. Holborow, *Chem. Eng. Sci.* **28**, 701 (1973).

24. R. M. Barrer and D. E. W. Vaughan, *J. Phys. Chem. Solids* **32**, 731 (1971).

25. D. M. Ruthven, *Zeolites* **2**, 242 (1982).

26. M. M. Dubinin, *Chem. Revs.* **60**, 235 (1960).

27. M. M. Dubinin, *Pure Appl. Chem.* **10**(4), 309 (1965).

28. B. P. Bering, M. M. Dubinin, and V. V. Serpinsky, *J. Colloid Interface Sci.* **38**(1), 185 (1972).

29. B. P. Bering, M. M. Dubinin, and V. V. Serpinsky, *J. Colloid Interface Sci.* **21**, 378 (1966).

30. M. M. Dubinin and V. A. Astakhov, *Adv. Chem.* **102**, 69 (1971).

31. M. Polanyi, *Trans. Faraday Soc.* **28**, 316 (1932).

32. M. Polanyi, *Z. Elektrochem.* **35**, 431 (1929).

33. L. Berenyi, *Z. Phys. Chem. Leipzig* **94**, 628 (1920) and **105**, 55 (1923).

34. M. M. Dubinin, A. F. Fomkin, I. I. Seliverstova, and V. V. Serpinsky, *Proceedings of the Fifth International Conference on Zeolites, Naples, June 1980*, L. V. C. Rees (ed.). Heyden, London, 1980.

35. R. P. Danner, Engineering Foundation Conference on Fundamentals of Adsorption, Schloss Elmau, Bavaria, May 1983.

4

CORRELATION, ANALYSIS,
AND PREDICTION OF
ADSORPTION EQUILIBRIA

Information concerning the relevant adsorption equilibria is generally an essential requirement for the analysis and design of an adsorption separation process. In Chapter 3 we considered adsorption equilibrium from the thermodynamic perspective and developed a number of simple idealized expressions for the equilibrium isotherm based on various assumptions concerning the nature of the adsorbed phase. The extent to which these models can provide a useful representation of the behavior of real systems was considered only superficially and is reviewed in this chapter. Since many practical adsorption systems involve the simultaneous adsorption of more than one component, the problems of correlating and predicting multicomponent equilibria from single-component data are of particular importance and are therefore considered in some detail.

4.1. LOCALIZED ADSORPTION

Ideal Langmuir Model

The Langmuir model is based on the assumption of ideal localized adsorption without interaction on a set of identical sites as outlined in Section 2.4. The special case of sorption of CH_4 or Ar in sodalite[1] was noted in Section 3.5 as an example of a system for which the basic assumptions of the Langmuir model are in fact fulfilled and for which the isotherms conform, as expected, to the Langmuir equation [Eq. (2.28)]. Sorption of normal tri- or tetradecane in 5A zeolite is another example of a zeolitic system in which each cage can accommodate only one sorbate molecule. Approximate conformity

(a) Kr   Cs = 11

(b) Xe   Cs = 8

c - molecule / covity
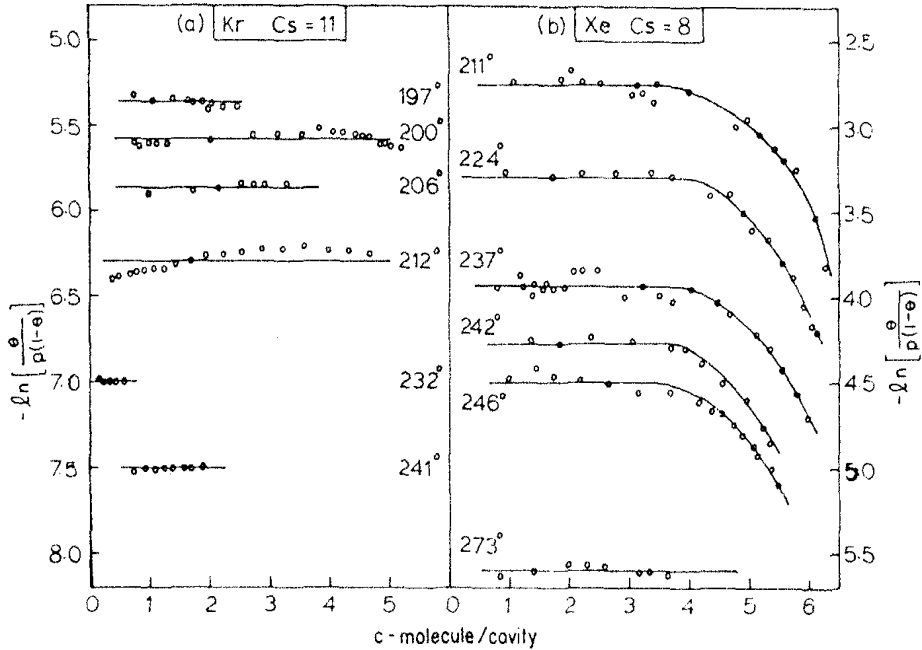
FIGURE 4.1. Langmuir "constants" calculated according to Eq. (3.78) for Kr and Xe in 5A zeolite. (Temperatures are in kelvin. Saturation capacities: Kr, $q_s = 11$ molecules/cage; Xe, $q_s = 8.0$ molecules/cage). (From ref. 3; reprinted by permission of the National Research Council of Canada from the *Canadian Journal of Chemistry*, Volume 53, 1975.)

with the Langmuir isotherm has been reported for these systems[2] although, since the windows of the 5A zeolite are larger than those of sodalite, the assumption of no interaction between molecules in neighboring cages may not be fulfilled quite as well as for the rare gases in sodalite. Systems which conform accurately to the Langmuir model are, however, exceptional; for most systems the basic assumptions of the Langmuir model are not fulfilled and the equilibrium isotherms deviate to a greater or lesser extent from the Langmuir form.

It was shown in Section 3.3 that an expression of the same general form as the Langmuir isotherm [Eq. (3.38)] is obtained as an approximation for ideal mobile adsorption at low sorbate concentrations. As a result it is not uncommon to find that the equilibrium isotherm obeys the Langmuir model at low concentrations with deviations becoming serious as saturation is approached. An example of such behavior is given in Figure 4.1 which shows the Langmuir "constants" $[b = \Theta/(1 - \Theta)p]$ for Kr and Xe in 5A zeolite plotted against sorbate concentration.[3]

The data of Barrer and Wasilewski[4] for the sorption of I_2 on 5A and 13X zeolites (Figure 4.2) are remarkable since they show conformity with the simple Langmuir model over very wide concentration ranges. More detailed analysis reveals that the heat of sorption varies strongly with sorbate concentration, as may be seen from Figure 4.2c. A constant heat of sorption is one of the requirements of the Langmuir model so the variation of heat of adsorption
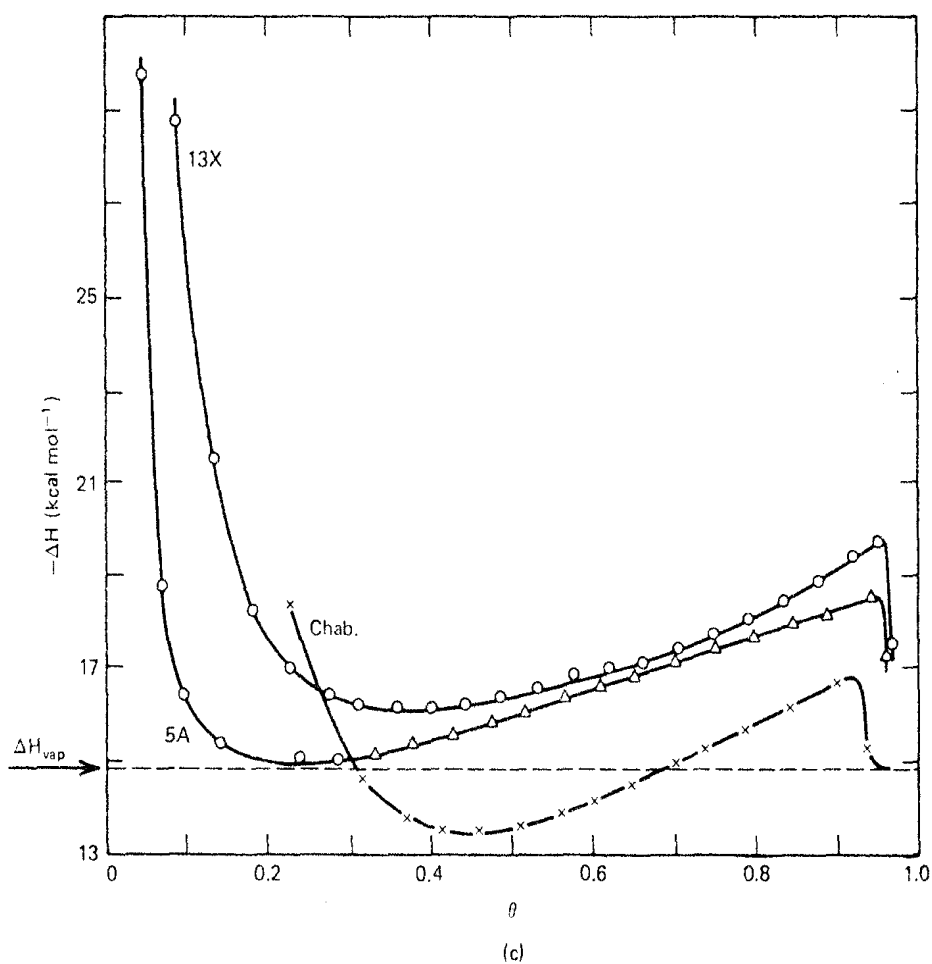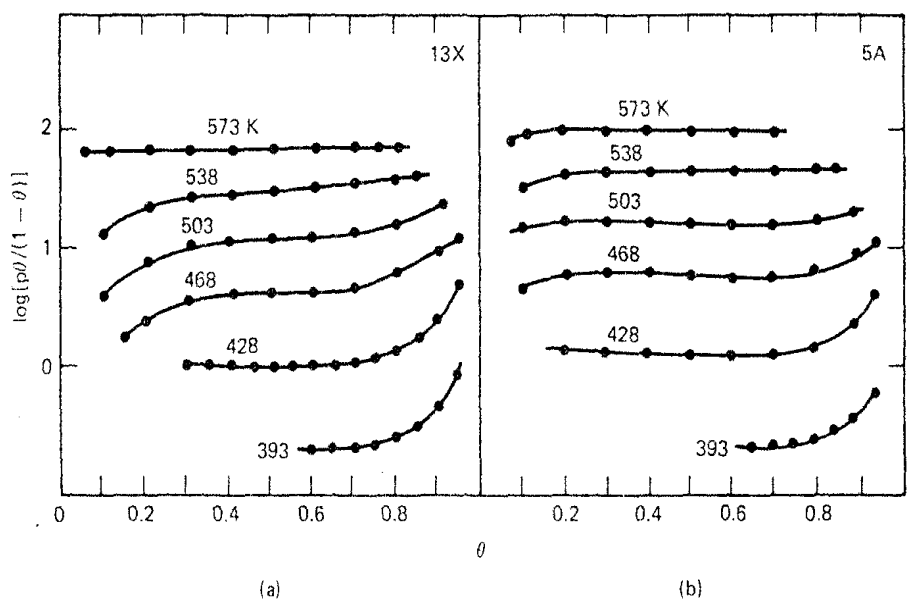
FIGURE 4.2. Langmuir "constants" [(a) and (b)] and heats of adsorption (c) plotted against fractional coverage (Θ) for I_2 on 5A and 13X zeolites. Heats of adsorption data for I_2 on chabazite as well as the heat of condensation of molecular iodine ($-\Delta H_c$) are also shown. (From ref. 4, with permission.)

with coverage implies that the basic postulates of the Langmuir theory are not in fact obeyed in this system. The constancy of the Langmuir "constants" evidently results from an almost exact compensation between the variation of the thermal entropy and heat of sorption with loading.

Deviations from Ideal Langmuir Model

In the systems so far discussed the ideal Langmuir model gives an appropriate representation of the system behavior at low concentration but breaks down in the saturation region where the effects of molecular interaction become pronounced. However, even at low sorbate concentrations, not all systems conform to the Langmuir model. Deviations can occur due to either heterogeneity of sites or interaction between adsorbed molecules. A pattern of behavior which has been observed for several systems is illustrated in Figure 4.3.[5] In the low-concentration region the Langmuir "constant" declines exponentially with loading and then falls off more rapidly as saturation is approached. Such behavior can be accounted for by several different models.

As a first-order deviation from the Langmuir model one may consider ideal adsorption on a set of localized sites with weak interaction between adsorbed molecules on neighboring sites. Such a model has been investigated theoretically by Lacher[6] and by Fowler and Guggenheim.[7] If the interaction is sufficiently weak that the random distribution of the adsorbed molecules is not significantly affected the resulting expression for the isotherm is

$$\frac{\Theta}{p(1 - \Theta)} = b \exp\left(\frac{-2w\Theta}{RT} \right) \tag{4.1}$$

where $2w$ is the pair interaction energy (negative for attraction, positive for repulsion). For $w \rightarrow 0$ Eq. (4.1) reverts to the Langmuir expression. The same form of equation may be derived from the vacancy solution model by assuming regular behavior of the adsorbed phase (see Section 3.4). According to this model a plot of $\log[\Theta/(1 - \Theta)p]$ versus sorbate concentration should be linear with a slope proportional to w. In the low-concentration region the data of Figure 4.3 conform to this behavior, giving $w \sim 200$–500 cal/mole. This is very much smaller than the heat of adsorption ($-\Delta H \sim 18$ kcal/mole) and would be consistent with a modest repulsive interaction between adsorbed molecules.

Sorption on a set of independent pairs of identical sites with interaction energy $2w$ when both sites of the pair are occupied yields Eq. (3.86) which, expressed in terms of the Henry constant becomes

$$q = 2\Theta = \frac{K'p + \frac{1}{2}(K'p)^2 e^{-2w/RT}}{1 + K'p + \frac{1}{4}(K'p)^2 e^{-2w/RT}} \tag{4.2}$$

while sorption on a set of independent pairs of nonequivalent sites with no interaction between adsorbed molecules yields the sum of two Langmuir
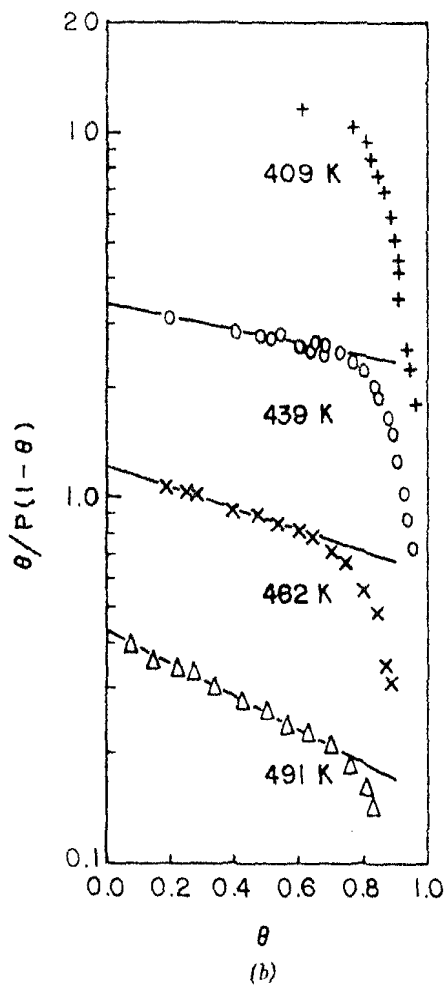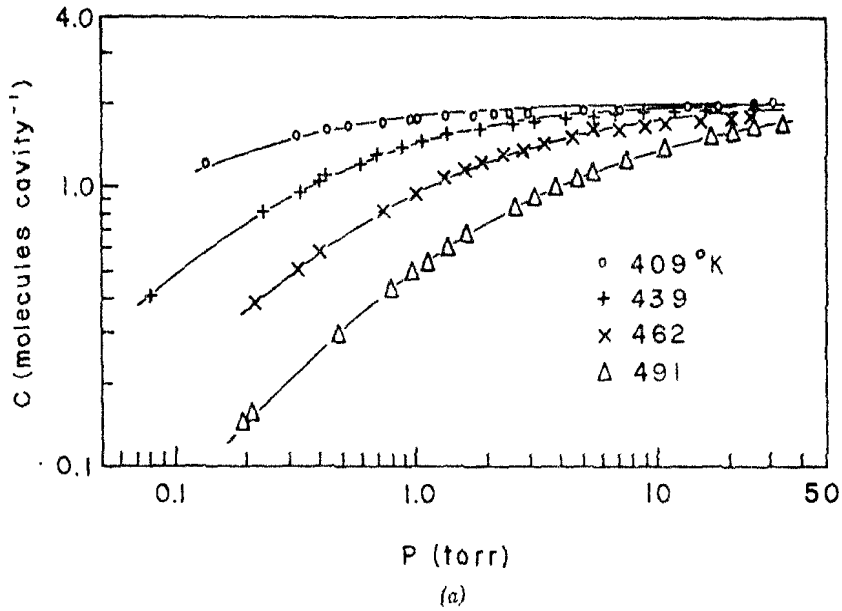
FIGURE 4.3. (a) Equilibrium isotherms and (b) variation of Langmuir "constant" with coverage for n-heptane in 5A zeolite. (From ref. 5; reproduced by permission of the National Research Council of Canada from the *Canadian Journal of Chemistry*, Volume 52, 1974.)

terms:

$$q = \frac{K_1'p}{1 + K_1'p} + \frac{K_2'p}{1 + K_2'p} \tag{4.3}$$

The cage of 5A zeolite is large enough to contain just two molecules of n-heptane at ordinary pressures so the models represented by both Eqs. (4.2) and (4.3) appear physically reasonable. Both equations contain two parameters $(K', w$ and $K_1', K_2')$ and both fit the experimental data well over the entire concentration range. Since Eq. (4.3) may be written in the form

$$q = \frac{(K_1' + K_2')p + 2K_1'K_2'p^2}{1 + (K_1' + K_2')p + K_1'K_2'p^2} \tag{4.4}$$

it is clear that both Eqs. (4.2) and (4.3) are of the same mathematical form $[K_1' + K_2' = K', \ K_1'K_2' = (K'^2/4)e^{-2w/RT}]$ and it is therefore not possible to distinguish between them simply from the analysis of experimental equilibrium data. The physical basis of the two models is, however, different since in the model leading to Eq. (4.2) the deviations from ideal Langmuir behavior are attributed to sorbate–sorbate interaction while in the model of Eq. (4.3) these deviations are ascribed to energetic heterogeneity. This illustrates a basic limitation in the use of model isotherms since it is often possible to obtain more than one physically reasonable model which provides an accurate representation of the experimental data, and it is not always possible to distinguish between the models by thermodynamic analysis.

4.2. MOBILE ADSORPTION

Simple Statistical Model Isotherm

For zeolitic adsorbents the assumptions of the simplified statistical models [Eq. (3.101) or (3.104)] are more reasonable than the assumptions of the Langmuir model, at least for nonpolar sorbates which show a good deal of intracage mobility. For systems such as CH_4-4A, for example, the results of neutron-scattering experiments show clearly that, in accordance with the assumptions of the statistical model, the molecule has essentially complete translational freedom within the zeolite cavity, with transitions to neighboring cages occurring only relatively infrequently.[8] Equation (3.101) has been shown to provide a good correlation of the experimental isotherms for several zeolitic systems[9-15] and representative examples are illustrated in Figure 4.4. The model contains two parameters; the Henry constant and the ratio β/v (effective molecular volume/cage volume). The volume of the zeolite cage is known from structural information while the van der Waals co-volume (b) provides a good first approximation to β so the model is really a single-parameter model. However, the fit of an experimental isotherm may generally
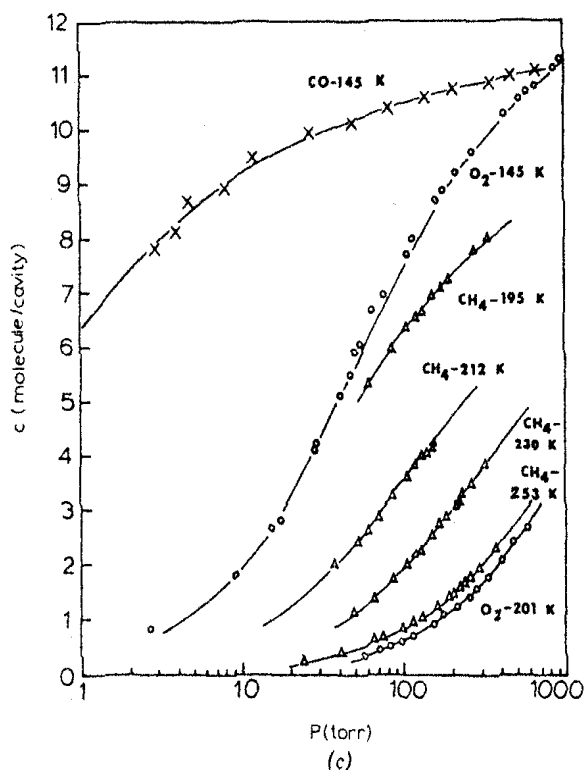
(a)

(b)
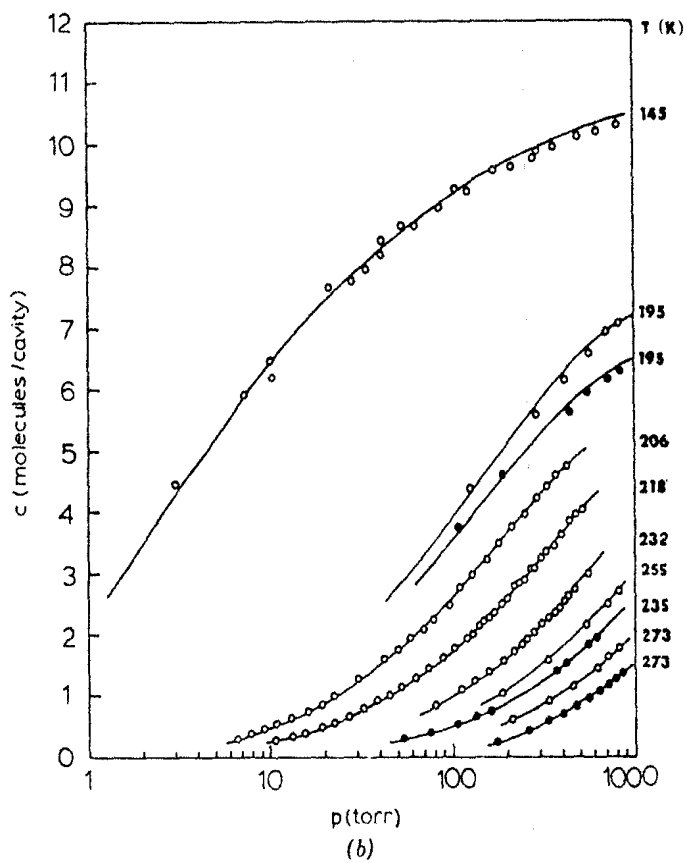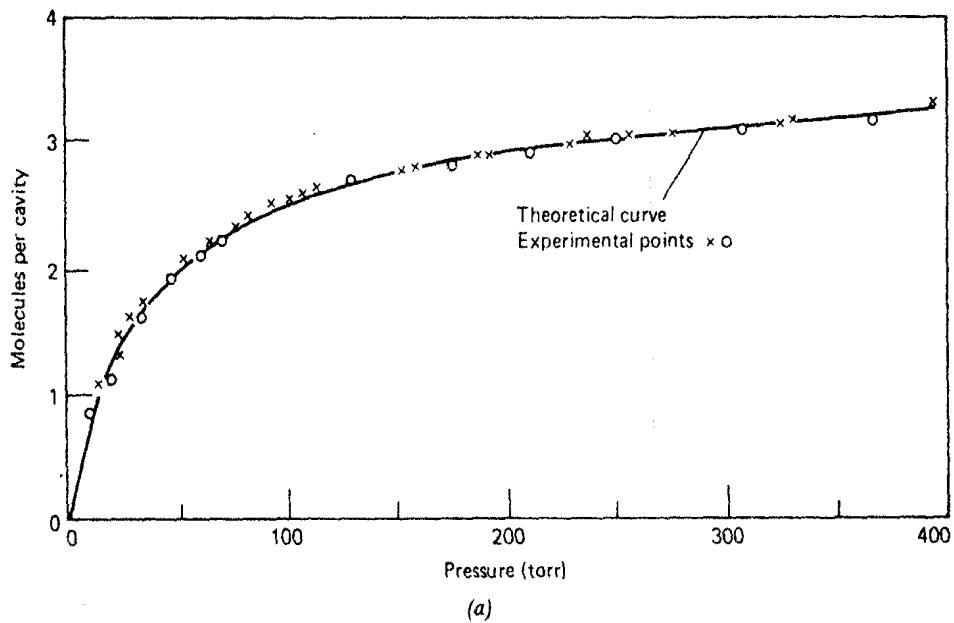
FIGURE 4.4. Single-component isotherms for (a) C_3H_8-5A; (b) N_2-5A (O) and N_2-4A (●); and (c) O_2-5A (O), CO-5A (×) and CH_4-5A (△) showing comparison between the theoretical curves calculated from Eq. 3.101 and experimental data. Parameters are given in Table 4.1. [From refs. 9 and 12; (a) reprinted by permission from *Nature*, **232**, p. 70. Copyright © 1971 Macmillan Journals Limited; (b) and (c) reprinted with permission.)

be improved by treating β as an additional parameter. The values obtained are of the same order as the van der Waals co-volumes but generally show a modest increase with temperature, as illustrated in Table 4.1.

In the original version of this model an attractive term based on Lennard–Jones potential constants was included in order to account for intermolecular attraction between adsorbed molecules.[9] However, it was found that the fit of the experimental isotherm was not significantly improved by the inclusion of these factors[10] so they were omitted in later studies.[12] This observation suggests that, at least for nonpolar sorbates, the adsorption equilibrium behavior is governed by the attractive potential of the framework, which determines the Henry constant, and the repulsive interaction between molecules due to their finite size. Attractive forces between adsorbed molecules appear to be of only secondary importance.

With nonpolar sorbates an increase in heat of adsorption with coverage is commonly observed, as illustrated in Figure 4.5 and this is commonly attributed to the effect of intermolecular attraction forces. The statistical model isotherm, however, suggests an alternative explanation. If the effective molecular volume increases with temperature, as it generally does, the isosteric heats

TABLE 4.1. Henry's Law Constants and Molecular Volumes Calculated from the Single-Component Isotherms[a]

System	T (°K)	K' (molecule/ cavity.Torr)	v/β	β (Å³)
N_2–5A	$T_c = 126$			$b = 65$
	145	3.7	13.5	57.5
	195	0.11	12	65
	205.5	0.062	10	
	218	0.034	10	
	232	0.015	10	
	252	0.007	10	77
	255	0.008	10	
	273	0.0037	10	
	298	0.0016	10	
N_2–4A	195	0.1	11	70
	235	0.0063	10	77
	273	0.0024	10	77
O_2–5A	$T_c = 155$			$b = 53$
	145	0.31	17	46
	201	0.007	17	46
	298	0.00041	15	52
CO–5A	$T_c = 133$			$b = 66$
	145	50	13	59
	298	0.011	8	97
CH_4–5A	$T_c = 191$			$b = 71$
	190	0.33	13.5	57.5
	212	0.083	12	64.5
	230	0.033	12	64.5
	253	0.011	12	64.5
	273	0.007	10	77
C_3H_8–5A	$T_c = 370$			$b = 140$
	358	0.14	5	140

Source: From Ref. 12.

[a] Volume of zeolite cavity = 776 Å³. A sorbate concentration of 1 molecule/cavity is equivalent to 0.45 mmole/g Linde peelet or 0.56 mmole/g anhydrous zeolite crystals.
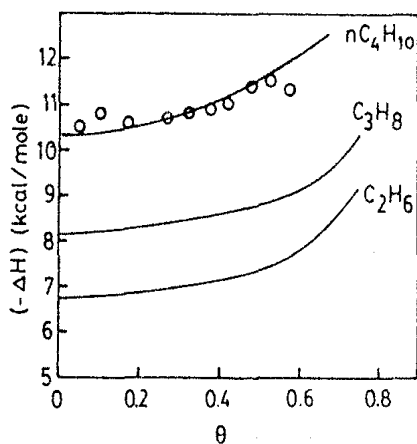
FIGURE 4.5. Variation of isosteric heat of sorption with coverage, calculated from Eq. (3.101), for light paraffins in 5A zeolite. Points are experimental data of Schirmer et al.[2] for butane-5A. (From ref. 10.)

of sorption calculated from the model [Eq. (3.101)] with no attraction term show an increase with loading similar to that which is observed experimentally.[10] The calculated values for butane are shown in Figure 4.5. According to the model this variation in isosteric heat arises because as the sorbate molecule expands the distribution of the molecules between cages is changed, reducing the average level of occupation at a given pressure. To maintain a constant adsorbed phase concentration the pressure must be increased to compensate and this translates to an increase in the isosteric heat. Isosteric heats calculated at constant volume fraction are independent of coverage.

The basic assumptions of this model may be regarded as a reasonable approximation for nonpolar sorbates at modest concentration levels. The model cannot be expected to apply in the high-concentration region approaching the saturation limit or for highly polar sorbates such as NH_3 or H_2O which are almost certainly localized. The model has, however, been found to provide an adequate representation of the behavior of quite strongly quadrupolar sorbates such as CO_2 on several zeolites.[13,14] At lower temperatures adsorption may be expected to become more localized leading to deviations from the model.

The application of Eq. (3.104) to the correlation of experimental equilibrium data for benzene on 13X zeolite[16] is illustrated in Figure 4.6. This equation is more recent and has been applied less widely than Eq. (3.101). However, except when the saturation limit is less than about four molecules
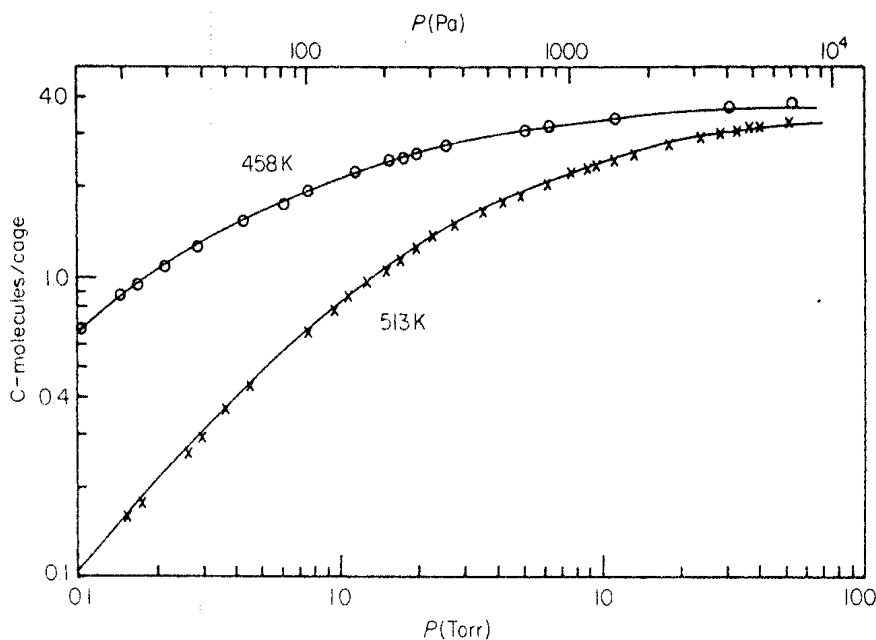
FIGURE 4.6. Experimental isotherms for benzene in 13X zeolite crystals at 458 and 513 K. Points are experimental, curves are calculated from Eq. (3.104) with $v/\beta = 5.0$, $K' = 8.8$ molecules/cage Torr at 458 K, and $K' = 1.25$ molecule/cage Torr at 513 K. [Reproduced from ref. 16 by permission of the publishers, Butterworth & Co (Publishers) Ltd. ©.]

per cage, both expressions are similar except for a small difference in the numerical value of the Henry constant so one may expect that the application of Eq. (3.104) will lead to results which are essentially the same as those derived from Eq. (3.101).

General Statistical Correlation

Since the assumptions from which Eqs. (3.101) and (3.104) are derived cannot be more than rough approximations which may be expected to break down at high sorbate concentrations, an alternative approach based on Eq. (3.105) has been adopted for the correlation and analysis of equilibrium data for strongly adsorbed species such as the xylenes on X and Y zeolites. By integration of the Gibbs equation one may calculate the spreading pressure (or surface potential Φ) as a function of equilibrium vapor pressure or sorbate concentration, directly from an experimental isotherm [Eq. (3.50)]. It follows from Eqs. (3.90), (3.94), and (3.99) that

$$\frac{\Phi}{RT} = \ln \xi = \int_0^{p^\circ} q^\circ(p)\, \frac{dp}{p}$$

$$= \ln\left\{ 1 + K'p^\circ + \frac{A_2(K'p^\circ)^2}{2!} + \frac{A_3(K'p^\circ)^3}{3!} + \cdots \right\} \qquad (4.5)$$

where q is expressed as molecules per cage. Knowing the Henry constant, which is found from the initial slope of the isotherm, it is thus possible to determine the values of the coefficients $A_2, A_3, \ldots$, from a least squares fit. It is of course possible to proceed directly by matching the experimental isotherm to Eq. (3.105), but such a procedure proves less satisfactory in practice due to compensation between the various terms in the numerator and denominator.

TABLE 4.2. Correlation of Equilibrium Isotherms for Hydrocarbons on Zeolite NaX and NaY According to Eq. (3.105)

Sorbent	Sorbate	T (K)	$K \left(\dfrac{\text{Molecule}}{\text{Cage torr}} \right)$	A_2	A_3	$KA_3^{1/3}$
NaX	cyclohexane	439	0.38	0.99	1.45	—
NaX	toluene	513	4.95	0.81	0.001	—
NaY	o-xylene	477	8.7	1.04	1.01	7.8
NaY	m-xylene	477	5.9	0.98	2.3	7.8
NaY	p-xylene	477	5.7	1.16	4.8	9.6
NaY	ethylbenzene	477	15.9	0.97	0.007	3.04

Affinity sequence (C_8 aromatics-NaY):
Low concentration (K):   EB > OX > MX~PX
High concentration ($KA_3^{1/3}$):   PX > OX > MX > EB

Results of an experimental study[17] of the sorption of several hydrocarbons on NaX and NaY zeolites are summarized in Table 4.2 and Figure 4.7. For these species at all temperatures investigated the saturation capacity was found to be close to 3.0 molecules/cage so only two coefficients (A_2 and A_3) are required in Eq. (4.5). The Henry constants were found from the limiting slopes of the isotherm at low pressure. Values of ξ were then calculated by integration of the isotherms [Eq. (4.5)], and the values so obtained were matched to the theoretical expression:

$$\xi = 1 + K'p + \frac{A_2}{2}(K'p)^2 + \frac{A_3}{6}(K'p)^3 \tag{4.6}$$

in order to determine the constants A_2 and A_3. The conformity of the experimental data to Eq. (4.6) is shown in Figure 4.7 in which the function $(\xi - 1 - K'p)/(K'p)^2$ is plotted against $K'p$. The values of A_2 derived from the intercepts of such plots were, in all cases, very close to unity suggesting that as long as a cage contains less then 2.0 sorbate molecules, there is very little sorbate–sorbate interaction. The values of A_3, however, range from 0.007 for ethylbenzene to about 5 for paraxylene, indicating that when three molecules are present in the same cage there are significant interactions which may result in either a net repulsion or a net attraction, depending on the sorbate.

If there are no significant nonideal interactions in a mixed adsorbed phase then a comparison of the equilibrium pressures for the two pure sorbates at the same temperature and spreading pressure (or the same value of ξ) provides
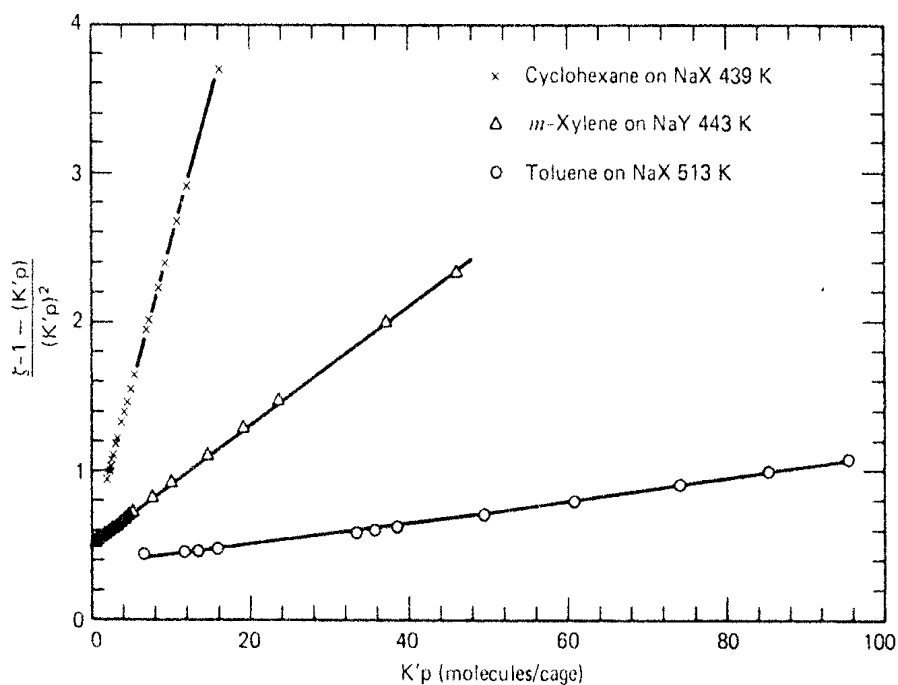
FIGURE 4.7. Experimental equilibrium data for hydrocarbons in NaX and NaY zeolite showing conformity of the isotherms to Eq. (4.6).

an estimate of the separation factor. At low concentrations this reduces simply to the ratio of the Henry constants, while at high sorbate concentrations approaching saturation the separation factor depends also on the third-order coefficients A_{31} and A_{32}:

$$q \to 0 \qquad \alpha_0 = \frac{K_1'}{K_2'}$$

$$q \to q_s \qquad \alpha_{12} = \frac{K_1'}{K_2'}\left(\frac{A_{31}}{A_{32}}\right)^{1/3} = \alpha_0\left(\frac{A_{31}}{A_{32}}\right)^{1/3} \qquad (4.7)$$

The separation factor at high concentration (as in a liquid phase system) may therefore bear little relationship to the separation factor at low concentration, as determined from the ratio of the Henry constants. By comparing the values of K and $KA_3^{1/3}$ it may be seen that, for the C_8 aromatic systems considered here, at low concentrations, ethylbenzene is the most strongly adsorbed species and p-xylene is held least strongly whereas at high concentrations the relative affinity for these species is reversed. It appears that at high loadings sorbate–sorbate intermolecular interactions are at least as important as sorbate–sorbent interactions in determining the selectivity.

4.3. GENERAL THERMODYNAMIC CORRELATIONS

Dubinin–Polanyi Theory

Because of the limited success which has been achieved by detailed isotherm models, a number of alternative approaches to correlation of sorption equilibrium data have been followed. Perhaps the most familiar of these is the correlation in terms of the Dubinin–Polanyi "characteristic curve." No specific model for the adsorbed phase is required and data over a wide range of conditions can often be correlated successfully in this way. Representative examples of characteristic curves taken from Dubinin's work[18] are shown in Figure 4.8. For adsorption on nonpolar adsorbents, such as activated carbon, the basic assumptions of the theory are reasonably well fulfilled since the adsorption potential for these systems is due entirely to van der Waals forces which are independent of temperature. The application to systems such as water on NaX zeolites is less easy to justify theoretically since, for such systems, temperature-dependent electrostatic forces make a significant contribution to the energy of adsorption. However, the influence of the electrostatic forces is dominant only at low coverage and at higher coverage the data conform approximately to the Dubinin theory, suggesting that dispersion–repulsion forces are dominant. Thus, even for systems such as water on zeolites the concept of a temperature-independent characteristic curve can provide a useful and concise engineering correlation, at least at moderate to high coverage.
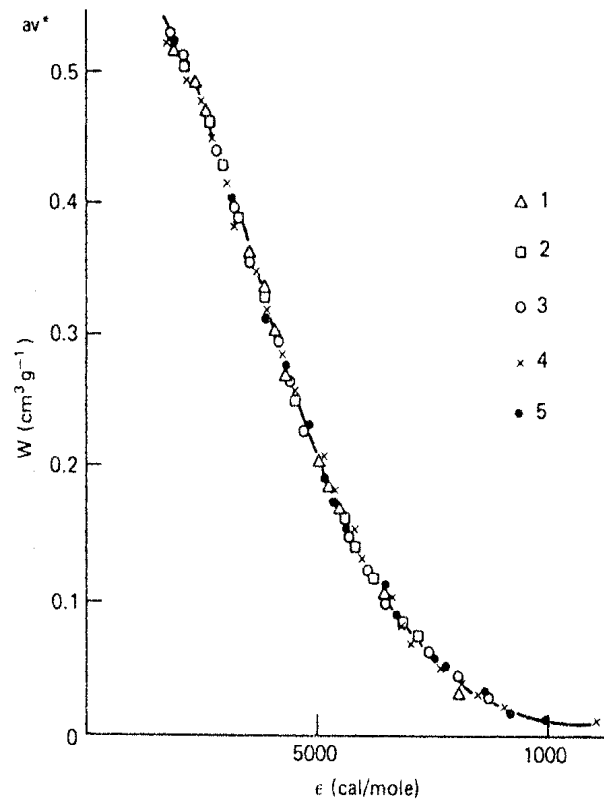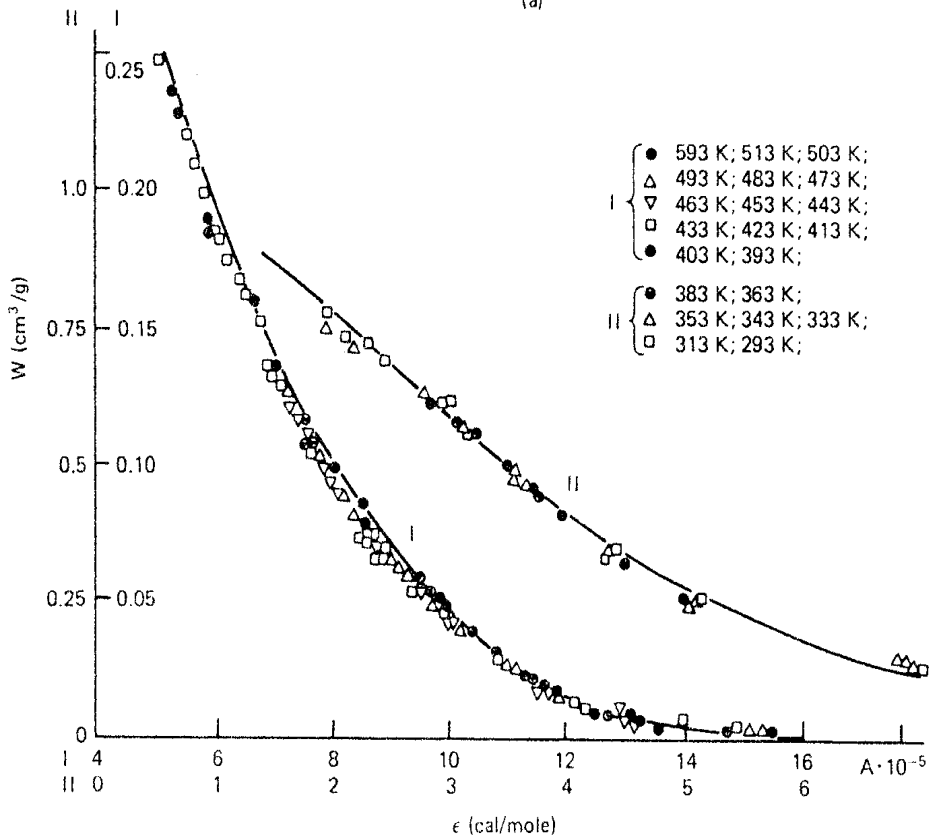
FIGURE 4.8. Experimental equilibrium data for (*a*) benzene-activated carbon and (*b*) water-NaX zeolite plotted as "characteristic curves" showing volume adsorbed against adsorption potential [defined by Eq. (3.106)]. (Reprinted with permission from ref. 32. Copyright 1971 American Chemical Society.)

99

Virial Isotherm

The virial isotherm [Eq. (3.43)] has also been widely used to correlate experimental equilibrium data.[19-21] With two virial coefficients in addition to the Henry constant it is possible to correlate the equilibrium data for many systems with high accuracy. However, little detailed information concerning the nature of the adsorbed phase can be deduced from the virial coefficients so the method is essentially one of empirical data correlation. As such it is less convenient than the Dubinin–Polanyi approach since more parameters, each one in principle dependent on temperature, are required. However the virial isotherm reduces naturally to Henry's law in the low-concentration limit, and this is a significant advantage over the Dubinin–Polanyi approach, the validity of which becomes questionable at low concentrations.

Generalized Equilibrium Isotherm

The Henry's law constant provides a direct measure of the interaction between an adsorbed molecule and the most favorable adsorption sites on the surface. Although the form of the equilibrium isotherm at higher sorbate concentrations is sensitive to a number of complicating effects arising from sorbate–sorbate interaction and energetic heterogeneity, one may expect that,

Henry constant (mol/cage. torr)	Temp. (K)	
9.03	409	o
2.75	437	×
1.16	457	□
0.42	487	△
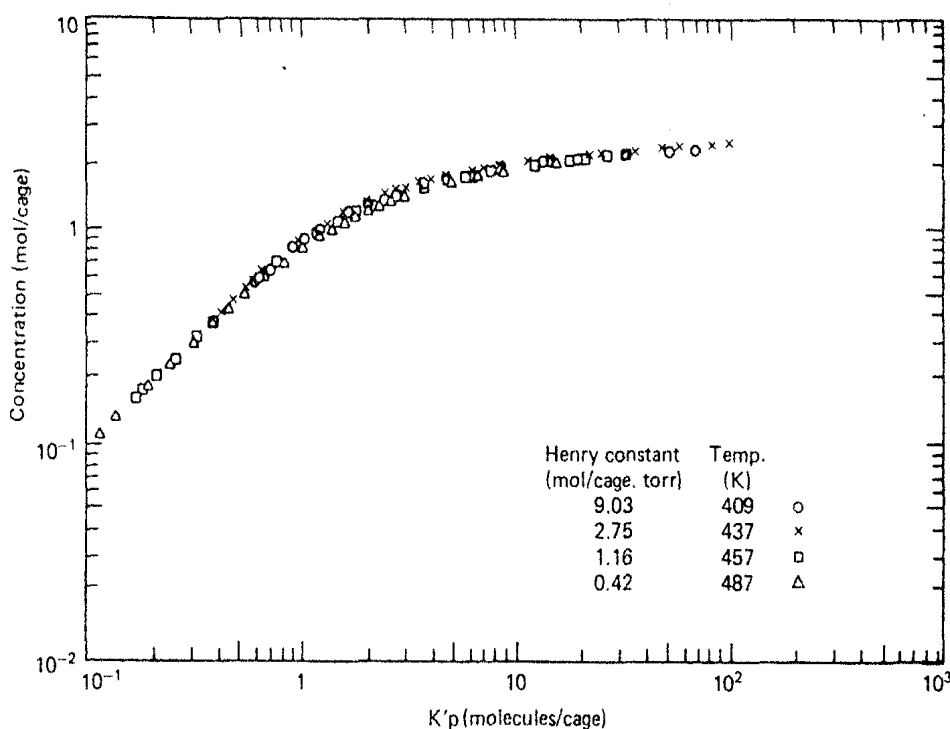
FIGURE 4.9. Equilibrium isotherms for n-heptane on 13X zeolite plotted in terms of K_p' to provide a generalized isotherm. (The experimental data were obtained by Doetsch at the University of New Brunswick.)

as long as the adsorbent is reasonably uniform, the Henry constant should prove to be a useful scale factor so that when plotted as adsorbed phase concentration versus $K'p$ the isotherms for a given system should approximate a single curve. This requires that the temperature dependence of the parameters $A_2, A_3, \ldots$, in Eq. (3.105) must be small compared with the temperature dependence of the Henry constant, and this proves to be a useful approximation for many systems. Such a correlation is illustrated in Figure 4.9 for the adsorption of n-heptane on 13X zeolite.

Although not exact, the generalized curve appears to provide a simple and practically useful method of data correlation and extrapolation. The only parameter required is the Henry's law constant which is easily determined from low-concentration isotherm data and which is readily extrapolated for temperature according to Eq. (2.19) or directly from a van't Hoff plot. This correlation has two advantages over the Dubinin–Polanyi approach: it is rigorously valid in the low-concentration region and it is somewhat easier to use since the uncertainties involved in estimation of the molecular volume of the sorbate are eliminated. The method works well for nonpolar molecules but cannot be expected to apply for small polar molecules such as water and ammonia on polar adsorbents, since the isotherms for such systems are strongly influenced by energetic heterogeneity.

4.4. HEATS OF ADSORPTION

According to the ideal Langmuir model the heat of adsorption should be independent of coverage, but this requirement is seldom fulfilled in real systems because the effects of surface heterogeneity and sorbate–sorbate interaction are generally significant. Information concerning the magnitude of the heat of adsorption and its variation with coverage can provide useful information concerning the nature of the surface and the adsorbed phase.

Commonly observed trends are illustrated in Figures 4.10–4.12. For the sorption of nonpolar molecules on a homogeneous surface the heat of sorption is generally almost independent of coverage at low coverage and increases modestly as the saturation limit is approached. Such behavior, illustrated in Figure 4.10 by the data for the paraffins, SF_6 and CF_4 on zeolites A and X, is commonly ascribed to the effect of intermolecular attraction. An alternative explanation based on repulsion forces was discussed in Section 4.2. By contrast, in silicalite, the heats of sorption of n-butane, 1-butene and benzene are almost constant over a wide range of concentration and almost the same ($\sim$11.5 kcal/mole) for the three different sorbates.[62]

The extent to which an adsorbent appears energetically heterogeneous depends to some extent on the size of the sorbate molecule since, if the favorable sites extend only over small regions of space, they may be accessible only to very small molecules. The surface may appear almost energetically
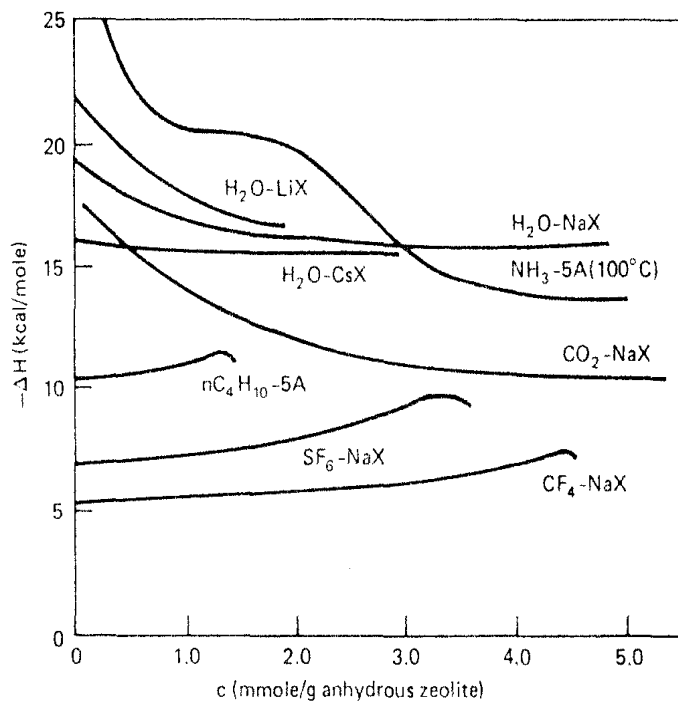
FIGURE 4.10. Variation of isosteric heat of adsorption with coverage showing the difference in trends between polar and nonpolar sorbates. nC_4H_{10}-5A, data of Schirmer et al.[2]; CF_4-NaX, SF_6-NaX, data of Barrer and Reucroft[22]; CO_2-NaX, data of Huang and Zwiebel[23]; NH_3-5A, data of Schirmer et al.[24]; H_2O-LiX, NaX, and CsX, data of Avgul et al.[25] (Reprinted from Ref. 26, p. 189, by courtesy of Marcel Dekker, Inc.)

uniform to a larger molecule which sees only the potential averaged over a larger region.

The increasing effect of electrostatic contributions to the heat of adsorption resulting from the exchange of $2Na^+$ for Ca^{2+} in zeolite A as well as the increasing energetic heterogeneity in the sequence CH_4 (nonpolar), N_2 (small quadrupole), CO (small dipole) is shown clearly in Figure 4.11.[27] For the
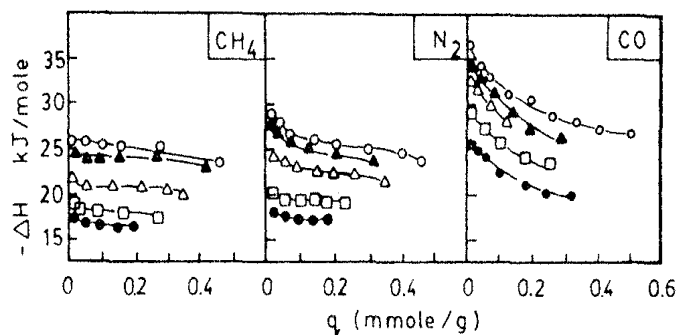
FIGURE 4.11. Variation of heat of sorption with coverage for CH_4, N_2, and CO on various NaCaA zeolites (●, NaA; □, 30% Ca-NaA; △, 46% Ca-NaA; ▲, 85% Ca-NaA; and ○, CaA). (From ref. 27, copyright John Wiley & Sons, Inc., 1980; reprinted with permission.)
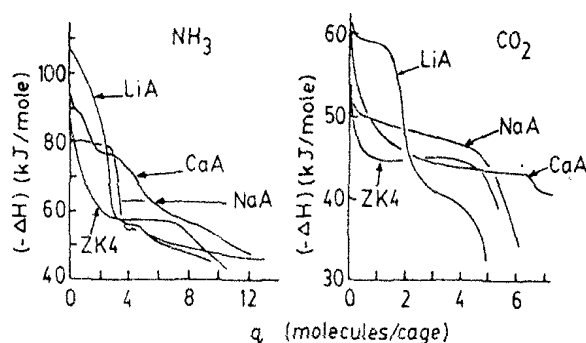
FIGURE 4.12. Variation of heat of adsorption with coverage for NH_3 and CO_2 on various type A zeolites. (From ref. 28, copyright John Wiley & Sons, Inc., 1980; reprinted with permission.)

more strongly quadrupolar CO_2 and dipolar NH_3 molecules the decrease in heat of adsorption with coverage becomes more pronounced and the form of the curve is greatly influenced by both the number and nature of the cations present, as may be seen from Figure 4.12. The greatest energetic heterogeneity is shown by LiA, reflecting the high polarizing power of the Li cation. Similar trends may be seen from Figure 4.10 where data for water on LiX, NaX, and CsX zeolites[25] are compared. The CsX sieve shows little variation of heat of adsorption with coverage suggesting that the electrostatic contribution is minor. It is sometimes possible to make quite detailed deductions concerning the location of the cations from accurate measurements of the heat of sorption as a function of sorbate concentration, and a more detailed interpretation of the data shown in Figure 4.12 may be found in the original article.[28]

In zeolitic adsorbents the cation density is governed by the Si/Al ratio. Dealumination therefore leads to an energetically more uniform surface and a reduction in the variation of heat of adsorption with coverage. This is clearly illustrated by the data of Barrer and Murphy,[29] shown in Figure 4.13. The difference between the heats of sorption of CO_2 (quadrupolar) and Kr (nonpolar) is shown as a function of coverage for various mordenites subjected to increasingly severe dealumination by acid leaching. The difference in the heats of sorption is greatest for the parent mordenite and least for the most ·
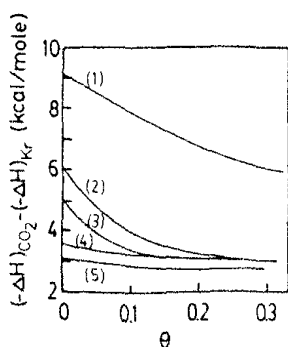
FIGURE 4.13. Difference between isosteric heats of sorption of CO_2 in Kr in different mordenite samples showing effect of dealumination in reducing energetic heterogeneity. (1) parent Na mordenite (Si/Al = 4.8); (2) H-mordenite; (3) treated with 2N HCl; (4) treated with 6N HCl; (5) treated with 12N HCl (Si/Al = 17.5). (From ref. 29, with permission.)
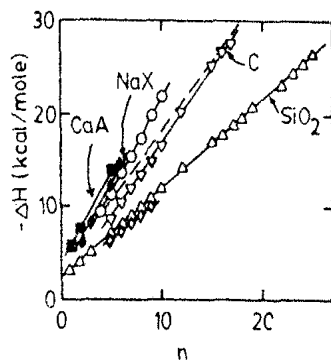
FIGURE 4.14. Dependence of limiting heat of sorption at zero coverage on chain length (n) for n-paraffins on various adsorbents. (From Kiselev and Shcherbakova.[30])

TABLE 4.3. Group Contributions for Estimation of Heats of Adsorption in 5A Zeolite

	Increment (kcal) for $\Theta = 0$	Increment (kcal) for $\Theta = 0.5$
$-CH_4$	2.95	3.5
$-CH_2-$	2.5	2.7
$-CH=CH_2$	8.35	7.0
$-NH_2$ (amines)	16.0	11.5

Source: From Ref. 31.

strongly dealuminated form. The near constant value of this quantity for the most strongly dealuminated samples suggests that the surface is energetically almost uniform.

In homologous series such as the linear paraffins, the heat of sorption, for a given adsorbent, increases linearly with chain length, as illustrated in Figure 4.14. The presence of double bonds or polar groups in the molecule gives rise to an additional electrostatic contribution to the heat of adsorption, and an approximate group contribution method for estimating heats of adsorption has been suggested by Schirmer et al.[31] (See Table 4.3). The variation of the heats of sorption of linear olefins in X and Y zeolites is more complex with a well defined oscillation superimposed on the general increasing trend of ΔH with carbon number. This has been attributed to the effect of the small electrostatic contribution since the dipole moments of the odd numbered species are slightly higher than those of the even numbered species.[63]

4.5. ENTROPY AND HEAT CAPACITY

Additional information concerning the nature of an adsorbed species may sometimes be obtained from a detailed analysis of the entropy of sorption. The absolute molar entropy of a gaseous molecule may be calculated from the Sackur–Tetrode equation, or its extension for a polyatomic species.[32] Equa-

tion (3.10) may therefore be used to calculate the partial molar entropy of the adsorbed phase once the heat of adsorption has been determined. Just as a complex partition function may be factorized into the contributions corresponding to different degrees of freedom, so the partial molar entropy may be regarded as the sum of the thermal ($\bar{S}_{th}$), translational ($\bar{S}_T$), and configurational ($\bar{S}_c$) entropies:

$$\bar{S}_s = \bar{S}_{th} + \bar{S}_T + \bar{S}_c \tag{4.8}$$

For localized adsorption $\bar{S}_T = 0$ and for adsorption or a set of uniform sites, as in the Langmuir or Lacher models [Eq. (4.1)] the configurational entropy may be shown, by differentiation of Eq. (3.58) and the application of Stirling's theorem, to be given by

$$\bar{S}_c = R \ln\left(\frac{1 - \Theta}{\Theta} \right) \tag{4.9}$$

The thermal entropy may therefore be calculated by difference from Eq. (4.8). Values derived in this way should be independent of coverage and of physically reasonable magnitude in the sense that they correspond with reasonable values of vibration frequency. A similar approach is possible for the mobile models (Volmer and van der Waals) but is somewhat more complicated because of the need to allow for the translational entropy. The main difficulty with this approach is that, for energetically heterogeneous adsorbents, the configurational and translational contributions to the entropy for real systems generally do not conform to the expressions derived from the simple models, making the values derived for the thermal entropies unreliable.

Measurements of the partial molar heat capacity ($\bar{C}_s$), which is related to the partial molar entropy by

$$\bar{C}_s = T\left(\frac{\partial \bar{S}_s}{\partial T} \right)_{n_s} \tag{4.10}$$

have proved more useful in determining the physical state of the adsorbed molecule. Available information has been reviewed by Barrer.[33] Elementary equipartition theory suggests $\bar{C}_s/R = n/2$ where n is the number of degrees of freedom (or "squared energy terms") for the adsorbed molecule. (In computing the value of n, vibrational degrees of freedom contribute two squared terms and are therefore counted twice.) The maximum possible values of $\bar{C}_s/R$ calculated on this basis are summarized in Table 4.4 for simple molecules in which internal degrees of freedom are not significantly excited.

Experimental heat capacity data for Kr in several different zeolites give $\bar{C}_s/R \sim 2.5$, suggesting two vibrational and one translational degrees of freedom. Values for adsorbed CO_2 (linear) and NH_3 and CH_4 (tetrahedral), however, exceed the maximum values estimated on this basis and show a complex temperature dependence which can best be explained by changes in the distribution of adsorbed molecules between different types of sites. For more complex molecules the interpretation of heat capacity data is complicated by contributions from internal degrees of freedom.

TABLE 4.4. Maximum Values of Heat Capacity from Equipartition

Molecule	$(\bar{C}_s/R)_{max}$	State
Monatomic	3	3 vibrations
Linear	5	$\begin{cases} \text{3 vibrations of} \\ \quad \text{center of mass} \\ \\ \text{2 rotational} \\ \quad \text{oscillations} \end{cases}$
Nonlinear	6	$\begin{cases} \text{3 vibrations of} \\ \quad \text{center of mass} \\ \\ \text{3 rotational} \\ \quad \text{oscillations} \end{cases}$

4.6. ADSORPTION OF MIXTURES

The experimental measurement of multicomponent adsorption isotherms is time consuming because of the large number of variables involved, and the problem of predicting binary and multicomponent equilibria from single-component adsorption data has therefore attracted much attention. A brief review of the various approaches which have been followed is given in this section. For simple systems considerable success has been achieved but there is still no established method with universal proven applicability, and this problem remains one of the more challenging obstacles to the development of improved methods of process design.

Extended Langmuir Model

The derivations given in Sections 2.4 and 3.3 may be easily extended to binary or multicomponent systems. The resulting expression for the isotherm is

$$\frac{q_1}{q_{s1}} = \frac{b_1 p_1}{1 + b_1 p_1 + b_2 p_2 + \cdots} , \qquad \frac{q_2}{q_{s2}} = \frac{b_2 p_2}{1 + b_1 p_1 + b_2 p_2 + \cdots} \qquad (4.11)$$

Kemball, Rideal, and Guggenheim[34] and independently Broughton[35] have shown that thermodynamic consistency requires $q_{s1} = q_{s2}$. For physical adsorption of molecules of widely different size such an assumption is unrealistic. If the extended Langmuir equation is regarded as an analytical description rather than a physical model, the use of different values of q_s for each component becomes permissible although the equations cannot then be expected to apply over the entire concentration range and extrapolation on such

a basis must be made with caution. This approach was followed by Markham and Benton[36] who showed that binary equilibrium data for O_2-CO and CO-CO_2 mixtures on silica gel are well correlated by Eq. (4.11) with different values of q_s for the two components.

The separation factor for a system described by Eq. (4.11) is given simply by the ratio of the adsorption equilibrium constants for the two components:

$$\alpha_{12} = \frac{X_1/X_2}{Y_1/Y_2} = \frac{b_1}{b_2} \tag{4.12}$$

and, as such is evidently independent of concentration. This result may be generalized for any number of adsorbed components:

$$\alpha_{ij} = \frac{b_i}{b_j} = \alpha_{ik}\alpha_{kj}, \qquad \alpha_{ji} = \frac{1}{\alpha_{ij}} \tag{4.13}$$

This assumption of a constant separation factor leads to considerable simplifi-
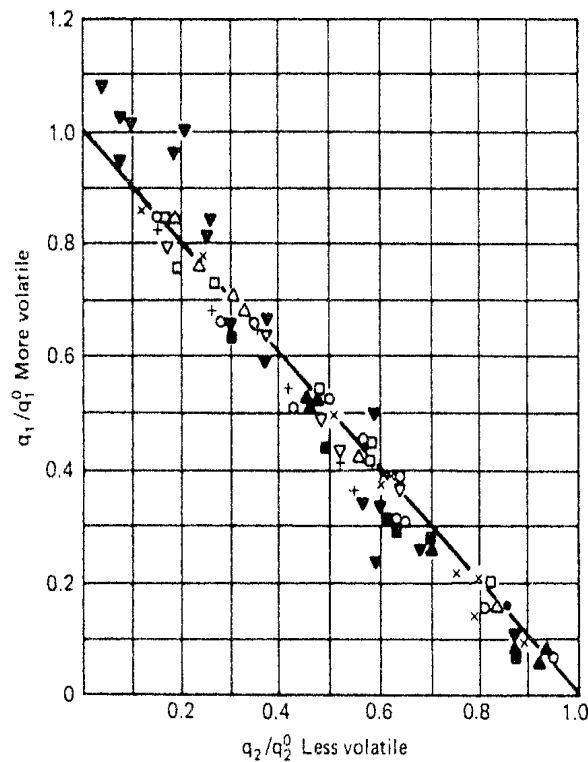
FIGURE 4.15. Test of the Lewis correlation [Eq. (4.14)] for sorption of hydrocarbons on silica gel and two activated carbons.

PCC Carbon	Columbia Carbon	Silica Gel
O, C_2H_4-C_3H_8	▽, CH_4-C_2H_4	▼, CH_4-C_2H_4
△, C_2H_6-C_3H_8	●, C_2H_4-C_2H_6	+, C_2H_6-C_3H_8
□, i-C_4H_{10}-1-C_4H_8	■, C_2H_4-C_3H_6	×, i-C_4H_{10}-1-C_4H_8
	▲, C_3H_6-C_3H_8	

(From ref. 37.)

cations in the analysis of adsorption column dynamics and is therefore widely used as an approximation even though it is accurate only for relatively few systems.

It follows from Eq. (4.11) that if q_1^0 and q_2^0 are the adsorbed phase concentrations for the pure components at pressures p_1^0 and p_2^0 and q_1, q_2 are the corresponding quantities for a mixture at partial pressures p_1, p_2 then, if $p_1^0 = p_2^0 = p_1 + p_2 = P$,

$$\frac{q_1}{q_1^0} + \frac{q_2}{q_2^0} = 1.0 \quad (\text{constant } T, P) \tag{4.14}$$

This result (the Lewis correlation)[37] has been found empirically to be of more general applicability than the Langmuir equations from which it is derived. Representative data, taken from the work of Lewis et al.,[37] showing the approximate conformity of experimental data for sorption of several binary hydrocarbon mixtures on silica gel are shown in Figure 4.15. Combining Eq. (4.14) with Eq. (3.57) and the definition of separation factor (α) [Eq. (1.1)] yields

$$\frac{\alpha - 1}{\alpha/q_2^0 - 1/q_1^0} \ln\left(\frac{\alpha q_1^0}{q_2^0}\right) = (q_2^0 - q_1^0)\ln(p_1 + p_2) - \int_0^{q_2^0} \ln p_2 \, dq_2$$

$$+ \int_0^{q_1^0} \ln p_1 \, dq_2 \tag{4.15}$$

which provides a convenient means of calculating the separation factor from experimental equilibrium data.

Langmuir–Freundlich Equations

Because of the limited success of the Langmuir model in predicting mixture equilibria, several authors have modified the equations by the introduction of a power law expression of Freundlich form[38]:

Pure components

$$\frac{q_1}{q_{s1}} = \frac{b_1 p_1^{n_1}}{1 + b_1 p_1^{n_1}}, \qquad \frac{q_2}{q_{s2}} = \frac{b_2 p_2^{n_2}}{1 + b_2 p_2^{n_2}} \tag{4.16a}$$

Binary mixture

$$\frac{q_1}{q_{s1}} = \frac{b_1 p_1^{n_1}}{1 + b_1 p_1^{n_1} + b_2 p_2^{n_2}}, \qquad \frac{q_2}{q_{s2}} = \frac{b_2 p_2^{n_2}}{1 + b_1 p_1^{n_1} + b_2 p_2^{n_2}} \tag{4.16b}$$

Although not thermodynamically consistent, these expressions have been shown to provide a reasonably good empirical correlation of binary equilibrium data for a number of simple gases on molecular sieve adsorbents[39] and are widely used for design purposes.[40] However, because of the lack of a proper theoretical foundation this approach should be treated with caution.

Statistical Model Isotherm

The extension of the simple statistical model to adsorption of a binary mixture is given by Eq. (3.102) and further extension to multicomponent systems follows naturally.[41] The parameters of the model (the Henry constant and effective molecular volume for each component) are derived from the single-component isotherms so that an *a priori* prediction of the mixture
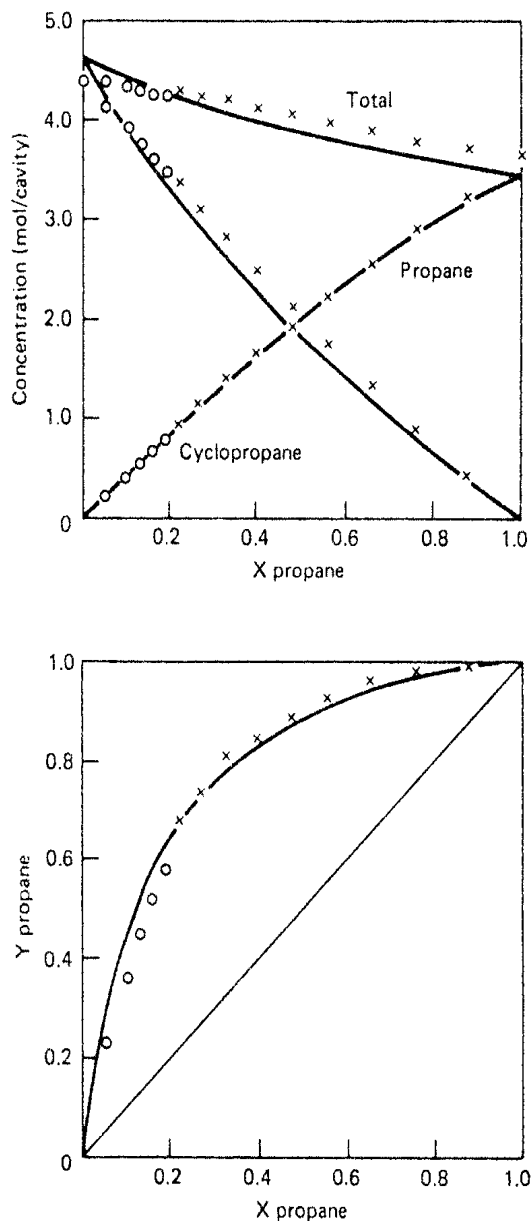
FIGURE 4.16. Equilibrium diagram (*a*) and *X*–*Y* diagram (*b*) for sorption of propane-cyclopropane mixtures on 5A zeolite at $P = 8$ torr, $T = 273$ K. Theoretical curves are calculated from Eq. (3.102) with the parameters derived from the single-component isotherms. (Reprinted with permission from ref. 42. Copyright 1977 American Chemical Society.)
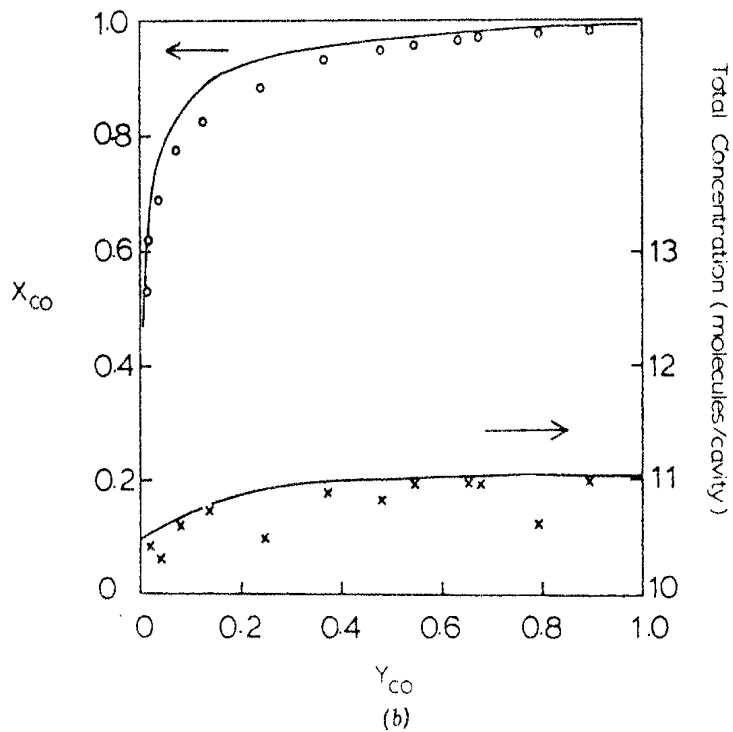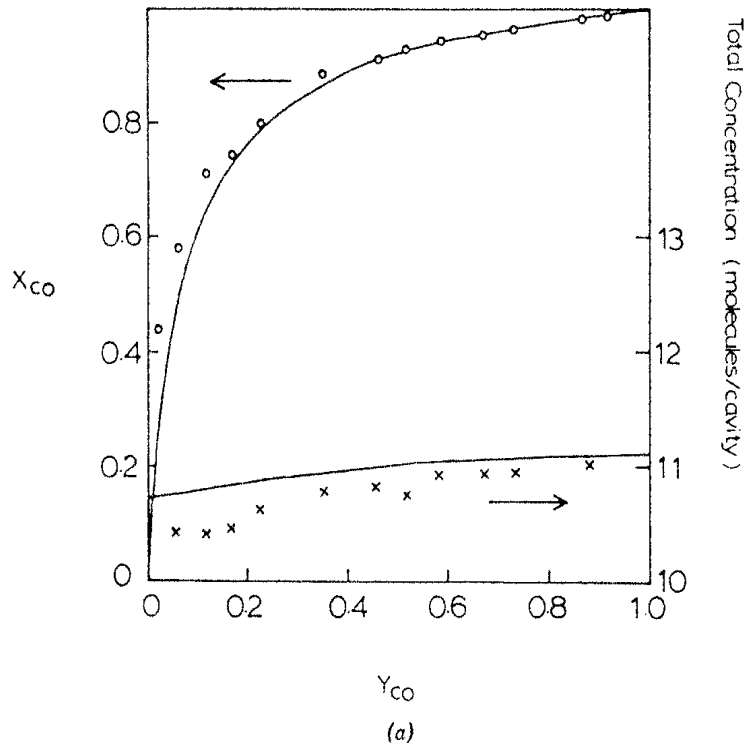
FIGURE 4.17. $X - Y$ diagrams and variation of total sorbate concentration with composition for binary systems (a) CO-N_2 and (b) CO-O_2 on 5A zeolite. Theoretical curves are calculated from Eq. (3.102) using the parameters derived from the single-component isotherms. (From ref. 12, reprinted with permission.)

110

isotherm is, in principle, possible. This model has been shown to provide reasonably good predictions of binary equilibrium data for systems such as C_2H_6-CO_2, C_2H_6-nC_4H_{10} and C_3H_8-cyclo C_3H_6[41-43] as well as for binary mixtures of O_2, N_2, CO, and CH_4[12] on 5A zeolite. Representative data for the C_3H_8-cyclo C_3H_6, CO-N_2, and O_2-CO systems are shown in Figures 4.16 and 4.17. For these systems the $X-Y$ diagrams are almost symmetric and show no strong deviations from ideality such as azeotrope formation or selectivity reversal. Highly nonideal behavior including azeotrope formation and selectivity reversal is shown by the experimental isotherms for hydrocarbon mixtures such as C_2H_4-C_3H_8 and C_2H_4-cyclo C_3H_6, and the mixture isotherms for these systems are not correctly predicted by the model [Eq. (3.102)], as may be seen from Figure 4.18. By the introduction of an additional parameter a reasonably good correlation of the experimental data for these systems may be obtained, but the predictive value of the model is lost by this approach.

Azeotrope formation and selectivity reversal appear to be fairly common features of binary adsorption equilibrium behavior but are not predicted by most of the simpler models such as Eqs. (4.11) or (4.16). Such behavior is predicted by Eq. (3.102) when the effective molecular volumes of the components are different and the component with the smaller volume also has the smaller Henry constant but only at relatively high sorbate concentrations.[41] The experimental data for C_2H_4-C_3H_8 in 5A show that selectivity reversal occurs even at relatively low loading (high temperatures) and is much more
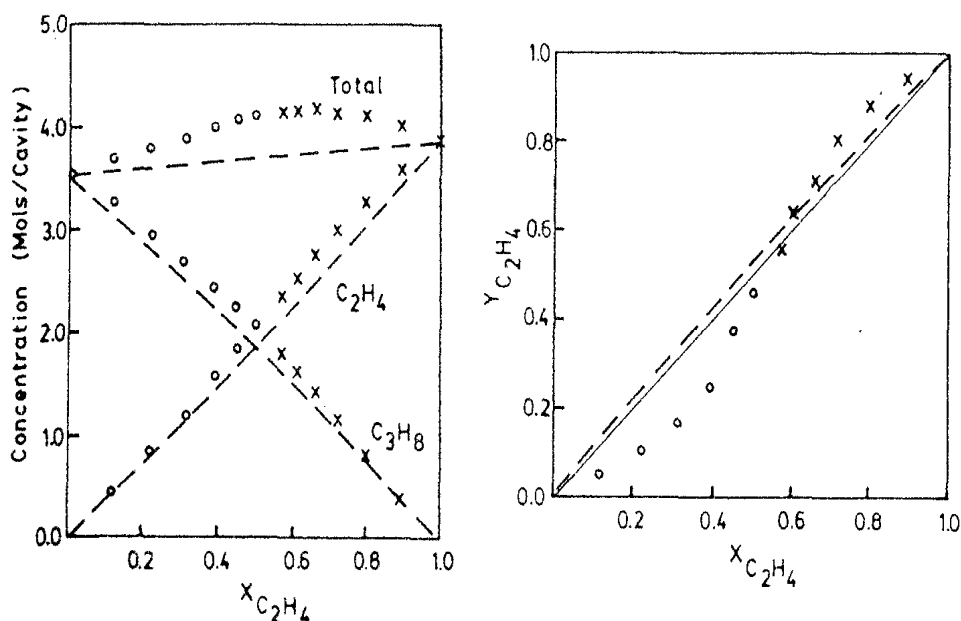
FIGURE 4.18. Comparison of experimental equilibrium data for the system C_2H_4-C_3H_8-5A sieve at 273 K, 8 torr, with the predictions of the ideal adsorbed solution theory (---). For this system the simplified statistical model leads to essentially the same predictions as the ideal adsorbed solution theory and the formation of an azeotrope is not predicted by either approach. (Reprinted with permission from ref. 42. Copyright 1977 American Chemical Society.)

pronounced than is suggested by the model. Such behavior may be attributed either to nonideal sorbate–sorbate interaction such as packing effects arising from the difference in the shape of the molecules, to strong intermolecular attraction, or to localized adsorption. Although present evidence is inconclusive, the latter appears the more likely possibility in view of the obvious tendency for localization of ethylene at the cation sites. To account for such behavior a more detailed statistical model is clearly required.

General Statistical Model

In Section 3.5 a general form of isotherm equation [Eq. (3.105)] was suggested in which the configuration integrals are in effect retained as empirical parameters. The corresponding expression for a binary mixture may be written:

$$q_1 = \frac{K_1 p_1 + \sum_j \sum_i \left[(K_1 p_1)^i (K_2 p_2)^j / (i-1)! \, j! \right] A_{ij}}{1 + K_1 p_1 + K_2 p_2 \sum_j \sum_i \left[(K_1 p_1)^i (K_2 p_2)^j / i! \, j! \right] A_{ij}} \tag{4.17}$$

with a similar expression for q_2. As with Eq. (3.102) the summation is carried out over all cages satisfying the requirement that $i\beta_1 + j\beta_2 \leqslant v$. The main difficulty in using such a model to predict mixture equilibria is that it is not obvious how the parameters A_{ij} representing the configuration integrals for the mixture are related to the values for the pure components. One possibility is to assume a geometric mean expression:

$$A_{ij} = \left(A_{1s}^i A_{2s}^j \right)^{1/(i+j)} \tag{4.18}$$

where A_{1n}, A_{2n} represent the nth-order coefficients for components 1 and 2 in the pure systems. This is equivalent to assuming that in a cage containing i molecules of component 1 and j molecules of component 2 the configuration integral is given by

$$Z(i,j) a_1^i a_2^j = \frac{(K_1' p_1)^i (K_2' p_2)^j}{i! \, j!} \left(A_{1s}^i A_{2s}^j \right)^{1/(i+j)} \tag{4.19}$$

Wong[44] has shown that with the coefficients derived from the single-component isotherms, Eqs. (4.17) and (4.18) provide a good representation of the binary isotherms for several systems. Representative data for cyclohexane–n-heptane on 13X zeolite are shown in Figure 4.19.

The approximation represented by Eqs. (4.17) and (4.18) is in fact equivalent to the assumption of an ideal adsorbed phase, defined in accordance with the Myers–Prausnitz formulation.[52] For either pure component the spreading pressure at an equilibrium vapor pressure p^0 is given by Eq. (4.6), which with Eq. (4.18) becomes

$$\exp\left(\frac{\phi_0}{RT} \right) = \xi_0 = 1 + K' p^0 + \left(\frac{K'' p^0}{2} \right)^2 + \left(\frac{K''' p^0}{3!} \right)^3 + \cdots \tag{4.20}$$
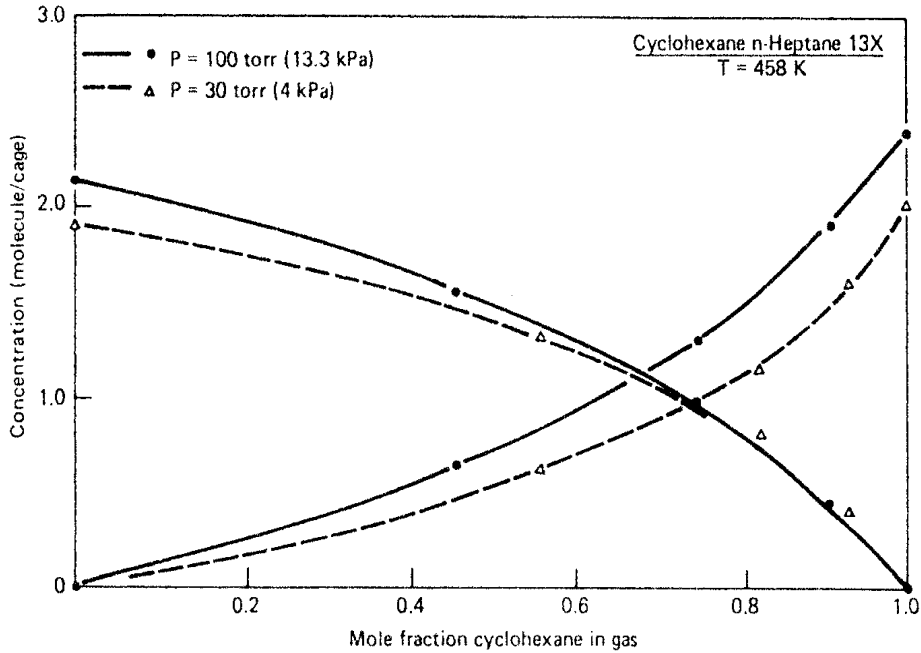
FIGURE 4.19. Comparison of experimental equilibrium data for the system n-heptane-cyclohexane on 13X zeolite with the theoretical predictions of the generalized statistical model [Eq. (4.18)] based on single-component data. (From ref. 17.)

where $K'' = K'A_2^{1/2}$, $K''' = K''A_3^{1/3}$ .... The spreading pressure for the mixture is given by

$$\exp\left(\frac{\phi}{RT}\right) = \xi = 1 + K_1'p_1 + K_2' + \sum\sum \frac{(K_1'p_1)^i(K_2'p_2)^j}{i!\,j!} A_{ij} \quad (4.21)$$

and with the same approximation [Eq. (4.18)] this becomes

$$\exp\left(\frac{\phi}{RT}\right) = \xi = 1 + K_1'p_1 + K_2'p_2 + \frac{1}{2}\left(K_1''p_1 + K_2''p_2\right)^2$$

$$+ \frac{1}{3!}\left(K'''p_1 + K'''p_2\right)^3 + \cdots \quad (4.22)$$

The adsorbed phase concentrations are given by $q_1 = (\partial \ln \xi/\partial \ln p_1)_{p_2}$ and $q_2 = (\partial \ln \xi/\partial \ln p_2)_{p_1}$ so that

$$X_1 = \frac{K_1'p_1 + K_1''p_1(K_1''p_1 + K_2''p_2) + \frac{1}{2}K_1'''p_1(K_1'''p_1 + K_2'''p_2)^2 + \cdots}{\left(K_{p_1}' + K_2'p_2\right) + \left(K_1''p_1 + K_2''p_2\right)^2 + \frac{1}{2}\left(K_1'''p_1 + K_2'''p_2\right)^3 + \cdots}$$

$$(4.23)$$

If

$$K_1'p_1^0 = K_1'p_1 + K_2'p_2 = K_2'p_2^0, \qquad K_1''p_2^0 = K_1''p_1 + K_2''p_2 = K_2''p_2^0 \cdots \quad (4.24)$$

we have

$$\phi_{01} = \phi_{02} = \phi, \qquad X_1 = \frac{p_1}{p_1^0}, \qquad X_2 = \frac{p_2}{p_2^0} \quad (4.25)$$

which is the definition of an ideal adsorbed solution [see Eqs. (4.31)–(4.35)]. Conformity of the binary isotherm to Eqs. (4.17) and (4.18), as observed for cyclohexane-n-heptane on NaX, therefore implies ideality of the binary adsorbed phase.

The volume-filling statistical model [Eqs. (3.101) and (3.102)] may be regarded as a special case of the more general model [Eqs. (3.105) and (4.17)] in which

$$A_{1s} = \left(1 - \frac{s\beta_1}{v}\right)^s, \qquad A_{2s} = \left(1 - \frac{s\beta_2}{v}\right)^s, \qquad A_{ij} = \left(1 - \frac{i\beta_1}{v} - \frac{j\beta_2}{v}\right)^{i+j}$$

(4.26)

Clearly, if $\beta_1 = \beta_2$ the condition represented by Eq. (4.18) will be fulfilled, and it follows that the mixture will show ideal behavior. Thus significant differences between the predictions of this model and IAST are to be expected only when there is a large difference in the molar volumes of the components.

Other Model Isotherms

Volmer's equation [Eq. (3.39)] has been extended to an ideal mobile binary monolayer[34] but since Volmer's equation seldom provides a good representation of single-component isotherms this approach is of limited practical value for the prediction of mixture isotherms for real systems. The multicomponent extension of the BET equation has been given by Hill[45] and for the adsorption of mixtures of oxygen and argon on chromia gel at $-196\,^\circ$C, White and Schneider[46] found fairly good agreement with Hill's expressions for the binary isotherm. However, for the system C_2H_6-CO_2 on chromia gel agreement was poor.[47] Since it appears that the theory is successful only for sorption of very similar molecules, its general value is somewhat limited.

Hoory and Prausnitz[48] have suggested extending the van der Waals isotherm [Eq. (3.41)] to a binary system using the approximations

$$\beta_{12} = X_1\beta_1 + X_2\beta_2$$

$$\alpha_{12} = \sqrt{\alpha_1\alpha_2}$$

(4.27)

The resulting equations for a binary mixture are

$$\ln(K_1'p_1) = \ln\left(\frac{X_1\beta_1}{\sigma - \beta_{12}}\right) + \left(\frac{\beta_1}{\sigma - \beta_{12}}\right) - \frac{2}{\sigma RT}(\alpha_1 X_1 + \alpha_{12}X_2)$$

$$\ln(K_2'p_2) = \ln\left(\frac{X_2\beta_2}{\sigma - \beta_{12}}\right) + \left(\frac{\beta_2}{\sigma - \beta_{12}}\right) - \frac{2}{\sigma RT}(\alpha_2 X_2 + \alpha_{12}X_1)$$

(4.28)

where σ is the average area/molecule which is proportional to the reciprocal of total adsorbed phase concentration. Danner and Choi[49] found that these equations give a good correlation of the binary equilibrium data for C_2H_6-C_2H_4 on 13X sieve, but the method gave poor results when applied to data for

the same sorbates on 10X sieve.[50] One may speculate that due to the presence of the Ca^{2+} cations there is a greater degree of localization of ethylene on 10X sieve giving more pronounced deviations from ideality, similar to those observed for sorption on 5A sieve.

Dubinin–Polanyi Theory

The Dubinin–Polanyi theory was extended to binary mixtures by Bering, Serpinsky, and Surinova.[51] It was suggested that if the characteristic curves for the single components are given by Eq. (3.107) then the curve for the mixture should be given by

$$\frac{(q_1 + q_2)V_m}{W_0} = \exp\{-k\epsilon^2\} \tag{4.29}$$

where

$$V_m = X_1\bar{V}_1 + X_2\bar{V}_2$$

$$\frac{1}{\sqrt{k}} = \frac{X_1}{\sqrt{k_1}} + \frac{X_2}{\sqrt{X_2}} \tag{4.30}$$

$$\epsilon = -RT\ln\left(\frac{p_1 + p_2}{p_{s12}}\right)$$

and p_{s12} is the equilibrium vapor pressure for the bulk mixture of both components which has the same composition as that of the equilibrium vapor over the adsorbent. Since the characteristic curve relates only the total sorbate concentration to the total equilibrium pressure, an additional relation is needed to define the system. Bering et al.[51] suggested using the Lewis equation [Eq. (4.14)] and showed that on this basis a good correlation was obtained for the binary equilibrium data for ethylchloride-diethylether and chloroform-diethylether on activated carbon. Although the approach is in effect a semiempirical correlation, it is relatively straightforward and could prove practically useful. The extent to which it can be applied to sorption on more polar adsorbents such as the zeolites does not appear to have been examined.

Ideal Adsorbed Solution Theory[15]

If the adsorbed phase is thermodynamically ideal, it is possible to derive the equilibrium relationships for an adsorbed mixture directly from the pure-component isotherms using the methods outlined in Section 3.4 without postulating a specific model for the adsorbed phase. For an ideal binary system Eq. (3.49) becomes

$$p_1 = p_1^0(\pi)X_1, \qquad p_2 = p_2^0(\pi)X_2 \tag{4.31}$$

Integration of the pure-component isotherm according to the Gibbs equation [Eq. (3.50)] yields, for each component, the relationship between spreading pressure and equilibrium pressure:

$$\frac{\pi_1^0 \mathscr{A}}{RT} = f_1(p_1^0), \qquad \frac{\pi_2^0 \mathscr{A}}{RT} = f_2(p_2^0) \tag{4.32}$$

and for mixing at constant temperature and spreading pressure:

$$\pi_1^0 = \pi_2^0 = \pi_{\text{mixture}} \tag{4.33}$$

We also have

$$X_1 + X_2 = 1.0, \qquad Y_1 + Y_2 = 1.0 \tag{4.34}$$

giving seven equations relating the nine unknowns $(P, X_1, X_2, Y_1, Y_2, p_1^0, p_2^0, \pi_1^0, \pi_2^0)$ so that if two independent variables, for example, P and Y_1 are specified, all other variables may be calculated. These relationships are shown in Figure 4.20. The total adsorbed phase concentration follows from the principle that for an ideal solution there is no change in the area/molecule on mixing:

$$\frac{1}{q_1 + q_2} = \frac{X_1}{q_1^0} + \frac{X_2}{q_2^0} \quad (\text{constant } T \text{ and } \pi) \tag{4.35}$$

Prediction of the mixture isotherm in this way requires experimental single-component isotherm data for the less strongly adsorbed species up to pres-
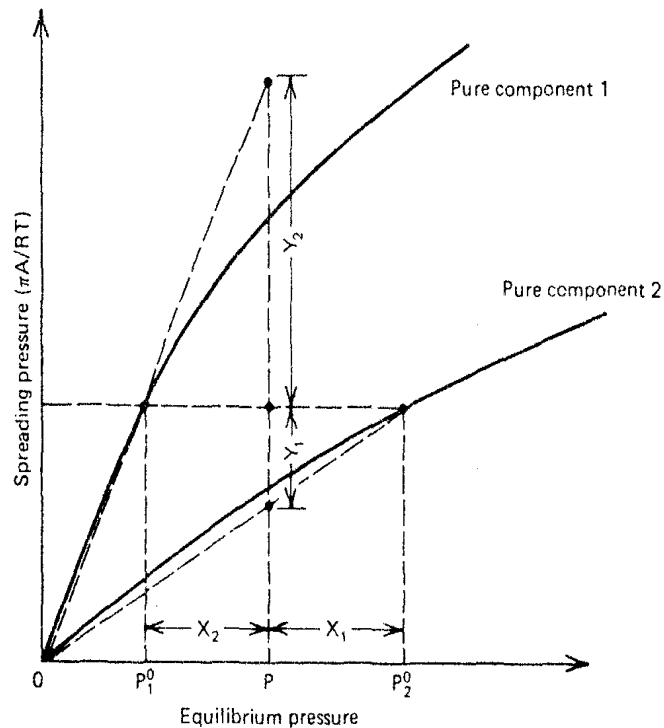
FIGURE 4.20. Calculation of mixture adsorption equilibria from pure-component spreading pressures.[52]

TABLE 4.5. Some Systems Showing Ideal Adsorbed Solution Behavior

Reference	Sorbate	Sorbent
Sorial et al.[59]	O_2-N_2	5A
Glessner and Myers[53]	C_2H_6-nC_4H_{10}	5A
Danner and Choi[49]	C_2H_6-C_2H_4	13X
Myers and Prausnitz[52]	CO-O_2	Silica gel
	C_2H_4-CO_2	Active carbon
	C_3H_8-C_3H_6	Silica gel
	CH_4-C_2H_6	Active carbon
Kaul[55]	CH_4-C_2H_6-C_2H_4	Active carbon[a]
	C_2H_4-C_2H_6-C_3H_6	

[a] Data of Costa et al.[56] The original authors claimed that their data could not be accounted for on the basis of the ideal adsorbed solution theory but this conclusion has been shown to be incorrect.[55]

sures exceeding the total pressure for the binary mixture. However, such data are generally easily obtained.

At first sight the assumption of ideal behavior in the adsorbed phase seems highly improbable, but it has been shown that a number of systems conform closely to this model. Some examples are listed in Table 4.5 but by no means all adsorbed mixtures show ideal behavior. Glessner and Myers[53] observed
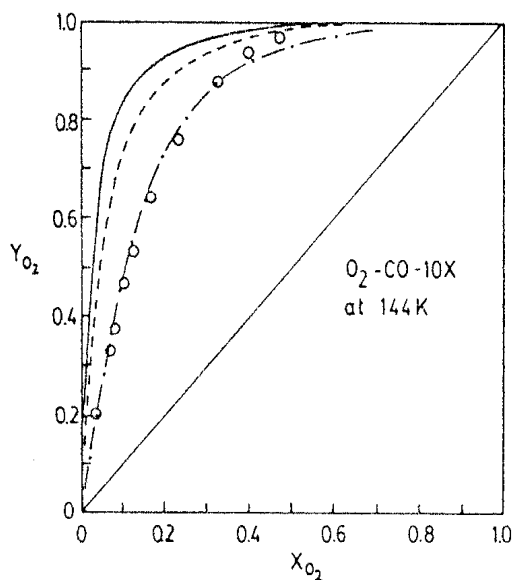
FIGURE 4.21. X–Y diagram for adsorption of O_2-CO on 10X zeolite at 144 K, 760 torr, showing comparison of experimental data of Danner and Wenzel[54] (○), with theoretical predictions of ideal adsorbed solution theory (----), vacancy solution theory without sorbate–sorbate interaction (——————), and vacancy solution theory with sorbate–sorbate interaction (—·—·—·—). (Reprinted with permission from ref. 55. Copyright 1984 American Chemical Society.)

significant deviations from ideality in the system C_2H_6-CO_2-5A sieve and similar deviations were observed by Holborow and Loughlin[42,43] for C_2H_4-C_3H_8, C_2H_4-cycloC_3H_6, and C_2H_4-CO_2 in 5A. Examples of some nonideal systems are shown in Figures 4.18, 4.19, and 4.21. For C_2H_4-C_3H_8-5A (Figure 4.18) the predictions of ideal adsorbed solution theory and the simple statistical model [Eq. (3.102)] are similar and neither theory correctly predicts the formation of an azeotrope which is shown clearly by the experimental data.

Vacancy Solution Theory

The assumptions of the ideal adsorbed solution theory are of limited applicability, and the theory cannot therefore provide a general method for the prediction of binary or multicomponent equilibria from single-component data. By contrast, the vacancy solution theory[57] depends on only the most general assumptions concerning the nature of the adsorbed phase. The adsorption equilibrium constant, saturation capacity, and the parameters giving the concentration dependence of the activity coefficients may be derived in a straightforward manner from the single-component isotherm. The theory is summarized in Section 3.4. The prediction of the relevant parameters for the mixture depends on well-established principles derived from solution thermodynamics and although the algebra may be tedious, the computations are straightforward.

This theory has been shown to provide a good representation of the experimental data for a variety of different systems, some of which are listed in Table 4.6. However, the majority of the systems for which this approach has been tested show only modest deviations from ideality. For example the behavior of the systems O_2-N_2, O_2-CO, and N_2-CO on 10X can all be

TABLE 4.6.   Systems to which Vacancy Solution Model Has Been Successfully Applied

Reference	Sorbate	Sorbent
Suwanayuen and Danner[57]	CH_4-C_2H_6 C_2H_4-C_2H_6 C_2H_6-C_3H_8 CO_2-C_2H_4	Silica gel
	O_2-$N_2{}^a$ O_2-CO^a N_2-CO^a	10X
Kaul[55]	CH_4-C_2H_6-C_2H_4 C_2H_4-C_2H_6-C_3H_6	Active carbon
Hyun[58]	iC_4H_{10}-C_2H_4	13X

[a] For these systems the deviations of the binaries from the predictions of the vacancy solution model are significant and the deviations of the ternaries are even more pronounced.[55]
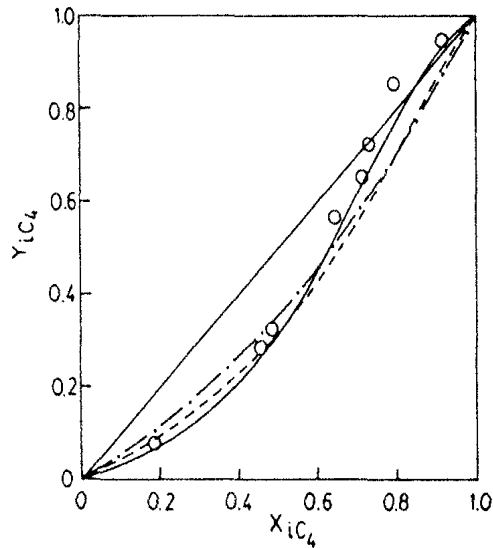
FIGURE 4.22. $X-Y$ diagram for adsorption of isobutane-ethylene on 13X sieve at 50°C, 20 psi (absolute), showing comparison of predictions from statistical model (----), ideal adsorbed solution theory (—·—·), and vacancy solution model (———) (without sorbate–sorbate interaction coefficient) with experimental data of Hyun. (Reprinted with permission from ref. 58. Copyright 1982 American Chemical Society.)

accounted for as well, if not better, by the simple statistical model[57] while the silica gel and active carbon systems are well correlated by the ideal adsorbed solution theory.[55] By contrast the system C_2H_4-iC_4H_{10}-13X shows the formation of an azeotrope, and the data for this sytem are not well predicted by either the ideal adsorbed solution theory or the statistical model (see Figure 4.22). For this system the predictions of the vacancy solution theory are significantly better than those of the other theories, even when no cross coefficient is included [see Eq. (3.70)], but at higher concentrations it is generally necessary to include the cross coefficient in order to obtain a good fit of the binary isotherms, as may be seen from Figure 4.21. Although approximate methods of estimation for the cross coefficients are available, this appears to be the most severe limitation of the vacancy solution theory.

Comparison of Models

Comparisons between the binary isotherm predictions derived from the varous theoretical approaches have been presented by Danner and Choi[49] for C_2H_6-C_2H_4-13X sieve, by Kaul[55] for mixtures of O_2, CO, CH_4, C_3H_6, etc., on activated carbon, and by Sorial, Granville, and Daly[59] for O_2-N_2-5A sieve (see Section 11.3). When the molecular volumes of both components are similar, there is little difference between the predictions of the ideal adsorbed solution theory and the simple statistical model as is to be expected from Eqs. (4.17)–(4.26). Both approaches generally give good predictions for sorption of mixtures of saturated hydrocarbons and other nonpolar species. However, the

extent to which these models can predict the behavior of binary hydrocarbon mixtures containing C_2H_4 seems to depend on the adsorbent. Both models give good predictions for the system C_2H_4-C_2H_6-13X but only rather poor predictions for C_2H_4-C_3H_8 and C_2H_4-cycloC_3H_6 in 5A sieve.[42,43] Sorial, Granville, and Daly[59] found that for the system N_2-O_2 on 5A the vacancy solution provides a less accurate prediction than the ideal adsorbed solution theory or the simple statistical model, as may be seen from Figure 4.23. Kaul points out the necessity of including empirical cross coefficients in the vacancy solution model in order to correlate data at high sorbate concentrations but, with the cross coefficients included, the vacancy solution theory is capable of representing large deviations from ideality.[55]

The same is true of the classical Myers-Prausnitz theory with activity coefficients introduced in order to account for nonideality of the adsorbed phase and of the general statistical model [Eq. (4.17)] with the cross coefficients retained as parameters. Since the cross coefficients cannot, as yet, be predicted theoretically from the single-component isotherms, this reduces somewhat the predictive value of these models. However, it has been shown that, for the system N_2-O_2-CO-10X, the vacancy solution theory with the cross coefficients evaluated from limited binary data provides a good prediction of the ternary equilibrium data.[55] The same approach may be extended to multicomponent systems provided data for all constituent binaries are available. The vacancy solution theory thus provides a practically useful means of data correlation and makes possible the prediction of multicomponent equilibrium behavior from binary data. The potential for the application of classical solution theory or of the statistical models in a similar way has not yet been investigated to the same extent.
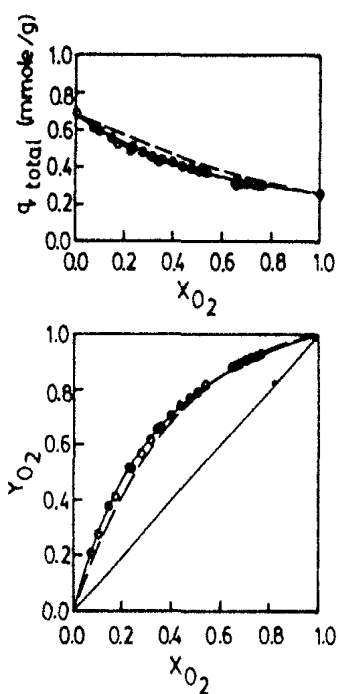
FIGURE 4.23. Equilibrium data for O_2-N_2 on 5A sieve at 278 K, 1.7 bar, showing comparison of experimental data and predictions from ideal adsorbed solution theory (————), the statistical model (----), and vacancy solution theory (—·—). In the $X-Y$ diagram the curves for the statistical and IAST models coincide. From Sorial, Granville and Daly[59] copyright 1983, Pergamon Press Ltd.

4.7. ADSORPTION FROM THE LIQUID PHASE

Despite its industrial importance, adsorption from the liquid phase has been studied much less extensively than adsorption from the vapor phase. There is no difference in principle between adsorption from liquid and vapor phases since, thermodynamically, the adsorbed phase concentration in equilibrium with a liquid must be precisely the same as that which is in equilibrium with the saturated vapor. The differences arise in practice because in adsorption from the liquid phase one is almost invariably concerned with high adsorbed phase concentrations close to the saturation limit. The simple model isotherms, developed primarily to describe adsorption from the vapor phase, are at their best at low sorbate concentrations and become highly unreliable as saturation is approached. Such models are therefore of only very limited applicability for the correlation of liquid phase adsorption data.

The classical thermodynamic approach has been applied to liquid phase adsorption by Larionov and Myers[60] and by Minka and Myers.[61] It was shown that for sorption of carbon tetrachloride-isooctane and benzene-carbon tetrachloride on aerosil the adsorbed solutions show approximately ideal behavior whereas adsorbed mixtures of benzene, ethyl acetate, and cyclohexane on activated carbon showed appreciable deviations from ideality. However, it is shown that the activity coefficients and hence the adsorption equilibrium data for the ternary systems may be successfully predicted, by classical methods, from data for the constituent binaries.

In unpublished work the generalized statistical model [Eq. (4.17)] has been successfully applied to the correlation of liquid phase adsorption equilibrium data for C_8 aromatics on faujasite zeolites. For these systems the saturation limit corresponds to approximately three molecules/cage, and at equilibrium with the liquid the adsorbent is essentially saturated so that each cage can be assumed to contain three sorbate molecules. This simplifies the model since only the terms corresponding to $i + j = 3$ in Eq. (4.17) need be retained, and the expression for the separation factor, assuming an ideal binary fluid phase, becomes

$$\frac{\alpha_{12}}{k_1/k_2} = \frac{1 + 2A_{21}\left(\dfrac{k_2 Y_2}{k_1 Y_1}\right) + A_{12}\left(\dfrac{k_2 Y_2}{k_1 Y_1}\right)^2}{\left(\dfrac{k_2 Y_2}{k_1 Y_1}\right)^2 + 2A_{12}\left(\dfrac{k_2 Y_2}{k_1 Y_1}\right) + A_{21}} \tag{4.36}$$

where $k_1 = K_1 A_{31}^{1/3}$, $k_2 = K_2 A_{32}^{1/3}$. If the cross coefficients are unity ($A_{12} = A_{21} = 1.0$) this expression reduces simply to a constant separation factor given by $\alpha_{12} = k_1/k_2$. However, if the cross coefficients are not unity, the separation factor may be strongly concentration dependent. The same approach may be extended to ternary systems and has been shown to provide a good prediction of experimental ternary data using the cross coefficients derived from data for the constituent binaries.

REFERENCES

1. R. M. Barrer and D. E. W. Vaughan, *J. Phys. Chem. Solids* **32**, 731 (1971).

2. W. Schirmer, G. Friedrich, A. Grossman, and H. Stach, in *Molecular Sieves*, Proceedings of the First International Conference on Molecular Sieves, London, 1967. Society of Chemical Industry, London, 1968.

3. R. I. Derrah and D. M. Ruthven, *Can. J. Chem.* **53**, 996 (1975).

4. R. M. Barrer and S. Wasilewski, *Trans. Faraday Soc.* **57**, 1140 and 1153 (1961).

5. I. H. Doetsch, D. M. Ruthven, and K. F. Loughlin, *Can. J. Chem.* **52**, 2717 (1974).

6. J. R. Lacher, *Proc. Roy. Soc.* **A161**, 525 (1937).

7. R. H. Fowler and E. A. Guggenhiem, *Statistical Thermodynamics*. Cambridge University Press, Cambridge, 1939.

8. E. Cohen de Lara and R. Kahn, *Adsorption of Hydrocarbons in Zeolites*, Preprints of Workshop held at the Academy of Sciences of the GDR, November 1982, Vol. 2, p. 60. *See also Proceedings of the Sixth International Conference on Zeolites, Reno, Nevada, July 1983*, Butterworths, Guildford, England, 1984.

9. D. M. Ruthven, *Nature Phys. Sci.* **232**(29), 70 (1971).

10. D. M. Ruthven and K. F. Loughlin, *J. Chem. Soc. Faraday Trans. I* **68**, 696 (1972).

11. D. M. Ruthven, K. F. Loughlin, and R. I. Derrah, *J. Chem. Soc. Faraday Trans. I* **68**, 1947 (1972).

12. D. M. Ruthven, *AIChE J.* **22**, 753 (1976).

13. B. Coughlin and S. Kilmartin, *J. Chem. Soc. Faraday Trans. I* **71**, 1809 (1975).

14. B. Coughlin, J. McEntee, and R. G. Shaw, *J. Colloid Sci.* **52**, 386 (1975).

15. J. L. Zuech, A. L. Hines, and E. D. Sloan, *Ind. Eng. Chem. Process Design Develop.* **22**, 172 (1983).

16. D. M. Ruthven, *Zeolites* **2**, 242 (1982).

17. M. Goddard and D. M. Ruthven, Engineering Foundation Conference on Fundamentals of Adsorption, Schloss Elmau, Bavaria, May 1983; *Proceedings of the Sixth International Conference on Zeolites, Reno, Nevada, July 1983*, Butterworths, Guildford, England, 1984.

18. M. M. Dubinin, *Adv. Chem.* **102**, 62 (1971).

19. R. M. Barrer and J. A. Davies, *Proc. Roy. Soc.* **A320**, 289 (1970).

20. R. M. Barrer and B. Coughlin, in *Molecular Sieves*, Proceedings of the First International Conference on Zeolites, London, 1967. Society of Chemical Industry, London, 1968.

21. A. V. Kiselev, *Adv. Chem.* **102**, 37 (1971).

22. R. M. Barrer and P. J. Reucroft, *Proc. Roy. Soc.* **A258**, 431 and 449 (1960).

23. A. A. Huang and I. Zwiebel, *Adv. Chem.* **121**, 374 (1973).

24. W. Schirmer, K. H. Sichert, M. Bulow, and A. Grossmann, *Chem. Techn.* **23**, 476 (1971).

25. N. N. Avgul, A. G. Bezus, and O. M. Dzhigit, *Adv. Chem.* **102**, 184 (1971).

26. D. M. Ruthven, *Separation and Purification Methods* **5**(2), 189 (1976).

27. T. Masuda, K., Tsutsumi, and H. Takahashi, *Proceedings of the Fifth International Conference on Zeolites, Naples, June 1980*, L. V. C. Rees (ed.). Heyden, London, 1980, p. 483.

28. S. S. Khvoshchev, V. E. Skazyvaev, and E. A. Vasiljeva, *Proceedings of the Fifth International Conference on Zeolites, Naples, June 1980*, L. V. C. Rees (ed.). Heyden, London, 1980, p. 476.

29. R. M. Barrer and E. V. T. Murphy, *J. Chem. Soc. A*, 2506 (1970).

30. A. V. Kiselev and K. D. Shcherbakova, in *Molecular Sieves*, Proceedings of the First International Conference on Zeolites, London 1967. Society of Chemical Industry, London, 1968.

31. W. Schirmer, *Chem. Techn.* **23**(2), 98 (1971).

32. T. L. Hill, *Introduction to Statistical Thermodynamics.* Addison Wesley, Reading, Mass., 1960.

33. R. M. Barrer, *Zeolites and Clay Minerals.* Academic Press, London, 1978, Chap. 5.

34. C. Kemball, E. K. Rideal, and E. A. Guggehnheim, *Trans. Faraday Soc.* **44**, 952 (1948).

35. D. B. Broughton, *Ind. Eng. Chem.* **40**, 1506 (1948).

36. E. C. Markham and A. F. Benton, *J. Amer. Chem. Soc.* **53**, 497 (1931).

37. W. K. Lewis, E. R. Gilliland, B. Chertow, and W. H. Hoffman, *J. Amer. Chem. Soc.* **42**, 1319 (1950).

38. R. Sips, *J. Chem. Phys.* **16**, 490 (1948).

39. C. M. Yon and P. H. Turnock, *AIChE Symp. Ser.* **67**(117), 75 (1971).

40. R. T. Maurer, *ACS Symp. Ser.* **135**, 73 (1980).

41. D. M. Ruthven, K. F. Loughlin, and K. A. Holborow, *Chem. Eng. Sci.* **28**, 701 (1973).

42. K. A. Holborow and K. F. Loughlin, *ACS Symp. Series* **40**, 379 (1977).

43. K. F. Loughlin, K. A. Holborow, and D. M. Ruthven, *AIChE Symp. Ser.* **71**, (152), 24 (1976).

44. F. Wong, M.Sc. thesis, University of New Brunswick, Fredericton, N.B., Canada, 1979.

45. T. L. Hill, *J. Chem. Phys.* **14**, 46 and 268 (1946).

46. L. White and C. H. Schneider, *J. Amer. Chem. Soc.* **71**, 2593 (1949).

47. L. White, C. H. Schneider, and W. W. Robinson, *J. Amer. Chem. Soc.* **74**, 5796 (1952).

48. S. E. Hoory and J. M. Prausnitz, *Chem. Eng. Sci.* **22**, 1025 (1967).

49. R. P. Danner and E. C. F. Choi, *Ind. Eng. Chem. Fund.* **17**, 248 (1978).

50. R. P. Danner, private communication (1980).

51. B. P. Bering, V. V. Serpinsky, and S. I. Surinova, *Dokl. Akad. Nauk SSSR* **153**(1), 129 (1963).

52. A. L. Myers and J. M. Prausnitz, *AIChE J.* **11**, 121 (1965).

53. A. J. Glessner and A. L. Myers, *C.E.P. Symp. Series* **65**(96), 73 (1969).

54. R. P. Danner and L. A. Wenzel, *AIChE J.* **15**, 515 (1969).

55. B. K. Kaul, AIChE Annual Meeting, Paper 91b, Los Angeles, November 1982, to be published in *Ind. Eng. Chem. Fund.*

56. E. Costa, J. L. Sotelo, G. Calleja, and C. Marron, *AIChE J.* **27**, 5 (1981).

57. S. Suwanayuen and R. P. Danner, *AIChE J.* **26**, 68 and 76 (1980).

58. S. H. Hyun and R. P. Danner, *J. Chem. Eng. Data* **27**, 196 (1982).

59. G. A. Sorial, W. H. Granville, and W. O. Daly, *Chem. Eng. Sci.*, **38**, 1517 (1983).

60. O. G. Larionov and A. L. Myers, *Chem. Eng. Sci.* **26**, 1025 (1971).

61. C. Minka and A. L. Myers, *AIChE J.* **19**, 453 (1973).

62. H. Lechert and W. Schweitzer, *Proceedings of the Sixth International Conference on Zeolites, Reno, Nevada, July 1983,* Butterworths, Guildford, England, 1984.

63. H. Herden, W-D. Einicke, U. Messow, K. Quitzsch, and R. Schöllner, *J. Colloid Interface Sci.* (in press).

5

DIFFUSION IN
POROUS MEDIA

Rates of adsorption and desorption in porous adsorbents are generally con-
trolled by transport within the pore network, rather than by the intrinsic
kinetics of sorption at the surface. Since there is generally little, if any, bulk
flow through the pores, it is convenient to consider intraparticle transport as a
diffusive process and to correlate kinetic data in terms of a diffusivity defined
in accordance with Fick's first equation:

$$J = -D(c)\frac{\partial c}{\partial x} \tag{5.1}$$

Such a definition provides a convenient mathematical representation, but it
does not imply that the diffusivity is independent of concentration, only that it
is not dependent on the concentration gradient. Since the true driving force
for any transport process is the gradient of chemical potential, rather than the
gradient of concentration, ideal Fickian behavior in which the diffusivity is
independent of sorbate concentration is realized only when the system is
thermodynamically ideal.

Pore diffusion may occur by several different mechanisms depending on
the pore size, the sorbate concentration, and other conditions. In fine micro-
pores such as the intracrystalline pores of zeolites, the diffusing molecule
never escapes from the force field of the adsorbent surface and transport
occurs by an activated process involving jumps between adsorption "sites."
Such a process is often called "surface diffusion," but the implication of a
two-dimensional surface is unnecessarily restrictive since the micropore struc-
ture in a zeolite crystal is often three-dimensional. The more general terms
"micropore" or "intracrystalline" diffusion are therefore used here to describe
transport in such systems, while diffusion in larger pores such that the
diffusing molecule escapes from the surface field is referred to as "macropore"
diffusion. This distinction between micropore and macropore diffusion is
useful since, in a zeolitic adsorbent, the diameter of the intracrystalline

micropores is generally much smaller than that of the smallest intercrystalline macropores (See Figure 1.2).

5.1. DRIVING FORCE FOR DIFFUSION

The relationship between the Fickian diffusivity, defined by Eq. (5.1), and the mobility $B(c)$, defined by

$$J = -Bc \frac{\partial \mu}{\partial x} \tag{5.2}$$

is easily derived. Considering equilibrium with an ideal vapor phase:

$$\mu = \mu^0 + RT \ln a = \mu^0 + RT \ln p \tag{5.3}$$

$$\frac{\partial \mu}{\partial x} = RT \frac{\partial \ln a}{\partial x} = RT \frac{d \ln p}{dc} \frac{\partial c}{\partial x} \tag{5.4}$$

$$J = -BRTc \frac{d \ln p}{dc} \frac{\partial c}{\partial x} = -BRT \frac{d \ln p}{d \ln c} \frac{\partial c}{\partial x} \tag{5.5}$$

Comparing Eqs. (5.1) and (5.5) we see that the Fickian diffusivity is given by

$$D = BRT \frac{d \ln p}{d \ln c} = D_0 \frac{d \ln p}{d \ln c} \tag{5.6}$$

where $D_0 = BRT$ is the corrected diffusivity.

In the vapor phase or in a liquid or adsorbed phase at low concentration, Henry's law is obeyed and the activity is directly proportional to concentration. Under these conditions $d \ln a / d \ln c \approx 1.0$ and the diffusivity approaches a constant limiting value. There is no sound theoretical reason to expect the corrected diffusivity to be independent of sorbate concentration at higher concentration levels outside the Henry's law region, although such behavior has been observed experimentally for a number of systems.[1-3] For binary liquid phase systems the concentration dependence of D_0 is generally less pronounced than that of D, but it is still significant in most systems.[4,5]

Experimental Evidence

Direct experimental proof that the true driving force for diffusive transport is the gradient of chemical potential rather than the concentration gradient is provided by the experiments of Haase and Siry[6,7] who studied diffusion in binary liquid mixtures near the consolute point. At the consolute point the chemical potential (and the vapor pressure) are independent of composition so, according to Eq. (5.6), the diffusivity should be zero. The consolute point for the system n-hexane-nitrobenzene occurs at 20°C at a mole fraction 0.422 of nitrobenzene. The system shows complete miscibility above this temperature and forms two separate phases at lower temperatures. Opposite behavior is shown by the system water-triethylamine, for which the consolute tempera-
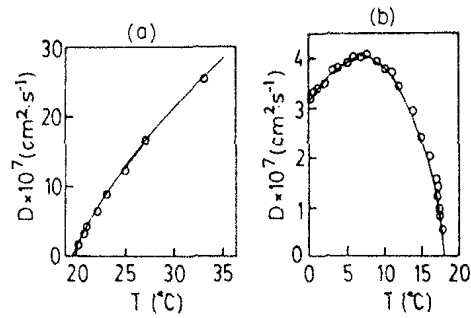
FIGURE 5.1. Variation of Fickian diffusivity with temperature for liquid mixtures of critical composition. (*a*) *n*-hexane-nitrobenzene (mole fraction nitrobenzene = 0.42, consolute temperature, 20°C). (*b*) Water-triethylamine (mole fraction triethylamine = 0.087, consolute temperature . = 18°C. [Reprinted from *Chem. Eng. Sci.* **30**, Turner (ref. 7). Copyright 1975, Pergamon Press, Ltd.]

ture is 18°C at a mole fraction of triethylamine of 0.08. The mixture is completely miscible below 18°C and separates into two phases at higher temperatures. The results of the diffusion measurements are shown in Figure 5.1. In both systems the Fickian diffusivity approaches zero as the consolute temperature is approached, as required by Eq. (5.6). The behavior of the system water-triethylamine is especially noteworthy since the diffusivity actually decreases with increasing temperature as the upper consolute temperature of 18°C is approached. Such behavior, which follows naturally from the assumption of chemical potential as the driving force, cannot be easily accounted for by a strictly Fickian model.

Despite the compelling evidence provided by the Haase and Siry study the contrary view has been expressed that diffusive transport is a stochastic process, for which the true driving force is the gradient of concentration.[8] Implicit in this argument is the assumption that the occurrence of a molecular jump is a random process which occurs with equal *a priori* probability in any direction. Such a model leads directly to Fick's equation [Eq. (5.1)] since the net flux of a particular species in a specified direction will be directly proportional to the difference in concentration over the average jump distance, that is, to the gradient of concentration. In fact, in the presence of a gradient of chemical potential, the jump probabilities are not the same in all directions. To reconcile the stochastic view of diffusive transport with the irreversible thermodynamic formulation requires only the additional assumption that the jump probability is directly proportional to the gradient of chemical potential.

Diffusive Transport and Self-Diffusion

At a specified concentration level the transport diffusivity (D) relating the flux to the concentration gradient, in accordance with Eq. (5.1), is in general different from the self-diffusivity ($\mathscr{D}$) which defines the rate of tracer exchange of marked molecules under equilibrium conditions in a system with no

net concentration gradient. The general form of the relationship may be derived from irreversible thermodynamics.[9,10] Considering self-diffusion of a marked tracer in a mixture of A and A^* we may write for the flux of A[11]:

$$J_A = -L_{AA}\frac{\partial \mu_A}{\partial x} - L_{AA^*}\frac{\partial \mu_{A^*}}{\partial x} \tag{5.7}$$

where $L_{AA}(c_A, c_{A^*})$ and $L_{AA^*}(c_A, c_{A^*})$ are the straight and cross coefficients of irreversible thermodynamics. For diffusive transport in a system containing only molecules of type A we have by comparison with Eq. (5.5)

$$J_A = -RTL_{AA}(c_A, 0)\frac{d\ln a_A}{dc_A}\frac{\partial c_A}{\partial x} \tag{5.8}$$

where $L_{AA}(c_A, 0) = Bc_A$. Assuming an ideal vapor phase it may be shown that the relationship between the transport and self-diffusivities is of the form[10]

$$D(c) = \mathscr{D}(c)\frac{d\ln p}{d\ln c}\left[1 - \frac{c^2}{c_A c_{A^*}}\frac{L_{AA^*}(c_A, c_{A^*})}{L_{AA}(c_A, 0)}\right]^{-1} \tag{5.9}$$

where $c = c_A + c_{A^*}$ is the total concentration of the diffusing species and the transport diffusivity is defined by

$$D(c) = L_{AA}(c_A, 0)RT\frac{d\ln p}{dc_A} = BRT\frac{d\ln p}{d\ln c} \tag{5.10}$$

A slightly modified form of expression was obtained by Ash and Barrer[9] who used a somewhat different definition of the transport diffusivity. If the cross coefficient can be neglected ($L_{AA^*} \approx 0$), Eq. (5.9) reduces to Eq. (5.6) with $D_0 = \mathscr{D}$, which is the familiar Darken equation,[12] originally derived for the interdiffusion of two alloys. While Eq. (5.6), being essentially a definition of D_0, is always valid it is evident that the assumption that $D_0 = \mathscr{D}$ is only true in the limiting case where $L_{AA^*} \to 0$. In general both D_0 and $\mathscr{D}$ are concentration dependent and since both L_{AA^*} and $L_{AA}(c_A, 0)$ are intrinsically positive, one may expect $D_0 \geqslant \mathscr{D}$.

For an activated zeolitic diffusion process, involving transition through a window between two cages, an expression of the same general form as Eq. (5.9) may be derived from simple microdynamic considerations if it is assumed that the interference effect represented by the cross coefficient in Eq. (5.7) arises from the periodic blocking of the window with a probability proportional to the counterdiffusing flux.[13]

5.2. EXPERIMENTAL MEASUREMENT OF DIFFUSIVITIES

Wicke–Kallenbach Method

The classical method of measuring intraparticle or macropore diffusivities is due to Wicke and Kallenbach.[14] The apparatus is shown schematically in Figure 5.2. Knowing the thickness of the pellet and the concentrations and
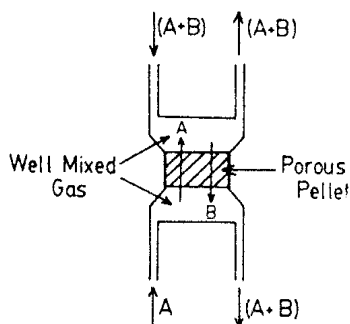
FIGURE 5.2. Schematic diagram showing essential features of the Wicke–Kallenbach apparatus for measuring intraparticle diffusivities.

flow rates of both streams, the fluxes in both directions and hence the effective diffusivity may be calculated. By making measurements over a range of concentrations it is possible, within the transition region, to determine also the relative contributions of Knudsen and molecular diffusion [see Eq. (5.18)].

The method has the advantage that it depends on a steady-state measurement and it is not affected by finite heat transfer. Effective intraparticle diffusivities determined in this way are commonly somewhat smaller than the values derived for the same adsorbent under similar conditions from transient uptake rate measurements. This is because blind pores, which contribute to the flux in a transient measurement, make no contribution in a Wicke–Kallenbach system.

The method is in principle applicable also to the measurement of micropore or intracrystalline diffusivities, but the practical difficulties of mounting and sealing a single small zeolite crystal have hitherto prevented such applications. However, these difficulties have been overcome and the results of two studies have been recently reported[15,16] in which diffusion through a single (100 μm) zeolite crystal, mounted in a metal plate, was measured by this method.

Uptake Rate Measurement

The uptake rate in a particle which is exposed to a step change in the surface concentration of an adsorbable species is determined by the diffusional time constant (D/r^2). The time constant and hence the diffusivity may therefore be determined, in principle, by matching the experimental uptake curve to the appropriate transient solution of the diffusion equation. To determine intraparticle or macropore diffusivities by this method is straightforward since the intrusion of heat transfer effects may be eliminated by the use of sufficiently large adsorbent particles and the effect of nonlinearities may be eliminated by making the experimental measurement over a small differential concentration change. The validity of the isothermal diffusion model may be confirmed by varying the particle size and the concentration step. Details of the relevant solutions for the uptake curve are given in Section 6.2.

The same method is also applicable, in principle, to the measurement of micropore diffusivities in zeolite crystals but, except when micropore diffusion

is relatively slow or the crystals are large, it may be difficult to find experimental conditions such that the uptake rate is controlled by intracrystalline diffusion, rather than by heat transfer or other extracrystalline resistances to mass transfer. In any experimental study it is desirable to confirm directly the dominance of intracrystalline resistance by varying both the configuration of the adsorbent sample and the crystal size, as well as to confirm linearity of the system by varying the concentration step.

Even if the intrusion of heat transfer or bed diffusional resistance cannot be entirely eliminated, it may still be possible to derive values for the diffusional time constant by using the appropriate solution of the diffusion equation. Some relevant solutions to the coupled heat and mass transfer equations for such systems are given in Section 6.3.

The initial rate measurement is sensitive to any intrusion of macropore (bed diffusion) resistance while the long time region of the uptake curve is sensitive to the effects of finite heat transfer resistance and crystal size distribution. In calculating the diffusivity from an experimental uptake curve greatest weight should therefore be assigned to the region of intermediate uptake ($0.2 < m_t/m_\infty < 0.5$). This means that it is generally necessary to use the full solution for the uptake curve [Eq. (6.4)] rather than either of the simplified forms [Eq. (6.6) or (6.8)].

Chromatography

As an alternative to conventional sorption rate measurements it is also possible to derive diffusional time constants from the dynamic response of a packed column to a change in sorbate concentration. In a chromatographic system the broadening of the response peak results from the combined effects of axial dispersion and mass transfer resistance. By making measurements over a range of gas velocities it is possible to separate the dispersion and mass transfer effects and so to determine the effective overall mass transfer coefficient or the diffusional time constant. Further details are given in Section 8.5.

The method is applicable to the measurement of both macropore and micropore time constants; but, if both resistances are significant, it may not be easy to determine their relative importance although, in principle, this can be established by varying the particle size.

Tracer Exchange

All the above methods measure transport diffusivities rather than self-diffusivities. Self-diffusivities may, however, be measured in a modified uptake rate experiment in which the absorbent particle is exposed to a change in the concentration of an isotopically labeled tracer at constant total sorbate concentration. This method is particularly convenient when one of the isotopes is radioactive since the activity count then provides a simple and accurate means of monitoring the concentration of the labeled species. Self-

diffusion of CO_2 in 5A zeolite was studied in this way by Sargent and Whitford.[17]

Nonradioactive isotopes may also be used but are somewhat less convenient since it is then necessary to follow the progress of the exchange by mass spectrometric analysis of the surrounding vapor. This method was used by Quig and Rees[18] and Lindsley and Rees[19] to study the self-diffusion of hydrocarbons in zeolite A and chabazite.

Nuclear Magnetic Resonance (NMR) Methods

NMR techniques provide a somewhat more convenient and widely used method for the measurement of self-diffusivities. The method is, however, restricted to species such as hydrocarbons which contain a sufficiently high concentration of unpaired nuclear spins. In comparing the results of NMR and uptake rate measurements it follows from Eqs. (5.6) and (5.9) that one should compare the NMR self-diffusivity with the corrected diffusivity from the uptake rate measurements. Exact agreement can be expected only when the cross coefficient is zero, but this is normally a good approximation at low concentrations.

Relaxation Measurements

In the earlier NMR studies[20] the self-diffusivity was derived indirectly from measurements of the spin-lattice relaxation time over a range of temperatures. The correlation time τ_c, which is roughly equivalent to the average time between successive molecular jumps, may be derived from such information and the self-diffusivity is then estimated from the Einstein relation using an assumed mean square jump length $\bar{\lambda}^2$. For an isotropic cubic lattice

$$\mathscr{D} = \frac{1}{6} \frac{\bar{\lambda}^2}{\tau_c} \tag{5.11}$$

The obvious disadvantage of this approach is that the mean square jump distance is seldom known with any accuracy and cannot be easily estimated *a priori*.

Pulsed Field Gradient (PFG) Method

The pulsed field gradient method of self-diffusion measurement was originally developed by Stejskal and Tanner[21] for the measurement of diffusion in liquids. The self-diffusivity is measured directly and no prior estimate of jump distance is needed so the results are, in principle, more reliable. The development and application of this technique to the study diffusion in zeolites and zeolitic adsorbents has been achieved largely through the researches of Pfeifer, Kärger, and their co-workers at the Karl Marx University in Leipzig.
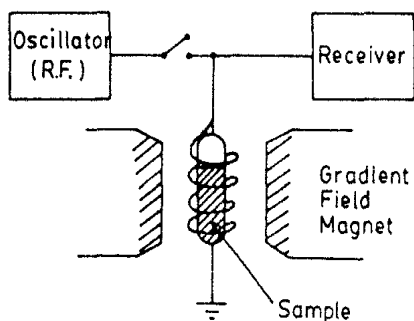
FIGURE 5.3. Schematic diagram showing the principal features of NMR pulse field gradient spectrometer.

Application of this method to the measurement of macropore diffusivities presents no great problem since effective macropore diffusivities [Eq. (6.16)] are commonly of the same order as liquid phase diffusivities.[25] To adapt the method to the measurement of intracrystalline diffusion proved more difficult since intracrystalline diffusivities are commonly much smaller than liquid diffusivities, necessitating the use of very large magnetic field gradients.[22,23]

The essential features of the PFG apparatus are shown in Figure 5.3 and the principle of operation is illustrated in Figure 5.4. A pulsed magnetic gradient field is applied to a sample in which the nuclear spins have been excited by a radio frequency magnetic pulse of suitable duration and intensity. This starts the nuclear spins precessing with an angular velocity determined by the position of the molecule at time zero. After a known time interval the gradient pulse is reversed. If there were no diffusion, the second gradient pulse would exactly counteract the effect of the first pulse, leaving all spins in phase. However, as a result of molecular migration the cancellation is incomplete and
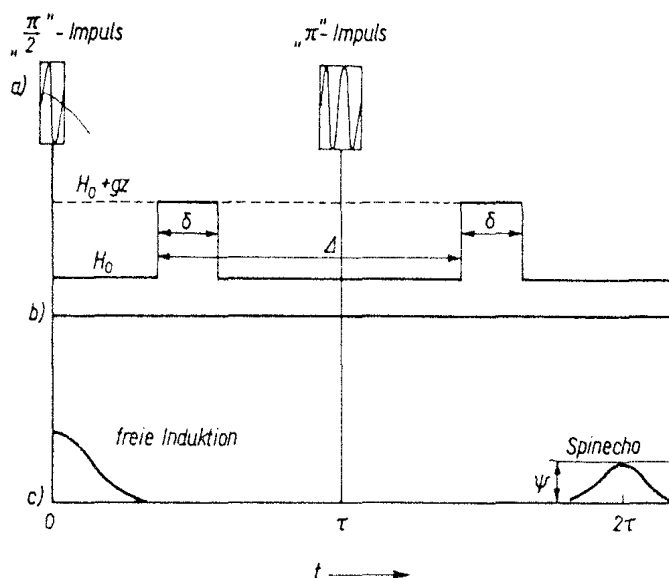
FIGURE 5.4. The sequence of pulses used in the pulsed field gradient self-diffusion measurement. (a) rf pulse; (b) Gradient pulse sequence (90°, 180°); (c) Response signal. (From ref. 22, with permission.)

the attenuation of the signal provides a direct measurement of the mean square displacement during the known time interval between gradient pulses. In practice, instead of reversing the gradient pulse it is easier to use two rf pulses with a phase difference of 90°, as sketched in Figure 5.4. The net effect of such a pulse sequence is the same as that of reversing the gradient pulse. A number of conditions concerning the duration of the time interval relative to the relaxation time must be fulfilled and the rms displacement must be less than the crystal diameter.[22,24] The result of these limitations is to restrict the method to relatively rapidly diffusing systems ($\mathscr{D} > \sim 10^{-8}$ cm^2 s^{-1}).

The variation in apparent diffusivity with temperature and crystal size is of the form illustrated in Figure 5.5. At lower temperatures and in larger crystals the rms displacement is always smaller than the crystal diameter, and under these conditions the intracrystalline diffusivity is measured directly. At higher
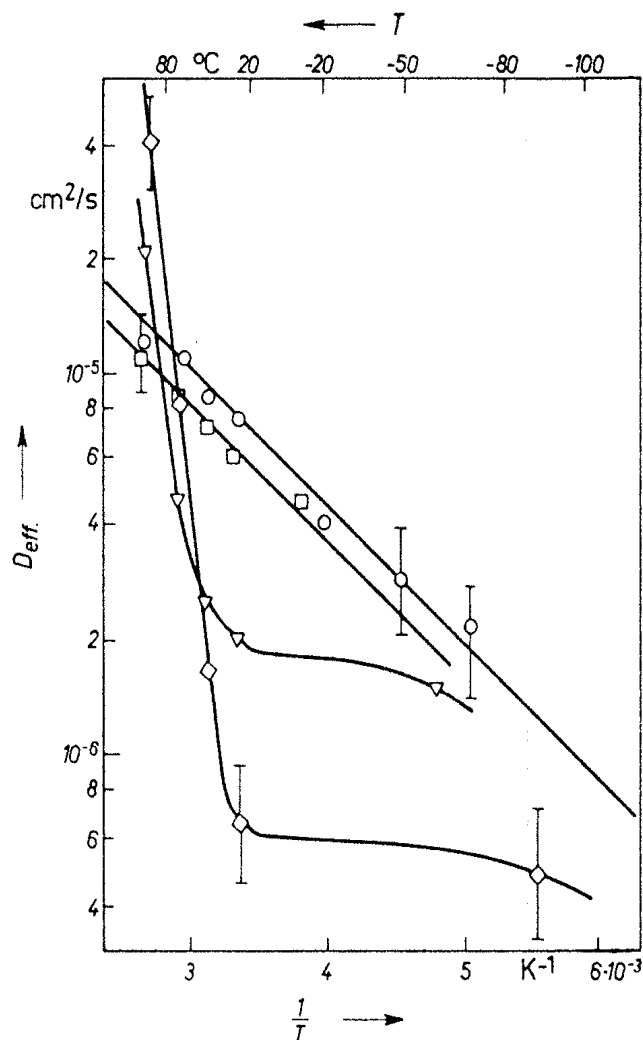
FIGURE 5.5. Arrhenius plot showing results of NMR diffusion measurements for n-hexane in NaX zeolite crystals. $r_c = 0.9$ μm, $\lozenge$ ($\Theta = 0.49$); $r_c = 2$ μm, ∇ ($\Theta = 0.39$); $r_c = 9$ μm, $\square$ ($\Theta = 0.35$); $r_c = 25$ μm, $\bigcirc$ ($\Theta = 0.29$). (Saturation limit $= 215$ mg/g.) (From ref. 22, with permission.)

temperatures and for smaller crystals the molecule escapes from the crystal during the time interval of the measurement and the apparent diffusivity corresponds to the long-range effective extracrystalline or macrodiffusivity. In the intermediate region there is a plateau region of restricted diffusion in which the molecules do not have sufficient energy to escape from the crystal and are reflected from the surface. The diffusivity at the plateau is simply related to the crystal size and this provides a direct check on the consistency of the method. Other simple tests such as blocking the intercrystalline space with CCl_4 have also been performed in order to confirm that the NMR signal is associated with intracrystalline rather than extracrystalline diffusion.[24]

Combining the PFG self-diffusion measurement with a measurement of the correlation time provides a means of determining directly the mean jump distance.

Fast-Tracer Desorption

There are many zeolitic systems in which intracrystalline diffusion is too slow to measure directly by the PFG method. A modification of this method which makes it possible, under certain conditions, to measure much slower diffusion processes has recently been introduced by Kärger.[27,28] By increasing the time interval in a PFG experiment, an increasing fraction of the molecules escapes from the crystal during the time interval of the measurement. If there is a sufficiently large difference between the intracrystalline and effective extracrystalline diffusivities, it becomes possible to determine the fraction escaping during the time interval of the measurement from the variation of the signal attenuation with the intensity of the gradient pulse. By varying the time interval it is then possible to determine the desorption curve for the spin-labeled molecules under equilibrium conditions. The diffusional time constant is found by matching this desorption curve to Eq. (6.4). Comparison with time constants measured directly by the PFG method can provide direct evidence concerning the significance of any "surface barrier" to mass transport.

5.3. DIFFUSION IN MACROPORES

Macropore diffusion has been widely studied in connection with its influence on the overall kinetics of heterogeneous catalytic reactions.[29] Four distinct mechanisms of transport may be identified: molecular diffusion, Knudsen diffusion, Poiseuille flow, and surface diffusion. The effective macropore diffusivity is thus a complex quantity which often includes contributions from more than one mechanism. Although the individual mechanisms are reasonably well understood, it is not always easy to make an accurate a priori prediction of the effective diffusivity since this is strongly dependent on the details of the pore structure.

In analyzing macropore diffusion it is usually assumed that the transport occurs only through the pores and the flux through the solid can be neglected. It is therefore convenient to define a pore diffusivity (D_p) based on the pore cross-sectional area:

$$J = -\epsilon_p D_p \frac{\partial c}{\partial x} \qquad (5.12)$$

D_p is smaller than the diffusivity in a straight cylindrical pore as a result of two effects; the random orientation of the pores, which gives a longer diffusion path and a reduced concentration gradient in the direction of flow, and the variation in the pore diameter. Both these effects are commonly accounted for by a "tortuosity factor" (τ):

$$D_p = \frac{D}{\tau} \qquad (5.13)$$

where D is the diffusivity under the same conditions in a straight cylindrical pore. Since the tortuosity is essentially a geometric factor it should be independent of either temperature or the nature of the diffusing species. For straight, randomly oriented, cylindrical pores it may be shown that $\tau = 3$, the mean value of $\cos^{-2}\theta$ averaged with equal probability over all possible orientations.[30,31] The same value was derived by Dullien for diffusion in a cubic pore structure built up from the same repeating unit.[32] Experimental tortuosity factors generally fall within the range 2–6. There is a general correlation between tortuosity and porosity (tortuosity varies inversely with porosity) and the higher tortuosity factors or low effective macropore diffusivities are generally found for highly compacted low-porosity pellets. The higher values may also reflect the intrusion of some intracrystalline diffusional resistance while values of less than 2.0, which are occasionally observed, may reflect either surface diffusion or a significant contribution to long-range transport from the intracrystalline flux.[26]

Dullien[33] has shown that, if the pore structure is characterized in detail, a reasonably accurate theoretical prediction of the tortuosity may be made, but this requires detailed measurement of both the pore shape and pore size distribution. However, it is generally simpler and more accurate to treat the tortuosity as an empirical constant which is determined experimentally for any particular adsorbent.

Molecular Diffusion (Gases)

If transport within the macropores occurs only by molecular diffusion, the pore diffusivity is given by

$$D_p = \frac{D_m}{\tau} \qquad (5.14)$$

where D_m is the molecular diffusivity which, for gaseous systems, may be estimated with confidence from the Chapman–Enskog equation.[34] For a

binary gas mixture

$$D_m = \frac{0.00158 T^{3/2} (1/M_1 + 1/M_2)^{1/2}}{P\sigma_{12}^2 \Omega(\epsilon/kT)} \quad (\mathrm{cm^2\,s^{-1}}) \quad (5.15)$$

where M_1, M_2 are the molecular weights, P is the total pressure in atmospheres, $\sigma_{12} = \frac{1}{2}(\sigma_1 + \sigma_2)$ is the collision diameter from the Lennard-Jones potential, expressed in Angstroms, and Ω is a function of ϵ/kT where $\epsilon = \sqrt{\epsilon_1\epsilon_2}$ is the Lennard-Jones force constant and k is the Boltzmann constant. Tabulations of the force constants are given by Hirschfelder, Curtis, and Bird[34] and by Satterfield.[29] The theory of diffusion in multicomponent mixtures is more complex, but a reasonably reliable estimate of the diffusivity of an individual component may be obtained from the simple approximate relationship

$$\frac{D_{1m}}{1 - Y_1} = \left(\sum_{j=2}^{n} \frac{Y_j}{D_{1j}} \right)^{-1} \quad (5.16)$$

The molecular diffusivity of a binary gas mixture is essentially independent of composition. In multicomponent mixtures the diffusivity becomes, in principle, concentration dependent, but such variations are generally relatively small so that the assumption of a concentration-independent diffusivity is usually a good approximation for most gaseous systems. Other important general conclusions which follow from Eq. (5.15) are that the molecular diffusivity is inversely dependent on total pressure and proportional to a low power of temperature. The combined effect of the $T^{3/2}$ factor in the numerator and the temperature-dependent function $\Omega(\epsilon/kT)$ in the denominator yields an overall temperature dependence of approximately $T^{1.7}$.

Molecular Diffusion (Liquids)

Diffusion in liquid-filled pores occurs by essentially the same mechanism as in gaseous systems. However, methods of correlation and prediction are less accurate since the fundamental theory of diffusion in the liquid phase is less well developed than the theory of molecular diffusion in the vapor phase. Correlations based on the Stokes–Einstein and Nernst–Einstein equations must be treated with caution. A wide range of empirical and semiempirical correlations is available[4,5,35] but it is generally necessary to select the appropriate correlation with care, taking due account of the nature of the components. Predictive methods are at their best for mixtures of two nonpolar species and at their worst for mixtures of a polar and nonpolar species.

In nonideal liquid mixtures both the transport diffusivity and the self-diffusivity are commonly concentration dependent. The thermodynamic correlation factor seldom exceeds 10 so the difference between corrected and uncorrected diffusivities in the liquid phase is much smaller than for an

adsorbed phase (see Section 5.4). At ordinary temperatures liquid phase diffusivities generally fall within the range 10^{-4}–10^{-6} cm^2 s^{-1}, except for polymers and other very large molecules, so the range of variation is also much smaller than that commonly encountered in adsorbed phases.

Knudsen Diffusion

In molecular diffusion the resistance to flow arises from collisions between diffusing molecules. The effect of the pore is merely to reduce the flux as a result of geometric constraints which are accounted for by the tortuosity factor. Molecular diffusion will be the dominant transport mechanism whenever the mean free path of the gas (i.e., the average distance traveled between molecular collisions) is small relative to the pore diameter. However, in small pores and at low pressure the mean free path is greater than the pore diameter and collisions of molecules with the pore walls occur more frequently than collisions between diffusing molecules. Under these conditions the collisions between molecule and pore wall provide the main diffusional resistance and we have what is known as Knudsen diffusion or Knudsen flow.

When a molecule strikes the pore wall it does not bounce like a tennis ball. Rather the molecule is instantaneously adsorbed and re-emitted in a random direction. The direction in which the molecule is emitted bears no relation to its original direction before the collision and it is this randomness which provides the characteristic feature of a diffusive process.

The Knudsen diffusivity may be estimated from the expression

$$D_K = 9700 r \left(\frac{T}{M} \right)^{1/2} \quad \text{(cm}^2\text{ s}^{-1}\text{)} \tag{5.17}$$

where r is the mean pore radius (cm), T is in kelvin, and M is the molecular weight of the diffusing species. The derivation of this equation together with a full discussion of the Knudsen flow regime are given by Kennard.[36] It is evident that in the Knudsen regime each species diffuses independently so that the diffusivity does not depend on either composition or total gas concentration. The temperature dependence is slight and there is the usual inverse dependence on the square root of molecular weight.

Transition Region

It is evident from the above discussion that there must be a wide range of conditions under which both Knudsen and molecular diffusion are significant. Indeed, in a given adsorbent it is quite possible for molecular diffusion to be dominant in the larger pores while Knudsen flow is dominant in the smaller pores. Because of the dependence of mean free path on pressure, for any given adsorbent and adsorbate there will be a transition from molecular diffusion at high pressure to Knudsen flow at low pressures. In the intermediate regime both wall collisions and intermolecular collisions contribute to the diffusional

resistance and the effective diffusivity depends on both the Knudsen and molecular diffusivities.

Essentially the same expression was derived almost simultaneously by Evans, Watson, and Mason[37] and Scott and Dullien.[38] For a binary gas in a porous solid at constant pressure the combined diffusivity is given by

$$\frac{1}{D} = \frac{1}{D_K} + \frac{1}{D_m}\left[1 - \left(1 + \frac{J_2}{J_1}\right)Y_1\right] \tag{5.18}$$

where J_1, J_2 are the fluxes of components 1 and 2 and Y_1 is the mole fraction of component 1. For equimolar counter diffusion $J_1 = -J_2$ and Eq. (5.18) reduces to the simple reciprocal addition law:

$$\frac{1}{D} = \frac{1}{D_m} + \frac{1}{D_K} \tag{5.19}$$

Although strictly valid only for equimolar counterdiffusion, this equation is often used as an approximation under other conditions.

The conditions under which either Knudsen or molecular diffusion becomes the dominant transport mechanism follow directly $(D_K \gg D_m$ or $D_K \ll D_m)$. Since D_m varies inversely with pressure Eq. (5.19) correctly predicts the transition from Knudsen to molecular diffusion with increasing pressure.

Surface Diffusion

Both the Knudsen and molecular diffusion mechanisms involve flow through the gas phase within the pore. There is in addition the possibility of a direct contribution to the flux from transport through the physically adsorbed layer on the surface of the macropore, and this is referred to as surface diffusion. Although the mobility of the adsorbed phase will generally be much smaller than that of the gas phase, the concentration is very much higher; so, under conditions such that the thickness of the adsorbed layer is appreciable, a significant contribution to the flux is possible. Significant physical adsorption is thus seen as a prerequisite for the contribution from surface diffusion to be noticeable, and this requires temperatures not too far above the boiling point of the species considered. At high temperatures the thickness of the adsorbed layer decreases and any surface flux becomes small compared with the flux through the gas phase.

Direct measurement of surface diffusion is not feasible since the flux due to diffusion through the gas phase is always present in parallel. In order to study surface diffusion it is therefore necessary to eliminate the gas phase contribution. The normal procedure, which is illustrated by the study of Schneider and Smith,[39] involves making measurements over a wide range of temperatures. The flux through the gas phase is determined from the high temperature measurements since under these conditions the surface flux can be neglected. The flux through the gas phase at the lower temperature is then found by extrapolation and subtracted from the measured flux in order to estimate the

TABLE 5.1.   Surface Diffusion of Propane on Silica Gel

Temperature (°C)	$D_e \times 10^3$ (cm^2 s^{-1})	$D_K \times 10^3$ (cm^2 s^{-1})	$\left(\dfrac{1 - \epsilon_p}{\epsilon_p}\right) KD_s \times 10^3$ (cm^2 s^{-1})	$D_s \times 10^3$ (cm^2 s^{-1})
50	1.54	0.42	1.12	0.74
75	1.45	0.44	1.01	1.31
100	1.33	0.45	0.88	1.95
125	1.22	0.47	0.75	2.8

Source: From ref. 39.

surface flux. Surface diffusion is significant only in small diameter pores in which the flux through the gas phase can generally be attributed entirely to Knudsen diffusion, and this simplifies considerably the extrapolation.

Representative data for surface diffusion of propane in a silica gel adsorbent (average pore diameter 22 Å), taken from the paper of Schneider and Smith,[39] are summarized in Table 5.1. The overall diffusivity is given by

$$D = D_K + \left(\frac{1 - \epsilon_p}{\epsilon_p}\right) KD_s \tag{5.20}$$

Surface diffusion is an activated process which is in some ways analogous to micropore or intracrystalline diffusion. The temperature dependence may be correlated by an Eyring equation:

$$D = D_* e^{-E/RT} \tag{5.21}$$

The contribution of surface diffusion to the overall effective diffusivity, however, depends on the product KD_s rather than on the surface diffusivity alone [Eq. (5.20)]. Since the diffusional activation energy (E) is generally smaller than the heat of sorption, this product, and therefore the relative contribution of surface diffusion, normally decreases with increasing temperature. Such a trend is illustrated by the data given in Table 5.1.

The surface diffusivity is generally found to be strongly concentration dependent, except within the Henry's law region, as illustrated by the data shown in Figure 5.6, taken from the work of Gilliland et al.[40,41] It seems logical to suggest that the concentration dependence probably arises largely from the nonlinearity of the equilibrium relationship [Eq. (5.6)], and in correlating the dependence of diffusivity on concentration and temperature it would have been desirable to eliminate the thermodynamic factor and examine the variation of the corrected diffusivity. However, such an approach was not taken and the diffusivity data were correlated directly with the heat of sorption.[41] It remains to be seen whether or not a correlation for the corrected diffusivity would be more accurate. The surface diffusivities considered vary over 11 orders of magnitude with the highest values being obtained
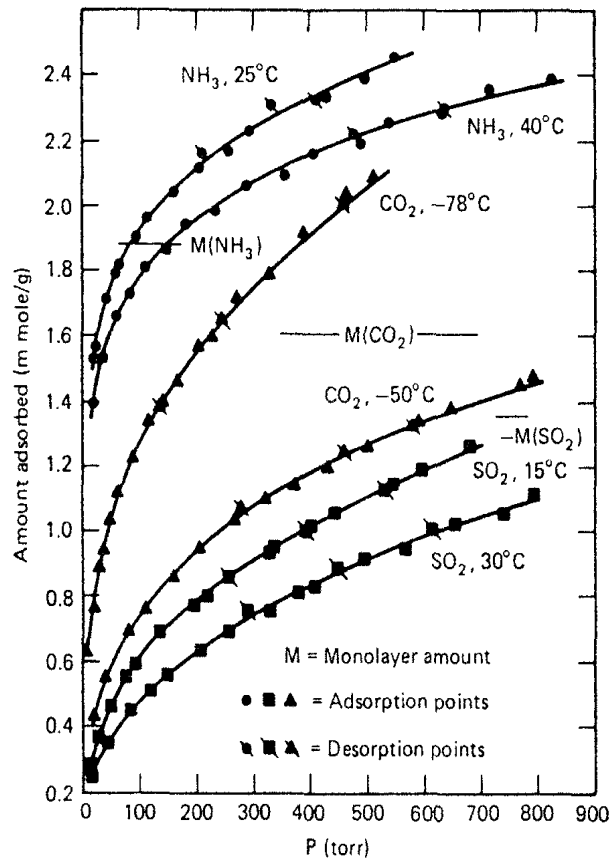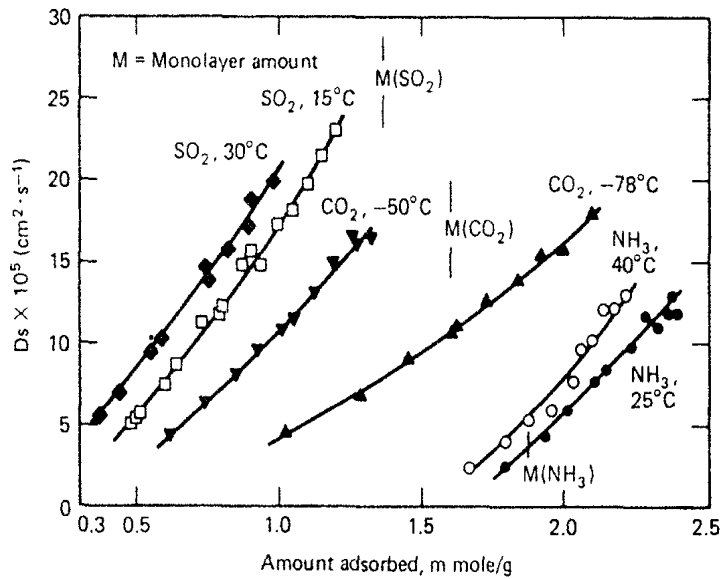
FIGURE 5.6. (a) Equilibrium isotherms and (b) variation of surface diffusivity with adsorbed phase concentration. (Reprinted with permission of ref. 40. Copyright 1974 American Chemical Society.)

TABLE 5.2.   Relative Importance of Molecular and Knudsen Diffusion
and Poiseuille Flow for a Straight Cylindrical Pore at 20°C, 1 atm

D_m	r (cm)	D_K	D	$D_{\text{Poiseuille}}$	D_{Total}	$D_{\text{Poiseuille}}/D_{\text{Total}}$
	10^{-6}	0.03	0.027	0.0007	0.027	0.026
0.2	10^{-5}	0.3	0.121	0.07	0.19	0.37
	10^{-4}	3.0	0.19	7.0	7.2	0.97

[D is given by $1/D = 1/D_K + 1/D_m$. Values of D in $cm^2 \ s^{-1}$]

for weakly adsorbed nonpolar species on nonpolar surfaces and the smallest values for strongly chemisorbed species such as hydrogen on metals.

In the adsorption of water and other rapidly diffusing species in zeolitic adsorbents, a significant additional contribution to the long-range intraparticle diffusivity may arise from intracrystalline transport. Such effects which, like surface diffusion, lead to an additional flux in parallel with the pore diffusion flux have been discussed by Jury[42,43] and Kärger et al.[26]

Poiseuille Flow

If there is a difference in total pressure across a particle, then there will be a direct contribution to the adsorption flux from forced laminar flow through the macropores. This effect is generally negligible in a packed bed since the pressure drop over an individual particle is very small. The effect may be of greater significance in the direct laboratory measurement of uptake rates in a vacuum system. From Poiseuille's equation it may be shown that the equivalent diffusivity is given by

$$D = \frac{P r^2}{8\mu} \tag{5.22}$$

where P is the absolute pressure (dynes/cm^2), μ is the viscosity in poise, and r is the mean pore radius in cm. Any flux due to Poiseuille flow simply adds to the diffusional flux through the pore. A simple order of magnitude calculation, the results of which are summarized in Table 5.2, shows that for air at 20°C and atmospheric pressure, the effect of Poiseuille flow becomes dominant in pores of radius 10^{-5}–10^{-4} cm. At lower pressures the Poiseuille diffusivity is reduced while the molecular diffusivity is increased proportionately.

5.4. MICROPORE DIFFUSION IN ZEOLITES AND CARBON MOLECULAR SIEVES

Micropore diffusion in zeolites and carbon molecular sieves has been widely studied. The subject has been reviewed by Barrer,[44] Kärger et al.,[45]

and Ruthven,[46] but the picture presented by the published literature is confusing. Most of the earlier reported diffusivities were derived from uptake measurements and the extent to which uptake rates may be affected by extraneous heat and mass transfer resistances, as discussed in Chapter 6, was not always fully appreciated. However, by the application of other experimental techniques such as chromatography and NMR methods as well as by more detailed sorption rate measurements with larger zeolite crystals, the general features of the diffusional behavior have now been established for several systems.

The relationship between sorbate activity and concentration for zeolitic systems is highly nonlinear; so, except at very low concentrations approaching the Henry's law region, the thermodynamic correlation factor $d\ln p/d\ln c$ [Eq. (5.6)] is large, approaching infinity in the saturation region of the isotherm. In analyzing the dependence of diffusivity on concentration and temperature, it is therefore important to consider the corrected diffusivity or the self-diffusivity rather than the transport diffusivity.

Intracrystalline diffusion is an activated process and the temperature dependence can generally be correlated according to Eq. (5.21). In small-port zeolites in which the free aperture of the window is only slightly greater than the critical diameter of the sorbate molecule, the activation energy correlates directly with critical molecular diameter suggesting that the rate-limiting step is the passage of the molecule through the sieve window.

Diffusion in Zeolite A

The channels of zeolite A are constricted by eight-membered oxygen rings having a free diameter of about 4.2 Å in the unobstructed Ca^{2+} or Mg^{2+} form (5A) and a somewhat smaller free diameter in the obstructed Na^+ (4A) form (see Section 1.4). For all but the smallest sorbate molecules, passage through the window is hindered by a significant repulsive barrier, and diffusional activation energies are typically several kcal/mole. As a result, intracrystalline diffusion is relatively slow and generally less than about 10^{-8} cm^2 s^{-1}, except for very small molecules in 5A. Diffusivities of this order of magnitude are small enough to allow reliable determination from uptake rate measurements, particularly if larger crystals (20–50 μm), which are easily synthesized by Charnell's method,[47] are employed. Diffusivities of light hydrocarbons in 5A zeolite may also be measured by the pulsed field gradient NMR method; but diffusion in 4A, or of higher hydrocarbons in 5A, is too slow for that technique.

Results of a series of uptake rate measurements performed with different crystal size fractions are summarized in Figures 5.7–5.9.[2,48,49] For butane in both 27.5 and 55 μm 5A crystals and for CO_2 in 21.5 and 34 μm 4A crystals the uptake rate is relatively slow and is evidently controlled by intracrystalline diffusion since the time constants show the expected dependence on the
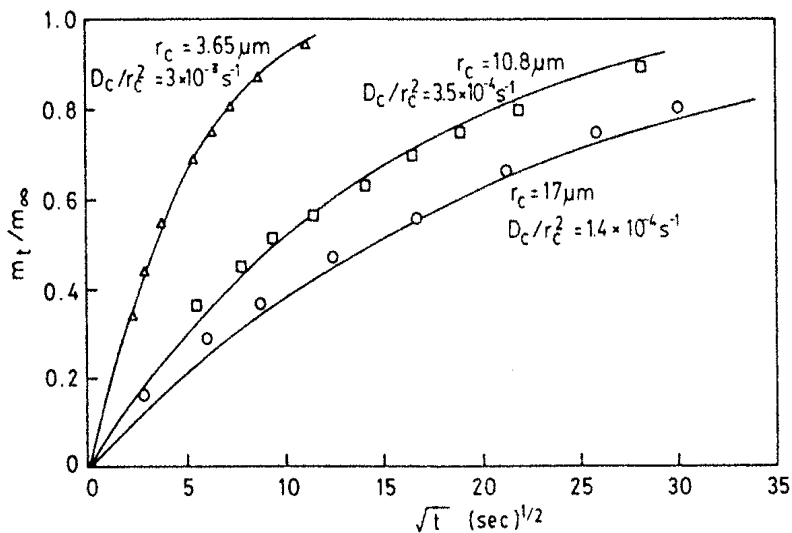
FIGURE 5.7. Experimental uptake curves for N_2 in three different size fractions of 4A zeolite crystals. Lines are theoretical curves calculated according to Eq. (6.4) with $D_c = 4.05 \times 10^{-10}$ cm^2 s^{-1}. (From ref. 48, with permission.)
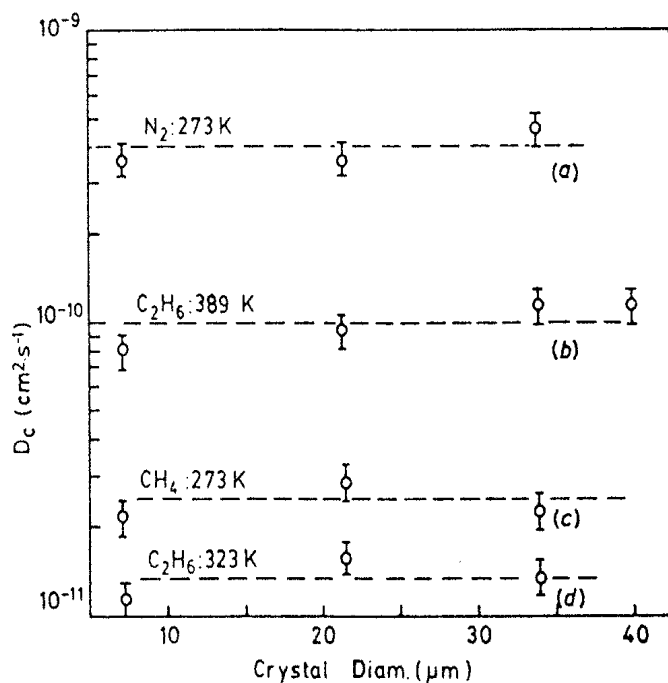
FIGURE 5.8. Diffusivities calculated from uptake curves measured with different size fractions of 4A zeolite crystals. Error bars show $\pm 15\%$ which was the scatter of individual time constants for each size fraction. (From ref. 48, with permission.)

square of the crystal radius. For CO_2 in the smaller 4A crystals (7.3 μm) heat effects are significant. Values of D_c/r_c^2 calculated from the simple isothermal model are anomalously low in comparison with the values for the larger crystals, but the values obtained from the nonisothermal model [Eqs. (6.67) and (6.68)] are consistent with the data for the larger crystals, confirming both the dominance of intracrystalline diffusional resistance and the utility of the nonisothermal model for analysis of the uptake curves for fast diffusing systems.

Concentration and Temperature Dependence

The dependence of diffusivity on concentration and temperature for some representative systems is illustrated in Figures 5.10 and 5.11.[1-3] Similar behavior for n-pentane in 5A zeolite has been reported by Kossaczky and Bobok.[50] The differential diffusivity generally shows a strong decrease with sorbate concentration, but this is due mainly to the thermodynamic correction factor. Corrected diffusivities calculated according to Eq. (5.6) using the values of $d\ln p/d\ln c$ from the equilibrium isotherm are essentially independent of concentration. The temperature dependence of the corrected diffusivity is correlated by Eq. (5.21), and the activation energy depends strongly on the diameter of the sorbate molecule relative to the sieve window, as is to be expected if the major energy barrier is the repulsive energy involved in passing through the window between adjacent cages. For a given sorbate the activation energy for diffusion in a 4A sieve is considerably greater than that for 5A, reflecting the difference in the effective aperture. In Figure 5.12 the van der Waals radius has been used as a measure of molecular diameter; but, although the correlation is good, it is evident that molecular shape is also important since molecules such as isobutane ($\sigma_0\sim$4.5 Å) and cyclohexane ($\sigma_0\sim$4.8 Å) cannot penetrate the 5A lattice while linear paraffins with much larger van der Waals radius can penetrate relatively easily.

Effect of Ion Exchange in Na-CaA Zeolites

The variation of the corrected diffusivity of n-butane with the degree of Ca^{2+} exchange in Na-CaA zeolite is shown in Figure 5.13. The results are consistent with a simple model based on a random distribution of "open" and "closed" windows.[3] If one assumes that both Na^+ and Ca^{2+} occupy the type I cation sites in preference to the type II sites within the eight-rings, then for any specified degree of Ca^{2+} exchange one may calculate the fraction of the windows which are obstructed by cations ("closed"). A random number routine was used to distribute the "open" and closed windows throughout the theoretical lattice, and the diffusivity was calculated by a random walk
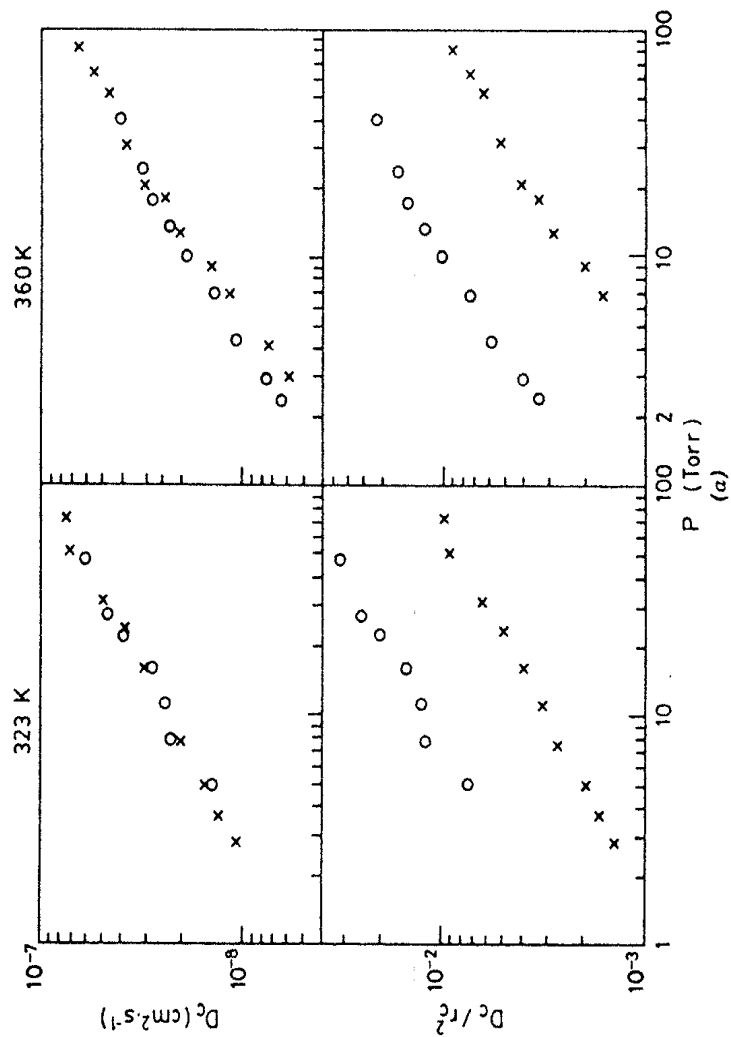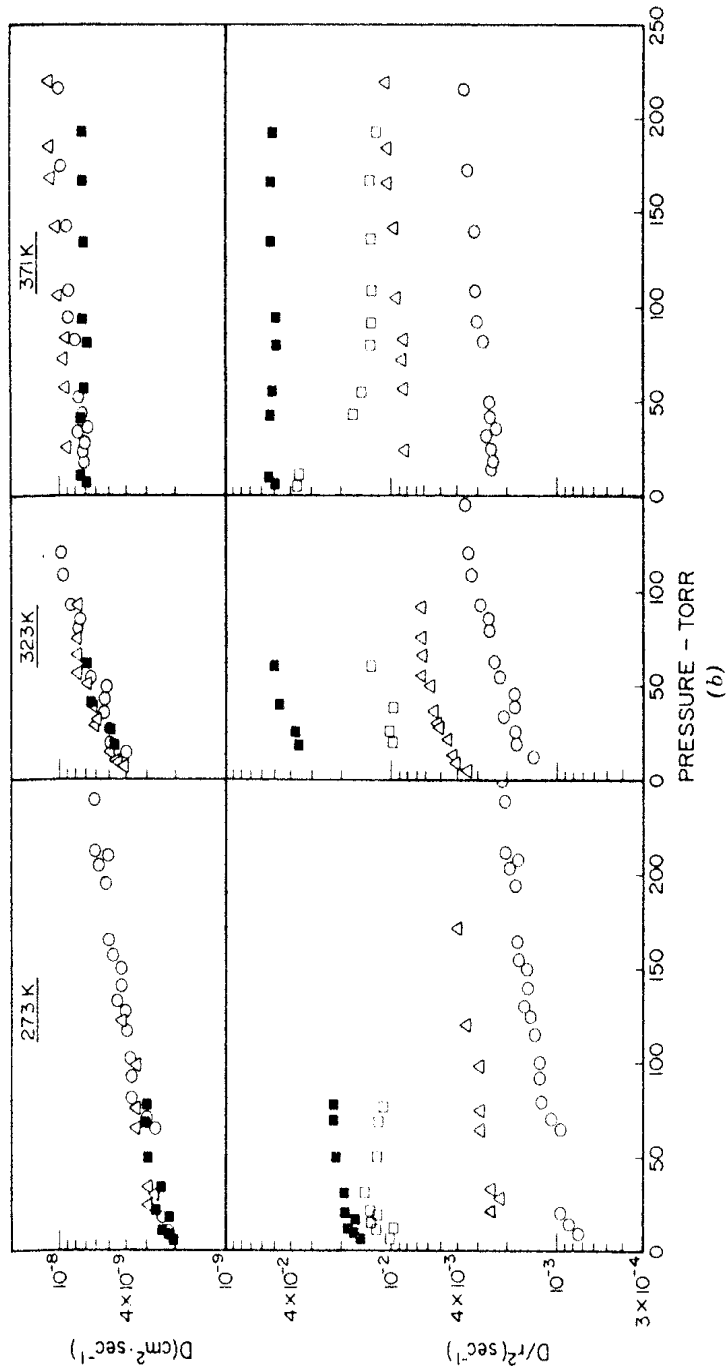
FIGURE 5.9. Variation of diffusional time constant with sorbate pressure for (a) n-butane in 55-μm (×) and 27.5-μm (O) crystals of 5A zeolite; (b) CO_2 in 34-μm (O), 21.5-μm (△), and 7.3-μm (□) crystals of 4A zeolite. Values for CO_2 in the 7.3-μm crystals derived from the nonisothermal model are shown by filled squares (see Figure 6.13). For the other systems diffusion is slow enough for heat effects to be neglected. (From refs. 2 and 49, with permission.)
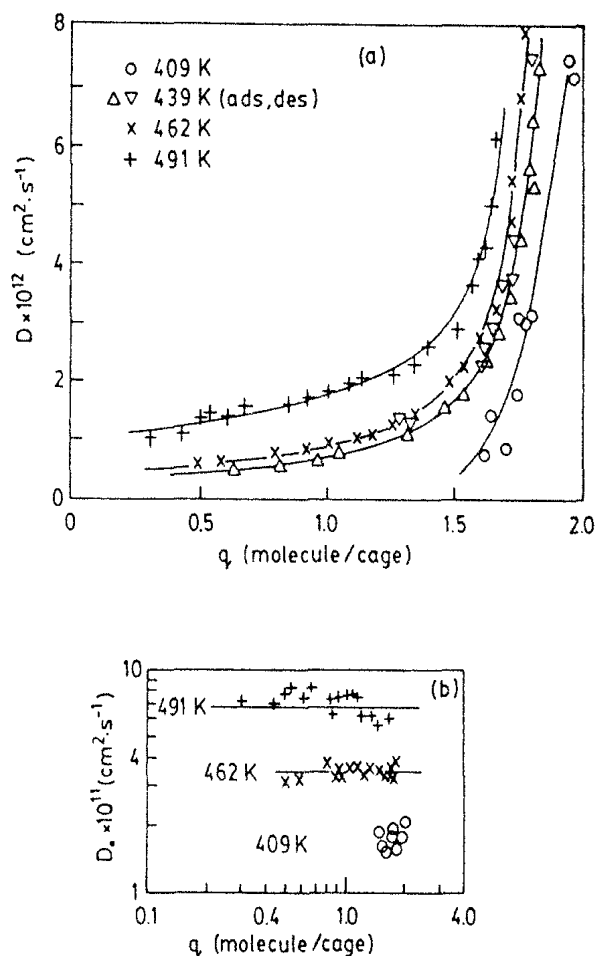
FIGURE 5.10. Variation of (a) diffusivity and (b) corrected diffusivity D_0 [Eq. (5.6)] with sorbate concentration for n-heptane in Linde 5A zeolite crystals ($r_c = 1.8$ μm). (Data from ref. 1; (a) reproduced by permission of the National Research Council of Canada from the *Canadian Journal of Chemistry*, Volume 52, 1974.)

procedure. Starting at the center of the lattice the probe molecule was assumed to attempt to move with equal probability in each of the six principal directions. If the molecule encounters an open window it passes through to the next cage and the procedure is repeated. If it encounters a closed window a random number routine is used to decide whether the transition is successful or not. The probability of a successful transition through a closed window is taken as the ratio of the diffusivities of the limiting forms, 4A (all windows closed) and 5A (all windows open). The results of such a calculation reveal that if the ratio of the diffusivities in the open and closed sieves is large the system will show a dramatic increase in diffusivity and a corresponding decrease in diffusional activation energy when one-third of the windows are open, corresponding to 10 cations per cell or one-third of the Na^+ replaced by
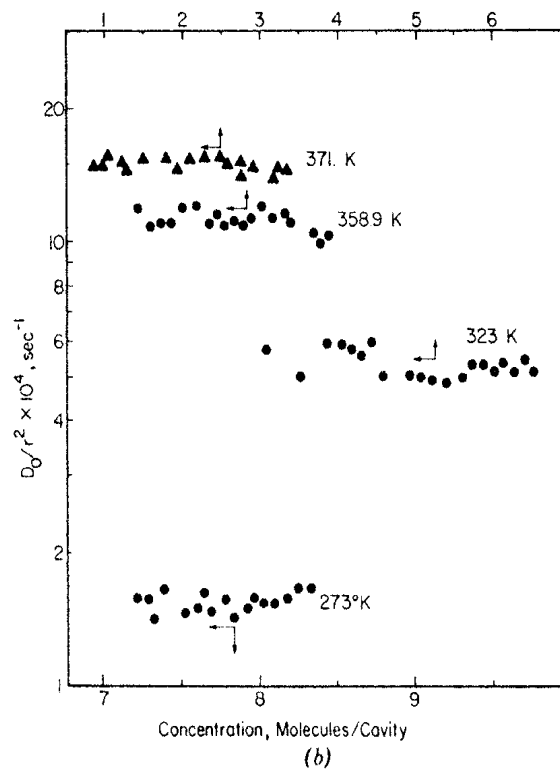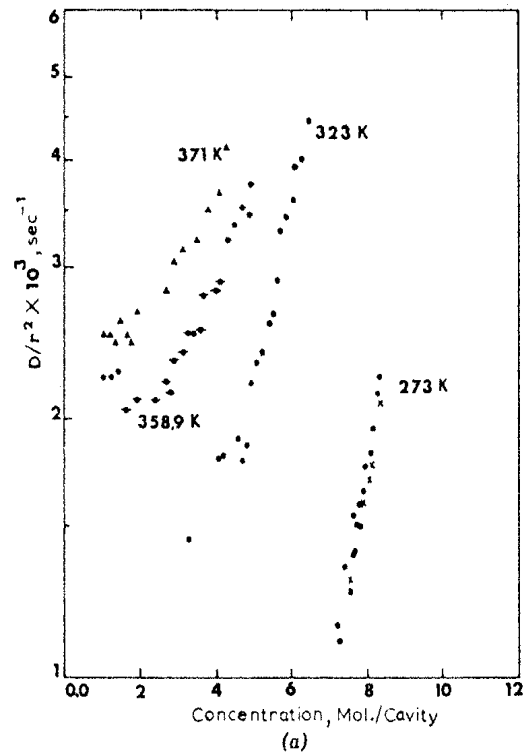
FIGURE 5.11. Variation of (a) diffusivity and (b) corrected diffusivity for CO_2 in 4A zeolite crystals ($r_c = 17 \ \mu m$). (From ref. 2.)
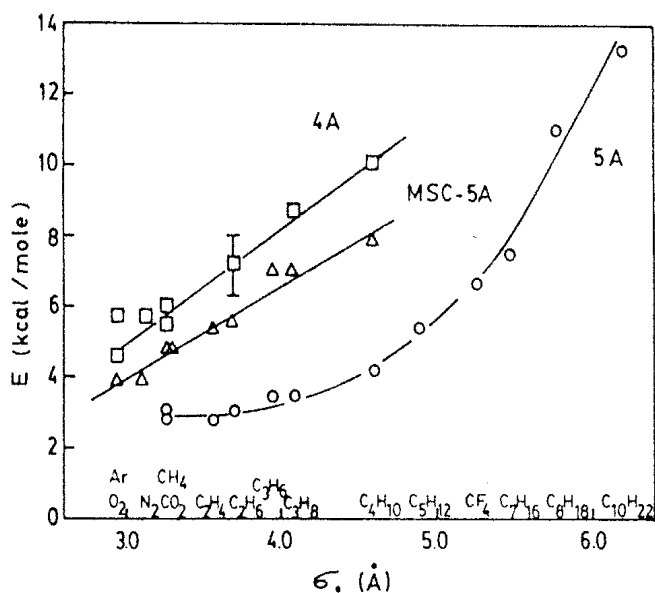
FIGURE 5.12. Variation of diffusional activation energy with van der Waals diameter for diffusion in 4A and 5A zeolites and 5A molecular sieve carbon.[81] Van der Waals diameters are estimated according to Eq. (2.5) from values of the van der Waals co-volume (b) given in the *Handbook of Physics and Chemistry*, 55th ed. C.R.C. Press 1974. (Diffusivity data are from refs. 1–3, 48, 49, 51–53, and 81.)
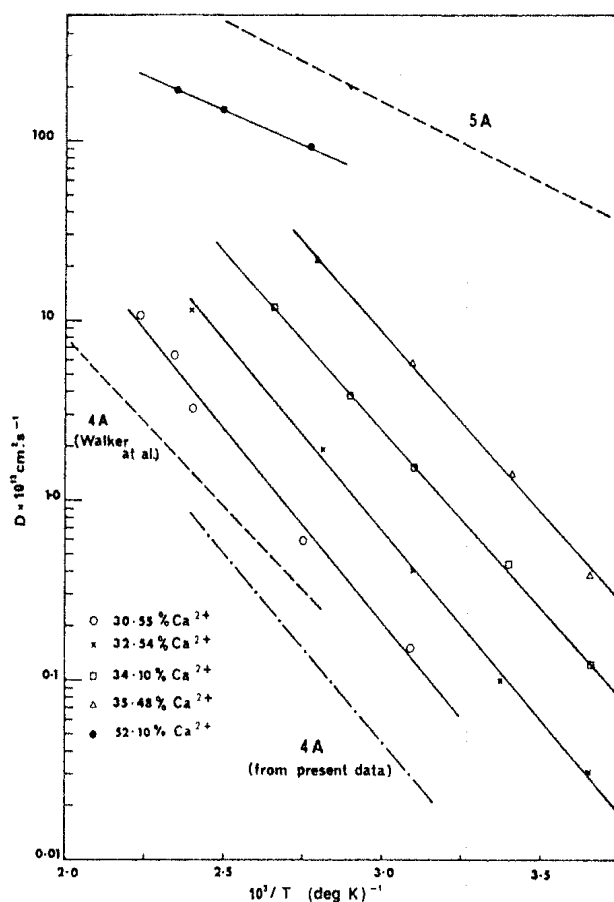
FIGURE 5.13(a). Arrhenius plot showing temperature dependence of diffusivity for butane in various partially exchanged Na-Ca A zeolite crystals. Data for the extreme forms NaA(4A) and CaA(5A) are also shown for comparison. (From ref. 53; reproduced by permission of the National Research Council of Canada from the *Canadian Journal of Chemistry*, Volume 52, 1974.)

148
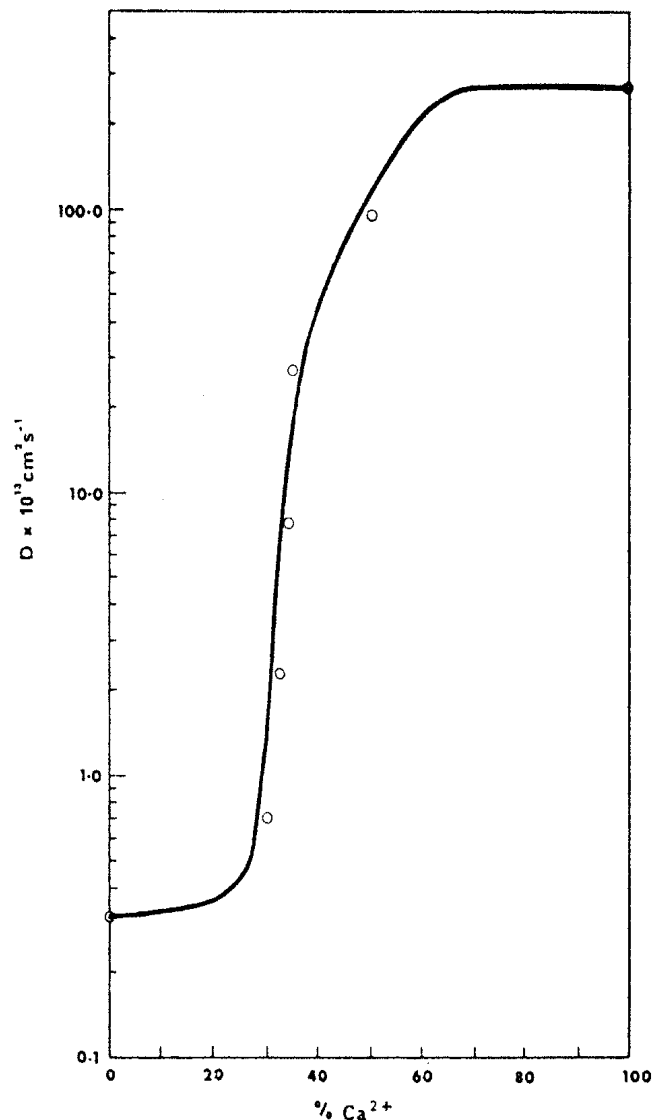
FIGURE 5.13(b). Variation of diffusivity of n-butane in Na-Ca A zeolites at 91° showing comparison of experimental points with theoretical curve calculated from the window blocking model using the values of D for 4A and 5A sieves. (From ref. 53; reproduced by permission of the National Research Council of Canada from the *Canadian Journal of Chemistry*, Volume 52, 1974.)

Ca^{2+}. For systems in which the diffusivity ratio is smaller a more gradual variation in diffusivity and diffusional activation energy with ion exchange is predicted. The theoretical curve calculated from this model provides a good representation of the experimental data for diffusion of butane in Na-Ca zeolite A, as may be seen from Figure 5.13b.

Differences in Diffusivity for Different Zeolite Samples

Measurements for a given sorbate in several different samples of 4A and 5A zeolites (Figures 5.14 and 5.15) revealed large differences in diffusivity but only a modest variation in activation energy.[2,48,49] In general, diffusivities for
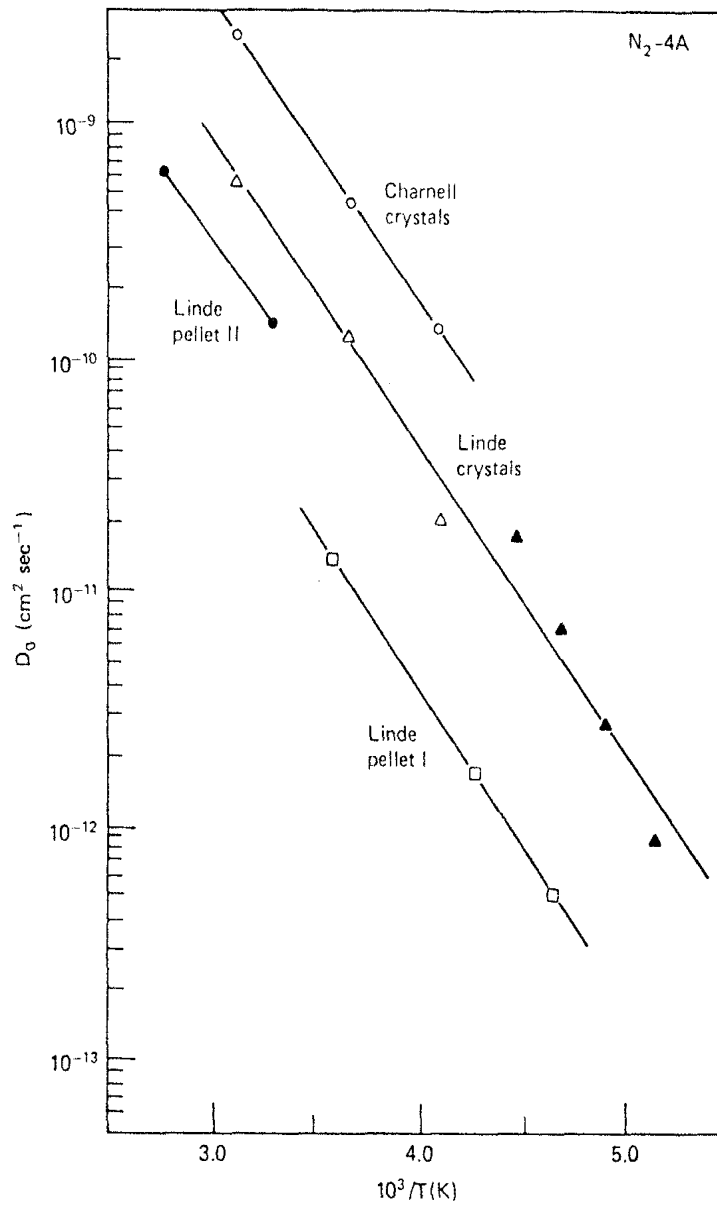
FIGURE 5.14. Arrhenius plot showing temperature dependence of limiting diffusivity for N_2 in various samples of 4A zeolite. O, 7.3–34-μm crystals synthesized by Yucel; △, ▲, 4.1-μm Linde crystals; ●, □, two different samples of Linde pellets. (From ref. 48, with permission.)

the small commercial zeolite crystals are substantially smaller than for large laboratory synthesized crystals.

Diffusion of n-butane and propane in large Charnell crystals of 5A has been measured by both sorption and NMR (PFG) methods with consistent results, as may be seen from Figure 5.16.[54] However, whereas NMR measurements showed little difference in self-diffusivity between the large Charnell crystals and the small commercial Linde 5A crystals, the uptake measurements revealed rather large differences. This and other similar observations
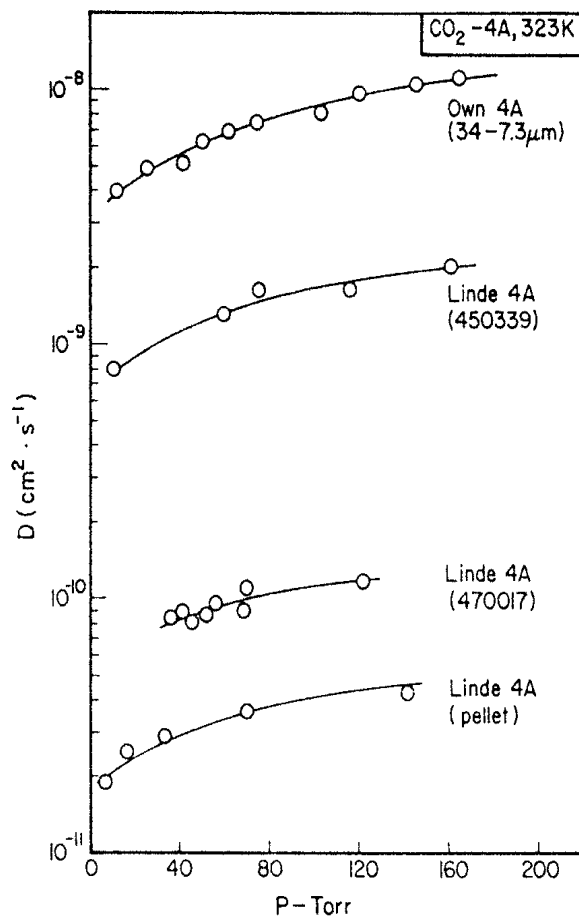
FIGURE 5.15. Diffusivity data from CO_2 in 4A zeolite showing large differences in diffusivity between different zeolite samples. (From Yucel and Ruthven.[2])

led to the suggestion that the uptake rate in the small Linde crystals may be limited by a surface barrier rather than by a true diffusional resistance.[24] In apparent support of this hypothesis it was observed that the apparent diffusivities derived from uptake rate measurements showed a strong decrease with crystal size.[55] However, detailed analysis suggests that the effect of crystal size was probably due mainly to the intrusion of heat transfer resistance, which is negligible in the larger crystals but becomes important when the crystal size is reduced. A similar study of the CO_2-4A system carried out by Yucel and Ruthven, in which the effect of heat transfer was allowed for in the analysis of the uptake curves, showed the diffusivity to be essentially independent of crystal size.[2]

With the development of the fast-tracer desorption method[27,28] a more detailed investigation of these systems became possible, but the evidence is still somewhat contradictory. Results obtained in a fast-tracer desorption study of the diffusion of C_2H_6 in 5A zeolite are shown in Figure 5.17. A sample of an 8-μm diameter 5A sieve showed no evidence of a surface barrier
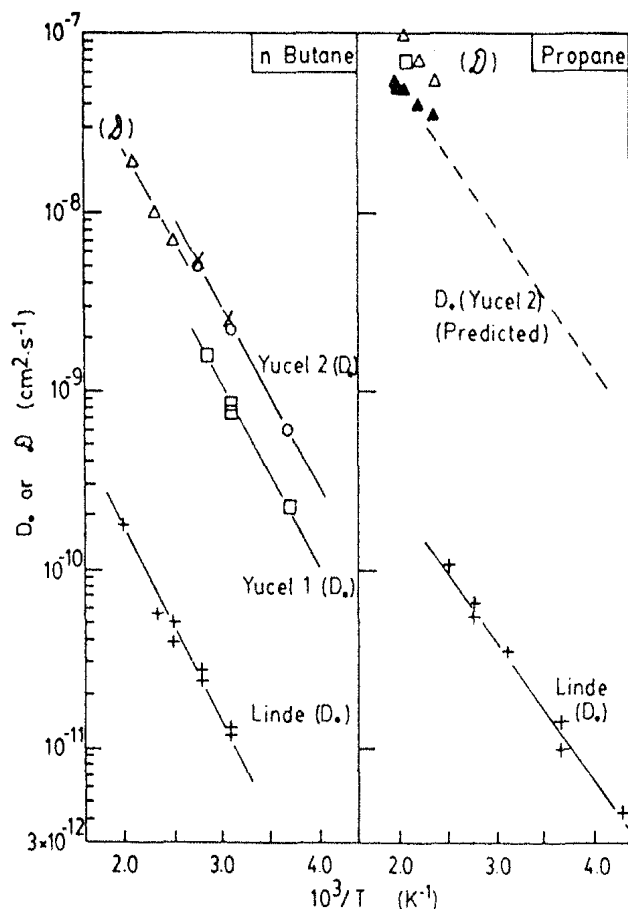
FIGURE 5.16. Diffusivity data for n-butane and propane in 5A zeolite crystals showing comparison between NMR self-diffusivities ($\mathscr{D}$) and corrected diffusivities from uptake rate measurements (D_0) $\cdot$ ×, ○, 55- and 27.5-μm diameter crystals synthesized by Yucel; □, ■, 34- and 7.3-μm crystals synthesized by Yucel; +, 3.6-μm Linde crystals; △, 21.5-μm crystals synthesized by Shdanov ($\mathscr{D}$). (From ref. 54, with permission.)

even when dehydrated at 600°C, rather than at the usual temperature of 400°C, since the diffusivities determined by fast-tracer desorption where essentially the same as those obtained from NMR PFG measurements. Similar diffusivities were obtained by both desorption and PFG measurements for a sample of small (0.5-μm) crystals dehydrated at 400°C. However, when a sample of the small crystals was dehydrated at 600°C a dramatic reduction in the desorption rate and a corresponding increase in the activation energy of desorption (from 1.3 to 2.8 kcal/mole) were observed.

The size of these crystals and the conditions of dehydration are essentially similar to those used in the preparation of commercial 5A adsorbents. It is remarkable that the diffusional activation energy determined from the tracer desorption results for the small crystals dehydrated at high temperature (2.8 kcal/mole) is almost the same as the value determined from the earlier adsorption rate measurements with small commercial Linde crystals (3.0 kcal/mole).[52] The absolute values of the diffusivities for the severely de-
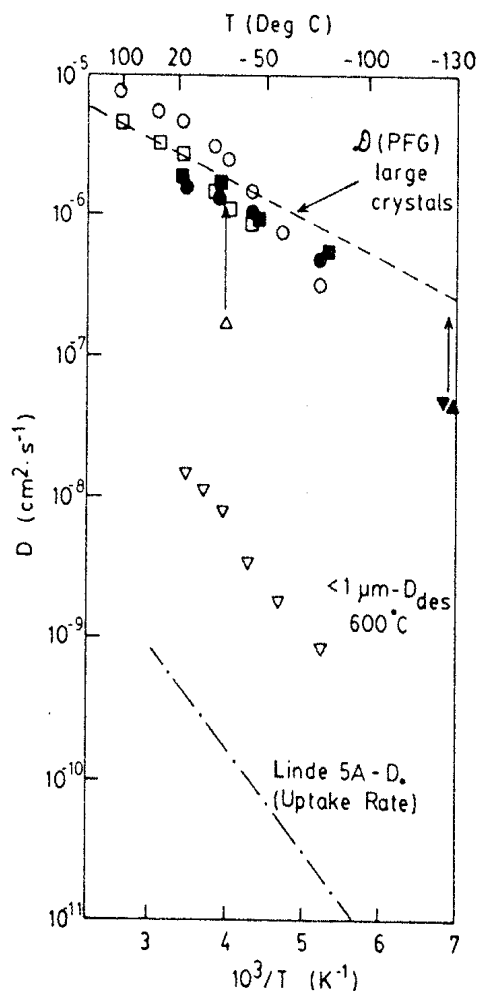
FIGURE 5.17. Results of tracer desorption study of diffusion of C_2H_6 in 5A zeolite crystals showing effect of crystal size and dehydration temperature. Filled symbols represent NMR (PFG) intracrystalline self-diffusivities. Open symbols represent tracer desorption diffusivities. Earlier self-diffusivity data for larger crystals (----) and uptake rate data[52] [D_0 defined by Eq. (5.6)] (—·—·) are shown for comparison. (After Kärger et al.[28])

	400°C	600°C
8 μm	O, ●	□, ■
< 1 μm	△, ▲	▽▲

hydrated small crystals and the commercial crystals also agree within an order of magnitude and are two or three orders of magnitude smaller than the intracrystalline self-diffusivities determined from NMR (PFG) measurements with the larger crystals or with the small crystals dehydrated under less severe conditions. Unfortunately in this study it was not possible to measure directly by the PFG method the self-diffusivity in the small severely dehydrated crystals and so to establish definitively whether the increased resistance to mass transfer is due to a decrease in the intracrystalline diffusivity or to the creation of a surface barrier.

Despite the large difference in the apparent diffusivities derived from uptake rate measurements, measurements of the intracrystalline self-diffusivity (for C_2H_6-5A) by the NMR (PFG) method show little difference between the large laboratory synthesized crystals and the small Linde crystals, thus favoring the surface barrier hypothesis.[56] The increase in activation energy, which is observed for this system on severe hydrothermal pretreatment of the smaller crystals, is also consistent with a change from intracrystalline diffusion to surface barrier control. Detailed sorption rate studies with the system n-butane-5A, however, support the opposite conclusion that the differences in

uptake rate between large laboratory synthesized crystals, dehydrated carefully at temperatures not exceeding 400°C, and the small commercial crystals, which are dehydrated at higher temperatures under deep-bed conditions, are due to differences in intracrystalline diffusivity rather than to the creation of a surface barrier. Where diffusion was slow enough to permit reliable measurement of initial uptake rates, the initial rate data generally conformed to the "$\sqrt{t}$ law" [Eq. (6.18)] rather than to a simple linear (or exponential) dependence on time as required by the surface barrier model. The observation that the large differences in apparent diffusivity are associated with changes in the pre-exponential factor with little change in activation energy[49] may also be taken as tentative evidence in favor of the diffusion model. Such behavior would be consistent with blocking of a certain fraction of the windows by a redistribution of the exchangeable cations, whereas a change from intracrystalline diffusion, which is clearly the rate-controlling process in the larger crystals, to surface barrier control as postulated for the small hydrothermally treated crystals would normally be expected to involve a change in activation energy. Tentative evidence of cation rearrangement at elevated temperatures is provided by the data of Roethe et al.[57]

From the practical point of view the important result is that these studies show clearly that the adsorption–desorption kinetics in zeolite crystals may be profoundly affected by the conditions of dehydration and that small crystals are more sensitive than large crystals to severe conditions of dehydration. These findings support and extend the conclusions reached by Kondis and Dranoff[58] who showed that the apparent diffusivity of ethane in commercial 4A pellets is much lower than in the unaggregated crystals and that by hydrothermal treatment the crystal diffusivity is reduced to a value approaching that for the pellets. The reason for the greater sensitivity of the small crystals is not fully established. There is some evidence that structural breakdown under hydrothermal conditions occurs more readily with very small crystals, presumably reflecting the greater relative importance of the inherently less stable surface layer of atoms in the crystal. However, the overall rate of a surface-limited sorption process will vary in proportion to the specific external surface area, which is inversely proportional to crystal radius, while the rate of the diffusive process depends on the time constant D/r^2. One may therefore expect that even without any structural breakdown the effect of surface resistance will always be more apparent in the smaller crystals. Thus, while small crystals are generally desirable in order to minimize intracrystalline diffusional resistance, any such advantage may easily be offset by decreased hydrothermal stability and increased surface resistance.

Diffusion in Zeolites X and Y

The lattice of the faujasite zeolites (types X and Y) is much more open than that of zeolite A. The windows consist of 12-membered oxygen rings which are unobstructed by cations. The free diameter (~ 7.5 Å) is large enough to

admit quite large molecules such as naphthalene, mesitylene, neopentane, and tertiary amines. Diffusion is rapid and generally too fast to measure by conventional gravimetric or chromatographic methods except in large crystals. Recent experimental studies[59] and detailed theoretical analysis[60,61] reveal that earlier reported diffusivities for hydrocarbons in zeolite X, determined from uptake rate measurements,[62-65] were almost certainly in error due to the intrusion of extracrystalline mass and/or heat transfer resistance. A significant repulsive energy barrier associated with passage through the sieve windows is observed only with very large molecules such as triethylamine or tributylamine and, in contrast to the hydrocarbons, diffusion of these species is slow enough to be determined from uptake rate measurements.[66]

Saturated Hydrocarbons

A detailed study of the diffusion of a series of linear paraffin and cyclohexane in NaX has been reported by Karger, Pfeifer, et al.[67] The results of these investigations reveal a consistent pattern of behavior which differs in several significant ways from diffusion in zeolite A. The general features are illustrated in Figures 5.18-5.20. The self-diffusivity in all cases decreases strongly with increasing sorbate concentration but this decrease in diffusivity is not due to an increase in diffusional activation energy which, in the case of the linear paraffins, is essentially independent of loading.
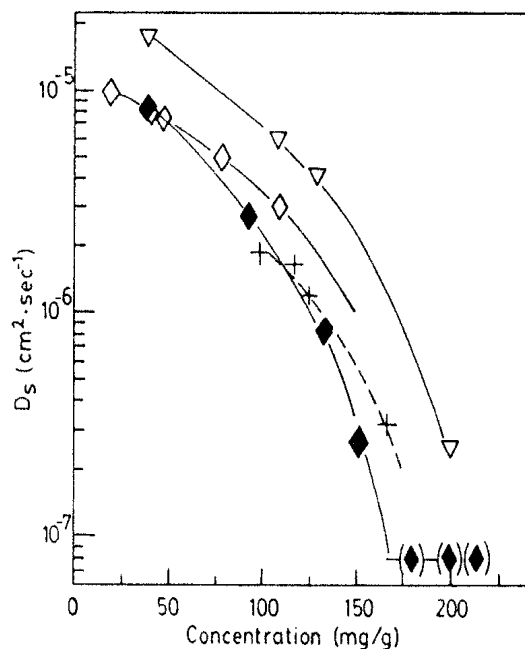
FIGURE 5.18. Concentration dependence of NMR self-diffusivity for paraffin hydrocarbons in Shdanov 13X zeolite crystals at $358 K_0$. $\triangledown$, n-heptane; $\lozenge$, n-octane; $+$, n-decane; $\blacklozenge$, isooctane. Points in parenthesis refer to pore-filling factors greater than 1.0, the contribution of the extracrystalline fluid to the NMR signal having been eliminated in the data analysis. (From ref. 54, with permission.)
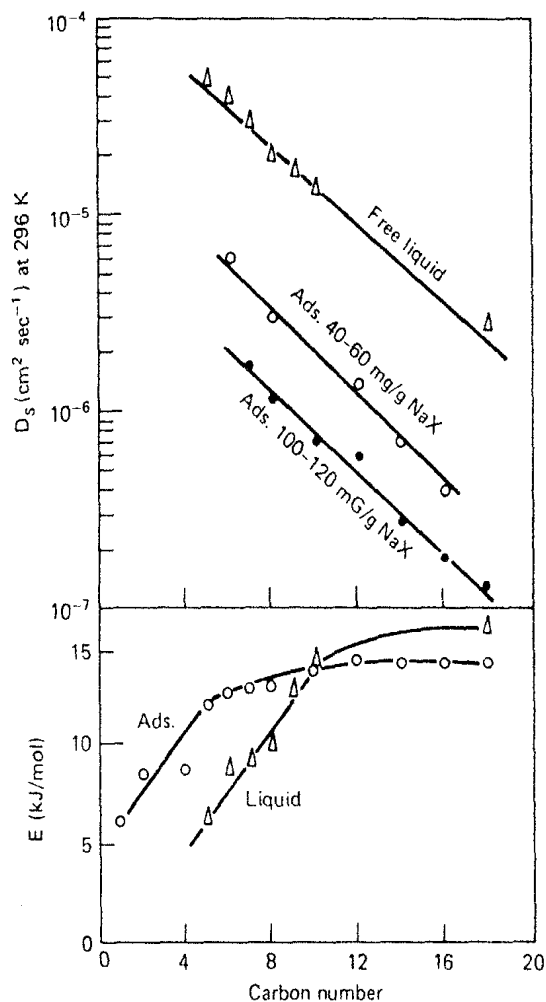
FIGURE 5.19. Comparison of self-diffusivities and diffusional activation energies for linear paraffins as free liquids and adsorbed on 13X zeolite crystals. Data of Kärger et al.[67] (Reprinted with permission from ref. 46. Copyright 1983 American Chemical Society.)

Comparison of PFG self-diffusion measurements and relaxation measurements shows that the reduction in diffusivity arises from a reduction in the rms jump distance which falls to about 1 Å at high loadings (see Figure 5.20), presumably as a result of the increasing importance of intermolecular collisions. The comparison of diffusivity and diffusional activation energy for the adsorbed phase and free liquid (Figure 5.19) suggests that at higher loadings intracrystalline diffusion occurs by essentially the same mechanism as liquid diffusion. Indeed the free volume theory has been successfully extended to intracrystalline diffusion.[67]

The behavior of cyclohexane[68] and isoparaffins[54] is basically similar to that of the linear alkanes. Activation energies are somewhat lower than for the linear paraffins with the same carbon number and, in the case of cyclohexane, the activation energy decreases with loading (3.0–2.1 kcal).
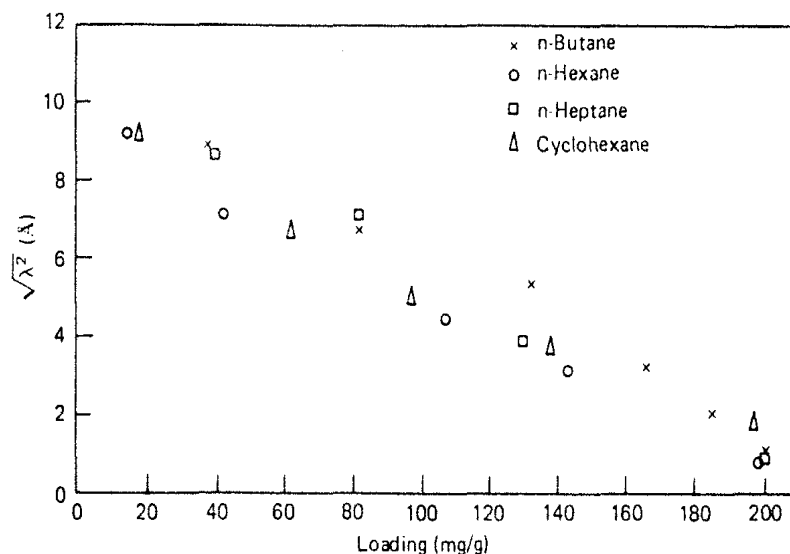
FIGURE 5.20. Variation of rms jump distance with sorbate concentration for saturated hydrocarbons on NaX zeolite. Data of Kärger et al.[67] (Reprinted with permission from ref. 46. Copyright 1983 American Chemical Society.)

Benzene

Benzene diffuses much less rapidly than cyclohexane and the activation energy is higher (~5 kcal/mole). Detailed studies by Lechert and co-workers[69-71] reveal that in zeolite Y, which has no delocalized cations, the benzene molecules tend to occupy tetrahedrally disposed sites with the molecules oriented parallel to the six-ring at a distance 3.2 Å from the S_2 cation. Up to a coverage of 4 molecules/cage the rms jump distance remains reasonably constant (3-4 Å) and is approximately consistent with the site-site distance.

Olefins

The diffusivity in NaX zeolite decreases by about a factor of 10 in the sequence n-butane > t-butene > 1-butene > cis-butene.[72] Activation energies for all these species are similar and increase somewhat with loading. Correlation times are also similar and the difference in diffusivity is due to a difference in the rms jump distance, which evidently varies as a result of different degrees of steric hindrance to passage through the 12-membered O ring. Thus for every jump between cages, the slowest diffusing species (cis-butene) makes, on average, about eight jumps within a cage compared with only about two $intra$cage jumps for $trans$-buten. This difference is attributed to the orienting effect of the small but significant dipole moment of cis-butene.

Partial ion exchange of Na^+ for Ag^+ leads to a dramatic reduction in diffusivity for the olefins (more than two orders of magnitude at 20% ex-

TABLE 5.3. Comparison of Theoretical and Experimental Values of K_0 and D_* for Hydrocarbons in NaX Zeolites

	Experimental Values				
	V_0 (kcal/mole)	$D_* \times 10^3$ (cm² s⁻¹)	$K_0 \times 10^9$ (molecule/cage Pa)	$\dfrac{(D_*)_{theory}}{(D_0)_{expt}}$	$\dfrac{(K_0)_{theory}}{(K_0)_{expt}}$
CH_4	1.6	3.5	7.6	1.3	1.5
C_2H_6	2.3	5.0	5.0	0.8	1.2
nC_4H_{10}	2.5	1.9	1.5	1.5	3.9
nC_6H_{14}	3.5	6.3	1.5	0.5	1.9
nC_7H_{12}	3.0	1.6	2.3	1.6	1.6
cyclo-C_6H_{12}	3.7	6.4	1.5	0.5	1.7

(sorbate concentration 15–30 mg/g)

Source: After Kärger et al.[76]

158

change) as a result of the strong olefin-Ag$^+$ interaction.[73] There is a parallel increase in correlation time, reflecting a dramatic increase in the mean residence time at an adsorption site rather than any change in rms jump distance. Ion exchange for Tl$^+$ has the opposite effect, increasing the diffusivity relative to the Na$^+$ form. The reasons are less obvious.

Theoretical Model

Following Hill[74] and Ruthven and Doetsch,[75] one may as a simple model represent the potential field within the zeolite by a symmetric three-dimensional sinusoidal function:

$$U = U_0 + \frac{1}{2} V_0\left(1 - \cos \frac{2\pi x}{a}\right) + \frac{1}{2} V_0\left(1 - \cos \frac{2\pi y}{a}\right) + \frac{1}{2} V_0\left(1 - \cos \frac{2\pi z}{a}\right)$$

(5.23)

From this model, one may derive theoretical expressions for the Henry's law equilibrium constant:

$$K_c = K_0 \exp\left(-\frac{U_0}{kT}\right), \qquad K_0 = \left[\exp\left(-\frac{V_0}{2kT}\right) I_0\left(\frac{V_0}{2kT}\right)\right]^3 \left(\frac{v}{kT}\right) \quad (5.24)$$

and for the diffusivity at low concentration

$$D = D_* \exp\left(-\frac{V_0}{kT}\right), \qquad D_* = \frac{a}{\sqrt{2}} \left(\frac{V_0}{m}\right)^{1/2} \quad (5.25)$$

Using for V_0 the experimental value of the diffusional activation energy, one may estimate theoretical values for the pre-exponential factors D_* and K_0, which may then be compared with the experimental values. Such a comparison, from the data of Karger et al.,[76] is shown in Table 5.3 for the diffusion of several hydrocarbons in NaX zeolite, and it is evident that in spite of the obvious approximations, the model provides a good representation of the behavior of these systems at low concentrations.

NMR Sorption Comparison

Diffusion of the large triethylamine molecule is sufficiently slow that reliable diffusivities can be determined from uptake rate measurements in ~50 μm crystals,[66] at least over a limited range of conditions. A comparative study, carried out with the same zeolite samples showed good agreement between the sorption and PFG NMR measurements, both as to the magnitude of the diffusivity ($\sim 10^{-8}$ cm^2 s^{-1} at 445 K) and the trends with concentration and temperature.[54] Good agreement between sorption and NMR diffusivities has recently been demonstrated for benzene in 120-μm crystals of NaX.[89]

Diffusion in Pentasil Zeolites

Only limited studies of diffusion in the Pentasil zeolites have so far been reported. Intracrystalline self-diffusion of ethane, propane, and water in ZSM-5 at temperature of 293–363 K has been studied recently by Kärger using the NMR PFG method.[77] The relaxation times were too short to permit detailed measurements but for all three species diffusion was found to be very fast ($\mathscr{D} \geqslant 10^{-5}$ cm^2 s^{-1}). For the hydrocarbons this is comparable

TABLE 5.4. Diffusion in Pentasil Zeolites (cm^2 s^{-1})

Sorbate	Investigator	Temp. (K)	D (cm^2 s^{-1})	E (kcal/mole)
n-butane	Paravar and Hayhurst[16]	297	5.7×10^{-8}	3.5
		334	1.1×10^{-7}	
i-butane	Paravar and Hayhurst[16]	297	1.9×10^{-8}	5.7
		334	5.5×10^{-8}	
methane	Paravar*	298	107×10^{-8}	
ethane			22×10^{-8}	
propane			7.3×10^{-8}	
n-butane			3.7×10^{-8}	
n-pentane			2.4×10^{-8}	
n-hexane	Wu et al.[79]	303	7.5×10^{-12}	
benzene	Wu et al.[79]	303	8.6×10^{-12}	
benzene	Doelle and Riekert[78]	303	2.4×10^{-10}	
p-xylene	Wu et al.[79]	303	1×10^{-11}	
m-xylene	Doelle and Riekert[78]	303	2.3×10^{-10}	
dimethylether	Wu et al.[79]	303	7.5×10^{-11}	
dimethylether	Doelle and Riekert[78]	303	1.3×10^{-9}	
2,2-dimethylbutane	Post et al.[86]	373 (373–555)	10^{-14}	15.8

*Additional data kindly provided by A. Paravar.

with the diffusivities observed in NaX and much higher than the diffusivities in 5A, but for water the diffusivity in ZSM-5 is larger than in either 5A or 13X by more than an order of magnitude, presumably reflecting the hydrophobic nature of the surface.

Diffusivities derived from uptake rate measurements and by other classical methods are summarized in Table 5.4. Post et al.[86] used both gravimetric and chromatographic methods and the diffusivities obtained by both these methods showed good agreement. Paravar and Hayhurst[16] used the Wicke-Kallenbach method with a single large crystal (100 μm) as the membrane. Their values are presumably reliable since in this method there is no intrusion of heat transfer or extracrystalline resistance to mass transfer. The diffusivity values (for n-butane) are of the expected order of magnitude, lying between the values for 5A zeolite ($D_0 \sim 10^{-9}$ cm^2 sec^{-1} from Figure 5.16) and 13X zeolite [$D_0 \sim 10^{-5}$ cm^2 s^{-1} as determined by both membrane diffusion and from NMR (PFG) measurements[15]]. The values given by Doelle et al. also appear reasonable, being somewhat smaller than the self-diffusivity values obtained for benzene in 13X zeolite by the NMR (PFG) method ($\mathscr{D} \sim 10^{-7}$ cm^2 s^{-1} at 300 K).[54] The values of Wu et al.[80] which were obtained for apparently similar systems are, however, smaller by a factor of about 20. It is not clear whether this difference is genuine, resulting from real differences in the zeolite crystals or an artifact arising from the intrusion of extraneous heat and mass transfer resistance. The data of Paravar for $C_1 - C_5$ alkanes show clearly the effect of increasing chain length, while comparison of the activation energies for n-butane, isobutane, and 2,2-dimethylbutane shows the effect of molecular diameter.

Diffusion in Carbon Molecular Sieves

A detailed study of diffusion in "5A" carbon molecular sieve has been published by Chihara, Suzuki, and Kawazoe[81-83] who used both the chromatographic and gravimetric methods. The concentration dependence of the
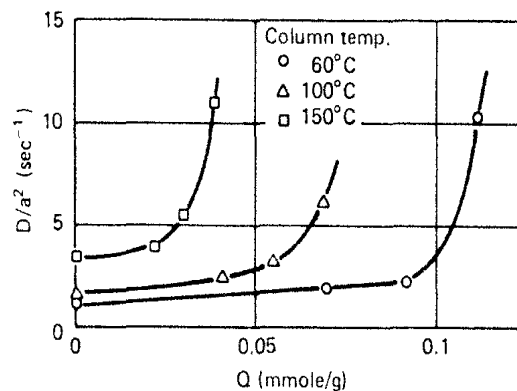
FIGURE 5.21. Concentration dependence of diffusional time constant for N$_2$ in molecular sieve carbon. (From ref. 82, with permission.)
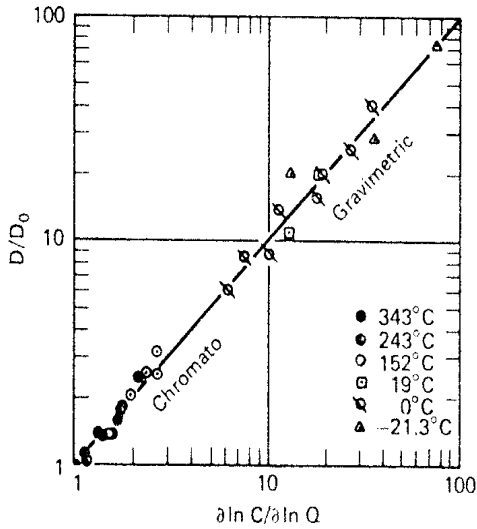
FIGURE 5.22. Correlation of micropore diffusivity for propene in MSC "5A" with thermodynamic correction factor. (From ref. 82, with permission.)

diffusivity was measured gravimetrically by the differential step method and chromatographically by using a mixed carrier stream, with consistent results by both methods. Representative data are shown in Figures 5.21–5.23. The general trends are similar to those observed for diffusion in small-port zeolites (Figures 5.10 and 5.11). As with the zeolite systems the concentration dependence of the diffusivity arises mainly from the thermodynamic correction factor with the corrected diffusivities, calculated according to Eq. (5.6), being almost independent of concentration. This is illustrated, for propylene, in Figure 5.22 in which the ratio D/D_0 is plotted against the factor $d\ln p/d\ln q$.
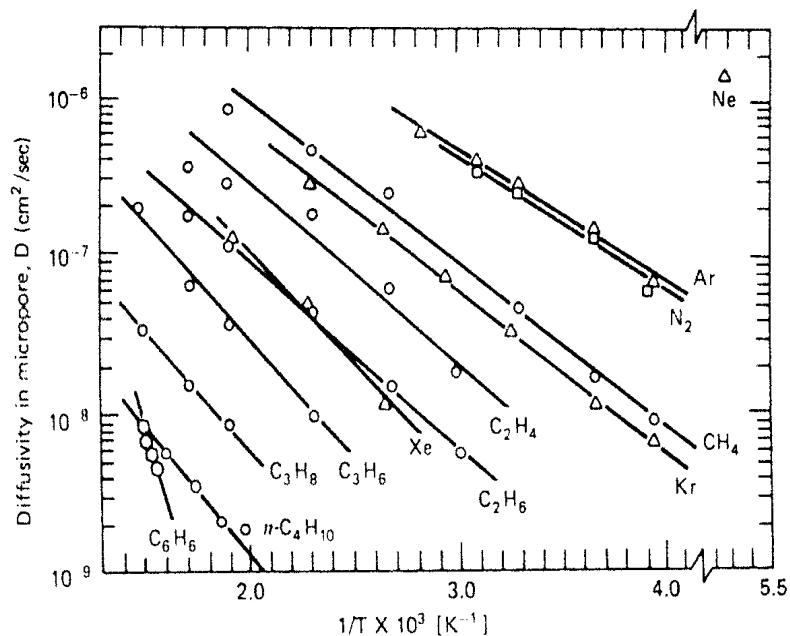
FIGURE 5.23. Arrhenius plot showing temperature dependence of limiting diffusivity for small molecules in molecular sieve carbon MSC-5A. (From ref. 81, reprinted with permission.)

The temperature dependence of the corrected diffusivity is illustrated in Figure 5.23, and the correlation of diffusional activation energy with van der Waals radius is indicated in Figure 5.12. It is evident that the trend is very similar to that observed with 4A zeolite although the magnitude is somewhat larger.

Essentially the same model as applied by Karger et al.[76] to diffusion in 13X zeolite [Eqs. (5.23)–(5.25)] was used to interpret the diffusivity data for the carbon sieve.[83] The experimental diffusivities showed approximately the expected relationship between D_* and E as expressed by Eq. (5.25). By comparing the experimental heat of sorption and activation energies with values derived from theoretical potential calculations, it was shown that the mean slit width of the sieve must be about 4.4 Å. Consistent results were obtained from the data for Ar, Kr, and Xe, thus supporting the proposed model.

Interest in carbon molecular sieves has been greatly stimulated by the development of a commercial sieve which can separate O_2 and N_2[84,85] on the basis of a difference in micropore diffusivity. Rudimentary kinetic and equilibrium data for this material are presented in Figure 11.23. More detailed diffusivity data as well as correlations between the kinetic and equilibrium properties of carbon sieves have been given by Seewald, Klein, and Jüntgen[87] and Seewald.[88]

REFERENCES

1. I. H. Doetsch, D. M. Ruthven, and K. F. Loughlin, *Can. J. Chem.* **52**, 2717 (1974).

2. H. Yucel and D. M. Ruthven, *J. Colloid Interface Sci.* **74**, 186 (1980).

3. A. P. Vavlitis, D. M. Ruthven, and K. F. Loughlin, *J. Colloid. Interface Sci.* **84**, 526 (1981).

4. R. K. Ghai, H. Ertl, and F. A. L. Dullien, *AIChE J.* **19**, 881 (1974).

5. H. Ertl, R. K. Ghai, and F. A. L. Dullien, *AIChE J.* **20**, 1 (1974).

6. R. Haase and M. Siry, *Z. Phys. Chem.* (Frankfurt) **57**, 56 (1968).

7. J. C. R. Turner, *Chem. Eng. Sci.* **30**, 1304 (1975).

8. P. V. Danckwerts, in *Diffusion Processes*, Vol. 2, J. N. Sherwood, A. V. Chadwick, W. M. Muir, and F. L. Swinton (eds.). Gordon and Breach, London, 1971, p. 45.

9. R. Ash and R. M. Barrer, *Surface Sci.* **8**, 461 (1967).

10. J. Kärger, *Surface Sci.* **36**, 797 (1973).

11. I. Prigogine, *Thermodynamics of Irreversible Processes*, 3rd ed. John Wiley, New York, 1967, p. 45.

12. L. S. Darken, *Trans. AIME* **175**, 184 (1948).

13. J. Kärger, *Surface Sci.* **59**, 749 (1976).

14. E. Wicke and R. Kallenbach, *Kolloid Z.* **97**, 135 (1941).

15. D. L. Wernick and E. J. Osterhuber, *Proceedings of the Sixth International Conference on Zeolites, Reno, Nevada, July 1983.* Butterworths, Guildford, England, 1984.

16. A. Paravar and D. T. Hayhurst, *Proceedings of the Sixth International Conference on Zeolites, Reno, Nevada, July 1983.* Butterworths, Guildford, England, 1984.

17. R. W. H. Sargent and C. J. Whitford, *Adv. Chem.* **102**, 155 (1971).

18. A. Quig and L. V. C. Rees, *J. Chem. Soc. Faraday Trans. I* **72**, 771 (1976).

19. G. I. Lindsley and L. V. C. Rees, Workshop on Adsorption of Hydrocarbons in Zeolites, Berlin DGR Nov. 1979. Preprints Vol. 2, p. 43 (Paper No. 5.)

20. H. Resing and J. S. Murday, *Adv. Chem.* **121**, 414 (1973).

21. E. O. Stejskal and J. E. Tanner, *J. Chem. Phys.* **42**, 288 (1965) and **49**, 1768 (1968).

22. J. Kärger and H. Pfeifer, *Z. Chemie* **16**, 85–90 (1976).

23. H. Pfeifer, *Phys. Reports (Phys. Letters C)* **26**, 293 (1976).

24. J. Kärger and J. Caro, *J. Chem. Soc. Faraday Trans. I* **73**, 1363 (1977).

25. J. Kärger, M. Rauscher, and H. Torge, *J. Colloid Interface Sci.* **76**, 525 (1980).

26. J. Kärger, M. Kocirik, and Z. Zikanova, *J. Colloid Interface Sci.* **84**, 240 (1981).

27. J. Kärger, *AIChE J.* **28**, 417 (1982).

28. J. Kärger, H. Pfeifer, M. Rauscher, M. Bulow, N. Sumuewitc, and S. P. Shdanov, *Z. Phys. Chem.* (Leipzig), **262**, 567 (1981).

29. C. N. Satterfield, *Mass Transfer in Heterogeneous Catalysis.* MIT Press, Cambridge, Mass., 1970.

30. M. F. L. Johnson and W. E. Stuart, *J. Catalysis* **4**, 248 (1965).

31. R. E. Haring and R. A. Greenkorn, *AIChE J.* **16**, 477 (1970).

32. F. A. L. Dullien, *AIChE J.* **21**, 299 (1975).

33. F. A. L. Dullien, *Porous Media, Fluid Transport and Pore Structure.* Academic Press, New York, 1979, Chap. III.

34. J. O. Hirschfelder, C. F. Curtiss, and R. B. Bird, *Molecular Theory of Gases and Liquids.* Wiley, New York, 1954.

35. R. C. Reid, J. M. Prausnitz, and T. K. Sherwood, *The Properties of Gases and Liquids,* 3rd ed. McGraw-Hill, New York, 1977.

36. E. H. Kennard, *Kinetic Theory of Gases.* McGraw-Hill, New York, 1938, p. 302.

37. R. B. Evans, G. M. Watson, and E. A. Mason, *J. Chem. Phys.* **33**, 2076 (1961).

38. D. S. Scott and F. A. L. Dullien, *AIChE J.* **8**, 113 (1962).

39. P. Schneider and J. M. Smith, *AIChE J.* **14**, 762 (1968).

40. E. R. Gilliland, R. F. Baddour, G. F. Perkinson, and K. J. Sladek, *Ind. Eng. Chem. Fund.* **13**, 95 (1974).

41. K. J. Sladek, E. R. Gilliland, and R. F. Baddour, *Ind. Eng. Chem. Fund.* **13**, 100 (1974).

42. S. H. Jury, *Can. J. Chem. Eng.* **55**, 538 (1977).

43. S. H. Jury, *J. Franklin Inst.* **305**, 79 (1978).

44. R. M. Barrer, *Zeolites and Clay Minerals as Adsorbents and Molecular Sieves.* Academic Press, London, 1978, Chap. XI.

45. J. Kärger, H. Pfeifer, and W. Heink, "NMR Diffusion Studies in Zeolites," presented at the Sixth International Conference on Zeolites, Reno, Nevada, July 1983.

46. D. M. Ruthven, *Am. Chem. Soc. Symp. Ser.* **218**, 345 (1983).

47. J. F. Charnell, *J. Crystal Growth* **8**, 291 (1971).

48. H. Yucel and D. M. Ruthven, *J. Chem. Soc. Faraday Trans. I* **76**, 60 (1980).

49. H. Yucel and D. M. Ruthven, *J. Chem. Soc. Faraday Trans. I* **76**, 71 (1980).

50. E. Kossaczky and D. Bobok, *Chem. Zvesti* **28**, 166, (1974).

51. D. M. Ruthven and R. I. Derrah, *J. Chem. Soc. Faraday Trans. I* **71**, 2031 (1975).

52. D. M. Ruthven, R. I. Derrah, and K. F. Loughlin, *Can. J. Chem.* **51**, 3514 (1973).

53. D. M. Ruthven, *Can. J. Chem.* **52**, 3523 (1974).

54. J. Kärger and D. M. Ruthven, *J. Chem. Soc. Faraday Trans. I* **77**, 1485 (1981).

55. J. Kärger and J. Caro, *Z. Chem.* **16**, 331 (1976).

56. J. Kärger, W. Heink, H. Pfeifer, and M. Rauscher, *Zeolites* **2**, 275 (1982).

57. K. P. Roethe, A. Roethe, and H. Kosslick, Workshop on Adsorption of Hydrocarbons in Zeolites, Berlin, GDR Nov. 1979. Preprints Vol. 2, p. 108 (Paper No. 12).

58. E. F. Kondis and J. S. Dranoff, *Ind. Eng. Chem. Process Design Develop.* **10**, 108 (1971).

59. L. Riekert and H. J. Doelle, *Angew. Chem.* **18**, 266 (1979).

60. D. M. Ruthven, L-K. Lee, and H. Yucel, *AIChE J.* **26**, 16 (1980).

61. D. M. Ruthven and L-K. Lee, *AIChE J.* **27**, 654 (1981).

62. T. Y. Lee and Y. H. Ma, *A.C.S. Symp. Ser.* **40**, 428, (1977).

63. Y. H. Ma and T. Y. Lee, *AIChE J.* **22**, 147 (1976).

64. Y. H. Ma and S. Y. Ho, *AIChE J.* **20**, 279 (1974).

65. D. M. Ruthven and I. H. Doetsch, *AIChE J.* **22**, 882 (1976).

66. D. M. Ruthven, A. M. Graham, and A. Vavlitis, *Proceedings of the Fifth International Conference on Zeolites, Naples, June 1980.* Heyden, London, 1980, p. 535.

67. J. Kärger, H. Pfeifer, M. Rauscher, and A. Walter, *J. Chem. Soc. Faraday Trans. I* **76**, 717 (1980).

68. J. Kärger, P. Lorenz, H. Pfeifer, and M. Bulow, *Z. Phys. Chem.* (Leipzig) **257**, 209 (1976).

69. H. Lechert, K. P. Wittern, and W. Schweitzer, *Acta. Phys. Chem.* **24**, 201 (1978).

70. H. Lechert, W. Schweitzer, and H. Kacirek, "Adsorption of Hydrocarbons in Zeolites II," Preprints of the Academy of Sciences of GDR, Berlin, 1979, p. 23.

71. K. P. Wittern, Ph.D. thesis, University of Hamburg, W. Germany, 1979.

72. J. Kärger and D. Michel, *Z. Phys. Chem. (Leipzig)* **257**, 983 (1976).

73. J. Kärger, D. Michel, A. Penzold, J. Caro, H. Pfeifer, and R. Schollner, *Z. Phys. Chem. (Leipzig)* **257**, 1009 (1976).

74. T. L. Hill, *Introduction to Statistical Thermodynamics.* Addison-Wesley, Reading, Mass., 1960, p. 172.

75. D. M. Ruthven and I. H. Doetsch, *J. Chem. Soc. Faraday Trans. I* **72**, 1043 (1976).

76. J. Kärger, M. Bulow, and K. Haberlandt, *J. Colloid Interface Sci.* **60**, 386 (1977).

77. J. Kärger, W. Krause, and H. Pfeifer, *Z. Phys. Chem. Leipzig* **263**, 840 (1982).

78. H.-J. Doelle, J. Heering, and L. Riekert, *J. Catalysis* **71**, 27 (1981).

79. P. Wu, A. Debebe, and Y. H. Ma, AIChE Winter Meeting, Orlando, FL, Paper 55a, 1981.

80. P. Wu and Y. H. Ma, *Proceedings of the Sixth International Conference on Zeolites, Reno, Nevada, July 1983.* Butterworths, Guildford, England, 1984.

81. K. Chihara, M. Suzuki, and K. Kawazoe, *AIChE Jl* **24**, 237 (1978).

82. K. Kawazoe, M. Suzuki, and K. Chihara, *J. Chem. Eng. Japan* **7**, 151 (1974) and **11**, 153 (1978).

83. K. Chihara, M. Suzuki, and K. Kawazoe, *J. Coll. Interface Sci.* **64**, 584 (1978).

84. H. Jüntgen, *Carbon* **15**, 273 (1977).

85. K. Knoblauch, *Chem. Eng.* **85**(25), 87 (1978).

86. M. F. M. Post, J. Amstel, and H. W. Krouwenhoven, *Proceedings of the Sixth International Conference on Zeolites, Reno, Nevada, July 1983.* Butterworths, Guildford, England, 1984.

87. H. Seewald, J. Klein, and H. Jüntgen, Engineering Foundation Conference on Fundamentals of Adsorption, Schloss Elmau, Bavaria, May 1983.

88. H. Seewald, *Endöl und Kohle-Erdgas-Petrochemie vereinigt mit Brennstoff-Chemie* **35**, 418 (1982).

89. M. Bulow, W. Mietk, P. Struve, W. Schirmer, and M. Kocirik, *Proceedings of the Sixth International Conference on Zeolites, Reno, Nevada, July 1983.* Butterworths, Guildford, England, 1984.

6

KINETICS OF SORPTION
IN BATCH SYSTEMS

The rate of physical adsorption at a surface is generally high so that in a porous catalyst or adsorbent the overall rate of adsorption is always controlled by mass or heat transfer resistance, rather than by the intrinsic sorption kinetics. However, this is not always immediately obvious from a cursory examination of kinetic data since a diffusion-controlled process may exhibit many of the characteristic features commonly associated with a slow activated surface rate process. There are several distinct resistances to mass and heat transfer which may limit the sorption rate and without detailed analysis coupled with appropriately designed experiments it is not always obvious which resistance is rate controlling. Thus, although direct measurement of the transient uptake curve for a sample of adsorbent provides, in principle, a simple method of studying adsorption kinetics, the interpretation of such data presents more difficulties than might be expected. The basic theory required for the analysis and interpretation of transient uptake curves for batch systems is presented in this chapter, while the more complex problem of sorption kinetics in a packed bed is dealt with in Chapters 8 and 9.

6.1. RESISTANCES TO MASS AND HEAT TRANSFER

As noted in Section 1.5, many commercial adsorbents consist of small microporous crystals formed into a macroporous pellet. Such adsorbents offer two distinct diffusional resistances to mass transfer: the micropore resistance of the adsorbent crystals or microparticles and the macropore diffusional resistance of the pellet. When adsorption occurs from a binary (or multicomponent) fluid mixture, there may be an additional resistance to mass transfer associated with transport through the laminar fluid boundary layer surrounding the particle (see Section 6.7). The general situation is as sketched in Figure

166
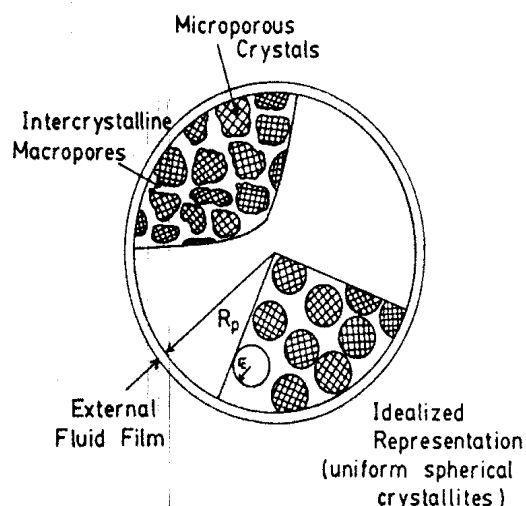
FIGURE 6.1. Schematic diagram of composite adsorbent pellet showing the three principal resistances to mass transfer.

6.1. The relative importance of micropore and macropore resistances depends on the ratio of the diffusional time constants which varies widely depending on the system and conditions. The time constant depends on the square of the particle radius; variation of the particle size therefore provides a simple and straightforward experimental test to confirm the nature of the controlling resistance.

Since adsorption is exothermic and the heat of sorption must be dissipated by heat transfer there is, in general, a difference in temperature between an adsorbent particle and the ambient fluid when sorption is taking place. Whether or not this temperature difference is significant depends on the relative rates of mass and heat transfer. By simple theoretical analysis it may be shown that in a batch adsorption experiment it is the dissipation of heat from the external surface of the adsorbent sample, rather than the conduction of heat within the adsorbent, which is generally the rate-limiting heat transfer process. The conditions under which heat transfer resistance may be neglected and the system treated as isothermal as well as a more detailed discussion of the analysis of nonisothermal behavior are given in Section 6.6.

6.2. ISOTHERMAL SINGLE-COMPONENT SORPTION: MICROPORE DIFFUSION CONTROL

Differential Step—Constant Diffusivity

The simplest case to consider is a single microporous adsorbent particle, such as a zeolite crystal, exposed to a step change in sorbate concentration at the external surface of the particle at time zero. Heat transfer is assumed to be sufficiently rapid, relative to the sorption rate, so that temperature gradients

both through the particle and between particle and surrounding fluid are negligible. For most particle shapes, representation as an equivalent sphere is an acceptable approximation and transport may therefore be described by a diffusion equation, written in spherical coordinates:

$$\frac{\partial q}{\partial t} = \frac{1}{r^2} \frac{\partial}{\partial r}\left(r^2 D_c \frac{\partial q}{\partial r} \right) \tag{6.1}$$

If the diffusivity is constant this equation simplifies to

$$\frac{\partial q}{\partial t} = D_c\left(\frac{\partial^2 q}{\partial r^2} + \frac{2}{r} \frac{\partial q}{\partial r} \right) \tag{6.2}$$

where D_c is the intracrystalline diffusivity and $q(r,t)$ is the adsorbed phase concentration. Even if the diffusivity is concentration dependent, the assumption of a constant diffusivity is still an acceptable approximation provided that the uptake curve is measured over a small differential change in adsorbed phase concentration.

If the uptake of sorbate by the adsorbent is small relative to the total quantity of sorbate introduced into the system, the ambient sorbate concentration will remain essentially constant following the initial step change, and the appropriate initial and boundary conditions are

$$q(r,0) = q_0', \qquad q(r_c,t) = q_0, \qquad \left(\frac{\partial q}{\partial r} \right)_{r=0} = 0 \tag{6.3}$$

The solution for the uptake curve is then given by the familiar expression

$$\frac{\bar{q} - q_0'}{q_0 - q_0'} = \frac{m_t}{m_\infty} = 1 - \frac{6}{\pi^2} \sum_{n=1}^{\infty} \frac{1}{n^2} \exp\left(- \frac{n^2 \pi^2 D_c t}{r_c^2} \right) \tag{6.4}$$

where $\bar{q}(t)$ is the average concentration through the particle, defined by

$$\bar{q} = \frac{3}{r_c^3} \int_0^{r_c} q r^2 \, dr \tag{6.5}$$

and m_t/m_∞ is the fractional approach to equilibrium. This expression [Eq. (6.4)] converges rapidly in the long time region since the higher terms of the summation become vanishingly small. For fractional uptakes greater than 70% we may retain only the first term to obtain

$$1 - \frac{m_t}{m_\infty} \approx \frac{6}{\pi^2} \exp\left(- \frac{\pi^2 D_c t}{r_c^2} \right) \tag{6.6}$$

At 70% uptake this expression deviates by less than 2% from the full solution [Eq. (6.4)].

In the long time region a plot of $\ln(1 - m_t/m_\infty)$ versus t should be linear with slope $-\pi^2 D_c/r_c^2$ and intercept $\ln(6/\pi^2)$, as illustrated in Figure 6.2. Such a plot provides, in principle, a simple method of both checking the conformity of an experimental uptake curve with the diffusion equation and determining the diffusional time constant.
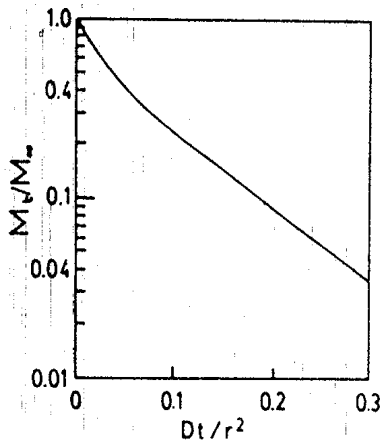
FIGURE 6.2. Theoretical uptake curve calculated according to Eq. (6.4), showing limiting behavior in the long time region.

At short times Eq. (6.4) converges very slowly and a more useful form of the solution is given by

$$\frac{m_t}{m_\infty} = 6\left(\frac{D_c t}{r_c^2}\right)^{1/2}\left[\frac{1}{\sqrt{\pi}} + 2\sum_{n=1}^{\infty} i\,\mathrm{erfc}\left(\frac{nr_c}{\sqrt{D_c t}}\right)\right] - 3\frac{D_c t}{r_c^2} \qquad (6.7)$$

which, for $m_t/m_\infty < 0.3$ reduces to

$$\frac{m_t}{m_\infty} \approx \frac{6}{\sqrt{\pi}}\left(\frac{D_c t}{r_c^2}\right)^{1/2} \qquad (6.8)$$

In the initial region diffusion occurs as if in a semi-infinite medium and the expression for the uptake curve for any particle shape may be written:

$$\frac{m_t}{m_\infty} \approx \frac{2A}{V}\left(\frac{D_c t}{\pi}\right)^{1/2} \qquad (6.9)$$

where A/V is the ratio of external area-to-particle volume which for a spherical particle is simply $3/r_c$. A plot of fractional uptake versus $\sqrt{t}$ should
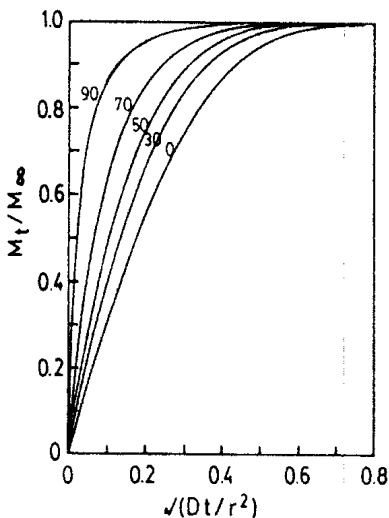
FIGURE 6.3. Theoretical uptake curves calculated according to Eqs. (6.10) and (6.11), showing the effect of finite system volume. Numbers on curve give Λ expressed as a percentage.

therefore yield a straight line through the origin with slope $2(A/V)\sqrt{D_c/\pi}$, as illustrated in Figure 6.3.

Effect of Finite System Volume

If the quantity of sorbate adsorbed or desorbed is not negligible compared with the quantity introduced or removed from the ambient fluid phase, the sorbate concentration in the fluid will not remain constant after the initial step, giving rise to a time-dependent boundary condition at the surface of the adsorbent particle. The solution for the uptake curve then becomes[1]

$$\frac{m_t}{m_\infty} = 1 - 6 \sum_{n=1}^{\infty} \frac{\exp(-D_c p_n^2 t / r_c^2)}{9\Lambda/(1-\Lambda) + (1-\Lambda)p_n^2} \tag{6.10}$$

where p_n is given by the nonzero roots of

$$\tan p_n = \frac{3p_n}{3 + (1/\Lambda - 1)p_n^2} \tag{6.11}$$

and $\Lambda \equiv (C_0 - C_\infty)/C_0$, the fraction of sorbate ultimately adsorbed by the adsorbent. A family of theoretical uptake curves, calculated according to Eqs. (6.10) and (6.11) is shown in Figure 6.3. It is evident that the effect of finite system volume becomes significant when Λ is greater than about 0.1 and under these conditions the assumption of a constant boundary condition will lead to an erroneously high apparent diffusivity.

Integral Step—Variable Diffusivity

In the preceding analysis we considered the diffusivity as constant but if the uptake curve is measured over a large concentration step this may be a poor approximation. In many zeolitic systems the concentration dependence of the intracrystalline diffusivity is given approximately by Eq. (5.6), with D_0 independent of concentration. If the adsorption equilibrium isotherm obeys the Langmuir equation this gives as the expression for the concentration dependence of the diffusivity

$$D_c = D_0 \left(1 - \frac{q}{q_s} \right)^{-1} \tag{6.12}$$

and the appropriate expression for the diffusion equation becomes

$$\frac{\partial q}{\partial t} = \frac{D_0}{r^2} \frac{\partial}{\partial r} \left(\frac{r^2}{(1 - q/q_s)} \frac{\partial q}{\partial r} \right) \tag{6.13}$$

This equation was solved numerically with the boundary conditions represented by Eq. (6.3) by Garg and Ruthven[2] and theoretical uptake curves calculated from this solution are reproduced in Figure 6.4. An essentially similar analysis was reported by Kocirik and Zikanova.[3] An additional
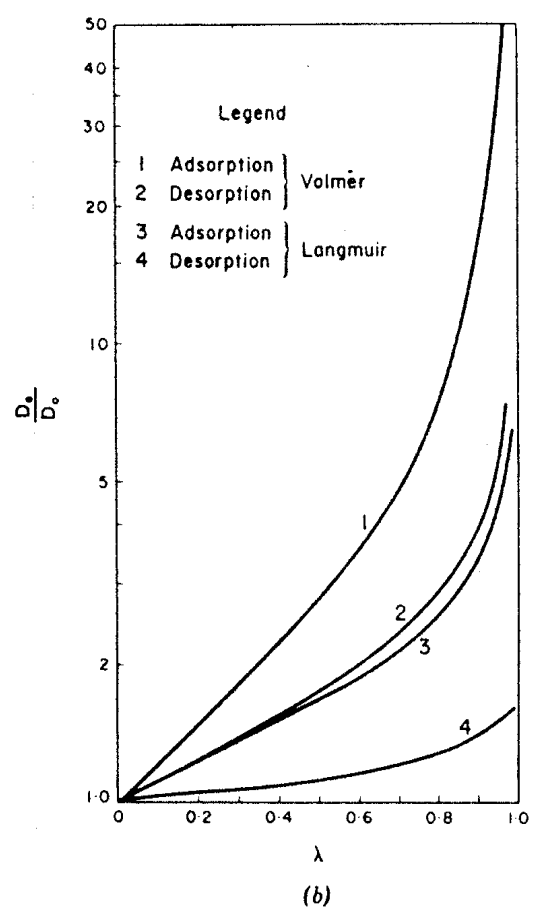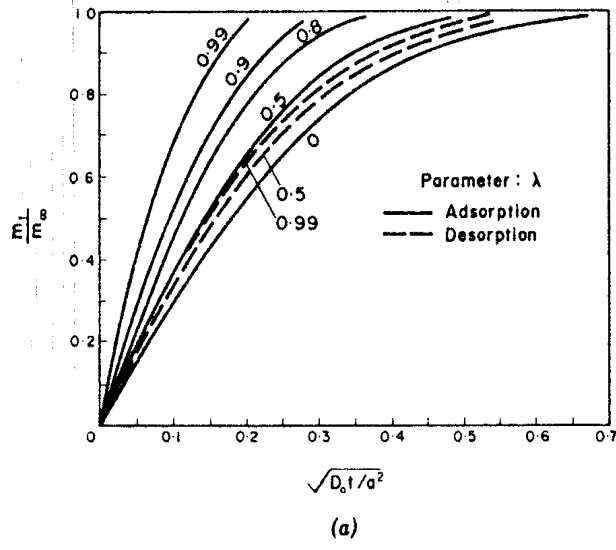
FIGURE 6.4. (a) Theoretical uptake curves for a Langmuir system with micropore diffusion control and (b) variation of effective diffusivity with sorbate concentration for a Langmuir system and a Volmer system calculated from the theoretical solution of Garg and Ruthven.[2] [Reprinted with permission from *Chem. Eng. Sci.* **27**, Garg and Ruthven (ref. 2). Copyright 1972, Pergamon Press, Ltd.]

parameter λ $(= q_0/q_s)$ representing the nonlinearity of the equilibrium relationship or the magnitude of the concentration step $(0 \rightarrow q_0)$ over which the uptake curve is measured is now required to define the system behavior. With appropriately redefined parameters $[\lambda = (q_0 - q_0')/(q_s - q_0')$, $D_0 \rightarrow D_0(1 - q_0'/q_s)^{-1}]$ the same solution is applicable to uptake curves measured from a finite initial concentration (q_0').

$\sqrt{t}\ -\ \sqrt{sec}$

(a)

$\sqrt{t}\ -\sqrt{sec}$

(b)
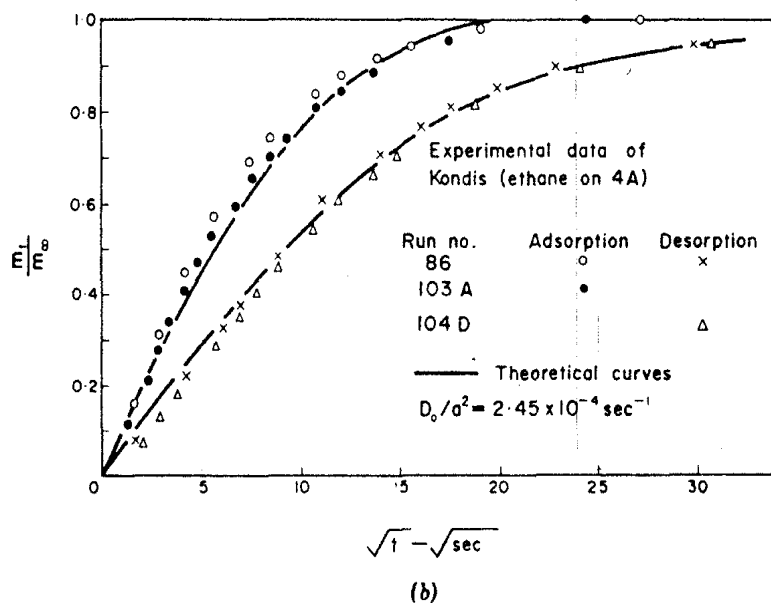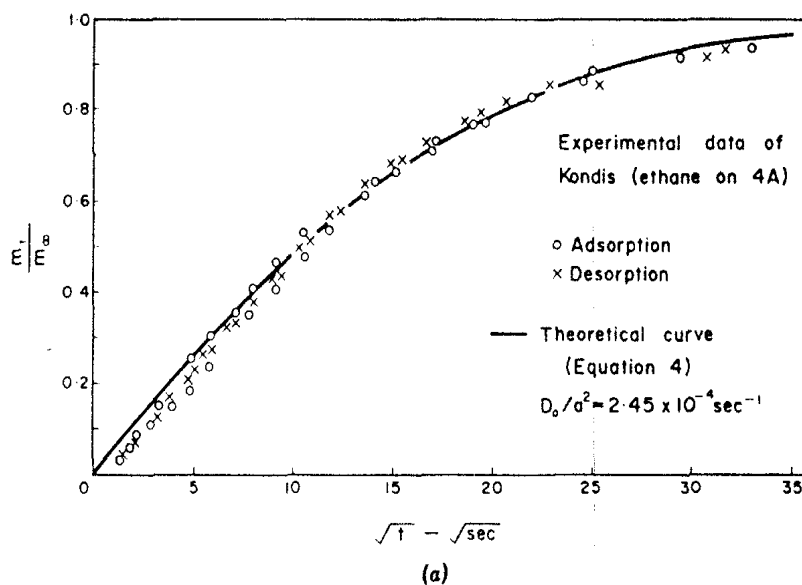
FIGURE 6.5. Comparison of theoretical and experimental uptake curves for C_2H_6 in 4A sieve. (a) Uptake curves measured differentially showing conformity to the isothermal diffusion model. (b) Integral uptake curves showing conformity to the theoretical curves calculated according to Eq. (6.13) with the values of D_0 derived from the low concentration data. [Reprinted with permission from Chem. Eng. Sci. 27, Garg and Ruthven (ref. 2). Copyright 1972, Pergamon Press, Ltd.]

The shape of the uptake curve does not differ greatly from the shape of the constant diffusivity curve but the uptake rate is modified. The effective diffusivity (D_e) thus becomes dependent on the step size, lying within the range

$$D_0 < D_e < \overline{D} \equiv \frac{1}{q_0} \int_0^{q_0} D(q) \, dq \tag{6.14}$$

where $\overline{D}$ is the average diffusivity over the concentration range $0 < q < q_0$. In a differential step the effect of the concentration dependence of diffusivity becomes insignificant. Equation (6.13) reduces to the constant diffusivity form and adsorption and desorption curves are mirror images. As the step size is increased the rate of adsorption increases rapidly while the desorption rate increases only slightly so that a large difference between adsorption and desorption rates develops. The general behavior is summarized in Figure 6.4.

Experimental data obtained by Kondis and Dranoff[4-6] for sorption of ethane in Linde 4A zeolite were analyzed according to this model (Figure 6.5). For small concentration steps adsorption and desorption curves were essentially identical and could be represented by Eq. (6.4), the solution for a constant diffusivity. For larger steps adsorption was much faster than desorption but both curves were well represented by the numerical solution to Eq. (6.13) using the value of D_0 derived from the low-concentration experiments. Large differences between adsorption and desorption rates have often been reported in the literature of zeolitic diffusion[7,8] but such results have generally been derived from integral diffusion measurements. The above analysis suggests that these differences probably arise from the concentration dependence of the diffusivity, rather than from any difference in intrinsic mobility.

6.3. ISOTHERMAL SINGLE-COMPONENT SORPTION: MACROPORE DIFFUSION CONTROL

In a composite adsorbent pellet (Figure 6.1) the uptake rate may be controlled by either micropore diffusion or macropore diffusion or by a combination of both resistances. If micropore resistance is dominant the concentration through the pellet is essentially uniform and the sorption rate should be independent of gross particle size. Under these conditions the system can be regarded simply as an assemblage of identical microparticles and the uptake curves may be analyzed in exactly the same way as for a single isolated microcrystal. On the other hand, if macropore resistance is dominant the concentration through an individual microparticle will be uniform but there will be a concentration profile through the macroparticle and the uptake rate will therefore depend on gross particle size. To derive an expression for the uptake curve for such a system we assume local equilibrium between the adsorbed phase and fluid phase within the macropore at any specified radial position.

Linear Equilibrium

The appropriate form of the diffusion equation for a macropore-controlled system may be obtained from a differential mass balance on a spherical shell element:

$$(1 - \epsilon_p) \frac{\partial q}{\partial t} + \epsilon_p \frac{\partial c}{\partial t} = \epsilon_p D_p \left(\frac{\partial^2 c}{\partial R^2} + \frac{2}{R} \frac{\partial c}{\partial R} \right) \qquad (6.15)$$

where we have taken the macropore diffusivity as independent of concentration, which is generally a good approximation. If the equilibrium isotherm is linear ($q^* = Kc$) this equation may be written

$$\frac{\partial c}{\partial t} = \frac{\epsilon_p D_p}{\epsilon_p + (1 - \epsilon_p)K} \left(\frac{\partial^2 c}{\partial R^2} + \frac{2}{R} \frac{\partial c}{\partial R} \right) \qquad (6.16)$$

which is identical with Eq. (6.2) except that D_c is replaced by the effective macropore diffusivity $\epsilon_p D_p / [1 + (1 - \epsilon_p)K]$. The initial and boundary conditions for a step change in surface concentration at time zero are also analogous to Eq. (6.3):

$$c(R, 0) = c_0', \qquad q(R, 0) = q_0'$$

$$c(R_p, t) = c_0, \qquad q(R_p, t) = q_0 \qquad (6.17)$$

$$\left(\frac{\partial c}{\partial R} \right)_{R=0} = \left(\frac{\partial q}{\partial R} \right)_{R=0} = 0$$

and the solution is therefore identical to Eq. (6.4) or (6.7) [or for a finite volume system, Eqs. (6.10) and (6.11)] with D_c / r_c^2 replaced by $(D_p / R_p^2) / [1 + (1 - \epsilon_p)K / \epsilon_p]$, the effective diffusional time constant.

The equilibrium constant which appears in the denominator of the time constant will vary with temperature according to a vant Hoff equation ($K = K_0 e^{-\Delta H / RT}$) whereas the temperature dependence of the pore diffusivity D_p is relatively weak. It follows that the apparent diffusivity will be strongly temperature dependent with an apparent energy of activation that approximates the heat of sorption. An apparent activation energy essentially equal to the heat of sorption may therefore be regarded as strong circumstantial evidence of macropore diffusion control. Since the equilibrium constant is commonly large, the effective diffusivity is generally small and no evidence concerning the nature of the controlling mass transfer resistance can be obtained from the magnitude of this quantity.

Provided that the uptake rate is measured over a small differential step, the same expression will apply outside the Henry's law region with the equilibrium constant K replaced by the local slope of the isotherm (dq^*/dc). Since the slope of the isotherm in general decreases with increasing concentration the effective diffusivity $D_p / [1 + (1 - \epsilon_p)(dq^*/dc)/\epsilon_p]$ will show an increase with increasing sorbate concentration.

Nonlinear Equilibrium

If the change in concentration over which the uptake curve is measured is large, the effect of nonlinearity of the equilibrium isotherm must be considered. For a Langmuir system

$$\frac{q^*}{q_s} = \frac{bc}{1+bc}, \qquad \frac{dq^*}{dc} = \frac{bq_s}{(1+bc)^2} = bq_s\left(1 - \frac{q}{q_s}\right)^2 \qquad (6.18)$$

If we are considering adsorption from the gas phase, $q \gg c$ and since $\partial c/\partial R = (\partial q/\partial R)(dc/dq^*)$, Eq. (6.15) becomes

$$\frac{\partial q}{\partial t} = \frac{\epsilon_p D_p}{(1-\epsilon_p)bq_s} \frac{1}{R_p^2} \frac{\partial}{\partial R}\left(\frac{R^2}{(1-q/q_s)^2} \frac{\partial q}{\partial R}\right) \qquad (6.19)$$

This is the standard diffusion equation in spherical coordinates with a concentration-dependent effective diffusivity given by

$$D_e = \frac{\epsilon_p D_p}{(1-\epsilon_p)(1-q/q_s)^2 bq_s} \qquad (6.20)$$

This is qualitatively similar to Eq. (6.13) which describes the behavior of a micropore-controlled system, except that the concentration dependence of the effective diffusivity is stronger. The solution for the uptake curve shows similar general features. The fractional uptake is a function of the dimensionless time variable $D_e t/R_p^2$ and the step size or nonlinearity, measured by the parameter $\lambda = q_0/q_s$. At small values of λ the system approaches linearity. The effective diffusivity becomes essentially constant and equal to the limiting value for the Henry's law region $[D_e \approx \epsilon_p D_p/(1-\epsilon_p)bq_s]$ and Eq. (6.19) reduces to the form of Eq. (6.16). Under these conditions adsorption and desorption curves are mirror images and the uptake rate is independent of step size but for larger concentration steps the rate becomes dependent on step size and adsorption is much faster than desorption.

Experimental studies of diffusion of several hydrocarbons in 5A zeolite pellets under conditions of macropore diffusion control have been reported by Ruthven and Derrah[9] and by Youngquist, Allen, and Eisenberg.[10] The experimentally observed behavior is in accordance with the theory outlined above. Sorption curves measured differentially over small concentration steps show no difference between adsorption and desorption curves measured at the same concentration. As a result of the decreasing slope of the equilibrium isotherm, the effective diffusivity increases rapidly with increasing concentration, as illustrated in Figure 6.6b. The corresponding pore diffusivities and the equilibrium isotherms from which the values of dq^*/dc could be found directly, show a modest decrease with increasing sorbate concentration. Such behavior is to be expected when molecular diffusion makes a significant contribution to macropore transport. The trends of the experimental values of
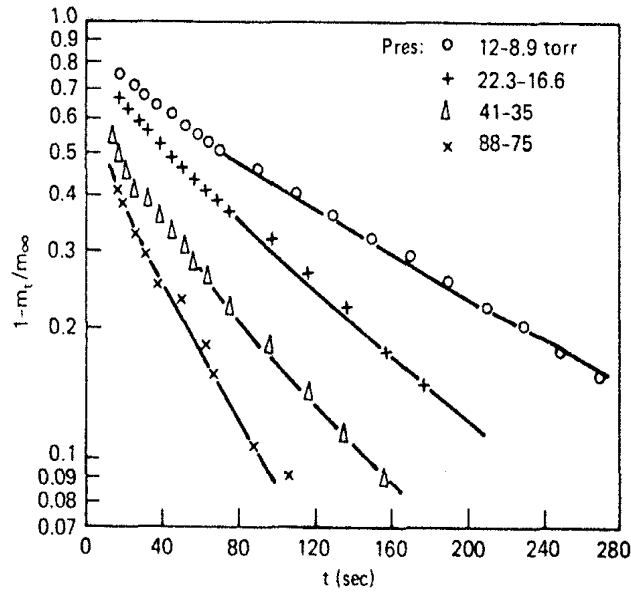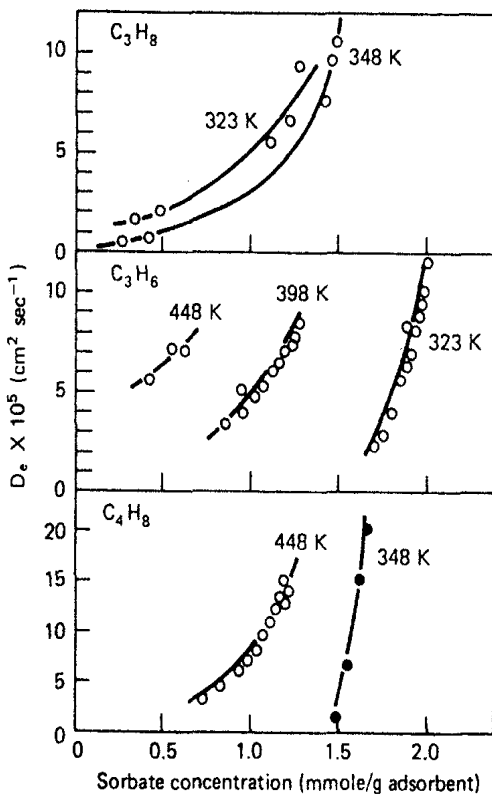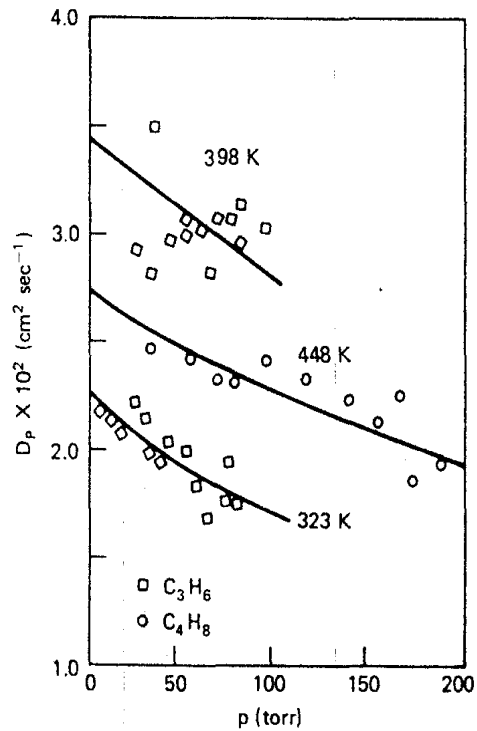
FIGURE 6.6. Sorption of light hydrocarbons in 5A molecular sieve pellets (Davison C-521) under conditions of macropore diffusion control. (a) Differential uptake curves for C_3H_6 at 323 K; (b) concentration dependence of effective diffusivities calculated from the experimental uptake curves [see Eq. (6.16)]; (c) pressure dependence of pore diffusivities calculated from effective diffusivities $D_e = D_p/[1 + (1 - \epsilon_p)(dq^*/dc)/\epsilon_p]$. (From ref. 9; reprinted from *Canadian Journal of Chemical Engineering.*)

TABLE 6.1. Physical Properties of Adsorbents

Zeolite	Linde 5A Pellets 5A	Davison C-521 5A	Davison C-626 5A
Form	Extrudates	Beads	Beads
Nominal pellet size	$\frac{1}{8}$ in.	4–8 mesh	4–8 mesh
R_p (cm)	0.16	0.23	0.26
ρ_p (g cm^{-3})	1.07	1.16	1.14
ϵ_p^a	0.34	0.36	0.32
ϵ_p^b	0.32	0.26	0.275
Wt. fraction of crystals	0.08	0.83	1.0
$\bar{r}$ (Å)	3,200	600	1600
Range of r (Å)	300–10,000	75–2,200	300–5,000
$\bar{R}_z$	1.8	0.35	0.35
Range of R_z (micron)	0.4–3.0	0.3–0.4	0.3–0.4

Source: From Ref. 9; reprinted from *Can. J. Chem. Eng.* with permission.

[a] These values were obtained from porosimetry.

[b] These values were calculated from density data taking the density of the anhydrous zeolite crystals as 1.57 g/cm^3 and were used in the calculation of D_p from D_e.

TABLE 6.2. Mean Pore Diffusion Coefficients and Tortuosity Factors

		C-521		C-626	
Sorbate	Temperature (K)	$\bar{D}_p$ cm^2 s^{-1}	τ	$\bar{D}_p$ cm^2 s^{-1}	τ
C_3H_8	348	0.030	4.9	—	—
	323	0.023	5.7	—	—
C_3H_6	323	0.020	6.8	(0.025)	
	398	0.030	5.2	0.076	4.5
	448	0.026	6.5	—	—
C_4H_8	348	0.020	6.6	(0.035)	
	448	0.023	6.2	—	

Source: From Ref. 9; reprinted from *Can. J. Chem. Eng.* with permission.

Values in parentheses are the means of a limited number of rather scattered values of D_p and are not considered reliable.

D_p shown in Figure 6.6c may be represented by theoretical curves calculated assuming a combination of Knudsen and molecular diffusion with the tortuosity factors given in Table 6.2:

$$\frac{1}{D_p} = \tau \left(\frac{1}{D_K} + \frac{1}{D_m} \right) \tag{6.21}$$

Relevant physical properties of the adsorbents are summarized in Table 6.1.

Integral uptake curves measured over large concentration steps show the expected large difference between adsorption and desorption rates as may be seen from Figure 6.7. The experimental curves are well approximated by theoretical curves calculated from the solution of Eq. (6.19) and the time constants obtained in this way are consistent with the values derived from differential measurements at low concentrations, as may be seen from Table 6.3.
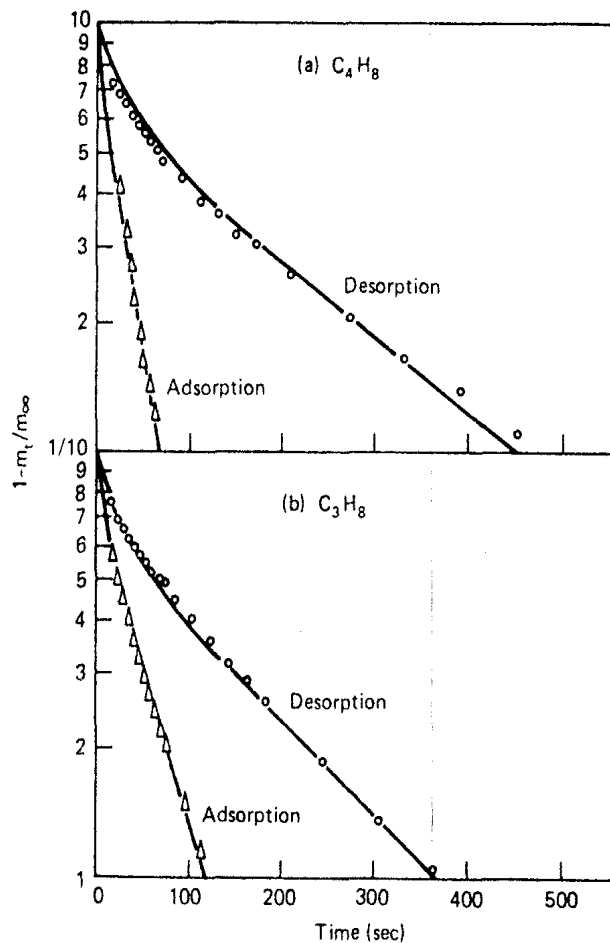
FIGURE 6.7. Integral uptake curves for C_3H_8 and C_4H_8 in Davison C-521 molecular sieve pellets showing difference between adsorption and desorption curves. Details are given in Tables 6.1–6.3. (From ref. 9; reprinted from *Canadian Journal of Chemical Engineering*.)

TABLE 6.3. Analysis of Sorption Curves for Large Step Changes

System		p_1 (torr)	p_2 (torr)	q_1 (mmole g^{-1})	q_2 (mmole g^{-1})	q_s (mmole g^{-1})	λ	$D' \times 10^5$ (cm^2 s^{-1})	$D'_0 \times 10^5$ (cm^2 s^{-1})
C_4H_8	Ads	1.1	86	1.35	1.68	1.71	0.92	14.1	0.64
	Des	86	1.1	1.35	1.68	1.71	0.92	2.2	0.51
C_3H_8	Ads	29	105	0.80	1.29	1.56	0.65	8.0	1.78[a]
	Des	100	12	0.51	1.27	1.56	0.72	2.7	1.15

Source: From Ref. 9; reprinted from *Can. J. Chem. Eng.* with permission.

[a] Value of D'_0 for propane derived from differential measurements at low sorbate concentration $\sim 2 \times 10^{-5}$ cm^2 s^{-1}.
D' = apparent diffusivity from sorption curve, D'_0 = limiting value of D_e as $q \rightarrow 0$.

Irreversible Equilibrium

For a large concentration step (zero to saturation) a highly favorable type I isotherm (e.g., a Langmuir isotherm) approaches the rectangular or irreversible form:

$$c = 0, \qquad q^* = 0, \qquad c > 0, \qquad q^* = q_s \qquad (6.22)$$

The rectangular isotherm therefore provides a convenient and mathematically tractible model for the analysis of sorption behavior for strongly adsorbed species. We consider a composite macroporous pellet in which most of the adsorption capacity lies in the microporous microparticles (e.g., zeolite crystallites) while the dominant mass transfer resistance is macropore diffusion in the channels between the microparticles. Intracrystalline diffusion is assumed to be sufficiently rapid to maintain the sorbate concentration essentially uniform through an individual crystallite and at equilibrium with the sorbate concentration in the macropore. Under these conditions the adsorption front penetrates into the particle as a shock transition separating the shrinking core region of the particle, into which adsorbent has not yet penetrated, from the saturated outer region in which the adsorbed phase concentration is uniform at the saturation level. Adsorption occurs entirely at this shock front $(R = R_f)$. The concentration profiles in adsorbed phase and fluid phase (along a macropore) are sketched in Figure 6.8.

Over the region $R_p > R > R_f$, the flux through the pores is constant since all adsorption takes place at R_f. The total flux into the particle is given by $4\pi\epsilon_p D_p R^2 \partial c/\partial R$ and is independent of R $[= k(t)]$. Integration at constant t yields

$$c = \frac{k(t)}{r} + \text{constant} \qquad (6.23)$$

and using the boundary conditions $R = R_f$, $c = 0$; $R = R_p$, $c = c_0$ (at the
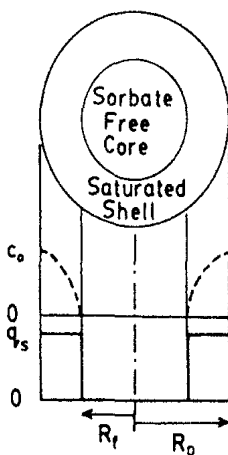
FIGURE 6.8.   Schematic diagram showing form of concentration profile through a macroporous pellet for sorption under conditions of macropore diffusion control with an irreversible isotherm.

particle surface) we obtain

$$R^2 \frac{\partial c}{\partial R} = \frac{c_0}{1/R_f - 1/R} \tag{6.24}$$

A mass balance at $R = R_f$ gives for the flow rate across the control surface

$$4\pi D_p \epsilon_p \left(R^2 \frac{\partial c}{\partial R} \right) = \frac{4\pi \epsilon_p D_p c_0}{1/R_f - 1/R} = -4\pi R_f^2 q_s \frac{dR_f}{dt} \tag{6.25}$$

Integrating from R_f to R_p gives

$$\frac{\epsilon_p D_p c_0 t}{R^2 q_s} = -\frac{1}{2} \left(\frac{R_f}{R_p} \right)^2 + \frac{1}{3} \left(\frac{R_f}{R_p} \right)^3 + \frac{1}{6} \tag{6.26}$$

Since $1 - m_t/m_\infty = (R_f/R_p)^3$ the uptake curve is given by[11]

$$\frac{t}{\tau} = 1 + 2 \left(1 - \frac{m_t}{m_\infty} \right) - 3 \left(1 - \frac{m_t}{m_\infty} \right)^{2/3} \tag{6.27}$$
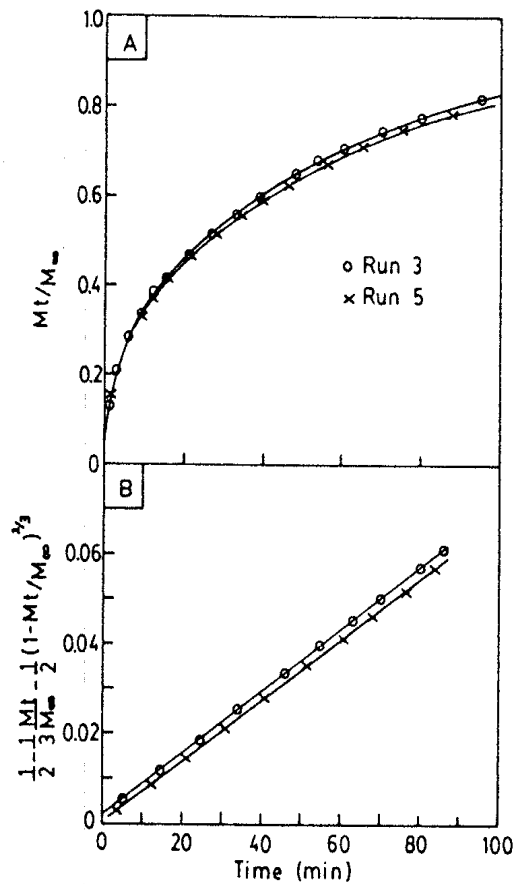
FIGURE 6.9. Experimental uptake curves for water in 4A molecular sieve pellets (Laporte) showing conformity to irreversible model [Eq. (6.27)]. (Data of Kyte.[13])

and the stoichiometric time (τ) at which $m_t/m_\infty = 1.0$ is given by

$$\tau = \frac{1}{6} \frac{R_p^2}{\epsilon_p D_p} \left(\frac{q_s}{c_0} \right) \tag{6.28}$$

Equation (6.27) may also be written in explicit form as[12]

$$1 - \frac{m_t}{m_\infty} = \left\{ \frac{1}{2} + \cos\left[\frac{\pi}{3} + \frac{1}{3} \cos^{-1}\left(1 - \frac{2t}{\tau}\right) \right] \right\}^3 \tag{6.29}$$

These expressions provide a simple and convenient model for the analysis of experimental uptake curves when the equilibrium isotherm is highly favorable and micropore diffusion is rapid. These conditions are amply fulfilled for the adsorption of water at or near ambient temperature in molecular sieve adsorbents. Experimental uptake curves for this system measured by Kyte[13] are shown in Figure 6.9. The experimental conditions and the effective diffusivity calculated according to Eq. (6.27) are given in Tables 6.4 and 6.5. Under the experimental conditions the estimated value of the Knudsen diffusivity [from Eq. (5.17)] is much larger than the molecular diffusivity

TABLE 6.4. Experimental Conditions for Single-Particle Uptake Measurements[13]

Adsorbent	Zeosorb 4A sieve (Laporte)
Particle radius (R_p)	2.93 mm
Particle weight	120 mg (dry)
Humidity	19,900 ppm
c_0	15×10^{-6} g H_2O/cm^3
q_0	0.198 g H_2O/cm^3 pellet
Temperature	30°C
Particle Re	43 and 104
Air flow rate	2.17 and 5.77 liters/min
Diameter of sample tube	2 cm
Macroporosity (ϵ_p)	0.34
Average macro-pore radius	10^{-4} cm

TABLE 6.5. Diffusivities Derived from Single-Particle Uptake Experiments

Run No.	$\epsilon_p D_p$ (cm^2 s^{-1})	D_p (cm^2 s^{-1})	D_K (cm^2 s^{-1})	D_M (cm^2 s^{-1})	Tortuosity Factor
3	0.0139	0.040	3.98	0.256	
5	0.0132	0.038	3.98	0.256	5

indicating that molecular diffusion is the dominant transport mechanism within the macropores. On this basis a value of 5 for the tortuosity factor is obtained which is of the expected order and is in fact similar to the values derived by Ruthven and Derrah from the uptake curves for propane, propene, and 1-butene (Tables 6.1–6.3).

6.4. ISOTHERMAL SINGLE-COMPONENT SORPTION: BOTH MACROPORE AND MICROPORE RESISTANCES SIGNIFICANT

In the situations so far considered a single diffusional resistance (either micropore or macropore) has been regarded as rate controlling with all other rate processes assumed to be essentially at equilibrium. However, in many practical systems the macropore and micropore diffusional time constants are of similar magnitude and under these conditions the overall uptake rate will depend on both time constants. Such a system appears to have been first analyzed by Ruckenstein et al.[14] in relation to microreticular ion exchange resins. A composite macroporous spherical particle composed of microporous spherical microparticles was considered, as sketched in Figure 6.1. Assuming a linear equilibrium relation and an infinitely large system (constant boundary condition) an analytic solution was derived for the uptake curve assuming a step change concentration at the external surface of the macroparticle.

Essentially the same problem was considered by Ma and Lee[15] and by Lee[16] who extended the analysis to include the case of a finite volume system in which the external fluid concentration changes as uptake progresses. This is the practically important solution for the analysis of uptake curves for experimental liquid phase systems in which the sorption curve is followed by monitoring the external fluid phase concentration.

The system is described by the following set of equations:

Intracrystalline diffusion in microparticle

$$\frac{\partial q}{\partial t} = \frac{1}{r^2} \frac{\partial}{\partial r} \left(r^2 D_c \frac{\partial q}{\partial r} \right) \tag{6.30}$$

$$\frac{\partial q}{\partial r}(0,t) = 0, \qquad q(r_c,t) = Kc(R,t) \tag{6.31}$$

$$\bar{q}(R,t) = \frac{3}{r_c^2} \int_0^{r_c} qr^2 \, dr \tag{6.32}$$

Macropore diffusion

$$\frac{1}{R^2} \frac{\partial}{\partial R} \left(R^2 D_p \frac{\partial c}{\partial R} \right) = \frac{\partial c}{\partial t} + \left(\frac{1 - \epsilon_p}{\epsilon_p} \right) \frac{\partial \bar{q}}{\partial t} \tag{6.33}$$

$$\frac{\partial c}{\partial R}(0,t) = 0, \qquad c(R_p,t) = c_0, \qquad q(r,0) = c(R,0) = 0 \tag{6.34}$$

The solution for the uptake curve for an infinitely large system (constant surface boundary condition) is

$$\frac{m_t}{m_\infty}$$

$$= 1 - \frac{18}{\beta + 3\alpha} \sum_{m=1}^{\infty} \sum_{n=1}^{\infty} \left(\frac{n^2\pi^2}{p_{n,m}^4}\right) \frac{e^{-p_{n,m}^2 D_c t/r_c^2}}{\left\{\alpha + \frac{\beta}{2}\left[1 + \frac{\cot p_{n,m}}{p_{n,m}}(p_{n,m}\cot p_{n,m} - 1)\right]\right\}}$$

(6.35)

where $p_{n,m}$ is given by the solution of the equation

$$\alpha p_{n,m}^2 - n^2\pi^2 = \beta(p_{n,m}\cot p_{n,m} - 1)$$

(6.36)

and the parameters α and β are defined by $\alpha \equiv (D_c/r_c^2)/(D_p/R_p^2)$, $\beta \equiv 3\alpha(1 - \epsilon_p)q_0/\epsilon_p c_0$. This expression is equivalent to the form given by Ruckenstein but since only one double summation is involved it is somewhat more convenient for numerical evaluation. If the accumulation of sorbate in the macropores can be neglected ($\beta \gg \alpha$), and this is generally a good approximation for sorption from the vapor phase, Eq. (6.35) may be simplified to

$$\frac{m_t}{m_\infty} = 1 - \sum_{m=1}^{\infty} \sum_{n=1}^{\infty} \frac{36n^2\pi^2\exp\left(-p_{n,m}^2 D_c t/r_c^2\right)}{\beta^2 p_{n,m}^4\left[1 + \frac{\cot p_{n,m}}{p_{n,m}}(p_{n,m}\cot p_{n,m} - 1)\right]}$$

(6.37)

where $p_{n,m}$ is given by

$$\beta(p_{n,m}\cot p_{n,m} - 1) = -n^2\pi^2$$

(6.38)

The more general solution, which allows for the change in external fluid concentration during sorption is

$$\frac{m_t}{m_\infty} = 1 - \frac{1}{\Lambda} \sum_{m=1}^{\infty} \sum_{n=1}^{\infty} \frac{\exp\left(-p_{n,m}^2 D_c t/r_c^2\right)}{1 + \frac{1}{4}\left[9\gamma/\beta - p_{n,m}^2(1 + \beta p_{n,m}^2/9\gamma)/u_n^2\right]L_{n,m}}$$

(6.39)

where

$$L_{n,m} = \left(2\alpha + \frac{\beta}{1 - \Lambda}\right) - \left(\frac{u_n^2 + \alpha p_{n,m}^2}{p_{n,m}^2}\right) - \left[1 + \frac{(1 - \Lambda)(u_n^2 + \alpha p_{n,m}^2)}{\beta}\right]$$

(6.40)

with $p_{n,m}$ given by the roots of

$$u_n^2 = \frac{\beta}{1 - \Lambda}(p_{n,m}\cot p_{n,m} - 1) - \alpha p_{n,m}^2$$

(6.41)
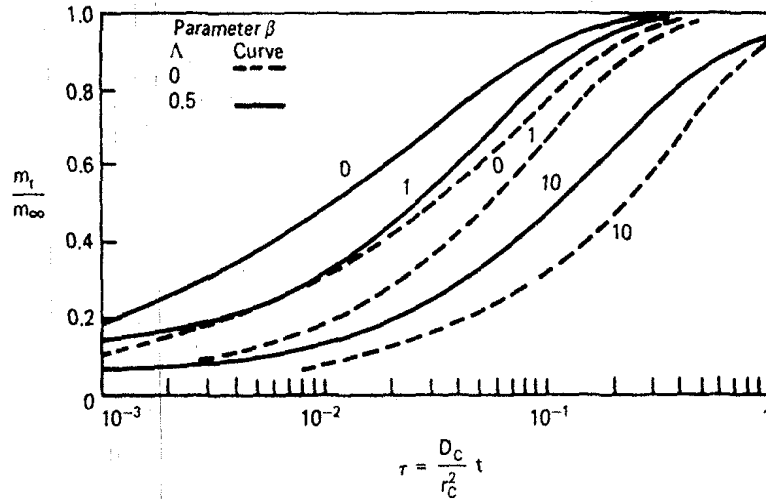
FIGURE 6.10. Theoretical uptake curves for a biporous adsorbent calculated according to Eqs. (6.39)–(6.42) showing the transition from micropore to macropore diffusion control and the difference in the shape of the uptake curve for intermediate values of β. (From ref. 16, with permission.)

and u_n given by the roots of

$$u_n \coth u_n = 1 + \frac{p_{n,m}^2 \beta}{9\gamma}$$

$$\Lambda = \frac{C_0 - C_\infty}{C_0}$$

$$\gamma = \frac{\beta \Lambda}{\beta + 3\alpha(1 - \Lambda)}$$

(6.42)

It is obvious if the sorption curve is to be followed by monitoring the composition of the fluid phase the experimental conditions must be chosen to ensure that $\Lambda \gg 0$.

For $\Lambda \to 0$ Eqs. (6.39)–(6.42) reduce to Eqs. (6.35) and (6.36), the solution for a constant external boundary condition. The limiting cases of macropore control ($\beta \to \infty$) and micropore control ($\beta > 0$), under which conditions Eqs. (6.39) and (6.42) reduce to the forms of Eqs. (6.10) and (6.11) [or Eq. (6.4) for $\Lambda \to 0$], may also be derived. For intermediate values of β the curves have a different shape and cannot be represented by a simple solution to the diffusion equation with a single time constant. The transition from micro- to macrocontrol (for $\Lambda = 0$) is illustrated in Figure 6.10.

6.5. DIFFUSION IN A BED OF POROUS PARTICLES

In the measurement of micropore diffusivities by the uptake rate method it is generally necessary to use an assemblage of microparticles (such as zeolite
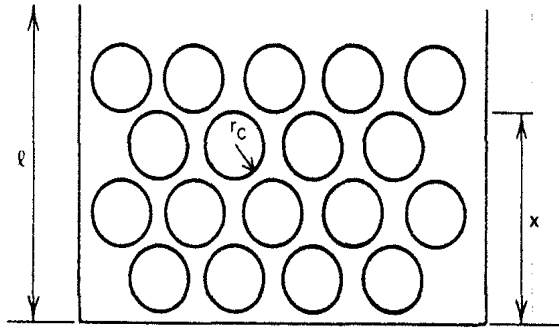
FIGURE 6.11. Idealized bed of uniform spherical microporous crystals.

crystals) rather than a single isolated particle. This introduces the possibility of an additional diffusional resistance associated with transport through the crystal bed. To analyze this system we consider an idealized bed of uniform spherical microparticles as sketched in Figure 6.11. The depth of the bed is assumed to be much greater than the diameter of an individual particle so that the concentration does not change significantly over the particle surface. Equilibrium is assumed between the adsorbed phase and fluid phase at the particle surface and the equilibrium relationship is taken to be linear. The system is considered isothermal and both intraparticle and extraparticle transport are represented by Fickian equations. The system is described by the following set of equations:

Micropore diffusion

$$\frac{1}{r^2} \frac{\partial}{\partial r} \left(r^2 D_c \frac{\partial q}{\partial r} \right) = \frac{\partial q}{\partial t} \tag{6.43}$$

$$\frac{\partial q}{\partial r}(0,t) = 0, \qquad q(r_c, t) = Kc(x,t) \tag{6.44}$$

$$\bar{q}(x,t) = \frac{3}{r_c^2} \int_0^{r_c} q r^2 \, dr \tag{6.45}$$

Bed diffusion

$$D_p \frac{\partial^2 c}{\partial x^2} = \frac{\partial c}{\partial t} + \left(\frac{1-\epsilon}{\epsilon} \right) \frac{\partial \bar{q}}{\partial t} \tag{6.46}$$

$$\frac{\partial c}{\partial x}(0,t) = 0, \qquad c(l,t) = C(t), \qquad q(r,0) = Kc(x,0) = 0 \tag{6.47}$$

where l is the bed depth and ϵ is the bed voidage. The fractional uptake is given by

$$\frac{m_t}{m_\infty} = \frac{1}{1 + \left(\frac{3\alpha}{\beta} \right)(1 - \Lambda)} \int_0^l \left[\frac{\bar{q}}{q_\infty} + \left(\frac{3\alpha}{\beta} \right) \frac{c}{C_0} \right] \frac{dx}{l} \tag{6.48}$$

where α is now defined as $(D_c/r_c^2)/(D_p/l^2)$. Except for the difference in geometry the problem is formally similar to the dual resistance macropore-micropore diffusion problem discussed in Section 6.4, and the solution may be obtained by the same method. The general expression for the uptake curve is

$$1 - \frac{m_t}{m_\infty} = \frac{1}{\Lambda} \sum_{n=1}^{\infty} \sum_{m=1}^{\infty} \frac{e^{-p_{n,m}^2 \tau}}{1 + LM}$$

$$L = \left\{ \alpha + \frac{\beta}{(1-\Lambda)} \left[1 + \frac{\cot p_{n,m}}{p_{n,m}} (p_{n,m}\cot p_{n,m} - 1) \right] \right\} \quad (6.49)$$

$$M = \left\{ \frac{-p_{n,m}^2}{2u_n\coth u_n} + \frac{3\Lambda}{\beta + 3\alpha(1-\Lambda)} \left(\frac{1}{2} + \frac{1}{2u_n\coth u_n} \right) \right\}$$

where u_n and $p_{n,m}$ are given by the roots of

$$\frac{\coth u_n}{u_n} = \frac{3\Lambda}{p_{n,m}^2\left[\beta + 3\alpha(1-\Lambda) \right]}$$

$$u_n^2 = \frac{\beta}{1-\Lambda} (p_{n,m}\cot p_{n,m} - 1) - \alpha p_{n,m}^2 \quad (6.50)$$

It should be noted that p is always real but u may be either real or imaginary. When u is imaginary $(u = iv)$, Eq. (6.50) becomes

$$\frac{\cot v}{v} = \frac{-3\Lambda}{p_{n,m}^2\left[\beta + 3\alpha(1-\Lambda) \right]} \quad (6.51)$$

In the limiting case of infinitely large volume systems $(\Lambda \to 0)$, $u \to i(n + \frac{1}{2})\pi$ and the expression for the uptake curve reduces to

$$1 - \frac{m_t}{m_\infty}$$

$$= \frac{6}{(\beta + 3\alpha)} \sum_{m=1}^{\infty} \sum_{n=1}^{\infty} \frac{(n + \frac{1}{2})^2 \pi^2 e^{-p_{n,m}^2 \tau}}{p_{n,m}^4 \left\{ \alpha + \frac{\beta}{2} \left[1 + \frac{\cot p_{n,m}}{p_{n,m}} (p_{n,m}\cot p_{n,m} - 1) \right] \right\}}$$

$$(6.52)$$

where $p_{n,m}$ is given by the roots of

$$\beta(p_{n,m}\cot p_{n,m} - 1) - \alpha p_{n,m}^2 = -(n + \frac{1}{2})^2\pi^2 \quad (6.53)$$

This is the analog of Eqs. (6.35) and (6.36). For zeolitic adsorbents $\Delta q/\Delta c \gg 1$ or $\alpha/\beta \to 0$ and these expressions reduce to the simpler forms analogous to Eqs. (6.37) and (6.38).

$$1 - \frac{m_t}{m_\infty} = \frac{12}{\beta^2} \sum_{n=1}^{\infty} \sum_{m=1}^{\infty} \frac{(n + \frac{1}{2})^2\pi^2 e^{-p_{n,m}^2 \tau}}{p_{n,m}^4 \left\{ 1 + \frac{\cot p_{n,m}}{p_{n,m}} (p_{n,m}\cot p_{n,m} - 1) \right\}} \quad (6.54)$$

with $p_{n,m}$ given by

$$\beta(p_{n,m}\cot p_{n,m} - 1) = -(n + \tfrac{1}{2})^2\pi^2 \tag{6.55}$$

If $\beta \to \infty$, $p \to 0$ and $p\cot p \to 1 - p^2/3$, the first term of the series expansion. Equations (6.54) and (6.55) then reduce to the limiting case of bed diffusion control:

$$1 - \frac{m_t}{m_\infty} = \sum_{n=0}^{\infty} \frac{2}{(n + \tfrac{1}{2})^2\pi^2} \exp\left[-\left(n + \frac{1}{2}\right)^2 \frac{\pi^2 D_e t}{l^2} \right] \tag{6.56}$$

$$\beta p_{n,m}^2 = 3(n + \tfrac{1}{2})^2\pi^2$$

where

$$\frac{D_e t}{l^2} = \frac{\epsilon_p D_p C_0 t}{(1 - \epsilon_p)q_0 l^2} = \frac{3\tau}{\beta} \tag{6.57}$$

which is identical to the expression given by Crank for uptake into a parallel-sided adsorbent slab.[18] In the other limit $\beta \to 0$, $p \to m\pi$, and Eq. (6.56) reduces to the familiar expression for intracrystalline diffusion control:

$$1 - \frac{m_t}{m_\infty} = \sum_{n=1}^{\infty} \frac{6}{n^2\pi^2} e^{-n^2\pi^2\tau} \tag{6.58}$$

which is the standard expression for uptake into a set of uniform spherical particles from an infinite reservoir [Eq. (6.4)].

In the more general case of Λ finite, the bed diffusion limit ($\beta \to \infty$) is obtained as

$$1 - \frac{m_t}{m_\infty} = \frac{1}{\Lambda} \sum_{n=1}^{\infty} \frac{2e^{-p_n^2\tau}}{\left(\dfrac{1}{1 - \Lambda}\right) + \dfrac{p_n^2\beta}{3\Lambda}} \tag{6.59}$$

where

$$p_n^2 = \frac{3(1 - \Lambda)q_n^2}{\beta} \tag{6.60}$$

and q_n is given by the roots of

$$\frac{\tan q_n}{q_n} = \frac{-\Lambda}{1 - \Lambda} \tag{6.61}$$

In the other limit of intraparticle diffusion control $\beta \to 0$ and Eqs. (6.49) and (6.50) reduce to Eqs. (6.10) and (6.11).

These expressions provide the basis for analysis of transient uptake curves for strongly adsorbed species for which the effects of bed diffusion resistance can be important.

6.6. NONISOTHERMAL SORPTION

Because the heat effects associated with adsorption are comparatively large, the assumption of isothermal behavior is a valid approximation only when uptake rates are relatively slow. The problem of nonisothermal sorption under conditions typical of a gravimetric uptake rate experiment has been analyzed by Lee and Ruthven.[19-21] Two distinct situations were considered: non-isothermal sorption in a single particle under conditions such that intraparticle diffusional resistance is the dominant resistance to mass transfer and sorption in a bed of particles under conditions such that the mass transfer rate is controlled by diffusion into the particle bed rather than by intraparticle diffusion.

In a nonisothermal system there are two effects: the temperature dependence of the equilibrium adsorbed phase concentration at the adsorbent surface and the temperature dependence of the diffusivity. The latter effect may be eliminated by reducing the size of the concentration step over which the uptake curve is measured, but the former effect is independent of step size.

Heat conduction through an adsorbent particle or through an assemblage of adsobent particles is generally much faster than heat transfer at the external surface so it is usually a good approximation to consider the particle as essentially isothermal with all heat transfer resistance concentrated in the external film.[19] This is essentially the same situation as in a nonisothermal catalyst particle.[22]

Particle Diffusion Control

Subject to this approximation and assuming intracrystalline diffusion to be the rate-controlling mass transfer process the response of a crystal to a small differential step change in sorbate concentration at the external surface is described by the following set of equations:

$$\frac{\partial q}{\partial t} = \frac{1}{r^2} \frac{\partial}{\partial r}\left(r^2 D_c \frac{\partial q}{\partial r}\right) \tag{6.62}$$

$$\bar{q} = \frac{3}{r_c^3} \int_{r=0}^{r_c} r^2 q \, dr \tag{6.63}$$

$$(-\Delta H)\frac{d\bar{q}}{dt} = C_s \frac{dT}{dt} + ha(T - T_0) \tag{6.64}$$

$$q(r,0) = 0, \qquad \frac{\partial q}{\partial r}(0,t) = 0 \tag{6.65}$$

The equilibrium relationship at the crystal surface is assumed to be linear:

$$\frac{q' - q_0'}{q_0 - q_0'} = 1 + \left(\frac{\partial q^*}{\partial T}\right)_p \left(\frac{T - T_0}{q_0 - q_0'}\right) \tag{6.66}$$

where $q'(t)$ is the adsorbed phase concentration at the crystal surface and

$(\partial q^* / \partial T)_p$ is the slope of the equilibrium line which is taken as constant over the step. The expression for the uptake curve is

$$\frac{m_t}{m_\infty} = 1 - \sum_{n=1}^{\infty} \frac{9\left[(p_n \cot p_n - 1)/p_n^2\right]^2 \exp\left(-p_n^2 D_c t / r_c^2\right)}{\frac{1}{\beta} + \frac{3}{2}\left[p_n \cot p_n (p_n \cot p_n - 1)/p_n^2 + 1\right]} \quad (6.67)$$

where p_n is given by the roots of the equation

$$3\beta'(p_n \cot p_n - 1) = p_n^2 - \alpha' \quad (6.68)$$

and the parameters α' and β' are defined by

$$\alpha' = \frac{ha}{C_s}\frac{r_c^2}{D_c}, \qquad \beta' = \frac{\Delta H}{C_s}\left(\frac{\partial q^*}{\partial T}\right)_p$$

The corresponding expression for the temperature history is

$$\frac{(T - T_0)}{(q_0 - q_0')}\left(\frac{\partial q^*}{\partial T}\right)_p = \sum_{n=1}^{\infty} \frac{-3\left[(p_n \cot p_n - 1)/p_n^2\right]\exp\left(-p_n^2 D_c t / r_c^2\right)}{\frac{1}{\beta'} + \frac{3}{2}\left[p_n \cot p_n (p_n \cot p_n - 1)/p_n^2 + 1\right]} \quad (6.69)$$

If macropore diffusion within the particle is controlling, the equations are
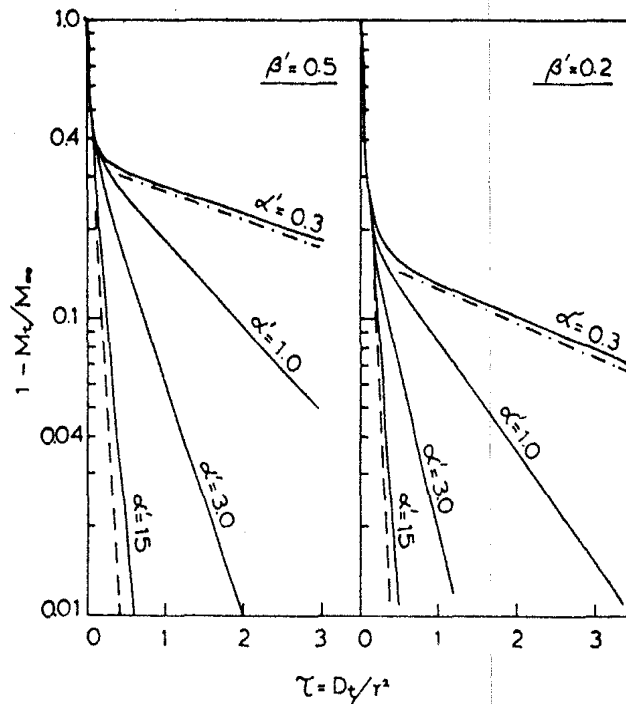
FIGURE 6.12.   Theoretical uptake curves calculated according to Eqs. (6.67) and (6.68) showing the effect of heat transfer resistance. As $\alpha' \to \infty$ the curves approach the limiting isothermal curve calculated from Eq. (6.4) (---) while for $\alpha' \to 0$ the curves approach the limiting case of heat transfer control given by Eq. (6.70) (—·—·). (From ref. 20, with permission.)

similar but with D_c/r_c^2 replaced by D_e/R_p^2. The solution for the more exact model including both internal heat conduction and external heat transfer resistance has recently been given by Haul and Stremming[37] but for most purposes the simpler model, outlined above, is fully adequate since the external resistance is normally dominant.

The general features of the uptake curves are shown in Figure 6.12. The limiting case of isothermal behavior [Eq. (6.4)] is obtained when either $\alpha \to \infty$ (infinitely high heat transfer coefficient) or $\beta \to 0$ (infinitely large heat capacity). When diffusion is rapid (α' small) the kinetics of sorption are controlled entirely by heat transfer. The limiting behavior may be derived by considering the asymptotic form of $(p_n \cot p_n - 1)$, which for small values of p may be replaced by the series expansion $-(p^2/3 + p^4/45 + \cdots)$. For small values of α' the first root of Eq. (6.68) is thus given by $p_1^2 = \alpha'/(1 + \beta')$ and the
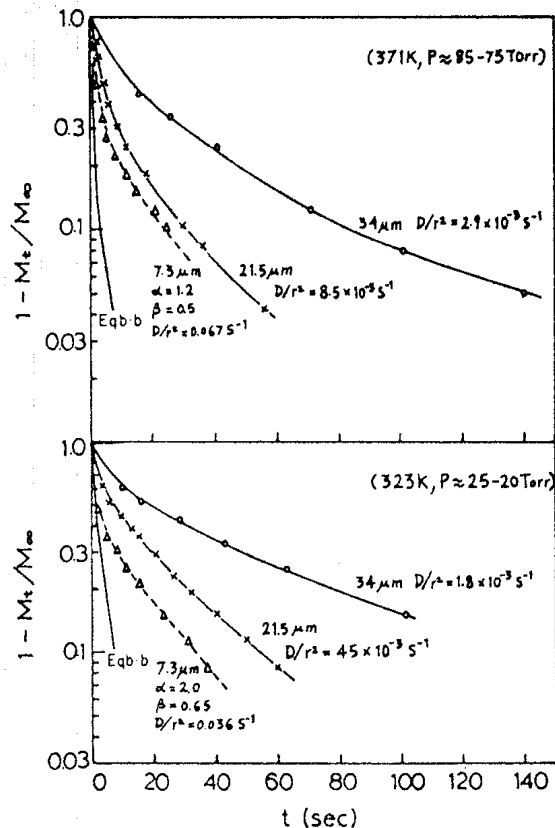
FIGURE 6.13. Experimental uptake curves for CO_2 in 4A zeolite crystals showing near isothermal behavior in the large (34- and 21.5-μm) crystals ($D \approx 9 \times 10^{-9}$ cm^2 s^{-1} at 371 K and 5.2×10^{-9} cm^2 s^{-1} at 323 K). The solid lines are the theoretical curves for isothermal diffusion from Eq. (6.4) with the appropriate value of D_c/r_c^2. The uptake curves for the small (7.3-μm) crystals show considerable deviation from the isothermal curves but conform well to the theoretical nonisothermal curves calculated from Eqs. (6.67) and (6.68) with the value of D estimated from the data for the large crystals, the value of β' calculated from the equilibrium data, and the value of α' estimated using heat transfer parameters estimated from uptake rate measurements with a similar system under conditions of complete heat transfer control. The curve marked Eq. (6.6) is the limiting isothermal curve. (From ref. 20, with permission.)

asymptotic expression for the uptake curve is

$$\frac{m_t}{m_\infty} = 1 - \left(\frac{\beta'}{1+\beta'}\right)\exp\left[-\frac{hat}{C_s}\frac{1}{(1+\beta')}\right]$$ (6.70)

This limiting form may be derived directly from the heat balance assuming that equilibrium between adsorbed phase concentration and external fluid phase concentration is maintained at all times.

When heat transfer is controlling, the uptake curves commonly show a rapid initial uptake followed by a slow approach to equilibrium and the observation of a distinct break in an experimental uptake curve therefore provides a useful clue that heat transfer resistance may be important. For all values of the parameters α' and β' the uptake curves in the long time region show a simple exponential approach to equilibrium and so give straight lines when plotted as $\ln(1 - m_t/m_\infty)$ versus t. If the process is substantially isothermal the intercept of such a plot should be $6/\pi^2$, and a significant deviation from this value can provide useful evidence of the intrusion of heat transfer effects. However, it is clear from Eq. (6.70) that when β' is 1.5 the same intercept will be obtained under conditions of complete heat transfer control. It is therefore not possible to determine unequivocally the significance
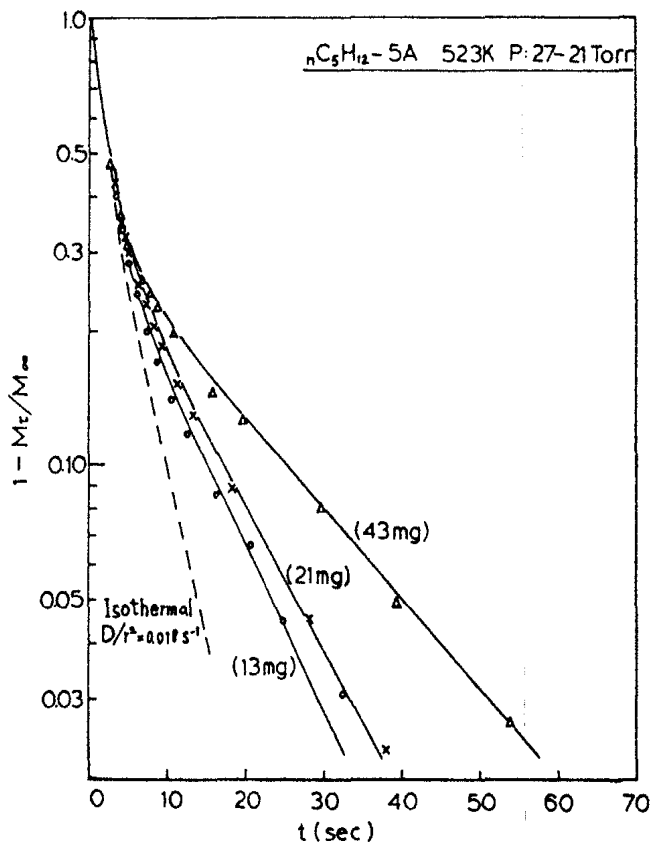
FIGURE 6.14. Experimental uptake curves of n-pentane in Linde 5A crystals (3.6 μm) showing effect of sample size. The uptake curve for the thin bed (13-mg sample) is close to the limiting isothermal curve, but as the depth of the sample bed is increased the deviations become increasingly pronounced. (From ref. 20, with permission.)

of heat effects simply from an examination of a single uptake curve. A more definite conclusion can however be drawn if a family of curves is available showing the variation with concentration. Variation of the configuration of the adsorbent sample provides a convenient experimental test for intrusion of both heat transfer and external (bed) diffusional resistance.

Examples of experimental uptake curves illustrating the transition from isothermal diffusion to heat transfer control are shown in Figures 6.13 and 6.14. Adsorption of CO_2 in larger crystals of 4A zeolite (21.5 and 34 μm) is relatively slow and the uptake curves are essentially controlled by isothermal diffusion and are independent of the quantity of adsorbent used in the experiment. In the smaller crystals, however, heat effects become significant, and in the later stages there is significant deviation from the expected curve for isothermal diffusion. The same situation is seen for n-pentane-5A zeolite in Figure 6.14. In the initial region thermal effects are unimportant and the uptake curve is essentially independent of sample size. In the later region of the uptake the curves for the different sample sizes diverge, the deviation from the isothermal curve being greatest for the largest sample for which heat transfer is slowest. The nonisothermal curves are well predicted by Eqs. (6.67)
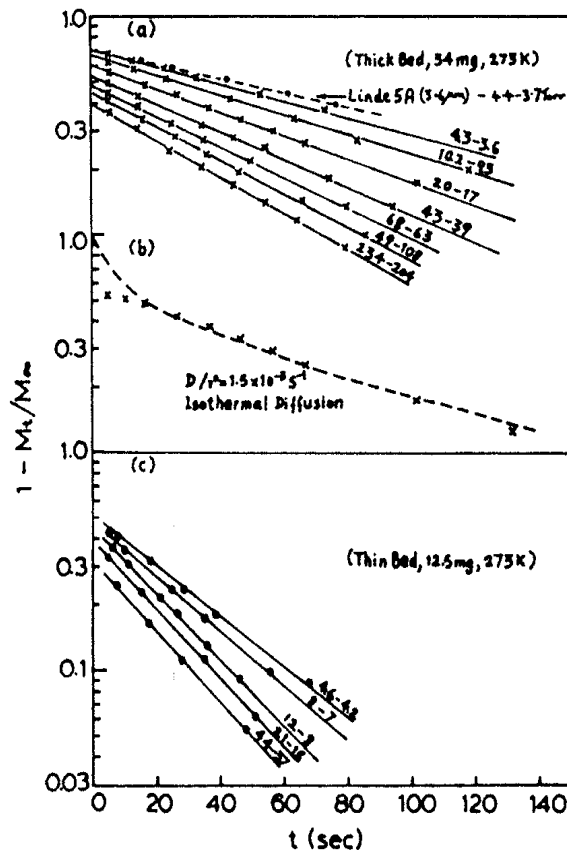
FIGURE 6.15. Experimental uptake curves for CO_2 in 5A zeolite crystals at 273 K showing limiting case of heat transfer control [Eq. (6.70)]. Note that the rate of approach to equilibrium is faster in the thin bed as a result of the greater surface area–volume ratio. Curve (b) shows a case where the heat transfer limited uptake curve lies (fortuitously) close to the ideal curve for isothermal diffusion except in the initial region. (From ref. 20, with permission.)

and (6.68) with the parameters D_c/r_c^2 and ha/C_s determined from experiments carried out with large crystals under isothermal conditions and with small crystals under conditions of complete thermal control.

The extreme case of complete heat transfer control for CO_2–5A is illustrated in Figure 6.15. For this system diffusion is much faster and even in relatively large crystals the uptake rate is controlled by heat transfer. Uptake curves are essentially independent of crystal size but vary with sample size due to changes in the effective heat capacity and external area-to-volume ratio for the sample. Analysis of the uptake curves according to Eq. (6.70) yields consistent values for the overall heat capacity (34 mg sample $C_p \approx 0.32$ and 12.5 mg sample $C_p \approx 0.72$ cal/g deg.). The variation of effective heat capacity with sample size arises from the increasing importance of the heat capacity of the containing pan when the adsorbent weight is small.

Bed Diffusion Control

The problem of nonisothermal uptake under conditions such that the main resistance to mass transfer is the diffusional resistance of the particle bed,[21] rather than the intraparticle resistance, is similar and the expression for the uptake curve may be derived in the same way. The response of the system to a step change in sorbate concentration is described by the following set of equations:

$$\frac{\partial q}{\partial \tau'} = \frac{\partial^2 q}{\partial x^2} \tag{6.71}$$

$$q(x,0) = q_0', \qquad q(1,\tau') = q', \qquad \left.\frac{\partial q}{\partial x}\right|_{x=0} = 0, \qquad \bar{q} = \frac{1}{l}\int_0^l q\,dx \tag{6.72}$$

$$(-\Delta H)\frac{d\bar{q}}{d\tau'} = C_s \frac{dT}{d\tau'} + \frac{ha(T - T_0)}{D_e/l^2} \tag{6.73}$$

where q' is given by Eq. (6.66) and

$$D_e = \frac{\epsilon D}{(1 - \epsilon)} \bigg/ \left.\frac{dq^*}{dc}\right|_{T=T_0}, \qquad \tau' = \frac{D_e t}{l^2} \tag{6.74}$$

The expression for the uptake curve is

$$1 - \frac{m_t}{m_\infty} = \sum_{n=0}^{\infty} \frac{2e^{-p_n^2\tau'}}{p_n^2\cot^2 p_n(1 + 2/\beta') + p_n^2 + p_n\cot p_n} \tag{6.75}$$

and for the temperature response

$$\left(\frac{T - T_0}{q_0 - q_0'}\right)\frac{\partial q^*}{\partial T} = \sum_{n=0}^{\infty} \frac{2e^{-p_n^2\tau'}}{p_n\cot p_n(1 + 2/\beta') + 1 + p_n\tan p_n} \tag{6.76}$$
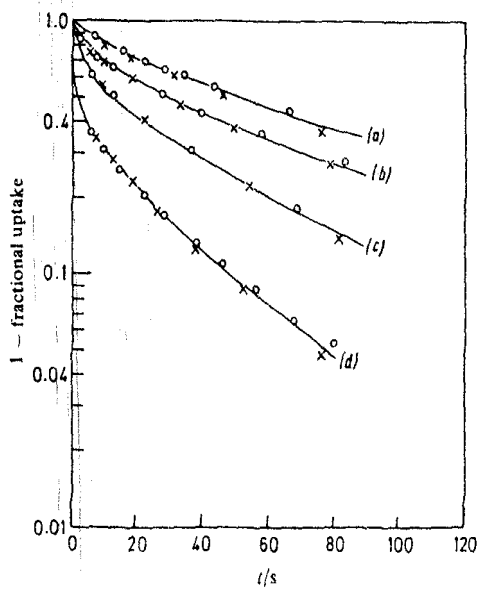
FIGURE 6.16. Comparison of experimental uptake curves for isooctane in 13X zeolite at 403 K measured over similar pressure steps with two different sizes of crystal ($\times$, 24 μm; $\bigcirc$, 39 μm). Pressure steps in torr (a) 0.0019–0.0075; (b) 0–0.0019; (c) 0.0195–0.03; (d) 0.17–0.53; 0.38–0.8. (From ref. 21, with permission.)
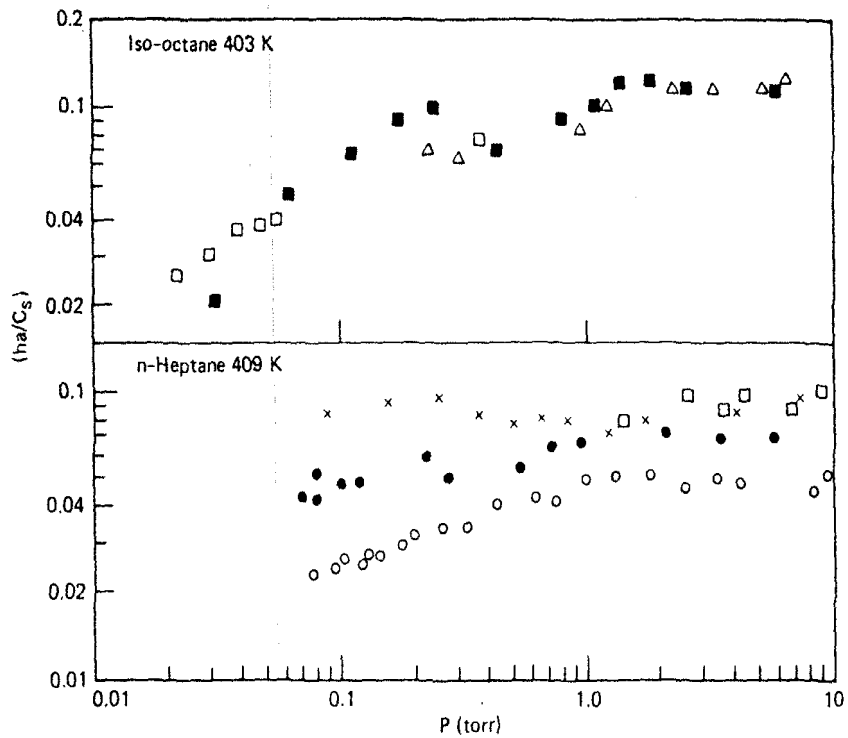
FIGURE 6.17. Variation of heat transfer parameter (ha/C_s) with sorbate pressure for sorption of *i*-octane and *n*-heptane ($\times$, 22-mg Linde 13X; $\bigcirc$, 20-mg, 17-μm 13X; $\bullet$, 28-mg, 17-μm 13X; on wide pan; $\square$ 14-mg, 39-μm 13X; $\blacksquare$, 14-mg, 24-μm 13X; $\triangle$, 14-mg, 55-μm 13X). Note that the value of ha/C_s depends on the bed configuration (sample weight) and pan diameter and is independent of crystal size or nature of the sorbate. (From ref. 21, with permission.)

where p_n is given by the roots of

$$\cot p_n = \frac{\beta' p_n}{\alpha' - p_n^2} \qquad (6.77)$$

and α' is redefined as $(ha/C_s)(l^2/D_e)$. In the limiting case of rapid diffusion Eqs. (6.76) and (6.77) reduce to Eq. (6.70), the expression for heat transfer control.

An example of a system (i-octane-13X zeolite) in which the uptake rate is controlled by the combined effects of heat transfer and bed diffusion is shown in Figure 6.16. The uptake curves for 24- and 39-μm crystals are essentially the same, showing that intracrystalline diffusion is sufficiently rapid even in these relatively large crystals to have no effect on the uptake rate. At low pressures heat transfer resistance also has little effect; the uptake rate is controlled by bed diffusion and the uptake curves conform to Eqs. (6.52) and (6.53). As the sorbate concentration is increased thermal effects become increasingly important leading to a change in the shape of the uptake curves which, at higher concentration, follow Eqs. (6.75) and (6.77).

The variation of the heat transfer time constant (ha/C_s) and the bed diffusional time constant D/l^2 with pressure is shown, for several different
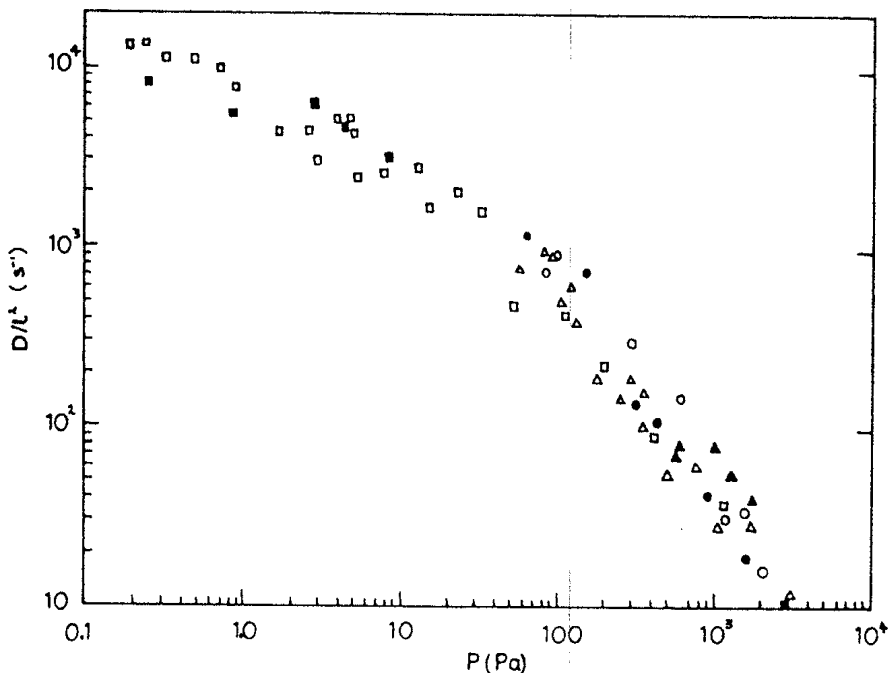
FIGURE 6.18. Pressure dependence of macrodiffusional time constant D/l^2 for sorption in 13X zeolite crystals. Data are for temperatures of 370–430 K with comparable adsorbent bed configuration. i-octane: 39-μm crystals, □; 24-μm crystals, ■. n-heptane: 39-μm crystals, △; 17-μm crystals, ▲. Benzene: 17-μm crystals, ●. Cyclohexane: 17-μm crystals, ○. Note that time constant is approximately independent of either sorbate or crystal size as may be expected for bed diffusion with sorbates of comparable molecular weight. Note also the transition from Knudsen diffusion (D_p independent of pressure) to molecular diffusion ($D_p \propto 1/p$) as pressure is increased. (From ref. 21, with permission.)

systems, in Figures 6.17 and 6.18. The heat transfer parameter (ha/C_s) is insensitive to the nature of the sorbate or the crystal size of the adsorbent but depends on the volume and configuration of the adsorbent sample. At pressures greater than about 1 torr the thermal conductivity of the gas phase, and hence the heat transfer coefficient and the time constant, become essentially independent of pressure, but at lower pressures the mean free path becomes comparable with the diameter of the hangdown tube containing the adsorbent sample and the heat transfer coefficient decreases. The effective heat capacity (C_s) includes the contribution from the containing pan. As the quantity of adsorbent is decreased the specific area increases leading to an increase in the heat transfer group, but the relationship is not straightforward since the effective heat capacity, which includes the contribution from the containing pan, also varies. The diffusional time constants are independent of crystal size, as expected if diffusion through the adsorbent bed is the rate-limiting process. At low pressures diffusion occurs mainly by Knudsen diffusion and under these conditions the diffusional time constant becomes essentially independent of pressure. As the pressure is increased molecular diffusion becomes increasingly important and the bed diffusivity becomes inversely dependent on the system pressure. The difference in molecular weights and diffusivities between isooctane, n-heptane, and cyclohexane is quite small so that the data for all three sorbates follow essentially the same curve.

Controlling Heat Transfer Resistance

It may be seen from Eq. (6.70) that the time constant for external heat transfer is given by $(ha/C_s)/(1 + \beta')$. Except for a difference in the definition of the specific area a, precisely the same expression holds for heat transfer from a single adsorbent particle or from the external surface of an adsorbent sample containing many individual particles. The specific external surface area of the assemblage of particles will always be less than that of an individual particle, so under stagnant conditions such that heat transfer occurs primarily by conduction and radiation with no significant convection, heat dissipation from the external surface of the adsorbent sample will always be slower than heat transfer between the individual particles within the sample.

In order to assess the relative importance of internal and external heat transfer resistances for an individual particle we note that for a system in which the uptake rate is controlled entirely by internal heat conduction, the uptake curve is given by

$$1 - \frac{m_t}{m_\infty} = \frac{6}{\pi^2} \sum_{n=1}^{\infty} \frac{1}{n^2} \exp\left[\frac{-n^2\pi^2\lambda_s t}{r_c^2 C_s(1 + \beta')} \right] \tag{6.78}$$

This is of the same form as Eq. (6.4) with D_c/r_c^2 replaced by $\lambda_s/C_s(1 + \beta')r_c^2$. The ratio of the time constants for internal and external heat transfer is given

by

$$\delta = \frac{\pi^2 \lambda_s}{C_s(1 + \beta')r_c^2} \Big/ \frac{ha}{C_s(1 + \beta')} = \frac{\pi^2 \lambda_s}{har_c^2} = \frac{\pi^2 \lambda_s}{3hr_c} \qquad (6.79)$$

The limiting Nusselt number for heat transfer from an isolated particle is given by $Nu = 2hr_c/\lambda_g = 2.0$ so that

$$\delta = \frac{\pi^2}{3} \frac{\lambda_s}{\lambda_g} \qquad (6.80)$$

Since the thermal conductivity of even a porous solid (λ_s) is much higher than that of the gas (λ_g) it follows that $\delta \gg 1.0$, implying that internal heat conduction within an adsorbent particle is always much faster than heat dissipation from the external surface of the particle. The assumption that under nonisothermal conditions all heat transfer resistance is concentrated at the external surface and the temperature is essentially uniform throughout the adsorbent sample thus appears to be a good approximation for most systems.

Experimental Measurement of Temperature Rise

Direct experimental measurements of the temperature rise during sorption in a batch system have been reported by Eagan et al.,[23] Doelle and Riekert,[24] and Ilavsky et al.[25] The observed temperature response curves were in all cases of the expected form, showing a rapid initial rise followed by a slow return to the ambient temperature. The absence of any significant intraparticle temperature gradient was confirmed directly by Ilavsky et al. who
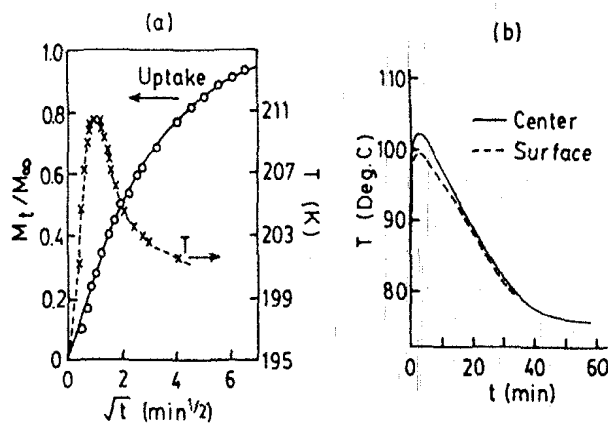
FIGURE 6.19. Experimental uptake curves showing nonisothermal behavior. (a) Adsorption of N_2 at 195 K on 4A zeolite crystals. (b) Adsorption of n-heptane on 5A zeolite pellets. Measurements of the temperature rise show little difference between the center and surface of the particle. [After refs. 23 and 25; (a) reprinted with permission from ref. 23. Copyright 1971 American Chemical Society. (b) Reprinted with permission from Chem. Eng. Sci. 35, Ilavsky et al., Copyright 1980, Pergamon Press, Ltd.]

measured temperatures at the center and surface of an adsorbent particle. Representative results are shown in Figure 6.19.

6.7. SORPTION IN BINARY SYSTEMS

In the earlier sections of this chapter attention has been focused on the sorption of a single component, with the implicit assumption that if a second (inert) component is present in the system it does not affect the sorption rate. Such an assumption requires further examination since whenever a second component is present, there is in principle a possibility of external resistance to mass transfer. Furthermore, if the second component is adsorbed it may also affect the intraparticle diffusion rate.

External Mass Transfer Resistance

The problem of eliminating external fluid film resistance in the measurement of sorption rates is similar to the problem of eliminating external resistance in the study of catalytic reaction kinetics. Both the "Carberry mixer"[26] in which the adsorbent particles are rotated on an impeller and the "Berty reactor,"[27,28] which consists of a small differential bed through which the fluid is rapidly circulated, have been applied in adsorption studies. A high relative velocity between fluid and adsorbent particle is required in order to ensure a high mass transfer coefficient. This is easily achieved in the Berty reactor system merely by increasing the circulation rate. It is less easily achieved in the Carberry mixer since the fluid tends to rotate with the adsorbent particles so that the relative velocity may be quite small. This problem becomes particularly serious if a basket containing several pellets rather than a single adsorbent pellet is used in the Carberry mixer since in such a system the flow between the pellets may be minimal.

A modified Carberry mixer was used by Ma and Lee[29] to measure uptake rates for C_4 hydrocarbons in 13X molecular sieve pellets using a helium carrier. Adsorption rates were slow and they concluded that the rate-controlling mass transfer process was intracrystalline diffusion with a diffusivity of order 10^{-14} cm^2 s^{-1} at 35°C. An independent study by Doelle and Riekert[24] using large crystals of 13X zeolite (~ 100 μm) showed that the diffusivity of butane is, under comparable conditions, very much higher ($\sim 10^{-6}$–10^{-7} cm^2 s^{-1}). The discrepancy appears to have arisen from the intrusion of external mass transfer resistance in the Carberry mixer.

A very similar experimental system was used by Taylor[30] who showed that the uptake rate in such systems could be correlated directly with the molecular diffusivity of the gas phase, strongly suggesting that external resistance was dominant. This conclusion was confirmed by detailed analysis of the experimental results which revealed that the measured mass transfer rates were consistent with established mass transfer correlations. The effect of
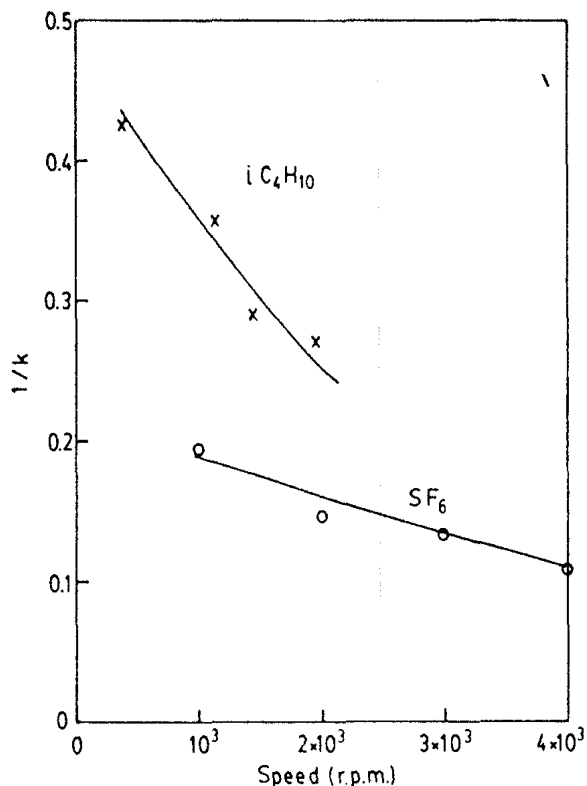
FIGURE 6.20. Test of the spinning basket adsorber. Overall rate coefficients for adsorption of propane on Linde 5A at 54°C were measured at several speeds of rotation in the presence of 500 Torr of either iC_4H_{10} or SF_6. These species are both too large to penetrate the sieve. The uptake rate correlates with the gas phase molecular diffusivity indicating external mass transfer control. (Data of Taylor.[30])

rotation speed on the mass transfer coefficient was shown to be modest so the usual test of varying the rotation speed to confirm the absence of significant external resistance is valid only if the tests cover a very wide range of impeller speeds. Some of Taylor's results are shown in Figure 6.20.

Diffusion in a Binary Adsorbed Phase

The analysis of macropore diffusion in binary or multicomponent systems presents no particular problems since the transport properties of one component are not directly affected by changes in the concentration of the other components. In an adsorbed phase the situation is more complex since in addition to any possible direct effect on the mobility, the driving force for each component (chemical potential gradient) is modified, through the multicomponent equilibrium isotherm, by the concentration levels of all components in the system. The diffusion equations for each component are therefore directly coupled through the equilibrium relationship. Because of the complexity of the problem, diffusion in a mixed adsorbed phase has been studied to only a limited extent.

A theoretical study of diffusion in a binary adsorbed phase was presented by Round, Newton, and Habgood[31] and an essentially similar analysis was reported independently by Kärger and Bulow.[32] Starting from the irreversible thermodynamic formulation and neglecting the cross coefficients, the fluxes of the two components are given by

$$J_A = -D_{OA}\left(\frac{\partial \ln p_A}{\partial \ln q_A}\right)\frac{\partial c_A}{\partial x}, \qquad J_B = -D_{OB}\left(\frac{\partial \ln p_B}{\partial \ln q_B}\right)\frac{\partial c_B}{\partial x} \qquad (6.81)$$

where $p_A(q_A, q_B)$ and $p_B(q_A, q_B)$ are the vapor pressures at equilibrium with an adsorbed phase of composition (q_A, q_B) and $D_{OA} = B_A RT = D_{OA} = B_B RT$. If it is then assumed that D_{OA} and D_{OB} are independent of adsorbed phase composition and the equilibrium relationship obeys a binary Langmuir equation:

$$\Theta_A = \frac{q_A^*}{q_s} = \frac{b_A p_A}{1 + b_A p_A + b_B p_B}, \qquad \Theta_B = \frac{q_B^*}{q_s} = \frac{b_B p_B}{1 + b_A p_A + b_B p_B} \qquad (6.82)$$

A differential mass balance for a spherical shell element yields for the relevant form of the diffusion equation:

$$\frac{\partial \Theta_A}{\partial t} = \frac{D_{AO}}{(1 - \Theta_A - \Theta_B)}\left\{(1 - \Theta_B)\left(\frac{\partial^2 \Theta_A}{\partial r^2} + \frac{2}{r}\frac{\partial \Theta_A}{\partial r}\right) + \Theta_A\left(\frac{\partial^2 \Theta_B}{\partial r^2} + \frac{2}{r}\frac{\partial \Theta_B}{\partial r}\right)\right\}$$

$$+ \frac{D_{AO}}{(1 - \Theta_A - \Theta_B)^2}\left\{(1 - \Theta_B)\frac{\partial \Theta_A}{\partial r} + \Theta_A\frac{\partial \Theta_B}{\partial r}\right\}\left\{\frac{\partial \Theta_A}{\partial r} + \frac{\partial \Theta_B}{\partial r}\right\}$$

$$(6.83)$$

with a similar expression for Θ_B. To describe binary diffusion we evidently require two coefficients, D_{AO} and D_{BO}, and the sorption process cannot, in general, be represented as a simple diffusion process characterized by a single effective diffusivity.

Counterdiffusion

Representation of the exchange process as a simple diffusive process is possible in the special case of equimolar counterdiffusion which requires $D_{OA} = D_{BO}$, $b_A = b_B$, and $\Theta_{A_\infty} - \Theta_{AO} = -(\Theta_{B_\infty} - \Theta_{BO})$. Under these conditions Eq. (6.85) reduces to

$$\frac{\partial \Theta_A}{\partial t} = -\frac{\partial \Theta_B}{\partial t} = D_{AO}\left\{\frac{\partial^2 \Theta_A}{\partial r^2} + \frac{2}{r}\frac{\partial \Theta_A}{\partial r}\right\} = -D_{BO}\left\{\frac{\partial^2 \Theta_B}{\partial r^2} + \frac{2}{r}\frac{\partial \Theta_B}{\partial r}\right\}$$

$$(6.84)$$

which is of the same form as the single-component diffusion equation with the effective diffusivity given by $D_{AO} = D_{BO} = D_e$.
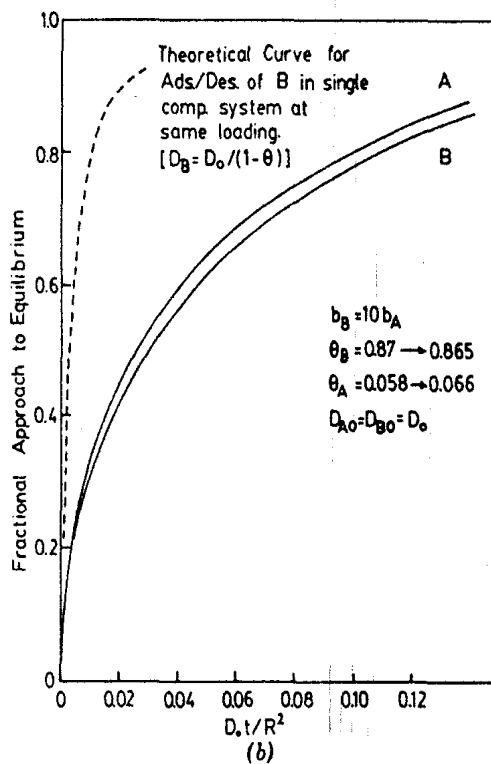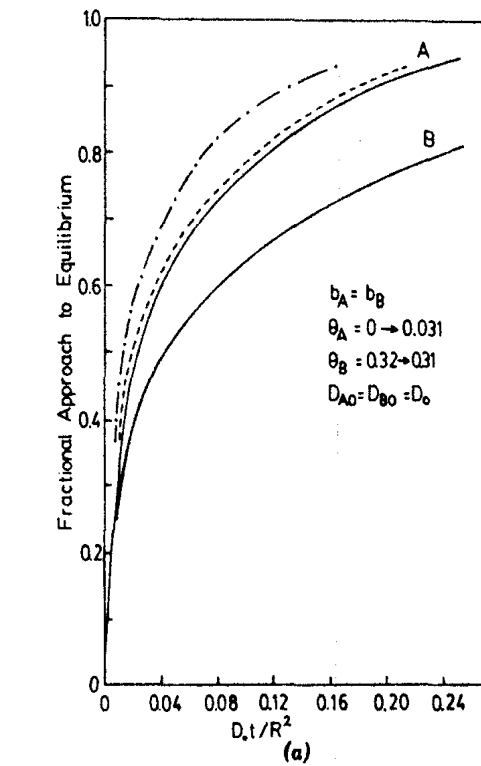
FIGURE 6.21. Theoretical uptake curves for counterdiffusion. A is adsorbing, B is desorbing, and $D_{AO} = D_{BO} = D_0$. Theoretical adsorption and desorption curves for both A and B, calculated from Eq. (6.83) are shown by continuous lines. In (a) the uptake curve for A is similar to the curve calculated from Eq. (6.4) with $D = D_0$ (---). (The curve for $D = D_0/(1 - \Theta)$ is shown, —·—·—). In (b) the uptake curves for A and B are both close to the simple diffusion curve [Eq. (6.4)] with $D = D_0$ and much slower than the curves for $D = D_0/(1 - \Theta)$.

Theoretical counterdiffusion curves calculated numerically from Eq. (6.83) are shown in Figure 6.21. Component A is the adsorbing species and the initial and final concentrations of both components are indicated. It is evident that the curves for components A and B are different, showing that the exchange process cannot be properly represented by a single effective diffusivity. Even though $D_{OA} = D_{OB}$ and $b_A = b_B$ the adsorption of A is substantially faster than desorption of B as a result of the different initial concentrations of the two components. In Figure 6.21a the adsorption of A is not greatly affected by the presence of component B since the uptake curve for A is close to the theoretical curve from Eq. (6.4) with $D_e = D_{OA}$. The desorption curve for component B is however of a different shape and does not follow Eq. (6.4). Attempts to match the desorption curve for B to Eq. (6.4) lead to effective diffusivities which decrease with time. The rate of desorption of B has been significantly reduced by the presence of a small amount of component A as a result of the effect on the equilibrium isotherm which controls the driving force.

At higher loading (Figure 6.21b) the behavior approaches more closely the simple case of equimolar counterdiffusion. The adsorption curve for component A and the desorption curve for component B approach one another and approximate to a simple diffusion curve with an effective diffusivity which in this case is given by $D_{AO} = D_{BO} = D_e$. If $D_{AO} \ll D_{BO}$ the behavior is broadly similar but the effective diffusivity is given by D_{AO} while for $D_{BO} \ll D_{AO}$ the effective diffusivity is given by D_{BO}.

In these calculations only differential changes in sorbate concentration have been considered. The behavior of a system involving large changes in concentration will be more complex although in principle the uptake curves may still be derived by numerical solution of Eq. (6.83) subject to the appropriate initial and boundary conditions.

Satterfield, Katzer, and co-workers[33-35] have measured counterdiffusion rates for various liquid hydrocarbons in small NaY crystals. Measurements were generally made over relatively large concentration steps and the validity of representing the exchange behavior in terms of a single effective diffusivity was not considered. Desorption was found to be slower than adsorption and exchange in a binary system was found to be much slower than adsorption in a single-component system. Effective diffusivities calculated according to Eq. (6.4) were found to vary strongly with fractional uptake, decreasing as equilibrium was approached. This is precisely the behavior to be expected, according to the above analysis, when the loading of the desorbing component is high and that of the adsorbing component is low, as in Figure 6.21a.

Co-Diffusion

In a co-diffusion experiment, in which the concentrations of both components are increased, the uptake curves have the general form sketched in Figure 6.22. The faster diffusion species is adsorbed initially to a concentra-
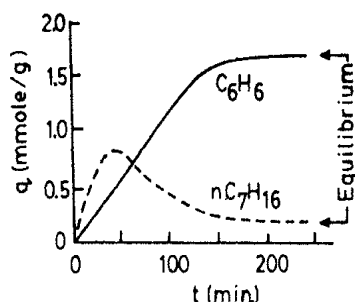
FIGURE 6.22. Experimental uptake curve for *n*-heptane benzene mixture on 13X zeolite at 359 K ($P_{benzene} = 24.3$ torr, $P_{heptane} = 50.6$ torr) showing the overshoot in the *n*-heptane concentration (faster diffusing, less strongly adsorbed). [Reprinted with permission from *Chem. Eng. Sci.* **30**, Kärger and Bülow (ref. 32). Copyright 1975, Pergamon Press, Ltd.]

tion level which exceeds the final equilibrium value. It then desorbs to the equilibrium level as the slower diffusing species penetrates. Such behavior has been observed experimentally for the sorption of *n*-heptane-benzene mixtures on 5A zeolite[32] and for N_2-CH_4[36] mixtures on 4A zeolite. The form of the uptake curves is qualitatively predicted by the solution to Eq. (6.85). Quantitative agreement is not expected since the equilibrium isotherms for these systems do not conform to the simple Langmuir model.

REFERENCES

1. J. Crank, *Mathematics of Diffusion*. Oxford University Press, London, 1956, Chap. VI.
2. D. R. Garg and D. M. Ruthven, *Chem. Eng. Sci.* **27**, 417 (1972).
3. M. Kocirik, A. Zikanova, and J. Dubsky, *Ind. Eng. Chem. Fund.* **12**, 440 (1973).
4. E. F. Kondis and J. S. Dranoff, *Adv. Chem.* **102**, 171 (1970).
5. E. F. Kondis and J. S. Dranoff, *Ind. Eng. Chem. Process Design Develop.* **10**, 108 (1971).
6. E. F. Kondis, Ph.D. thesis, Northwestern University, Evanston, Illinois, 1969.
7. P. E. Eberly, *Ind. Eng. Chem. Fund.* **8**, 25 (1969).
8. C. N. Satterfield and A. J. Frabetti, *AIChE J* **13**, 731 (1967).
9. D. M. Ruthven and R. I. Derrah, *Can. J. Chem. Eng.* **50**, 743 (1972).
10. G. R. Youngquist, J. L. Allen, and J. Eisenberg, *Ind. Eng. Chem. Prod. Res. Develop.* **10**, 308 (1971).
11. R. L. Dedrick and R. B. Beekman, *Chem. Eng. Prog. Symp. Series* **63**(74), 68 (1967).
12. V. Brauch and E. U. Schlunder, *Chem. Eng. Sci.* **30**, 540 (1975).
13. W. S. Kyte, Ph.D. thesis, University of Cambridge, 1970.
14. E. Ruckenstein, A. S. Vaidyanathan, and G. R. Youngquist, *Chem. Eng. Sci.* **26**, 1306 (1971).
15. Y. H. Ma and T. Y. Lee, *AIChE J.* **22**, 147 (1976).
16. L-K. Lee, *AIChE Jl* **24**, 531 (1978).
17. L-K. Lee and D. M. Ruthven, *Can. J. Chem. Eng.* **57**, 65 (1979).
18. J. Crank, *Mathematics of Diffusion*. Oxford University Press, London, 1956, Chap. IV.
19. L-K. Lee and D. M. Ruthven, *J. Chem. Soc. Faraday Trans. I* **75**, 2406 (1979).
20. D. M. Ruthven, L-K. Lee, and H. Yucel, *AIChE J* **26**, 16–23 (1980).
21. D. M. Ruthven and L-K. Lee, *AIChE J* **27**, 654 (1981).
22. J. J. Carberry, *Ind. Eng. Chem. Fund.* **14**, 129 (1975).
23. J. D. Eagan, B. Kindl, and R. B. Anderson, *Adv. Chem.* **102**, 164 (1971).
24. H. J. Doelle and L. Riekert, *Angew. Chem. Int. Ed.* **18**, 266 (1979).
25. J. Ilavskyk, A. Brunovska, and V. Hlavacek, *Chem. Eng. Sci.* **35**, 2475 (1980).

26. J. J. Carberry, *Ind. Eng. Chem.* **56**(11), 39 (1964).

27. J. M. Berty, *Chem. Eng. Prog.* **70**, 78 (1974).

28. J. M. Berty, *Catalysis Rev.* **19**, 1 (1979).

29. Y. H. Ma and T. Y. Lee, *AIChE J* **22**, 147 (1976).

30. R. A. Taylor, Ph.D. thesis, University of New Brunswick, Fredericton, N.B., Canada, 1979.

31. G. F. Round, H. W. Habgood, and R. Newton, *Sep. Sci.* **1**, 219 (1966).

32. J. Kärger and M. Bulow, *Chem. Eng. Sci.* **30**, 893 (1975).

33. C. N. Satterfield and J. R. Katzer, *Adv. Chem.* **102**, 193 (1971).

34. C. N. Satterfield and C. S. Cheng, *AIChE J.* **18**, 724 (1972).

35. R. Moore and J. R. Katzer, *AIChE J.* **18**, 816 (1972).

36. H. W. Habgood, *Can. J. Chem.* **36**, 1384 (1958).

37. R. Haul and H. Stremming, *J. Colloid Interface Sci.* (in press).

7

FLOW THROUGH
PACKED BEDS

In most adsorption processes the adsorbent is contacted by the fluid phase in a packed column. Such variables as the particle size, fluid velocity, and bed dimensions determine the pressure drop and have an important impact on the economics of the process since they determine the pumping cost as well as the extent of axial mixing and the heat transfer properties. The hydrodynamics of flow through packed beds have been extensively studied, and detailed accounts may be found in many chemical engineering textbooks.[1] The present review is therefore limited to a brief summary of the principal features of the flow behavior which are important in the design of fixed bed absorbers.

7.1. PRESSURE DROP

Pressure drop in flow through packed columns has been investigated by Furnas,[2] Chilton and Colburn,[3] and more recently by Leva[4] and Ergun.[5] The same general trends were observed in all these investigations, although the experimental data show considerable scatter, probably due to differences in voidage and/or wall effects for which corrections were not always applied. The data may be conveniently correlated in terms of a dimensionless friction factor (f), defined by

$$f \approx \left(\frac{2R_p}{L} \right) \frac{\Delta p}{\rho_f(\epsilon v)^2} \tag{7.1}$$

where Δp is the pressure drop, expressed in absolute units (Nm^{-2}, poundals ft^{-2}, etc.), across a length L of packed column and ϵv is the superficial fluid velocity. Two commonly used correlations for the friction factor are

206

Chilton–Colburn[3]

$$Re < 40 \quad f = 805/Re$$

$$Re > 40 \quad f = 38/Re^{0.15}$$

(7.2)

Ergun[5]

$$f = \left(\frac{1 - \epsilon}{\epsilon^3} \right) \left[\frac{150(1 - \epsilon)}{Re} + 1.75 \right]$$

(7.3)

The Reynolds number used in these correlations is based on particle diameter (or equivalent diameter) and superficial gas velocity. Although the numerical forms of these expressions are different, they show reasonably close numerical agreement when the bed voidage is about 0.35, as may be seen from Figure 7.1. The Ergun expression shows clearly the dependence on bed voidage and may therefore be considered preferable.

Except when the bed diameter is large relative to the particle diameter, the pressure drop may be significantly reduced by wall effects. The correction factor may be estimated from the correlation given by Furnas[2] which is shown in Figure 7.2.
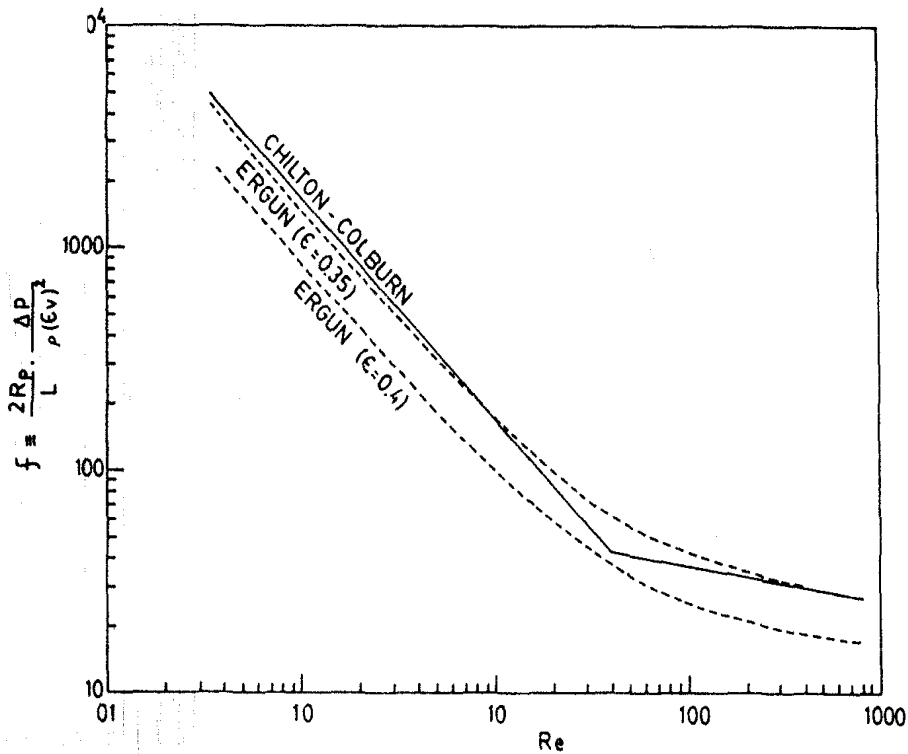
FIGURE 7.1. Comparison of friction factors for flow through packed beds according to Chilton and Colburn[3] and Ergun.[5]
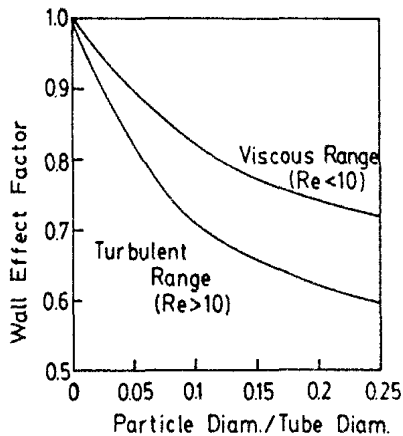
FIGURE 7.2. Dependence of wall factor on particle–tube diameter ratio (after Furnas.[2])

To prevent attrition from the movement of particles within the bed it is normal practice to limit the allowable velocity in upflow to less than about 80% of the minimum fluidization velocity:

$$v_{max} = 0.8 v_{mf} \approx 6 \times 10^{-4} g \frac{(2R_p)^2}{\mu} (\rho - \rho_f) \qquad (7.4)$$

For air at 298 K ($\mu = 1.84 \times 10^{-4}$ Poise) and for a typical adsorbent with particle density of 1.1 g/cm^3 Eq. (7.4) gives about 35 cm/s for the maximum allowable interstitial velocity for upflow through a bed of 1-mm diameter particles. Somewhat higher velocities up to about 1.8 times the minimum fluidization velocity may be tolerated in downflow, and it is therefore usual practice in reverse-flow systems to arrange that the higher velocity flow is passed through the bed in the downflow direction.

7.2. AXIAL DISPERSION IN PACKED BEDS

When a fluid flows through a packed bed there is a tendency for axial mixing to occur. Any such mixing is undesirable since it reduces the efficiency of separation. The minimization of axial dispersion is therefore a major design objective, particularly when the separation factor is small.

Flow through a packed bed may generally be adequately represented by the axial dispersed plug flow model:

$$-D_L \frac{\partial^2 c}{\partial z^2} + \frac{\partial}{\partial z}(vc) + \frac{\partial c}{\partial t} + \left(\frac{1-\epsilon}{\epsilon}\right)\frac{\partial \bar{q}}{\partial t} = 0 \qquad (7.5)$$

In this model the effects of all mechanisms which contribute to axial mixing are lumped together into a single effective axial dispersion coefficient. More detailed models which include, for example, radial dispersion are generally not necessary and in many cases it is in fact possible to neglect axial dispersion altogether and assume ideal plug flow.

Gases

Dispersion in gaseous systems has been reviewed by Langer et al.[6] Ignoring effects due to nonuniformity of packing (which, if the ratio of bed-to-particle diameters is not sufficiently large, can give rise to significant additional dispersion from wall effects), there are two main mechanisms which contribute to axial dispersion: molecular diffusion and turbulent mixing arising from the splitting and recombination of flows around the adsorbent particles. To a first approximation these effects are additive so that the dispersion coefficient may be represented by

$$D_L = \gamma_1 D_m + \gamma_2 2 R_p v \qquad (7.6)$$

where γ_1 and γ_2 are constants which normally have values of about 0.7 and 0.5, respectively. Expressed in terms of an axial Peclet number Eq. (7.6) becomes

$$\frac{1}{Pe'} = \frac{D_L}{2vR_p} = \gamma_1 \frac{D_m}{2vR_p} + \gamma_2 = \frac{\gamma_1 \epsilon}{Re\,Sc} + \gamma_2 \qquad (7.7)$$

Considering the bed as an assemblage of randomly oriented cylindrical pores suggests $\gamma_1 = 1/\sqrt{2}$, which is close to the experimental values derived from dispersion measurements for gases at low Reynolds number. More detailed investigation reveals that the bed tortuosity $(1/\gamma_1)$ is related to the voidage. Wicke[7] has suggested:

$$\gamma_1 = 0.45 + 0.55\epsilon \qquad (7.8)$$

which, for typical bed voidages in the range 0.35–0.4, gives $\gamma_1 = 0.64$–0.67.

The second term on the right-hand side of Eq. (7.6) accounts for turbulent mixing and a simple model of the bed as a series of mixing chambers, separated on average by the mean particle diameter[8] leads to $\gamma_2 \approx 0.5$ or $Pe'_\infty = 1/\gamma_2 = 2.0$, where Pe'_∞ is the limiting value of Peclet number at high Reynolds number. The dispersion data of a number of authors conform to this limit in the fully turbulent region, but at intermediate Reynolds numbers, dispersion is commonly somewhat greater than predicted by Eq. (7.6) or (7.7). Edwards and Richardson[9] have suggested

$$\frac{D_L}{2vR_p} = \gamma_1 \frac{D_m}{2vR_p} + \frac{1}{Pe'_\infty\left(1 + \beta\gamma_1 \dfrac{D_m}{2vR_p}\right)}$$

$$\text{or} \qquad \frac{1}{Pe'} = \frac{\gamma_1 \epsilon}{Re\,Sc} + \frac{1}{Pe'_\infty\left(1 + \dfrac{\beta\gamma_1 \epsilon}{Re\,Sc}\right)} \qquad (7.9)$$

with $\gamma_1 = 0.73$, $\beta = 13.0$, and $Pe'_\infty = 2.0$. The correlation of Hsu and Haynes[27] (Figure 7.3a) is similar but with somewhat different coefficients.
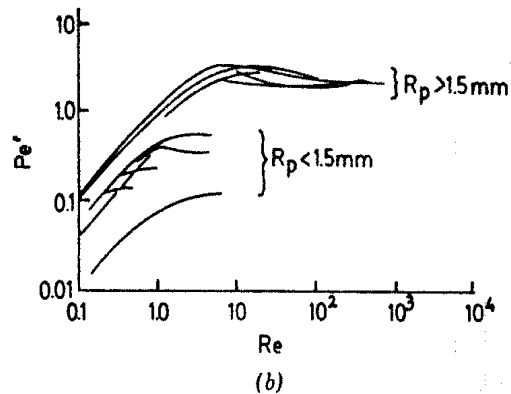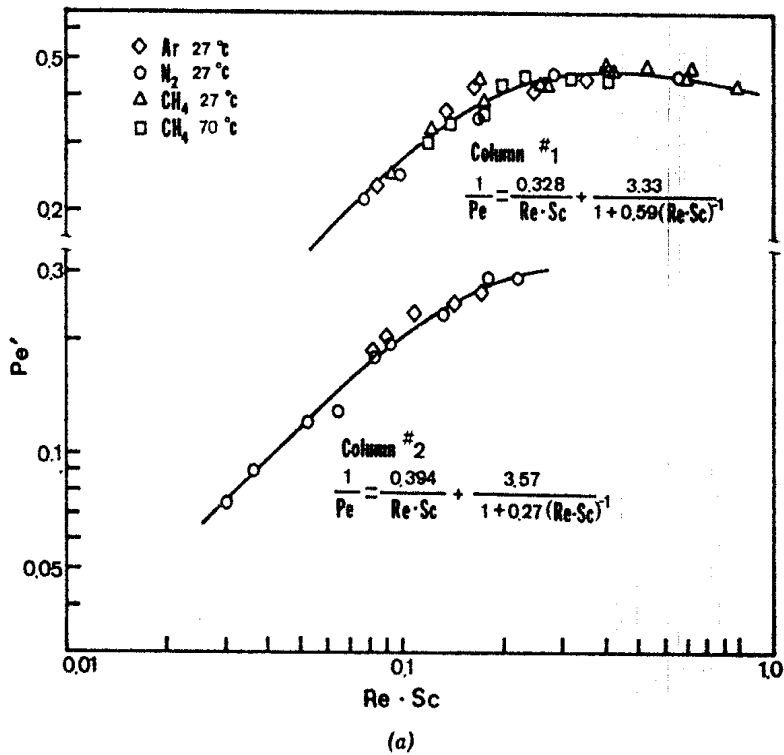
FIGURE 7.3. Variation of Peclet number with Reynolds number for flow of gases through packed beds. (a) Data of Hsu and Haynes[27] (column 1, $R_p = 0.36$ mm; column 2, $R_p = 0.17$ mm). (b) Comparison of results obtained by several authors showing large variation in Pe_∞ for small particles. [(a) is reprinted with permission from $AIChEJl$ (ref. 27), (b) is from ref. 6. Copyright 1978, Pergamon Press, Ltd.]

The derivation and physical meaning of this equation have been discussed by Bischoff[10] and Wicke.[7] The term $\beta\gamma_1 D_m/vd$ accounts for the effect of radial dispersion on the concentration gradient caused by axial dispersion. The data of a number of authors, correlated according to Eq. (7.9), are summarized in Figure 7.3b and Table 7.1.[6]

The data for the larger particles ($R_p > 0.15$ cm) appear generally consistent and show limiting Peclet numbers close to the theoretically expected value of 2.0. The data for the smaller particles ($R_p < 0.15$ cm), however, show very

TABLE 7.1. Summary of Experimental Axial Dispersion Data for Gases in Packed Columns Correlated According to Eq. (7.9)

Author	L/d	$2R_p$ (cm)	γ_1	β	Pe'_∞
McHenry–Wilhelm	18	0.323	—	—	1.88
Edwards–Richardson[9]	10	0.0377–0.607	0.73	13	2.0
Evans–Kenney	164	0.196	0.67	10	2.0
Urban–Gomezplata	16	0.6, 1.6	0.73	19	2.0
	16	0.15	0.73	10	1.0
	59	1.6	0.75	29	2.0
Scott–Lee–Papa	63	0.7, 0.87	0.64	39	2.0
	53	0.87	0.57	42	2.0
Suzuki–Smith	204	0.01–0.08	—	—	0.13–0.77
van Deemter	408	0.0056	—	—	0.125
et al.		0.0225	—	—	0.333
Kawazoe et al.	97	0.067	—	—	0.51
	45	0.141	—	—	1.20
Hsu–Haynes[27]	28	0.072	0.76	1.8	0.3
	39	0.034	0.90	0.7	0.28

Source: Reprinted with permission from *Int. J. Heat and Mass Trans.*, **21**, Langer et al. Copyright 1978, Pergamon Press, Ltd. (For references to the original data see ref. 6.)

much smaller limiting Peclet numbers. There is no correlation with the ratio of particle-to-tube diameters but a rather clear correlation with the absolute value of the particle diameter, as may be seen from Figure 7.4. For particles with diameters less than about 0.3 cm the limiting Peclet number is given, approximately, by

$$R_p < 0.15 \text{ cm}, \qquad Pe'_\infty \approx 3.35 R_p \qquad (7.10)$$

This pattern of behavior is explained by the tendency of the smaller particles to stick together to form clusters which act effectively as single particles in their effect on the fluid flow.

These observations are of considerable practical importance since it is evident that the advantage of reduced pore diffusional resistance which is gained by reduction of particle size can easily be offset by the increased axial dispersion once the particle diameter is reduced below about 0.3 cm.
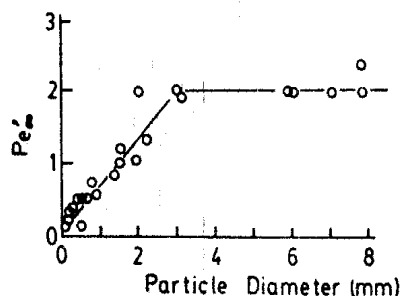
FIGURE 7.4. Variation of limiting Peclet number with particle diameter for flow through packed beds. [Reprinted with permission from *Int. J. Heat and Mass Trans.* **21**, after Langer et al. (ref. 6). Copyright 1978, Pergamon Press, Ltd.]
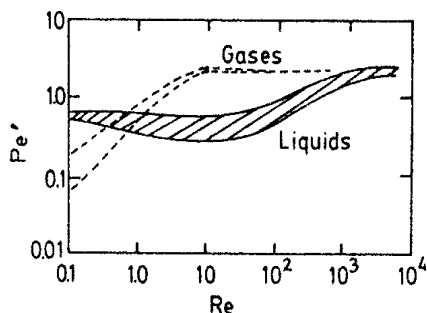
FIGURE 7.5. Variation of Peclet number with Reynolds number—comparison of experimental data for liquids and gases. (After ref. 11, copyright John Wiley & Sons, Inc., 1972; reprinted with permission.)

Liquids

Liquid systems have been studied less extensively than gaseous systems, but the general features of their behavior are well established. The variation of Peclet number with Reynolds number is shown in Figure 7.5.[11] In the high Reynolds number region the Peclet number approaches the theoretical limit of 2.0 ($D_L/vL = 0.5$), but at lower Reynolds numbers dispersion is somewhat greater for liquids than for gases. This has been attributed to the effect of the greater hold-up of liquid in the laminar boundary layer surrounding the particles which, combined with small random fluctuations in the flow, can lead to greater axial mixing. The molecular diffusivities of liquids are too small to contribute significantly to axial dispersion, even at low Reynolds numbers. The complexities of behavior observed in gaseous systems with small particles have not been reported for liquid systems.

Porous Particles

Most experimental studies of axial dispersion have been performed either with nonporous particles or with porous particles under nonadsorbing conditions, and it has been tacitly assumed that the dispersion coefficients measured in this way can be applied to an adsorption column packed with porous adsorbent particles. Wakao[12-14] has, however, shown that this assumption is not necessarily valid.* If adsorption (or reaction) within the particle is sufficiently strong and rapid, the concentration profile through the particle becomes asymmetric, and this can lead to a significant additional contribution to axial dispersion arising from direct transport through the solid. This effect is only important in the low Reynolds number regime since at high Reynolds number there is sufficient turbulent mixing to ensure an essentially uniform boundary concentration around any individual particle. The contribution to the axial dispersion coefficient from intraparticle diffusion depends on the effective intraparticle diffusivity and the magnitude of the concentation gradient through the particle, but for gases at low Reynolds number the effect can be considerable. The effect becomes most significant when all adsorption occurs at the outside of the particle as in the initial stages of the uptake.

*See also R. Chao and H. E. Hoelscher, AIChEJ 12, 271 (1966).

Wakao suggests as a limiting expression for a system with a rectangular isotherm

$$\frac{D_L}{2vR_p} = \frac{20}{\epsilon}\left(\frac{D_m}{2vR_p}\right) + \frac{1}{2} = \frac{20}{\text{Re Sc}} + \frac{1}{2} \qquad (7.11)$$

which is equivalent to Eq. (7.7) with $\gamma_1 = 20/\epsilon$ and $\gamma_2 = 0.5$. With a typical bed voidage of 0.4 this gives $\gamma_1 \sim 50$ compared with about 0.7 for nonporous particles. The practical consequence of this is that with strongly adsorbed species under laminar flow conditions, axial dispersion may be important even when, according to correlations such as that of Edwards and Richardson, it would be insignificant for nonporous particles.

7.3. MASS TRANSFER RESISTANCE OF ADSORBENT PARTICLES

The practical requirement to maintain an acceptable pressure drop at relatively high flow rates means that in a large-scale adsorption process it is generally necessary to use relatively large adsorbent particles (typically 1–3 mm in diameter). The particles generally have a bidisperse pore structure, as indicated in Figure 6.1, and can therefore be regarded as offering two internal diffusional resistances to mass transfer in addition to the external film resistance which is, in principle, always present with any adsorbent, except when the fluid phase contains only a single component. Depending on the particular system and the conditions, any one of the three potential resistances to mass transfer may be controlling or indeed more than one resistance may be important. Intraparticle diffusion was discussed in Chapters 5 and 6 and, apart from the difference in the boundary condition at the external surface, is essentially the same for a particle in a packed bed as for an isolated particle in a batch system. The external fluid film resistance is, however, determined by the hydrodynamic conditions.

The condition of no slip at a solid boundary means that each particle in the bed is surrounded by a laminar sublayer, through which mass transfer occurs by molecular diffusion. The thickness of the laminar sublayer, and hence the mass transfer coefficient, is determined by the hydrodynamic conditions. It is convenient to correlate mass transfer rates in terms of an effective mass transfer coefficient (k_f), defined according to a linear driving force equation:

$$\frac{\partial \bar{q}}{\partial t} = k_f a(c - c^*) = \frac{3k_f}{R_p}(c - c^*) \qquad (7.12)$$

where a is the external surface area per unit particle volume $(3/R_p$ for spherical particles) and $\bar{q}$ is the adsorbed phase concentration averaged over a particle.

The appropriate dimensionless group characterizing film mass transfer is the Sherwood number, defined by $\text{Sh} \equiv 2R_p k_f/D_m$ which is the analog of the Nusselt number for heat transfer. A simple analysis of heat conduction from

an isolated spherical particle surrounded by a stagnant fluid leads to the conclusion that the limiting value of Nusselt number for low Reynolds number flows is 2.0, and by analogy this should also be the lower limit for the Sherwood number. At higher Reynolds numbers convective effects become significant and a correlation of the form Sh = f(Sc, Re) is to be expected.

The correlation of Ranz and Marshall[15]:

$$Sh = \frac{2k_f R_p}{D_m} = 2.0 + 0.6 Sc^{1/3} Re^{1/2} \qquad (7.13)$$

which was derived from the results of an experimental study of mass transfer rates for freely falling solid spheres, has been widely applied to packed beds. This equation implies that the Sherwood number approaches a limiting value of 2.0 at low velocities, as for an isolated sphere.

Experimental mass transfer data at low Reynolds numbers show a great deal of scatter, but most of the reported values fall somewhat below the limit of 2.0 predicted from the Ranz–Marshall correlation. For example, expressed in terms of Sherwood number, the correlation of Petrovic and Thodos[16] for gases is equivalent to

$$3 < Re < 2000, \qquad Sh = \frac{0.357}{\epsilon} Re^{0.64} Sc^{0.33} \qquad (7.14)$$

while, for liquids, Wilson and Geankoplis[17] suggest

$$0.0015 < Re < 55, \qquad Sh = \frac{1.09}{\epsilon} Re^{0.33} Sc^{0.33}$$

$$55 < Re < 1050, \qquad Sh = \frac{0.25}{\epsilon} Re^{0.69} Sc^{0.33} \qquad (7.15)$$

There has been much debate as to whether the low-velocity limit Sh → 2.0, derived for an isolated sphere, is really applicable to a packed bed. The subject has been well reviewed by Wakao and Funazkri[14] who reanalyzed most of the available experimental data for both gas and liquid systems. Most experimental mass transfer coefficients for packed beds have been obtained from measurements of the transient response of the bed to a change in concentration of an adsorbable or reacting species. Axial dispersion and finite resistance to mass transfer have similar effects on the transient response so the assumption of plug flow or of an erroneously low axial dispersion coefficient leads to erroneously low values for the apparent mass transfer coefficient. It was pointed out in Section 7.2 that in the low Reynolds number region, the axial dispersion coefficient for beds packed with porous adsorbent particles are often much higher than those determined for nonporous particles under similar conditions, but this was not generally recognized until recently. It thus appears that in most of the earlier studies the extent of axial dispersion in the low Reynolds number region was underestimated, leading to erroneously low apparent mass transfer coefficients. Wakao and Funazkri[14] showed that when the results of the earlier measurements were corrected for axial dispersion a consistent correlation of the data for both gas and liquid systems
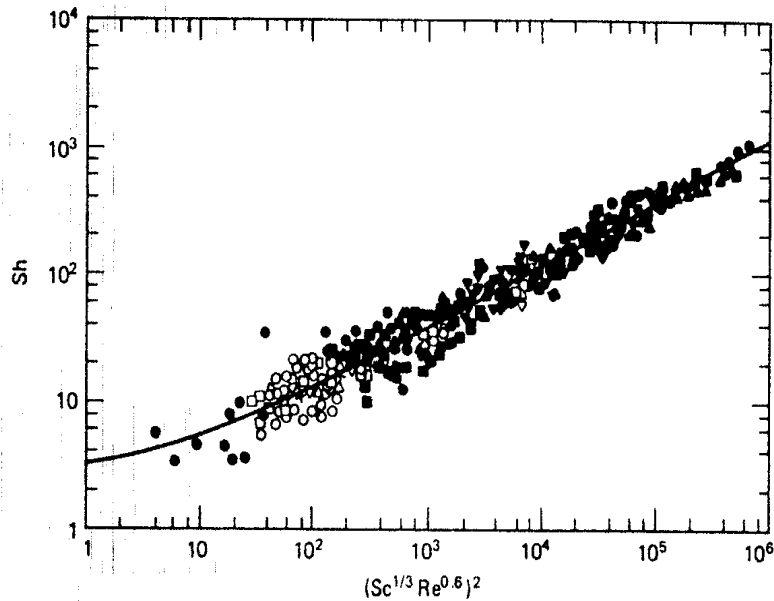
FIGURE 7.6. Correlation of Sherwood number with $Sc^{1/3}Re^{0.6}$ for gas and liquid systems. [Reprinted with permission from *Chem. Eng. Sci.* 33, Wakao and Funazkri (ref. 14). Copyright 1978, Pergamon Press, Ltd.]

emerged:

$$3 < Re < 10^4, \qquad Sh = 2.0 + 1.1Sc^{1/3}Re^{0.6} \qquad (7.16)$$

The correlation of the data from many different authors is shown in Figure 7.6.

Equation (7.16) is similar to the Ranz–Marshall correlation [Eq. (7.13)] and shows the same limiting behavior at low Reynolds number, but both the coefficient and power of the Reynolds number are somewhat larger. In the application of this expression it is important to note that axial dispersion coefficients must be properly estimated [e.g., according to Eq. (7.11) if the isotherm is highly favorable] otherwise the overall dispersion arising from external mass transfer resistance and axial mixing may be underestimated.

7.4. AXIAL HEAT CONDUCTION AND HEAT TRANSFER

For a nonisothermal system the differential heat balance for the fluid phase (see Section 8.1) may be written as

$$-\frac{\lambda_L}{C_f}\frac{\partial^2 T_f}{\partial z^2} + v\frac{\partial T_f}{\partial z} + \frac{\partial T_f}{\partial t} + \left(\frac{1-\epsilon}{\epsilon}\right)\left(\frac{C_s}{C_f}\right)\frac{\partial T_s}{\partial t}$$

$$= \left(\frac{1-\epsilon}{\epsilon}\right)\left(\frac{-\Delta H}{C_f}\right)\frac{\partial \bar{q}}{\partial t} - \frac{4h_w}{\epsilon dC_f}(T_f - T_w) \qquad (7.17)$$

The terms on the left-hand side of this equation are analogous to the terms in

Eq. (7.5), while the terms on the right-hand side give the difference between the rate of heat generation within a particle and the rate of transfer of heat to the column wall. In an adiabatic system the wall heat transfer coefficient is zero so the last term drops out, while in an isothermal system the wall heat transfer coefficient is infinite so that $T_f = T_s = T_w$ (constant).

The heat balance for an individual adsorbent particle may be written

$$C_s \frac{\partial T_s}{\partial t} = \frac{3h}{R_p} (T_f - T_s) + (-\Delta H) \frac{\partial \bar{q}}{\partial t} \qquad (7.18)$$

Convective transport of heat and mass occur by the same mechanism, so if the contribution from radiation, which is normally small except at high temperatures, is neglected one has from the similarity condition

$$\mathrm{Nu} \equiv \frac{2hR_p}{\lambda_f} = \mathrm{Sh} \equiv \frac{2k_f R_p}{D_m}, \qquad \mathrm{Pr} \equiv \frac{C_f \mu}{\rho_f \lambda_f} = \mathrm{Sc} \equiv \frac{\mu}{\rho_f D_m}$$

$$h = k_f C_f, \qquad \lambda_f = C_f D_m \qquad (7.19)$$

In analogy with Eq. (7.16) the fluid-particle heat transfer coefficient is therefore given by

$$\mathrm{Nu} = 2.0 + 1.1 \mathrm{Pr}^{1/3} \mathrm{Re}^{0.6} \qquad (7.20)$$

while the effective axial thermal conductivity is given by

$$\lambda_L = C_f D_L \qquad (7.21)$$

Experimental measurements of fluid-particle heat transfer[18-21] in general confirm the validity of the analogy with mass transfer, particularly at higher Reynolds numbers. In the low Reynolds number range there is, however, a great deal of experimental scatter. As with mass transfer this is almost certainly due to the breakdown of the assumption of a uniform surface boundary condition leading to errors in the estimation of the effective axial thermal conductivity and corresponding errors in the values of heat transfer coefficients derived from the experimental data. On the basis of Wakao's analysis[12,13] it seems reasonable to use Eq. (7.20) for the estimation of particle heat transfer coefficients but, as with mass transfer, it is essential to make due allowance for the effect of axial heat conduction in the low Reynolds number region[12] [Eqs. (7.21) and (7.17)]. In laboratory studies with small diameter columns the effect of heat conduction in the column wall can also contribute significantly to the effective axial conductivity, but this effect is generally negligible in large commercial columns.

7.5. RELATIVE IMPORTANCE OF INTERNAL AND EXTERNAL RESISTANCES

In this analysis it has been tacitly assumed that the temperature can be considered uniform throughout an individual adsorbent particle, implying that

the major resistance to heat transfer lies in the external fluid film rather than within the particle. This is in fact a good approximation as has been shown by Lee and Luss[22] and Carberry[23] in relation to the analysis of nonisothermal behavior of catalyst particles.

The Biot numbers for mass and heat transfer, which measure the ratio of internal-to-external gradients, are defined by:

$$(Bi)_m = \frac{k_f R_p}{3\epsilon_p D_p}, \qquad (Bi)_h = \frac{h R_p}{3\lambda_s} \tag{7.22}$$

or, in terms of Sherwood and Nusselt numbers:

$$(Bi)_m = \frac{Sh}{6} \frac{D_m}{\epsilon_p D_p}, \qquad (Bi)_h = \frac{Nu}{6} \frac{\lambda_f}{\lambda_s} \tag{7.23}$$

Since $Sh \geqslant 2$ and $D_p \leqslant D_m/\tau$, the minimum value of $(Bi)_m$ is given by $\tau/3\epsilon$ ($\sim$3.0). Thus, even under these rather extreme assumptions the internal concentration gradient is appreciably greater than the external gradient. Any additional resistance to mass transfer from either Knudsen diffusion or intracrystalline diffusion will decrease D_p further, so one may conclude that under most practically realisable conditions the intraparticle resistance is more important than film resistance in determining the mass transfer rate.

For heat transfer the relative importance of the internal and external resistances is reversed. For a gaseous system $\lambda_s/\lambda_f \sim 10^2$–$10^3$ so it is evident from Eqs. 7.20 and 7.23 that at any reasonable Reynolds number $(Bi)_h \ll 1.0$, indicating that the external temperature gradient is much greater than the temperature gradient within the particle. The model of an isothermal particle in which all resistance to mass transfer is due to intraparticle diffusion while resistance to heat transfer is confined to the external film thus emerges as a realistic representation for most conditions of practical importance. The validity of this approximation has been verified experimentally for a single isolated adsorbent particle.[24]

For liquid systems $\lambda_s/\lambda_g \sim 1.0$, so the internal and external resistances to heat transfer may be comparable. However, since the thermal capacity of the fluid is then much higher, the absolute magnitude of the temperature rise is generally small, except when the sorbate concentration is very high.

7.6. HEAT TRANSFER TO COLUMN WALL

Heat transfer between packed beds and the external column wall has been widely studied because of its relevance to the design and operation of wall-cooled catalytic reactors.[1] In the one-dimensional model, which is the basis of Eq. (7.17), the overall heat transfer resistance may be represented as the sum of the internal, external, and wall resistances:

$$\frac{1}{dh_w} = \frac{1}{dh_i} + \frac{1}{d_e h_e} + \frac{x}{\lambda_w d_{im}} \tag{7.24}$$

Cooling at the external surface is normally by natural convection and the value of the external heat transfer coefficient (h_e) is given, approximately, by[25]

$$h_e \, (\text{BTU}/\text{hr ft}^2 \, ^\circ\text{F}) = 0.27\Delta T \, (^\circ\text{F}) \qquad (7.25)$$

where ΔT is the temperature difference between the external surface and the surroundings. For metal-walled vessels the heat transfer resistance of the wall can generally be neglected; but, of course, this term becomes important if the wall is insulated. The heat transfer coefficient at the internal surface may be estimated from Leva's correlation[4]:

$$\text{Nu}_i \equiv \frac{h_i d}{\lambda_f} = 0.813 \text{Re}^{0.19} e^{-12R_p/d} \qquad (7.26)$$

The results of Ruthven, Garg, and Crawford[26] who estimated wall heat transfer coefficients directly from the temperature profiles measured in an adsorption column are in satisfactory accord with this formula. ($h_w = 3$–5×10^{-4} cal/cm s deg. for $\frac{1}{8}$-in. diameter particles in a tube of diameter 1.5 in. at Re ~ 15 compared with a predicted value of $h_w = 4.5 \times 10^{-4}$ cal/cm s deg.) The significance of heat loss from the column wall may be estimated by comparing the overall heat loss with the rate at which heat is generated within the column. In general, large industrial columns operate under near adiabatic conditions whereas small laboratory scale columns may approach isothermal operation. However, except when the concentration of the absorbable component is low and the heat of adsorption is small, it is often difficult to obtain a really good approximation to isothermal operation even in a small column.

A more detailed review and summary of the correlations for estimation of heat transfer coefficients in packed beds has been given by Rodrigues et al.[28]

REFERENCES

1. G. F. Froment and K. B. Bischoff, *Chemical Reaction Analysis and Design*. Wiley, New York, 1979, Chap. 11.

2. C. C. Furnas, U.S. Bureau of Mines Bulletin No. 307 (1929).

3. T. H. Chilton and A. P. Colburn, *Trans. Am. Inst. Chem. Eng.* **26**, 178 (1931).

4. M. Leva, *Chem. Eng.* **56**, 115 (1949).

5. S. Ergun, *Chem. Eng. Prog.* **48**, 89 (1952).

6. G. Langer, A. Roethe, K-P. Roethe, and D. Gelbin, *Int. J. Heat and Mass Trans.* **21**, 751 (1978).

7. E. Wicke, *Ber. Bunsenges* **77**, 160 (1973).

8. R. Aris and N. R. Amundson, *AIChE J.* **3**, 280 (1957).

9. M. F. Edwards and J. F. Richardson, *Chem. Eng. Sci.* **23**, 109 (1968).

10. K. B. Bischoff, *Chem. Eng. Sci.* **24**, 607 (1969).

11. O. Levenspiel, *Chemical Reaction Engineering*, 2nd ed. Wiley, New York, 1972, p. 282.

12. N. Wakao, *Chem. Eng. Sci.* **31**, 1115 (1976).

13. N. Wakao, S. Kaguei, and N. Nagai, *Chem. Eng. Sci.* **33**, 183 (1978).

14. N. Wakao and T. Funazkri, *Chem. Eng. Sci.* **33**, 1375 (1978).

15. W. E. Ranz and W. R. Marshall, *Chem. Eng. Prog.* **48**, 173 (1952).

16. L. J. Petrovic and G. Thodos, *Ind. Eng. Chem. Fund.* **7**, 274 (1968).

17. E. J. Wilson and C. J. Geankoplis, *Ind. Eng. Chem. Fund.* **5**, 9 (1966).

18. D. Kunii and M. Suzuki, *Int. J. Heat and Mass Trans.* **10**, 845 (1967).

19. M. Sagaro, P. Schneider, and J. M. Smith, *Chem. Eng. J.* **1**, 47 (1970).

20. H. Littman, R. G. Barile, and A. H. Pulsifer, *Ind. Eng. Chem. Fund.* **7**, 554 (1968).

21. D. Gelbin, K-H. Radeke, B. Rosahl, and N. Stein, *Int. J. Heat and Mass Trans.* **19**, 987 (1976).

22. J. C. M. Lee and D. Luss, *Ind. Eng. Chem. Fund.* **8**, 596 (1969).

23. J. J. Carberry, *Ind. Eng. Chem. Fund.* **14**, 129 (1975).

24. J. Ilavsky, A. Brunovska, and V. Hlavacek, *Chem. Eng. Sci.* **35**, 2475 (1980).

25. J. H. Perry (ed.), *Chemical Engineers' Handbook*, 3rd ed. McGraw-Hill, New York, 1950, p. 474.

26. D. M. Ruthven, D. R. Garg, and R. M. Crawford, *Chem. Eng. Sci.* **30**, 803 (1975).

27. L-K. P. Hsu and H. W. Haynes, *AIChE J.* **27**, 81 (1981).

28. A. Rodrigues, C. Costa, R. Ferreira, J. Loureiro, and S. Azevedo, NATO ASI Zeolites, Sintra-Estoril, Portugal, May, 1983.

8

DYNAMICS OF ADSORPTION COLUMNS
Single-Transition Systems

In Chapter 6 we discussed the kinetics of adsorption for a single adsorbent particle exposed to a known concentration of sorbate at its external surface. This is the appropriate perspective when considering the analysis of experimental uptake curves for batch systems, but in the practical application of adsorbents the situation is generally more complex since the adsorbent is usually contacted by fluid flowing through a packed bed, rather than in a well-mixed system of uniform composition. It is the overall dynamics of the packed-bed system, rather than the adsorption kinetics for a single particle, which control the design and determine the efficiency of such a process.

In an ideal plug flow system with no resistance to mass transfer, the outlet concentration response would replicate the input with a time delay corresponding to the hold-up in the column. In a real system the outlet response is also dispersed as a result of the combined effects of axial dispersion and mass transfer resistance. Measurement of the time delay therefore provides information concerning the adsorption equilibrium while measurement of the dispersion of the response provides information on the sorption kinetics and the extent of axial mixing in the column. To extract this information, the experimental response must be matched with the theoretical response curve, calculated from a suitable dynamic model for the system. From the perspective of the design engineer the inverse problem, that is, prediction of the breakthrough curve from basic kinetic and equilibrium data, is also important since this provides, in principle, a method of predicting the dynamic capacity of the column without recourse to extensive experimentation.

In studying the dynamics of a fixed-bed adsorption column it is convenient to consider the response of an initially sorbate free column to either a step change in sorbate concentration at the column inlet (step input) or to the

injection of a small pulse of sorbate at the column inlet (pulse input). The response to a step input is commonly called the breakthrough curve while the pulse response is often referred to as the chromatographic response. Since a delta function (perfect pulse) is the derivative of the Heaviside function (perfect step) for a linear system, the chromatographic response is simply the derivative of the breakthrough curve. Exactly the same information may therefore be derived from the response to either input and the choice is therefore determined by practical convenience rather than by more fundamental theoretical considerations.

It is convenient to classify adsorption systems in the first instance according to the number of transitions or mass transfer zones in the dynamic response to a change in feed composition. The simplest type of system is an isothermal system with one adsorbable component in an inert carrier. Such systems exhibit only a single mass transfer zone and the dynamic behavior may be analyzed in considerable detail. Systems with two adsorbable species (no inert present) also show only a single mass transfer zone but analysis of the dynamic behavior is somewhat more difficult because of coupling between the equilibrium isotherms and the rate equations for the two species. In this chapter consideration is limited to single transition systems and the discussion is concerned primarily with systems containing only one adsorbable component. More complex systems including multicomponent and adiabatic systems are discussed in Chapter 9.

8.1. MATHEMATICAL MODEL OF AN ISOTHERMAL, SINGLE-TRANSITION ADSORPTION COLUMN

The differential mass balance equations for an element of the adsorption column and for an adsorbent particle within such an element provide the starting point for development of a mathematical model to describe the dynamic behavior of the system. We consider an element of the bed, as sketched in Figure 8.1, through which a fluid stream containing concentration $c(z,t)$ of an adsorbable species is flowing. If the flow pattern can be represented as axially dispersed plug flow the differential fluid phase mass bal-
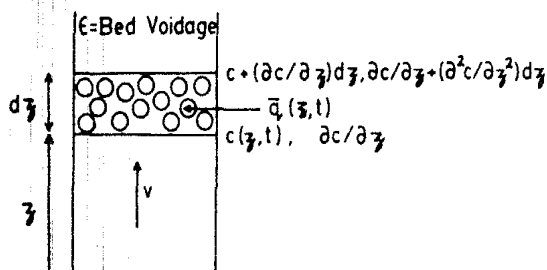
FIGURE 8.1. Element of packed bed.

ance is

$$-D_L \frac{\partial^2 c}{\partial z^2} + \frac{\partial}{\partial z}(vc) + \frac{\partial c}{\partial t} + \left(\frac{1-\epsilon}{\epsilon}\right)\frac{\partial \bar{q}}{\partial t} = 0 \qquad (8.1)$$

The mass balance for an adsorbent particle yields the adsorption rate expression, which may be written

$$\frac{\partial \bar{q}}{\partial t} = f(q, c) \qquad (8.2)$$

Although written here as a single equation, the mass transfer rate expression is commonly a set of equations comprising one or more diffusion equations with associated boundary conditions, incorporating the equilibrium constraints to which the mass transfer rate expression must reduce at sufficiently long times.

The dynamic response of the column is given by the solution $[c(z,t), \bar{q}(z,t)]$ to Eqs. (8.1) and (8.2) subject to the initial and boundary conditions imposed on the column. The response to a perturbation in the feed composition involves a mass transfer zone or concentration front which propagates through the column with a characteristic velocity determined by the equilibrium isotherm. The location of the front at any time may be found simply from an overall mass balance, but to determine the form of the concentration front Eqs. (8.1) and (8.2) must be solved simultaneously.

If the system contains two adsorbable components, rather than one adsorbable component in an inert carrier, mass balance equations analogous to Eqs. (8.1) and (8.2) may be written for both species. However, since the continuity condition must also be satisfied ($c_1 + c_2 = C$ = constant) these equations are not independent and there is still only one mass transfer zone. The behavior of a system which contains an inert carrier in addition to the two adsorbable species is entirely different since two distinct mass transfer zones are then formed. The discussion of such systems is deferred until Chapter 9.

8.2. EQUILIBRIUM CONSIDERATIONS

The general nature of a concentration front or mass transfer zone is determined entirely by the equilibrium isotherm although the shape of the concentration profile may be significantly modified by kinetic effects. Three general cases can be distinguished depending on whether the equilibrium relationship is linear, favorable, or unfavorable over the concentration range corresponding to the transition considered. The meaning of these terms can be understood by reference to Figure 8.2 which shows possible general forms for the equilibrium isotherm and the $X-Y$ diagram. The $X-Y$ diagram is simply a nondimensional representation of the equilibrium relationship, expressed in terms of the reduced variables $(q^* - q_0')/(q_0 - q_0')$ and $(c - c_0')/(c_0 - c_0')$, where $q_0 - q_0'$ and $c_0 - c_0'$ represent the respective changes in adsorbed phase and fluid phase concentrations over the mass transfer zone for the component considered.
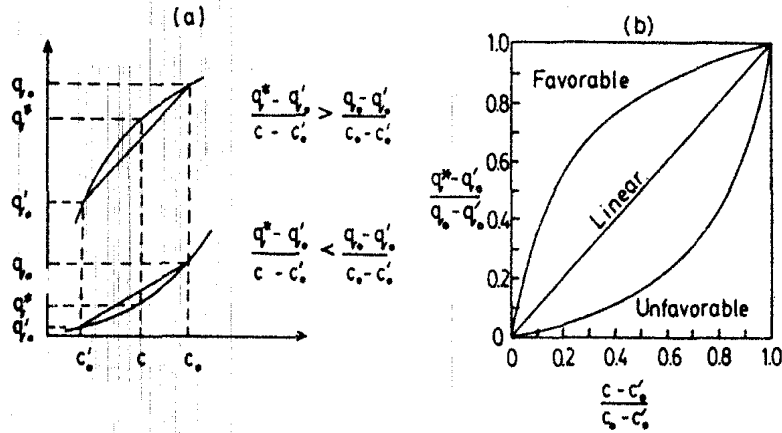
FIGURE 8.2. (*a*) Equilibrium isotherms and (*b*) equilibrium diagram showing distinction between "favorable," "unfavorable," and "linear" systems.

The three general cases illustrated in Figure 8.2 correspond to:

Favorable
$$\frac{q^* - q'_0}{q_0 - q'_0} > \frac{c - c'_0}{c_0 - c'_0}$$

Linear
$$\frac{q^* - q'_0}{q_0 - q'_0} = \frac{c - c'_0}{c_0 - c_0}$$

Unfavorable
$$\frac{q^* - q'_0}{q_0 - q'_0} < \frac{c - c'_0}{c_0 - c'_0}$$

One may define an equilibrium factor (β) for the transition in a manner analogous to relative volatility or separation factor:

$$\beta_{c'_0 \to c_0} \equiv \frac{\left(\dfrac{c - c'_0}{c_0 - c'_0}\right) \Big/ \left(\dfrac{q^* - q'_0}{q_0 - q'_0}\right)}{\left(1 - \dfrac{c - c'_0}{c_0 - c'_0}\right) \Big/ \left(1 - \dfrac{q^* - q'_0}{q_0 - q'_0}\right)} = \left(\frac{c - c'_0}{c - c_0}\right)\left(\frac{q^* - q_0}{q^* - q'_0}\right) \quad (8.3)$$

It is evident that if the sorbent is initially free of sorbate ($c'_0 = q'_0 = 0$):

$$\beta_{0 \to c_0} = \left(\frac{c}{q^*}\right)\left(\frac{q_0 - q^*}{c_0 - c}\right), \qquad \beta_{c'_0 \to c_0} = \frac{\beta_{0 \to c_0}}{\beta_{0 \to c'_0}} \quad (8.4)$$

For a desorption process the values of c'_0, c_0 and q'_0, q_0 are interchanged and it follows that the equilibrium factors defined by Eq. (8.3) are reciprocally related:

$$\beta_{\text{des}} = \frac{1}{\beta_{\text{ads}}} \quad (8.5)$$

The criteria for favorable, linear, and unfavorable equilibria are, respectively, $\beta_{0 \to c_0} < 1.0$, $\beta_{0 \to c_0} = 1.0$, and $\beta_{0 \to c_0} > 1.0$ so it is clear that if an isotherm is

favorable for adsorption it will be unfavorable for desorption. Only in the case of a linear isotherm are adsorption and desorption symmetrically equivalent processes.

It is evident from Eq. (8.3) that the equilibrium factor is in general concentration dependent. However, in the special case of a Langmuir equilibrium isotherm

$$\frac{q^*}{q_s} = \frac{bc}{1 + bc}, \qquad \beta_{c_0' \to c_0} = \frac{1 + bc_0'}{1 + bc_0} = \frac{1 - q_0/q_s}{1 - q_0'/q_s} \qquad (8.6)$$

it may be seen that β is constant and depends only on the magnitude of the concentration change, relative to the saturation limit. This is an important advantage of the Langmuir model which, in the discussion of adsorption column dynamics, is often referred to as the "constant separation factor" approximation.

For systems in which the equilibrium isotherm is linear or unfavorable the mass transfer zone broadens continuously as the front propagates through the column. Such behavior is commonly referred to as dispersive or "proportionate pattern" since the width of the mass transfer zone increases in direct proportion to the distance traveled through the column. When the isotherm is favorable a completely different type of behavior is observed. In the initial region the mass transfer front broadens but after some distance it attains "constant-pattern" form and thereafter it progresses through the column with no further change in shape. This type of behavior, which is of considerable practical importance, is discussed in greater detail in Section 8.7.

8.3. CLASSIFICATION OF SINGLE-TRANSITION SYSTEMS

The dynamic behavior of an adsorption system may be classified according to the nature of the mass transfer front and the complexity of the mathematical model required to describe the system. The nature of the mass transfer front is determined solely by the form of the equilibrium relationship, as outlined above, while the complexity of the mathematical model depends on the concentration level, the choice of rate equation, and the choice of flow model. The following classification scheme provides a useful framework for more detailed analysis.

1. *Nature of Equilibrium Relationship*
   (a) *Linear Isotherm.* Dispersive behavior. Analytic solutions for step or pulse response can generally be found.
   (b) *Favorable Isotherm.* Concentration front approaches constant-pattern form. Analytic solutions for the asymptotic constant-pattern profile are easily obtained, but a general analytic solution for the breakthrough curve or pulse response is only possible in a few special cases.

(c) *Unfavorable Isotherm.* Dispersive behavior. Most commonly observed during desorption of a favorably adsorbed species. Analytic solutions are generally not possible.

2. *Isothermal or Near Isothermal*

   (a) *Isothermal.* Heat transfer resistance can be neglected. The spreading of the concentration front is due entirely to axial dispersion and mass transfer resistance. This is the usual situation in a chromatographic system in which the adsorbable component is present only at low concentration in an inert carrier.

   (b) *Near Isothermal.* Heat transfer between fluid and solid is slow enough to cause additional broadening of the concentration front although heat transfer between the column and surroundings is still fast enough to prevent the formation of a distinct thermal front and associated secondary mass transfer zone. This situation, which can occur in a chromatographic system when the adsorbable species has a high heat of adsorption or is present at a relatively high concentration level, is discussed in Section 8.7.

When adiabatic behavior is approached the concentration profile shows two distinct fronts. The discussion of such systems is deferred until Chapter 9.

3. *Concentration Level of Adsorbable Components*

   (a) *Trace Systems.* The adsorbable component is present only at low concentration in an inert carrier. Changes in fluid velocity across the mass transfer zone are therefore negligible.

   (b) *Nontrace Systems.* The adsorbable species are present at sufficiently high concentration levels to cause a significant variation in fluid velocity across the mass transfer zone. Such effects are usually significant only for gaseous systems.

4. *Flow Model*

   (a) *Plug Flow.* Axial dispersion is neglected so that the term $-D_L \partial^2 c / \partial z^2$ can be dropped, reducing Eq. (8.1) to a first-order hyperbolic equation.

   (b) *Dispersed Plug Flow.* Axial dispersion is significant so that the term $-D_L \partial^2 c / \partial z^2$ must be retained in Eq. (8.1).

5. *Complexity of Kinetic Model*

   (a) *Negligible Mass Transfer Resistance.* Instantaneous equilibrium is assumed at all points in the column.

   (b) *Single Mass Transfer Resistance.*

      (i) Linear rate expression:

$$\frac{\partial \bar{q}}{\partial t} = k(q^* - q) \quad \text{or} \quad k'(c - c^*)$$

The rate coefficient is an overall effective mass transfer coefficient (lumped parameter).

   (ii)   Diffusion model:

The dominant mass transfer resistance is intraparticle diffusion which is described by the diffusion equation with associated boundary conditions.

(c)   *Two Mass Transfer Resistances.*

   (i)   External fluid film resistance plus intraparticle diffusion.

   (ii)   Two internal diffusional resistances (macropore–micropore).

(d)   *Three Mass Transfer Resistances.*

   External film resistance plus two intraparticle diffusional resistances (macropore–micropore).

   Such a model is sufficiently general to provide a realistic description of almost all practical systems.

8.4.   ISOTHERMAL, SINGLE-TRANSITION SYSTEM: EQUILIBRIUM THEORY

Trace Systems

In accordance with our classification the simplest system to consider is an isothermal plug flow system in which a trace of an adsorbable species is adsorbed from an inert carrier under conditions such that mass transfer resistance is negligible. Although such systems are not common in practice, their analysis can provide useful insight into the behavior of more complex systems. For such a system the differential fluid phase mass balance for the adsorbable species [Eq. (8.1)] reduces to

$$v\frac{\partial c}{\partial z} + \frac{\partial c}{\partial t} + \left(\frac{1-\epsilon}{\epsilon}\right)\frac{\partial \bar{q}}{\partial t} = 0 \tag{8.7}$$

Representing the equilibrium isotherm in general form by

$$q^* = f(c) \tag{8.8}$$

and assuming mass transfer equilibrium:

$$\left(\frac{\partial \bar{q}}{\partial t}\right)_z = \left(\frac{\partial q^*}{\partial t}\right)_z = \frac{dq^*}{dc}\left(\frac{\partial c}{\partial t}\right)_z \tag{8.9}$$

$$\left(\frac{\partial c}{\partial t}\right)_z + \frac{v}{\left[1 + \left(\frac{1-\epsilon}{\epsilon}\right)\left(\frac{dq^*}{dc}\right)\right]}\left(\frac{\partial c}{\partial z}\right)_t = 0 \tag{8.10}$$

This equation has the form of the kinematic wave equation. The velocity with

which the disturbance propagates through the column is given by

$$w(c) = \left(\frac{\partial z}{\partial t}\right)_c = -\frac{(\partial c/\partial t)_z}{(\partial c/\partial z)_t} = \frac{v}{\left[1 + \left(\frac{1-\epsilon}{\epsilon}\right)\left(\frac{dq^*}{dc}\right)\right]} \tag{8.11}$$

and the mean retention time is given by

$$\bar{t} = \frac{L}{v}\left[1 + \left(\frac{1-\epsilon}{\epsilon}\right)\left(\frac{dq^*}{dc}\right)\right] \tag{8.12}$$

a result which may also be obtained directly from a mass balance over the column.

Equation (8.11), which was first derived by deVault,[1] shows how the basic pattern of behavior of a chromatographic system depends on the form of the equilibrium isotherm. If the equilibrium is unfavorable, dq^*/dc is a continuously increasing function of concentration and the propagation velocity increases from the initial to the final state, leading to a dispersive wave which spreads out continuously as it propagates through the column. If the isotherm is favorable the reverse situation occurs and the propagation velocity corresponding to the initial state is higher than that of the final state. This would lead to the physically unrealistic situation of an overhanging concentration profile as sketched in Figure 8.3. In fact the limiting behavior of this type of
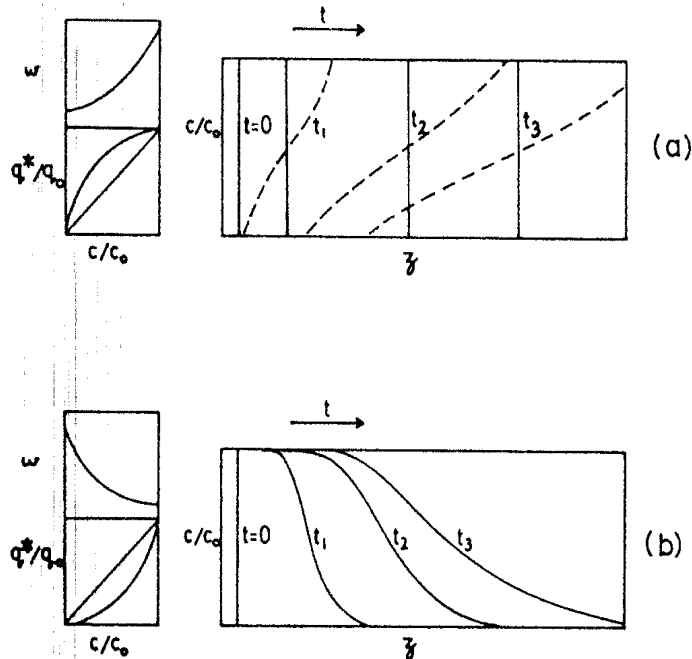
FIGURE 8.3. (a) Development of physically unrealistic overhanging concentration profile and corresponding shock profile for a favorable isotherm ($\beta < 1.0$). (b) Development of dispersive (proportionate-pattern) concentration profile for desorption of a uniformly saturated bed when the isotherm is favorable for adsorption, unfavorable for desorption ($\beta_{ads} < 1.0$; $\beta_{des} > 1.0$) (after Rodrigues[3]).

compressive wave is a shock transition which travels through the column with a velocity determined by the mass balance over the front:

$$w' = \frac{v}{1 + \left(\dfrac{1-\epsilon}{\epsilon}\right)\dfrac{\Delta q^*}{\Delta c}} \tag{8.13}$$

A perfect step transition will be attained only in a system in which there are no dispersive effects (no axial dispersion or mass transfer resistance). In a real system the profile will converge to a limiting form in which the dispersive effects are exactly counterbalanced by the compressive effect of the equilibrium relationship. When this form is reached the profile will progress through the column without any further change in shape and with the velocity given by Eq. (8.13). This is referred to as "constant-pattern" behavior and is discussed in greater detail in Section 8.7.

In most adsorption systems the isotherm is favorable for adsorption and therefore unfavorable for desorption. In desorption the mass transfer zone is therefore dispersive, leading to a continuously spreading concentration profile (proportionate-pattern behavior) while in adsorption the mass transfer zone is compressive, leading to constant-pattern behavior. For example, for a system which obeys the Langmuir isotherm [Eq. (8.6)]

$$\frac{dq^*}{dc} = \frac{bq_s}{(1 + bc)^2} \tag{8.14}$$

Substitution in Eq. (8.11) followed by integration yields as the asymptotic expression for the breakthrough curve for desorption of a uniformly saturated bed (c_0, q_0) with pure carrier[2]:

$$\frac{c}{c_0} = \frac{\beta}{(1-\beta)}\left[\left(\frac{\xi}{\tau}\right)^{1/2} - 1\right], \qquad \frac{1}{\beta^2} > \frac{\xi}{\tau} > 1 \tag{8.15}$$

where the dimensionless variables are defined by

$$\beta = 1 - \frac{q_0}{q_s} = (1 + bc_0)^{-1} \quad [\text{Eq. (8.6)}] \quad \text{and} \quad \frac{\xi}{\tau} = \frac{(bq_s)z}{(vt - z)}\left(\frac{1-\epsilon}{\epsilon}\right).$$

Equation (8.10) is a standard hyperbolic equation of the form

$$\left(\frac{\partial c}{\partial t}\right)_z + w(c)\left(\frac{\partial c}{\partial z}\right)_t = 0 \tag{8.16}$$

which may be expressed more concisely in terms of the modified coordinate $z' = z - wt$:

$$\left(\frac{\partial c}{\partial t}\right)_{z'} = 0 \tag{8.17}$$

The concentration profile can thus be thought of as propagating along characteristic lines of slope w in the $z-t$ plane. The form of the characteristics and the corresponding concentration profiles for desorption of a uniformly saturated bed (favorable isotherm) are sketched in Figure 8.4. The characteris-
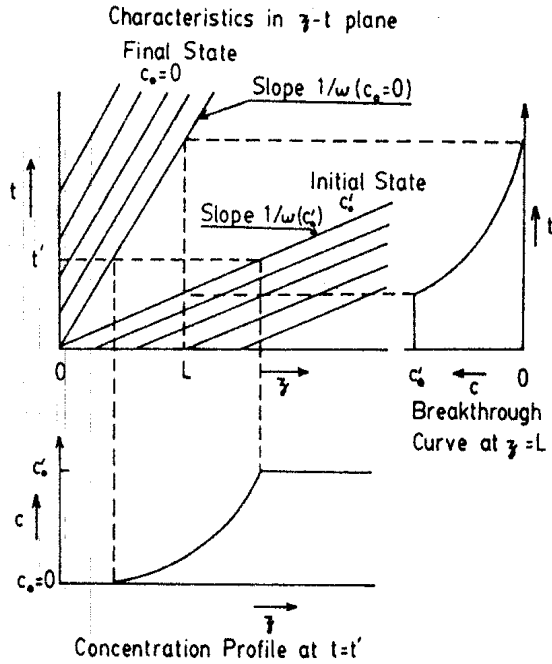
FIGURE 8.4. Characteristics, concentration profile, and breakthrough curve for desorption of a uniformly saturated bed. (Isotherm is favorable for adsorption, unfavorable for desorption.)

tic lines diverge since w is larger for the final state than for the initial state, leading to the proportionate-pattern type of profile. The inverse situation which occurs during saturation of a clean bed is shown in Figure 8.5. The characteristics cross and instead of a simple dispersive wave we have a shock front which propagates with the characteristic shock velocity given by Eq. (8.13).

In the case of an isotherm which has an inflection, such as the BET isotherm, the equilibrium is favorable at low concentrations and unfavorable at high concentrations. The resulting concentration front is a composite wave composed of a shock transition followed by a dispersive front, as illustrated in Figure 8.6. At the transition point $(c'/c_0, q'/q_0)$ the shock velocity and the wave velocity are the same [Eqs. (8.11) and (8.13)] so that $dq^*/dc = \Delta q^*/\Delta c$. The transition point is thus seen to be given by the tangent which passes through the origin. If the equation of the isotherm is defined, the form of the dispersive front which is obtained for $c/c_0 > c'/c_0$ is easily calculated from Eq. (8.11) since at any given concentration $t = L/w$. The complete breakthrough curve may then be constructed since the transition point is known.[3]

The effect of isotherm nonlinearity on the chromatographic response can also be seen from Eq. (8.10). If the isotherm is linear then, under equilibrium conditions, there will be no dispersion. All concentration levels travel at the same velocity (since dq^*/dc is constant) and the outlet response replicates the input with a time delay corresponding to the hold-up in the column. However, for a nonlinear system the different concentration levels travel at different velocities since dq^*/dc is concentration dependent. A delta function input is
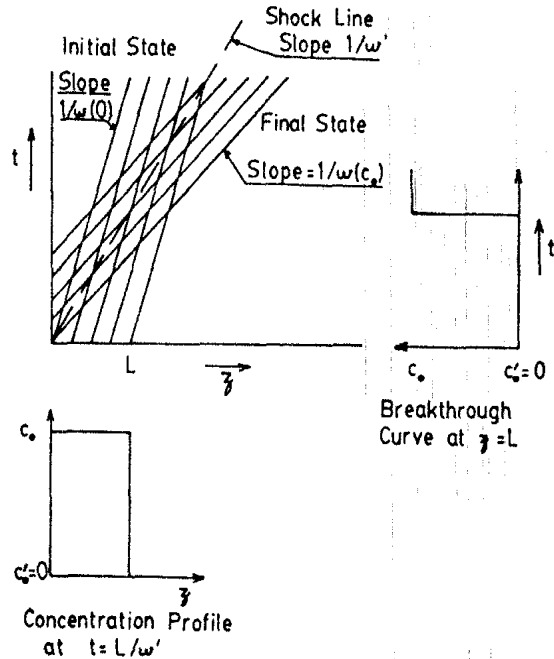
FIGURE 8.5. Characteristics, concentration profile, and breakthrough curve for adsorption with an initially clean bed. (Favorable adsorption isotherm.)

merely two steps, adsorption and desorption, separated by an infinitesimal time interval. The leading concentration front is thus an adsorption transition which, in an equilibrium system with favorable adsorption isotherm, propagates as a step. The trailing front is a desorption transition which propagates as a dispersive proportionate-pattern profile. The pulse therefore progresses through the column as a peak with a sharp front followed by a broadening tail as indicated in Figure 8.7. In a linear system both the retention time and the shape of chromatographic peak are independent of pulse size, but in a
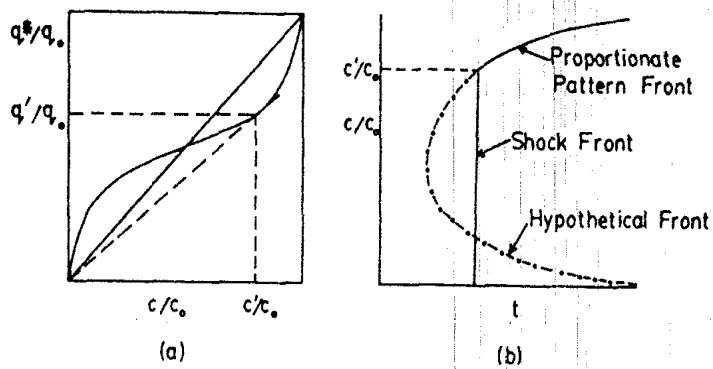
FIGURE 8.6. $X-Y$ diagram (a) and corresponding breakthrough curve (b) for adsorption with a favorable–unfavorable (BET) type of isotherm. The broken curve is the hypothetical curve calculated according to equilibrium theory from Eq. (8.11). The actual profile (continuous line) consists of a shock front combined with a proportionate-pattern front. The intersection of these two fronts is at c'.
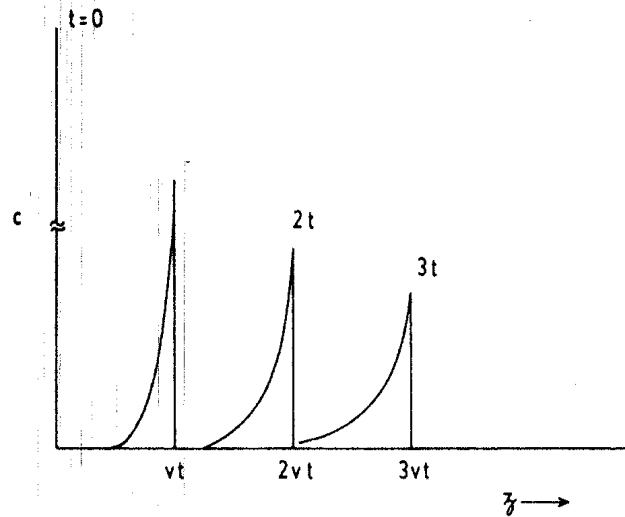
FIGURE 8.7. Schematic diagram showing propagation of a chromatographic pulse under nonlinear equilibrium conditions. (The isotherm is assumed to be favorable for adsorption.)

nonlinear (favorable equilibrium) system the retention time will decrease and the peak will become more dispersed with increasing pulse size. Variation of pulse size thus provides a simple experimental test for system linearity.

Broadening of the chromatographic response can also be caused by other effects such as finite mass transfer resistance, and this is the basis of the chromatographic method for measuring mass transfer coefficients. Clearly in any application of this method it is essential to confirm that the system is indeed linear and the peak broadening results from mass transfer resistance rather than from nonlinearity of the isotherm. With strongly adsorbed species this may require working at extremely low concentration levels at which accurate measurements may be difficult.

Nontrace Systems

In the preceding analysis the term $c\partial v/\partial z$ was dropped from the differential fluid phase mass balance [Eq. (8.1)]. This is justified provided that the concentration of the adsorbable species is sufficiently small, that is, for a trace component in an inert carrier. However, if this condition is not fulfilled a more detailed analysis is required since the variation in fluid velocity over the mass transfer zone must be accounted for. For generality we first consider a two-component (isothermal) system in which both components are adsorbable. For such a system we can write two differential fluid phase mass balance equations, one for each component:

$$-D_L \frac{\partial^2 c_1}{\partial z^2} + v \frac{\partial c_1}{\partial z} + c_1 \frac{\partial v}{\partial z} + \frac{\partial c_1}{\partial t} + \left(\frac{1-\epsilon}{\epsilon} \right) \frac{\partial q_1}{\partial t} = 0 \qquad (8.18)$$

The equation for component 2 is similar. These two equations are not

independent since the continuity condition $c_1 + c_2 = C$ must be obeyed. For gaseous systems, where the pressure drop is small, the total concentration in the fluid phase (C) remains constant and this is approximately true also for liquid mixtures when the components have similar molar volumes. The equations for the two components may be combined to give

$$-D_L \frac{\partial^2 Y}{\partial z^2} + v \frac{\partial Y}{\partial z} + \frac{\partial Y}{\partial t} + \frac{1}{C}\left(\frac{1-\epsilon}{\epsilon}\right)\left[(1-Y)\frac{\partial \bar{q}_1}{\partial t} - Y\frac{\partial \bar{q}_2}{\partial t}\right] = 0 \quad (8.19)$$

where Y is the mole fraction of component 1 in the fluid phase. For small differential changes the equilibrium relationship may be considered linear:

$$\frac{\partial \bar{q}_1}{\partial t} = C\frac{dq_1^*}{dc_1}\frac{\partial Y}{\partial t}, \qquad \frac{\partial \bar{q}_2}{\partial t} = -C\frac{dq_2^*}{dc_2}\frac{\partial Y}{\partial t} \quad (8.20)$$

Substitution in Eq. (8.19) yields

$$-D_L \frac{\partial^2 Y}{\partial z^2} + v\frac{\partial Y}{\partial z} + \frac{\partial Y}{\partial t}\left\{1 + \left(\frac{1-\epsilon}{\epsilon}\right)\left[(1-Y)\frac{dq_1^*}{dc_1} + Y\frac{dq_2^*}{dc_1}\right]\right\} = 0$$

$$(8.21)$$

which, if axial dispersion is neglected, is analogous to Eq. (8.10) with dq^*/dc replaced by the term in square brackets, a function of Y which may be considered as the effective equilibrium "constant." The propagation velocity of the mass transfer front, which is given by

$$w = \frac{v}{1 + \left(\frac{1-\epsilon}{\epsilon}\right)\left[(1-Y)\frac{dq_1^*}{dc_1} + Y\frac{dq_2^*}{dc_2}\right]} \quad (8.22)$$

may be seen to depend on the equilibria for both components. If $Y = 0$ we recover Eq. (8.11) for a trace component. However, if Y is finite, then even when the carrier is inert $(dq_2^*/dc_2 = 0)$, the propagation velocity will vary with composition according to

$$w = \frac{v}{\left[1 + \left(\frac{1-\epsilon}{\epsilon}\right)(1-Y)\frac{dq_1^*}{dc_1}\right]} \quad (8.23)$$

Measurement of the retention time for a system with a mixed carrier stream of known composition containing both an inert and adsorbable component yields immediately dq_1^*/dc_1 as a function of c_1. The equilibrium isotherm $q_1^*(c_1)$ may be found directly by integration.[4,5]

The variation of fluid velocity through the column is given by

$$\frac{\partial v}{\partial z} = -\frac{dq_1^*}{dc_1}\left(\frac{1-\epsilon}{\epsilon}\right)\frac{\partial Y}{\partial t} \quad (8.24)$$

For simplicity we consider a linear system and set $dq_1^*/dc = K$ (independent of Y). Combining Eqs. (8.24) and (8.16) gives for the variation in fluid velocity

through the column

$$\frac{dv}{dY} = \frac{K\left(\frac{1-\epsilon}{\epsilon}\right)v}{1 + K\left(\frac{1-\epsilon}{\epsilon}\right)(1 - Y)} \qquad (8.25)$$

which may be integrated between $Y = 0$, $v = v_0$, and Y, v:

$$\ln\left(\frac{v}{v_0}\right) = \int_0^Y \frac{K\left(\frac{1-\epsilon}{\epsilon}\right)dY'}{\left[1 + K\left(\frac{1-\epsilon}{\epsilon}\right)(1 - Y')\right]} = \ln\left[\frac{1 + K\left(\frac{1-\epsilon}{\epsilon}\right)}{1 + K\left(\frac{1-\epsilon}{\epsilon}\right)(1 - Y)}\right] \qquad (8.26)$$

whence

$$w = \frac{v_0\left[1 + K\left(\frac{1-\epsilon}{\epsilon}\right)\right]}{\left[1 + K\left(\frac{1-\epsilon}{\epsilon}\right)(1 - Y)\right]^2} \qquad (8.27)$$

This is clearly an increasing function of Y. Thus, for a nontrace system, the sorption effect (variation in fluid velocity due to sorption of the adsorbable species) leads to an increase in the propagation velocity with increasing concentration. The effect is thus qualitatively similar to the effect of curvature of the equilibrium isotherm and leads to the chromatographic response having a sharp front and a broadening tail as sketched in Figure 8.7.

Two Adsorbable Components

As a result of the continuity condition a binary isothermal system with two adsorbable components (no carrier) has a single mass transfer zone which propagates with velocity given by Eq. (8.22). This provides the basis of a simple chromatographic method for the experimental determination of binary equilibrium isotherms.[4,5] The propagation velocity for a small perturbation is measured over a range of compositions for the binary mixture. The variation with composition of the apparent equilibrium constant defined by

$$K = (1 - Y)\frac{dq_1^*}{dc_1} + Y\frac{dq_2^*}{dc_2}$$

is then fitted to a polynomial expression:

$$K = A_0 + A_1 Y + A_2 Y^2 + A_3 Y^3 \qquad (8.28)$$

The isotherms for the individual components are then expressed in polynomial form with unknown coefficients:

$$\frac{dq_1^*}{dc_1} = B_0 + B_1 Y + B_2 Y^2, \qquad \frac{dq_2^*}{dc_2} = C_0 + C_1 Y + C_2 Y^2 \qquad (8.29)$$
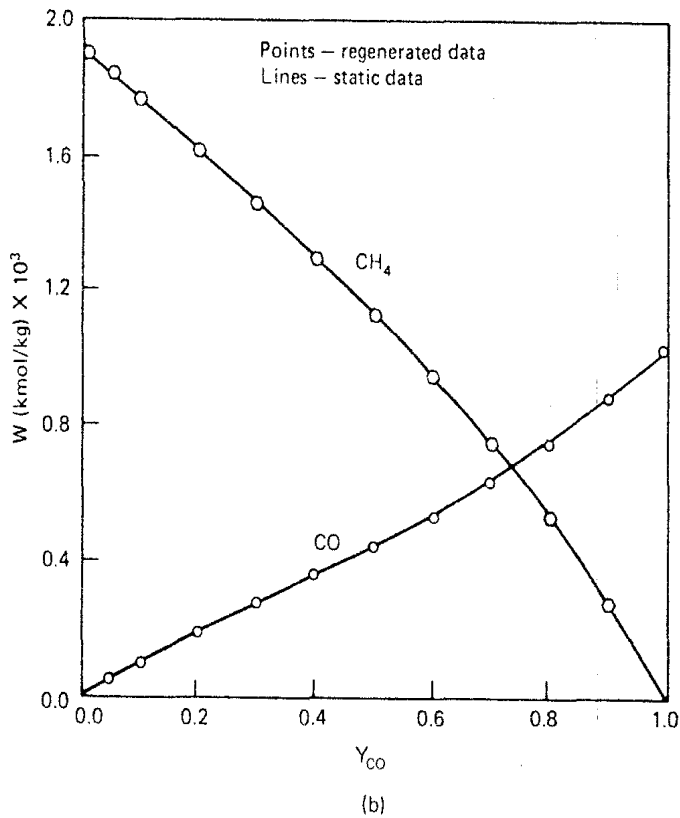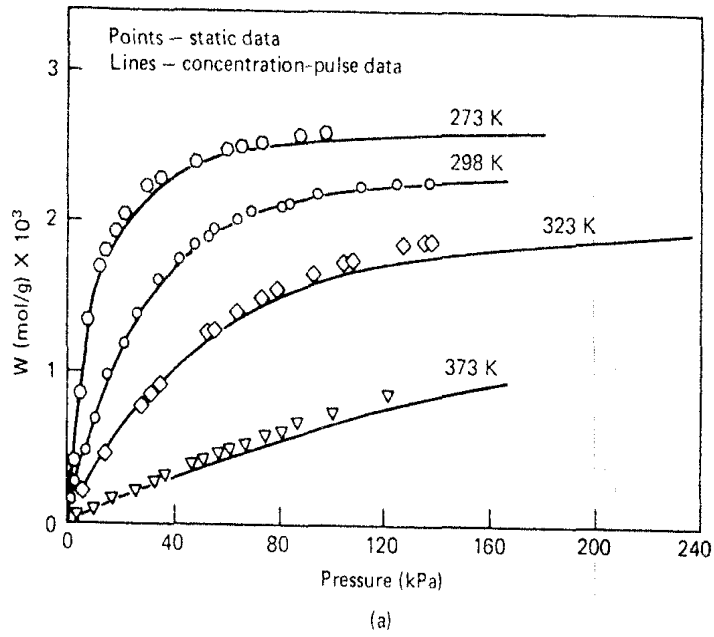
FIGURE 8.8. Comparison of (a) single-component equilibrium isotherms for C_2H_6 on 13X sieve and (b) binary isotherms for CO-CH$_4$ on activated carbon, as determined by static and chromatographic methods. (From ref. 6, reprinted with permission.)

Hence

$$K = (1 - Y)\frac{dq_1^*}{dc_1} + Y\frac{dq_2^*}{dc_2}$$

$$= B_0 + (B_1 + C_0 - B_0)Y + (B_2 + C_1 - B_1)Y^2 + (C_2 - B_2)Y^3 \quad (8.30)$$

The equilibrium adsorbed phase concentrations for the individual components are found by integration of Eq. (8.29) (from $Y = 0$ to Y for component 1 and from $Y = 1$ to Y for component 2):

$$q_1^* = C\left[B_0 Y + \frac{B_1 Y^2}{2} + \frac{B_2 Y^3}{3} \right]$$

$$q_2^* = C\left[C_0(1 - Y) + \frac{C_1}{2}(1 - Y^2) + \frac{C_2}{3}(1 - Y^3) \right]^\dagger$$

$$(8.31)$$

Comparing coefficients between Eqs. (8.28) and (8.30) provides four relations between the six unknown coefficients $B_0, B_1, B_2, C_0, C_1, C_2$. Two further equations are obtained from the single-component isotherms which fix the values of q_1^* at $Y = 1$ and q_2^* at $Y = 0$. Solution of these six simultaneous equations gives the coefficients in Eq. (8.31) and hence the individual isotherms for both components in the mixture.

Examples of single-component and binary isotherms showing good agreement between the experimental isotherms determined by chromatographic and static methods are shown in Figure 8.8.[6] It should be noted that this method is restricted to binary systems and cannot be easily extended to ternary or multicomponent mixtures.

8.5. ISOTHERMAL, SINGLE-TRANSITION SYSTEMS: FINITE MASS TRANSFER RESISTANCE (LINEAR EQUILIBRIUM)

Analytic Solutions

If the equilibrium isotherm is linear, analytic expressions for the concentration front and the breakthrough curve may, in principle, be derived, however complex the kinetic model, but except when the boundary conditions are simple, the solutions may not be obtainable in closed form. With the widespread availability of fast digital computers the advantages of an analytic solution are less marked than they once were. Nevertheless, analytic solutions generally provide greater insight into the behavior of the system and have played a key role in the development of our understanding of the dynamics of adsorption columns.

---

† This relation is printed incorrectly in ref. 5.

TABLE 8.1. Summary of Analytic Solutions for Breakthrough Curve for Linear, Isothermal Trace Component Systems

1. Linearized Rate Expression: $\dfrac{\partial \bar{q}}{\partial t} = k(q^* - q) = kK(c - c^*)$

Flow Model	Author	Solution for Breakthrough Curve
1a. Plug Flow [Eq. (8.7)]	Anzelius[7] Walter[2] Furnas[8] Nusselt[9], etc. Klinkenberg[10]	$\dfrac{c}{c_0} = e^{-\xi}\displaystyle\int_0^\tau e^{-u} I_0\left(2\sqrt{\xi u}\right) du + e^{-(\tau+\epsilon)} I_0\left(2\sqrt{\tau\xi}\right)$ $\tau = k(t - z/v)$, $\xi = \dfrac{kKz}{v}\left(\dfrac{1-\epsilon}{\epsilon}\right)$ $\dfrac{c}{c_0} = \dfrac{1}{2}\text{erfc}\left(\sqrt{\xi} - \sqrt{\tau} - \dfrac{1}{8}\sqrt{\xi} - \dfrac{1}{8}\sqrt{\tau}\right)$ (approx. solution; error $< 0.6\%$ for $\xi > 2.0$) $\dfrac{c}{c_0} = \dfrac{1}{2}\text{erfc}\left(\sqrt{\xi} - \sqrt{\tau}\right)$ (asymptotic form for large ξ)
1b. Dispersed Plug Flow [Eq. (8.32)]	Lapidus and Amundson[11]	$\dfrac{c}{c_0} = \exp\left(\dfrac{vz}{2D_L}\right)\left(F(t) + k\displaystyle\int_0^t F(t)\, dt\right)$ $F(t) = e^{-kt}\displaystyle\int_0^t I_0\left\{2k\left[K\left(\dfrac{1-\epsilon}{\epsilon}\right)u(t-u)\right]^{1/2}\right\} \dfrac{z}{2\sqrt{\pi D_L u^3}}\exp\left[\dfrac{-z^2}{4D_L u} - \dfrac{v^2 u}{4D_L} - kKu\left(\dfrac{1-\epsilon}{\epsilon}\right) - ku\right] du$
	Levenspiel and Bischoff[12]	$\dfrac{c}{c_0} = \dfrac{1}{2}\text{erfc}\left\{\dfrac{1 - t/\bar{t}}{2\left[\dfrac{D_L}{vz}\left(\dfrac{t}{\bar{t}}\right)\right]^{1/2}}\right\}$, $\quad \bar{t} = \dfrac{z}{v}\left\{1 + K\left(\dfrac{1-\epsilon}{\epsilon}\right)\right\}$ (asymptotic form for $k \to \infty$, long column)

2. Intraparticle Diffusion Control: (no external mass transfer resistance)

$$\frac{\partial q}{\partial t} = \frac{1}{R^2}\frac{\partial}{\partial R}\left(DR^2\frac{\partial q}{\partial R}\right), \qquad q(R_p, t - z/v) = q^* = Kc$$

$$\bar{q} = \frac{3}{R_p^3}\int_0^{R_p} qR^2\, dR, \qquad \frac{\partial q}{\partial R}(0, t - z/v) = 0$$

Flow Model	Author	Solution for Breakthrough Curve
2a. Plug Flow [Eq. (8.7)]	Rosen[13,14]	
2b. Dispersed Plug Flow [Eq. (8.32)]	Rasmuson and Neretnieks[15]	

Rosen[13,14]:

$$\frac{c}{c_0} = \frac{1}{2} + \frac{2}{\pi}\int_0^\infty \exp\left[-\xi H_1(\lambda)/5\right]\sin\left[2\lambda^2\tau/15 - \xi H_2(\lambda)/5\right]\frac{d\lambda}{\lambda}$$

$$H_1(\lambda) = \lambda[\sinh(2\lambda) + \sin(2\lambda)]/[\cosh(2\lambda) - \cos(2\lambda)] - 1$$
$$H_2(\lambda) = \lambda[\sinh(2\lambda) - \sin(2\lambda)]/[\cosh(2\lambda) - \cos(2\lambda)]$$

$$\xi = \frac{15D}{R^2}\frac{Kz}{v}\left(\frac{1-\epsilon}{\epsilon}\right), \qquad \tau = \left(\frac{15D}{R^2}\right)(t - z/v)$$

$$\frac{c}{c_0} = \frac{1}{2}\,\text{erfc}\left(\frac{\xi - \tau}{2\sqrt{\xi}}\right) \qquad \text{(asymptotic form for large } Z\text{)}$$

Rasmuson and Neretnieks[15]:

$$\frac{c}{c_0} = \frac{1}{2} + \frac{2}{\pi}\int_0^\infty \exp\left[\frac{vz}{2D_L} - z\left(\frac{\sqrt{x^2(\lambda) + y^2(\lambda)} + x(\lambda)}{2}\right)^{1/2}\right.$$

$$\left.\times \sin\left[\frac{2Dt\lambda^2}{R^2} - z\left(\frac{\sqrt{x^2(\lambda) + y^2(\lambda)} - x(\lambda)}{2}\right)^{1/2}\right]\right]\frac{d\lambda}{\lambda}$$

$$x(\lambda) = \frac{v^2}{4D_L} + \frac{3D(1-\epsilon)}{R^2 D_L \epsilon}H_1(\lambda)$$

$$y(\lambda) = \frac{2D}{R^2 D_L}\lambda^2 + \frac{3D(1-\epsilon)}{R^2 D_L \epsilon}H_2(\lambda)$$

237

TABLE 8.1. (*Continued*)

3. Intraparticle Diffusion with External Film Resistance

$$\frac{\partial q}{\partial t} = \frac{1}{R^2}\frac{\partial}{\partial R}\left(DR^2\frac{\partial q}{\partial R}\right), \qquad D\frac{\partial q}{\partial R}(R_p, t) = \frac{3k_f}{R_p}[c(z,t) - q(R_p,t)/K]$$

$$\bar{q} = \frac{3}{R_p^3}\int_0^{R_p} qR^2\,dR, \qquad \frac{\partial q}{\partial R}(0,t) = 0$$

Flow Model	Author	Solution for Breakthrough Curve
3a. Plug Flow [Eq. (8.7)]	Rosen[13,14]	As in 2a (above) with $H_1(\lambda)$ and $H_2(\lambda)$ replaced by $H_1(\lambda, \nu)$ and $H_2(\lambda, \nu)$ $H_1(\lambda, \nu) = [H_1 + \nu(H_1\lambda^2 + H_2^2)]/[(1 + \nu H_1)^2 + (\nu H_2)^2]$ $H_2(\lambda, \nu) = H_2/[(1 + \nu H_1)^2 + (\nu H_2)^2]$ $\nu = DK/R_p k_f$, [$H_1(\lambda)$ and $H_2(\lambda)$ defined above]
3b. Dispersed Plug Flow [Eq. (8.32)]	Rasmuson and Neretnieks[15]	As in 2b (above) with $H_1(\lambda)$ and $H_2(\lambda)$ replaced by $H_1(\lambda, \nu)$ and $H_2(\lambda, \nu)$

4. Macropore–Micropore Diffusion with External Film Resistance

$$\frac{\partial q}{\partial t} = \frac{1}{r^2}\frac{\partial}{\partial r}\left[r^2 D_c \frac{\partial q}{\partial r}\right], \quad \epsilon_p \frac{\partial c}{\partial t} + (1-\epsilon_p)\frac{\partial \bar{q}}{\partial t} = \frac{1}{R^2}\frac{\partial}{\partial R}\left[\epsilon_p D_p R^2 \frac{\partial c}{\partial R}\right]$$

$$q(r_c, t) = K_c(R, t), \qquad \frac{\partial Q}{\partial t} = \frac{3}{R_p}k_f[c(R_p, t) - C(z, t)], \qquad q(r, 0) = 0$$

$$\frac{\partial q}{\partial r}(0, t) = 0, \qquad \frac{\partial c}{\partial R}(0, t) = 0, \qquad c(R, 0) = 0, \qquad q(r, 0) = 0$$

$$\bar{q} = \frac{3}{r_c^3}\int_0^{r_c} r^2 q\, dr, \qquad Q = (1-\epsilon_p)\bar{q} + \epsilon_p^z$$

$$= (1-\epsilon_p)\frac{3}{R_p^3}\int_0^{R_p}\bar{q}R^2\, dR + \frac{3\epsilon_p}{R_p^2}\int_0^{R_p}cR^2\, dR$$

Flow Model	Author	Solution for Breakthrough Curve
4a. Plug Flow	Kawazoe and Takeuchi[16]	As in 3a with $H_1(\lambda)$ and $H_2(\lambda)$ replaced by $H_1(\phi_1)$ and $H_2(\phi_2)$ where $$\phi_1 = \frac{h}{\sqrt{2}}\left[\sqrt{H_1^2(\lambda) + H_2^2(\lambda)} - H_1(\lambda)\right]^{1/2}$$ $$\phi_2 = \frac{h}{\sqrt{2}}\left[\sqrt{H_1^2(\lambda) + H_2^2(\lambda)} + H_1(\lambda)\right]^{1/2}$$ $$h = \left[\frac{3(D_c/r_c^2)}{K(\epsilon_p D_p/R_p^2)}\right]^{1/2}$$
4b. Dispersed Plug Flow	Rasmuson[17]	As in 3b with $H_1(\lambda)$ and $H_2(\lambda)$ replaced by $H_1(\phi_1)$ and $H_2(\phi_2)$

239

For a system containing only a single adsorbable component at low concentration, the differential fluid phase mass balance [Eq. (8.1)] becomes

$$-D_L \frac{\partial^2 c}{\partial z^2} + v \frac{\partial c}{\partial z} + \frac{\partial c}{\partial t} + \left(\frac{1-\epsilon}{\epsilon} \right) \frac{\partial \bar{q}}{\partial t} = 0 \qquad (8.32)$$

where

$$\bar{q} = \left(\frac{3}{R_p^3} \right) \int_0^{R_p} R^2 q \, dR$$

This reduces to Eq. (8.7) if axial dispersion is neglected.

The initial and boundary conditions for an initially sorbate free column subjected to a step change in sorbate concentration at the inlet at time zero are

$$\begin{aligned} t < 0, \qquad & q(R,0,z) = c(0,z) = 0 \\ t \geqslant 0, \qquad & c(t,0) = c_0 \end{aligned} \qquad (8.33)$$

To obtain the solution for the breakthrough curve it is necessary to solve Eq. (8.32), subject to these boundary conditions, together with the appropriate adsorption rate equation, which must be consistent with the equilibrium isotherm. The various mathematical models differ only in the form of the rate expression and the choice between Eqs. (8.7) and (8.32) to represent the fluid phase mass balance. Some of the solutions which have been obtained are summarized in Table 8.1.

For the simplest model [the linear rate law with plug flow (model 1a)] the model equations, written in dimensionless variables, assume the form:

$$\text{Fluid mass balance} \qquad \frac{\partial \phi}{\partial \xi} + \frac{\partial \psi}{\partial \tau} = 0 \qquad (8.34a)$$

$$\text{Rate equation} \qquad \frac{\partial \psi}{\partial \tau} = \phi - \psi \qquad (8.34b)$$

where $\phi = c/c_0$, $\psi = \bar{q}/q_0$, and the dimensionless bed length and time parameters are defined by

$$\xi = \frac{kKz}{v} \left(\frac{1-\epsilon}{\epsilon} \right), \qquad \tau = k(t - z/v)$$

These equations are precisely analogous to those used to describe heat transfer in a packed bed or in a double crossflow heat exchanger, and many of the earliest solutions such as that of Anzelius[7] were derived for the analogous heat transfer problem.

The solutions for the breakthrough curve given in Table 8.1 for the more realistic models (2b; 3a,b; 4a,b) are too cumbersome to be of much practical value. For some ranges of parameters the convergence of the oscillating integrals to which these diffusion models all reduce is slow, making numerical evaluation time consuming. Indeed it has recently been shown that for model 2b, direct numerical solution of the model equations by orthogonal collocation

provides a faster computation of the response curve than numerical evaluation of the exact solution.[18]

To avoid the complexity of the diffusion solutions it is common practice to use the simple linear driving force model with the effective rate constant estimated from Eq. (8.41). Fortunately the error involved in this approach is smaller than might be expected.

Although the expressions for the breakthrough curve derived from the various models are algebraically different, the numerical difference is quite small when the comparison is made on an equivalent basis. A comparison between the breakthrough curves calculated from the linear rate model (1a) and the Rosen solution (model 2a) is shown in Figure 8.9. It is evident that with the equivalent rate constant defined as $15D/R_p^2$ the curves show good agreement. This was first pointed out by Glueckauf[19,20] who showed that, provided the system is linear, the equivalence between a linear rate model with $k = 15D/R_p^2$ and the diffusion model holds for a variety of different boundary conditions. The factor 15 has therefore been incorporated in the definitions of the dimensionless time and bed length parameters for the diffusion models, thus making these quantities numerically equivalent to the corresponding quantities for the linear rate model. Since, for any boundary conditions, the solution of the linear rate model is much easier and faster than the solution of a diffusion model this approximation has found widespread application. However, while this approximation works well for linear and nearly linear systems it breaks down when the isotherm is highly nonlinear (see Section 8.6).

The approximate additivity of the effects of axial dispersion and mass transfer resistance was first deduced by van Deemter et al.[21] by considering the asymptotic form of model 1b. The same conclusion may be reached in a simpler way from moments analysis and leads to Eq. (8.42) as the definition for an overall effective rate coefficient incorporating both the effects of axial dispersion and finite mass transfer resistance.
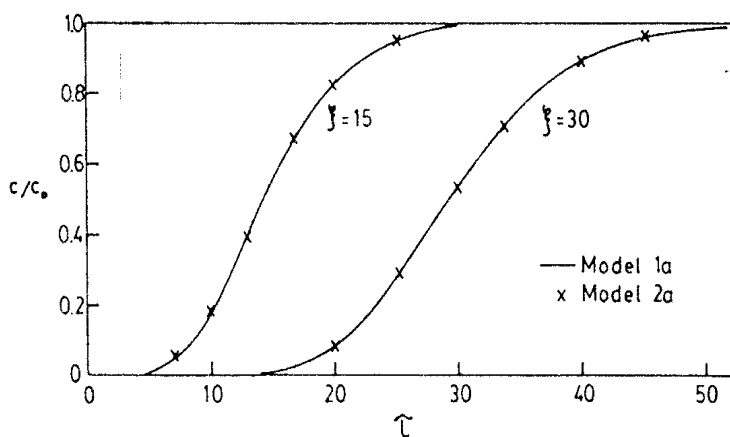
FIGURE 8.9. Comparison of theoretical breakthrough curves calculated from the Rosen solution [model 2a with $\tau = (15D/r^2)(t - z/v)$, $\xi = (15D/R^2)Kz(1 - \epsilon)/v\epsilon$] and linearized rate model [model 1a with $\tau = k(t - z/v)$, $\xi = kKz(1 - \epsilon)/v\epsilon$].

Moments Analysis

The solutions given in Table 8.1 were all obtained by Laplace transformation. To obtain the solution of the model equations in the Laplace domain is straightforward but inversion of the transform to obtain an analytic expression for the breakthrough curve or pulse response is difficult. Simple analytic expressions for the moments of the pulse response may, however, be derived rather easily directly from the solution in Laplace form by the application of van der Laan's theorem:[22]

First moment

$$\mu \equiv \bar{t} \equiv \frac{\int_0^\infty ct\, dt}{\int_0^\infty c\, dt} = -\lim_{s \to 0} \frac{\partial \tilde{c}}{\partial s} \frac{1}{c_0} \qquad (8.35a)$$

Second moment

$$\sigma^2 = \frac{\int_0^\infty c(t - \mu)^2 dt}{\int_0^\infty c\, dt} = \lim_{s \to 0} \frac{\partial^2 \tilde{c}}{\partial s^2}\left(\frac{1}{c_0}\right) - \mu^2 \qquad (8.35b)$$

By this procedure Haynes and Sarma[23] obtained the expressions for the first and second moments of the pulse response for model 4b, which is a sufficiently general model to provide a realistic representation of most chromatographic columns:

$$\mu = \frac{L}{v}\left[1 + \left(\frac{1-\epsilon}{\epsilon}\right)\epsilon_p + \left(\frac{1-\epsilon}{\epsilon}\right)(1 - \epsilon_p)K_c\right] = \frac{L}{v}\left[1 + \left(\frac{1-\epsilon}{\epsilon}\right)K\right] \qquad (8.36)$$

where $K = \epsilon_p + (1 - \epsilon_p)K_c$

$$\sigma^2 = \left(\frac{2L}{v}\right)\left(\frac{D_L}{v^2}\right)\left[1 + \left(\frac{1-\epsilon}{\epsilon}\right)\epsilon_p + \left(\frac{1-\epsilon}{\epsilon}\right)(1 - \epsilon_p)K_c\right]^2$$

$$+ \frac{2}{3}\left(\frac{L}{v}\right)\left(\frac{R_p}{k_f}\right)\left(\frac{1-\epsilon}{\epsilon}\right)[\epsilon_p + (1 - \epsilon_p)K_c]^2$$

$$+ \frac{2}{15}\left(\frac{L}{v}\right)\left(\frac{R_p^2}{\epsilon_p D_p}\right)\left(\frac{1-\epsilon}{\epsilon}\right)[\epsilon_p + (1 - \epsilon_p)K_c]^2$$

$$+ \frac{2}{15}\left(\frac{L}{v}\right)\left(\frac{r_c^2}{D_c}\right)\left(\frac{1-\epsilon}{\epsilon}\right)(1 - \epsilon_p)K_c \qquad (8.37)$$

Provided that $K \gg \epsilon_p$, which is usually true, this expression may be simplified

to

$$\frac{\sigma^2}{2\mu^2} = \frac{D_L}{vL} + \left(\frac{v}{L}\right)\left(\frac{\epsilon}{1-\epsilon}\right)\left(\frac{R_p}{3k_f} + \frac{R_p^2}{15\epsilon_p D_p} + \frac{r_c^2}{15KD_c}\right)\left(1 + \frac{\epsilon}{(1-\epsilon)K}\right)^{-2}$$

(8.38)

For a strongly adsorbed species $\epsilon/(1-\epsilon)K$ is small and Eq. (8.38) simplifies further to

$$\frac{\sigma^2}{2\mu^2} = \frac{D_L}{vL} + \left(\frac{v}{L}\right)\left(\frac{\epsilon}{1-\epsilon}\right)\left(\frac{R_p}{3k_f} + \frac{R_p^2}{15\epsilon_p D_p} + \frac{r_c^2}{15KD_c}\right)$$

(8.39)

It is evident that the contributions of axial dispersion and the various mass transfer resistances are linearly additive.

The corresponding expression for the second moment for the simple linear rate model (model 1b) is

$$\frac{\sigma^2}{2\mu^2} = \frac{D_L}{vL} + \frac{v}{L}\left(\frac{\epsilon}{1-\epsilon}\right)\frac{1}{kK}\left(1 + \frac{\epsilon}{(1-\epsilon)K}\right)^{-2}$$

(8.40)

In order to match the second moments we must set

$$\frac{1}{kK} = \frac{R_p}{3k_f} + \frac{R_p^2}{15\epsilon_p D_p} + \frac{r_c^2}{15KD_c}$$

(8.41)

This relationship provides an extension of the Glueckauf approximation for systems in which more than one mass transfer resistance is significant.

A further generalization of the Glueckauf approximation is suggested by comparison of the moments for the simple linear rate plug flow model (model 1a) and the general diffusion model with axial dispersion (model 4b). One may define an overall effective rate coefficient (k') which includes both the effects of axial dispersion and mass transfer resistance:

$$\frac{1}{Kk'} = \frac{D_L}{v^2}\left(\frac{1-\epsilon}{\epsilon}\right) + \frac{R_p}{3k_f} + \frac{R_p^2}{15\epsilon_p D_p} + \frac{r_c^2}{15KD_c}$$

(8.42)

Response curves and concentration profiles calculated according to the simple model with an overall effective rate coefficient defined by Eq. (8.42) provide a reasonably good approximation to the exact solutions, calculated from model 4b. This is illustrated in Figure 8.10. The dimensionless parameters are defined by

$$\tau' = k'(t - z/v), \qquad \xi' = \frac{k'Kz}{v}\left(\frac{1-\epsilon}{\epsilon}\right), \qquad \delta = \frac{kKD_L}{v^2}\left(\frac{1-\epsilon}{\epsilon}\right)$$

with k' related to the diffusion, dispersion, and mass transfer coefficients by Eq. (8.42). The relationship with the dimensionless parameters used by
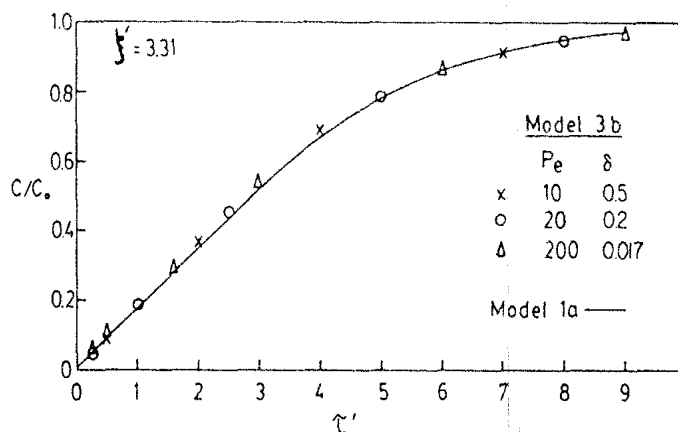
FIGURE 8.10. Comparison of linear driving force approximation (model 1a) with modified mass transfer coefficient defined by Eq. (8.42) and exact solution for breakthrough curve with axial dispersion, external mass transfer and diffusional resistances (model 3b). (Linear system)

Raghavan and Ruthven[18] is

$$\tau' = \frac{\theta\tau - 1/\psi}{1/Pe + (\theta/15)(1 + 5/\xi)}, \qquad \xi' = \frac{1}{1/Pe + (\theta/15)(1 + 5/\xi)}$$

The curves calculated in this way at constant ξ for different combinations of Pe and δ [i.e., for different combinations of axial dispersion and mass transfer resistance but the same linear combination $1/Pe + \theta(1 + 5/\xi)/15$] show close agreement with each other and with the curve calculated from the simple linearized rate model using an overall lumped coefficient to account for the combined effects of axial dispersion, diffusion, and external mass transfer resistance.

It is evident that for linear systems the precise nature of the dispersive forces, whether external film resistance, diffusional resistance, or axial dispersion, has only a very minor effect on the shape of the transient concentration response. This observation has two practically important consequences.

1. In the modeling of adsorption and chromatographic columns under linear equilibrium conditions it is seldom worth using a model more complex than model 1a.[†]

2. In the analysis of breakthrough curves or chromatographic response peaks, a single response curve can provide reliable information only on the combined effects of mass transfer resistance and axial dispersion.

[†]This conclusion is not necessarily valid for liquid systems. When the macropore hold-up is significant the form of the breakthrough curve derived from the dual-resistance diffusion model may differ significantly from the curves derived from single-resistance models (See W. J. Weber, Conference on Fundamentals of Adsorption, Schloss Elmau, Bavaria, May 1983, proceedings published by Engineering Foundation.)

Chromatographic Measurement of Diffusional Time Constants

In a chromatographic experiment a small packed adsorption column is subjected to a perturbation in the inlet concentration of an adsorbable species and the dynamic response at the column outlet is measured. Such measurements provide, in principle, a simple and rapid means of studying adsorption kinetics and equilibria. This method has been widely applied to gaseous sorbates but similar techniques are in principle applicable with liquids. In practice it is usual to employ either a pulse or a step input although other types of perturbation may also be used. The choice between step or pulse depends entirely on practical convenience since exactly the same information may be obtained from either experiment.

In the interpretation and analysis of chromatographic data it is assumed that the system is linear. Kinetic and equilibrium parameters are determined by matching the experimental response curve to the dimensionless theoretical curve calculated from a suitable dynamic model for the system. The assumption of linearity is a valid approximation provided that the concentration change over which the response is measured is sufficiently small. In the linear regime the normalized response is independent of the magnitude of the perturbation, and variation of the pulse (or step) size therefore provides a simple and direct test of system linearity.

For the measurement of intraparticle and intracrystalline diffusional time constants the chromatographic method offers the significant advantage over direct uptake rate measurements that, as a result of the improved heat transfer in a flow system and the presence of an excess of inert carrier, the intrusion of heat transfer is much less significant. This is an important consideration especially for systems in which diffusion is rapid. However, for the measurement of intracrystalline diffusivities, this advantage is offset to some extent by the intrusion of axial disperson and macropore diffusional resistance. In most molecular sieve zeolite adsorbents the microporous zeolite crystals are too small to use in a chromatographic column in unaggregated form without introducing inordinately high pressure drop. The use of a pelleted adsorbent introduces macropore diffusional resistance which must be allowed for in the analysis of the chromatograms. It is however possible to grow synthetic zeolite crystals of up to about 100 μm in diameter, and crystals of this size could be used directly in a chromatographic column without pelletization. The difficulty of synthesizing large crystals in sufficient quantity appears to have prevented any application of this potentially useful method.

Various methods of analyzing chromatographic data have been developed. The simplest approach depends on matching first and second moments. Expressions for the first and second moments for a general chromatographic system including axial dispersion, external film resistance, and macropore and micropore diffusion were given in Eqs. (8.36)–(8.40). The corresponding expressions for simpler models follow naturally by dropping the terms which

are considered negligible. Matching the experimental first moment to Eq. (8.36) yields directly the adsorption equilibrium constant, while matching the second moment yields one equation for the axial dispersion coefficient and overall mass transfer resistance. In order to determine the individual values of the axial dispersion coefficient and the various mass transfer parameters additional information is obviously required. It is in principle possible to obtain additional equations by matching higher order moments. However, as a result of the insensitivity of the response peaks to the individual dispersion and mass transfer resistances, the additional equations obtained in this way are almost degenerate. The accuracy with which the higher moments can be determined experimentally decreases rapidly with order so the method has little practical value.

The ease with which the individual mass transfer parameters and the axial dispersion coefficient can be determined depends on the relative magnitude of the various resistances. If mass transfer is rapid the dispersion of the chromatogram will be caused mainly by axial dispersion, and under these conditions it is not possible to derive any information concerning the diffusional time constants. In the low Reynolds number regime $Sh \equiv 2k_fR_p/D_m \approx 2.0$ so Eq. (8.39) may be written

$$\frac{\sigma^2}{2\mu^2}\frac{L}{v} \approx \frac{D_L}{v^2} + \left(\frac{\epsilon}{1-\epsilon}\right)\left(\frac{R_p^2}{3D_m} + \frac{R_p^2}{15\epsilon_pD_p} + \frac{r_c^2}{15KD_c}\right)\left(1 + \frac{\epsilon}{(1-\epsilon)K}\right)^{-2}$$

$$(8.43)$$

It is evident that in this regime both the external mass transfer and macropore resistances are directly proportional to the square of the particle radius. The contribution of these terms may therefore be reduced to an insignificant level by using sufficiently small particles. Furthermore, in the low Reynolds number regime, the axial dispersion coefficient becomes independent of particle size so variation of the particle size provides a convenient experimental test for the significance of external film and macropore diffusion resistances.

It follows from Eq. (8.43) that within the low Reynolds number regime a plot of $(\sigma^2/2\mu^2)(L/v)$ versus $1/v^2$ should be linear with slope D_L and intercept corresponding to the total mass transfer resistance:

$$\frac{\epsilon}{(1-\epsilon)}\left(\frac{R_p^2}{3D_m} + \frac{R_p^2}{15\epsilon_pD_p} + \frac{r_c^2}{15KD_c}\right)\left(1 + \frac{\epsilon}{(1-\epsilon)K}\right)^{-2}$$

Such a plot provides a convenient way of separating the mass transfer and axial dispersion terms. If the experiments are repeated with two or more different particle sizes the individual values of the intracrystalline and macropore plus film time constants may be found.

A representative plot for several sorbates in 4A zeolite is shown in Figure 8.11.[24] The molecules of CF_4 and isobutane are too large to penetrate the lattice of the 4A zeolite so for these sorbates the mass transfer resistance is small and insensitive to temperature, corresponding only to the external film
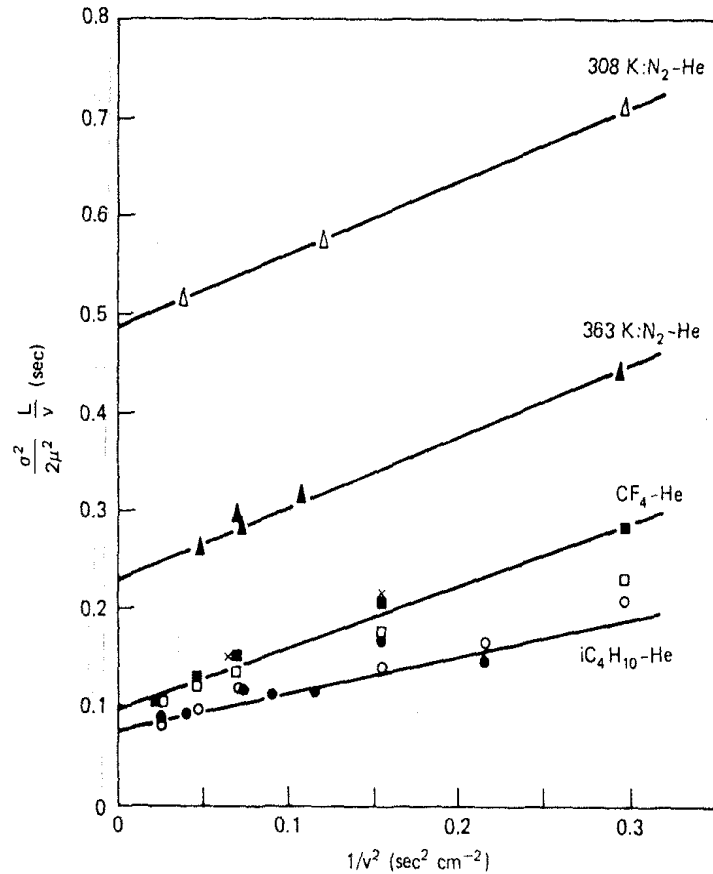
FIGURE 8.11. $\sigma^2/2\mu^2(L/v)$ plotted against $1/v^2$ for N_2, CF_4, and $i\text{-}C_4H_{10}$ in 4A molecular sieve. (From ref. 24; reprinted with permission from the *Canadian Journal of Chemical Engineering* **60**, 495, 1982.)

and macropore diffusion terms. The intercept for N_2 is very much higher and strongly temperature dependent, reflecting the dominance of the intracrystalline resistance. To determine the micropore time constant (D_c/r_c^2) the contribution from external film and macropore diffusion must be subtracted. This contribution may be estimated either from the data obtained with a nonpenetrating sorbate such as CF_4 or $i\text{-}C_4H_{10}$ or by repeating the experiments with particles of different size.

To avoid the errors associated with moments analysis various more sophisticated methods such as Fourier transformation and combinations of Fourier transform and moments methods have been developed.[25-28] The advantages of such methods have, however, been largely eliminated by the availability of a full analytic solution for the general model (model 4b) in the time domain[17] and by the development of improved numerical techniques which allow the time domain solutions to be calculated rapidly, directly from the model equations.[29-31] With these developments the best approach appears to be a combination of the moments method to determine initial estimates of the parameter values coupled with a final optimization by direct matching of the response curves in the time domain.

Plate Theory of Chromatography

In the preceding discussion the fundamental behavior of an adsorption column has been described in terms of the differential mass balances for the fluid and adsorbed phases in an element of the column. The mathematical description of the system dynamics is then obtained from the solution of these differential equations. An alternative approach, originally developed by Martin and Synge[32] has also been widely used. This approach, which is directly analogous to the "tanks in series" model for a nonideal flow reactor, depends on representing the column by a finite number of hypothetical well-mixed stages, the number of stages being a direct measure of axial dispersion and mass transfer resistance in the system. Although physically less realistic, this model gives results which are very similar to those obtained from the continuous theory and provides a direct link with the classical theory of countercurrent processes.

The discussion given below concerning the equivalence of the discrete and continuous representations of a chromatographic column is taken from Villermaux.[33] We consider an ideal mixing cell in which mass transfer occurs between fluid phase and adsorbed phase (Figure 8.12). Transient mass balances for the two phases yield

$$\epsilon v c_0 = \epsilon v c + V_f \frac{dc}{dt} + V_s \frac{d\bar{q}}{dt} \qquad (8.44)$$

$$(1 - \epsilon) l \frac{d\bar{q}}{dt} = k(q^* - \bar{q}) \qquad (8.45)$$

The expression for the transfer function is obtained directly from the Laplace transforms of these equations:

$$\frac{\tilde{c}}{\tilde{c}_0} = \left[1 + \frac{sl}{v} \left[1 + \frac{\left(\frac{1-\epsilon}{\epsilon} \right) K}{1 + (s/k)} \right] \right]^{-1} \qquad (8.46)$$

where $K = q^*/c$. For N identical stages in series

$$\frac{\tilde{c}}{\tilde{c}_0} = \left[1 + \frac{sl}{v} \left[1 + \frac{\left(\frac{1-\epsilon}{\epsilon} \right) K}{1 + (s/k)} \right] \right]^{-N} \qquad (8.47)$$
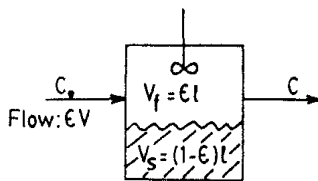
FIGURE 8.12. Hypothetical equilibrium stage as represented in the plate theory of chromatography.

The expression for the moments may be found from van der Laan's theorem[22] [Eq. (8.35)]:

$$\frac{\sigma^2}{2\mu^2} = \frac{1}{2N} + \frac{v}{Nl}\left(\frac{\epsilon}{1-\epsilon}\right)\frac{1}{kK}\left[1 + \frac{\epsilon}{(1-\epsilon)K}\right]^{-2} \qquad (8.48)$$

Comparison shows that Eqs. (8.40) and (8.48) are identical provided that $N = L/l = vl/2D_L$. N is then the number of theoretical plates (NTP) to which the column is equivalent. The definition of the height equivalent to a theoretical plate (HETP) follows naturally:

$$\text{HETP} = \frac{\sigma^2}{\mu^2}L = 2\frac{D_L}{v} + 2v\left(\frac{\epsilon}{1-\epsilon}\right)\frac{1}{kK}\left[1 + \frac{\epsilon}{(1-\epsilon)K}\right]^{-2} \qquad (8.49)$$

Combining this equation with Eq. (7.46) for D_L yields an expression of the same general form as the van Deemter equation:

$$\text{HETP} = \frac{A_1}{v} + A_2 + A_3 v \qquad (8.50)$$

where $A_1 = 2\gamma_2 R_p$, $A_2 = 2\gamma_1 D_m$, $A_3 \approx 2[\epsilon/(1-\epsilon)]/kK$, and we have assumed $K \gg 1.0$. The variation of HETP with fluid velcoity is shown in Figure 8.13.

Provided that N is sufficiently large ($> \sim 10$) the transfer function for the stage model [Eq. (8.47)] becomes numerically equivalent to the transfer function for the linear rate model (Table 8.1, model $1a$). Therefore, for a linear system the HETP–NTP representation is evidently equivalent to the representation in terms of an overall effective mass transfer coefficient defined according to Eq. (8.42). This model of an adsorption column as a number of equivalent theoretical stages is often extended to nonlinear systems. While this would appear to be generally acceptable as an engineering approximation it
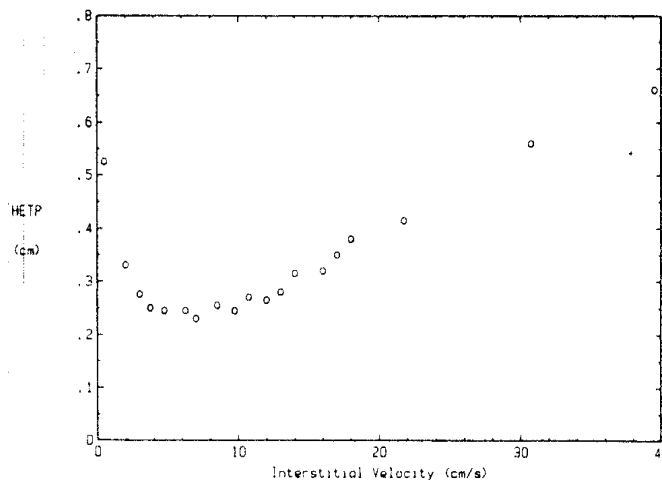
FIGURE 8.13. Van Deemter plot showing dependence of HETP on gas velocity for Ar-He-3A sieve ($R_p = 0.1$ cm) at 300 K. [Data of P. E. Eberly, *Ind. Eng. Chem. Fund.* **8**, 25 (1969). Copyright 1969 American Chemical Society.]

should be recognized that for a nonlinear system the equivalence between the discrete and continuous representation is no longer exact and if the isotherm is highly nonlinear such a representation may lead to serious error.

8.6. ISOTHERMAL, SINGLE-TRANSITION SYSTEMS: FINITE MASS TRANSFER RESISTANCE (NONLINEAR EQUILIBRIUM)

Analytic Solutions for Irreversible Equilibrium

When the equilibrium relationship is nonlinear it is generally not possible to determine a general analytic solution for the breakthrough curve. Such solutions have been obtained, however, for a number of special cases of which the irreversible or rectangular isotherm is the simplest. The irreversible isotherm, sketched in Figure 8.14, may be considered as the extreme limit of a favorable type I isotherm for which $\beta \to 0$ and, as such, it represents an important limiting case.

The earliest solution for the breakthrough curve for an irreversible system appears to be due to Bohart and Adams[34] who used a quasi-chemical kinetic rate expression.

The solutions for linear rate expressions with either solid or fluid driving force are readily obtained. In contrast to the situation with a linear isotherm, where the solution for a linear rate expression is the same with either fluid or solid phase driving force, in the case of an irreversible isotherm the response curves for these two models are quite different.

The rate expression for solid diffusion control is obtained directly by differentiation of the expression for the uptake curve for a spherical adsorbent particle subjected to a step change in sorbate concentration at the external surface [Eq. (6.4)]. Pore diffusion control with an irreversible isotherm leads to the shrinking core model and the uptake rate is therefore given by the differential of Eq. (6.27).

A summary of some of the available solutions for irreversible systems is given in Table 8.2. All solutions assume plug flow. The limiting cases of solid diffusion control and pore diffusion control were solved by Cooper[35] and by Cooper and Libermann[36] while the solution for the case of combined pore diffusion and external mass transfer resistance was obtained by Weber and Chakravorti[37] using the method of Cooper and Libermann. Weber and
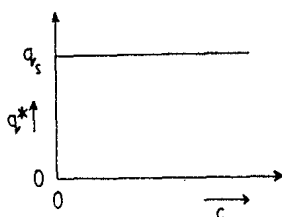
FIGURE 8.14. The irreversible or rectangular isotherm.

TABLE 8.2. Summary of Analytic Solutions for Breakthrough Curve for Systems with Irreversible Isotherm

Model	Rate Equation	Author	Solution for Breakthrough Curve
1	$\dfrac{\partial \bar{q}}{\partial t} = kc(q_s - \bar{q})$ (quasichemical)	Bohart and Adams[34]	$\dfrac{c}{c_0} = \dfrac{e^\tau}{e^\tau + e^\xi - 1}$, $\quad \xi = \dfrac{kq_0 z}{v}\left(\dfrac{1-\epsilon}{\epsilon}\right)$ $\tau = kc_0\left(t - \dfrac{z}{v}\right)$,
2	$\dfrac{\partial \bar{q}}{\partial t} = k(q_s - \bar{q})$ (linear rate— solid film)	Cooper[35]	$\dfrac{c}{c_0} = 1 - \xi e^{-\tau}$, $\qquad \xi \le 1.0$ $\dfrac{c}{c_0} = 1 - e^{\xi - \tau - 1}$, $\quad 1 \le \xi \le 1 + \tau$ $\dfrac{c}{c_0} = 0$, $\qquad\qquad \xi \ge 1 + \tau$ $\tau = k\left(t - \dfrac{z}{v}\right)$, $\quad \xi = \dfrac{kq_0 z}{c_0 v}\left(\dfrac{1-\epsilon}{\epsilon}\right)$
3	$\dfrac{\partial \bar{q}}{\partial t} = k'(c - c^*)$ (linear rate— fluid film)		$\dfrac{c}{c_0} = e^{-\xi}$, $\qquad\qquad 0 \le \tau \le 1$ $\dfrac{c}{c_0} = e^{\tau - \xi - 1}$, $\quad 1 \le \tau \le 1 + \xi$, $\quad \tau = \dfrac{k'c_0}{q_0}\left(t - \dfrac{z}{v}\right)$, $\quad \xi = \dfrac{k'z}{v}\left(\dfrac{1-\epsilon}{\epsilon}\right)$ $\dfrac{c}{c_0} = 1.0$, $\qquad\qquad \tau \ge 1 + \xi$

TABLE 8.2. (*Continued*)

Model	Rate Equation	Author
4	$$\frac{\partial \bar{q}}{\partial t} = q_s \frac{6D}{R^2} \sum_1^\infty \exp\left[\frac{-n^2\pi^2 D(t - t_f)}{R^2} \right]$$ (solid diffusion)	Cooper[35]
5	$$\frac{\partial \bar{q}}{\partial t} = \frac{3\epsilon_p D_p c(z,t)}{R_p^2 \left[(1 - \bar{q}/q_s)^2 - 1 \right]}$$ (pore diffusion)	Cooper and Liberman[36]
6	$$\frac{\partial \bar{q}}{\partial t} = \frac{3\epsilon_p D_p c_s}{R_p^2 \left[(1 - \bar{q}/q_s)^2 - 1 \right]}$$ $$= \frac{3k_f}{R_p}(c - c_s)$$ (film + pore diffusion)	Weber and Chakravorti[37]

$$\frac{c}{c_0} = S\left(t - \frac{z}{v}\right) - \frac{6}{\pi^2} \sum_{n=1}^{\infty} \frac{1}{n^2} \left[\exp\left(\frac{-n^2\pi^2}{15}\right)(\tau - \tau_f) - \exp\left(\frac{-n^2\pi^2\tau}{15}\right) \right]$$

$$\times \left(\frac{-4}{\pi^2}\right) \sum_{n=1}^{\infty} \exp\left(\frac{-n^2\pi^2\tau}{15}\right) \sum_{n=1}^{\infty} \frac{\exp\left[(n^2 - \sigma_i^2)(\pi^2/15)\tau_f - 1\right]}{n^2 - \sigma_i^2}$$

σ_i given by roots of: $\tan(\pi\sigma_i) = \pi\sigma_i$

$$\tau = \frac{15D}{R^2}\left(t - \frac{z}{v}\right), \qquad \xi = 1 + \tau_f - \frac{10}{\pi^2} \sum_{n=1}^{\infty} \frac{\exp(-\pi^2\sigma_i\tau_f/15)}{\sigma_i^2}$$

$$-\xi''(\tau, \psi) = \frac{15}{\sqrt{3}} \tan^{-1}\left[\frac{2(1 - \psi)^{1/3} + 1}{\sqrt{3}} \right] - \frac{15}{2} \ln[1 + (1 - \psi)^{1/3} + (1 - \psi)^{2/3}]$$

$$- \frac{15}{\sqrt{3}} \tan^{-1}\sqrt{3} + \frac{15}{2} \ln 3, \qquad \tau'' \leqslant \frac{5}{2}$$

$$\tau'' - \xi''(\tau, \psi) = \frac{15}{3} \tan^{-1}\left[\frac{2(1 - \psi)^{1/3} + 1}{\sqrt{3}} \right] - \frac{15}{2} \ln[1 + (1 - \psi)^{1/3} + (1 - \psi)^{2/3}]$$

$$+ \frac{5}{2} - \frac{5\pi}{2\sqrt{3}}, \qquad \tau'' \geqslant \frac{5}{2}$$

$$\frac{c}{c_0} = \frac{\phi(\tau'', \xi'')}{\phi(\tau'', 0)}$$

$$\tau'' = 5\left\{ \frac{3}{2} - \frac{3}{2}[1 - \psi(\tau'', 0)]^{2/3} - \psi(\tau'', 0) \right\}, \qquad 0 \leqslant \tau'' \leqslant \frac{5}{2}$$

$$\psi = 1.0, \qquad \tfrac{5}{2} \leqslant \tau''$$

$$\xi'' = \frac{15\epsilon_p D_p}{R_p^2}\left(\frac{z}{v}\right)\left(\frac{1 - \epsilon}{\epsilon}\right), \qquad \tau'' = \frac{15\epsilon_p D_p}{R_p^2}\left(\frac{c_0}{q_s}\right)\left(t - \frac{z}{v}\right), \qquad \psi = q/q_s$$

$$-\xi'' = \frac{15}{\sqrt{3}} \tan^{-1}\left[\frac{2(1 - \psi)^{1/3} + 1}{3} \right] - \frac{15}{2} \ln[1 + (1 - \psi)^{1/3} + (1 - \psi)^{2/3}]$$

$$- \frac{15}{\sqrt{3}} \tan^{-1}\sqrt{3} + \frac{15}{2} \ln 3 + \gamma \ln \psi, \qquad \tau'' \leqslant \frac{5}{2} + \gamma$$

$$\tau'' - \xi'' = \frac{15}{\sqrt{3}} \tan^{-1}\left[\frac{2(1 - \phi)^{1/3} + 1}{3} \right] - \frac{15}{2} \ln[1 + (1 - \psi)^{1/3} + (1 - \psi)^{2/3}]$$

$$+ \frac{5}{2} - \frac{5\pi}{2\sqrt{3}} + \gamma(\ln \psi + 1); \qquad \tau'' \geqslant \frac{5}{2} + \gamma$$

$$\frac{c}{c_0} = \frac{\psi(\tau'', \xi'')}{\psi(\tau'', 0)}, \qquad \tau'' = 5\left\{ \frac{3}{2} - \frac{3}{2}[1 - \psi(\tau'', 0)]^{2/3} - \psi(\tau'', 0) \right\}, \qquad 0 \leqslant \tau'' \leqslant \frac{5}{2} + \gamma$$

$$s\psi = 1.0, \qquad \frac{5}{2} + \gamma \leqslant \tau''$$

$$\gamma = \frac{15\epsilon_p D_p}{R_p^2} \frac{R_p}{3k_f}, \qquad \xi'' = \frac{15\epsilon_p D_p}{R_p^2}\left(\frac{z}{v}\right)\left(\frac{1 - \epsilon}{\epsilon}\right), \qquad \tau'' = \frac{15\epsilon_p D_p}{R_p^2}\left(\frac{c_0}{q_s}\right)\left(t - \frac{z}{v}\right)$$
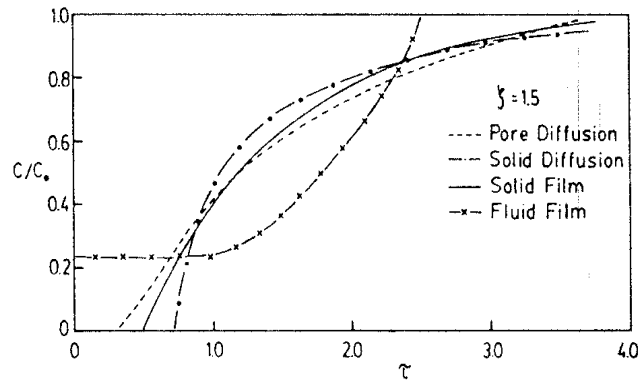
FIGURE 8.15. Comparison of theoretical breakthrough curves for a system with irreversible equilibrium, calculated according to linear rate models with solid and fluid resistances and the solid and pore diffusion models (models 2–5 of Table 8.2).

Chakravorti also pointed out that combined external film and solid diffusion is not physically possible with the irreversible model. However, it has recently been shown that this conclusion is not strictly correct and a useful analytic solution for this case has been derived.[58]

It may be seen that the expressions for the concentration profiles assume different forms in the different regions of the bed. The region $\xi < 1$ for the linear rate models or $\xi \leqslant 2.5$ for the pore diffusion model corresponds to the developing region in which the concentration profile is changing as it progresses. At $\xi = 1$ (or $\xi = 2.5$ for the pore diffusion model) the constant-pattern limit is reached and thereafter the front progresses with no further change in shape.

A comparison between theoretical breakthrough curves calculated from the pore diffusion, solid diffusion and linear rate models is shown in Figure 8.15. The curves for the four models show quite large differences. The linear rate
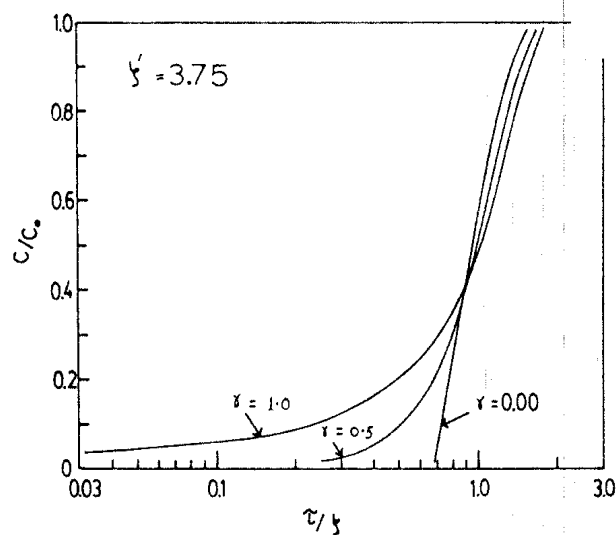
FIGURE 8.16. Theoretical breakthrough curves, calculated from the model of Weber and Chakravorti,[37] showing effect of external mass transfer resistance on breakthrough time (see Table 8.2).

model with solid phase driving force may be considered to provide a fair approximation to the diffusion models but, particularly in the initial region, the approximation is much poorer than for a linear equilibrium system. The deviation between fluid and solid phase driving force models is large and the fluid phase linear rate model leads to a somewhat unrealistic form for the response curve.

The effect of external mass transfer resistance on the breakthrough curve for a pore diffusion-controlled system, calculated from the model of Weber and Chakravorti,[37] is illustrated in Figure 8.16. It is clear that the breakthrough time is strongly affected by the intrusion of external mass transfer resistance even though the effect on the higher concentration region of the response curve is comparatively small. An accurate estimate of the external mass transfer resistance is therefore necessary in order to predict the dynamic capacity of an irreversible system with pore diffusion control. It should be noted that deviation of the equilibrium isotherm from the rectangular model leads to a qualitatively similar effect on the breakthrough curve. In the analysis of experimental data it is therefore not always easy to decide whether premature breakthrough is due to external mass transfer resistance or to deviation of the isotherm from rectangular form.

The Thomas Equation

A general analytical solution for a nonlinear (Langmuir) system with a pseudo second-order reaction kinetic rate law has been found by Thomas.[38] His model is summarized in Table 8.3. The numerical values of $\tau(\xi, \beta)$ have

TABLE 8.3. The Thomas Model[38]

Dimensional Equations	Dimensionless Equations
$v\dfrac{\partial c}{\partial z} + \dfrac{\partial c}{\partial t} + \left(\dfrac{1-\epsilon}{\epsilon}\right)\dfrac{\partial \bar{q}}{\partial t} = 0$	$\dfrac{\partial(c/c_0)}{\partial \xi} + \dfrac{\partial(\bar{q}/q_0)}{\partial T} = 0$
$\dfrac{\partial \bar{q}}{\partial t} = k[c(q_s - q) - \beta q(c_0 - c)]$	$\dfrac{\partial(\bar{q}/q_0)}{\partial T} = \left(\dfrac{c}{c_0}\right)\left(1 - \dfrac{\bar{q}}{q_s}\right) - \beta\left(\dfrac{\bar{q}}{q_0}\right)\left(1 - \dfrac{c}{c_0}\right)$
$\tau = (kc_0)(t - z/v);$	$\xi = \dfrac{kq_0 z}{v}\left(\dfrac{1-\epsilon}{\epsilon}\right)$

$$\text{Solution} \qquad \frac{c}{c_0} = \frac{J(\beta\xi, \tau)}{J(\beta\xi, \tau) + [1 - J(\xi, \beta\tau)]\exp[(\beta - 1)(\tau - \xi)]}$$

$$J(\alpha, \beta) = 1 - \int_0^\alpha \exp(-\beta - \alpha)I_0\left(2\sqrt{\beta\xi}\right)d\xi$$

Source: From ref. 38.

Note: With $\beta = 1$ this expression reduces to the solution for a linear system given in Table 8.1, model 1a, while for $\beta = 0$ it reduces to the form given by Bohart and Adams[32] for an irreversible system.

TABLE 8.4. Summary of Mathematical Models for Non-Linear Systems

Fluid mass balance:
$$v\frac{\partial c}{\partial z} + \frac{\partial c}{\partial t} + \left(\frac{1-\epsilon}{\epsilon}\right)\frac{\partial \bar{q}}{\partial t} = 0$$

Initial conditions:

Adsorption, $\bar{q}(z,0) = 0$, $\quad c(0,t) = 0$;

Desorption, $\bar{q}(z,0) = q_0$, $\quad c(0,t) = 0$

Equilibrium:

Freundlich, $\quad q^* = Kc^{1/n}$, $\quad$ Langmuir, $\quad \dfrac{q^*}{q_s} = \dfrac{bc}{1+bc}$

1. Linear Rate Models	2. Solid Diffusion	3. Pore Diffusion
(a) Fluid film resistance		
$\dfrac{\partial \bar{q}}{\partial t} = \dfrac{3k_f}{R_p}(c - c^*)$	$\dfrac{\partial q}{\partial t} = \dfrac{1}{r^2}\dfrac{\partial}{\partial r}\left(D_c r^2 \dfrac{\partial q}{\partial r}\right)$	$\epsilon_p \dfrac{\partial c}{\partial t} + (1 - \epsilon_p)\dfrac{\partial \bar{q}}{\partial t} = \dfrac{\epsilon_p D_p}{R^2}\dfrac{\partial}{\partial R}\left(R^2 \dfrac{\partial c}{\partial R}\right)$
	(i) $D_c = $ constant	D_p constant
	(ii) $D_c = D_0(1 - q/q_s)^{-1}$	
(b) Solid film resistance		
$\dfrac{\partial \bar{q}}{\partial t} = k(q^* - \bar{q})$	$q(r,0) = 0 \text{ or } q_0$	$\bar{q}(r,0) = 0 \text{ or } q_0$
	$q(r_c, t - z/v) = q^*(z,t)$	$\bar{q}(R_p, t - z/v) = q^*(z,t)$
	$\dfrac{\partial q}{\partial r}(0, t - z/v) = 0$	$\dfrac{\partial \bar{q}}{\partial R}(0,t) = 0$
	$\bar{q} = \bar{q} = \dfrac{3}{r_c^3}\displaystyle\int_0^{r_c} qr^2 dr$	$\bar{q} = \dfrac{3}{R_p^3}\displaystyle\int_0^{R_p}[\bar{q}(1 - \epsilon_p) + \epsilon_p c]R^2 dR$

Model No.	Author	Equilibrium	Rate Expression	Comments
1a	Zwiebel et al.[41]	Langmuir	Fluid film	Comparison with diffusion models
1b	Garg and Ruthven[40]	Langmuir	Solid film	
1c	Tien and Thodos[42]	Freundlich	External film + solid film	
2a	Antonson and Dranoff[43]	Langmuir	Solid diffusion (i)	$\xi = 15X(1-\lambda)$, $\tau = 15T$
2b	Kyte[44]	Freundlich	Solid diffusion (i)	
2c	Garg and Ruthven[40,46]	Langmuir	Solid diffusion (ii)	
3a	Carter and Husain[45]	Langmuir	Pore diffusion	
3b	Garg and Ruthven[47]	Langmuir	Pore diffusion	$\xi = 15X'$, $\tau = 15T'(1-\lambda)^{-1}$

Note: The definitions of the dimensionless column length and time parameters used in this book and their relationship to the parameters used by Garg and Ruthven (X, X', T, T', λ) are

$$\beta = (1 - \lambda)$$

Solid diffusion $\xi = \left(\dfrac{15D_0}{r_c^2}\right)\left(\dfrac{z}{v}\right)\left(\dfrac{q_0}{c_0}\right)\left(\dfrac{1-\epsilon}{\epsilon}\right) = 15X(1-\lambda)$ $\qquad \tau = \left(\dfrac{15D_0}{r_c^2}\right)\left(t - \dfrac{z}{v}\right) = 15T$

Pore diffusion $\xi = \left(\dfrac{15\epsilon_p D_p}{R_p^2}\right)\left(\dfrac{z}{v}\right)\left(\dfrac{1-\epsilon}{\epsilon}\right) = 15X'$ $\qquad \tau = \left(\dfrac{15\epsilon_p D_p}{R_p^2}\right)\left(\dfrac{c_0}{q_0}\right)\left(t - \dfrac{z}{v}\right) = \dfrac{15T'}{(1-\lambda)}$

been calculated from this model for a wide range of parameters and the results were presented in graphical form by Hiester and Vermeulen.[39] Such plots provide a simple means of assessing the importance of mass transfer resistance in any system for which the rate constant and equilibrium parameters are known.

Although based on a somewhat unrealistic form of rate expression this model provides a useful description of the behavior of nonlinear systems and shows clearly the effect of the isotherm shape on the breakthrough curve. The difference between breakthrough curves calculated from the Thomas model and from the more realistic diffusion equation model is small.

Numerical Results for Nonlinear Systems

Theoretical breakthrough curves for nonlinear systems may be calculated by numerical solution of the model equations using standard finite difference or collocation methods. Such solutions have been obtained by many authors and a brief summary is given in Table 8.4. In all cases plug flow was assumed and the equilibrium relationship was taken to be of either Langmuir or Freundlich form. As linearity is approached ($\beta \to 1.0$) the linearized rate models approach the Anzelius model (Table 8.1, model 1a) while the diffusion models approach the Rosen model (Table 8.1, model 2a). The conformity of the numerical solution to the exact analytic solution in the linear limit was confirmed by Garg and Ruthven.[40]

For many zeolitic systems the equilibrium isotherm can be represented in an approximate way by the Langmuir model while the intracrystalline diffusivity varies with concentration according to Eq. (6.12). Model 2c is intended to describe the dynamic behavior of such systems under conditions of intracrystalline diffusion control.

Representative adsorption and desorption curves are shown in Figure 8.17. The curves for the various models are qualitatively similar and show the same general trends. When the isotherm approaches linearity ($\beta \to 1.0$) the adsorption and desorption curves become mirror images and coincide with the theoretical curve calculated from Rosen's analysis. The adsorption curves for the nonlinear system show the expected approach to the constant-pattern form. As the isotherm becomes increasingly favorable ($\beta \to 0$) the distance required to approach the constant-pattern limit decreases and the form of the constant-pattern breakthrough curve approaches eventually the form calculated for an irreversible isotherm (Table 8.3). Meanwhile the desorption curves approach proportionate-pattern behavior so a pronounced asymmetry develops between adsorption and desorption curves.

Figure 8.17 also shows the comparison between pore diffusion and intracrystalline diffusion models. For moderately favorable isotherms ($1 > \beta > 0.5$) the differences between the theoretical curves are small, but as the isotherm becomes highly favorable ($\beta < 0.5$), approaching the irreversible
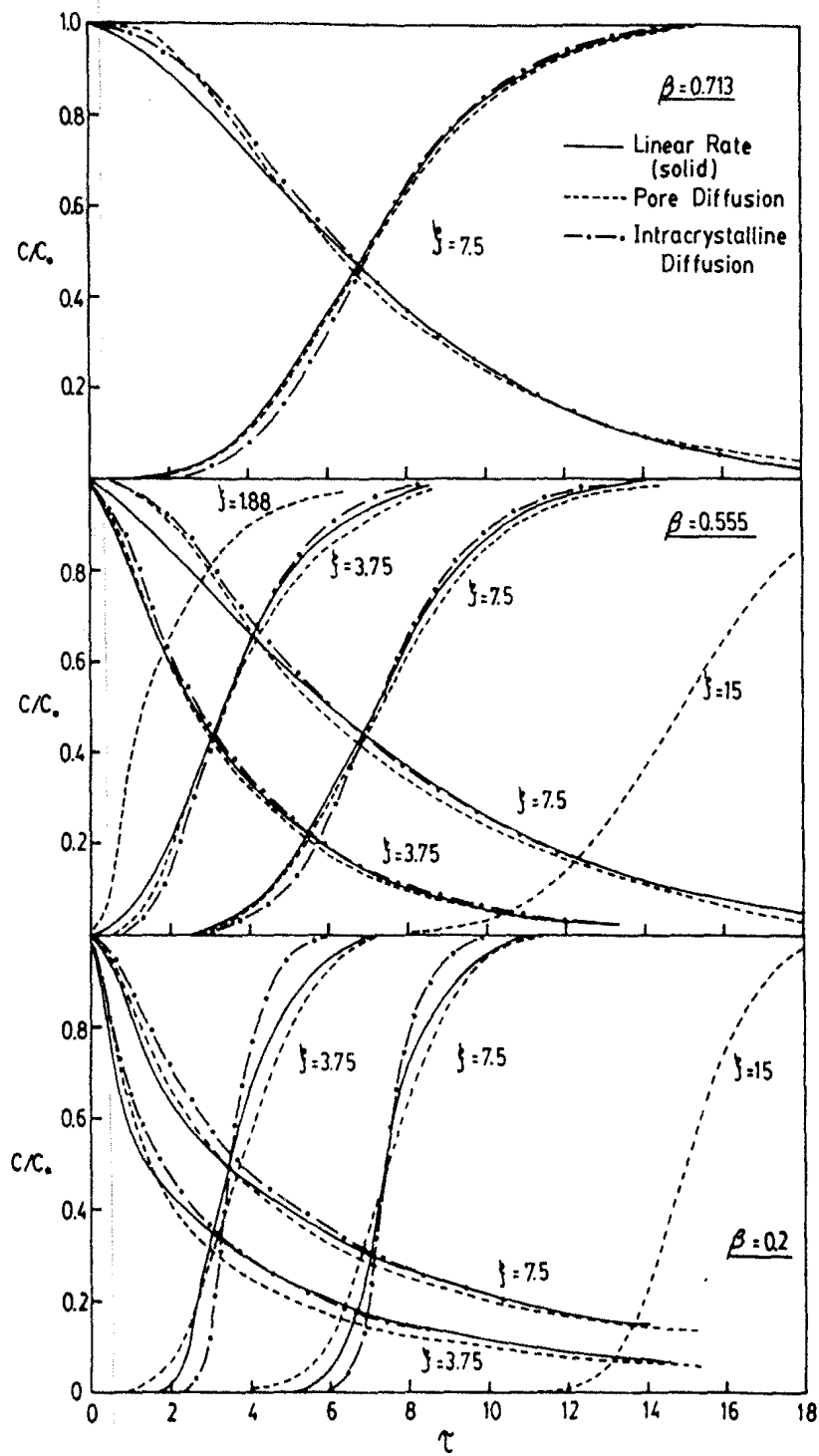
FIGURE 8.17. Theoretical breakthrough curves for nonlinear (Langmuir) systems showing comparison between linear rate, pore diffusion, and intracrystalline diffusion models. (See Table 8.4, models 1*b*, 2*c*, 3*b*.)

limit, the differences become large and are more pronounced for adsorption than for desorption.

An alternative perspective follows from the recognition that $\beta_{des} = 1/\beta_{ads}$. One may therefore regard the desorption curves as equivalent to adsorption curves for an unfavorable equilibrium. Figure 8.18b in which the adsorption curves are compared with the desorption curves plotted on an inverted concentration scale may therefore be thought of as illustrating the change in the shape of the breakthrough curve as the isotherm changes from highly favorable to highly unfavorable.

The adequacy of the Glueckauf linear rate approximation may be judged by comparing the curves calculated from the diffusion models with the curves calculated fom the linear rate expression, which are also shown in Figure 8.17. The linearized rate approximation provides a good representation of the desorption curves over the entire range of nonlinearity. The approximation is

(a)

(b)
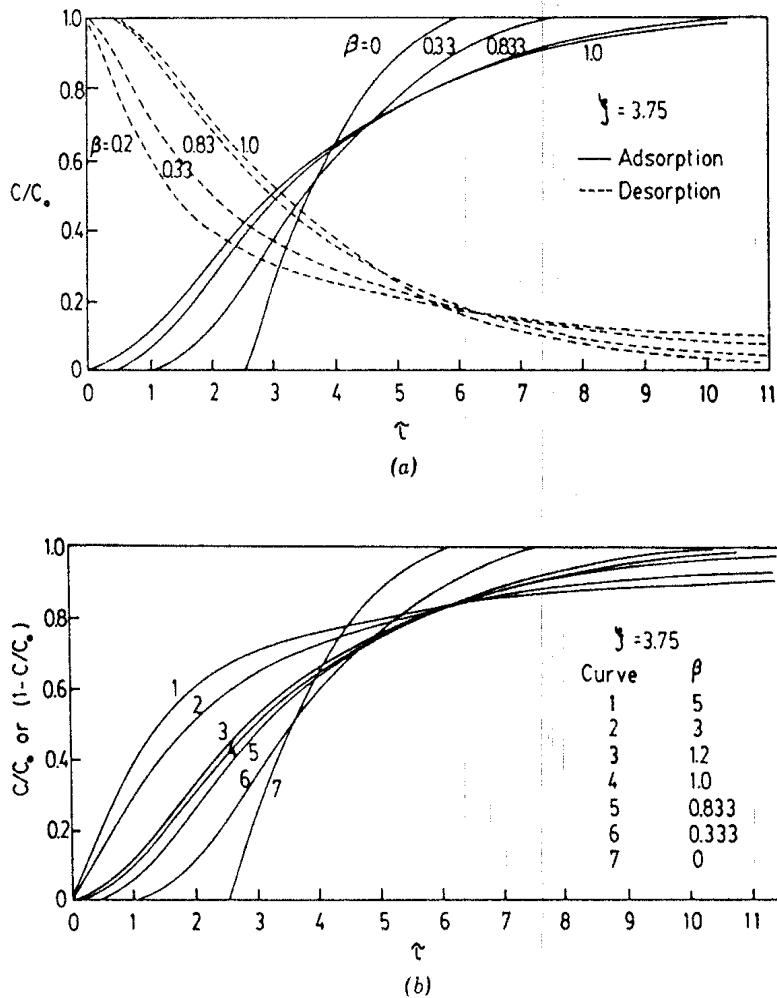
FIGURE 8.18. Theoretical breakthrough curves calculated for a nonlinear (Langmuir) system according to the pore diffusion model (model 3b, Table 8.4) showing effect of nonlinearity. In (b) the desorption curves of (a) are shown plotted on an inverted concentration scale with $\beta = 1/\beta_{des}$.

also adequate for the adsorption curves for moderately favorable isotherms $(1 > \beta > 0.5)$ but breaks down when the isotherm is highly favorable $(\beta < 0.5)$. One may thus conclude that the simple linearized model is a useful engineering approximation for unfavorable, linear, or moderately favorable isotherms $(1 > \beta > 0.5)$ but should be used only with caution when the equilibrium is highly favorable.

The breakdown of the linear rate approximation for nonlinear systems was noted by Vermuelen[48] who developed modified lumped parameter approximations which represent the diffusion models more accurately than the simple linear rate expression. For solid diffusion (model $2a$ or $2b$) a "quadratic driving force approximation" is recommended:

$$\frac{\partial \bar{q}}{\partial t} = k \frac{(q^{*2} - \bar{q}^2)}{\bar{q}} f(\beta)$$

$$f(\beta) = 0.59(1 - 0.41\beta)^{-1} \tag{8.51}$$

while as an approximation to the pore diffusion model (model 3) Vermeulen and Quilici[49] recommend

$$\frac{\partial \bar{q}}{\partial t} = \frac{15\epsilon_p D_p}{R_p^2} \left(\frac{c_0}{q_0}\right) \frac{(q^* - \bar{q})}{[1 + (\beta - 1)\bar{q}/q_0]^{1/2}} \tag{8.52}$$

Although these expressions provide a good representation of the breakthrough behavior for diffusion-controlled systems, a major advantage of the linear model, linear addition of mass transfer resistances, is lost by the introduction of a nonlinear driving force.

8.7. CONSTANT-PATTERN BEHAVIOR

When the equilibrium relationship is linear or unfavorable the mass transfer zone continues to expand as it progresses through the column. However, when the isotherm is favorable (type I) the pattern of behavior is quite different. In the initial region the mass transfer front spreads as it progresses, but some distance from the inlet it reaches an asymptotic form and thereafter it progresses as a stable mass transfer zone with no further change in shape. These trends are evident from the breakthrough curves plotted in Figure 8.17. The distance required to approach the constant-pattern limit depends on the degree of nonlinearity of the isotherm and on the kinetics of sorption. For many practical systems however this distance is very small. The constant-pattern approximation is therefore a very useful design tool since the calculation of the form of the mass transfer front under constant-pattern conditions is very simple.

A mathematical proof of the existence of a constant-pattern limit for any system with a favorable isotherm has been given by Cooney and Lightfoot.[50] Although not rigorous the following qualitative argument may be helpful in
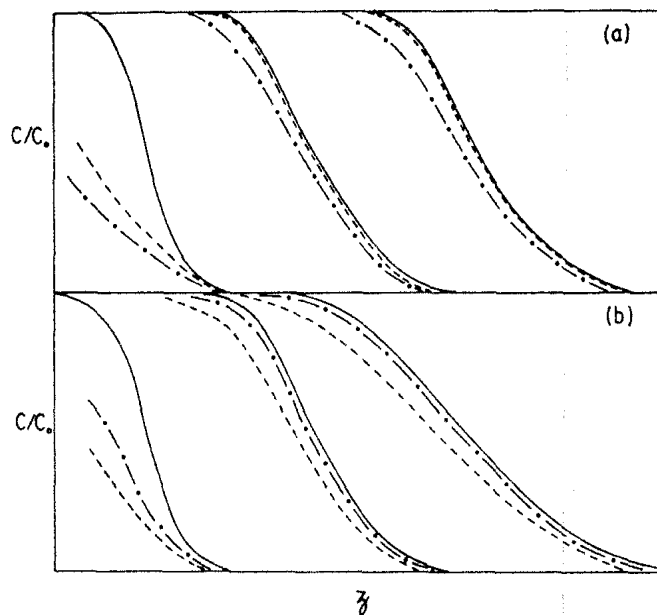
FIGURE 8.19. Schematic diagram showing (a) approach to constant-pattern behavior for a system with a favorable isotherm ($\beta < 1.0$) and (b) approach to proportionate-pattern (equilibrium) limit for a system with an unfavorable isotherm ($\beta > 1.0$) (c/c_0, ———; $\bar{q}/q_0$, ---; c^*/c_0, —·—).

understanding the physical reason for constant-pattern behavior. For a favorable isotherm ($q^*/q_0 > c/c_0$) the adsorbed phase concentration front must lie below the fluid phase concentration front (c/c_0) and above the equilibrium fluid phase concentration front (c^*/c_0) as sketched in Figure 8.19a. There is therefore a driving force, proportional to $c - c^*$, and mass transfer will occur from fluid to solid. As mass transfer proceeds the adsorbed phase concentration is built up while the fluid phase concentration is reduced so that the fluid

TABLE 8.5. Derivation of Constant-Pattern Breakthrough Curve for Linear Rate Model

Rate expression	$\dfrac{\partial \bar{q}}{\partial t} = k(q^* - q)$
Equilibrium	$\dfrac{q^*}{q_s} = \dfrac{bc}{1 + bc}$, $\quad \beta = 1 - \dfrac{q_0}{q_s}$
Constant-pattern condition	$\dfrac{c}{c_0} = \dfrac{\bar{q}}{q_0}$
	$\dfrac{\partial \bar{q}}{\partial t} = kq_s\left(\dfrac{bc_0(q/q_0)}{1 + bc_0(q/q_0)}\right) - \dfrac{q}{q_s}$
Integrated form	$k(t_2 - t_1) = \dfrac{1}{1 - \beta}\ln\left(\dfrac{\phi_2(1 - \phi_1)}{\phi_1(1 - \phi_2)}\right) + \ln\left(\dfrac{\phi_1}{\phi_2}\right)$
	$\left[\phi_1 = \dfrac{c_1}{c_0}, \phi_2 = \dfrac{c_2}{c_0}\right]$

TABLE 8.6. Summary of Asymptotic Constant-Pattern Solutions for Breakthrough Curve for Langmuir Equilibrium

	Model	Author	Rate Equation	Solution for Breakthrough Curve
1a.	Linear rate, fluid film	Michaels[51]	$\dfrac{\partial \bar{q}}{\partial t} = k'(c - c^*)$	$\dfrac{k'c_0}{q_0}(t_2 - t_1) = \dfrac{1}{\lambda}\ln\left(\dfrac{\phi_2(1 - \phi_1)}{\phi_1(1 - \phi_2)}\right) + \ln\left(\dfrac{1 - \phi_2}{1 - \phi_1}\right)$
1b.	Linear rate, solid film	Hall et al.[52]	$\dfrac{\partial \bar{q}}{\partial t} = k(q^* - q)$	$k(t_2 - t_1) = \dfrac{1}{\lambda}\ln\left(\dfrac{\phi_2(1 - \phi_1)}{\phi_1(1 - \phi_2)}\right) + \ln\left(\dfrac{\phi_1}{\phi_2}\right)$
2a.	Solid diffusion (constant D)	Hall et al.[52]	$\dfrac{\partial q}{\partial t} = D_c\left(\dfrac{2\partial q}{r\partial r} + \dfrac{\partial^2 q}{\partial r^2}\right)$	Numerical tabulation
2b.	Solid diffusion $[D = D_0(1 - q_0/q_s)^{-1}]$	Garg and Ruthven[40]	$\dfrac{\partial q}{\partial t} = \dfrac{1}{r^2}\dfrac{\partial}{\partial r}\left(r^2 D \dfrac{\partial^2 q}{\partial r^2}\right)$	Graphs of c/c_0 vs. τ
3a.	Pore diffusion	Hall et al.[52]	$\epsilon_p \dfrac{\partial c}{\partial t} + (1 - \epsilon_p)\dfrac{\partial \bar{q}}{\partial t} = \dfrac{\epsilon_p D_p}{R^2}\dfrac{\partial}{\partial R}\left(R^2 \dfrac{\partial c}{\partial R}\right)$	Numerical tabulation
3b.	Pore diffusion	Garg and Ruthven[40]	$\epsilon_p \dfrac{\partial c}{\partial t_t} + (1 - \epsilon_p)\dfrac{\partial \bar{q}}{\partial t} = \dfrac{\epsilon_p D_p}{R^2}\dfrac{\partial}{\partial R}\left(R^2 \dfrac{\partial c}{\partial R}\right)$	Graphs of c/c_0 vs. τ

Note: Plug flow with constant linear velocity is assumed in all cases. Constant-pattern conditions: $c/c_0 = \bar{q}/q_0$. Isotherm: $q^*/q_s = bc(1 + bc)^{-1}$ or $bc^* = (q/q_s)(1 - q/q_s)^{-1}$, $\lambda = 1 - \beta$.

phase and adsorbed phase fronts tend to approach one another. It is physically impossible for the adsorbed phase concentration front to overtake the fluid phase front so the asymptotic limit is reached when the two fronts coincide $(c/c_0 = \bar{q}/q_0)$. Thereafter the fronts remain coincident and propagate further without change in shape. For a system with axial dispersion the constant-pattern condition cannot be expressed quite so simply but the qualitative behavior is still similar.

To derive an expression for the asymptotic form of the breakthrough curve for a plug flow system under constant-pattern conditions it is only necessary to integrate the rate expression subject to the constant-pattern condition
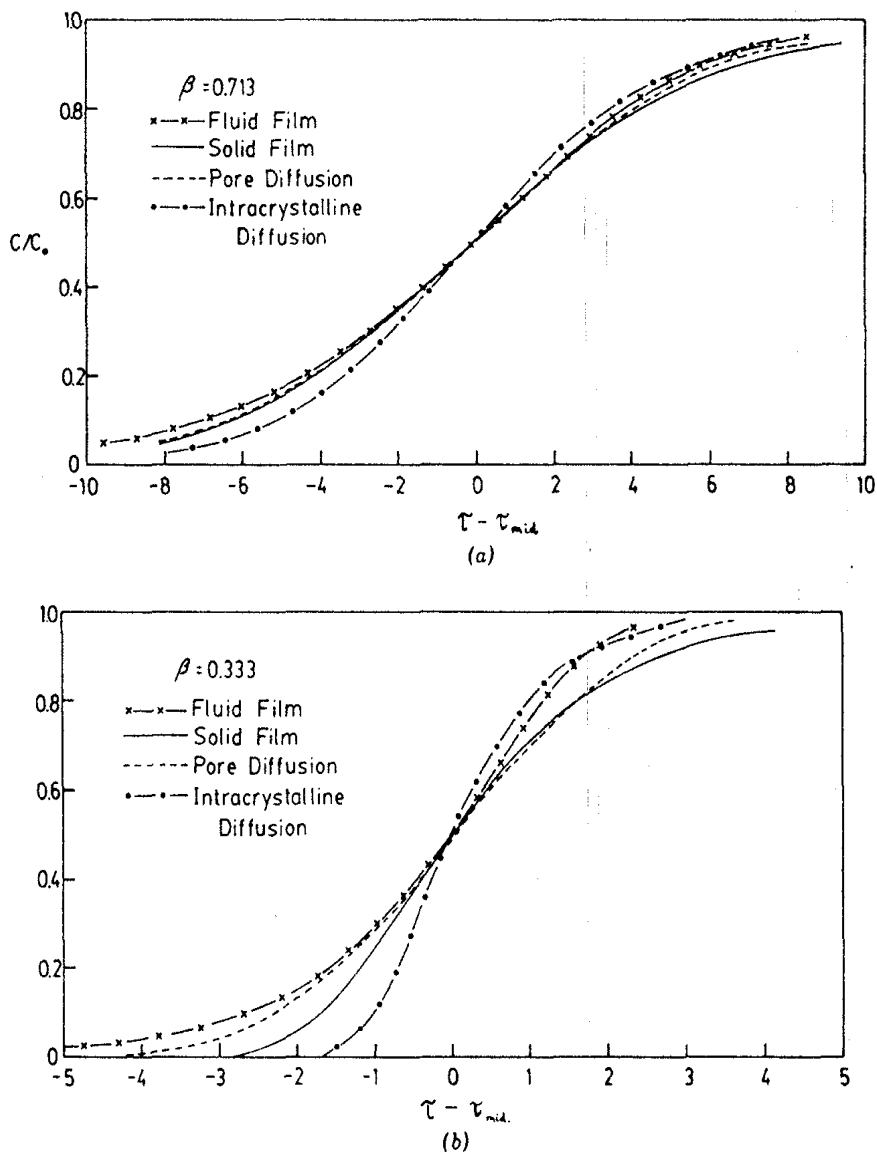
FIGURE 8.20. Theoretically calculated constant-pattern breakthrough curves for a favorable Langmuir system showing comparison between linear rate, intracrystalline, and pore diffusion models (Table 8.6, models 1a, 1b, 2b, 3b) for (a) $\beta = 0.713$ and (b) $\beta = 0.333$. [To illustrate the difference in shape the curves are matched at the midpoint (τ_{mid}) rather than at the stoichiometric time. For a symmetric curve $\tau_{mid} = \xi$.]

$c/c_0 = \bar{q}/q_0$. To illustrate the procedure we consider, in Table 8.5, a simple plug flow Langmuir system in which the adsorption rate is described by a linearized rate equation and in which the change in sorbate concentration across the mass transfer zone is small enough to allow the assumption of constant fluid velocity.

Some of the solutions which have been obtained in this way are summarized in Table 8.6. For a nonlinear system the linearized rate expression written in terms of a fluid phase concentration as the driving force is not exactly equivalent to the "solid film" driving force model and the expression obtained for the breakthrough curves for these two cases are therefore different.

The forms of the constant-pattern breakthrough curves for these models are compared in Figure 8.20. When the deviation from linearity is small $(1 > \beta > 0.7)$ the differences between the four models are quite minor, although it should be noted that such differences are at their greatest in the initial time region so that the error in predicting the breakthrough time may be significant if the wrong rate model is used. For highly nonlinear systems the differences between the predictions of the various models are much greater and it is evident that under these conditions the use of an incorrect kinetic model can lead to very large errors in the prediction of dynamic capacity.

By comparing the concentration profiles derived from the full solution to the differential model equations with the asymptotic profiles calculated from the constant-pattern condition it is possible to determine the dimensionless distance required to approach constant-pattern behavior. The results of such calculations are summarized in Figure 8.21.
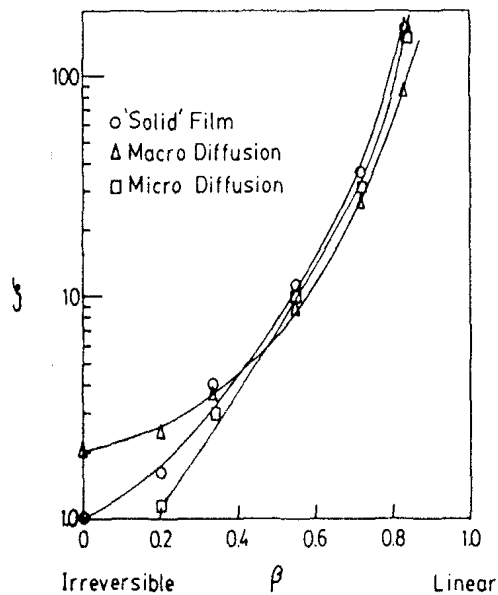
FIGURE 8.21. Comparison of dimensionless bed lengths required to approach within 5% of the constant-pattern solution, as measured by the 10–90% times, according to the linear rate (solid film), intracrystalline, and pore diffusion models (Table 8.6, models 1b, 2b, and 3b) showing effect of isotherm nonlinearity.

Effect of Axial Dispersion

The effect of axial dispersion on the form of the asymptotic constant-pattern breakthrough has been discussed by Acrivos[53] and by Garg and Ruthven.[54] A set of theoretical constant-pattern breakthrough curves calculated for $\beta = 0.33$ from the fluid film linear rate model, including axial dispersion, is shown in Figure 8.22. The curves are calculated for various values of the parameter

$$\delta = \left(\frac{1 - \epsilon}{\epsilon} \right) \left(\frac{3k'_f}{R_p} \right) \left(\frac{D_L}{v^2} \right)$$
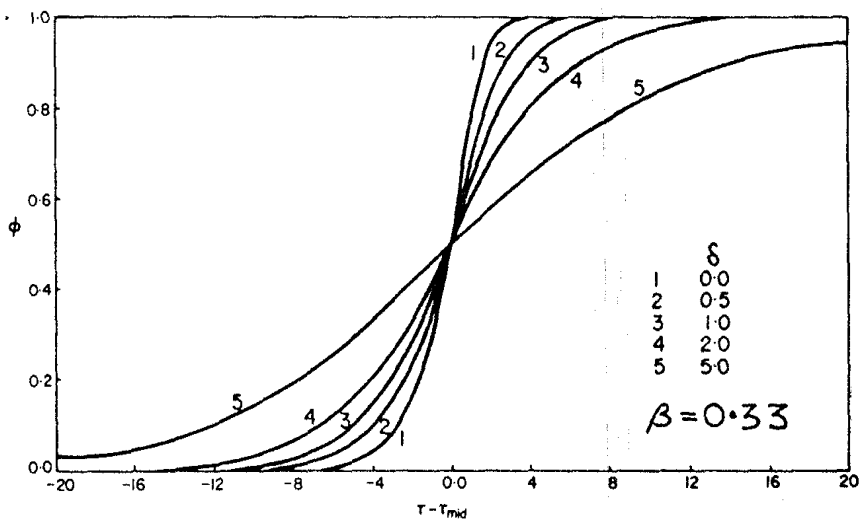
(a)
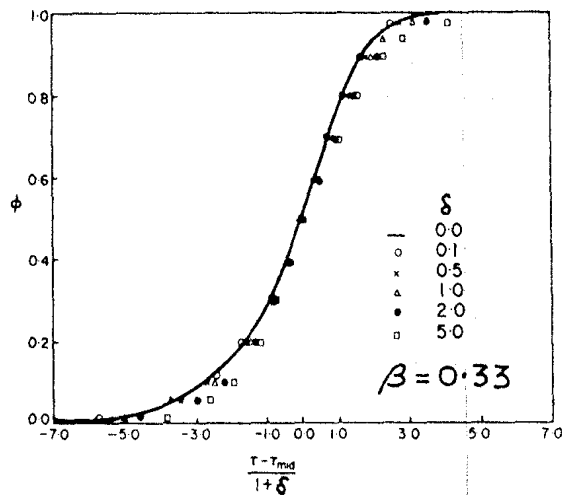
(b)

FIGURE 8.22. Combined effects of axial dispersion and mass transfer resistance for a favorable Langmuir equilibrium system ($\beta = 0.33$). (a) Constant pattern breakthrough curves for various values of δ (fluid film resistances + axial dispersion). (b) The same curves plotted on a modified time scale with $\tau' = \tau/(1 + \delta)$. [Reprinted with permission from *Chem. Eng. Sci.* **30**, Garg and Ruthven (ref. 54). Copyright 1975, Pergamon Press, Ltd.]
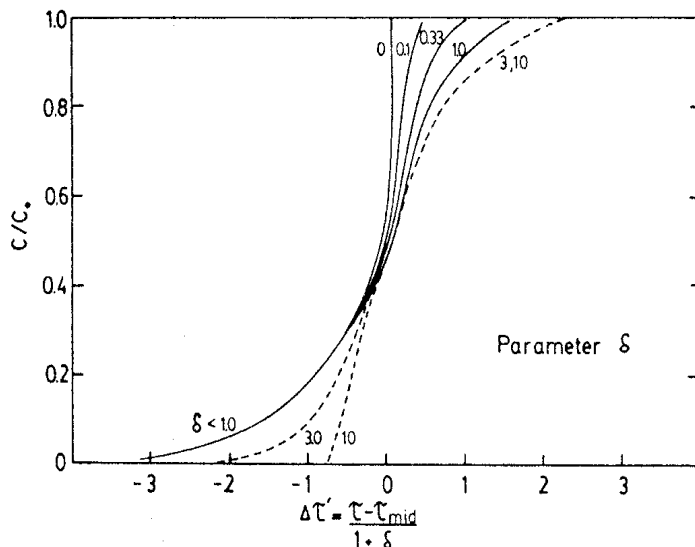
FIGURE 8.23. Theoretical constant-pattern breakthrough curves for irreversible adsorption showing combined effects of axial dispersion and (external) mass transfer resistance. $\delta < 1.0$ corresponds essentially to plug flow with external film resistance while $\delta \to \infty$ corresponds to axial dispersion with negligible mass transfer resistance. Curves are calculated from expression given by Acrivos.[53]

which measures the relative importance of axial dispersion and mass transfer resistance. These curves are replotted in Figure 8.23 on the modified time scale defined by

$$\frac{\Delta\tau}{1+\delta} = \frac{t - \bar{t}}{\left[\frac{R_p}{3k_f} + \left(\frac{1-\epsilon}{\epsilon}\right)\left(\frac{D_L}{v^2}\right)\right]\left(\frac{q_0}{c_0}\right)} = k'(t - \bar{t}) = \Delta\tau' \quad (8.53)$$

where k' is an effective rate coefficient defined according to Eq. (8.42) and τ' is the corresponding dimensionless time parameter.

If the effects of mass transfer resistance and axial dispersion were linearly additive, as they are for a linear system, then the breakthrough curve plotted in terms of the modified time parameter τ' would be independent of δ. That this is approximately, though not exactly, true may be seen from Figure 8.22b. However, the deviation from the linear addition rule becomes important only when δ is large and the isotherm is highly nonlinear ($\beta < 0.5$). Even for a highly nonlinear isotherm ($\beta = 0.33$) the linear addition principle evidently provides a useful approximation except in the extreme case of low mass transfer resistance and large axial dispersion ($\delta \geqslant 5$).

As the isotherm becomes progressively more rectangular the validity of the linear addition principle breaks down and in the irreversible limit the approximation is no longer valid. An analytic expression for the asymptotic constant-pattern breakthrough curve or concentration profile for a system with an irreversible isotherm was derived by Acrivos.[53] Theoretical breakthrough curves calculated from this expression and plotted against the modified dimensionless time variable τ' [$= \tau/(1 + \delta)$] are shown in Figure 8.23. It is

evident that the shape of the curves varies greatly with the value of δ indicating that in the irreversible limit the linear addition principle does not hold. It is of interest to note that the initial breakthrough time is more sensitive to mass transfer resistance than to axial dispersion whereas the situation is reversed in the saturation region. As a result, when plotted against the modified time variable, the curves for large values of δ show later breakthrough than the curves for small values of δ. However, for $\delta < 1.0$, in the initial region, a common curve is obtained showing that in this region the principle of linear addition is still applicable and may be used to estimate the breakthrough capacity even when the isotherm is rectangular.

An equivalent analysis of the combined effects of axial dispersion and mass transfer resistance has been presented by Rhee and Amundson,[55,56] based on shock layer theory. From the mass balance over the shock layer it may be shown that the propagation velocity [Eq. (8.13)] is not affected by mass transfer resistance or axial dispersion. For an equilibrium system with axial dispersion the differential mass balance [Eq. (8.1)] becomes, under constant-pattern conditions,

$$- \frac{1}{Pe} \frac{d^2c}{dz'^2} + (1 - w') \frac{dc}{dz'} - w' \left(\frac{1 - \epsilon}{\epsilon} \right) \frac{d\bar{q}}{dz'} = 0 \qquad (8.54)$$

where $z' = z - w't$. The corresponding expression for a system in which mass transfer resistance is finite it

$$- \frac{w'}{PeSt} \frac{d^2c}{dz'^2} \left(\frac{1}{Pe} + \frac{w'(1 - w')}{St} \right) \frac{dc}{dz'} - w' \left(\frac{1 - \epsilon}{\epsilon} \right) \frac{d\bar{q}}{dz'} = 0 \quad (8.55)$$

It is evident that the dispersion and mass transfer resistance play essentially equivalent roles in Eq. (8.55). Except when the isotherm approaches the irreversible limit the second-order term is much smaller than the first-order term and it shown that to a good approximation the profile depends only on the value of the combined parameter $1/Pe + w'(1 - w')/St$. Since $Pe/St = \delta$ this is equivalent to the previous result.

Nonisothermal Constant-Pattern Behavior

In an adiabatic adsorption column the temperature front generally travels at a velocity which is different from the velocity of the primary mass transfer front and, since adsorption equilibrium is temperature dependent, a secondary mass transfer zone is established coincident with the thermal front. In a system with finite heat loss from the column wall one may approach either the isothermal situation with a single mass transfer zone or the adiabatic situation with two mass transfer zones, depending on the relative rates of heat generation and dissipation from the column wall. In the former case the effect of finite heat transfer resistance is to widen the mass transfer zone relative to an isothermal system.

Provided that the deviation from isothermal behavior is not too large and the isothermal profile is of constant-pattern form, it is relatively simple to
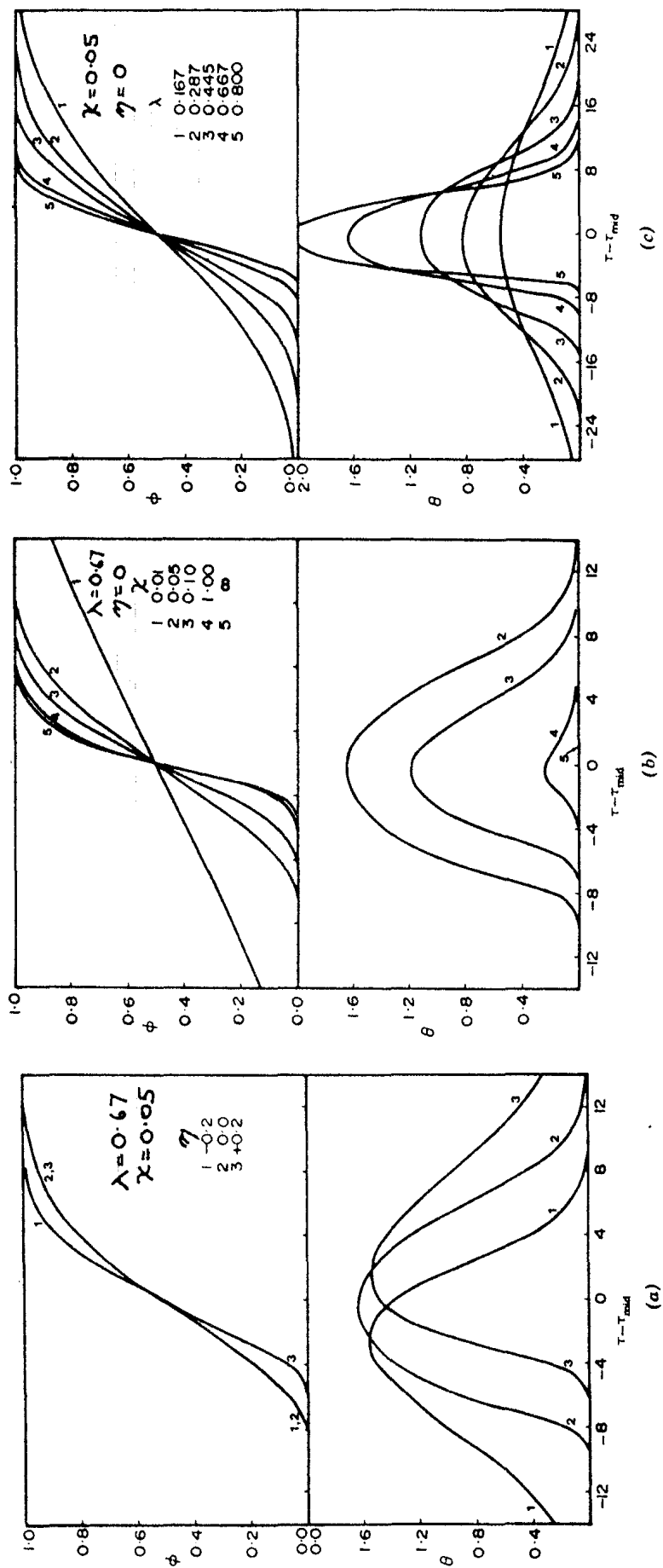
FIGURE 8.24. Theoretical curves showing effect of η and χ on constant-pattern breakthrough curves for a slightly nonisothermal Langmuir system. (a) Effect of η ($\chi = 0.05$, $\lambda = 0.67$); (b) Effect of χ ($\eta = 0$, $\lambda = 0.67$); (c) Effect of isotherm nonlinearity λ ($\chi = 0.05$, $\eta = 0$). [Reprinted with permission from *Chem. Eng. Sci.* 30, Ruthven, Garg, and Crawford (ref. 57). Copyright 1975, Pergamon Press, Ltd.]

269

calculate the profile under nonisothermal conditions since all that is required is a simultaneous integration of the heat and mass balance equations subject to the constant-pattern condition $c/c_0 = \bar{q}/q_0$. Such calculations have been carried out by Garg, Ruthven, and Crawford[57] for a Langmuir system using the "solid film" linear rate model. The solution for the breakthrough curve (c/c_0 vs. τ) is obtained as a function of two dimensionless parameters which characterize the heat transfer:

$$\eta = \frac{C_s/\Delta q - C_f/\Delta c}{R\left(\dfrac{-\Delta H}{RT_0}\right)^2}, \qquad \chi = \frac{4h_w}{k\Delta qd(1-\epsilon)R\left(\dfrac{-\Delta H}{RT_0}\right)^2}$$

·A representative set of breakthrough curves and corresponding temperature profiles is shown in Figure 8.24. The temperature profile consists of a peak which either precedes, coincides with, or lags behind the concentration profile, depending on the value of η, which measures the thermal capacity of the system relative to the rate of heat generation. As the parameter χ, which measures the relative rates of heat generation and heat loss from the wall increases, the magnitude of the temperature rise decreases, eventually to an insignificant level, and the breakthrough curve approaches the asymptotic form given in Table 8.5. However, when χ is small there is considerable broadening of the mass transfer zone. Interpretation of breakthrough curves obtained under these conditions according to the isothermal model will therefore lead to erroneously low values for the apparent mass transfer coefficient.

The effect on the breakthrough capacity of the column is greatest when η is negative ($C_f\Delta q/C_s\Delta c > 1.0$). Under these conditions the natural velocity of the thermal front is higher than the natural velocity of the concentration front so that the temperature profile leads the concentration profile, thus affecting the initial break point. This is by far the commonest situation in adsorption from the vapor phase and it may be seen that a significant loss of dynamic capacity can result from small departures from isothermal behavior.

Dynamic Capacity and Length of Unused Bed (LUB)

In the simplest type of adsorption processes in which an adsorption column is used to remove a trace impurity from a process stream, the main requirement for rational design is an estimate of the dynamic or breakthrough capacity of the bed. In such systems the adsorbable impurity is invariably strongly adsorbed with a favorable isotherm and the concentration profile therefore rapidly approaches constant-pattern form. The constant-pattern assumption provides the basis of a very simple design method which permits reliable scale-up from small-scale laboratory experiments.

The length of unused bed (LUB) is defined by

$$\text{LUB} = \left(1 - \frac{\bar{q}'}{q_0}\right)L = \left(1 - \frac{t'}{t}\right)L \tag{8.56}$$
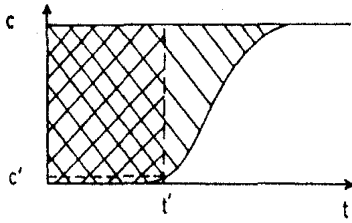
FIGURE 8.25. Sketch of breakthrough curve showing break time t' and method of calculation of stoichiometric time and LUB.

where $\bar{q}'$ is the capacity at the break time t'. The break time (t') and stoichiometric time $(\bar{t})$ may be determined from a single experimental breakthrough curve since

$$\bar{t} = \frac{L}{v}\left[1 + \left(\frac{1-\epsilon}{\epsilon}\right)\left(\frac{q_0}{c_0}\right)\right] = \int_0^\infty\left(1 - \frac{c}{c_0}\right)dt = \text{shaded area in Figure 8.25}$$

$$t' = \frac{L}{v}\left[1 + \left(\frac{1-\epsilon}{\epsilon}\right)\left(\frac{q^1}{c_0}\right)\right] = \int_0^{t'}\left(1 - \frac{c}{c_0}\right)dt = \text{hatched area in Figure 8.25}$$

t' is the breakthrough time at which the effluent concentration reaches its maximum permissible level. The LUB may thus be found from Eq. (8.56). Defined in this way the LUB depends on the sorbate and fluid velocity but is independent of the column length. The LUB may therefore be measured at the design velocity in a small laboratory column packed with the desired adsorbent. The full-scale adsorber bed may then be sized simply by adding the LUB to the length of bed needed to achieve the required stoichiometric capacity.

Since the method depends on constant-pattern behavior it should never be applied to a system in which equilibrium isotherm is unfavorable and it clearly does not provide any information concerning the required regeneration conditions.

The validity of this widely used procedure depends on the conditions in the laboratory column being similar to those in the full-scale unit. In particular, since large-diameter columns commonly operate adiabatically it is very important that the small-scale column should be very well insulated. If heat loss from the laboratory column is significant, the apparent LUB will be erroneously low leading to underdesign of the full-scale unit. Other factors such as axial dispersion, which may not be the same in the large and small column can also lead to discrepancies, but if caution is exercised the LUB concept provides a simple and practically useful design method.

Unfavorable Isotherm

If the isotherm is unfavorable $q/q_0 < c/c_0$ and the adsorbed phase concentration front lies below the fluid concentration front, as shown in Figure 8.19b. Under these conditions constant-pattern behavior can never be achieved since equilibrium would be reached first $(c/c_0 \rightarrow c^*/c_0)$. For a system with an unfavorable isotherm the asymptotic behavior in a long

column is simply represented by the equilibrium condition which leads to proportionate-pattern behavior, as discussed in Section 8.4.

REFERENCES

1. D. DeVault, *J. Am. Chem. Soc.* **65**, 532 (1943).

2. J. E. Walter, *J. Chem. Phys.* **13**, 229 and 332 (1945).

3. A. E. Rodrigues, in *Percolation Processes*, A. E. Rodrigues and D. Tondeur (eds.). Sijthoff and Noordhoff, Rockville, Md., 1981, p. 31.

4. E. van der Vlist and J. van der Meijden, *J. Chromatography* **79**, 1 (1973).

5. D. M. Ruthven and R. Kumar, *Ind. Eng. Chem. Fund.* **19**, 27 (1980).

6. S. H. Hyun and R. P. Danner, *AIChE Symp. Ser.* **78**(219), 19 (1982).

7. A. Anzelius, Z. *Angew. Math. Mech.* **6**, 291 (1926).

8. C. C. Furnas, *Trans. Am. Inst. Chem. Eng.* **24**, 142 (1930).

9. W. Nusselt, *Tech. Mech. Thermodynam.* **1**, 417 (1930).

10. A. Klinkenberg, *Ind. Eng. Chem.* **46**, 2285 (1954).

11. L. Lapidus and N. R. Amundson, *J. Phys. Chem.* **56**, 984 (1952).

12. O. Levenspiel and K. B. Bischoff, *Advances in Chemical Engineering*, Vol. 4, 95, Academic Press, New York, 1963.

13. J. B. Rosen, *J. Chem. Phys.* **20**, 387 (1952).

14. J. B. Rosen, *Ind. Eng. Chem.* **46**, 1590 (1954).

15. A. Rasmuson and I. Neretnieks, *AIChE J.* **26**, 686 (1980).

16. K. Kawazoe and Y. Takeuchi, *J. Chem. Eng. Japan* **7**, 431 (1974).

17. A. Rasmuson, *Chem. Eng. Sci.* **37**, 787 (1982).

18. N. S. Raghavan and D. M. Ruthven, *AIChE J.* **29**, 922 (1983).

19. E. Glueckauf, *Trans. Faraday Soc.* **51**, 1540 (1955).

20. E. Glueckauf and J. E. Coates, *J. Chem. Soc.* 1315 (1947).

21. J. J. van Deemter, F. J. Zuiderweg, and A. Klinberg, *Chem. Eng. Sci.* **5**, 271 (1956).

22. E. Th. van der Laan, *Chem. Eng. Sci.* **7**, 187 (1958).

23. H. W. Haynes and P. N. Sarma, *AIChE J.* **19**, 1043 (1973).

24. R. Kumar, R. C. Duncan, and D. M. Ruthven, *Can. J. Chem. Eng.* **60**, 493 (1982).

25. W. Boersma-Klein and J. A. Moulijn, *Chem. Eng. Sci.*, **34**, 959 (1979).

26. S. K. Gangwal, R. R. Hudgins, A. W. Bryson, and P. L. Silveston, *Can. J. Chem. Eng.* **49**, 113 (1971).

27. D. S. Scott, W. Lee, and J. Papa, *Chem. Eng. Sci.* **29**, 2155 (1974).

28. T. S. Chou and L. L. Hedgedus, *AIChE J.* **24**, 255 (1978).

29. H. W. Haynes, *Chem. Eng. Sci.* **30**, 955 (1975).

30. L-K. P. Hsu and H. W. Haynes, *AIChE J.* **27**, 81 (1981).

31. N. S. Raghavan and D. M. Ruthven, *Chem. Eng. Sci.* (to be published).

32. M. J. P. Martin and R. L. M. Synge, *Biochem. J.* **35**, 1359 (1941).

33. J. Villermaux, in *Percolation Processes*, A. E. Rodrigues and D. Tondeur (eds.). Sijthoff and Noordhoff, Rockville, Md., 1981, p. 83.

34. G. Bohart and E. Adams, *J. Am. Chem. Soc.* **42**, 523 (1920).

35. R. S. Cooper, *Ind. Eng. Chem. Fund.* **4**, 308 (1965).

36. R. S. Cooper and D. A. Liberman, *Ind. Eng. Chem. Fund.* **9**, 620 (1970).

37. T. W. Weber and R. K. Chakravorti, *AIChE J.* **20**, 228 (1974).

38. H. C. Thomas, *J. Am. Chem. Soc.* **66**, 1664 (1944); *Ann. N.Y. Acad. Sci.*, **49**, 161 (1948).

39. N. K. Hiester and T. Vermeulen, *Chem. Eng. Prog.* **48**, 505 (1952).

40. D. R. Garg and D. M. Ruthven, *Chem. Eng. Sci.* **28**, 791 and 799 (1973).

41. I. Zwiebel, R. L. Gariepy, and J. J. Schnitzer, *AIChE J.* **18**, 1139 (1972).

42. C. Tien and G. Thodos, *AIChE J.* **5**, 373 (1959).

43. C. R. Antonson and J. S. Dranoff, *AIChE Symp. Ser.* **65**(96), 20 and 27 (1969).

44. H. S. Kyte, *Chem. Eng. Sci.* **28**, 1853 (1973).

45. J. W. Carter and H. Husain, *Trans. I. Chem. Eng.* **50**, 69 (1972).

46. D. R. Garg and D. M. Ruthven, *Chem. Eng. Sci.* **29**, 571 (1974).

47. D. R. Garg and D. M. Ruthven, *Chem. Eng. Sci.* **29**, 1961 (1974).

48. T. Vermeulen, *Ind. Eng. Chem.* **45**, 1664 (1953).

49. T. Vermeulen and R. E. Quilici, *Ind. Eng. Chem. Fund.* **9**, 179 (1970).

50. D. O. Cooney and N. Lightfoot, *Ind. Eng. Chem. Fund.* **4**, 233 (1965).

51. A. S. Michaels, *Ind. Eng. Chem.* **44**, 1922 (1952).

52. K. R. Hall, L. C. Eagleton, A. Acrivos, and T. Vermeulen, *Ind. Eng. Chem. Fund.* **5**, 212 (1966).

53. A. Acrivos, *Chem. Eng. Sci.* **13**, 1 (1960).

54. D. R. Garg and D. M. Ruthven, *Chem. Eng. Sci.* **30**, 1192 (1975).

55. H-K. Rhee and N. R. Amundson, *Chem. Eng. Sci.* **26**, 1571 (1971).

56. H-K. Rhee and N. R. Amundson, *Chem. Eng. Sci.* **27**, 199 (1972).

57. D. M. Ruthven, D. R. Garg, and R. M. Crawford, *Chem. Eng. Sci.* **30**, 803 (1975).

58. Y. Yoshida and T. Kataoka, *Chem. Eng. Sci.* (to be published).

9

DYNAMICS OF ADSORPTION COLUMNS
Multiple-Transition Systems

In the preceding chapter we restricted our consideration of adsorption column dynamics to isothermal or near isothermal systems containing no more than two components. Indeed, most of the discussion was further restricted to systems containing only one adsorbable species in an inert carrier or solvent. The distinguishing feature of such systems is that the concentration profile shows only a single transition or mass transfer zone. In many adsorption systems of practical interest the situation is more complicated because the column is run adiabatically rather than isothermally and there are commonly more than one adsorbable components present in the feed. In such systems the concentration profile comprises more than one mass transfer zone.

The general principles governing the behavior of multicomponent adsorption systems are similar to those governing the behavior of single-component systems. Indeed, in the limiting case of an infinitely dilute isothermal system with a nonadsorbing carrier and all adsorbable species present at low concentrations within the Henry's law region, the extension of the single-component analysis is trivial. Under such conditions the equilibrium relationship for each component is not affected by the presence of the other components so the system is linear and uncoupled and the principle of superposition applies. The multicomponent response then consists simply of the sum of the individual responses for each component, for the same initial and boundary conditions. This is the situation which prevails in linear chromatography and it is on this basis that a chromatograph calibration, determined by injection of samples of individual components, may be used for the analysis of a multicomponent mixture.

At higher sorbate concentrations, and for nonisothermal systems this simple pattern of behavior no longer applies since, outside the Henry's law region,

the adsorption equilibrium for any particular component is affected by all other components present, as well as by the temperature. The differential heat and mass balance equations for the individual components are therefore coupled, which both complicates the analysis and introduces new features in the dynamic behavior. This coupling or "interference" between components is the central feature of multicomponent chromatography and the analysis of multicomponent adsorption systems. In many situations coupling may occur through the adsorption rate equations as well as through the equilibria since the diffusion coefficient may be strongly influenced by the presence of the other components. However, such systems have not yet been analyzed theoretically and we shall therefore consider only the effects of coupling between the temperature and the equilibrium relationships. This limitation is less severe than it may appear at first sight since the gross features of the dynamic behavior of the system are determined entirely by the equilibrium relationships. These features may be significantly modified by kinetic effects, but the general pattern of the dynamic behavior is not changed.

The difficulties associated with the mathematical modeling of the column dynamics increase rapidly with the number of components so that analytic solutions for the transient concentration and temperature profiles can be obtained only for a few limiting cases. A good qualitative understanding of the behavior of both multicomponent and nonisothermal systems can however be obtained from equilibrium theory. In general, numerical solution of the differential heat and mass balance equations offers the only feasible alternative. The numerical approach has the advantage that kinetic and dispersive effects may be included in the theoretical model but it has the disadvantage that solutions may be obtained only for specified sets of parameter values and the general trends of behavior are not always fully evident. The numerical computations are bulky and until recently it has not been practical to obtain numerical solutions for systems involving more than two transitions. However, with the development of improved numerical methods for the solution of differential equations and the concurrent improvement in the speed of computers the extension to more complex systems has now become practically feasible.

9.1. GENERAL MODEL FOR A NONISOTHERMAL, MULTICOMPONENT ADSORPTION COLUMN

As in Section 8.1 we consider an element of the bed through which a stream containing concentration $c_i(z, t)$ of adsorbable species i is flowing. Assuming that the flow pattern can be described by the axially dispersed plug flow model, the differential fluid phase mass balance equation for each component is

$$-D_L \frac{\partial^2 c_i}{\partial z^2} + \frac{\partial}{\partial z}(v c_i) + \frac{\partial c_i}{\partial t} + \left(\frac{1-\epsilon}{\epsilon}\right)\frac{\partial \bar{q}_i}{\partial t} = 0 \qquad (9.1)$$

The particle mass balance yields the adsorption rate equation for each component, which may be written in the generalized form

$$\frac{\partial \bar{q}_i}{\partial t} = f(q_i, q_j, \ldots, c_i, c_j, \ldots) \tag{9.2}$$

where it is understood that the function may in fact represent a set of diffusion equations with associated boundary conditions, rather than a simple algebraic expression. In addition, the continuity equation must also be satisfied, so these equations may not all be independent.

If the system is nonisothermal, heat balances for the column element and particle are also required to complete the formal description of the system.

$$-\lambda_L \frac{\partial^2 T_f}{\partial z^2} + C_f \frac{\partial(v T_f)}{\partial z} + \left(\frac{1-\epsilon}{\epsilon}\right) C_s \frac{\partial T_s}{\partial t} + C_f \frac{\partial T_f}{\partial t}$$

$$= \left(\frac{1-\epsilon}{\epsilon}\right) \sum_i (-\Delta H_i) \frac{\partial \bar{q}_i}{\partial t} - \frac{4h_w}{\epsilon d}(T_f - T_w) \tag{9.3}$$

$$C_s \frac{\partial T_s}{\partial t} - \frac{3h}{R_p}(T_f - T_s) = \sum_i (-\Delta H_i) \frac{\partial \bar{q}_i}{\partial t} \tag{9.4}$$

Since both the adsorption equilibrium and the adsorption kinetics are temperature dependent, it is evident that the dynamic behavior may be considerably altered by heat effects.

The dynamic response of the column is given by the solution $c_i(z,t), \bar{q}_i(z,t),$ $T(z,t)$ to Eqs. (9.1)–(9.4) subject to the boundary conditions imposed on the column. For an isothermal system with n components (including inert, non-adsorbing species if present) the response to a change in inlet concentration will generally consist of a set of $n - 1$ mass transfer zones which propagate through the column with characteristic velocities determined by the multicomponent equilibrium isotherm. This is always true for saturation of an initially clean bed or for elution of a saturated bed with an inert solvent but in certain limited situations which are noted below, additional transitions may arise or two transitions may become degenerate.

Since the adsorption equilibrium is temperature dependent, a nonisothermal system will include an additional mass transfer zone which propagates with the velocity of the temperature front. Thus, in a formal sense, one may consider an n-component nonisothermal system as equivalent to an isothermal system with $n + 1$ components.

Clearly, the problem defined in this way is much too complex to allow a general solution to be found, and to make further progress it is necessary to restrict the generality of the mathematical representation by the introduction of appropriate approximations. The various models which are commonly used to represent the dynamic behavior of an adsorption column differ in their generality depending on the extent and severity of the approximations introduced.

9.2. CLASSIFICATION OF ADSORPTION SYSTEMS

The complexity of the dynamic behavior of an adsorption column is directly related to the number of components and the nature of the operation (isothermal or adiabatic) since these factors determine the number of transitions or mass transfer zones. It is therefore convenient to classify systems, in order of increasing complexity, according to the following scheme.

1. Single-Transition Systems

    (a) One adsorbable component plus inert carrier, isothermal or near isothermal operation.

    (b) Two adsorbable components (no carrier), isothermal or near isothermal operation.

2. Two-Transition Systems

    (a) Two adsorbable components plus inert carrier, isothermal operation.

    (b) Three adsorbable components (no carrier), isothermal operation.

    (c) One adsorbable component plus inert carrier, adiabatic operation.

    (d) Two adsorbable components (no carrier), adiabatic operation.

3. Multiple-Transition Systems

    (a) Four or more components, isothermal operation.

    (b) Three or more components, adiabatic operation.

    (c) Three components, isothermal operation with selectivity reversal.

    (d) Two components, adiabatic operation, with selectivity reversal.

The additional complexity which can arise in a limited range of compositions due to selectivity reversal is discussed in Section 9.4.

Numerical solutions to the coupled heat and mass balance equations have been obtained for both isothermal and adiabatic two- and three-transition systems but for more complex systems only equilibrium theory solutions have so far been obtained. In the application of equilibrium theory a considerable simplification becomes possible if axial dispersion is neglected and the plug flow assumption has therefore been widely adopted. Under plug flow conditions the differential mass and heat balance equations assume the hyperbolic form of the kinematic wave equations and solutions may be obtained in a straightforward manner by the method of characteristics. In a numerical simulation the inclusion of axial dispersion causes no real problem. Indeed, since axial dispersion tends to smooth the concentration profiles the numerical solution may become somewhat easier when the axial dispersion term is included. Nevertheless, the great majority of numerical solutions obtained so far have assumed plug flow.

9.3. ADSORPTION EQUILIBRIUM IN MULTICOMPONENT SYSTEMS

In Chapter 8 the equilibrium factor for a single adsorbed species was defined by analogy with the relative volatility. This definition is easily extended to a binary or multicomponent system. For competitive sorption the binary separation factor is defined by

$$\beta_{ij} = \frac{\phi_i \psi_j^*}{\psi_i^* \phi_j} \tag{9.5}$$

where $\phi_i = c_i/c_0$, $c_0 = c_i + c_j + c_k + \cdots =$ total concentration of adsorbable species in fluid.

$$\psi_i^* = \frac{q_i^*}{q_0}, \qquad q_0 = q_i + q_j + q_k + \cdots = \text{total concentration in adsorbed phase}$$

Thus $\psi_i = X_i =$ mole fraction in adsorbed phase and if no inerts are present $\phi_i = Y_i =$ mole fraction in fluid phase. It is apparent that

$$\beta_{ij} = \frac{1}{\beta_{ji}}, \qquad \beta_{ik} = \beta_{ij}\beta_{jk} \tag{9.6}$$

The equilibrium factor measures the affinity of the adsorbent for a particular component relative to the same component in the fluid phase whereas the binary separation factor measures the relative preference of the adsorbent for two different competing adsorbates. If the equilibrium obeys the multicomponent Langmuir model:

$$\frac{q_i^*}{q_s} = \frac{b_i c_i}{1 + b_i c_i + b_j c_j + b_k c_k + \cdots} \tag{9.7}$$

it may be shown by simple algebra that $\beta_{ij} = b_j/b_i$ while the affinity factor is given by $\beta_i = (1 + b_i c_0)^{-1}$. For such a system the separation factor is clearly independent of composition. This leads to considerable simplifications in the equilibrium theory analysis of adsorption column dynamics and the Langmuir model or "constant separation factor approximation" has therefore been widely adopted. The equation for the multicomponent isotherm [Eq. (9.7)] may be conveniently written in terms of the dimensionless concentration variables with the separation factors as parameters:

$$\frac{\phi_i}{\psi_i^*} = \phi_i + \phi_j \beta_{ij} + \phi_k \beta_{ik} + \cdots \tag{9.8}$$

With the definition given above, the smaller the value of β_{ij} the more strongly held is component i relative to component j. Following Helfferich[3] and Vermeulen[4] it has become conventional to define the separation factor for a multicomponent system (α_{ij}) as the reciprocal of β_{ij}:

$$\alpha_{ij} \equiv \frac{1}{\beta_{ij}} \equiv \beta_{ji} \equiv \frac{\phi_j \psi_i^*}{\psi_j^* \phi_i} = \left(\frac{b_i}{b_j} \text{ for Langmuir system} \right) \tag{9.9}$$
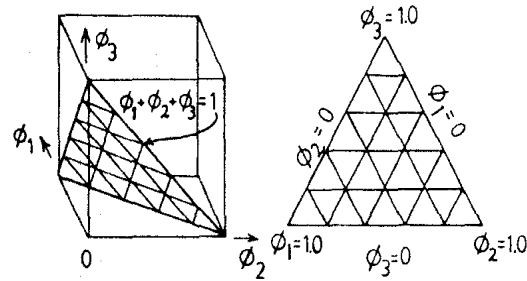
FIGURE 9.1. Orthogonal concentration coordinates for a three-component system and representation as a triangular composition diagram.

With this definition, which is adopted for the remainder of this chapter, the separation factor measures directly the affinity of the adsorbent for component i relative to component j; the higher the separation factor the more strongly is component i adsorbed relative to component j.

For a ternary system the composition of the fluid phase (or the adsorbed phase) can be naturally represented in three-dimensional space with three orthogonal concentration coordinates, as indicated in Figure 9.1. However, if the concentrations are expressed in normalized form (ϕ_i or ψ_i) the normalization requires that $\phi_i + \phi_j + \phi_k = 1.0$ so that all possible compositions are confined to the plane formed by the equilateral triangle defined by the diagonals of the cube containing the concentration axes. The concentrations may therefore be conveniently represented in two-dimensional form using a standard triangular diagram. Such a diagram may be drawn for either fluid phase or adsorbed phase composition. Similarly the dimensionless compositions in a four-component system may be conveniently represented in three-dimensional form as points within a regular tetrahedron but in the present discussion we shall not be concerned with systems of more than three components.

9.4. EQUILIBRIUM THEORY OF ADSORPTION COLUMN DYNAMICS FOR ISOTHERMAL SYSTEMS

The equilibrium theory of binary and multicomponent isothermal adsorption systems appears to have been first developed by Glueckauf.[1] More general and comprehensive treatments have been developed by Rhee, Aris, and Amundson[2] and by Helfferich and Klein.[3] The former treatment exploits the analogy between chromatographic theory and the theory of kinematic waves. The detailed quantitive theory has been developed only for ideal Langmuir systems without axial dispersion or mass transfer resistance and in which the initial and boundary conditions represent constant steady states. Subject to these constraints the treatment is sufficiently general to allow the dynamic behavior to be predicted for systems with any number of components, provided only that the separation factors are known. In the

development of the theory, however, considerable prior knowledge of the theory of the first-order wave equation is assumed.

The development of Helfferich and Klein[3] is equally comprehensive with somewhat greater emphasis on physical understanding. However, the generality of the treatment and the extensive use of an elegant nonlinear transformation (the h-transformation), while contributing greatly to the understanding of the behavior of the more complex systems, tends to obscure the comparatively simple behavior observed with two- and three-component systems. The original treatment of Glueckauf,[1] although less general, provides a somewhat easier introduction to the subject and is therefore followed here.

A key concept in the equilibrium theory of multicomponent adsorption is the concept of coherence. Coherent behavior was assumed by most of the early workers, including Glueckauf, but the nature of this assumption appears to have been recognized only more recently by Helfferich.[3] For a dilute equilibrium plug flow system the differential fluid phase mass balance [Eq. (9.1)] may be written for each component in the form

$$v\left(\frac{\partial c_i}{\partial z}\right)_t + \left(\frac{\partial c_i}{\partial t}\right)_z + \left(\frac{1-\epsilon}{\epsilon}\right)\left(\frac{\partial q_i^*}{\partial t}\right)_z = 0 \tag{9.10}$$

The equilibrium adsorbed phase concentration q_i^* depends only on the local concentrations of all adsorbable components:

$$q_i^* = q_i^*(c_i, c_j, c_k, \dots)$$

$$\therefore \frac{dq_i^*}{dc_i} = \left(\frac{\partial q_i^*}{\partial c_i}\right)_{c_j, c_k} + \left(\frac{\partial q_i^*}{\partial c_j}\right)_{c_i, c_k}\frac{dc_j}{dc_i} + \cdots = \left(\frac{\partial q_i^*}{\partial c_i}\right)_z \tag{9.11}$$

$$\therefore \left(\frac{\partial q_i^*}{\partial t}\right)_z = \left(\frac{\partial q_i^*}{\partial c_i}\right)_z\left(\frac{\partial c_i}{\partial t}\right)_z = \frac{dq_i^*}{dc_i}\left(\frac{\partial c_i}{\partial t}\right)_z$$

Equation (9.10) may therefore be written in the form of the kinematic wave equation:

$$w_i\left(\frac{\partial c_i}{\partial q}\right)_t + \left(\frac{\partial c_i}{\partial t}\right)_z = 0, \qquad w_i(c_i, c_j, \dots) = \frac{v}{1 + \left(\dfrac{1-\epsilon}{\epsilon}\right)\left(\dfrac{dq_i^*}{dc_i}\right)_{c_i, c_j, \dots}} \tag{9.12}$$

For a shock transition the equivalent expression is

$$w_i'\left(\frac{\partial c_i}{\partial z}\right)_t + \left(\frac{\partial c_i}{\partial t}\right)_z = 0, \qquad w' = \frac{v}{1 + \left(\dfrac{1-\epsilon}{\epsilon}\right)\dfrac{\Delta q_i^*}{\Delta c_i}} \tag{9.13}$$

When there is only one adsorbable species these equations reduce to Eqs. (8.11) and (8.13).

A coherent concentration front may be defined as consisting of traveling loci of constant compositions. By contrast, in a noncoherent boundary, the concentrations of the species shift relative to one another as the species

migrate and a particular composition $(c_i, c_j, c_k, \ldots)$ exists only momentarily. Coherence requires that the characteristic velocity for a given composition $(c_i, c_j, c_k, \ldots)$ must be the same for all species:

$$w_i(c_i, c_j, c_k, \ldots) = w_j(c_i, c_j, c_k, \ldots) = w_k(c_i, c_j, c_k) = \cdots \qquad (9.14)$$

and this in turn requires, according to Eqs. (9.12) and (9.13),

$$\left(\frac{dq_i^*}{dc_i}\right)_{c_i, c_j, \ldots} = \left(\frac{\partial q_i}{\partial c_i}\right)_z = \left(\frac{\partial q_j}{\partial c_i}\right)_z \qquad (9.15a)$$

or (for a shock)

$$\left(\frac{\Delta q_i}{\Delta c_i}\right)_z = \left(\frac{\Delta q_i}{\Delta c_j}\right)_z \quad \text{(for all } i, j) \qquad (9.15b)$$

From Eq. (9.10) and the cyclic rule for partial differentials it follows that $(\partial q_i/\partial c_i)_z = (\partial q_i/\partial c_i)_t$ and this implies that all concentrations can be expressed as functions of z/t rather than as functions of z and t separately.

The mathematical justification for the assumption of coherent concentration fronts proceeds via the inverse of this argument. It has been shown that, in a system governed by the kinematic wave equation [Eq. (9.12)] involving a transition between two constant states (a Riemann problem), if a unique solution exists it is always a function of the combined variable z/t[5]; the requirement for a coherent boundary expressed by Eq. (9.15) therefore follows automatically.

Some reduction in algebraic complexity may be achieved by the use of an adjusted time variable $\hat{t} = t - z/v$. With the substitution Eq. (9.10) becomes

$$v\left(\frac{\partial c_i}{\partial z}\right)_{\hat{t}} + \left(\frac{1-\epsilon}{\epsilon}\right)\left(\frac{\partial q_i^*}{\partial \hat{t}}\right)_z = 0 \qquad (9.16)$$

The adjusted wave velocity $(\hat{w}_i)$ and the adjusted shock velocity $(\hat{w}_i')$ are seen to be given by

$$\hat{w}_i(c_i, c_j, \ldots) = \left(\frac{\partial z}{\partial \hat{t}}\right)_{c_i, c_j, \ldots} = \frac{v}{\left(\dfrac{1-\epsilon}{\epsilon}\right)\left(\dfrac{dq_i^*}{dc_i}\right)_{c_i, c_j, \ldots}}$$

$$\hat{w}_i' = \frac{v}{\left(\dfrac{1-\epsilon}{\epsilon}\right)\dfrac{\Delta q_i^*}{\Delta c_i}} \qquad (9.17)$$

The true and adjusted wave velocities are related by

$$\frac{1}{\hat{w}_i} = \frac{1}{w_i} - \frac{1}{v}, \qquad \frac{1}{\hat{w}_i'} = \frac{1}{w_i'} - \frac{1}{v} \qquad (9.18)$$

Three-Component Systems (Two Adsorbable Species with Inert Carrier)

To illustrate the detailed application of equilibrium theory we consider Glueckauf's treatment of a system with two adsorbable components (1 and 2)

present at low concentrations in an inert carrier. The system is considered isothermal and nondispersive so that the differential fluid phase mass balances obey Eq. (9.10). Assuming general functional forms for the equilibrium relationships

$$q_i^* = f_1(c_1, c_2), \qquad q_2^* = f_2(c_1, c_2) \tag{9.19}$$

we obtain from Eq. (9.12)

$$w_1 = \cfrac{v}{1 + \left(\cfrac{1-\epsilon}{\epsilon}\right)\left[\cfrac{\partial f_1}{\partial c_1} + \cfrac{\partial f_1}{\partial c_2}\cfrac{dc_2}{dc_1}\right]}$$

$$w_2 = \cfrac{v}{1 + \left(\cfrac{1-\epsilon}{\epsilon}\right)\left[\cfrac{\partial f_2}{\partial c_2} + \cfrac{\partial f_2}{\partial c_1}\cfrac{dc_1}{dc_2}\right]} \tag{9.20}$$

and from the coherence conditions [Eq. (9.14)]

$$\frac{\partial f_2}{\partial c_1}\left(\frac{dc_1}{dc_2}\right)^2 + \left(\frac{\partial f_2}{\partial c_2} - \frac{\partial f_1}{\partial c_1}\right)\frac{dc_1}{dc_2} - \frac{\partial f_1}{\partial c_2} = 0 \tag{9.21}$$

The partial derivatives $\partial f_2/\partial c_1$, $\partial f_2/\partial c_2$, $\partial f_1/\partial c_1$, and $\partial f_1/\partial c_2$ are all known from the equilibrium relation [Eq. (9.19)] so Eq. (9.21) may be regarded as a quadratic equation defining the total differential dc_1/dc_2. For all normal equilibrium relationships $(\partial f_z/\partial c_1)_{c_2}$ and $(\partial f_1/\partial c_1)_{c_1}$ are both negative. This means that Eq. (9.21) has two real roots, one positive and one negative:

$$\frac{dc_1}{dc_2} = g_1(c_1, c_2) \quad (+), \qquad \frac{dc_1}{dc_2} = g_2(c_1, c_2) \quad (-) \tag{9.22}$$

Corresponding to these two roots there are two different propagation velocities given by

$$w_+ = \cfrac{v}{1 + \left(\cfrac{1-\epsilon}{\epsilon}\right)\left[\cfrac{\partial f_2}{\partial c_2} + \cfrac{\partial f_2}{\partial c_1}\, g_1(c_1, c_2)\right]}$$

$$w_- = \cfrac{v}{1 + \left(\cfrac{1-\epsilon}{\epsilon}\right)\left[\cfrac{\partial f_2}{\partial c_2} + \cfrac{\partial f_2}{\partial c_2}\, g_2(c_1, c_2)\right]}$$

$$\hat{w}_+ = \cfrac{v}{\left(\cfrac{1-\epsilon}{\epsilon}\right)\left[\cfrac{\partial f_2}{\partial c_2} + \cfrac{\partial f_2}{\partial c_1}\, g_1(c_1, c_2)\right]} \tag{9.23}$$

$$\hat{w}_- = \cfrac{v}{\left(\cfrac{1-\epsilon}{\epsilon}\right)\left[\cfrac{\partial f_2}{\partial c_2} + \cfrac{\partial f_2}{\partial c_2}\, g_2(c_1, c_2)\right]}$$

Since $(\partial f_2/\partial c_1)_{c_2}$ is negative while g_1 is positive and g_2 is negative, it follows that, for any specified composition (c_1, c_2), w_+ (for which dc_1/dc_2 is positive) must be larger than w_- (for which dc_1/dc_2 is negative).
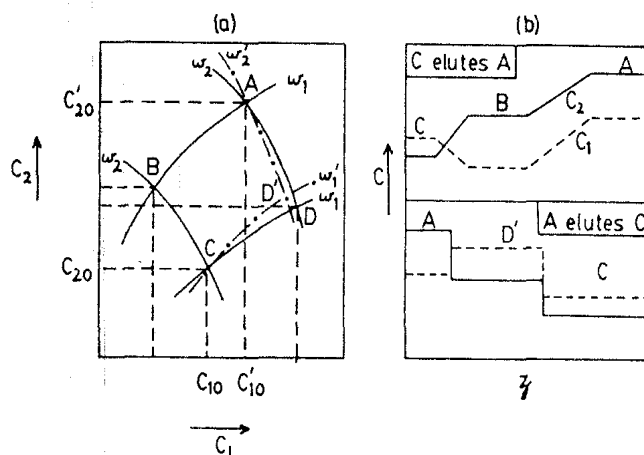
FIGURE 9.2. (a) Sketch of characteristics and (b) corresponding concentration profiles for transitions between states A and C.

If we consider an initially uniform steady-state concentration represented by (c'_{10}, c'_{20}) throughout the bed and a final steady concentration (c_{10}, c_{20}) we can represent the transition between these two states on a "hodograph" plot of c_1 versus c_2, as illustrated in Figure 9.2. To construct the hodograph the characteristic curves through initial point and feed point are first calculated from the equilibrium isotherm according to Eq. (9.24):

$$c''_2 = c'_{20} - \Delta c_2, \qquad c''_1 = c'_{10} - \frac{dc_1}{dc_2}\bigg|_{c'_{10}, c'_{20}} \Delta c_2$$

$$c'''_2 = c''_2 - \Delta c_2, \qquad c'''_1 = c''_1 \frac{dc_1}{dc_2}\bigg|_{c'_1, c'_2} \Delta c_2 \qquad (9.24)$$

$$\vdots \qquad\qquad \vdots$$

Point A represents the initial state of the bed and point C is the final state. Through both these points there are two characteristic curves corresponding to the propagation velocities w_1 and w_2. The solution for the breakthrough curve or concentration profile may be constructed directly from the hodograph. Since there are two different characteristic curves through both the initial and final points there appears to be some ambiguity. In fact there is no ambiguity since the initial state must propagate through the bed faster than the final state. This means that we must leave point A along a w_+ characteristic and approach point C along a w_- characteristic. The sequence $A-B$ represents the first mass transfer zone and the form of the concentration front may be easily calculated since the velocity at any point along $A-B$ is given by Eq. (9.23). Point B represents a plateau region between the two mass transfer zones while the sequence $B-C$ represents the second mass transfer zone. The velocity at any point along $B-C$ is again obtainable directly from Eq. (9.23).

If the concentration of the more strongly adsorbed component decreases over a transition, the velocity of the final state will be greater than that of the initial state. Under these conditions Eq. (9.12) breaks down and must be

replaced by the corresponding shock wave expression [Eq. (9.13)]. Knowing the equilibrium isotherm, the characteristic curve for a shock transition and the corresponding shock velocity may be calculated in a manner similar to that outlined above for a simple wave.

In Figure 9.2 component 2 is considered to be the more strongly adsorbed species. The simple wave velocity therefore decreases continuously along both $A \rightarrow B$ and $B \rightarrow C$ and both these transitions assume the form of simple proportionate-pattern waves. If a column initially in state A (c'_{10}, c'_{20}) is eluted with a solution corresponding to state C (c_{10}, c_{20}) the profile will therefore consist of two simple waves with a plateau corresponding to state B.

The reverse procedure, that is, elution of a column initially at state C with a solution corresponding to point A, leads to a shock wave profile. Since component 2 is the more strongly adsorbed species, the simple wave velocity increases along $C \rightarrow D$ so this transition must be replaced by the chain-dotted curve representing the corresponding shock transition. Similarly the transition $D \rightarrow A$ is replaced by the shock transition $D' \rightarrow A$ and the profile consists of two shocks separated by a plateau corresponding to D'.

As a specific example of the application of this general method we consider a two-component Langmuir system with the isotherm relation given by Eq. (9.7) with $b_2 = 2b_1$ or $\alpha_{21} = 2.0$. For such a system Eq. (9.21) assumes the form

$$p_1 \left(\frac{dp_1}{dp_2} \right)^2 - (1 + p_1 - p_2) \frac{dp_1}{dp_2} - p_1 = 0 \qquad (9.25)$$

where, following Glueckauf, we have introduced for convenience the modified concentration variables $p_1 = b_1 b_2 c_1 / (b_2 - b_1)$ and $p_2 = b_1 b_2 c_2 / (b_2 - b_1)$. Since component 2 is the more strongly adsorbed species $(b_2 > b_1)$ both p_1 and p_2 are always positive. It may be shown that the only physically realistic solutions to Eq. (9.25) $(c_1$ and c_2 or p_1 and p_2 both positive) are linear functions of the form

$$p_1 = \lambda p_2 - \frac{\lambda}{1 + \lambda}, \qquad c_1 = \lambda c_2 - \left(\frac{b_2 - b_1}{b_1 b_2} \right) \left(\frac{\lambda}{1 + \lambda} \right) \qquad (9.26)$$

where λ is a constant of integration which depends on the starting conditions. Equation (9.26) may be written as a quadratic in λ:

$$\lambda^2 + \lambda \left(1 - \frac{c_2}{c_1} - \frac{b_2 - b_1}{b_1 b_2 c_2} \right) - \frac{c_1}{c_2} = 0 \qquad (9.27)$$

which has one positive root (μ) and one negative root (ν). From the equations of the characteristics [Eq. (9.26)] we can write down directly expressions for the concentration in terms of the parameters μ and ν:

$$c_1 = \left(\frac{b_2 - b_1}{b_1 b_2} \right) \frac{-\mu\nu}{(1 + \mu)(1 + \nu)}, \qquad c_2 = \left(\frac{b_2 - b_1}{b_1 b_2} \right) \frac{1}{(1 + \mu)(1 + \nu)} \qquad (9.28)$$

From the equilibrium isotherm [Eq. (9.7)] we can also write down expressions

for the adsorbed phase concentration in terms of μ and ν:

$$q_1^* = \frac{-(\mu\nu)(b_2 - b_1)b_1 q_s}{(b_1\mu + b_2)(b_2\nu + b_2)}, \qquad q_2^* = \frac{(b_2 - b_1)b_2 q_s}{(b_1\mu + b_2)(b_1\mu + b_2)} \qquad (9.29)$$

The expressions for the corrected velocity may then be found by evaluating the partial derivatives $(\partial c_2/\partial\mu, \partial c_2/\partial\nu$ and $\partial c_1/\partial\mu, \partial c_1/\partial\nu)$ and substituting in Eq. (9.23):

$$\hat{w}_+ = \left.\frac{dz}{d\hat{t}}\right|_{c_1,c_2,\mu} = \frac{q_s}{\kappa}\left(\frac{\mu + \kappa}{\mu + 1}\right)\left(\frac{\nu + \kappa}{\nu + 1}\right)^2 \frac{\epsilon v}{(1 - \epsilon)}$$

$$\hat{w}_- = \left.\frac{dz}{d\hat{t}}\right|_{c_1,c_2,\nu} = \frac{q_s}{\kappa}\left(\frac{\mu + \kappa}{\mu + 1}\right)^2\left(\frac{\nu + \kappa}{\nu + 1}\right)\frac{\epsilon v}{(1 - \epsilon)} \qquad (9.30)$$

The corresponding shock velocities are given by

$$\hat{w}'_+ = \frac{q_s}{\kappa}\left(\frac{\mu + \kappa}{\mu + 1}\right)\left(\frac{\nu_1 + \kappa}{\nu_1 + 1}\right)\left(\frac{\nu_2 + \kappa}{\nu_2 + 1}\right)\frac{\epsilon v}{(1 - \epsilon)}$$

$$\hat{w}' = \frac{q_s}{\kappa}\left(\frac{\mu_1 + \kappa}{\mu_1 + 1}\right)\left(\frac{\mu_2 + \kappa}{\mu_2 + 1}\right)\left(\frac{\nu + \kappa}{\nu + 1}\right)\frac{\epsilon v}{(1 - \epsilon)} \qquad (9.31)$$

where $\kappa = b_2/b_1$ and $(\mu_1,\nu_1),(\mu_2,\nu_2)$ are the pairs of roots of Eq. (9.27) corresponding to the upper and lower concentrations of the shock transition.

For a Langmuir system the characteristic paths for a shock transition and for a simple wave transition between two defined states are the same although this is not generally true for any other form of isotherm. This degeneracy between the shock and simple wave characteristics follows from the linearity of the characteristics since for a straight line $dc_1/dc_2 = \Delta c_1/\Delta c_2$.

In elucidating equilibrium theory behavior the two basic rules formulated by Glueckauf provide useful guidance:

Rule 1. A concentration plateau c_1', c_2' is produced spontaneously in a boundary if the boundary in front of it travels along the positive characteristics of c_1', c_2' while the rear boundary travels along a characteristic where dc_1/dc_2 is negative or zero. (This eliminates any apparent ambiguity in the possible routes between two concentration states.)

Rule 2. Whenever the more strongly adsorbed solute increases in concentration along the column we have a diffuse boundary (simple proportionate-pattern wave) while where the concentration of the more strongly adsorbed component decreases along the column we have a shock transition.

The characteristics and corresponding profiles for a Langmuir system with $\kappa = b_2/b_1 = 2.0$ are shown in Figure 9.3. It may be seen that the profiles consist in all cases of a plateau region separated from the initial and final states by two mass transfer zones. The form of these mass transfer zones can
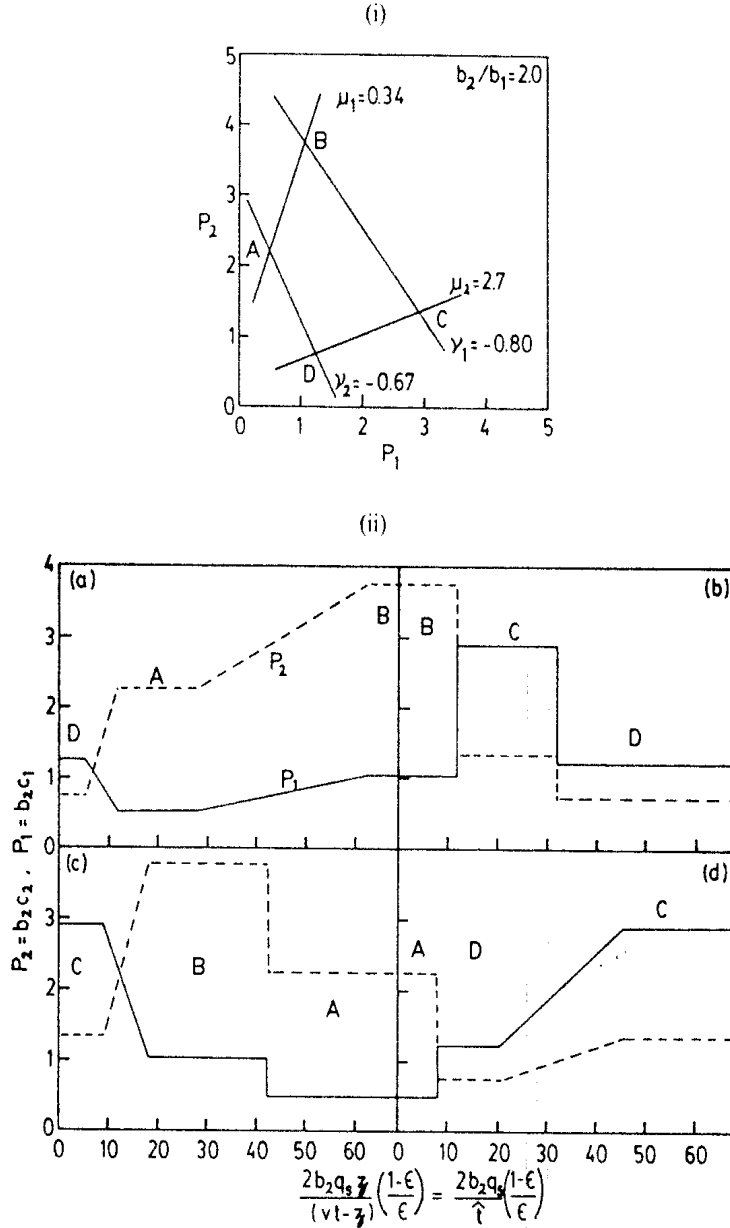
FIGURE 9.3. (i) Characteristics and (ii) concentration profiles for a Langmuir system. The profiles between the states A, B, C, and D are shown as follows: (a) D elutes B, (b) B elutes D, (c) C elutes A, and (d) A elutes C. $(p_1, \text{———}; p_2, \text{---}.)$ (From ref. 1, reprinted with permission.)

be deduced from rules 1 and 2 above while their position may be calculated from the velocity expressions, given in Eqs. (9.30) and (9.31), using the appropriate values of μ and ν.

It is evident that the intermediate plateau concentration of one of the components may exceed either the feed concentration or the initial concentration of that component. This is a common feature of multicomponent adsorption systems and is sometimes referred to as roll-up. The effect is due to displacement of the less strongly adsorbed species by the slower moving more strongly adsorbed component.

The development outlined here may be generalized for systems with more than two adsorbable components although the algebra becomes tedious.[6]

Displacement Development

A common operation in liquid chromatography and in some large-scale chromatographic separations involves the displacement of adsorbed components from a loaded column by a desorbent which is more strongly adsorbed than any of the components already present in the system. Since the desorbent is the most strongly adsorbed species its characteristic velocity will be smaller than that of any of the other components. Under these conditions in the displacement of a binary system, no ternary mixtures are formed, and for a Langmuir system the situation may be represented by two adjoining sets of linear characteristics as sketched in Figure 9.4.

The behavior is somewhat different depending on the concentration level of the desorbent relative to the other components. The original concentrations
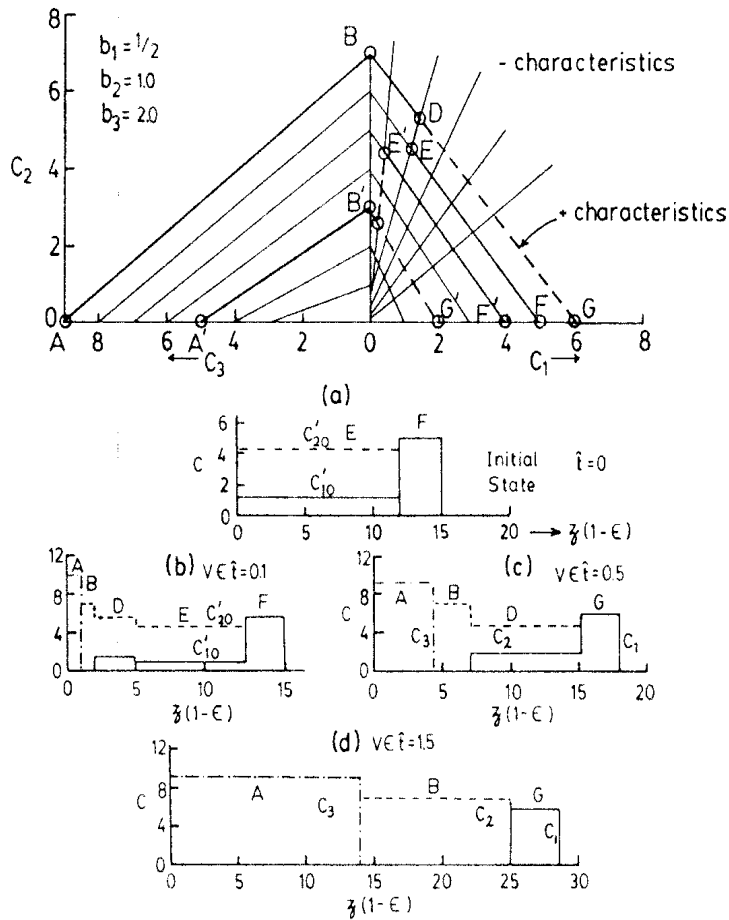
FIGURE 9.4. Characteristics for displacement of two solutes by a strong desorbent and concentration profiles showing the development of the profiles at successive times in the sequence (a), (b), (c), and (d) $(c_1,$ ———; $c_2,$ ---; $c_3,$ —·—·). (From ref. 1, reprinted with permission.)

c'_{10}, c'_{20} are represented by point E and the displacing solution containing concentration c_{30} of desorbent is represented by point A. When c_{30} is sufficiently high the path, according to rule 1, follows $ABDEF$. Points B, D, and F all correspond to stable plateaus since the forward transitions from these plateaus travel along positive characteristics (dc_1/dc_2 positive) while the rear transitions travel along negative characteristics. The original concentration plateau is unstable since the forward front lies on a negative characteristic while the near front is on a positive characteristic, so plateau E decreases in length as displacement progresses and eventually disappears from the column. The path from D to O then goes via G (Figure 9.4c). Under these conditions the previous plateaux D and F become unstable and eventually disappear so that the situation sketched in Figure 9.4a is reached in which all three solutes are concentrated in sharp bands arranged in order of affinity.

If the desorbent concentration (c_s^0) is smaller (A') the path will follow $A'B'D'E'F'$. The boundary $D'E'$ will now be diffuse and the plateau E' is unstable and eventually disappears leaving the plateaux $A'B'G'$. With even lower desorbent concentration there is no displacement development.

Systems with Three Adsorbable Components

For systems with three adsorbable components the composition paths are conveniently determined with the aid of a triangular composition diagram, as illustrated in Figure 9.5. For a Langmuir system the characteristics, plotted in this way, are linear so the diagram is easily constructed once the separation factors are known. An important property of the path grid is the existence of the watershed point W on the border $\phi_2 = 0$, where component 2 is the component with intermediate affinity. The location of the watershed point is given by $\phi_2 = 0$, $\phi_1 = (\alpha_{12} - 1)/(\alpha_{13} - 1)$. The 1–2 paths connecting the borders $\phi_1 = 0$ and $\phi_2 = 0$ all originate on one side of the point W while the 2–3 paths connecting the $\phi_2 = 0$ and $\phi_3 = 0$ borders all originate on the other side of W. There are no direct paths connecting $\phi_1 = 0$ and $\phi_3 = 0$. The rule of equal intercept ratios states that the intersection of each 1–2 composition path with the 1–3 border occurs at the same fractional distance between W and the component 1 corner as the other intercept from the component 2 corner along the 2–3 border. The same rule applies *mutatis-mutandis* to the 2–3 paths so that the path grid may be readily constructed.

Between any two points in the interior of the diagram there are two alternative coherent paths: along a 1–2 characteristic and then along a 2–3 characteristic or vice versa. Thus, referring to Figure 9.5, if a bed in which the initial state is given by point A is contacted with a feed corresponding to point C there are two coherent paths between A and C: ABC or ADC. B and D represent the plateau compositions for these two routes. The decision as to which is the correct path follows from Glueckauf's rule 1; that is, the velocity of the transition between the plateau and the initial state must be higher than the velocity of the transition between the feed state and the plateau. If component 1 is the most strongly adsorbed species and component 3 is the
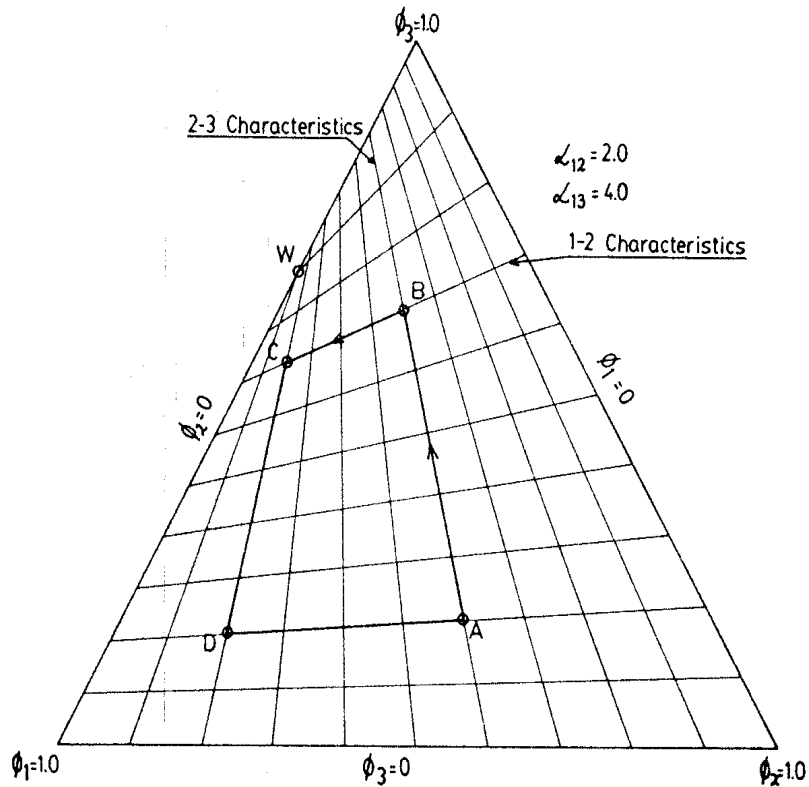
FIGURE 9.5. Equilibrium diagram for ternary Langmuir system showing possible coherent composition paths.

least strongly adsorbed species, for a given composition, the velocity along the 1–2 characteristic will always be lower than that along the 2–3 characteristic. The path must therefore follow ABC. (In the reverse situation of a bed of composition C contacted with feed of composition A the path would follow CDA by similar logic.)

When the concentration of the more strongly adsorbed species (component 1 in a 1–2 transition, component 2 in a 2–3 transition) decreases over the concentration front in the downstream direction the transition will be a shock, whereas when the concentration of the more strongly adsorbed species increases the transition will be gradual. Thus, in the example considered we deduce that the transition $A \rightarrow B$ is a gradual transition (ϕ_2 increases downstream) while the transition $B \rightarrow C$ will be a shock (ϕ_2 decreases downstream). The qualitative form of the profile is sketched in Figure 9.6. To deduce the detailed form of the profile it would be necessary to calculate the shock
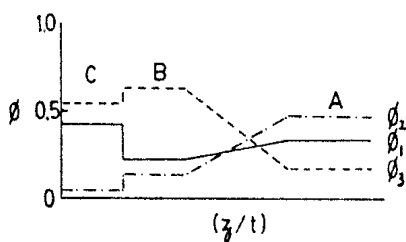
FIGURE 9.6. Sketch showing form of concentration profiles for the transition ABC (Figure 9.5).

velocity for the $B-C$ transition and the wave velocity variation along $A-B$ from Eqs. (9.12) and (9.13), as was done previously for the binary case.

When the separation factor is constant (Langmuir system) no selectivity reversal can occur and every point within the composition diagram can be connected to any other point by two alternative paths along 1–2 and 2–3 characteristics, intersecting at some particular plateau composition. This means that the concentration profile will always consist of two transitions separated by a plateau region, except in the special case where both the initial and final states lie on the same characteristic. Under these conditions only one transition will be observed and the system will behave like a binary system. This result may be generalized to multicomponent systems, leading to the general conclusion that in an n-component isothermal system with constant separation factors there can be no more than $n - 1$ transitions separating the constant initial and final states.

More Complex Systems

The present discussion of equilibrium theory has been concerned mainly with constant separation factor Langmuir systems and has been restricted to the analysis of the effect of a single step change in feed composition on a previously equilibrated bed. The Langmuir assumption greatly simplifies the analysis since, for such systems, the characteristics are linear and the same for gradual and shock transitions.

In the more general situation with concentration-dependent separation factors, the calculation of the characteristics is more complicated and requires numerical integration, as indicated in Eq. (9.24). Selectivity reversal becomes possible and if this occurs additional concentration fronts may be introduced so that, in these circumstances, a three-component isothermal system may show three transitions. Such problems have been considered in detail by Helfferich and Klein.[3]

The situation which arises when the adsorbent bed is subjected to successive changes in feed composition is also of some practical interest particularly in relation to the analysis of pulse chromatography in nonlinear interfering systems. Each change in feed composition introduces its own family of transitions (in general $n - 1$ transitions for an n-component system) which propagate through the bed at their characteristic velocities. It is possible for the velocity of one or more fronts from the second feed perturbation to travel with a velocity greater than that of some (or all) of the fronts from the earlier perturbation. Under these circumstances the concentration waves from the two perturbations will interact with each other leading to various types of combined wave fronts and additional complexity of the system response. Such problems are not considered here. It is in the elucidation of these more complex types of behavior that the wave theory analysis of Rhee et al.[2] has proved particularly useful and the reader is referred to Rhee's paper for a more complete discussion.

9.5. ISOTHERMAL SYSTEMS WITH FINITE MASS TRANSFER RESISTANCE

Extension of Equilibrium Theory

The effect of mass transfer resistance is to broaden the mass transfer zone relative to the profile deduced from equilibrium theory. Where equilibrium theory predicts a shock transition the actual profile will approach constant-pattern form. Since the location of the mass transfer zone and the concentration change over which the transition occurs are not affected by mass transfer resistance, the extension of equilibrium theory is in this case straightforward and requires only the integration of the rate expression, subject to the constant-pattern approximation, to determine the form of the concentration profile. This is in essence the approach of Cooney and Strusi[7] who show that for a Langmuir system with two adsorbable components a simple analytic expression for the concentration profile may be obtained when both mass transfer zones are of constant-pattern form.

A more detailed discussion has been given by Rhee and Amundson[8] who show that the constant-pattern analysis of the combined effects of mass transfer resistance and axial dispersion, as described in Section 8.7, may be extended to multicomponent systems. Such an approach has been used by Thomas and Lombardi[9] and by Bradley and Sweed.[10]

Representative profiles showing the form of the concentration fronts and the fit of the theoretical profiles calculated from the binary equilibrium data and the constant-pattern assumption are shown in Figure 9.7. Benzene is the
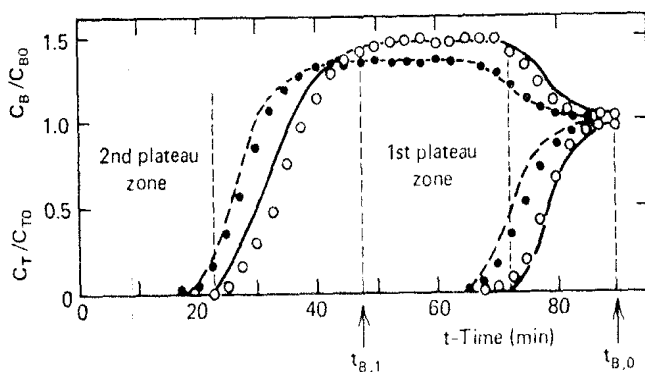
FIGURE 9.7. Comparison of experimental (●, ○) and theoretical (---, ———) breakthrough curves for benzene (B) and toluene (T) for vapor phase adsorption from a nitrogen carrier on an activated carbon adsorbent.

$$\text{○, } C_{B0}(\text{benzene}) = 1.07 \times 10^{-8} \text{ g mol/cm}^3$$
$$C_{T0}(\text{toluene}) = 20.6 \times 10^{-8} \text{ g mol/cm}^3 \quad \Bigg\rbrace \text{ flow rate}$$
$$\text{●, } C_{B0}(\text{benzene}) = 0.99 \times 10^{-8} \text{ g mol/cm}^3 \quad = 62 \text{ cm}^3/\text{min.}$$
$$C_{T0}(\text{toluene}) = 1.32 \times 10^{-8} \text{ g mol/cm}^3$$

[From ref. 9; reprinted by permission from *Trans. I. Chem. Engs.* **49** (1971).]

TABLE 9.1. Summary of Numerical Solutions for Isothermal Multicomponent Systems

Author	Rate Expression	Equilibrium Isotherm	Numerical Method	No. of Components	Experimental System
Carter and Husain[11]	Ext. fluid + Pore Diffusion	Modified Langmuir	Crank Nicolson + Forward finite difference	2 + carrier	CO_2-H_2O on 4A sieve
Zwiebel et al.[12,13]	Linear rate (fluid)	Langmuir	Characteristics	2 + carrier	CO_2-C_2H_6-Act. Carbon
Liapis and Rippin[14]a	Ext. fluid + Pore Diffusion	Empirical (nonlinear)	Collocation	2 + carrier	2-butanol + t-amylalcohol on Act. Carbon
Balzi, Liapis and Rippin[15]	1. Liquid Film 2. Solid Film 3. Ext. Fluid + Pore Diffusion	Empirical (nonlinear)	Finite Difference	3 + carrier	2-butanol + t-amyl alcohol + phenol on Act. Carbon
Santacesaria et al.[16]a	1. Pore Diffusion + Ext. Fluid 2. Linear Rate	Langmuir	Collocation	2 + carrier	C_8 Aromatics on KX, KY

a Axial dispersion is included. In the other papers plug flow is assumed.

less strongly adsorbed species and breaks through first with the concentration rising above the feed concentration. The theoretical curves, which were calculated according to the constant-pattern approximation with the "solid film" linearized rate model using overall mass transfer coefficients determined from single-component breakthrough curves, evidently provide a good representation of the behavior for the binary system.

General Numerical Simulation

The constant-pattern extension of equilibrium theory analysis is applicable only when the transition is, according to equilibrium theory, of shock form. When this condition is not met the only feasible approach to the prediction of the profile is the numerical solution of the coupled differential mass balance equations for the system. This approach has been followed by several authors and brief details of some of these studies are given in Table 9.1. As a representative example, the mathematical model used by Santacesaria et al.[14] is summarized in Table 9.2, while examples of some of the experimental breakthrough curves, together with the model predictions, are shown in Figure 9.8.

TABLE 9.2. The Model of Santacesaria et al.[16]

Fluid phase mass balance	$-D_L \dfrac{\partial^2 c_i}{\partial z^2} + v \dfrac{\partial c_i}{\partial z} + \dfrac{\partial c_i}{\partial t} + (\dfrac{1-\epsilon}{\epsilon}) \dfrac{\partial \bar{q}_i}{\partial t} = 0$
Mass transfer rate equation	$\dfrac{\partial \bar{q}_i}{\partial t} = k'(c_i - \bar{c}_i)$ $\dfrac{1}{k'} = \dfrac{R_p}{3k_f} + \dfrac{R_p^2}{15\epsilon_p D_p}$
Average conc. in adsorbed phase	$\bar{q}_i = (1 - \epsilon_p)q_i^*(\bar{c}_i) + \epsilon_p \bar{c}_i$
Equilibrium isotherm	$q_i^*(c_i) = \dfrac{bq_s c_i}{1 + \sum_j b_i c_i}$
Initial condition	$t = 0;\ \bar{c}_i(z,0) = c_{i0}'$ $\bar{q}_i(z,0) = q_i^*(c_{i0}') = b_i q_s c_{i0}'/(1 + \sum b_i c_{i0}')$
Boundary conditions	$z = 0;\ t > 0;\ vc_{i0} = vc_i(0,t) - D_L \left. \dfrac{\partial c_i(z,t)}{\partial z} \right|_{z=0}$ $z = L;\ t > 0;\ \left. \dfrac{\partial c_i(z,t)}{\partial z} \right|_{z=L} = 0$

(a)

(b)
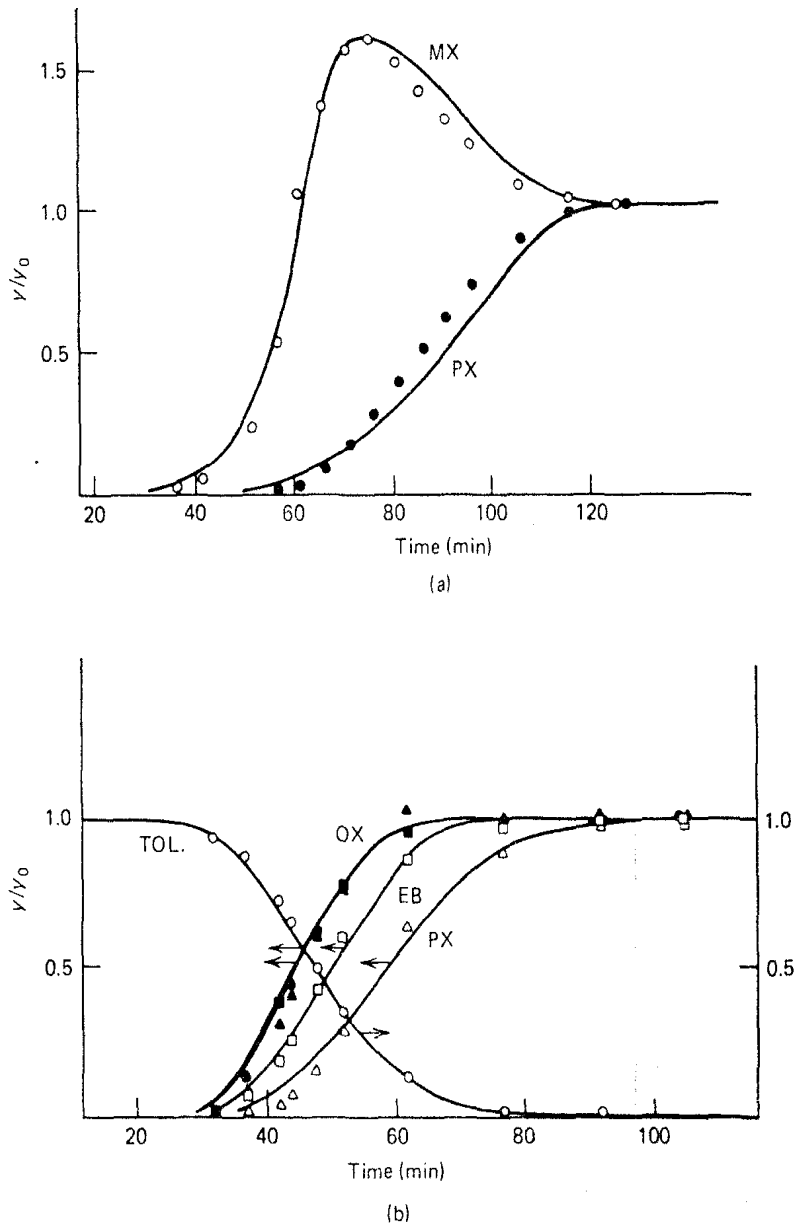
FIGURE 9.8. Comparison of theoretical and experimental breakthrough curves for C_8 aromatics on KY zeolite. (a) Initial composition, 100% i-octane. Feed composition, 5% m-xylene + 5% p-xylene + 90% n-octane (O, MX; ●, PX). (b) Initial composition, 100% toluene. Feed composition, 49% m-xylene, 9% o-xylene, 22% p-xylene, 13.5% ethylbenzene, 6.5% m-octane (O, T; ●, MX; ▲, OX; □, EB; △, PX). (Reprinted with permission from ref. 16. Copyright 1978 American Chemical Society.)

The model of Santacesaria et al.[16] is an extension of the linear driving force model, with fluid side resistance, for a nonlinear multicomponent Langmuir system. It includes axial dispersion, and the combined effects of pore diffusion and external fluid film resistance are accounted for through an overall rate coefficient. Intracrystalline diffusional resistance is neglected and equilibrium between the fluid in the macropores and in the zeolite crystals is

assumed. In typical commercial KY zeolite the crystal size is small (< 1 μm) and the assumption of negligible intracrystalline resistance may be justified on the basis of a comparison of the estimated time constants for intracrystalline and macropore diffusion. The validity of the Danckwerts boundary conditions under transient conditions has been confirmed by van Cauwenberghe[49].

In the calculation of the predicted response curves the axial dispersion coefficient and the external mass transfer coefficient were estimated from standard correlations and the effective pore diffusivity was determined from batch uptake rate measurements with the same adsorbent particles. The model equations were solved by orthogonal collocation and the computation time required for the collocation solution ($\sim$20 s) was shown to be substantially shorter than the time required to obtain solutions of comparable accuracy by various other standard numerical methods. It is evident that the fit of the experimental breakthrough curves is good. Since all parameters were determined independently this provides good evidence that the model is essentially correct and demonstrates the feasibility of modeling the behavior of fairly complex multicomponent dynamic systems.

9.6. EQUILIBRIUM THEORY OF ADSORPTION COLUMN DYNAMICS FOR ADIABATIC SYSTEMS

From the perspective of multicomponent chromatography, enthalpy can be considered as directly equivalent to an additional adsorbed species. There is therefore complete formal similarity between an n-component isothermal system and an $n - 1$ component adiabatic system. This however is true only in the limiting case of an adiabatic system in which enthalpy, like the total mass of each component, is conserved. In the general case of a nonisothermal system involving significant heat loss from the column wall, the analogy breaks down. Indeed, as heat losses increase, ideal isothermal behavior is eventually approached. Real systems therefore encompass the entire spectrum from near adiabatic to near isothermal, and since the behavior of isothermal and adiabatic systems is quite different it is important in the analysis of any particular system to know whether either of the extreme cases can be regarded as a reasonable representation or whether a more general model including finite heat loss is required.

The importance of heat effects in adsorption column dynamics appears first to have been recognized by Leavitt[17] in the early 1960s but detailed analysis came only some years later. The equilibrium theory of an adiabatic adsorption column, which is closely related to the equilibrium theory of multicomponent adsorption, was first developed by Amundson, Aris, and Swanson[18] and the analysis was extended by Pan and Basmadjian[19,20] who also verified some aspects of the theory in an experimental study of the adsorption of CO_2 and 5A molecular sieve. These initial developments were expanded into a more complete treatment by Rhee, Amundson, and Heerdt[21-25] as well as in later

work by Basmadjian et al.[26-28] The subject has been reviewed more recently by Sweed.[29]

For an adiabatic two-component system (one adsorbable species in an inert carrier) the concentration profile consists, in general, of two transitions or mass transfer zones, over which both concentration and temperature vary, separated by a plateau region of constant temperature and concentration. However, the first transition may be degenerate, involving only a change in temperature with no change in concentration. This is sometimes referred to as a pure thermal wave. Also in certain cases where the watershed is crossed an additional transition may occur.

As an example of the application of equilibrium theory to nonisothermal systems we consider here a plug flow system, with one adsorbable component, in which the concentration of adsorbable species and the temperature changes are both small enough to validate the constant velocity approximation. For such a system the differential mass and heat balance equations are

$$v\frac{\partial c}{\partial z} + \frac{\partial c}{\partial t} + \left(\frac{1-\epsilon}{\epsilon}\right)\frac{\partial \bar{q}}{\partial t} = 0 \tag{9.32}$$

$$v\frac{\partial T_f}{\partial z} + \frac{\partial T_f}{\partial t} + \left(\frac{1-\epsilon}{\epsilon}\right)\frac{C_s}{C_f}\frac{\partial T_s}{\partial t} = \left(\frac{1-\epsilon}{\epsilon}\right)\left(\frac{-\Delta H}{C_f}\right)\frac{\partial \bar{q}}{\partial t} \tag{9.33}$$

Assuming thermal and mass transfer equilibrium $T = T_f = T_s$, $\bar{q} = q^* = f(c, T)$, and $\partial \bar{q}/\partial t = (dq^*/dc)(\partial c/\partial t) = (dq^*/dT)(\partial T/\partial t)$ so that Eqs. (9.32) and (9.33) become

$$\frac{\partial T}{\partial z} + \frac{1}{v}\left[1 + \left(\frac{1-\epsilon}{\epsilon}\right)\frac{C_s}{C_f} - \left(\frac{1-\epsilon}{\epsilon}\right)\left(\frac{-\Delta H}{C_f}\right)\frac{dq^*}{dT}\right]\frac{\partial T}{\partial t} = 0 \tag{9.34}$$

$$\frac{\partial c}{\partial z} + \frac{1}{v}\left[1 + \left(\frac{1-\epsilon}{\epsilon}\right)\frac{dq^*}{dc}\right]\frac{\partial c}{\partial t} = 0 \tag{9.35}$$

These equations are of charcteristic hyperbolic form and represent kinematic waves with propagation velocities given by

$$w_T = \cfrac{v}{1 + \left(\cfrac{1-\epsilon}{\epsilon}\right)\cfrac{C_s}{C_f} - \left(\cfrac{1-\epsilon}{\epsilon}\right)\left(\cfrac{-\Delta H}{C_f}\right)\cfrac{dq^*}{dt}}, \qquad w_c = \cfrac{v}{1 + \left(\cfrac{1-\epsilon}{\epsilon}\right)\cfrac{dq^*}{dc}}$$

$$\tag{9.36}$$

Coherence requires that for any point (c, T) these velocities must be equal so in analogy with Eq. (9.15) we have

$$\frac{dq^*}{dc} = \frac{C_s}{C_f} - \left(\frac{-\Delta H}{C_f}\right)\frac{dq^*}{dT} \tag{9.37}$$

$$\frac{\partial q^*}{\partial c} + \frac{\partial q^*}{\partial T}\frac{dT}{dc} = \frac{C_s}{C_f} - \left(\frac{-\Delta H}{C_f}\right)\left(\frac{\partial q^*}{\partial T} + \frac{\partial q^*}{\partial c}\frac{dc}{dT}\right) \tag{9.38}$$

The analog of Eq. (9.21) is

$$\left(\frac{\partial q^*}{\partial T}\right)_c \left(\frac{dT}{dc}\right)^2 + \left[\left(\frac{\partial q^*}{\partial c}\right)_T - \frac{C_s}{C_f} + \left(\frac{-\Delta H}{C_f}\right)\left(\frac{\partial q^*}{\partial T}\right)_c\right]\left(\frac{dT}{dc}\right)$$

$$+ \left(\frac{\partial q^*}{\partial c}\right)_T\left(\frac{-\Delta H}{C_f}\right) = 0 \tag{9.39}$$

This equation may be considered as a quadratic for dT/dc. All derivatives may be evaluated from the equilibrium relationship, provided that the temperature dependence of the equilibrium constant is known. Since adsorption is generally exothermic, $(\partial q^*/\partial T)_c$ is negative and $(\partial q^*/\partial c)_T$ is positive. The equation therefore has two real roots, one positive and one negative, and two corresponding velocities [given by Eq. (9.36)]. The higher velocity is associated with the positive root. Corresponding to Eq. (9.13) the velocity of a shock transition is given by

$$w_T' = \frac{v}{1 + \left(\frac{1-\epsilon}{\epsilon}\right)\left(\frac{C_s}{C_f} - \left(\frac{-\Delta H}{C_f}\right)\frac{\Delta q^*}{\Delta T}\right)}, \qquad w_c' = \frac{v}{1 + \left(\frac{1-\epsilon}{\epsilon}\right)\frac{\Delta q^*}{\Delta c}}$$

$$\tag{9.40}$$

with the integral coherence requirement, analogous to Eq. (9.15), given by

$$\frac{\Delta q^*}{\Delta c} = \frac{C_s}{C_f} - \left(\frac{-\Delta H}{C_f}\right)\frac{\Delta q^*}{\Delta T} \tag{9.41}$$

Apart from the difference in the form of the equilibrium relationships there is complete formal similarity between the single-component adiabatic system and the general two-component isothermal system which was considered previously. However, for an adiabatic system, the $c - T$ (or $q - T$) characteristics are generally nonlinear so the simplicity of the ideal binary Langmuir

TABLE 9.3. Equilibrium Data for
Adsorption of Benzene on Charcoal[30]

$\epsilon = 0.5$

$C_s = 405$ cal/L K

$C_f = 2.7$ cal/L K

$$\frac{q^*}{q_s} = \frac{bc}{1 + bc}$$

$q_s = 5.5$ mole/L adsorbent

c is expressed in moles benzene/L gas

$b = b_0\sqrt{T}\,e^{-\Delta H/RT}$

$b_0 = 3.88 \times 10^{-5}$ L/mole K$^{1/2}$

$\Delta H = -10,400$ cal/mole

$T = $ temperature in K

$P = 10$ atm

isothermal system does not extend to the adiabatic case. This means that an adiabatic system commonly shows selectivity reversal and the shock and wave characteristics are not coincident.

In order to illustrate the application of this theory we consider the numerical example discussed by Rhee et al.[21-25] and later by Sweed[29]; the adsorption of benzene from a nitrogen carrier on a charcoal adsorbent. Equilibrium data for this system obtained by James and Phillips,[30] and correlated in the form of a Langmuir isotherm are summarized in Table 9.3.

For a nonisothermal system the characteristics are no longer linear and must be calculated by numerical integration from the analog of Eq. (9.24):

$$T' = T_0' - \Delta T, \qquad c' = c_0' - \frac{dc}{dT}\bigg|_{T_0', c_0'} dT$$

$$T'' = T' - \Delta T, \qquad c'' = c' - \frac{dc}{dT}\bigg|_{T', c'} dT \tag{9.42}$$

where dc/dT is given by the roots of Eq. (9.39). The hodograph plot (c vs. T) calculated in this way is shown in Figure 9.9. Corresponding to the two roots we get two different families of characteristic curves, and two corresponding
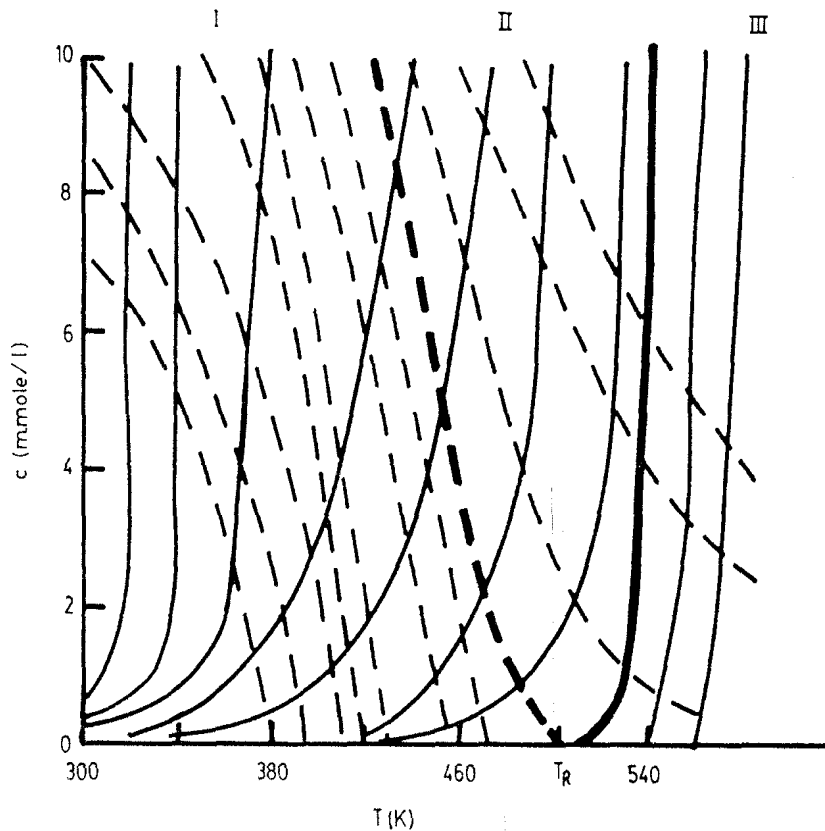
FIGURE 9.9. Hodograph plot for benzene–nitrogen–charcoal adiabatic system. Positive characteristics (Γ_+), ———; negative characteristics (Γ_-), ---. The critical characteristics passing through the point of selectivity reversal (T_R) are shown by heavy lines. (After refs. 21 and 29; reprinted with permission of Martinus Nijhoff Publishers.)

velocities at each point (T, c) given by Eq. (9.36), with the velocity for the positive root (corresponding to Γ_+) being always greater than that for the negative root (corresponding to Γ_-).

The watershed point (point of selectivity reversal T_R) occurs at $c = 0$, $T = 505$ K. The positive characteristic which passes through T_R divides the family of positive characteristics into those which intersect the T axis (high-temperature region) and those which are asymptotic to the T axis $(T < T_R)$. Similarly for $T < T_R$ the negative characteristics intersect the T axis while for $T > T_R$ the negative characteristics are asymptotic. The critical characteristics, passing through T_R, define three distinct regions (I, II, and III) in which there are important differences in the behavior of the bed.

The path between any initial state (c_0', T_0') and final state (c_0, T_0) may be deduced from the hodograph in the same way as for an isothermal binary system. Glueckauf's rule 1 allows the correct path to be selected from the two alternative coherent paths which may be drawn by following the characteristic curves. The distinction between a simple wave and a shock transition requires calculation of the wave velocities along the characteristics. A minor complication arises since the shock characteristic is no longer coincident with the characteristic for a simple wave transition and must be calculated separately from the equilibrium relation and the integral coherence condition [Eq. (9.41)].

The following examples illustrate the use of the hodograph plot for determining the form of the concentration and temperature profiles.

1. *Elution of Uniformly Saturated Bed with Pure Solvent (Figure 9.10a, b, c)*

Initial State (A)	Final State (B)
$c_0' = 10.0$	$c_0 = 0$
$q_0' = 5.27$	$q_0 = 0$
$T_0' = 350$	$T_0 = 350$

(c in mmole/L, q in mole/L solid adsorbent, T in K). The relevant $c - T$ characteristics are sketched in Figure 9.10a. The path follows ADB (Γ_+ from initial state to plateau D, Γ_- from plateau to feed point). The wave velocity, calculated from Eq. (9.36), decreases $A \to D \to B$ so both transitions are simple proportionate pattern waves. The $t - z$ characteristics, concentration, and temperature profiles are sketched in Figures 9.10b and c. There are two mass transfer zones, both of the simple wave type, separating a plateau region corresponding to point D.

2. *Saturation of a Clean Bed (Figure 10a, d, e)*

Initial State (B)	Final State (A)
$c_0' = 0$	$c_0 = 10.0$
$q_0' = 0$	$q_0 = 5.27$
$T_0' = 350$	$T_0 = 350$
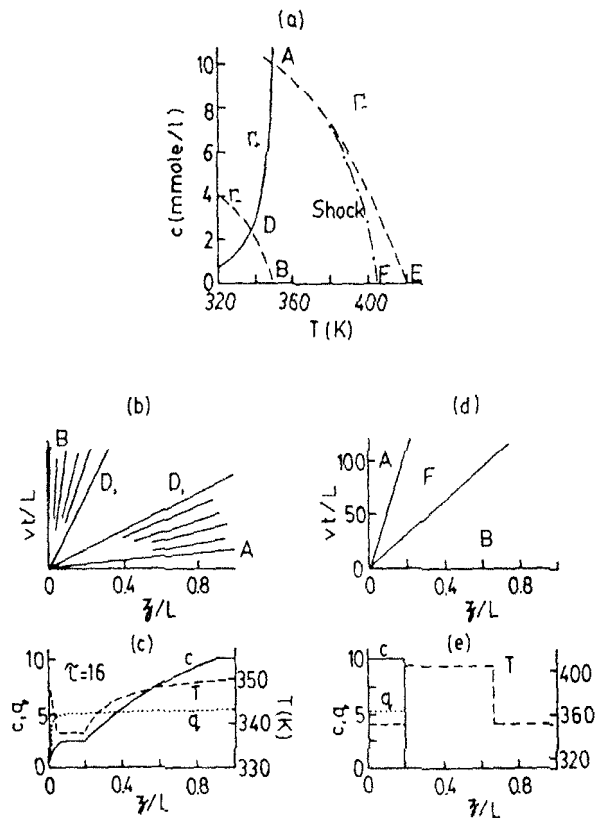
FIGURE 9.10. (a) Hodograph plot showing relevant characteristics for examples 1 and 2; (b) $z-t$ characteristics and (c) profiles for example 1; (d) $z-t$ characteristics and (e) profiles for example 2.[23,29] (Reprinted by permission from *Chem. Eng. J.*, 1 (1970) 279.)

This example is the inverse of example 1 involving a transition in the reverse direction between the same two points. Calculations according to Eq. (9.36) reveal that the wave velocity remains constant along BE and increases along $E \to A$ (or $B \to D$). To satisfy the requirement that the initial state propagate ahead of the feed and to avoid the physically unrealistic overhanging type of profile the path must follow BF (rather than BD) and the gradual wave transition $E \to A$ must be replaced by the shock $F \to A$. The shock characteristic and hence the location of point F is found from Eq. (9.40). The resulting $z - t$ characteristics and the corresponding concentration and temperature profiles are shown in Figures 9.10d and e.

The profile again shows a plateau region bounded by two transitions, but in this case both transitions are shocks and the leading transition is a "pure thermal wave" which is accompanied by no change in concentration. Changing the initial bed temperature affects only the magnitude of the leading thermal wave and has no effect on the mass transfer zone. This pattern of behavior occurs whenever the feed state is located within region I of Figure 9.9. This is the most common situation for adsorption from the vapor phase. There are important practical implications since it follows that the temperature at which adsorption occurs, and therefore the form of the mass transfer

front, is determined entirely by the condition of the feed and is not affected by the initial bed temperature. This means that in a thermal swing process the traditional cooling step which is included following the high-temperature regeneration cycle can be omitted with no adverse effect on the subsequent adsorption cycle. This condition has been verified experimentally by Basmadjian[28] for the CO_2-He-5A sieve system. (Figure 9.15, taken from Basmadjian's work, shows clearly that although the form of the breakthrough curve differs considerably from the shock front predicted by equilibrium theory, the conclusion that the breakthrough capacity is not affected by initial bed temperature is accurately fulfilled.)

3. *Elution with Selectivity Reversal (Figure 9.11a, b, c)*

Initial State (A′)	Feed State (B′)
$c_0' = 5.0$ mmole/L	$c_0 = 0$
$q_0' = 0.32$ mole/L	$q_0 = 0$
$T_0' = 550$ K	$T_0 = 480$ K

As in example (1) the path from the initial state follows the positive characteristic $A' - H$ but the feed point B' now lies on the other side of the watershed. From H to B' the path follows the T axis which for $H \rightarrow T_R$ is the limiting negative characteristic and for $T_R \rightarrow B'$ is the limiting positive characteristic. The wave velocity decreases along $A' \rightarrow H$ so the leading transition is a proportionate-pattern wave while $H \rightarrow B'$ is a pure thermal wave (shock). The $z - t$ characteristics and the concentration and temperature profiles are shown in Figure 9.11b and c. In this case we have an example of a pure thermal wave formed during desorption and lagging behind the mass transfer zone. Altering the temperature of the inlet stream merely modifies the form of the pure thermal wave with no effect on the concentration profile.

4. *Elution by Cool Feed (Figure 9.11a, d, e)*

Initial State (A′)	Feed State (B″)
$c_0' = 5.0$ mmole/L	$c_0 = 5.0$ mmole/L
$q_0' = 5.32$ mole/L	$q_0 = 2.054$ mole/L
$T_0' = 550$ K	$T_0 = 440$ K

The problem is similar to example 3 in that the feed and initial states lie on opposite sides of the watershed but the feed point no longer lies on the T axis. The problem can conveniently be divided into two problems: the paths $A' \rightarrow T_R$ and $T_R \rightarrow B''$. The path $A' \rightarrow T_R$ is affected by the initial condition of the bed (i.e., the location of A') but it is independent of the feed condition
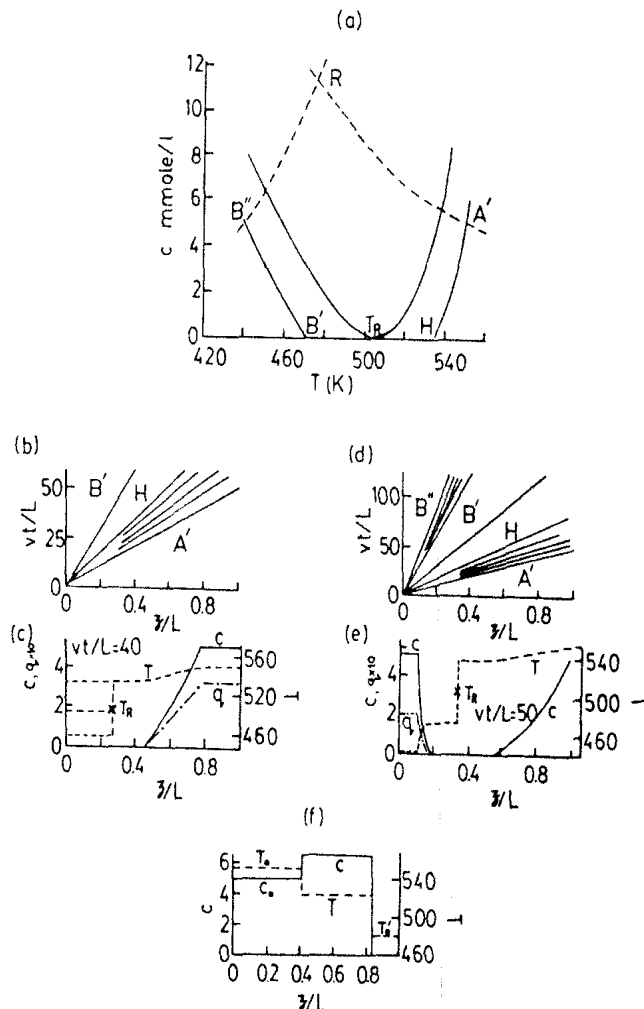
FIGURE 9.11. (a) Hodograph plot showing relevant characteristics for examples 3 and 4; (b) $z-t$ characteristics; (c) profiles for example 3; (d) $z-t$ characteristics; (e) profiles for example 4; and (f) $z-t$ profiles for saturation with hot feed.[23,29] (Reprinted by permission from *Chem. Eng. J.* **1** (1970) 279.)

(i.e., the location of point B''). The path $T_R \rightarrow B''$ is affected by the feed condition (i.e., the location of point B'') but it is independent of the initial bed condition (A'). For this particular example the path $A' \rightarrow T_R$ follows $A' \rightarrow H$ (proportionate-pattern wave) and $T_R \rightarrow B''$ (pure thermal wave), just as in example 3. The path $T_R \rightarrow B''$ follows $T_R - B'$ (pure thermal wave as in example 3) and then $B' \rightarrow B''$ along the negative characteristic. The wave velocity decreases along $B' \rightarrow B''$ so this transition is a proportionate-pattern wave. The $z - t$ characteristics and profiles are sketched in Figure 9.11d and e. It may be seen that there are now three transitions and two plateaux. A pure thermal wave lies between the leading front which is a desorption mass transfer zone, and the trailing front which is an adsorption mass transfer zone. Between these two mass transfer zones the sorbate concentration falls to zero. Whenever the initial state lies within region III, and the feed state lies within
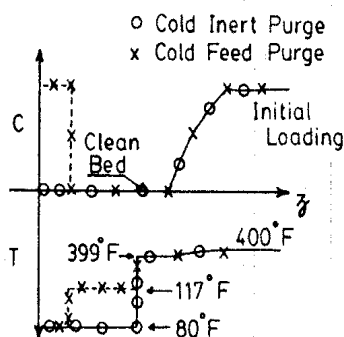
FIGURE 9.12. Theoretically calculated equilibrium profiles for desorption of a bed of 5A molecular sieve, saturated initially with CO_2 at 400 °F, with cold inert purge with cold-feed purge. (Reprinted with permission from ref. 26. Copyright 1975 American Chemical Society.)

region I (Figure 9.9), changes in the feed condition have no effect on the leading mass transfer (desorption) zone. The quantity of feed required for complete desorption is therefore independent of either the composition or temperature of the purge stream. This means that the adsorbent bed may be regenerated using a cool purge stream or even a cool stream of the same composition as that with which the bed was originally saturated. This possibility is illustrated in Figure 9.12, which shows theoretical profiles for desorption of CO_2 from a bed of 5A molecular sieve using a purge of clean cold inert and cold feed. The desorption profiles are seen to be the same in both cases.[26]

The behavior of a clean bed at initial temperature $T_0' < T_R$ (region I) when contacted with a feed in region III is illustrated in Figure 9.11f. The concentration profile shows "roll-up," that is, the plateau concentration is higher than either the initial state or the feed concentration. (The particular profile shown corresponds to a bed with initial state at or near B' contacted by a feed corresponding to point A' in Figure 9.11a.) If a bed in state B'' is contacted with hot feed corresponding to state A' the path goes via $B'' \rightarrow R$ and $R \rightarrow A'$ and the profile, which is qualitatively similar to Figure 9.11f, consists of two shocks separating a plateau region of high concentration and intermediate temperature ($c = 11.3$ mmole/L, $T = 478$ K). It is evident that a continuous cyclic separation may be achieved by a judiciously chosen sequence in which the bed is alternately contacted with hot and cool feed. For example for operation between the points A' and B'' there is an initial period during which the effluent concentration is equal to or lower than the feed followed by a period, corresponding to the region $H \rightarrow B'$, during which essentially sorbate-free carrier is eluted. During the hot cycle the effluent is initially in the same state as the cool feed (B''). There is then a period, corresponding to the plateau point R, during which an effluent enriched in sorbate is obtained. The hot cycle is terminated when the second front ($R - A'$) just reaches the outlet. The practical application of this concept has been demonstrated by Jacobs and Tondeur[31] for separation of a mixture of n- and isopentane on 5A sieve. Their cycle is illustrated in Figure 9.13.

The profiles sketched in Figure 9.11e illustrate an exception to the general rule that in an adiabatic system containing one adsorbable species in an inert carrier there are two transitions. An additional transition is introduced when the watershed is crossed unless either feed or initial state lies on the T axis
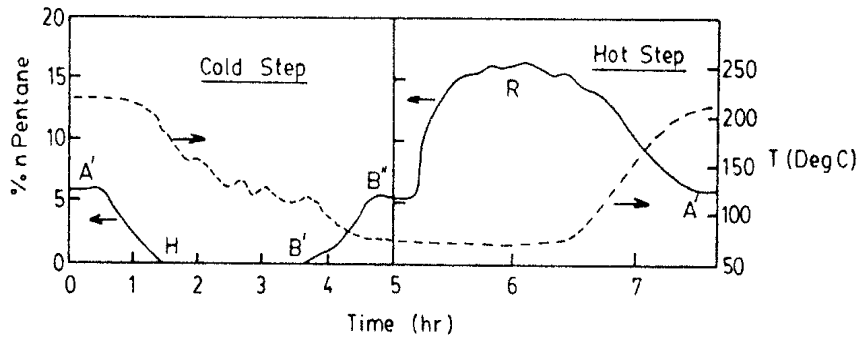
FIGURE 9.13. Experimental concentration and temperature at the bed outlet for thermal swing cyclic separation of n- and isopentane on 5A molecular sieve. The process operates between two points on opposite sides of T_R (such as B'' and A' in Figure 9.11a) and the trajectory during the hot step follows $B'' \rightarrow R \rightarrow A'$ and $A' \rightarrow H \rightarrow B' \rightarrow B''$ during the cold step. Pure i-pentane is withdrawn between H and B' and an enriched level of n-pentane is obtained at the plateau corresponding to point R. (Reprinted from Ref. 31, p. 1572, by courtesy of Marcel Dekker, Inc.)
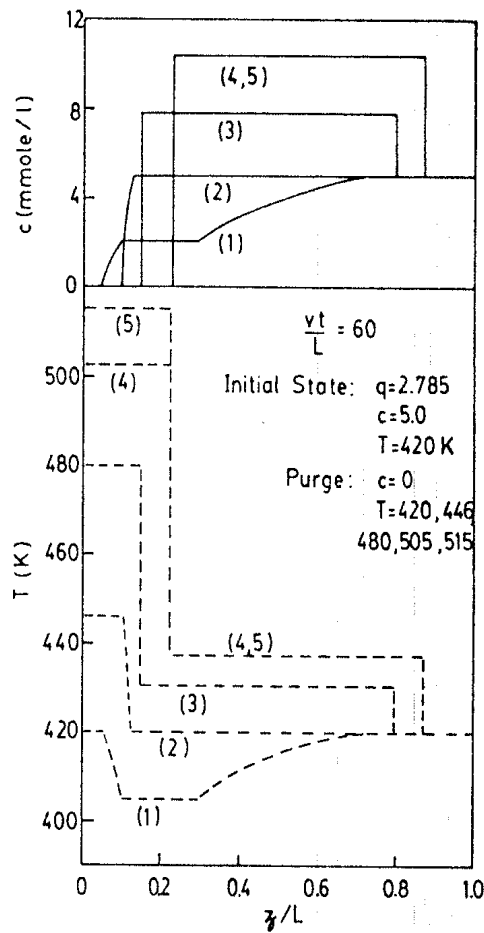
FIGURE 9.14. Calculated profiles for the system of Figure 9.9 showing the effect of purge temperature. In all cases the initial state corresponds to $c = 5.0$ mmole/L, $q = 2.785$ mole/L, $T = 420$ K. The purge stream is sorbate free.

(zero concentration). A further exception to this general rule occurs when both initial and feed states lie on the same characteristic. In such circumstances there is only one transition as illustrated in Figure 9.14, curve 2.

In the examples selected for detailed discussion the profiles have all had the form of either simple proportionate-pattern waves or simple shocks. When there is an inflection in the characteristic a combined wave, consisting partly of a shock and partly of a simple wave, may occur (see Section 8.4, Figure 8.6). However such details do not affect the broad pattern of the behavior of the system.

Conditions for Formation of Pure Thermal Wave

For a pure thermal wave to be formed during adsorption the temperature front must precede the mass transfer zone. This can occur only when the initial state lies on the T axis (i.e., a clean bed) and the feed state lies on the negative characteristic to the left of the critical characteristic in Figure 9.9 (region I). Under these conditions the T axis takes the place of the positive characteristic through the initial state.

A pure thermal wave, lagging behind the mass transfer zone, may also be formed during desorption. For this to occur the initial state must lie on a positive characteristic to the right of the critical characteristic in Figure 9.9 (region III) and the feed must contain no adsorbate. Under these conditions the T axis takes the place of the negative characteristic through the feed state.

A pure thermal wave is always a shock and from Eq. (9.36) it is clear that its velocity is given by $v/\{1 + [(1 - \epsilon)/\epsilon]C_s/C_f\}$ while the velocity of the mass transfer front is given by $v/\{1 + [(1 - \epsilon)/\epsilon]dq^*dc\}$. For the thermal wave to precede the concentration front (adsorption) therefore requires $(dq^*/dc)_{c=0} > C_s/C_f$ while for a pure thermal wave lagging the concentration front to be formed during desorption $(dq^*/dc)_{c=0} < C_s/C_f$. At the watershed point (T_R), $(dq^*/dc)_{c=0} = C_s/C_f$ and the velocity of the limiting proportionate-pattern wave is the same as that of the thermal shock. A more detailed discussion of the conditions of thermal wave formation and the practical importance of this type of behavior has been given by Basmadjian.[19]

Effect of Regeneration Temperature

Equilibrium theory provides useful insight into the choice of regeneration conditions for a thermal swing adsorption process. As illustrated in the preceding examples, three different patterns of behavior are observed, depending on the initial conditions of the bed in relation to the critical characteristics. The desorption behavior of a bed with an initial state located in region I of Figure 9.9 (the low-temperature region) is illustrated in Figure 9.14. This is the most common situation in a vapor phase system. With increasing regeneration

temperature the level of the plateaux of both temperature and concentration increases until at 446 K the initial state and the feed state lie on the same characteristic, as may be seen from Figure 9.9. At this point the plateau and initial states coincide and there is only one transition which is of the proportionate-pattern type. Further increase in purge temperature leads to "roll-up" (i.e., the concentration at the plateau rises above the initial concentration) and both front and rear transitions become shock waves. When the purge temperature reaches the watershed value (505 K for this system) the profile corresponding to curve 4 is obtained and further increase in temperature leads merely to an increase in the rear thermal shock wave without any effect on the concentration profile. It is evident that the time and therefore the purge volume required for complete regeneration of the bed decreases as the purge temperature is increased up to T_R, but further increase in temperature beyond T_R gives no further reduction and is therefore economically undesirable.

The behavior of a bed with initial loading in region II is somewhat similar except that in the case of a low-temperature purge the simple waves are replaced by shocks. This situation is discussed in detail by Rhee and Amundson.[23]

When the initial state lies in region III (high-temperature region), as in example (4), the pattern of behavior is quite different. The thermal wave lags behind the mass transfer zone and, as may be seen from Figure 9.11c, increasing the purge temperature merely affects the thermal wave with no effect on the concentration profile. These are the conditions under which the bed may be regenerated with a cold purge or even directly with cold feed and, since it is not necessary to cool the bed, a continuous cyclic adsorption–desorption operation may be carried out merely by changing the feed temperature, as illustrated in Figures 9.12 and 9.13.

Comparison with Experiment

Figures 9.15 and 9.16 show experimental data obtained by Basmadjian and co-workers with the system CO_2-5A sieve. Equilibrium theory predicts that at temperatures below the reversal temperature (region I of Figure 9.9) changes in the initial bed temperature have no effect on the concentration break-
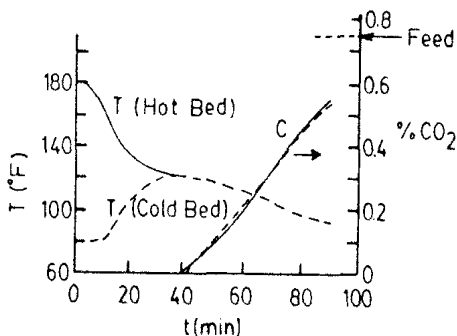
FIGURE 9.15. Experimental concentration and temperature breakthrough curves for adsorption of 0.75% mole CO_2 from He on 5A molecular sieve at 1 atm showing the effect of initial bed temperature (80 or 180°F). Feed temperature, 80°F. (From ref. 28; reprinted with permission from *Canadian Journal of Chemical Engineering* **53**, 234, 1975.)
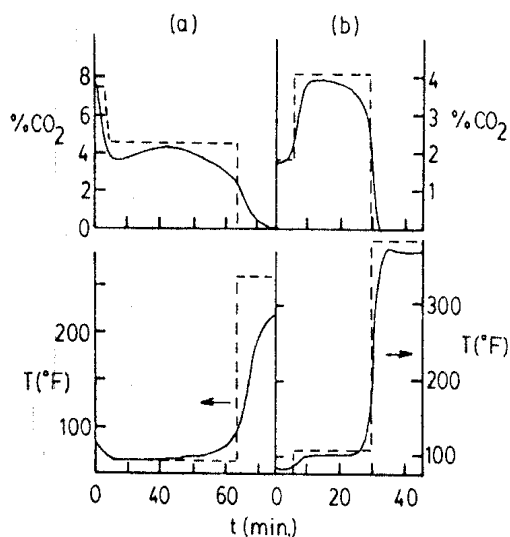
FIGURE 9.16. Comparison of experimental (———) and theoretical (---) equilibrium theory desorption curves for a bed of 5A molecular sieve saturated initially with CO_2-He and desorbed with pure He. (a) Initial bed temperature, 80°F, 7.5% CO_2 at 1 atm; (b) Initial bed temperature, 80°F, 1.8% CO_2 at 1 atm. (Reprinted with permission from ref. 27. Copyright 1975 American Chemical Society.)

through curve and this is seen to be verified (Figure 9.15). From Figure 9.16 it is evident that the theoretical curves from equilibrium theory provide a good approximation to the experimentally observed behavior although the precise form of the response curves is not predicted. To calculate the equilibrium theory profiles requires only a knowledge of the equilibrium relationship $q^* = q^*(c, T)$ over the relevant range of temperature and concentration and information on heat capacities of bed and fluid. On this basis it is possible to predict the effects of changes in operating conditions and to obtain useful guidance in the selection of optimal operating conditions for sorption processes. Design and final optimization may require more detailed calculations taking into account heat and mass transfer resistance, but the comparative simplicity of the equilibrium theory approach makes it an important initial step in preliminary process analysis, optimization, and design.

9.7. ADIABATIC AND NEAR ADIABATIC SYSTEMS WITH FINITE MASS TRANSFER RESISTANCE

Analytic Solution for Irreversible Equilibrium (One Adsorbable Component)

When mass transfer resistance is important the dynamic behavior of an adsorption column can generally be predicted only by numerical solution of the coupled differential heat and mass balance equations which describe the system. However, in the extreme case of an irreversible isotherm with q_s independent of temperature, the differential mass balance and mass transfer

rate equations become, to a first approximation, independent of temperature and therefore independent of the heat balance. Under these conditions a formal analytic solution may be derived, and if the mass transfer rate expression is sufficiently simple, the expressions for the concentration and temperature profiles may be obtained in closed form. Such solutions have been obtained by Ozil and Bonnetain[32] and by Yoshida and Ruthven.[33] These solutions provide considerable insight into the qualitative behavior of an adiabatic system and are therefore discussed in some detail.

Subject to the assumptions of plug flow, thermal equilibrium between fluid and solid and constant linear fluid velocity, the differential mass and heat balance equations for an adiabatic column are given by Eqs. (9.32) and (9.33), while for an irreversible system, the equilibrium isotherm is given by

$$q^* = 0, \quad c = 0, \quad q^* = q_s, \quad c > 0 \tag{9.43}$$

Expressed in dimensionless form Eqs. (9.32) and (9.33) become

$$\left(\frac{\partial \phi}{\partial \xi}\right)_\tau + \left(\frac{\partial \psi}{\partial \tau}\right)_\xi = 0 \tag{9.44}$$

$$\left(\frac{\partial \theta}{\partial \tau}\right)_\xi + \gamma \left(\frac{\partial \theta}{\partial \xi}\right)_\tau = \left(\frac{\partial \psi}{\partial \tau}\right)_\xi \tag{9.45}$$

where $\gamma = q_0 C_f / c_0 C_s$. If we put $\xi' = \xi - \gamma\tau$, Eq. (9.45) becomes

$$\left(\frac{\partial \theta}{\partial \tau}\right)_{\xi'} = \left(\frac{\partial \psi}{\partial \tau}\right)_\xi \tag{9.46}$$

The assumption of an irreversible equilibrium relationship means that the concentration profile is not affected by temperature and is therefore the same as for an isothermal system. The simplest kinetic model is the linear rate expression for which the solution for the concentration profile has been given by Cooper[34] (see Section 8.6):

$$\frac{\partial \bar{q}}{\partial t} = k(q^* - \bar{q}), \quad \left(\frac{\partial \psi}{\partial \tau}\right)_\xi = 1 - \psi \tag{9.47}$$

$$\xi < 1.0, \qquad \psi = 1 - e^{-\tau}, \qquad \phi = 1 - \xi e^{-\tau}, \qquad \left(\frac{\partial \theta}{\partial \tau}\right)_{\xi'} = e^{-\tau}$$

$$1 \leqslant \xi \leqslant 1 + \tau, \qquad \psi = \phi = 1 - e^{\xi - \tau - 1}, \qquad \left(\frac{\partial \theta}{\partial \tau}\right)_{\xi'} = e^{\xi - \tau - 1} \tag{9.48}$$

$$1 + \tau \leqslant \xi, \qquad \psi = \phi = 0, \qquad \left(\frac{\partial \theta}{\partial \tau}\right)_{\xi'} = 0$$

For saturation of an initially clean bed the appropriate initial and boundary conditions are

$$
\begin{array}{llll}
\tau = 0, & \theta = 0 & \text{for} & 0 < \xi < 1.0 \\
\tau > 0, & \theta = 0 & \text{at} & \xi = 0 \\
& \theta = 0 & \text{at} & \xi = 1 + \gamma\tau \quad (\gamma > 1.0) \\
\text{or} & \theta = 0 & \text{at} & \xi = 1 + \tau \quad (\gamma < 1.0)
\end{array}
\tag{9.49}
$$
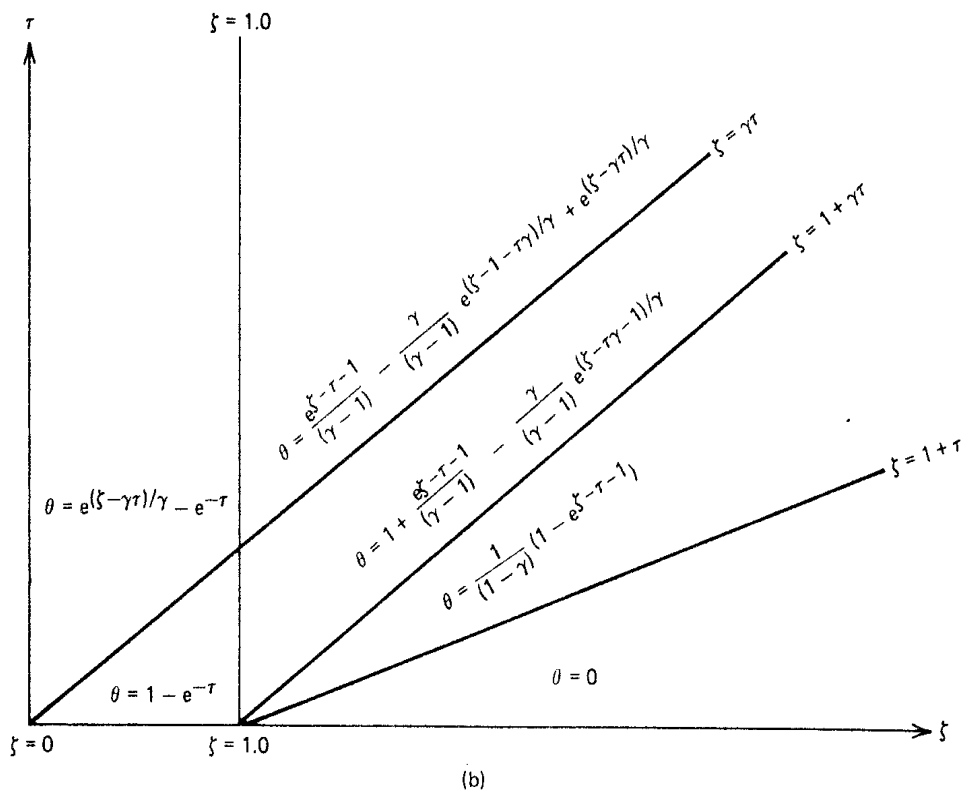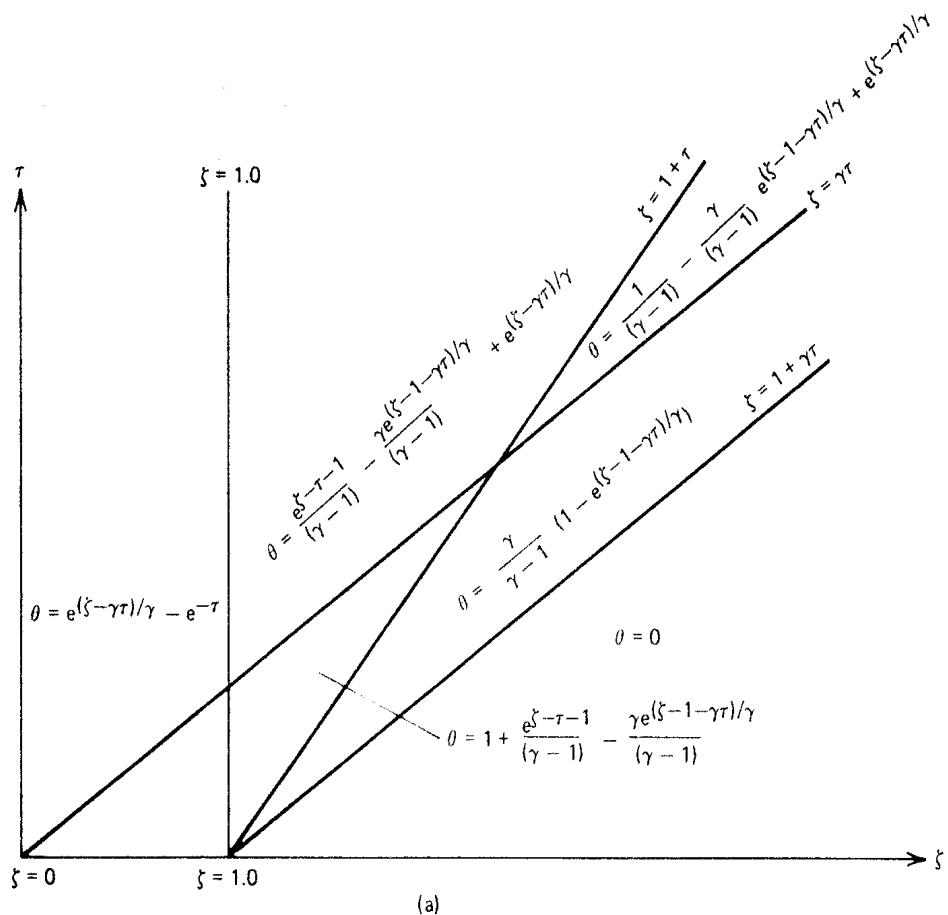
FIGURE 9.17. Theoretical solution for temperature response in an adiabatic system with irreversible equilibrium and linear rate expression: (a) Thermal front leads, $\gamma > 1.0$; (b) thermal front lags, $\gamma < 1.0$. [Reprinted with permission from *Chem. Eng. Sci.* **37**, Yoshida and Ruthven (ref. 33). Copyright 1983, Pergamon Press, Ltd.]

The solution for the temperature profile may be obtained by integrating Eq. (9.46) along the characteristics (ξ' constant), starting from any point in the $\xi - \tau$ plane at which θ is known and using the appropriate expression for $(\partial\psi/\partial\tau)_\xi$ from Eq. (9.47). Two distinct solutions are obtained depending on whether $\gamma > 1.0$ (velocity of thermal front greater than velocity of mass transfer front) or $\gamma < 1.0$ (velocity of thermal front less than velocity of mass transfer front). Since the expressions for $(\partial\psi/\partial\tau)_\xi$ are different in different regions of the bed, the final solution assumes different forms in the different regions.

The expressions for the temperature profile derived in this way are summarized in Figure 9.17. Representative profiles are shown in Figures 9.18 and 9.19. The profiles show two fronts separated by a plateau region within which the variation of temperature is relatively small. In the developing region ($\xi < 1.0$) these fronts intersect and there is no plateau region. For $\gamma > 1.0$ the leading front is a pure thermal wave which runs ahead of the mass transfer zone. In the region of the leading front ($\gamma\tau < \xi < 1 + \gamma\tau$) the profile is of constant-pattern form in the sense that it is a function only of the combined
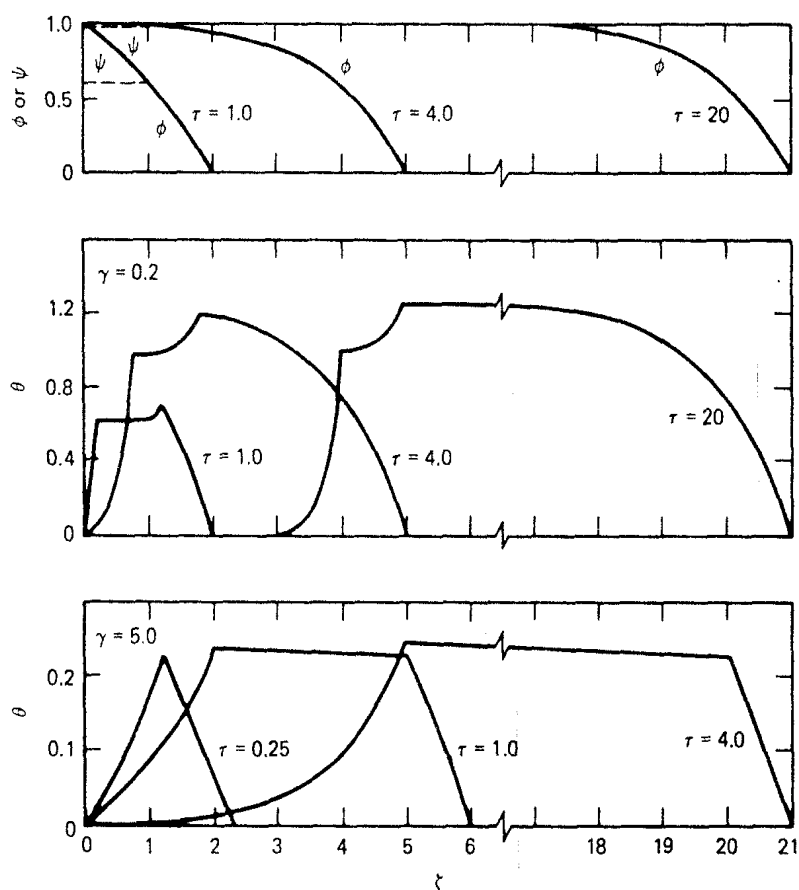
FIGURE 9.18. Theoretical concentration and temperature profiles for an irreversible adiabatic system. $\gamma < 1.0$, thermal front lags; $\gamma > 1.0$, thermal front leads. [Reprinted with permission from *Chem. Eng. Sci.* **37**, Yoshida and Ruthven (ref. 33). Copyright 1983, Pergamon Press, Ltd.]
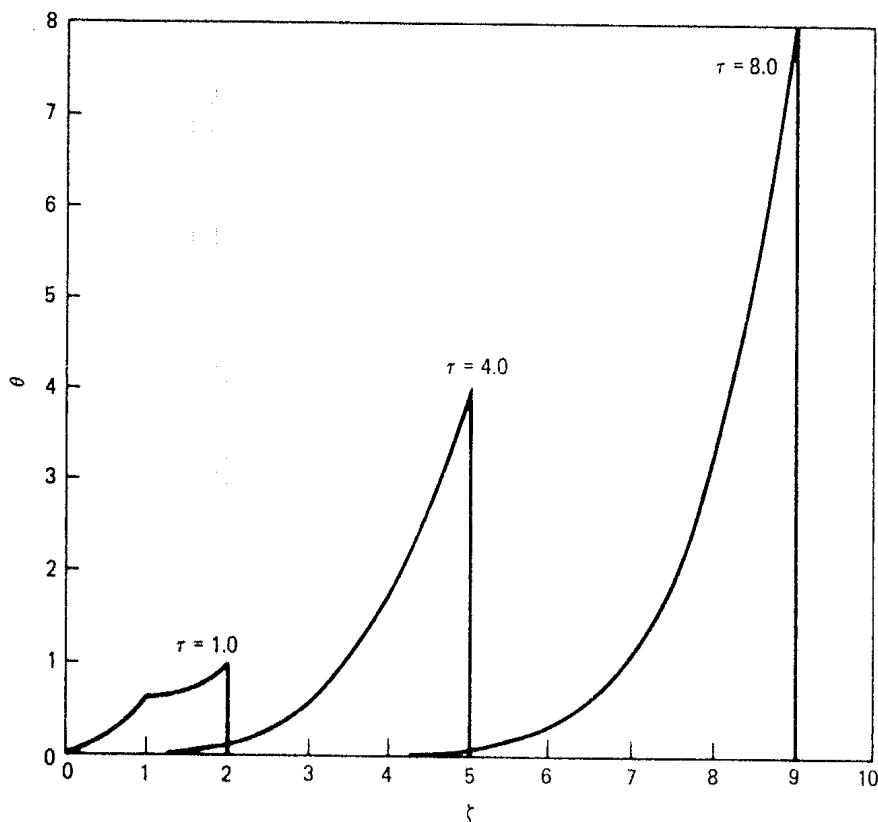
FIGURE 9.19. Theoretical temperature profiles for an irreversible adiabatic system with $\gamma = 1.0$ (velocities of thermal and concentration fronts are equal). [Reprinted with permission from *Chem. Eng. Sci.* **37**, Yoshida and Ruthven (ref. 33). Copyright 1983, Pergamon Press, Ltd.]

variable $(\xi - \gamma\tau)$ while the rear profile, which coincides with the mass transfer zone $(\xi < 1 + \tau)$, broadens as it progresses through the column. For $\gamma < 1.0$ the thermal wave lags behind the mass transfer zone so that the leading front now corresponds to the mass transfer zone. This front which extends over the region $1 + \gamma\tau < \xi < 1 + \tau$ is also of constant-pattern form $[\theta = f(\xi - \tau)]$. In the region $\gamma\tau < \xi < 1 + \gamma\tau$ there is a transitional profile which is not of constant-pattern form and this is followed by the thermal wave (cooling) over the region $\xi < \gamma\tau$. Thus in both situations $(\gamma > 1.0$ and $\gamma < 1.0)$ the general form of the profile consists of two fronts, moving with different velocities and separated by an expanding plateau region. The maximum temperature which occurs at $\xi = 1 + \tau$ for $\gamma > 1.0$ and at $\xi = 1 + \gamma\tau$ for $\gamma < 1.0$ approaches in both cases $\theta = (|\gamma - 1|)^{-1}$, provided that the column is sufficiently long for the concentration front to attain constant-pattern form $(\xi > 1.0)$.

Temperature Profile for $\gamma = 1.0$

An interesting special case arises when $\gamma = 1.0$. In this situation the natural velocities of the mass transfer front and the thermal wave are the same. Under these conditions the characteristics $\xi = 1 + \gamma\tau$ and $\xi = 1 + \tau$ become coinci-

dent so that the leading front becomes a step function. The limiting form for the temperature profile, which may be derived in a straightforward way using L'Hopital's rule, becomes

$$
\begin{aligned}
1 > \xi < \tau & \qquad \theta = e^{\xi-\tau} - e^{-\tau} \\
1 > \xi > \tau & \qquad \theta = 1 - e^{-\tau} \\
1 < \xi < \gamma\tau & \qquad \theta = e^{(\xi-\tau)}\left[1 + (\xi-2)e^{-1}\right] \\
\tau < \xi < 1 + \tau & \qquad \theta = 1 + (\xi-2)e^{\xi-\tau-1}
\end{aligned}
\tag{9.50}
$$

The form of this profile is shown in Figure 9.20. It may be seen that, under these conditions, the profile approaches a pulse of short duration and increasing magnitude ($\theta_{max} = \tau = \xi - 1$) so that an extremely high temperature, which could be sufficient to destroy the adsorbent, may be encountered if the column is sufficiently long. In most practical systems involving adsorption from the gas phase $\gamma \gg 1.0$, so this situation is unlikely to be encountered naturally. However, the condition $\gamma \approx 1.0$ may be achieved by diluting the adsorbent with inert material of high heat capacity. This is the basis of a recent patent[35] aimed at enhancing the recovery of high-grade heat in a cyclic system.

Temperature Profile for $\gamma \gg 1.0$ or $\gamma \ll 1.0$

Two further limiting cases which are of some interest arise for $\gamma \gg 1.0$ or $\gamma \ll 1.0$. In the former situation the characteristics $\xi = \gamma\tau$ and $\xi = 1 + \gamma\tau$ both approach the ξ axis ($\tau = 0$) while in the latter situation these characteristics approach the lines $\xi = 0$ and $\xi = 1.0$. Under these conditions the expressions for the temperature profile assume the simplified form:

	$\gamma \gg 1.0$	$\gamma \ll 1.0$	
$\gamma\tau < \xi < 1$	$\theta = 1 - e^{-\tau}$	$\theta = 1 - e^{-\tau}$	
$\gamma\tau > \xi < 1$	$\theta = 0$	—	
$1, \gamma\tau < \xi < 1 + \tau$	$\theta = 1 - e^{-\tau} + \dfrac{e^{\xi-\tau-1}}{(\gamma-1)}$	—	
$1 < \xi < 1 + \tau, \gamma\tau$	$\theta = \dfrac{e^{\xi-\tau-1}}{(\gamma-1)}$	—	(9.51)
$1 + \gamma\tau < \xi < 1 + \tau$	—	$\theta = 1 - e^{\xi-\tau-1}$	
$1 + \tau, \gamma\tau < \xi < 1 + \gamma\tau$	$\theta = 1 - e^{-\tau}$	—	
$1 + \tau < \xi < \gamma\tau$	$\theta = \dfrac{1}{\gamma-1}$	—	
$1 + \tau < \xi$	—	$\theta = 0$	
$1 + \gamma\tau < \xi$	$\theta = 0$	—	

The limit $\gamma \ll 1.0$ is unlikely to be realized in practice, but the limit $\gamma \gg 1.0$ represents a common situation for vapor phase adsorption.

Constant-Pattern Region

Within the constant-pattern region of the concentration front a more general treatment of the system is possible. The concentration profile may be represented by the general expression

$$\psi = f(\xi - \tau)$$

$$\left(\frac{\partial \psi}{\partial \tau}\right)_\xi = -f'(\xi - \tau) = \left(\frac{\partial \theta}{\partial \tau}\right)_{\xi'} \tag{9.52}$$

Integrating at constant ψ along the characteristic $\xi = \xi' + \gamma\tau$:

$$\theta = -\int f'[\xi' + (\gamma - 1)\tau] d\tau = \frac{-\phi}{\gamma - 1} + g(\xi') \tag{9.53}$$

For $\gamma > 1.0$ the boundary conditions require $\theta = 0$ for $\phi = 1.0$, whence $g(\xi') = 1/(\gamma - 1)$ and the temperature profile is given simply by

$$\theta = \frac{1 - \phi}{\gamma - 1} \tag{9.54}$$

For $\gamma < 1.0$ the boundary conditions for the constant-pattern region are $\theta = 0$, $\phi = 0$, so $g(\xi') = 0$ and the temperature profile becomes

$$\theta = \frac{\theta}{1 - \gamma} \tag{9.55}$$

Thus, in a column which is sufficiently long for the concentration profile to approach constant-pattern form, the temperature and concentration profiles are directly related in a simple way through Eq. (9.54) or (9.55). The temperature profile may therefore be predicted directly from the concentration profile (and vice versa) without knowledge of the mass transfer rate expression.

Comparison with Experimental Data

Although based on the idealized assumption of an irreversible isotherm and a rate expression which provides only an approximate representation of a diffusional process this simple model provides a fairly good representation of the breakthrough curves for strongly adsorbed species such as water on molecular sieve adsorbents for which the assumption of a rectangular isotherm is an appropriate approximation (see Figure 1.3). Theoretical and experimental temperature and concentration breakthrough curves are compared in Figure 9.20 and relevant parameters are summarized in Table 9.4. The diffusional time constants were estimated from the fit of the high-concentration region of the breakthrough curves since in this region the assumptions of the irreversible model are well fulfilled. It is evident that the simplified model provides a good representation of the experimentally observed behavior although there are small deviations in the initial region. As may be seen from Figure 4.21 such deviations become more pronounced for an alumina adsorbent for which the equilibrium isotherm is less rectangular. However, even
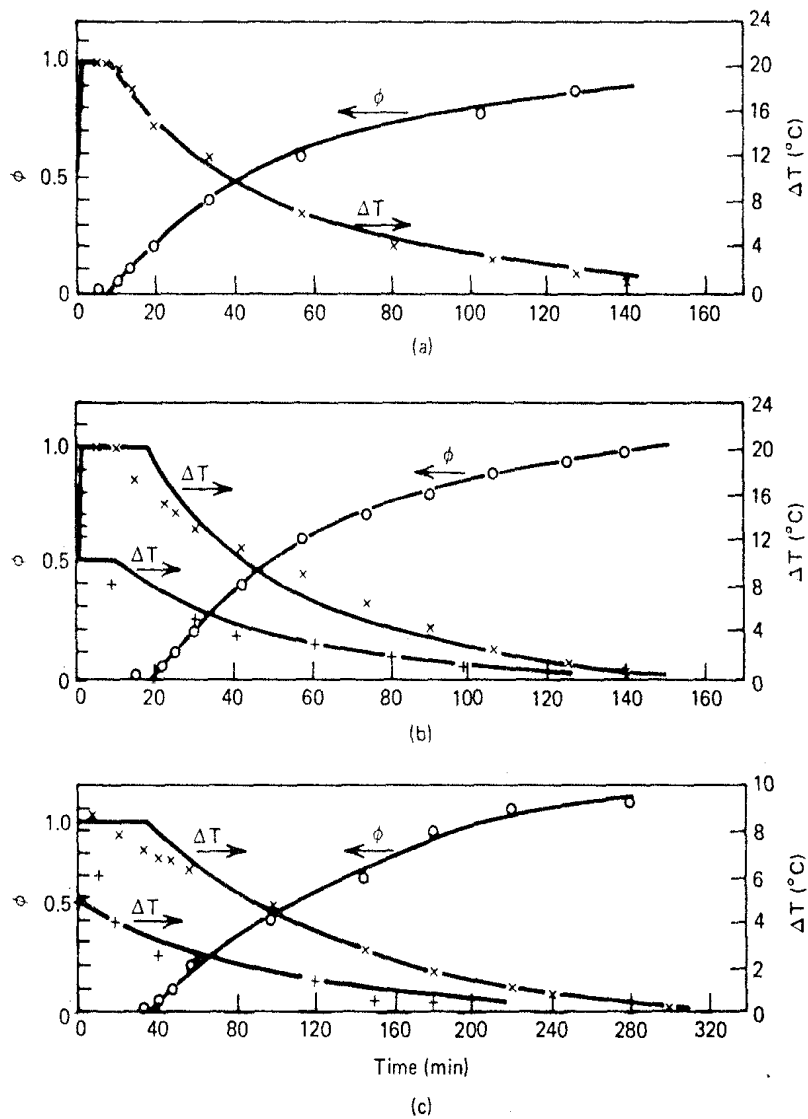
FIGURE 9.20. Experimental breakthrough curves for sorption of water in 4A molecular sieve showing comparison between experimental concentration (O) and temperature (×, +) break-through curves and theoretical curves (————) calculated for an irreversible adiabatic system. + represents temperatures measured at an intermediate point in the bed. Experimental conditions and model parameters are summarized in Table 9.4. [Reprinted with permission from *Chem. Eng. Sci.* **37**, Yoshida and Ruthven (ref. 33). Copyright 1983, Pergamon Press, Ltd.]

TABLE 9.4. Model Parameters for Experimental Breakthrough Curves Shown in Figures 9.20 and 9.21

Figure	Adsorbent	H_2O (ppm)	q_0 (g/g)	$-\Delta H$ (kcal/mole)	$10^4 \times k$ γ	(s^{-1})	ξ	ξ''
	a Davison 4A	8600	0.19	16.3	42	3.1	1.13	—
9.20	*b* Linde 4A	8600	0.19	16.3	42	4.3	1.54	0.6
	c Linde 4A	3300	0.18	17.5	107	1.7	1.35	0.53
9.21	Activated Alumina	4800	0.043	13.8	16.7	3.0	4.2	—

(ξ'' = dimensionless length to intermediate thermocouple).

314
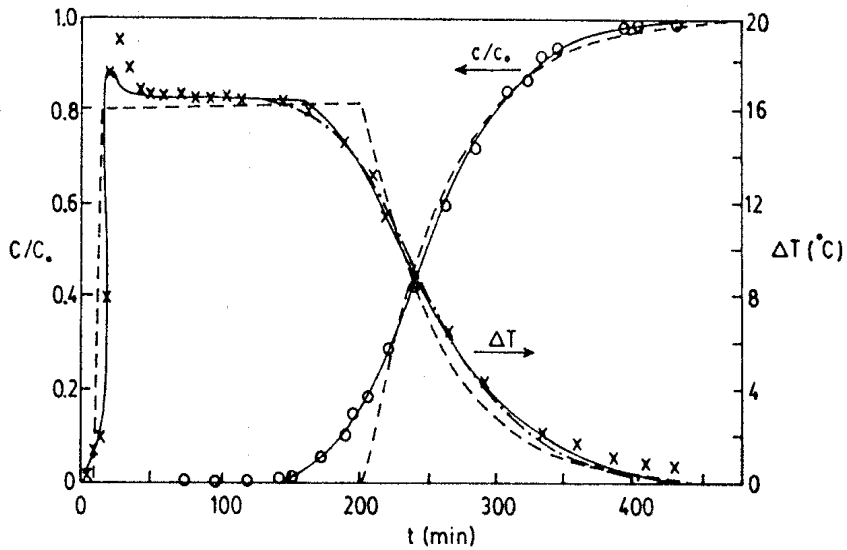
FIGURE 9.21. Experimental breakthrough curve (O) and corresponding temperature profile (×) for adiabatic adsorption of moisture on alumina.[37] The theoretical breakthrough curve and temperature profile calculated according to the irreversible adiabatic model [Eq. (9.48) and Figure 9.17] are shown by broken lines, while the temperature profile calculated directly from the concentration profile according to Eq. (9.54) is shown by — · — · —. Theoretical curves calculated from the model of Raghavan and Ruthven[44] (Langmuir isotherm, pore diffusion + external fluid film resistance) are shown by the solid line.

when the rectangular model does not hold, the simple relationship between the temperature and concentration fronts defined by Eq. (9.54) is still very accurate, justifying the measurement of temperature as a means of detecting the breakthrough time (see Figure 9.21).

In order to improve the accuracy with which the breakthrough time can be predicted for the more general case of a favorable equilibrium isotherm, a more detailed mathematical model has been developed as outlined below.[44]

General Numerical Solutions (One Adsorbable Component)

Except for the limiting case of the irreversible isotherm discussed above the prediction of the temperature and concentration profiles requires the simultaneous solution of the coupled differential heat and mass balance equations which describe the system. The earliest general numerical solutions for a nonisothermal adsorption column appear to have been given almost simultaneously by Carter[36-38] and by Meyer and Weber.[39,40] These studies all deal with binary adiabatic or near adiabatic systems with a small concentration of an adsorbable species in an inert carrier. Except for a difference in the form of the equilibrium relationship and the inclusion of intraparticle heat conduction and finite heat loss from the column wall in the work of Meyer and Weber, the mathematical models are similar. In both studies the predictive value of the mathematical model was confirmed by comparing experimental non-isothermal temperature and concentration breakthrough curves with the theoretical curves calculated from the model using the experimental equilibrium

TABLE 9.5. Summary of Numerical Solutions for Adiabatic Adsorption Columns with Finite Mass Transfer Resistance

Author	Equilibrium	Mass Transfer	Heat Transfer	Experimental System	Remarks
Carter (1966–68)[36,37]	Freundlich with $K = K_0 e^{-\Delta H/RT}$	Ext. film + pore diff.	Ext. film	H_2O-Al_2O_3	Similarity between heat and mass transfer. Finite difference calculation.
Carter and Barrett (1973)[38]	Freundlich with $K = K_0 e^{-\Delta H/RT}$	Ext. film + pore diff.	Ext. film	H_2O-Silica, Alumina, 4A Sieve	Similarity between heat and mass transfer. Finite difference calculation.
Meyer and Weber (1967–69)[39,40]	Empirical, nonlinear	Ext. film + pore diff.	Ext. film	CH_4-Act. Carbon	Wall heat loss included. Similarity between heat and mass transfer assumed. Finite difference calculation.
Cooney (1974)[41]	Langmuir $(b = b_0 e^{-\Delta H/RT})$	Linear rate	Ext. film	—	Finite difference.
Ikeda (1979)[42]	Langmuir Dubinin	Pore diff.	Thermal Equilib.	CO_2-5A Sieve	Mixing cell model. Finite difference.
Marcussen (1982)[43]	Freundlich	Pore diff.	Ext. film + internal conduction	H_2O-Alumina	Similarity assumed. Collocation solution.
Raghavan and Ruthven (1983)[44]	Langmuir	Ext. film + pore diff.	Ext. film	H_2O-4A Sieve	Similarity assumed. Axial dispersion included. Collocation solution.
Harwell et al. (1980)[45,47] Liapis and Crosser (1982)	Langmuir	Linear rate	Ext. film	CO_2-C_2H_6-5A	Two adsorbed species. Finite difference characteristics

data and reasonable estimates for the kinetic parameters. Brief details of these and other later studies are given in Table 9.5.

The qualitative effects of the variables on the form of the concentration and temperature profiles were investigated by Cooney[41] who used a linearized rate expression rather than a diffusion model. Cooney's equations are summarized in Table 9.6 as a representative example of the models for this class of systems.

A more detailed numerical investigation of a nonisothermal Langmuir system was recently undertaken by Raghavan and Ruthven[44] using a more

TABLE 9.6. Mathematical Model for an Adiabatic Adsorption Column

Fluid phase mass balance	$\dfrac{\partial c}{\partial t} + v \dfrac{\partial c}{\partial z} + \left(\dfrac{1-\epsilon}{\epsilon} \right) \dfrac{\partial \bar{q}}{\partial t} = 0$
Fluid phase heat balance	$\dfrac{\partial T_f}{\partial t} + v \dfrac{\partial T_f}{\partial z} + \dfrac{C_s}{C_f} \left(\dfrac{1-\epsilon}{\epsilon} \right) \dfrac{\partial T_s}{\partial t} + \dfrac{\Delta H}{C_f} \dfrac{\partial \bar{q}}{\partial t} \left(\dfrac{1-\epsilon}{\epsilon} \right) = 0$
	For gaseous systems $v = v(T)$ so the variation in v should be accounted for. This is neglected in Cooney's model, an approximation which is acceptable for moderate changes in temperature.
Mass transfer rate	$\dfrac{\partial \bar{q}}{\partial t} = k(q^* - \bar{q})$
	k is taken as independent of T although, in principle, $k = k(T_s)$. The temperature dependence of k could be included in the numerical scheme without undue difficulty.
Heat transfer rate	$\dfrac{\partial T_s}{\partial t} = ha(T_f - T_s) - \dfrac{\Delta H}{C_s} \dfrac{\partial \bar{q}}{\partial t}$
Equilibrium	$q^*/q_s = bc/(1 + bc)$ $b = b_0 e^{-\Delta H/RT}$
Initial condition	Bed initially sorbate free at $T = T_0$ throughout.
Boundary condition	Step change at time zero to feed of fixed concentration at $T = T_0$ at inlet.

Source: From Ref. 41.

complete mathematical model which includes finite heat transfer resistance and axial dispersion as well as external film and pore diffusional resistances to mass transfer. The model equations were solved by orthogonal collocation which proved much faster than standard finite difference methods. If similarity between heat and mass transfer is assumed the calculated difference in temperature between solid and gas is small showing that the effect of heat transfer resistance is minor and the assumption of thermal equilibrium is normally a good approximation. The effect of varying the nonlinearity of the isotherm and the degree of nonisothermality of the system (measured by the parameter $\Omega \equiv (-\Delta H)c_0/C_f T_0$) were investigated for a range of parameter values selected as being representative of air-water-zeolite systems. Representative adsorption and desorption curves are shown in Figure 9.22a and b. As the isotherm approaches rectangular form ($\lambda_0 \to 1.0$) the temperature and concentration curves for the adsorption step approach the form predicted by the irreversible model [Eqs. (9.48) and (9.51)] although, as a result of the
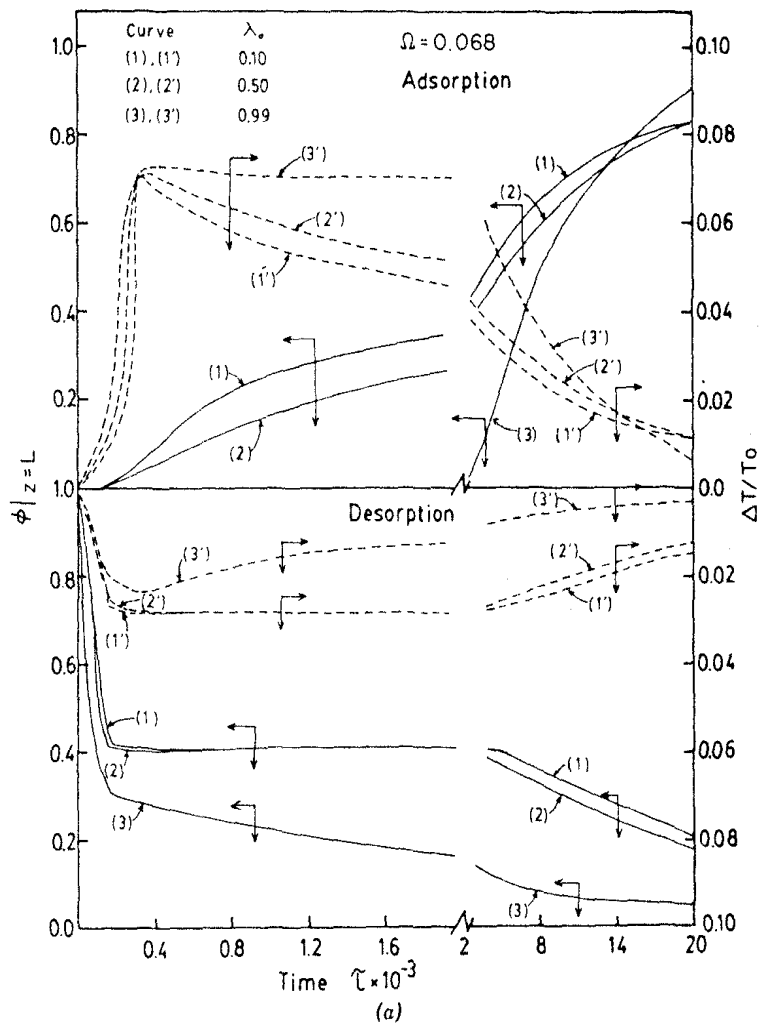
FIGURE 9.22(a). Theoretical concentration and temperature breakthrough curves for an adiabatic Langmuir system showing the effect of the nonlinearity parameter [$\lambda_0 = b_0 c_0/(1 + b_0 c_0)$, $b_0 = b(T_0)$]. (From Raghavan and Ruthven.[44])

inclusion of a finite resistance to heat transfer, the temperature rises slightly above the plateau value. As $\lambda_0 \rightarrow 0$, approaching a linear equilibrium relation, the concentration front becomes increasingly diffuse and eventually merges with the initial temperature front so that the well-defined plateau disappears.

Conversely, as $\lambda_0 \rightarrow 1.0$ the desorption curves become increasingly diffuse and the desorption profile changes from two well-defined fronts separated by a plateau, for near linear systems, to a more or less continuous curve as the rectangular limit is approached.

The effect of nonisothermality for a system in which the equilibrium isotherm is practically linear ($\lambda_0 = 0.05$) is shown in Figure 9.22b. At very low values of Ω (< 0.001) the system approaches isothermal behavior and the adsorption and desorption curves are mirror images. As the value of Ω is increased a pronounced asymmetry develops; the adsorption curve shows little change but the desorption curve, even for quite small Ω values, shows the development of two distinct fronts separated by a plateau. The practically
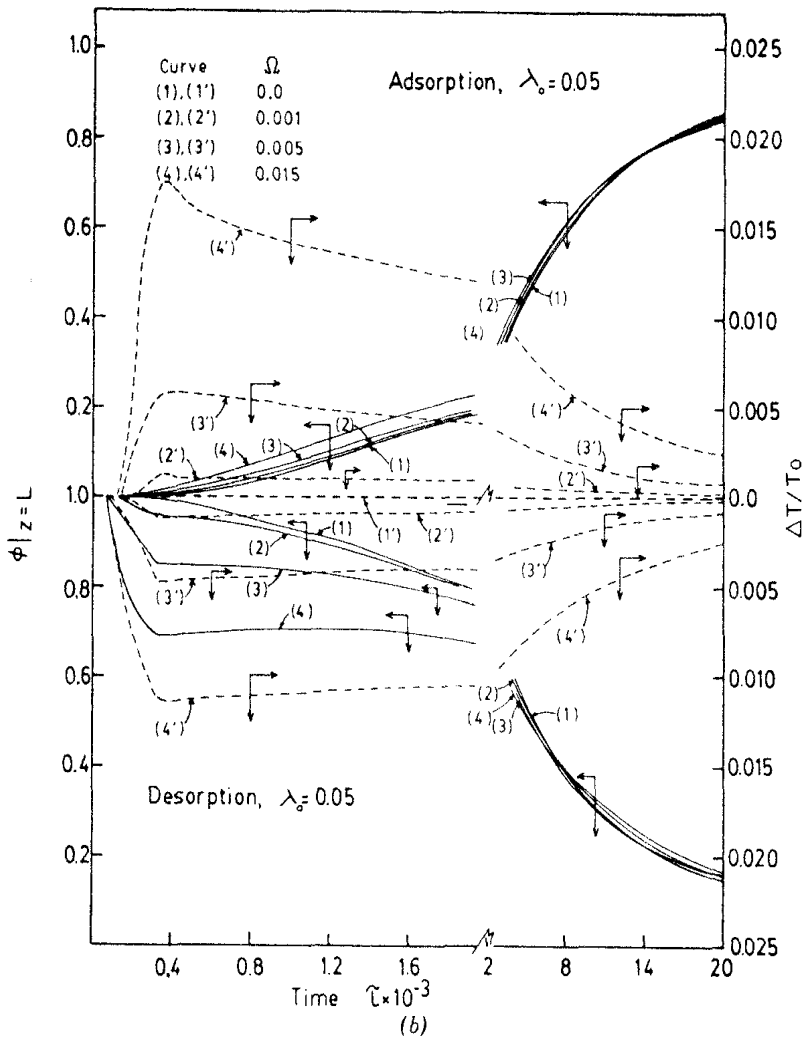
FIGURE 9.22(b). Theoretical concentration and temperature breakthrough curves for an adiabatic Langmuir system showing the effect of non-isothermal parameter $\Omega = (-\Delta H)c_0/C_f T_0$. (From Raghavan and Ruthven.[44])

important conclusion from this observation is that for real systems heat effects may often become significant even at low concentrations within the Henry's law range. Although the effect of a small temperature change on the break-through time for adsorption or on the time (or volume of purge) required to desorb the bed may be minor, such effects lead to significant differences in the shapes of the adsorption and desorption curves and may therefore be expected to cause significant distortion of the pulse shape in a chromatographic experiment. The effect of deviations from isotherm linearity in this respect is well known but it appears from this analysis that essentially a similar effect may arise, perhaps more commonly, as a result of small deviations from isothermality.

Parametric studies reveal that when the isotherm is highly favorable, the effects of external mass transfer resistance, axial dispersion, and small devia-tions of the isotherm from the limiting rectangular form all affect the initial region of the breakthrough curve in a similar way, leading to a reduction in dynamic capacity relative to the predictions of the simple irreversible model. Thus, in order to obtain an accurate *a priori* prediction of dynamic capacity a rather detailed mathematical model is required, even though the form of the breakthrough curve in the higher concentration region is well predicted from the simple irreversible model.

A comparison between the theoretical and experimental curves for the H_2O-alumina system is included in Figure 9.21 from which it may be seen that the model provides an excellent representation of the observed behavior.

General Numerical Solutions (Multicomponent Systems)

With the development of improved numerical methods for solution of differential equations and faster computers it has recently become possible to extend the numerical simulation to more complex systems involving more than one adsorbable species. Such a solution for two adsorbable species in an inert carrier was presented by Harwell et al.[45] The mathematical model, which is based on the assumptions of plug flow, constant fluid velocity, a linear "solid film" rate expression, and Langmuir equilibrium is identical with the model of Cooney (Table 9.6) except that the mass transfer rate and fluid phase mass balance equations are written for both adsorbable components, and the multicomponent extension of the Langmuir equation is used to represent the equilibrium. The solution was obtained by the method of orthogonal collocation.

This model has recently been used to interpet the experimental adiabatic breakthrough curves obtained by Wright and Basmadjian for CO_2-C_2H_6-N_2 on 5A sieves.[46,47] N_2 is treated as a nonadsorbing carrier. The binary equilibrium data were derived from the isotherms given by Glessner and Myers[48] and the temperature dependence of the overall rate coefficients was assumed to be given by an Arrhenius-type expression with activation energy
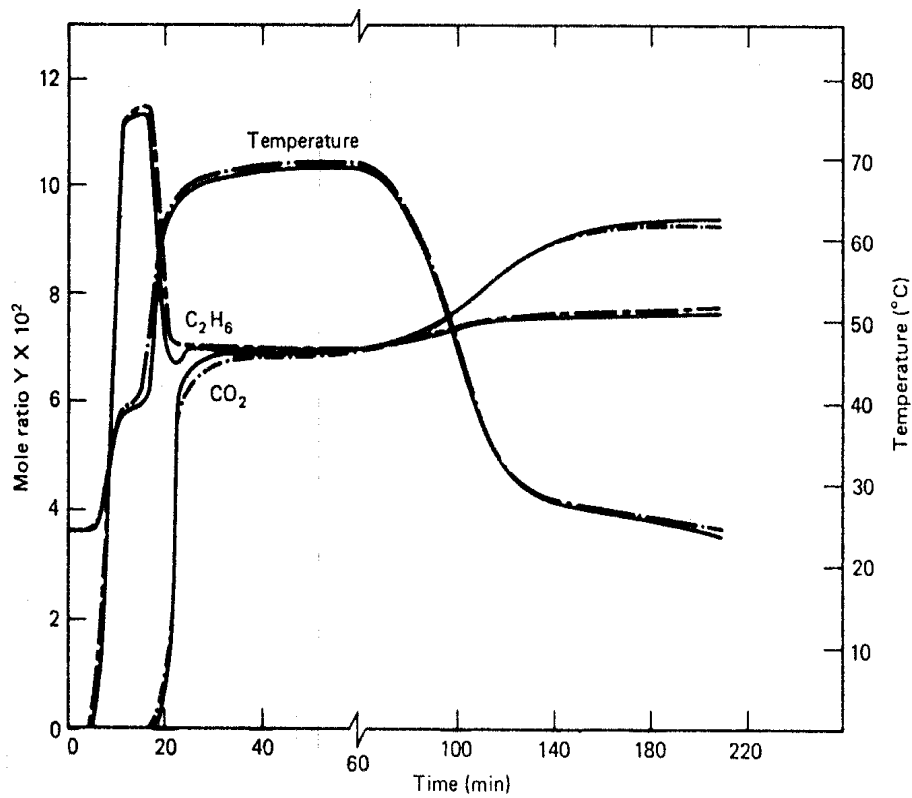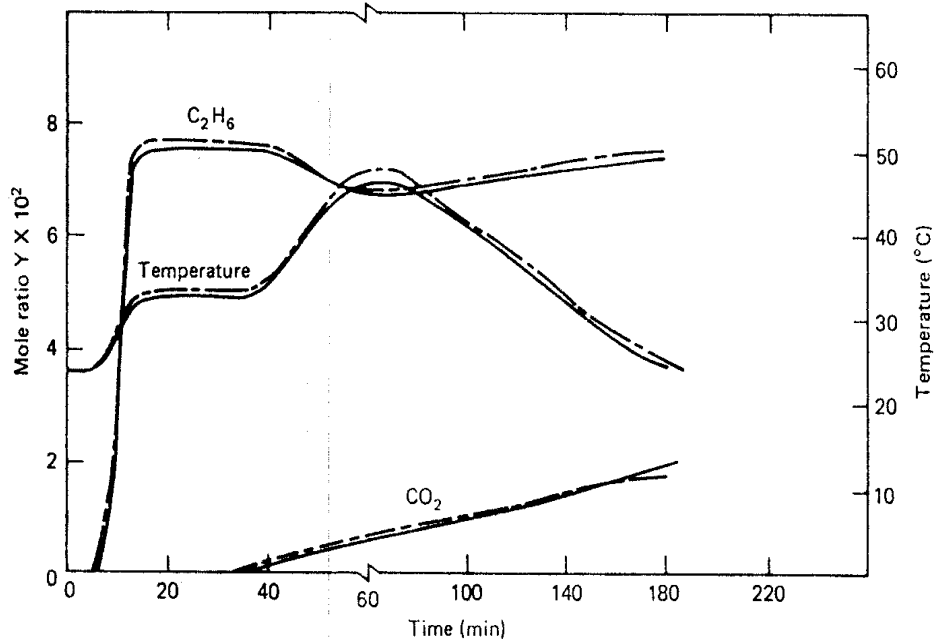
FIGURE 9.23. Comparison of theoretical (————) and experimental (—·—·—) concentration and temperature breakthrough curves for sorption of C_2H_6-CO_2 mixtures on 5A molecular sieve. (a) Basmadjian and Wright[46] Run B-14. $L = 48.3$ cm; feed 10.5 mole% CO_2; 7.03 mole% C_2H_6; 82.5 mole% N_2 at 24 °C, 1.15 atm. (b) Basmadjian and Wright Run B-9. $L = 48.3$ cm; feed 1.94 mole% CO_2; 6.98 mole% C_2H_6; 91 mole% N_2 at 24 °C, 1.15 atm. [Reprinted with permission from Chem. Eng. Sci., Liapis and Crosser (ref. 47). Copyright 1982, Pergamon Press, Ltd.]

321

taken as the activation energy for zeolitic diffusion. The pre-exponential factors for the two lumped mass transfer rate coefficients and the overall heat transfer coefficient were estimated from the best fit of the experimental curves. Representative results are shown in Figure 9.23 and it is evident that the model provides a good representative of the experimentally observed behavior.

The breakthrough curves consist, as expected, of four plateaux, including the initial and final states, separated by three mass transfer zones. CO_2 is evidently the more strongly adsorbed species and in Figure 9.23 the ethane concentration rises appreciably above the feed concentration (roll-up). When the CO_2 content of the feed is progressively reduced the level of the ethane plateau decreases significantly as the competition between ethane and CO_2 for the adsorption sites becomes less unequal. At the same time the thermal wave and the CO_2 wave begin to separate so that at low CO_2 feed concentrations the second temperature plateau precedes the CO_2 concentration front. Such behavior is consistent with equilibrium theory since, if $\gamma \equiv q^*C_s/c_0C_f \geqslant 1.0$, the velocity of the temperature front will exceed that of the concentration front leading to pure thermal wave formation. It is however of interest that the same behavior is observed in a multicomponent system.

REFERENCES

1. E. Glueckauf, *Disc. Faraday Soc.* **7**, 12 (1949).

2. H. K. Rhee, R. Aris, and N. R. Amundson, *Phil. Trans. Roy. Soc. London* **267A**, 419 (1970).

3. F. Helfferich and G. Klein, *Multicomponent Chromatography*. Marcel Dekker, New York, 1970.

4. T. Vermeulen, in *Chemical Engineers Handbook*, 5th ed., R. H. Perry and C. H. Chilton (eds.). McGraw-Hill, New York, 1973, section 16.

5. P. D. Lax, *Commun. Pure Appl. Math.* **10**, 537 (1957).

6. B. Davidson, *Disc. Faraday Soc.* **7**, 45 (1949).

7. D. O. Cooney and F. P. Strusi, *Ind. Eng. Chem. Fund.* **11**, 123 (1972).

8. H. K. Rhee and N. R. Amundson, *Chem. Eng. Sci.* **29**, 2049 (1974).

9. W. J. Thomas and J. L. Lombardi, *Trans. I. Chem. Eng.* **49**, 240 (1971).

10. W. G. Bradley and N. H. Sweed, *AIChE Symp. Ser.* **71**, (152) 59 (1975).

11. J. W. Carter and H. Husain, *Chem. Eng. Sci.* **29**, 267 (1974).

12. R. L. Gariepy and I. Zwiebel, *AIChE Symp. Ser.* **67**(117), 17 (1971).

13. I. Zwiebel, C. M. Kralik, and J. J. Schnitzer, *AIChE J.* **20**, 915 (1974).

14. A. I. Liapis, and D. W. T. Rippin, *Chem. Eng. Sci.* **33**, 593 (1978).

15. M. W. Balzi, A. I. Liapis, and D. W. T. Rippin, *Trans. I. Chem. Eng.* **56**, 145 (1978).

16. E. Santacesaria, M. Morbidelli, A. Servida, G. Storti, and S. Carra, *Ind. Eng. Chem. Process Design Develop.* **21**, 446 (1982).

17. F. W. Leavitt, *Chem. Eng. Prog.* **58**(8), 54 (1962).

18. N. R. Amundson, R. Aris, and R. Swanson, *Proc. Roy. Soc. London* **286A**, 129 (1965).

19. C. Y. Pan and D. Basmadjian, *Chem. Eng. Sci.* **25**, 1653 (1970).

20. C. Y. Pan and D. Basmadjian, *Chem. Eng. Sci.* **26**, 45 (1971).

21. H. K. Rhee, Ph.D. thesis, University of Minnesota, 1968.

22. H. K. Rhee and N. R. Amundson, *Chem. Eng. J.* **1**, 241 (1970).

23. H. K. Rhee, E. D. Heerdt, and N. R. Amundson, *Chem. Eng. J.* **1**, 279 (1970).

24. H. K. Rhee, E. D. Heerdt, and N. R. Amundson, *Chem. Eng. J.* **3**, 22 (1972).

25. H. K. Rhee and N. R. Amundson, *Chem. Eng. J.* **3**, 122 (1972).

26. D. Basmadjian, D. K. Ha, and C. Y. Pan, *Ind. Eng. Chem. Process Design Develop.* **14**, 328 (1975).

27. D. Basmadjian, D. K. Ha, and D. P. Proulx, *Ind. Eng. Chem. Process Design Develop.* **14**, 340 (1975).

28. D. Basmadjian, *Can. J. Chem. Eng.* **53**, 234 (1975).

29. N. H. Sweed, in *Percolation Processes*, NATO ASI No. 33, Espinho, Portugal 1978, A. E. Rodrigues and D. Tondeur (eds.). Sijthoff and Noordhoff, Rockville, Md., 1981.

30. D. H. James and C. S. G. Phillips, *J. Chem. Soc.* **1066** (1954).

31. P. Jacob and D. Tondeur, *Separation Sci. and Technology* **15**, 1563 (1980).

32. P. Ozil and L. Bonnetain, *Chem. Eng. Sci.* **33**, 1233 (1978).

33. H. Yoshida and D. M. Ruthven, *Chem. Eng. Sci.* **38**, 877 (1983).

34. R. S. Cooper, *Ind. Eng. Chem. Fund.* **4**, 308 (1965).

35. W. J. Asher and A. F. Venero, U.S. Patent No. 4,398,927 (Aug. 1983) to Exxon Research and Engineering.

36. J. W. Carter, *Trans. I. Chem. Eng.* **44**, T253 (1966).

37. J. W. Carter, *Trans. I. Chem. Eng.* **46**, T213 (1968).

38. J. W. Carter, *Trans. I. Chem. Eng.* **51**, T75 (1973).

39. O. A. Meyer and J. W. Weber, *AIChE J.* **13**, 457 (1967).

40. O. A. Meyer and J. W. Weber, *Can. J. Chem. Eng.* **47**, 60 (1969).

41. D. O. Cooney, *Ind. Eng. Chem. Proc. Design Develop.* **13**, 368 (1974).

42. K. Ikeda, *Chem. Eng. Sci.* **34**, 941 (1979).

43. L. Marcussen, *Chem. Eng. Sci.* **37**, 299 (1982).

44. N. S. Raghavan and D. M. Ruthven, *Chem. Eng. Sci.* (to be published).

45. J. H. Harwell, A. I. Liapis, R. Litchfield, and D. T. Hanson, *Chem. Eng. Sci.* **35**, 2287 (1980).

46. D. Basmadjian and D. W. Wright, *Chem. Eng. Sci.* **36**, 937 (1981).

47. A. I. Liapis and O. K. Crosser, *Chem. Eng. Sci.* **37**, 958 (1982).

48. A. J. Glessner and A. L. Myers, *CEP Symp. Ser.* **65**(96), 73 (1969).

49. A. R. van Cauwenberghe, *Chem. Eng. Sci.* **21**, 203 (1966).

10

CHROMATOGRAPHIC SEPARATION PROCESSES

In its broader sense the term chromatography is sometimes used to include any separation process which depends on partition between a flowing fluid and a solid adsorbent (or a solid-supported liquid phase). However, in this chapter we use the term in its more restricted sense to include only those processes in which the solid phase is contained in a packed column and the mixture to be separated is introduced as a pulse into a flowing stream of carrier, as in analytical gas or liquid chromatography.

An analytic chromatograph can provide highly efficient separation of even very similar molecular species and the possibility of scaling up such processes for large-scale production has therefore attracted much attention. Unfortunately the problems of scale-up have proved surprisingly difficult and although preparative scale chromatography is widely used in the production of pharmaceuticals and other fine chemicals, the scale of operation is generally relatively small (< 1 ton/day). In only a few instances have such processes actually been developed for full-scale industrial operations although there have been many theoretical studies suggesting the feasibility of large-scale units.

The subject has been reviewed by Conder[1] and the present discussion is therefore confined to brief review of some of the problems involved in scale-up. More detailed accounts of these aspects may be found in the articles of Valentin,[2] LeGoff and Midoux,[3] and Seko et al.[4] on which much of the present discussion is based.

10.1. PROCESS DESCRIPTION

A simplified flow sheet for a preparative scale chromatograph is shown in Figure 10.1. Since the system is, in essence, a batch process, it is common

Surge
tank

Compressor

Surge
tank

Flowmeter

Feed
tank

Feed
injection
system

Carrier
cleanup

Recorder and
automatic
control system

Column(s)

Oven

Detector

Product
fraction
collectors
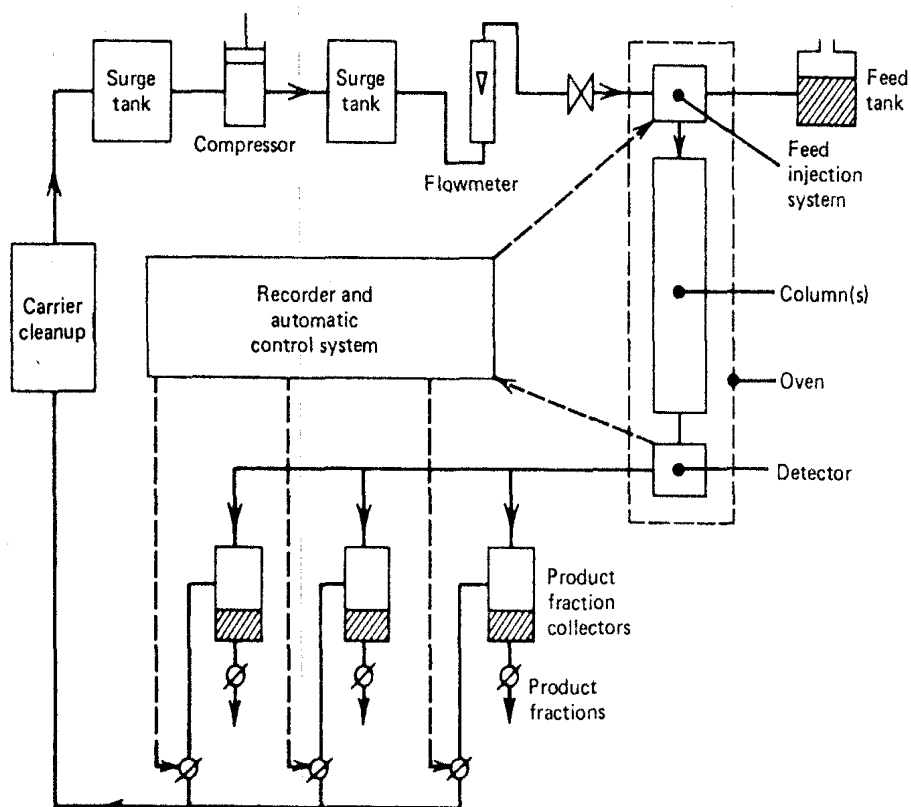
Product
fractions

FIGURE 10.1. Schematic diagram of production scale chromatographic process. (From ref. 1, copyright John Wiley & Sons, Inc., 1973; reprinted with permission.)

practice to use several columns, operating in parallel, in order to provide a more or less continuous flow of product. An automatic timing system controls the injection valves so that a pulse of feed is injected into each column in turn, according to a preprogrammed sequence. The injection cycle is adjusted so that by the time the injector is ready to introduce a second pulse into the first column, the first pulse has progressed far enough along the column that an acceptable separation is maintained.

The effluent from the column is directed alternately to the appropriate traps or receivers in which the products are separated and the carrier is then recycled to the inlet. The process scheme is essentially the same for both gas and liquid operation.

10.2. COLUMN EFFICIENCY

The separating power of a chromatographic process arises because during passage through the column each molecule of an adsorbable species is equilibrated many times between the mobile and stationary phases. Each equilibration is equivalent to one "equilibrium stage" or "theoretical plate." Even though the separation factor between two components may be small, with sufficient "theoretical plates," any desired resolution may be achieved.

The great advantage of a chromatographic system is that many theoretical plates can be contained within a column of moderate length.

The HETP for a chromatographic column (H) is given approximately by the van Deemter equation [Eq. (8.50)],

$$H = A + \frac{B}{v} + Cv \qquad (10.1)$$

and from Eqs. (7.6) and (8.49):

$$A \approx 2\gamma_2 R_p \qquad B \approx 2\gamma_1 D_m \qquad C \approx \frac{2\epsilon}{(1-\epsilon)kK}$$

The minimum value of H occurs at

$$v = \left(\frac{B}{C}\right)^{1/2} = \left[2\left(\frac{1-\epsilon}{\epsilon}\right)\gamma_1 D_m kK\right]^{1/2} \qquad (10.2)$$

and is given by

$$H_{min} = 2\gamma_2 R_p + 2\left[\frac{2\gamma_1 \epsilon D_m}{(1-\epsilon)kK}\right]^{1/2} \qquad (10.3)$$

To obtain a small HETP and therefore an efficient separation process, uniform packing is essential. This requires special packing procedures to eliminate variations in voidage through the bed. Any variation in voidage caused by nonuniformity of packing leads to an increase in the value of γ_2 and hence to an increase in the HETP. Such effects can be large as shown in Figure 10.2. Although wall effects can cause significant loss of efficiency in a small analytical column these are probably not important in preparative columns because of the much greater column diameter. The major cause of loss of efficiency in large diameter columns appears to be sorting of the adsorbent according to size during packing of the column and variation in local porosity due to unequal distribution of mechanical constraints during packing.[4] In supported liquid systems maldistribution of the liquid flow may be an additional problem.

The problem of uneven packing becomes increasingly severe as the diameter of the column is increased, leading to an increase in HETP. This has
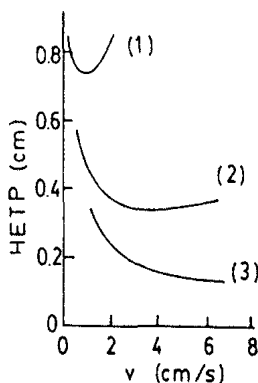
FIGURE 10.2. Effect of column packing on HETP. (1) loosely poured packing; (2) pouring + vibration; (3) pouring + vibration + controlled shocks. (From ref. 2, reprinted with permission of Martinus Nijhoff Publishers.)

proved to be a major obstacle to the scale-up of chromatographic processes. Baffles are commonly introduced at intervals through the column to act as flow redistributors,[5,6] but this is a less satisfactory solution than eliminating the problem by carefully controlled packing procedures. However, even in a very carefully packed column with closely sized adsorbent particles a significant increase in HETP with column diameter is still observed, as illustrated in Figure 10.3a.[4]

In order to assess the magnitude of H_{min} and its dependence on the size of the adsorbent particles, we may consider the three extreme cases of external film, macropore diffusion, and intracrystalline diffusion control.

For external film control we assume that with small particles the Reynolds number is not large even at high velocity and we therefore take the limiting case of $Sh = 2$ or $kK = D_m/R_p$ as an upper limit for the mass transfer coefficients. This leads to:

External film

$$\frac{H_{min}}{2} \geqslant \gamma_2 R_p + \left(\frac{2\gamma_1 R_p \epsilon}{1 - \epsilon} \right)^{1/2} \approx R_p + \sqrt{R_p} \qquad (10.4)$$

where we have assumed the typical values $\gamma_2 \approx 1.0$, $\gamma_1 = 0.7$, and $\epsilon = 0.4$.

For macropore diffusion control we assume molecular diffusion as the dominant mode of macropore transport and set $kK \approx 15\epsilon_p D_m/\tau R_p^2$, where τ is the tortuosity factor. This leads to the following expression for H_{min}:

Macropore diffusion

$$\frac{H_{min}}{2} \geqslant \gamma_2 R_p + R_p \left(\frac{2\gamma_1 \epsilon \tau}{15(1 - \epsilon)\epsilon_p} \right)^{1/2} \approx 1.8 R_p \qquad (10.5)$$

where we have again assumed $\gamma_2 \approx 1.0$, $\gamma_1 = 0.7$, $\epsilon = 0.4$, $\epsilon_p = 0.3$, and $\tau_1 = 3.0$. In order to maximize the number of stages in a given length of column it is clearly necessary to reduce the particle size as far as possible. The limit is set by pressure drop, which becomes unacceptably large if the particles are too small. In practice it is generally not economic in preparative chromatography to use particles smaller than about 100 mesh ($\sim$150 μm).

If intracrystalline (micropore) diffusional resistance is dominant $kK \approx 15KD_c/r^2$ and;

Intracrystalline diffusion

$$\frac{H_{min}}{2} = \gamma_2 R_p + r_c \left(\frac{2\gamma_1 \epsilon D_m}{15(1 - \epsilon)KD_c} \right)^{1/2} \qquad (10.6)$$

The role played by the particle size is now less important since the second term depends only on the crystal size. In this situation, depending on the relative magnitudes of the two terms, further reduction in particle size may

cis- and trans-pentene-2
25°C
N₂ Carrier
30% AgNO₃/TEG on C-22 supersupport, 60/80 mesh
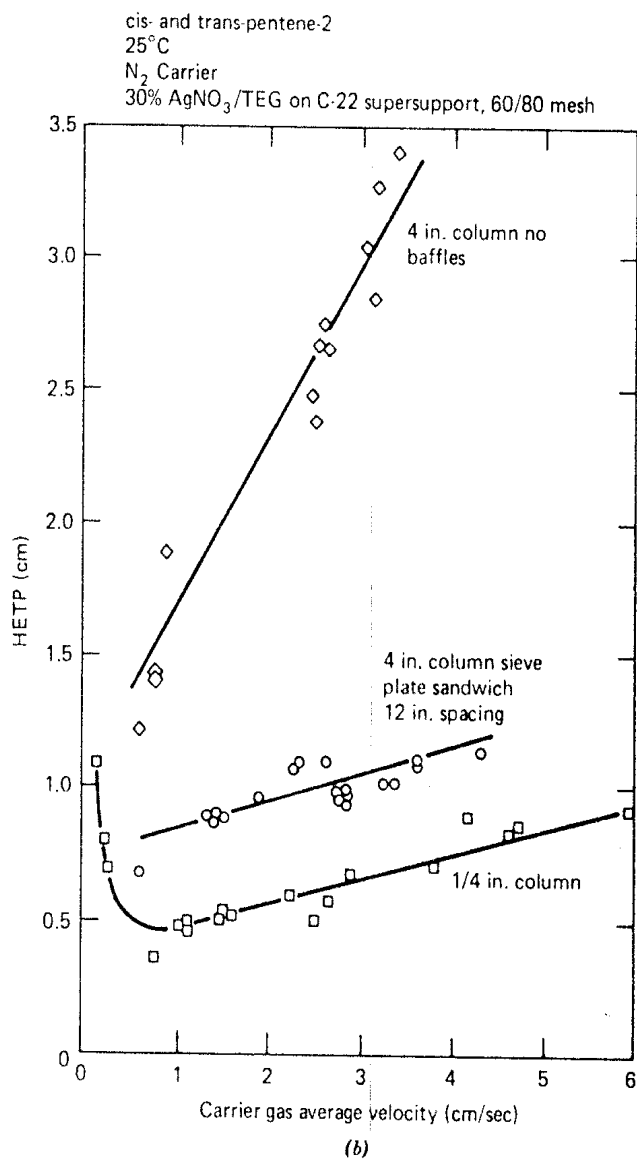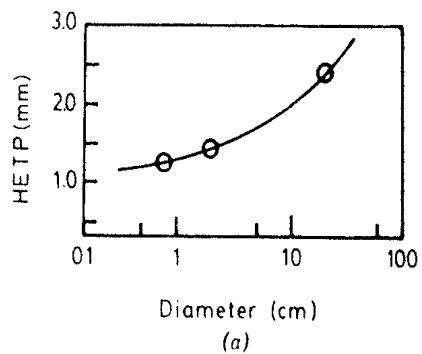
FIGURE 10.3. (a) Effect of column diameter in increasing HETP. (b) Reduction of HETP by introduction of baffles. [(a) reprinted with permission from ref. 4. Copyright 1982 American Chemical Society. (b) reprinted with permission from ref. 6.]

provide only a marginal reduction in H_{min}, and it may be necessary to change to an adsorbent with a smaller crystal size or higher intracrystalline diffusivity in order to reduce the HETP.

10.3. CHOICE OF OPERATING CONDITIONS FOR PREPARATIVE CHROMATOGRAPHY

In selecting operating conditions for an analytical chromatograph it is generally desirable to maximize the resolution, subject to some restriction on the maximum acceptable retention time. In preparative chromatography the constraints are more complex since the objective is generally to maximize the production rate with a given column or to minimize the column volume required for a given production rate, subject to allowable limits on product purity. In addition, for a true economic optimization it is necessary to consider, as well as the capital cost which is determined mainly by the column volume, the energy costs, which are determined mainly by the carrier flow rate and pressure drop. Since the production rate increases directly with the quantity of feed injected in each pulse, as well as with the injection frequency, it is common practice to run a preparative column under overload conditions (i.e., outside the Henry's law region) and to inject the sample as a square pulse of finite duration rather than as an ideal delta function. The column is also operated close to the minimum acceptable resolution and successive pulses of feed are injected as frequently as possible subject to the constraint imposed by minimum resolution requirements. It is evident that the basic assumptions of ideal chromatography (linear system, perfect pulse injection) are violated to a greater or lesser extent in a preparative system and conclusions deduced from the idealized theory will not be quantitatively correct. Nevertheless, the idealized theory provides useful approximate guidance concerning the optimal choice of operating conditions.

It may be shown that, provided the width ($4\sigma_i$) of a rectangular injection pulse is less than about 40% of the width of the response peak measured between the intersections of the tangents at the inflection points with the axis ($4\sigma_A$ or $4\sigma_B$), the standard deviation of the response peak (σ_A or σ_B) will not differ by more than 10% from the standard deviation for an ideal pulse injection. Under these conditions the number of theoretical stages in the column is given, approximately, by

$$N = \left(\frac{\bar{t}_A}{\sigma_A} \right)^2 = \left(\frac{\bar{t}_B}{\sigma_B} \right)^2 \tag{10.7}$$

The resolution between two adjacent peaks is defined by

$$R_{AB} = \frac{\bar{t}_A - \bar{t}_B}{4\sigma_{AB}}, \qquad \sigma_{AB} = \frac{\sigma_A + \sigma_B}{2} \tag{10.8}$$

At $R_{AB} = 1.0$ successive peaks are almost resolved while resolution is essentially complete for $R_{AB} \geqslant 1.5$. The number of theoretical stages required to achieve a given resolution in an ideal system is given by

$$N_0 \equiv \frac{L}{H} = 4R_{AB}^2\left(\frac{\alpha+1}{\alpha-1}\right)^2 \qquad (10.9)$$

where $\alpha = \bar{t}_A/\bar{t}_B$. For strongly adsorbed species $(K \gg 1.0)$, α defined in this way is equivalent to the separation factor defined by Eq. (1.1). In the case of a rectangular injection pulse, as illustrated in Figure 10.4, the number of theoretical stages required to achieve the same degree of resolution is given by

$$N = N_0\left(1 + \frac{\sigma_i}{\sigma_{AB}R_{AB}}\right)^2 = 4R_{AB}^2\left(\frac{\alpha+1}{\alpha-1}\right)^2\left(1 + \frac{\sigma_i}{\sigma_{AB}R_{AB}}\right)^2 \qquad (10.10)$$

Assuming the same minimum separation between peaks introduced in successive injections as between the peaks for adjacent components in the same injection, the time interval between successive injections is given by

$$T = 2\left(\bar{t}_A - \bar{t}_B\right) = 8(\sigma_i + R_{AB}\sigma_{AB}) \qquad (10.11)$$

and the relative duration of the injection pulse is given by

$$\theta = \frac{4\sigma_i}{T} = \frac{2}{2(1 + R_{AB}\sigma_{AB}/\sigma_i)} \qquad (10.12)$$

Using Eqs. (10.10) and (10.12), the required number of theoretical stages may be expressed as a function of θ with α and R_{AB} as parameters:

$$N(\theta) = 4R_{AB}^2\left(\frac{\alpha+1}{\alpha-1}\right)^2(1 - 2\theta)^{-2} \qquad (10.13)$$

The column length is given by $N(\theta)H(v)$ and the production rate (per unit cross-sectional area) by $\theta v\epsilon$ so that the production rate per unit column volume is given by

$$\frac{\theta v\epsilon}{NH} = \frac{\epsilon}{4R_{AB}^2}\left(\frac{\alpha-1}{\alpha+1}\right)^2\frac{v}{H(v)}\theta(1 - 2\theta)^2 \qquad (10.14)$$
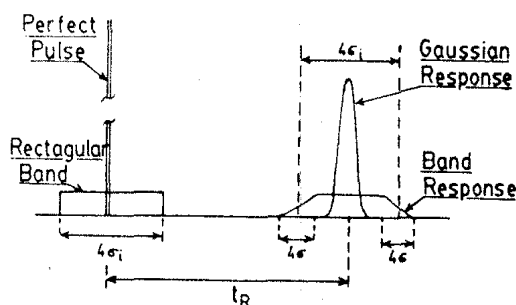
FIGURE 10.4. Idealized chromatographic response to (a) a perfect pulse injection and (b) a rectangular pulse injection.
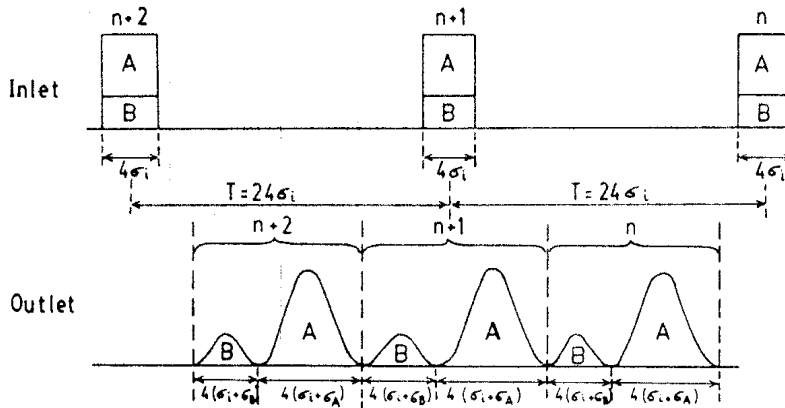
FIGURE 10.5. Optimal pulse sequence for production chromatography. Successive pulses of feed are introduced at intervals (T) such that $\theta = \frac{1}{6} = 4\sigma_i/T$, $T \approx 8(\sigma_i + \sigma_A)$, $\sigma_i = \sigma_A/2$. Components A and B are just resolved both within a given sample and between adjacent samples.

It is evident that, in order to maximize this quantity, θ should be chosen to maximize the function $\theta(1 - 2\theta)^2$, while the velocity should be chosen to minimize $H(v)/v$. This gives, for the optimal value of θ, $\theta = \frac{1}{6}$. More detailed analysis shows that under several different sets of simplifying assumptions, the requirement to minimize power consumption also suggests an optimal value of θ close to one-sixth. The optimal situation is shown in Figure 10.5.

From Eq. (10.1) it is clear that the requirement to minimize $H(v)/v$ leads to the conclusion that the fluid velocity should be as large as possible. Under these conditions

$$\frac{H(v)}{v} \approx \frac{2\epsilon}{(1 - \epsilon)kK} \tag{10.15}$$

The particle size should be as small as possible to maximize k, but the benefits of the reduction in the column volume must be balanced against the greater energy costs arising from the higher pressure drop with small adsorbent particles.

10.4. PROCESS APPLICATIONS

Separation of Pinenes

Both Abcor[6] and Elf-SRTI[2] have developed gas chromatographic processes for the separation of α and β pinenes. The processes, which are similar in general principle and differ mainly in the methods used to pack the column, are compared in Table 10.1. By improvements in column-packing technology Elf-SRTI were able to eliminate baffles and still achieve a reasonably low HETP in a production scale column. $(H \sim 1.0$ mm for a 40 cm. diameter column.) However, even in the largest of these units throughput is only about

TABLE 10.1. Comparison of Chromatographic Processes for
Separation of α and β Pinenes

	Abcor[6]	Elf-SRTI[2]	
Date	1968	1973	
Adsorbent	Chromasorb +	20% Carbowax	
T (°C)	160	160	
N (NTP)	275	275	
HETP (cm)	1.0	0.55	
Baffles	Yes	No	
Carrier	He	He or H_2	
Gas velocity (cm/s)	9.2	9-9.5	
Retention time (s)	80	80-65	
Column diameter (cm)	10	31	12.5	40
Column length L (cm)	275	?	150	150
Throughput (kg/day)	19	160	40	540

half a ton/day and it is not clear to what extent further scale-up is feasible simply by increasing the column diameter.

Separation of Xylene Isomers

A chromatographic process for separation of C_8 aromatic isomers has been recently developed by Asahi.[4,7] The process operates in the liquid phase and is put forward as an alternative to the UOP Sorbex process (see Section 12.5). The adsorbent is an X or Y zeolite but details of the ionic form have not been released. A schematic of the process, which uses three separation columns, is shown in Figure 10.6. The main column separates the mixed-feed stream into four cuts containing (a) ortho + meta + ethylbenzene (trace), (b) ortho + meta + ethylbenzene + paraxylene (trace), (c) paraxylene + ethylenebenzene, and (d) pure paraxylene. Cut (d) is passed directly to product while cut (b) is returned to the isomerization unit. Cuts (a) and (c) are passed to further columns in order to produce essentially pure ethylbenzene and paraxylene as products.

The process appears so far to have been operated only on a pilot scale but the performance of a full-scale unit (200 ton/day) has been predicted from a detailed numerical simulation. On the basis of projected costs it is claimed that the process requires only about half the adsorbent inventory and desorbent circulation rate of the Sorbex process. Such a claim can however be justified only on the basis of a substantial improvement in the separation factor since a simplified comparison between chromatographic and countercurrent systems suggests that, with the same adsorbent, the countercurrent
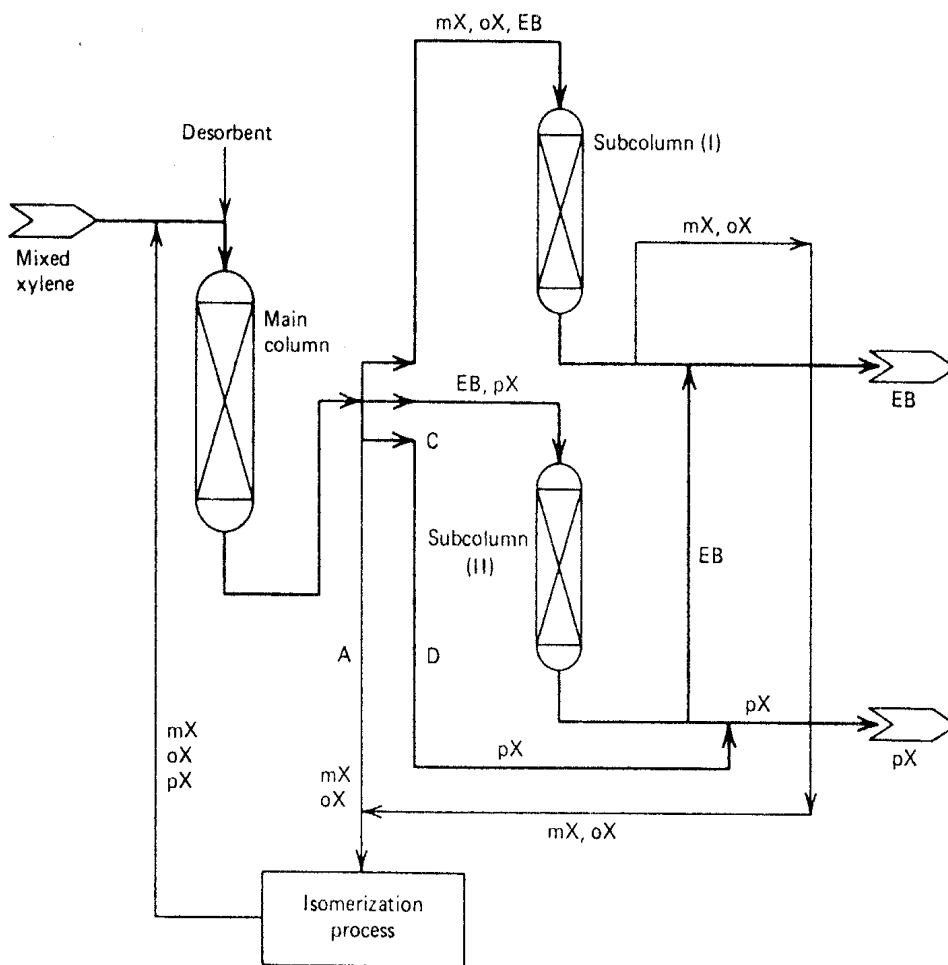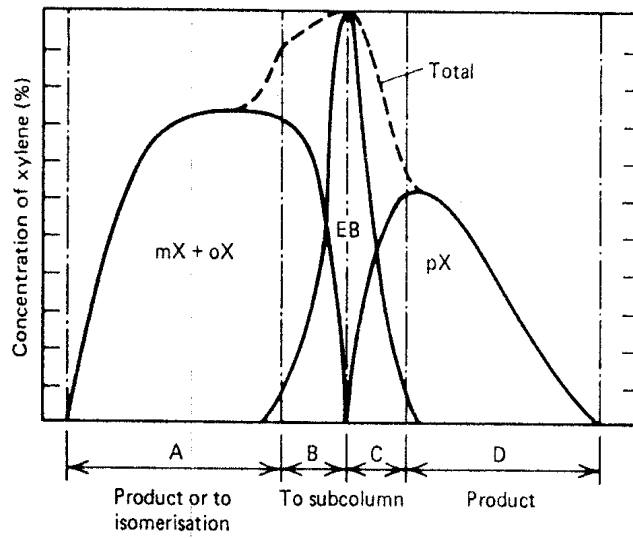
FIGURE 10.6. Schematic diagram of Asahi process for separation of C_8 aromatic isomers. (Reprinted with permission from ref. 7. Copyright 1979 American Chemical Society.)

process will generally be substantially more efficient than the chromatographic process (see Section 12.6).

Separation of Linear Paraffins

As an alternative to the conventional type of cyclic batch "Iso-Siv" process for separation of linear paraffins from light naphtha, a chromatographic process (Elf-N-Iself) has been recently developed.[8] A 300-ton/day demonstration unit was planned for 1983 but this has now been deferred until 1986.* Although the process operates in the chromatographic mode, the kinetic separation between linear and branched hydrocarbons on a 5A sieve is so sharp that only a very few theoretical plates are required in the column. The process may therefore be equally properly regarded as a variant of the traditional cyclic batch type of process (see Chapter 11) in which desorption is achieved by purge gas stripping with a circulating hydrogen or helium carrier rather than by thermal or pressure swing.

Process details have been given by Jacob.[9] The flow sheet is similar to Figure 10.1 with the addition of a fired heater and the necessary heat exchangers for feed vaporization and preheating. Five columns are operated in parallel with feed injected into each column in sequence over a period corresponding to one-fifth of the cycle time to achieve continuity of flow. The columns operate at 250°C, 13.2 atm, with a total cycle time of 268 s. The effluent concentration profile is similar to that shown in Figure 10.5 although since product purity is not critical the system is generally operated with greater overlap between the peaks. The *i*-paraffin/cyclic cut, which is normally the major fraction, is eluted first and is collected during approximately one-third of the cycle while the normal cut is collected during the rest of the cycle. The fraction which is recycled is determined by product purity specifications.

A numerical simulation of the system has been developed in order to allow optimization of the initial design and continuous optimization of the process conditions during operation to take account of slow deactivation of the adsorbent.

*Information provided by Elf-SRTI.

REFERENCES

1. J. R. Conder, "Production Scale Chromatography," in *New Developments in Gas Chromatography*, H. Purnell (ed.). Wiley, New York, 1973, pp. 137–185.

2. P. Valentin, in *Percolation Processes*, A. E. Rodrigues and D. Tondeur (eds.), NATO ASI No. 33. Sijthoff and Noordhoff, Alphen den Rijn, Holland, 1981, p. 141.

3. P. LeGoff and N. Midoux, in *Percolation Processes*, A. E. Rodrigues and D. Tondeur (eds.), NATO ASI No. 33. Sijthoff and Noordhoff, Alphen den Rijn, Holland, 1981, p. 197.

4. M. Seko, H. Takeuchi, and T. Inada, *Ind. Eng. Chem. Prod. Res. Develop.* **21**, 656 (1982).

5. R. Baddour, U. S. Patent No. 3, 250, 058 May 10 (1967).

6. J. M. Ryan, R. S. Timmins, and J. F. O'Donnell, *Chem. Eng. Prog.* **64**(8), 53 (1968).

7. M. Seko, J. Miyake, and K. Inada, *Ind. Eng. Chem. Prod. Res. Develop.* **18**, 263 (1979).

8. J. R. Bernard, J.-P. Gourlice, and M. Guttierrez, *Chem. Eng.* **88**(10), 92 (1981).

9. P. Jacob, NATO ASI Zeolites, Estoril-Sintra, Portugal, May, 1983 (Martinus Nijhoff, to be published).

11

ADSORPTION SEPARATION PROCESSES
I. Cyclic Batch Systems

Large-scale adsorptive separation processes may be conveniently divided into two broad classes; cyclic batch systems, in which the adsorbent bed is alternately saturated and regenerated in a cyclic manner, and continuous flow systems, generally involving continuous countercurrent contact between feed and adsorbent. The distinction between these two basic modes of operation is shown schematically in Figure 11.1. The present chapter is restricted to processes which operate in the cyclic mode while continuous contacting systems are discussed in Chapter 12.

It is convenient to distinguish purification processes, the aim of which is to remove an undesirable component or components from a feed stream without recovery, and true separations in which the feed is divided into two (or more) fractions of different composition where both fractions contain valuable products which are recovered. The process schemes used in these two types of separation are obviously somewhat different although the general principles of design and operation are similar.

11.1. METHODS OF REGENERATION

Cyclic batch adsorption processes differ from each other mainly in the methods by which the adsorbent is regenerated during the desorption cycle (see Table 11.1). Four basic methods are in common use although combinations of two or more methods may also be used with advantage in particular situations.

1. *Thermal Swing.* In thermal swing operation the bed is regenerated by heating, usually with a stream of hot gas (or less commonly with hot liquid), to
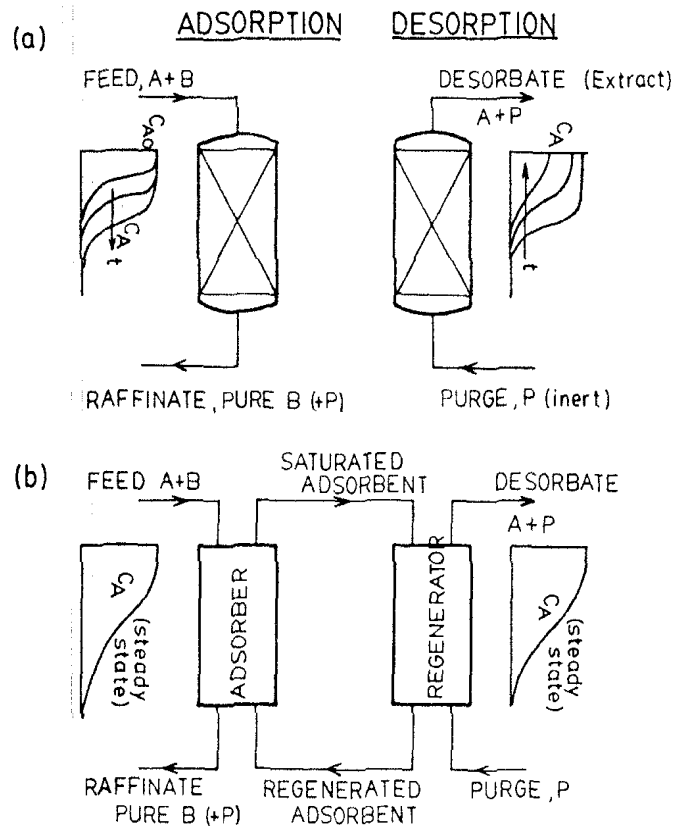
FIGURE 11.1. Schematic diagram showing the two basic modes of operation: (*a*) cyclic batch two-bed system; (*b*) continuous countercurrent system with adsorbent recirculation. Concentration profiles through the bed are indicated. *A* is the more strongly adsorbed species.

TABLE 11.1. Examples of Cyclic Adsorption Separation Processes

Process	Liquid (*L*) or Gas Phase (*G*)	Adsorbent	Selectivity	Regeneration Method
Drying of gas streams	*G*	13X, 4A, or 3A mol. sieve	Equilib.	*T* swing or *P* swing
Drying of solvents	*L*	4A sieve	Equilib.	*T* swing
Solvent recovery	*G*	Act. carbon	Equilib.	Steam stripping
H$_2$ recovery	*G*	Mol. sieve	Equilib.	*P* swing
Air separation	*G*	Carbon mol. sieve	Kinetic	*P* swing
		Zeolite	Equilib.	*P* swing
Linear paraffins separation	*G*	5A mol. sieve	Shape selective sieving	Displacement or vacuum
Waste water purification	*L*	Act. carbon	Equilib.	Steam stripping

337
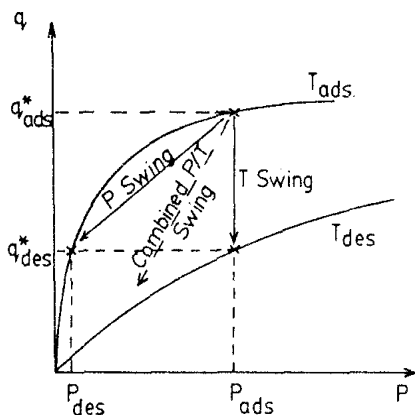
FIGURE 11.2. Schematic isotherms showing pressure swing, thermal swing and combined pressure–temperature swing operation for an adsorption process.

a temperature at which the adsorbed species are desorbed and removed from the bed in the fluid stream.

2. *Pressure Swing.* In a pressure swing process desorption is accomplished by reducing the pressure at essentially constant temperature and then purging the bed at low pressure. This mode of operation is obviously restricted to gaseous systems. The basic difference between pressure swing and thermal swing operation is shown schematically in Figure 11.2.

3. *Purge Gas Stripping.* The bed is regenerated at essentially constant pressure and temperature by purging with a nonadsorbing inert gas as in elution chromatography. This method of regeneration is applicable only when the adsorbed species are weakly held, otherwise the quantity of purge required would be prohibitive. Furthermore, the desorbate is normally present only at very low concentrations in the purge gas so the method would not normally be used where the desorbate is to be recovered.

4. *Displacement Desorption.* The temperature and pressure are maintained essentially constant, as in purge gas stripping, but instead of an inert purge the adsorbed species are displaced by a stream containing a competitively adsorbed species, as in displacement chromatography. The method is applicable to both gas and liquid systems.

Steam stripping, which is widely used in the regeneration of solvent recovery systems using an activated carbon adsorbent, can be considered as a combination of thermal swing and displacement desorption. Vacuum desorption, which is used in some versions of the Union Carbide IsoSiv process for separation of medium-chain linear paraffins as well as in some air separation systems can be considered as a special case of pressure swing.

Choice of Regeneration Method

The choice between the possible modes of regeneration, for any particular system, depends on economic factors as well as on technical considerations. For example, availability of a cheap source of steam or waste heat tends to favor thermal swing operation over the other alternatives. Nevertheless, there

are a number of general considerations which provide initial guidance. A brief summary is given in Table 11.2.

Thermal swing is probably the most common system. The temperature dependence of the adsorption equilibrium constant is governed by a vant Hoff equation [Eq. (2.20)]. Since adsorption is an exothermic process and since the more strongly adsorbed species generally have the higher heats of adsorption, a large decrease in the adsorbed phase concentration in equilibrium with a specified fluid concentration may be achieved by a comparatively modest increase in temperature. This means that at elevated temperatures the iso-

TABLE 11.2.   Summary of Factors Governing Choice of Regeneration Method

Method	Advantages	Disadvantages
Thermal swing	Good for strongly adsorbed species; small change in T gives large change in q^*	Thermal aging of adsorbent
	Desorbate may be recovered at high concentration	Heat loss means inefficiency in energy usage
		Unsuitable for rapid cycling so adsorbent cannot be used with maximum efficiency
	Gases and Liquids	In liquid systems high latent heat of interstitial liquid must be added.
Pressure swing	Good where weakly adsorbed species is required in high purity	Very low P may be required
		Mechanical energy more expensive than heat
	Rapid cycling—efficient use of adsorbent	Desorbate recovered at low purity
Displacement desorption	Good for strongly held species	Product separation and recovery needed (choice of desorbent is crucial)
	Avoids risk of cracking reactions during regeneration	
	Avoids thermal aging of adsorbent	

therm becomes much less favorable for adsorption (more favorable for desorption) and at sufficiently high temperatures even the most strongly adsorbed species may be desorbed with comparative ease and with relatively high concentrations in the desorbate effluent. This is illustrated by the isobars and isosteres for adsorption of water on 4A molecular sieve which are shown in Figure 11.3.

Provided that the adsorbent has adequate selectively, both the raffinate product (the less strongly adsorbed species which is removed from the bed outlet during the adsorption cycle) and the extract product (the more strongly adsorbed species which is desorbed during the desorption cycle) can be recovered. However, while the raffinate product is recovered at high purity, the extract product always contains an appreciable proportion of the less strongly adsorbed component. Because temperature is a more effective variable than pressure for changing the thermodynamic potential, thermal swing processes are generally preferred for strongly adsorbed species and for systems containing several adsorbates of widely different adsorption affinities. Such processes are applicable to both gas and liquid systems and are simple to design and flexible in operation. However, repeated thermal cycling can substantially reduce the life of an adsorbent[2] (see Section 1.5) and where reactive hydrocarbons are involved, exposure to elevated temperature during the desorption cycle can lead to coke formation.

The energy costs associated with a thermal swing operation are not insignificant and the time delays involved in heating and cooling the bed make such systems unsuitable for rapid cycling. This means that the inventory of adsorbent in a thermal swing system is generally relatively large with consequent adverse impact on the economics.

The pressure swing system is well suited to rapid cycling and this has the advantage of minimizing the adsorbent inventory and therefore the capital cost of the system. The raffinate product may be recovered at high purity, but the efficiency of recovery is lower than in a thermal swing system since a fraction of this product stream is used for purging the bed. The process is therefore well suited to separations where either the product which is required in high purity is the weakly adsorbed species or where a high-purity product is not essential. It is particularly useful when the feed stream is of relatively low value so that complete product recovery is not essential. These requirements are fulfilled in all three of the major large-scale applications of pressure swing systems; the heatless air drier, air separation processes, and hydrogen purification.

The use of isothermal purge gas stripping is relatively uncommon since such a process is applicable only for very weakly adsorbed components. More commonly a combination of purge gas stripping with a modest thermal swing is used. This permits desorption of somewhat more strongly held species while at the same time the temperature change is small enough to avoid most of the disadvantages associated with a standard thermal swing process.

Displacement desorption is useful for the separation of strongly adsorbed species where conditions of adsorbent stability or reactivity of the sorbate
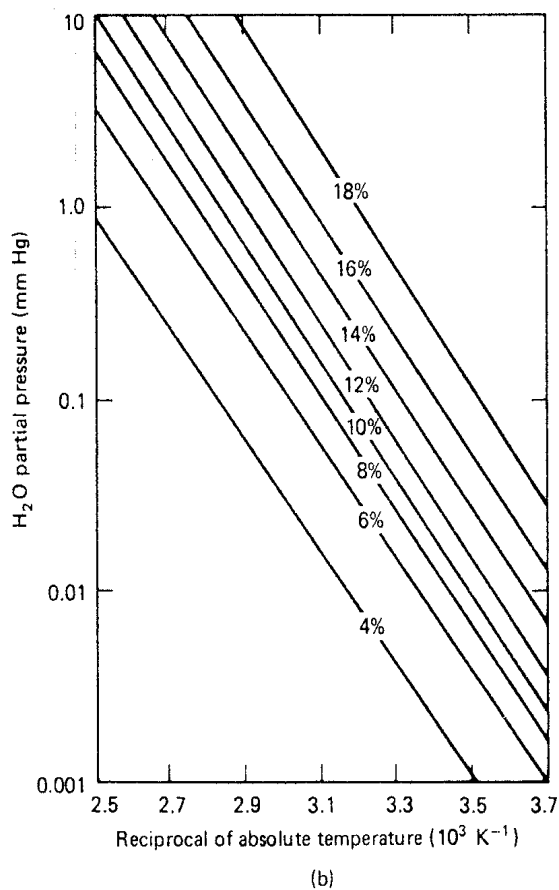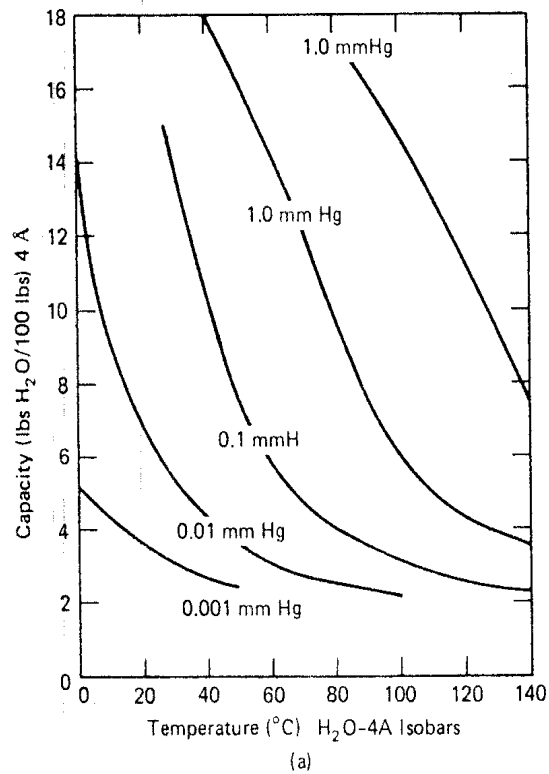
FIGURE 11.3. Equilibrium isobars (a) and isosteres (b) showing temperature and pressure dependence of equilibrium adsorption capacity for water on 4A sieve. (Courtesy of W. R. Grace.[1])

make thermal swing operation undesirable. In a displacement system product recovery is somewhat more complex than in a simple pressure swing or thermal swing system since both products are contaminated by the displacing agent and additional separation steps, involving flashing or distillation, are required. The choice of desorbent is crucial to the success of such a process. At the end of the adsorption cycle the adsorbent is loaded with the more strongly adsorbed of the feed components which is then displaced during the desorption cycle by the displacing agent or desorbent. In order for displacement to be possible the adsorption equilibrium must be such that a significant change in the composition of the adsorbed phase results from a change in the fluid phase composition. This requires that the desorbent should be adsorbed with about the same affinity as the more strongly adsorbed component of the feed (i.e., $\alpha \sim 1.0$ for feed component vs. desorbent). If the desorbent is too strongly adsorbed it cannot be effectively displaced from the bed during the adsorption cycle, leading to very low utilization of adsorbent capacity or poor product recovery, while if the desorbent is too weakly adsorbed, a very large desorbent flow rate and a long desorption period are required in order to desorb the adsorbed product during the regeneration cycle. It is also necessary that the intrinsic separation factor between the adsorbable species in the feed be not adversely affected by the presence of desorbent and that the desorbent be easily separable by distillation, or other simple means, from both components of the feed.

11.2. THERMAL SWING PROCESSES

General Design Considerations

The simplest version of the thermal swing process operates with two beds, one adsorbing and the other desorbing, in order to provide continuity of flow. The general scheme is as sketched in Figure 11.1a. In a two-bed system, the times of the adsorption and desorption cycles (including heating and cooling steps) must be equal and this limits flexibility and reduces somewhat the effectiveness with which the adsorbent capacity may be utilized. More efficient use of the adsorbent is obtainable in multiple-bed systems but since cost increases with complexity, multiple-bed systems are generally not justified except where adsorption rates are low. The basic two-bed system is standard for most vapor phase applications including gas driers, solvent recovery systems, and natural gas sweetening systems.

In a linear equilibrium system adsorption and desorption are symmetrically equivalent processes so the restriction to equal times for the adsorption and desorption cycles in a two-bed system does not limit the efficiency with which the adsorbent may be used. However, most cyclic adsorption separation processes operate under conditions such that the isotherm for the more strongly adsorbed species is of favorable (type I) form. Under these conditions

the desorption cycle becomes the limiting factor in the design of a cyclic two-bed process. This follows from straightforward equilibrium theory considerations. For a favorably adsorbed species the concentration front during adsorption tends to constant-pattern form and, under nondispersive conditions, approaches a shock front. During desorption the profile assumes the broadening proportionate-pattern form. Since the profile during desorption is more dispersed it follows that if temperature and flow rate are maintained constant throughout adsorption and desorption cycles, a longer period will be required for desorption than for adsorption of a given quantity of sorbate. The restriction to equal times for adsorption and desorption means that only a fraction of the sorbate present in the feed can be removed during the desorption cycle. A satisfactory separation for a favorably adsorbed component is therefore not possible since, whatever cycle time is chosen, the adsorbate will always break through during the adsorption cycle. In order to obtain a satisfactory cycle with a two-bed system it is therefore necessary that either the flow rate or the temperature be higher during desorption than adsorption. This conclusion, reached here by general qualitative arguments, is confirmed by the numerical simulations of Bunke and Gelbin.[3,4]

A low operating temperature during the adsorption cycle increases the capacity of the adsorbent and also generally improves selectivity. However, if the adsorbable species are too strongly adsorbed, an unduly large temperature swing may be needed for effective desorption during the regeneration cycle. In principle there is therefore an economic optimum temperature of operation, but in practice the adsorption cycle is generally operated at or near ambient temperature since substantial heating or cooling of the feed stream proves in most cases to be uneconomic.

Desorption is accomplished by heating the bed with either *in situ* steam coils or, more commonly, by heating with a hot purge gas stream. The regeneration temperature and purge gas flow rate during regeneration are related since any defined degree of regeneration may be achieved either by a relatively low temperature rise coupled with a high purge flow rate or by a higher temperature rise with a smaller purge. The optimal combination for any particular system depends on the cost, quality, and availability of steam relative to the cost of purge gas. In driers and natural gas sweetening systems it is common practice to use a small fraction of the product gas as the purge stream. Regeneration with hot feed is also common where product purity requirements are not too stringent. For systems in which the desorbate is to be recovered, a relatively high desorption temperature is desirable in order to increase the desorbate concentration in the effluent and thus reduce downstream recovery costs.

Forward- and Reverse-Flow Regeneration

In a practical adsorption system the adsorption cycle is generally terminated prior to breakthrough in order to ensure purity of the raffinate product.

This leaves a region of incompletely saturated adsorbent at the outlet of the bed. Similarly the time of the desorption cycle is limited so that in general the sorbate is not completely removed from the bed during desorption. If the bed were desorbed under forward-flow conditions the residual sorbate at the end of the desorption cycle would accumulate at the bed outlet and contaminate the raffinate during the next adsorption cycle. To obtain pure raffinate with forward-flow regeneration requires that desorption be carried essentially to completion during the regeneration cycle. This may require the use of either an inordinately high regeneration temperature or an uneconomically high purge rate. The problem is avoided by reverse-flow regeneration since then any residue of sorbate remaining at the end of the desorption cycle is concentrated at the bed inlet and does not affect the raffinate purity in the subsequent adsorption cycle. Reverse-flow regeneration is therefore standard practice and forward-flow regeneration is used only in special situations which preclude the use of reverse flow. For similar reasons, where a cooling step is included in the cycle, forward flow is generally employed during cooling so that any accumulation of adsorbable species from the coolant occurs near the bed inlet rather than at the outlet.

An example of a special situation requiring forward-flow desorption was discussed by Wunder[5] in relation to the drying of a natural gas stream containing significant quantities of higher hydrocarbons. In such a system the heavier hydrocarbons are adsorbed to some extent and during the adsorption cycle the hydrocarbon zone moves through the bed ahead of the moisture front. Thus at the end of the adsorption cycle there is a zone of these heavier hydrocarbons in the region of the bed outlet. If the bed were regenerated in reverse flow, contact with hot gas at the start of the desorption cycle could cause cracking and coking of the adsorbent. This problem is avoided by foward-flow regeneration since the entry region of the bed is essentially free of the heavier hydrocarbons. During forward-flow regeneration the hydrocarbon residue is displaced by relatively cool gas and water vapor so the risk of cracking is avoided.

When forward-flow regeneration is employed it is essential that the adsorption cycle should not be terminated prematurely otherwise desorption will be very inefficient since the sorbate must first be pushed through the unsaturated region of the bed before it can be removed from the outlet. The volume of purge required to desorb the partially saturated bed is therefore essentially the same as for a fully saturated bed. By contrast, with reverse-flow regeneration premature termination of the adsorption cycle means only that the full capacity of the adsorbent is not utilized and the purge requirement/mole desorbed is not increased by operating with an incompletely saturated bed.

A full discussion of these factors has been given by Carter[6] who has also presented a numerical simulation of the regeneration of an adiabatic air drier showing clearly the advantage of reverse flow.[7] In Carter's simulation[7] the initial moisture profile through the bed was taken as the profile at the end of the adsorption cycle, which was terminated just prior to breakthrough. The
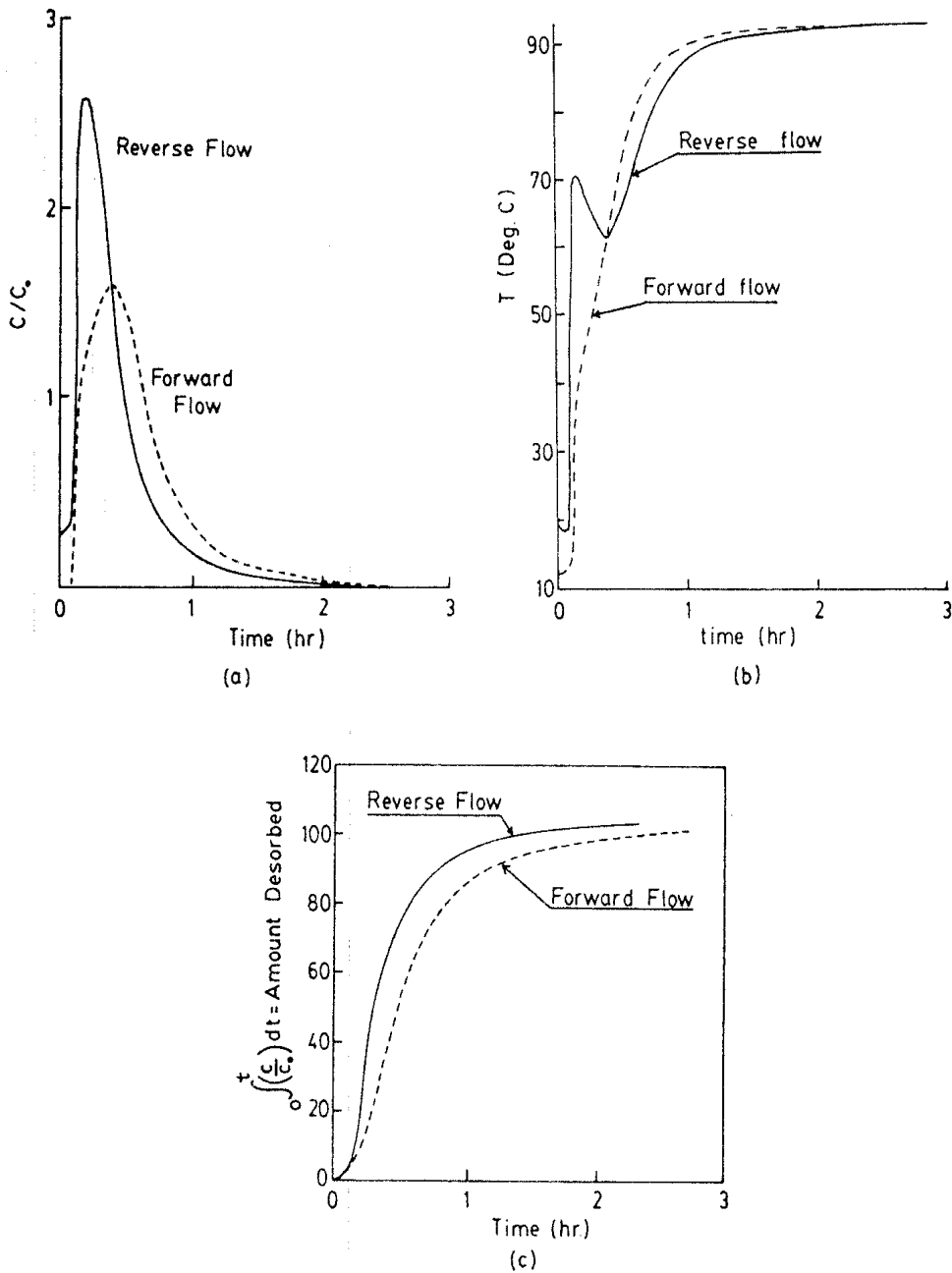
FIGURE 11.4. Simulated desorption curves for regeneration of a partially saturated bed (H_2O-Al_2O_3) in forward flow (---) and with reverse flow (————). (*a*) Effluent concentration, (*b*) effluent temperature, and (*c*) rate of removal of moisture. (After Carter.[7])

initial bed temperature was 21 °C. During regeneration dry air at 93 °C was introduced into the bed, first in the forward direction and then in reverse flow. The simulated desorption curves and corresponding outlet temperature histories are shown in Figure 11.4. The peak concentration of water in the effluent stream is higher and occurs earlier in reverse flow. Comparison of the integrated desorption curves, which are shown in Figure 11.4*c*, shows clearly that a given quantity of moisture is removed in a shorter time (i.e., with a

smaller volume of purge) in reverse flow. The dip in temperature which is observed during forward-flow regeneration is due to the adsorption and re-evaporation of water in the incompletely saturated outlet region of the bed. In a practical thermal swing drier a higher regeneration temperature would normally be used to reduce the time or purge volume required, but the qualitative trends remain the same.

Bed Cooling

In earlier adsorption systems it was general practice to include in the cycle a cooling step to return the bed to the adsorption temperature at the end of the regeneration cycle. It has been pointed out by Basmadjian[8-10] that the majority of adsorption processes operate at temperatures well below the temperature of selectivity reversal (see Table 11.3). Under these conditions inclusion of a cooling step is not required, as noted in Section 9.6. During the adsorption cycle the thermal wave runs ahead of the mass transfer zone and the temperature of the bed in the region of the mass transfer zone is therefore determined only by the feed temperature and is not affected by the initial bed temperature. Indeed, the inclusion of a cooling step may actually be a disadvantage since there is generally some loss of capacity due to contamination from the cooling purge gas.

TABLE 11.3. Reversal Temperatures
for Some Important Adsorption
Systems[9]

System	T_R (°C)
CO_2-CH_4-5A	111
H_2O-Air-5A	320
H_2O-Air-silica gel	122
H_2S-CH_4-5A	205
Acetone-air-C	150

Choice of Operating Conditions (Theoretical Considerations)

The choice of optimal operating conditions for a two-bed cyclic adsorption system presents a complex optimization problem since the effects of all the process variables (cycle time, bed length, adsorption and desorption temperatures, purge gas velocity) are coupled. However some general guidance may be derived from a comparatively simple theoretical analysis.

The mathematical models used to simulate the dynamic behavior of a cyclic adsorption system are essentially similar to those described in Chapters 8 and 9. There is however one important difference. In most of the models discussed in Chapters 8 and 9 an initially sorbate free-adsorbent bed was

assumed at the start of the adsorption process and a completely regenerated (or uniformly loaded) bed at the start of the desorption cycle. In practical systems both adsorption and desorption are seldom carried to completion so that at the start of the adsorption cycle there is a "heel" of undesorbed sorbate in the inlet region of the bed, while at the start of the desorption cycle there is a region of incompletely loaded adsorbent in the region of the outlet. This complicates somewhat the problem of mathematical simulation since the initial distribution of sorbate is not known *a priori*. If an accurate prediction of performance is required it is necessary to simulate both adsorption and desorption cycles. Starting from any arbitrary initial sorbate distribution the profiles will eventually converge to a cyclic steady state in which the concentrations at all positions at any time in the cycle remain the same in all subsequent cycles. The number of cycles required to approach the cyclic steady state varies widely depending on the system parameters and may be as high as 30. Such calculations can only be done by numerical simulation and the analytic solutions discussed in Chapters 8 and 9, although providing useful understanding and general guidance for design, cannot be used to give accurate predictions of the performance of a practical system.

.Theoretical simulations of a two-bed adsorption system with a single adsorbable component have been carried out by Tan and Spinner for linear systems[11,12] and by Bunke and Gelbin[3,4] and Chao[13] for nonlinear systems. In Gelbin's analysis the advantages of reverse-flow regeneration are clearly shown but the quantitative conclusions are of limited practical value since the analysis is restricted to systems in which both temperature and flow rate are maintained constant throughout the entire cycle. For the reasons already discussed it is impractical to operate an adsorption system in that way except when the adsorption isotherm is linear.

In Chao's analysis reverse-flow regeneration is assumed and allowance is made for differences in fluid velocity and adsorption equilibrium between the adsorption and desorption cycles but the temperature dependence of the adsorption rate coefficient is neglected. Both the adsorption and desorption cycles are considered to operate isothermally at their respective temperatures and no allowance is made for the time required for heating and cooling the adsorbent bed or for the transient behavior during the heating and cooling periods. Other assumptions include plug flow, constant fluid velocity, Langmuir equilibrium, and, in the modified version of Chao's analysis presented here, a linearized rate expression.

With these assumptions the behavior of the system is described by the following set of equations:

$$v \frac{\partial c}{\partial z} + \frac{\partial c}{\partial t} + \left(\frac{1 - \epsilon}{\epsilon} \right) \frac{\partial \bar{q}}{\partial t} = 0 \tag{11.1}$$

$$\frac{\partial \bar{q}}{\partial t} = k(q^* - \bar{q}) \tag{11.2}$$

$$\frac{q^*}{q_s} = \frac{bc}{1 + bc} \tag{11.3}$$

with the initial and boundary conditions:

Start of adsorption cycle (end of desorption cycle)

$$\bar{q}(z,0) = \bar{q}_e^d(z',t_c) = \bar{q}_0^a(z,0), \qquad c(0,t) = c_0 \qquad (11.4a)$$

Start of desorption cycle (end of adsorption cycle)

$$\bar{q}(z,0) = \bar{q}_0^d(z,0) = \bar{q}_e^a(z',t_c), \qquad c(0,t) = 0 \qquad (11.4b)$$

These conditions imply that the initial distribution of sorbate at the start of the adsorption cycle, $\bar{q}(z,0)$, is the same as the final distribution at the end of the desorption cycle, $\bar{q}(z',t_c)$, where t_c is the duration of both adsorption and desorption cycles. Distances during desorption are measured from the bed outlet (z') to take account of the flow reversal.

The equations were written in dimensionless form and solved by standard finite difference methods. The relevant dimensionless variables which determine the behavior of the system are

$$\phi = \frac{c}{c_0}, \qquad \psi = \frac{\bar{q}}{q_0}, \qquad \bar{\psi} = \text{value of } \psi \text{ averaged over adsorbent bed}$$

$$\tau = k(t - z/v), \quad \xi^a = \frac{kzq_0^a}{v^a c_0}\left(\frac{1-\epsilon}{\epsilon}\right), \quad \xi^d = \frac{kzq_0^d}{v^d c_0}\left(\frac{1-\epsilon}{\epsilon}\right), \quad r = \xi^d/\xi^a$$

$$\lambda^a = \frac{q_0^a}{q_s} \qquad \text{where} \quad q_0^a = q^*(c_0, T^a) = \frac{b(T^a)q_s c_0}{1 + b(T^a)c_0}$$

$$\lambda^d = \frac{q_0^d}{q_s} \qquad \text{where} \quad q_0^d = q^*(c_0, T^d) = \frac{b(T^d)q_s c_0}{1 + b(T^d)c_0}$$

$$\gamma = \frac{\lambda^d}{\lambda^a}$$

The superscripts a and d refer to the adsorption and desorption cycles. The magnitude of the temperature swing is represented by γ, the ratio of nonlinearity parameters for adsorption and desorption.

The general behavior in the cyclic steady state for a two-bed system with nonlinear equilibrium is shown schematically in Figure 11.5. In order to prevent contamination of the raffinate product the adsorption cycle must be terminated before the concentration front reaches the outlet of the bed. For a given bed length (and other system parameters) there is therefore a maximum allowable cycle time. Similarly for a given cycle time there is a maximum usable bed length. Any further increase in the bed length merely adds unusable capacity. At the end of the adsoption cycle there is an unsaturated region at the bed outlet while at the end of the desorption cycle there is an undesorbed heel of sorbate near the bed entrance. The area between the two extreme profiles ($\Delta\bar{\psi}$) represents the fractional utilization of the capacity of the adsorbent. The progress towards the cyclic steady state, which for this particu-
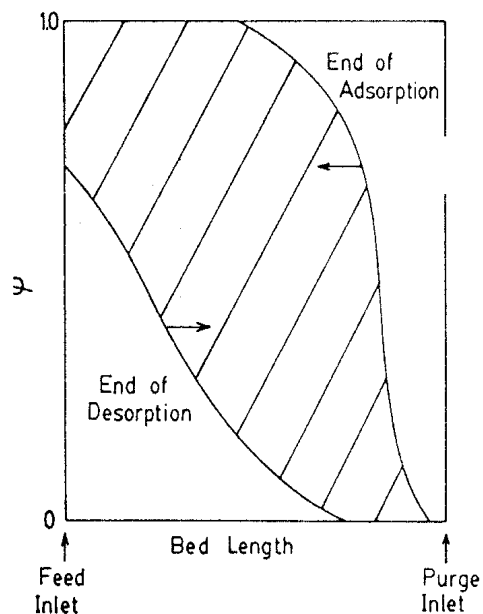
FIGURE 11.5. Simulated adsorbent loading profiles for the cyclic steady state in a two-bed thermal swing system. It is assumed that the adsorption cycle is terminated just prior to breakthrough in order to produce a pure raffinate product.
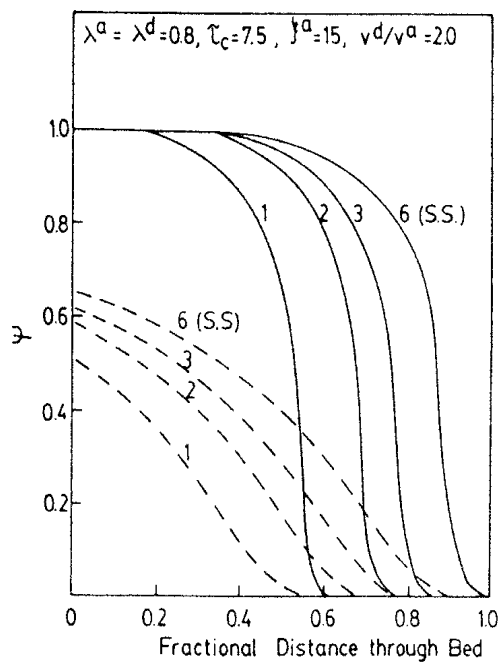
FIGURE 11.6. Simulated adsorption and desorption curves for a two-bed cyclic isothermal purge gas stripping system showing progress towards the cyclic steady state. Cycle numbers are indicated on the curves. Broken lines represent profiles at the end of the desorption cycle while solid lines represent profiles at the end of the adsorption cycle. (From Chao.[13])

349

lar choice of parameter values is reached in about six cycles, is shown in Figure 11.6.

The effects of the process variables on overall system performance may be examined by computing the cyclic steady-state profiles for a range of parameter values. We consider a simple system, such as a gas drier, with a single adsorbable component in an inert carrier. We assume that the feed composition, temperature, and flow rate are fixed and that the adsorption cycle should operate at the feed temperature. For a given adsorbent this fixes the capacity and the nonlinearity of the equilibrium relationship (λ^a). The designer then has the freedom to choose the regeneration temperature and purge flow rate, the cycle time, and the bed depth.

Efficient use of the adsorbent capacity requires that the bed length (ξ^a) be fixed at the minimum value required to just prevent breakthrough under the specified operating conditions since any increase in bed length beyond the minimum does not contribute useful capacity. If the system operates at constant temperature $(\lambda^a = \lambda^d)$ as in purge gas stripping, the only remaining variable is the purge flow rate or the ratio v^d/v^a. For any given cycle time (τ_c), there is therefore a range of bed lengths (ξ^a) with their corresponding purge rates (specified by $r = v^a/v^d$) which define acceptable conditions of operation. Such loci, calculated for two different cycle times and nonlinearity factors, are shown in Figure 11.7.

The effectiveness with which the adsorbent capacity is utilized is given by $\Delta\bar{\psi} = \tau_c/\xi^a$. However, the overall utilization depends on the product of the
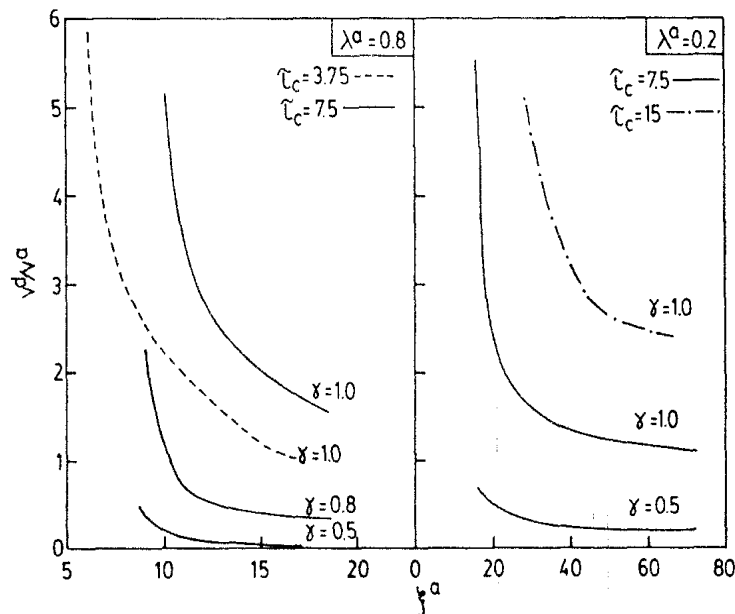
FIGURE 11.7. Variation of purge flow rate (v^d/v^a) with bed length for a two-bed cyclic system. Curves are calculated for two different isotherm nonlinearities $(\lambda^a = 0.8, 0.2)$, for three different levels of temperature swing $(\gamma = 0.5, 0.8, 1.0)$ and for three different cycle times $(\tau_c = 3.75, 7.5, 15)$. (Calculated from data presented by Chao.[13])
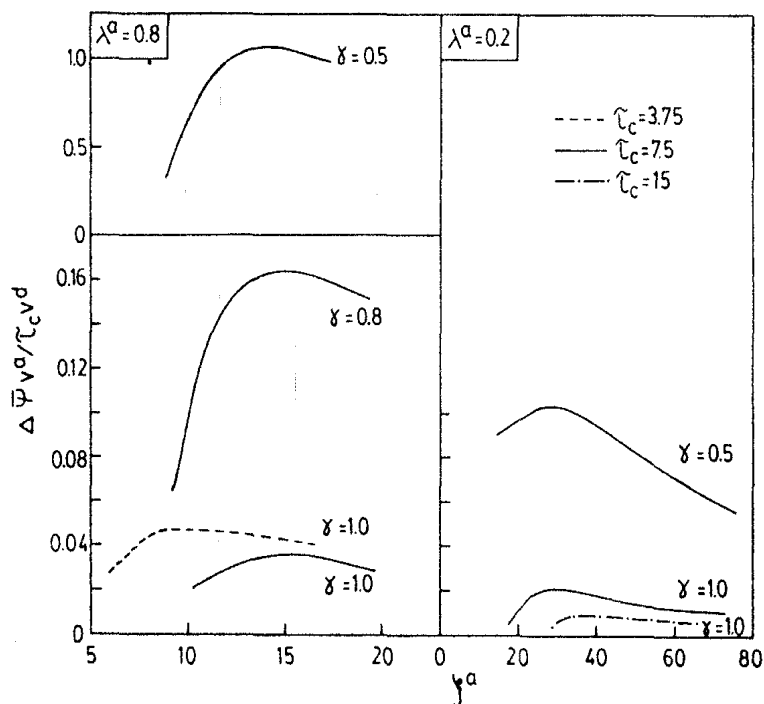
FIGURE 11.8. Variation of objective function $\Delta\bar{\psi}v^a/\tau_c v^d$ with bed length (ξ^a) for two different isotherm nonlinearities ($\lambda^a = 0.8$ and $\lambda^d = 0.2$) and three different temperature swings (measured by $\gamma = 0.5$, 0.8, and 1.0). (Calculated from data presented by Chao.[13])

capacity factor and the cycle frequency; $\Delta\bar{\psi}/\tau_c = 1/\xi^a$. The useful load per unit of purge flow rate is given by $(1/\xi^a)(v^a/v^d) = 1/\xi^d$ and the variation of this quantity with bed length, cycle time, and isotherm nonlinearity is shown in Figure 11.8. It is clear that for any specified cycle time and affinity factor there is a maximum which defines the most efficient operation.

The magnitude of this maximum increases as cycle time (and corresponding optimal bed length) are decreased, indicating that the operation is more efficient with a rapid cycle. However, it is generally not feasible to use very short cycle times because of the limitation imposed by the time required to heat and cool the adsorbent bed, which is ignored in the present analysis, and because the increased frequency of thermal cycling tends to reduce adsorbent life. Increasing the temperature of the desorption cycle has little effect on the utilization of the adsorbent but the purge requirement is dramatically reduced. This advantage must be offset against the increased cost of higher grade heat and by faster thermal aging of the adsorbent at higher temperature.

In practice the regeneration temperature is generally determined by an economic balance between the heating cost and the cost of purge gas while the cycle time is generally fixed by practical considerations. Once these have been fixed the analysis outlined here may be used to provide guidance concerning the optimal choice of bed length and purge gas flow rate, but because of the simplifications introduced into the theoretical model, such conclusions cannot be expected to be quantitatively accurate.

Drying of Air or Gas Streams

Figure 11.9 shows a schematic diagram of a typical two-bed thermal swing drier unit such as is widely used for the drying of air, natural gas, or other process streams.[14] The choice of adsorbent depends mainly on the nature of the gas stream and the level of dehydration required. When the humidity requirements are modest, silica gel is the preferred adsorbent because of its high capacity and easy regeneration but where low humidities are required, as in the drying of natural gas, molecular sieve (usually 4A) is generally employed (see Figure 11.10). For the drying of cracked gas and other hydrocarbon streams containing light olefins or other reactive species 3A sieve, which excludes the hydrocarbon molecules, is preferred since the risk of cracking and coking is minimized. Theoretical considerations suggest that when the moisture level is high it is advantageous to use a combination of two adsorbents. The first adsorbent, typically silica gel, has a high capacity and removes the bulk of the moisture at relatively high partial pressure while final dehydration is accomplished by the second adsorbent, usually a molecular sieve. With proper design, such a system can reduce significantly both the quantity of adsorbent and the regeneration gas requirements with no loss of product quality.

The design of both gas and liquid driers has been described in detail by
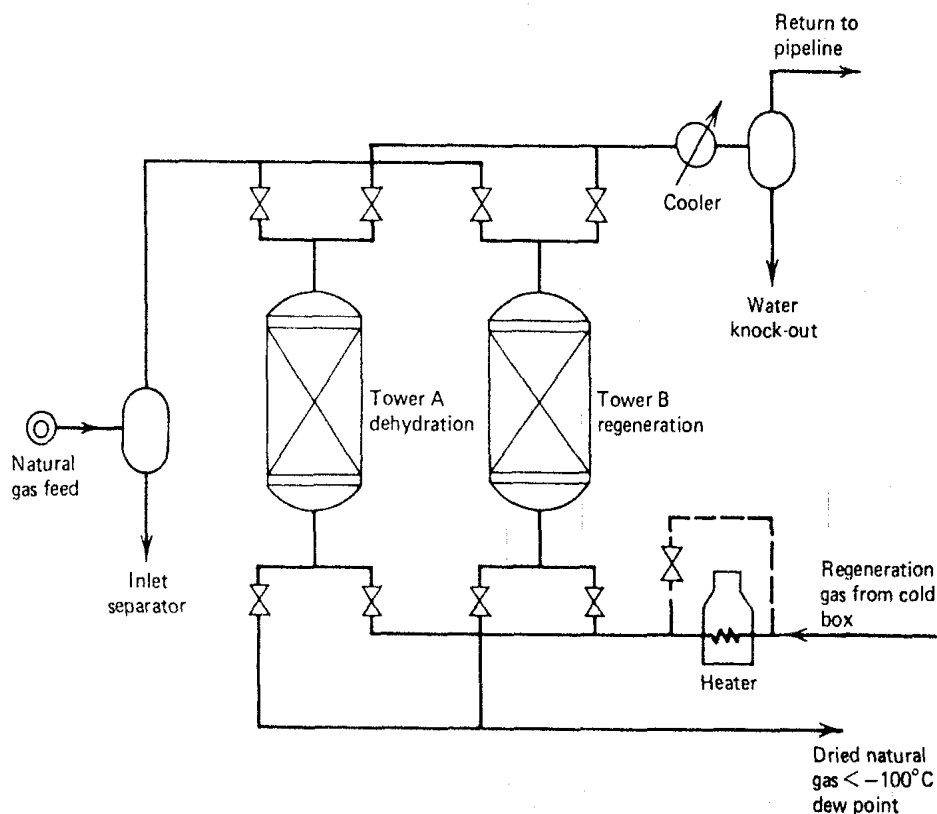
FIGURE 11.9. Schematic diagram of typical two-bed thermal swing gas dehydrator. (From ref. 14, copyright John Wiley & Sons, Inc., 1978; reprinted with permission.)

Basmadjian[15] and only a brief summary of some of the more important aspects is therefore given here.

Equilibrium Theory Analysis

Large-scale gas driers operate approximately adiabatically, and to predict the limiting performance from equilibrium theory the simultaneous integration of the differential heat and mass balance equations as outlined in Section 9.6 is required. In Chapter 9 we developed the equilibrium theory solutions as hodograph plots of fluid phase concentration against temperature. However, in the practical design of an adsorber one is concerned primarily with adsorbent bed size and purge gas requirements while the temperature history is of only secondary importance. It is therefore more convenient to display the results of the equilibrium theory solution in the form of the adiabatic equilibrium curves showing adsorbed phase versus fluid phase concentration for specified feed and initial bed conditions. Provided that the equilibrium relationship, the heat of adsorption, and the heat capacities of solid and gas are known, such curves may be calculated either by numerical integration [Eq. (9.42)] or by a simple graphical construction which has been described in detail by Basmadjian.[16,17]

The path which is followed may be determined directly from the form of adiabatic equilibrium curve and an approximate estimate of the bed volume and purge requirements per unit feed rate may be obtained from the slope of the relevant operating line. For adsorption along a (favorable) type I curve, the operating line is simply the chord connecting the initial bed state and the feed point. The corresponding breakthrough curve consists simply of a single shock transition. For desorption along an unfavorable (type III) curve the operating line is drawn between the purge gas state and the plateau state located at the intersection of the two different equilibrium curves through the feed state and the initial bed state. The corresponding desorption breakthrough curve consists of two transitions separated by a plateau, but the detailed form of the transitions depends on the purge temperature relative to the initial bed temperature, as illustrated in Figure 9.14.

Where the adiabatic equilibrium curve is sigmoidal, with a point of inflection, the operating line must be drawn from the initial or plateau point to the point of tangency. Under these conditions a composite front, partly sharp and partly diffuse, is obtained as shown in Figure 8.6 for an isothermal system with a BET isotherm.

The adiabatic adsorption and desorption equilibrium curves for two common desiccants (4A sieve and silica gel) are shown in Figure 11.10 and the corresponding adsorbent and purge requirements, calculated from the relevant operating lines are shown in Figures 11.11 and 11.12. These curves show the expected increase in both bed and regenerant requirements with feed moisture content as well as the pronounced advantage of the molecular sieve adsorbent at low humidities and the beneficial effects of an increase in regeneration temperature and of a decrease in regeneration pressure. They may be used to
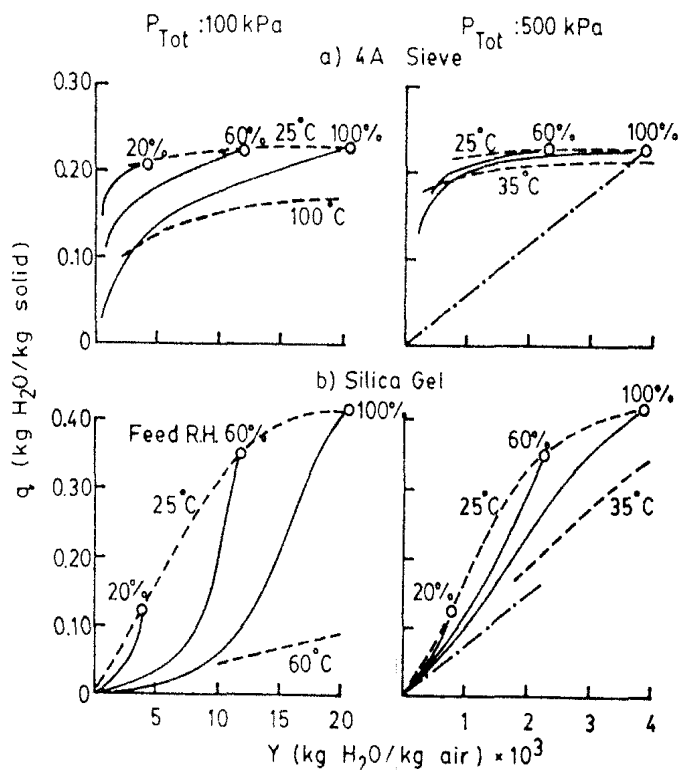
FIGURE 11.10. Isotherms (---) and adiabatic adsorption equilibrium curves (————) for (*a*) 4A sieve and (*b*) silica gel. Representative operating lines are shown as —·—·. The initial condition is taken as a clean bed. (From ref. 15, copyright Hemisphere Publishing Company, 1983; reprinted with permission.)

obtain initial design guidance over a wide range of practical operating conditions.

It may be seen from Figure 11.11 that the intersection of the two branches of the adiabatic desorption curves, corresponding to the plateau point, may occur at a point which lies above the saturation vapor pressure of the adsorbate, and under these conditions condensation will occur. Indeed, because of surface tension, condensation in the smaller macropores may occur at a vapor pressure appreciably below the saturation limit (Section 2.5). Friday and LeVan[18,19] have investigated this phenomenon in detail and have shown that condensation probably occurs in many gas driers under normal operating condition. (See Figure 11.13). In aqueous systems condensation is undesirable since most desiccants have limited hydrothermal stability and premature deterioration of the adsorbent is a likely consequence of such operation. The consequences with organic sorbates are generally less serious.

Condensation may be avoided by lowering the pure temperature or by ensuring that the purge temperature is raised to its final level sufficiently slowly. The penalty is an increase in the quantity of purge gas required for regeneration. A similar result may sometimes be achieved, either deliberately or fortuitously, by the intrusion of mass transfer resistance since if mass transfer resistance is sufficiently high the fluid phase concentration will never
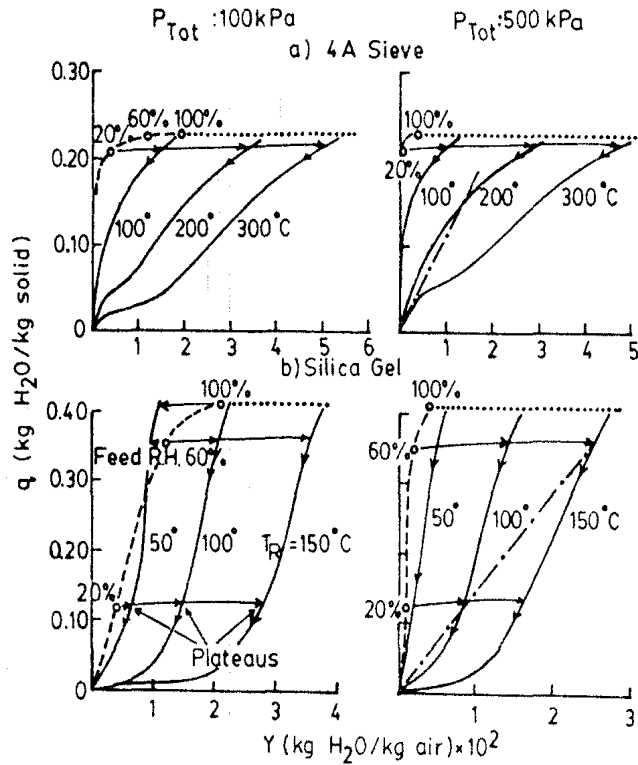
FIGURE 11.11. Adiabatic desorption equilibrium curves for (a) 4A sieve and (b) silica gel. Curves are calculated for a uniformly saturated bed at 25 °C at the indicated humidity, assuming bone-dry purge gas at the specified temperature. The 25 °C isotherm is shown as – – –, representative operating lines are shown as –·–· and the saturation limit is indicated by a dotted line. (From ref. 15, copyright Hemisphere Publishing Company, 1983; reprinted with permission.)
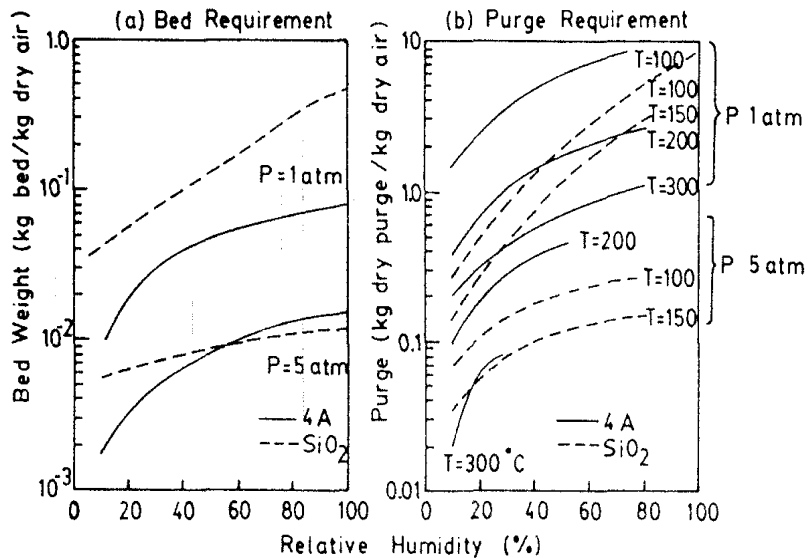
FIGURE 11.12. (a) Adsorbent bed requirement and (b) purge gas requirement per unit feed calculated from the equilibrium curves of Figures 11.11 and 11.12. Curves are shown for operation at atmospheric pressure and at 5 atm. (From ref. 15, copyright Hemisphere Publishing Company, 1983; reprinted with permission.)

355
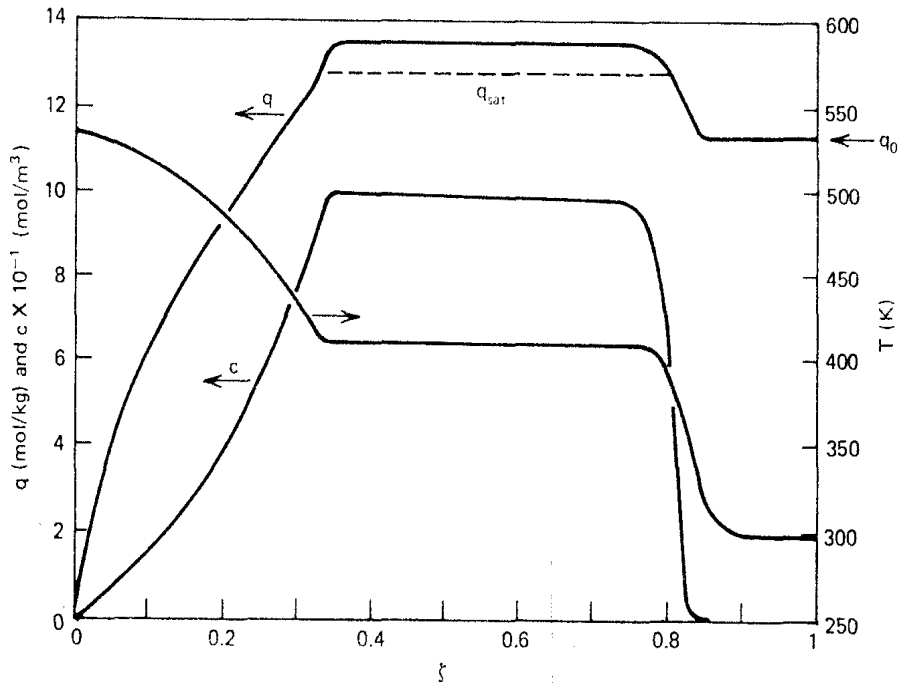
FIGURE 11.13. Theoretical profiles of concentration (c) and temperature (T) during thermal regeneration of an adiabatic natural gas drier showing "roll-up" effect leading to condensation in the bed. (From ref. 18, reprinted with permission.)

reach the plateau concentration predicted by equilibrium theory. This method has the obvious disadvantage that the dynamic capacity during adsorption is reduced correspondingly. A more satisfactory solution is to reduce the pressure during desorption.

Mass Transfer Resistance

To refine the preliminary equilibrium theory design it is necessary to consider mass transfer resistance. This is generally allowed for by using the LUB approach (Section 8.7) but provided that mass transfer coefficients or diffusivity data are available one may also use the Hiester–Vermeulen charts[20] (Section 8.6). However if an accurate design is required it is probably preferable to return to first principles and solve numerically the coupled heat and mass balance equations as outlined in Section 9.7 since it is only by such an approach that one may accurately account for the effect of incomplete regeneration and so optimize the choice of cycle time and regeneration conditions.

The Heat Balance

During the regeneration cycle the heat required to raise the temperature of the adsorbent bed as well as the heat of desorption and heat of evaporation of any residual liquid in the bed must be supplied by the purge gas. It is therefore essential to check the heat balance before the design conditions are finalized.

In a typical molecular sieve drier unit, the heat of desorption and the sensible heat required to raise the temperature of the adsorbent and vessel each contribute about equally to the total heat load. In the thermal regeneration of beds used for liquid phase adsorption the heat load is somewhat greater since the heat required to evaporate residual liquid from the macropores and surface of the adsorbent may be comparable with the heat required for desorption. A recent pilot plant study[21] showed that in a 4A sieve drier system the volume of purge required for desorption was about four to five times the theoretical volume required for heat transfer or about three to four times the actual purge volume required for heat transfer. Under these conditions the desorption cycle is mass transfer limited and the heat balance is automatically satisfied even by the minimum required purge. This is commonly the situation when regeneration is carried out at elevated pressure but if regeneration is carried out at atmospheric pressure the volume of purge required to desorb the bed is much smaller, particularly when regeneration is achieved by both lowering the pressure and raising the temperature. Under these conditions the cycle is commonly thermally limited and the minimum purge requirement may then be determined by the heat balance.
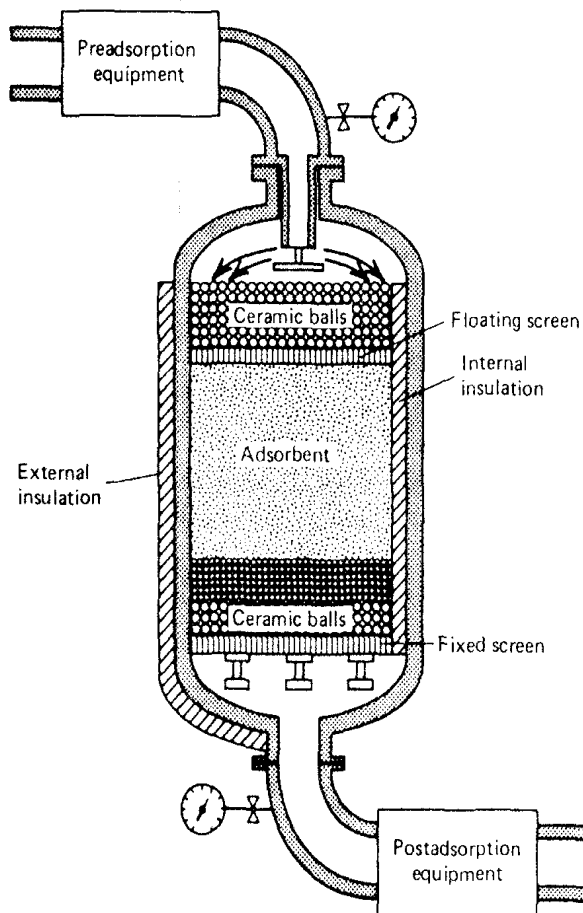
FIGURE 11.14. Schematic diagram showing typical arrangement for bed support and flow distribution in a fixed-bed drier. (Courtesy of W. R. Grace).

In a natural gas drier the bed is commonly regenerated by using as purge either a hot stream of purified product gas or, where ultimate dew point is less important, hot-feed gas. The purge requirement amounts typically to 5–10% of the feed but the precise figure varies quite widely depending on the humidity level required and the regeneration temperature.

Other Considerations

Other factors requiring detailed consideration are the choice of fluid velocity, particle size, and bed configuration. These have been discussed in Chapter 7. To obtain good flow distribution during both adsorption and regeneration and to prevent dune formation at the free surface it is common practice to support the adsorbent on a few inches of ceramic particles and to cover the surface of the adsorbent at the top of the bed in a similar way. Details of one typical arrangement are shown in Figure 11.14.

Theoretical considerations show that a cooling step is not required (see Section 9.6) but such a step is in fact included in many industrial units.

Sweetening of Sour Gas

The sweetening of sour gas provides a good example of a process which involves the adsorption of more than one species. A schematic of a typical system is shown in Figure 11.15.[22] In essential features the process is similar to the simple dehydration process but the profiles of concentration and temperature through the adsorbent bed are more complicated. It is usual to use a large-pore type X sieve as the adsorbent in order to adsorb mercaptans as well as H_2S.

The form of the mass transfer zones during the adsorption cycle is sketched in Figure 11.16 while typical breakthrough curves from a pilot plant study[19] are shown in Figure 11.17. There are three adsorbable components with adsorption affinities in the order $H_2O > H_2S > CO_2$. The concentration profile during adsorption thus consists of three constant-pattern adsorption zones separated by two plateau regions. In normal sweetening, removal of CO_2 is not necessary so the adsorption cycle is continued until the H_2S break point. It is therefore the form of the second mass transfer zone in which H_2S displaces CO_2 which determines the LUB. This zone is generally more diffuse than the rather sharp moisture adsorption zone which occurs in a drier and accurate estimation of the LUB is therefore more important. In estimating the LUB it is necessary to allow for both the width of the H_2S mass transfer zone and the fraction of the bed which is saturated with moisture. An empirical correlation for the LUB, based on pilot plant data, has been given by Chi and Lee.[23] A theoretical calculation based on the methods discussed in chapter 9 would also be possible given sufficiently detailed equilibrium and kinetic data. Apart from the additional complexity of the mass transfer zones the general design considerations are similar to those for a drier unit.
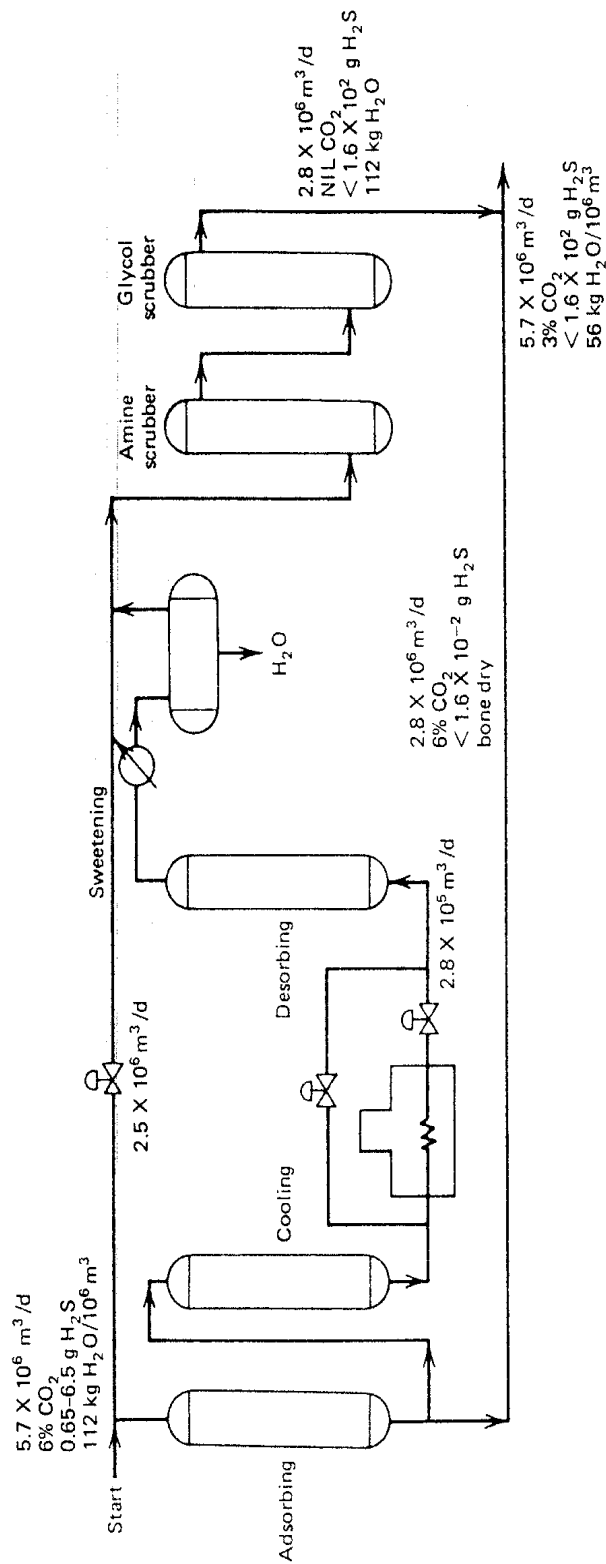
FIGURE 11.15. Schematic diagram of a typical thermal swing process for sweetening of sour gas. (From ref. 22, copyright John Wiley & Sons, Inc., 1978; reprinted with permission.)
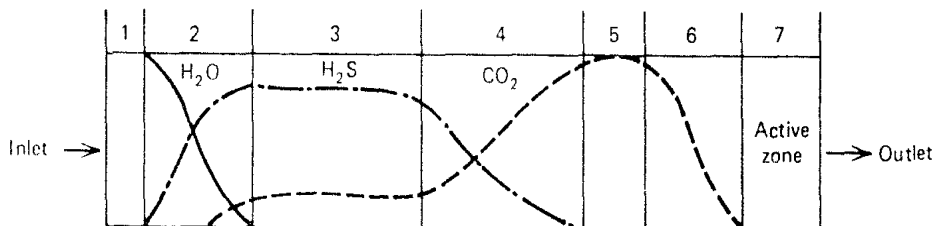
FIGURE 11.16. Schematic representation of the concentration profiles through the adsorbent bed during simultaneous adsorption of H_2O, H_2S, and CO_2 from sour gas. (From ref. 22, copyright John Wiley & Sons, Inc., 1978; reprinted with permission.)

Where the concentrated sour gas recovered during the regeneration cycle cannot be used as fuel, or otherwise disposed of, it is sometimes further treated by absorption in ethanolamine solution.

A particular problem in this process is the formation of COS by reaction between adsorbent CO_2 and H_2S:

$$CO_2 + H_2S \rightarrow COS + H_2O$$
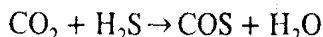
The formation of COS is undesirable since it passes through the system with CO_2 leaving significant sulphur in the gas and if the gas is fractionated to recover heavier hydrocarbons COS is concentrated in the propane fraction. In contact with traces of moisture the COS can be hydrolyzed back to H_2S with obvious undesirable consequences.

It has been found that Ca^{2+} exchanged sieves generally show less catalytic activity than the Na^+ forms for this reaction. Formation of COS can therefore
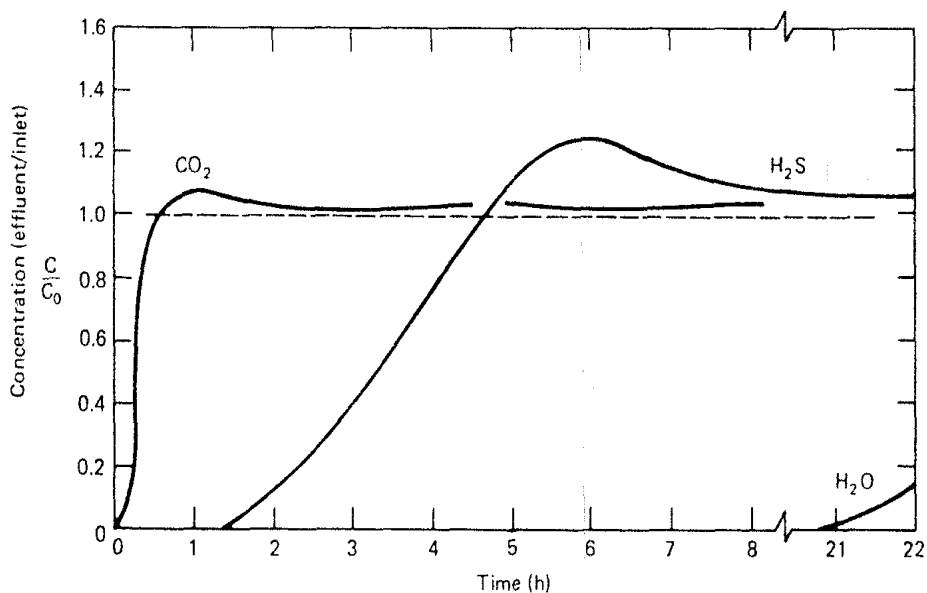
FIGURE 11.17. Experimental breakthrough curves of CO_2, H_2S, and H_2O obtained in a pilot plant study of the drying and sweetening of natural gas. (Feed: CO_2, 1.14%; H_2S, 730 ppm; $P = 68$ atm; $T = 298$ K). (From ref. 23, copyright John Wiley & Sons, Inc., 1978; reprinted with permission.)

be minimized by using the zeolite in its Ca^{2+} form (10X) and taking care to minimize the iron content of both zeolite and binder since traces of iron also catalyze this reaction.

11.3. PRESSURE SWING PROCESSES

In pressure swing adsorption (PSA) systems, regeneration of the adsorbent during the desorption cycle is achieved simply by reducing the total pressure and purging the bed at low pressure with a small fraction of the product stream. The process therefore operates between two different points on the same equilibrium isotherm as indicated in Figure 11.2. The original PSA system was the "heatless drier" developed by Skarstrom[24,25] for air drying, but in recent years processes of this kind have been developed for a wide range of industrially important separations. The PSA system in its basic form consists of two beds which are alternately pressurized and depressurized according to a preprogrammed sequence. The basic system is shown schematically in Figure 11.18 while the sequence of the cycle is indicated in Figure 11.19. This basic type of system is used in the heatless drier and in small-scale
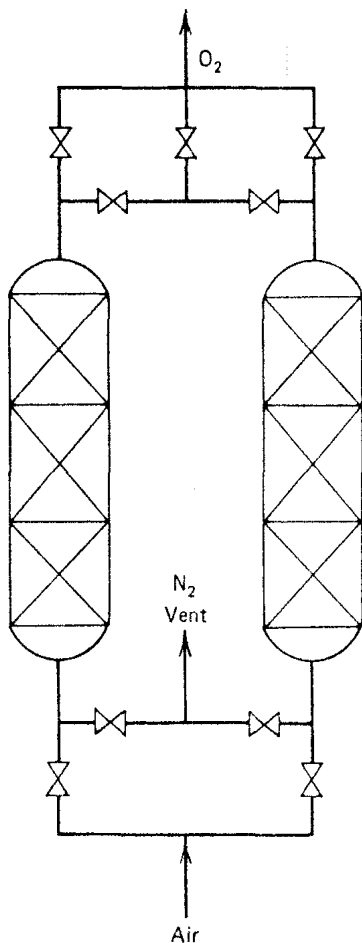
FIGURE 11.18. The basic two-bed pressure swing adsorption system. (After Skarstrom[24]; from ref. 32; reprinted with permission.)
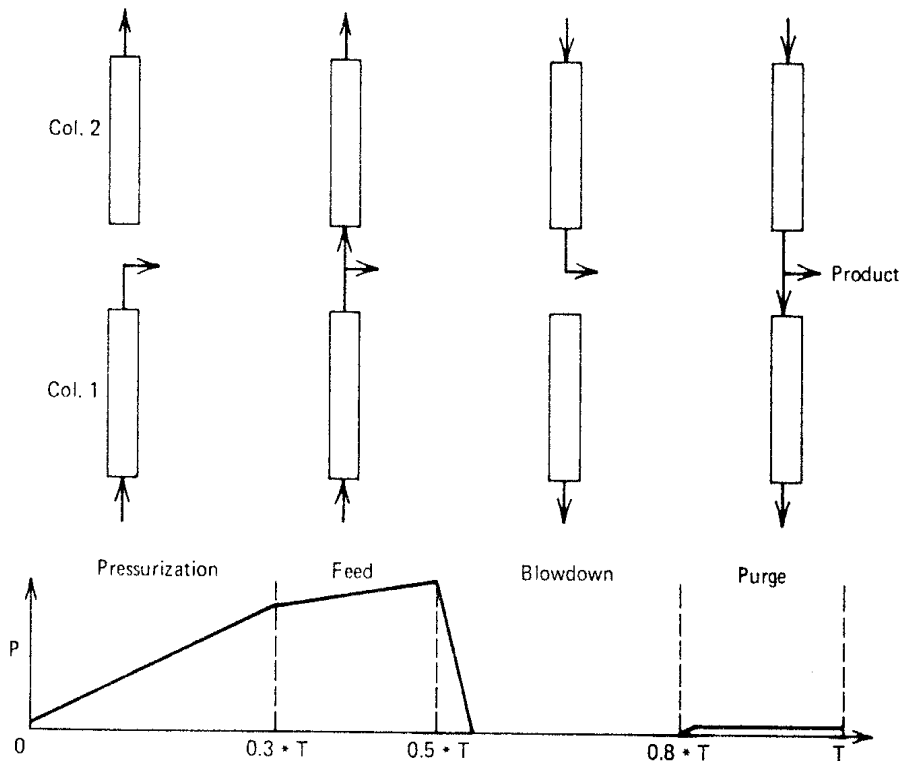
FIGURE 11.19. The sequence of steps in the basic PSA cycle.

air separation units, but in large-scale air separation and hydrogen purification systems more complex cycles involving three or four adsorbent beds are generally used in order to reduce power consumption.

From a thermodynamic perspective the essential difference between PSA and thermal swing processes is that in the PSA system the energy required to achieve the separation is put into the system as mechanical work rather than as heat. Since mechanical energy is generally more expensive than heat, efficient utilization of energy is essential for an economic PSA system. Such considerations become especially important in the larger scale units.

The pressure swing system is well suited to rapid cycling and generally operates at relatively low adsorbent loadings since selectivity is greatest in the Henry's law region. Low-temperature operation is also desirable to maximize capacity and selectivity but cooling below ambient temperature is generally not economic.

The purging step is essential for an efficient separation. Reverse-flow purge ensures that the more strongly adsorbed components are pushed back towards the bed inlet and do not contaminate the raffinate product in the next cycle. It is essential that sufficient purge is used to flush completely the void spaces within the bed as well as to desorb any of the more strongly adsorbed components from the outlet region of the bed. Product purity increases as the purge is increased but after a certain point the gain becomes marginal. In practice the volume of the purge, measured at low pressure, should generally be between one and two times the volume of the feed stream (measured at

high pressure). The increase in volume on depressurization means that the actual fraction of the product stream required for purging is quite small and decreases with the operating pressure. Thus high-pressure operation is desirable from the standpoint of minimizing purge loss but this gain is to some extent offset by the greater blowdown losses for a high-pressure system.

Theoretical Analysis

Most PSA processes depend on equilibrium selectivity and the simplest approach to the modeling of these systems is through equilibrium theory.[†] Such an analysis was first developed by Shendalman and Mitchell[26] for the case of a single adsorbable species in a nonadsorbing carrier. The theory was extended by Chan, Hill, and Wong[27] to a system with two adsorbable components subject to the restriction that the equilibrium relationships for both species are linear and the more strongly adsorbed species is present only at low concentration. The system is described by the following equations:

$$\frac{\partial c_1}{\partial t} + \frac{\partial}{\partial z}(vc_1) + \left(\frac{1-\epsilon}{\epsilon}\right)\frac{\partial q_1^*}{\partial t} = 0$$

$$\frac{\partial c_2}{\partial t} + \frac{\partial}{\partial z}(vc_2) + \left(\frac{1-\epsilon}{\epsilon}\right)\frac{\partial q_2^*}{\partial t} = 0$$
(11.5)

$$q_1^* = K_1 c_1, \qquad q_2^* = K_2 c_2$$
(11.6)

For a trace system with negligible pressure drop these equations may be combined to give

$$\left[1 + \left(\frac{1-\epsilon}{\epsilon}\right)K_1\right]\frac{\partial y}{\partial t} + v\frac{\partial y}{\partial z} + \left(\frac{1-\epsilon}{\epsilon}\right)(K_1 - K_2)y\frac{\partial \ln p}{\partial t} = 0$$
(11.7)

where y is the mole fraction of component 1. This is a quasilinear first-order equation from which the two following ordinary differential equations are obtained:

$$\frac{dt}{1 + \left(\frac{1-\epsilon}{\epsilon}\right)K_1} = \frac{dz}{v} = \frac{-d\ln p}{\left(\frac{1-\epsilon}{\epsilon}\right)(K_A - K_B)\frac{\partial \ln p}{\partial t}}$$
(11.8)

The solution may thus be obtained by integration along the characteristics which for this simple case are linear in the $z - t$ plane. By this method Chan, Hill, and Wong[27] were able to derive a number of useful relationships including the critical purge-feed ratio and the fractional recovery of major and minor components as a function of pressure ratio and separation factor. The

---

[†] A useful review has been given by Kenney and Kirby, NATO ASI, Sintra-Estoril, Portugal, May 1983. Proceedings to be published by Martinus Nijhoff, Holland. *See also* Flores, Fernandez, and Kenney, *Chem. Eng. Sci.* **38**, 827 (1983).
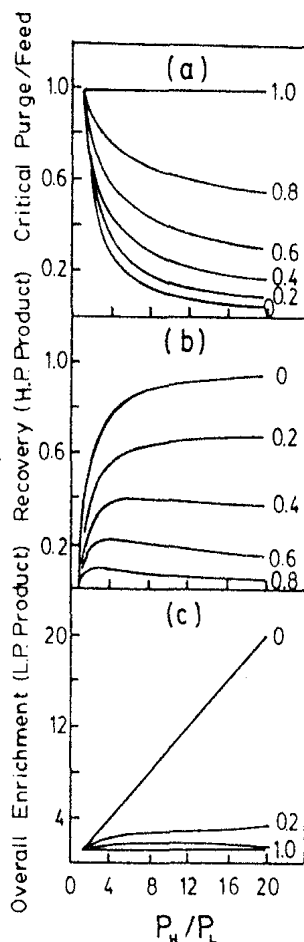
FIGURE 11.20.   Variation of (a) critical purge–feed ration, (b) fractional recovery of high-pressure product, and (c) enrichment of low-pressure product. Parameter β' (modified separation factor). [Reprinted with permission from *Chem. Eng. Sci.* **36**, after Chan, Hill, and Wong (ref. 27). Copyright 1981, Pergamon Press, Ltd.]

results are summarized in Figure 11.20 where the separation factor is expressed in terms of a modified parameter defined by

$$\beta' = \left[1 + \left(\frac{1-\epsilon}{\epsilon} \right) K_2 \right] \Big/ \left[1 + \left(\frac{1-\epsilon}{\epsilon} \right) K_1 \right] \qquad (11.9)$$

For large values of K_1 and K_2 this reduces to the same form as Eq. (9.9). The restriction that the more strongly adsorbed species be present only at low concentration has been relaxed in a more recent study.[28]

One important result which follows from the equilibrium theory analysis is that as long as the dimensionless bed length (kL/v) exceeds a critical minimum value a pure raffinate product will be obtained. However, the results of an experimental study carried out by Mitchell and Shendalman[29] with the CO_2-He-silica gel system showed considerable deviations from the predictions of simple equilibrium theory, indicating that kinetic or dispersive effects are important. A modified theory which included finite mass transfer resistance was developed but proved only marginally more successful in accounting for the observed behavior of the system.

TABLE 11.4. Dynamic Model for a PSA System[31]

Assumptions:	One adsorbable species, inert carrier.
	Axial dispersed plug flow.
	Linear rate expression and linear isotherm.
	Isothermal system.
Step 1:	High pressure flow in bed 2, low pressure (purge) in bed 1

External fluid

Bed 2:
$$-D_{LH}\frac{\partial^2 c_2}{\partial z^2} + v_2\frac{\partial c_2}{\partial z} + \frac{\partial c_2}{\partial t} + \left(\frac{1-\epsilon}{\epsilon}\right)\frac{\partial \bar{q}_2}{\partial t} = 0$$

Bed 1:
$$-D_{LL}\frac{\partial^2 c_1}{\partial z^2} + v_1\frac{\partial c_1}{\partial z} + \frac{\partial c_1}{\partial t} + \left(\frac{1-\epsilon}{\epsilon}\right)\frac{\partial \bar{q}_1}{\partial t} = 0$$

Mass transfer rate equations

Bed 2: $\quad \partial \bar{q}_2/\partial t = k_2(q_2^* - \bar{q}_2)$

Bed 1: $\quad \partial \bar{q}_1/\partial t = k_1(q_1^* - \bar{q}_1)$

Equilibrium

Bed 2: $\quad q_2^* = Kc_2$

Bed 1: $\quad q_1^* = Kc_1$

Boundary conditions

Bed 2:
$$D_{LH}\frac{\partial c_2}{\partial z}\bigg|_{z=0} = -v_2(c_1|_{z-0^-} - c_2|_{z=0^+})$$

$$\frac{\partial c_2}{\partial z}\bigg|_{z=L} = 0$$

Bed 1:
$$D_{LL}\frac{\partial c_1}{\partial z}\bigg|_{z=0} = -v_1\left(\frac{P_L}{P_H}c_z - c_1|_{z=0^+}\right)$$

$$\frac{\partial c_1}{\partial z}\bigg|_{z=L} = 0$$

Initial conditions $\quad c_2(z,0) = q_2(z,0) = c_1(z,0) = q_1(q,0) = 0$

Step 2 for bed 2

External fluid
$$-D_{LL}\frac{\partial^2 c_2}{\partial z^2} - \frac{\partial(vc_2)}{\partial z} + \frac{\partial c_2}{\partial t} = 0$$

$$\frac{\partial v}{\partial z} = \frac{1}{P}\frac{\partial P}{\partial t}$$

Boundary conditions

$$\frac{\partial c_2}{\partial z}\bigg|_{z=0} = 0; \qquad \frac{\partial c_2}{\partial z}\bigg|_{z=L} = 0; \qquad u|_{z=L} = 0$$

Note: Relevant equations for blowdown of bed 1 (step 4 of cycle) are similar but since the blowdown occurs from the opposite end of the bed the signs of the terms involving $\partial/\partial z$ are reversed. It is assumed that D_L is directly proportional to v and independent of P (high Re region) while $k \propto 1/P$ as for pore diffusion in the regime of molecular diffusional control.

A somewhat similar dynamic simulation of a PSA air drier has been recently presented by Carter and Wyszynski, *Chem. Eng. Sci.* **38**, 1093 (1983).

More recently, numerical simulations of the simple PSA process have been developed by Chihara,[30] who used conventional finite difference methods and Raghavan, Hassan, and Ruthven[31] who used the method of orthogonal collocation. For solutions of comparable accuracy the collocation method was shown to require considerably less computer time. Brief details of Raghavan's model are given in Table 11.4. Computed curves showing the approach to steady-state operation are given in Figure 11.21 and a comparison of the

(a)

$PeH = PeL = 10^3, \alpha = 20, \tau_{fH} = 5.56 \times 10^{-4}, \tau_{fL} = 27.8 \times 10^{-4}, K = 9084$

(b)
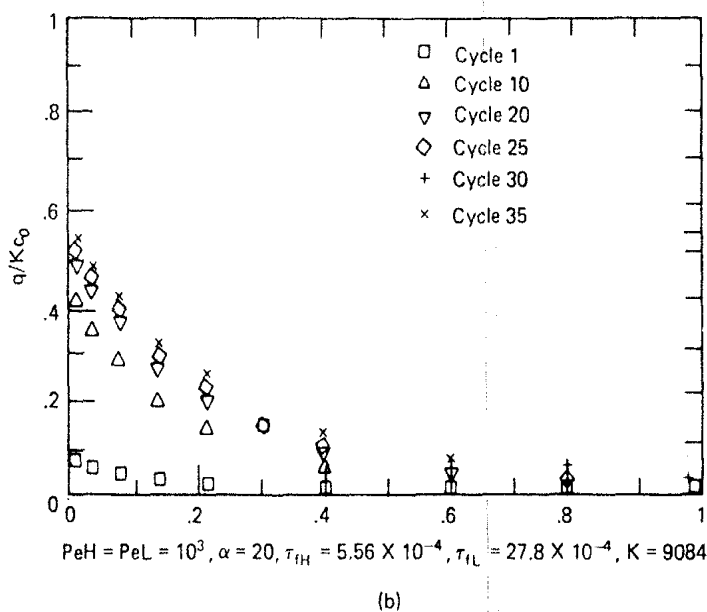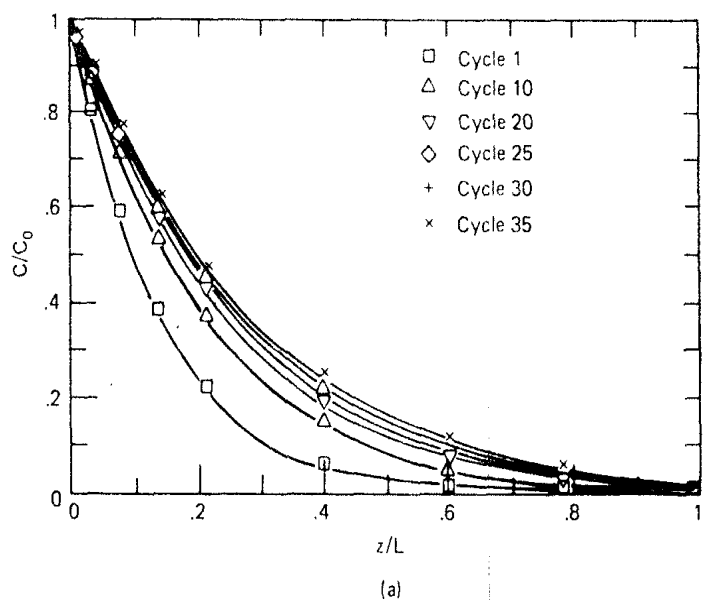
FIGURE 11.21. (a) Gas phase and (b) adsorbed phase concentration profiles at the end of the high-pressure (adsorption) step showing progress towards the cyclic steady state in a two-bed PSA system with parameters representative of an air drier system ($Pe_H = Pe_L = 10^3$, $v_L/v_H = 2.0$, $L = 0.5$ m, half-cycle time 270 s, $K = 9000$, $k = 2.8 \times 10^{-4}$ s^{-1}, $v_H = 25$ cm/s, $P_H = 5$ atm, $P_L = 1$ atm, $\epsilon = 0.4$). (From Raghavan, Hassan, and Ruthven.[31])

theoretical predictions with the experimental data of Mitchell and Shendalman is shown in Figure 11.22 and Table 11.5. The results of this simulation show clearly that modest deviations from plug flow and/or finite resistance to mass transfer lead to rather large deviations from the predictions of the simple equilibrium theory. Thus, although equilibrium theory can provide useful initial guidance concerning the selection of possible operating conditions a more detailed model is required to predict performance. For a linear system the performance is governed by the combination $(D_L/vL) + \epsilon v/(1 - \epsilon)kKL$, which measures the combined effects of axial dispersion and mass transfer resistance, rather than by the individual values of the Peclet number and mass transfer rate coefficient. To obtain a good prediction of system performance requires accurate estimates of this combined parameter for both high- and low-pressure flow conditions.

The sensitivity of the process to mass transfer resistance and axial dispersion also means that in order to achieve an efficient practical system it is essential to minimize these effects. In most practical PSA systems the mass transfer rate is controlled by macropore diffusion and the mass transfer
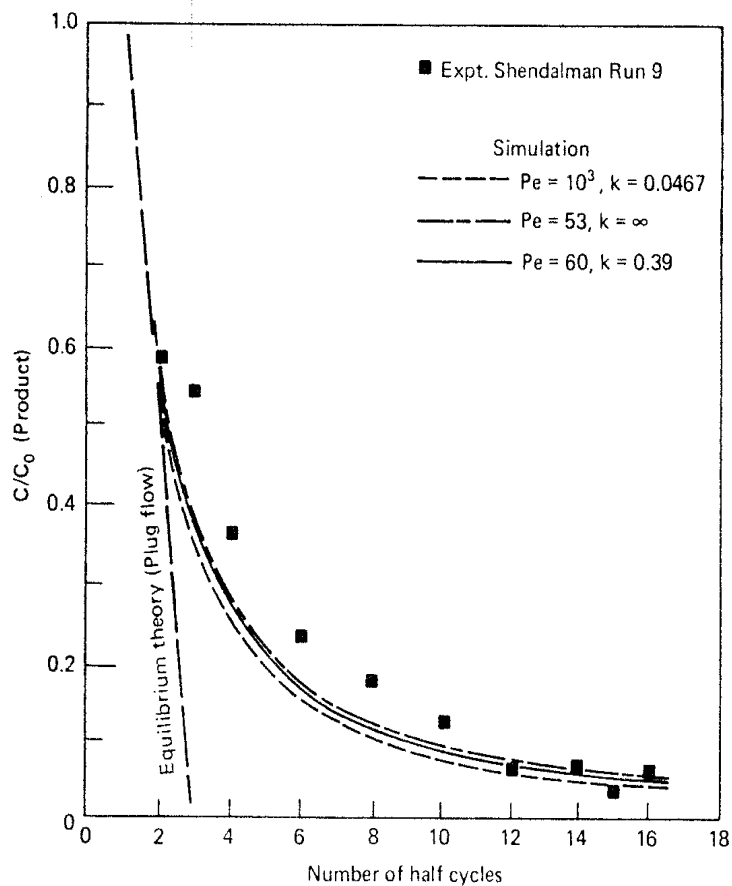
FIGURE 11.22. Comparison of experimental data of Mitchell and Shendalman[29] for separation of CO_2-He on silica gel (■) with theoretical curves calculated from the simulation of Raghavan et al.[31] The various combinations of Pe and k were selected to give a constant value for the linear combination $[1/Pe + \epsilon v_H/(1 - \epsilon)kKL]$. Details of experimental conditions and model parameters are given in Table 11.5.

TABLE 11.5. Parameters used in Calculation of Theoretical Curves for PSA Data of Shendalman and Mitchell (Figure 11.22)

Common Parameters	
Feed gas composition	1.09% CO_2 in He
Feed pressure	4.0 atm
Purge pressure	1.33 atm
Column length	61 cm
Cross-sectional area	11.4 cm^2
Bed porosity	0.42
Adsorption equilibrium constant K	52.7
Time for steps 2 and 4	$0.25t^*$
Temperature	25°C
Adsorbent	W. R. Grace Silica Gel (Tel-Tale, grade 92, 6-16 mesh)
$\alpha = v_L/v_H$	1.5
Feed rate (SCFM)	0.15
Time for steps 1 and 3 t^*(s)	180
Dimensionless time for steps 1 and 3 $t^* v_H / L$	10.91
Linear Combination $[(1/Pe + \epsilon v_H/(1 - \epsilon)kKL]$	0.0188
k (s^{-1})^a	0.0467

^{a}Experimentally measured value of k at high pressure assuming Pe → ∞. It is assumed that $k\alpha 1/P$.

resistance may therefore be minimized by using an adsorbent with relatively large pores and a small particle diameter. To minimize axial dispersion a carefully packed bed is required and the gas velocity should be kept high.

PSA Air Separation

Pressure swing units are widely used for air separation, both on a small scale for production of medical oxygen and, increasingly, on a large scale as an alternative to the cryogenic process for production of industrial oxygen and nitrogen. There are two different types of process in common use. Processes which utilize a zeolite adsorbent depend on the preferential adsorption of nitrogen under equilibrium conditions, whereas processes which use a carbon molecular sieve depend on a kinetic separation in which oxygen, the faster diffusing species, is preferentially adsorbed. The types of cycles, the conditions of operation, and the product purities are quite different for these two types of process.
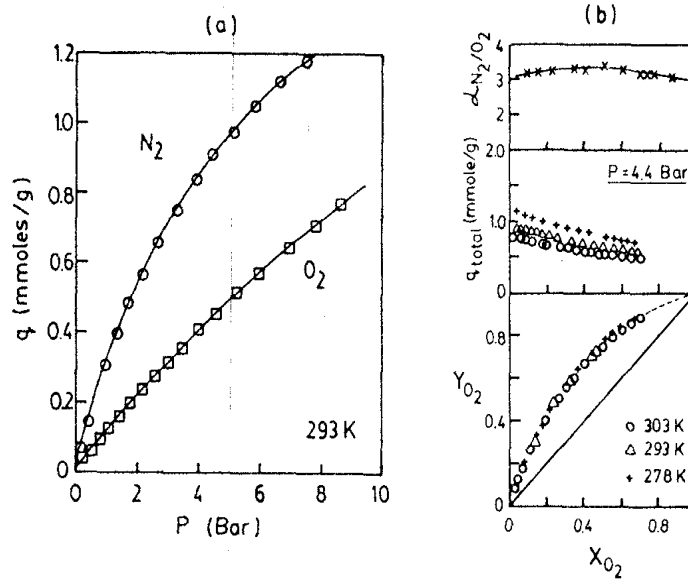
FIGURE 11.23. Equilibrium data for sorption of O_2, N_2, and O_2-N_2 binary mixtures on zeolite 5A showing (a) single-component isotherms and (b) variation of separation factor and total adsorbed phase concentration and $X-Y$ diagram. (From Sorial, Granville, and Daly.[33])

Zeolite Process

The earlier commercial units used either 5A or 13X sieves for which the equilibrium separation factor is about 3.0–3.5 at 25°C. Experimental equilibrium data for the O_2-N_2-5A system[33] are shown in Figure 11.23. Even with this modest separation factor, essentially complete removal of nitrogen may be achieved in a well-designed system. However, argon is not separated from oxygen so the maximum purity of the oxygen product is 96–97%. The presence of a small amount of argon causes no problem in many applications but it is a serious disadvantage in welding applications since the presence of even 2–3% argon leads to a significant reduction in the temperature.

The smaller PSA units generally use only two adsorbent beds and oxygen recovery is generally relatively low ($< 25\%$). Representative experimental data showing oxygen purity and fractional recovery are given in Figure 11.24.[25] For small-scale units the low oxygen recovery is not a serious disadvantage but, in the development of larger scale units, improvement of the oxygen recovery has been a major concern since power costs have a major impact on the overall process economics. A variety of process modifications have been suggested and these developments have been reviewed by Lee and Stahl.[32] The inclusion of a pressure equalization step, which is standard in most modern PSA systems, appears to have been first suggested by Berlin.[34] After the first bed has been purged and the second bed has completed the adsorption step, instead of blowing down the second bed directly, both beds are connected to equalize the pressure. The first bed is therefore partly pressurized with the oxygen-rich gas from the outlet region of the second bed. Following
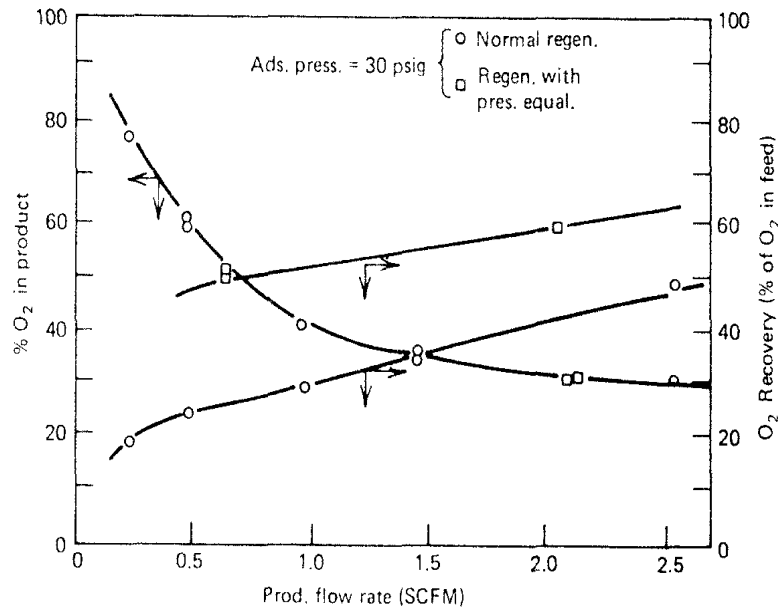
FIGURE 11.24. Purity and fractional recovery of O_2 in a bed PSA air separation unit showing improvement in recovery obtained by inclusion of a pressure equalization step. (Reprinted with permission from *Recent Developments in Separation Science*, copyright CRC Press Inc., Boca Roton, FL.)

pressure equilization the beds are disconnected and the first bed is pressurized with feed air while the second bed is vented to complete the blowdown. The resulting increase in recovery is shown in Figure 11.24.[25]

More complex schemes including three- and four-column systems have also been developed.[35] One such example is shown schematically in Figure 11.25. In this system, which utilizes four columns, one column is in the adsorption step and the other three columns are in various stages of pressurization, depressurization, or purging. The principle is a straightforward extension of the Berlin system. The process operates at two intermediate pressures between the feed pressure and the exhaust pressure (usually atmospheric). At the end of the adsorption step, column 1, which is at high pressure, is connected at the discharge end to column 2, which has just completed the purge step and is essentially at atmospheric pressure, and the pressures are equalized. In this way oxygen-rich gas is conserved and used for partial pressurization of bed 2. A fraction of the remaining gas from bed 1 is used for reverse-flow purging of bed 3. When the pressure in bed 1 has fallen to the required level, beds 1 and 3 are disconnected and the residual gas from bed 1 is vented to atmosphere from the bed inlet. Bed 1 is then purged in reverse flow with gas from the fourth bed and repressurized to the first intermediate pressure with gas from the second bed which has just completed the adsorption step. Final repressurization is accomplished using product gas and the feed is then connected to the inlet of bed 1. With this cycle, which is summarized in Figure 11.26, a considerable reduction in power is achieved compared with the two-bed system, but only at the expense of introducing additional columns and a more complex cycle.
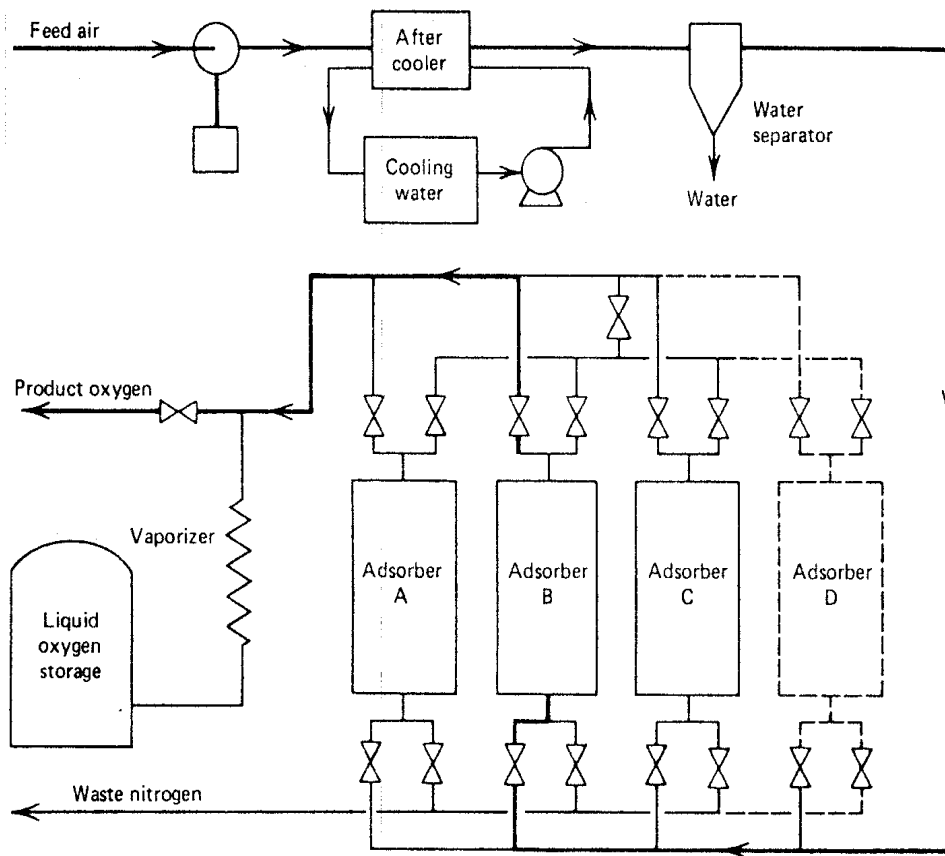
FIGURE 11.25. Schematic diagram of a four-bed PSA system for air separation. [From ref. 35; excerpted by special permission from Chemical Engineering, Oct. 16, 1978, p. 88. Copyright © 1978, by McGraw-Hill, Inc., New York, N.Y. 10020.]

Vessel
Number

1	Adsorption			EQ1 ↑	CD ↑	EQ2 ↑	CD ↓	Purge ↓	EQ2 ↓	EQ1 ↓	R ↓
2	CD ↓	Purge ↓	EQ2 ↓	EQ1 ↓	R ↓		Adsorption		EQ1 ↑	CD ↑	EQ2 ↑
3	EQ1 ↑	CD ↑	EQ2 ↑	CD ↓	Purge ↓	EQ2 ↓	EQ1 ↓	R ↓	Adsorption		
4	EQ1 ↓	R ↓	Adsorption				EQ1 ↑	CD ↑	EQ2 ↑	CD ↓	Purge ↓	EQ2 ↓

EQ—Equalization   ↑—Cocurrent flow
CD —Cocurrent depressurization   ↓—Countercurrent flow
CD —Countercurrent depressurization
R—Repressurization

FIGURE 11.26. Summary of cycle for a four-bed PSA unit. (Reprinted with permission from ref. 41. Copyright 1980 American Chemical Society.)

371

(a)   (b)
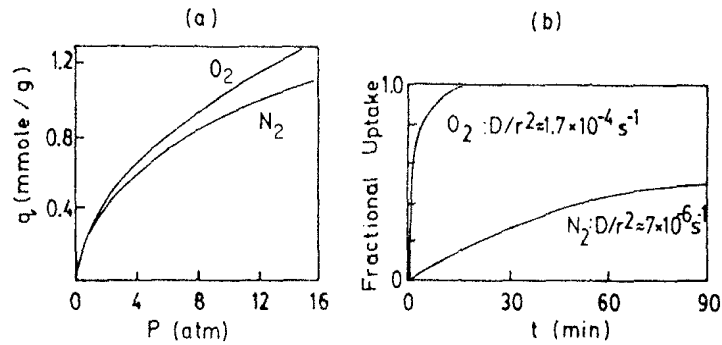
FIGURE 11.27.   Equilibrium isotherms (a) and experimental uptake curves (b) for sorption of O_2 and N_2 on Bergbau–Forschung carbon molecular sieve. [From ref. 37; excerpted by special permission from *Chemical Engineering*, Vol. 85, No. 25, 87 (1978). Copyright © 1978, by McGraw-Hill, Inc., New York, N.Y. 10020.]

Carbon Sieve Process

Equilibrium and kinetic data for the sorption of oxygen and nitrogen on the Bergbau–Forschung carbon molecular sieve[36] are shown in Figure 11.27.[37] It is apparent that there is little difference in equilibrium but a large difference in diffusivity with oxygen being the more rapidly adsorbed species. The high-pressure (raffinate) product in the carbon sieve process is therefore nitrogen, and purities as high as 99.9% may be attained in a properly designed
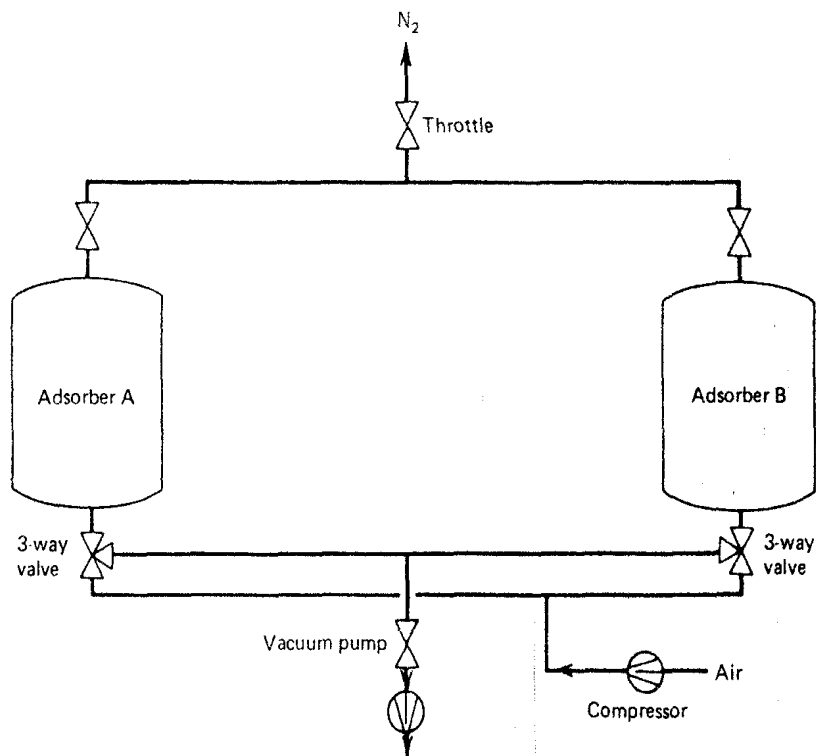
FIGURE 11.28.   Schematic diagram of the Bergbau–Forschung PSA air separation process. [From ref. 37; excerpted by special permission from *Chemical Engineering*, Vol. 85, No. 25, 87 (1978). Copyright © 1978, by McGraw-Hill, Inc., New York, N.Y. 10020.]
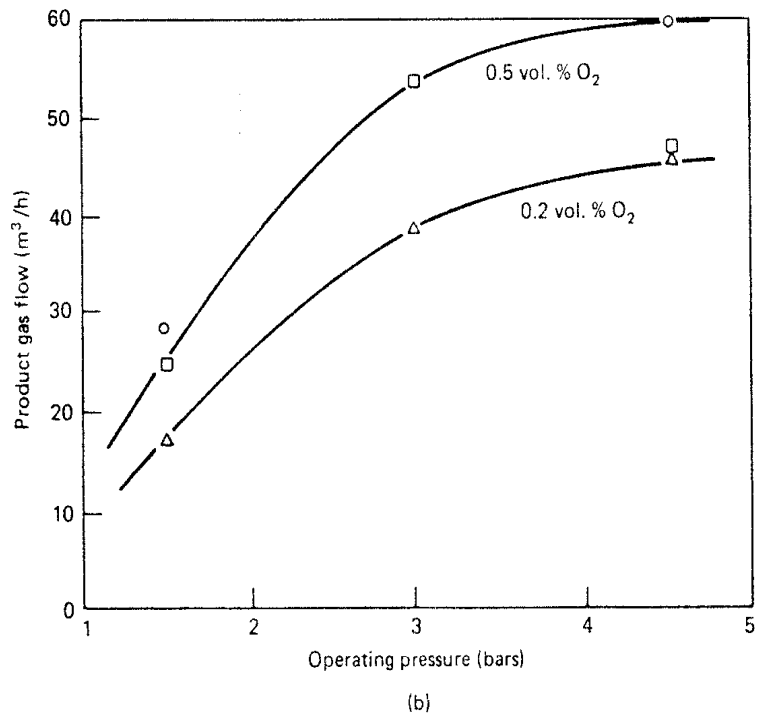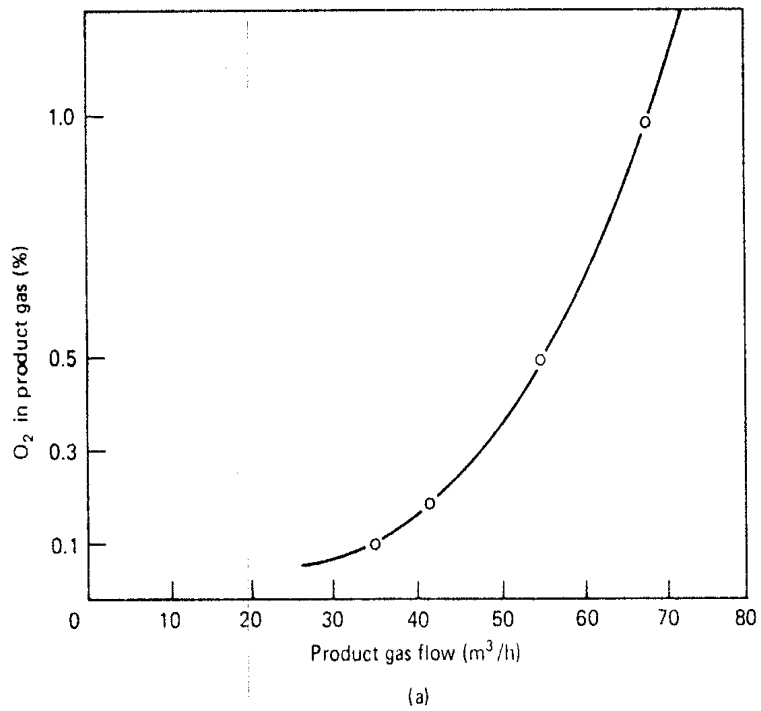
FIGURE 11.29. Effect of product flow rate and operating pressure on purity of the N_2 product in the Bergbau–Forschung PSA process. [From ref. 37; excerpted by special permission from *Chemical Engineering*, Vol. 85, No. 25, 87 (1978). Copyright © 1978, by McGraw-Hill, Inc., New York, N.Y. 10020.]

cycle. Oxygen is produced as the low-pressure (extract) product during the purge and blowdown and is obtained at relatively low concentrations (35–50%). CO_2 and water vapor are removed with oxygen in the blowdown while argon, which has about the same diffusivity as N_2, passes through into the raffinate product stream. The carbon sieve process is therefore preferable to the zeolite process where a pure nitrogen product is the primary requirement but is inferior as a process for oxygen production.

Vacuum desorption rather than a product purge is used to remove the adsorbed oxygen during regeneration in order to avoid the slow uptake of nitrogen which would eventually saturate the sieve and reduce the efficiency of oxygen capture. The cycle commonly operates between about 4 and 0.1 atm with a half cycle time of about 1 min.[37,38] The general scheme is shown in Figure 11.28 and typical performance data showing the effects of flow rate and pressure on product purity are given in Figure 11.29.

The possibility of using a carbon sieve which adsorbs oxygen in preference to argon in conjunction with a zeolite-based PSA process in order to produce both purified oxygen and argon appears technically feasible but such a process has not yet been commercialized.

PSA Hydrogen Purification

PSA systems are widely used for the recovery of pure hydrogen from refinery hydrogen streams containing a few percent of light hydrocarbons.[39-41] This is an ideal application for a PSA system since the desired product (H_2) is essentially nonadsorbed and can therefore be obtained at very high purity (99.9999%). The separation factor between hydrogen and hydrocarbon is very large on almost all zeolites so selection of a suitable adsorbent presents no serious problem. The feed stream is of only moderate value so, although a high recovery is desirable the blowdown and purge losses, which commonly amount to about 20%, do not render the process uneconomic.

The system used is very similar to the four-bed system for oxygen recovery. The cycle is illustrated in Figure 11.26. A plant to process 41MMSCFD was commissioned in 1977 at the Wintershell A. G. refinery in Lingen, West Germany. Essentially pure product hydrogen was obtained at 86% recovery[41] using a pressure swing between about 30 atm and atmospheric pressure.

Single-Column PSA Process

A modified type of PSA cycle[42] utilizing a single adsorbent column packed with small adsorbent particles to give a high pressure drop through the column was suggested by Turnock and Kadlec.[43] At one end of the column pressurized feed is alternately applied and the blowdown, containing the more strongly adsorbed species, exhausted on a rapid cycle while at the other end a more or less continuous stream of the less strongly adsorbed component is obtained. Successful operation requires a careful choice of the particle size

and cycle time to obtain the proper dynamic response with sufficient pressure drop to prevent breakthrough of the more strongly adsorbed species. A process of this type has recently been developed for production of medical oxygen on a small scale. Purity and recovery are comparable with a conventional PSA system but the inventory of adsorbent required for a given product rate is substantially reduced. However the very rapid pressure cycling may reduce adsorbent life and the overall economic comparison is not yet established.[42]

11.4. DISPLACEMENT DESORPTION

Displacement desorption requires a somewhat more complex process scheme than either the pressure swing or thermal swing system and it is therefore generally used only in situations where the simpler methods fail. As an example of this type of process we consider the widely used adsorption separation of medium molecular weight $(C_{10}-C_{18})$ linear paraffins from mixtures with branched chain and cyclic isomers.

There is considerable economic incentive for such a separation since the medium-chain paraffins are required for the manufacture of synthetic detergents while their removal reduces the freezing point of the raffinate stream, enhancing its value as jet fuel for high-flying aircraft. The difference in relative volatility between linear, branched, and cyclic isomers is small so that such a separation cannot be achieved simply by distillation.

Several different adsorption processes for the separation of linear paraffins have been developed including Ensorb (Exxon), IsoSiv (Union Carbide), T. S. F. (Texaco), the Shell process, and the Leuna Werke process. The latter has been called Parex (paraffin extraction) but the choice of name is unfortunate because of possible confusion with the UOP Parex process for separation of xylene isomers. All these processes use a 5A molecular sieve, generally in "binderless" form to minimize nonselective adsorption. The $C_{10}-C_{18}$ linear paraffins are strongly adsorbed even at temperatures as high as 350°C. Thermal swing desorption is not feasible since the temperature required for desorption is so high that coking would occur. The alternatives are therefore vacuum desorption, which is used in some versions of the IsoSiv process, or displacement desorption which is used in most if not all of the other processes.

A schematic diagram of the Exxon "Ensorb" process,[44,45] which uses ammonia as the desorbent, is shown in Figure 11.30 while Figure 11.31 shows one of the two large sieve beds in the operating unit at the Baytown refinery. The process operates at 550–600°F and slightly above atmospheric pressure with a cycle time which is varied from 12 to 30 min (complete cycle) depending on the condition of the sieve and the flow rate and linear paraffin content of the feed (typically 15–25%).[44]

Ammonia is a good choice as a desorbent since, because of its high dipole moment, it is much more strongly adsorbed than would be expected simply on
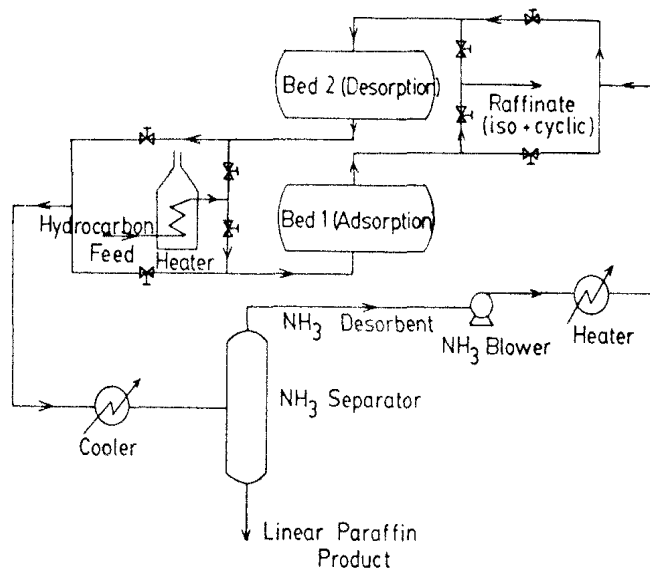
FIGURE 11.30. Simplified flow sheet of Exxon Ensorb Process for separation of medium-chain linear paraffins. (Courtesy of Aromatics Technology Division, Exxon Chemical Company.)
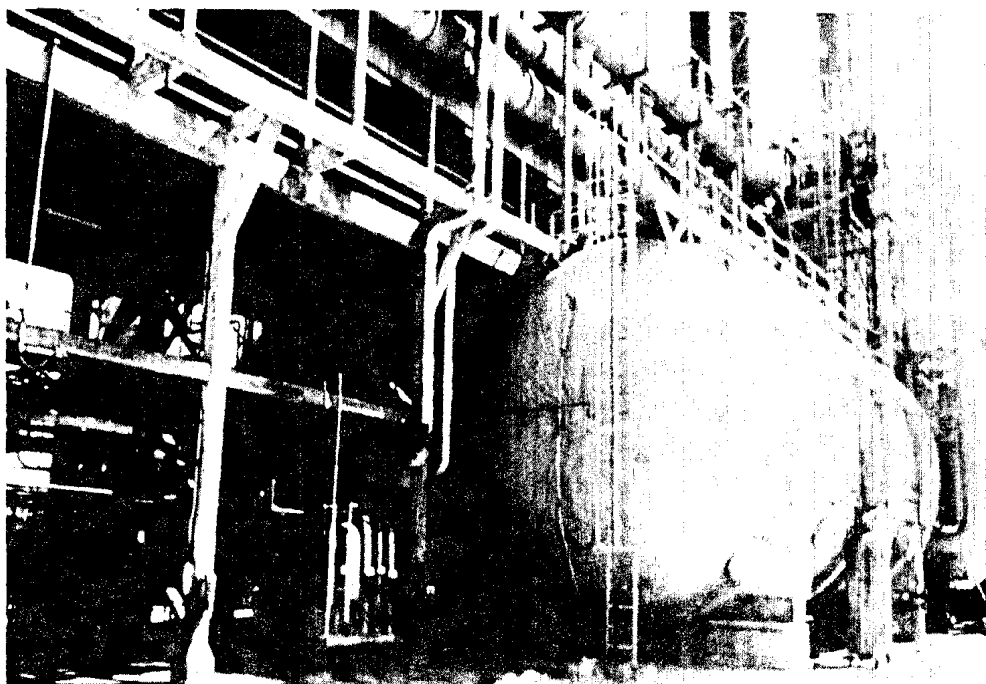
FIGURE 11.31. Photograph of sieve bed and associated ductwork for the Ensorb unit at Baytown refinery. (Courtesy of Aromatics Technology Division, Exxon Chemical Company.)
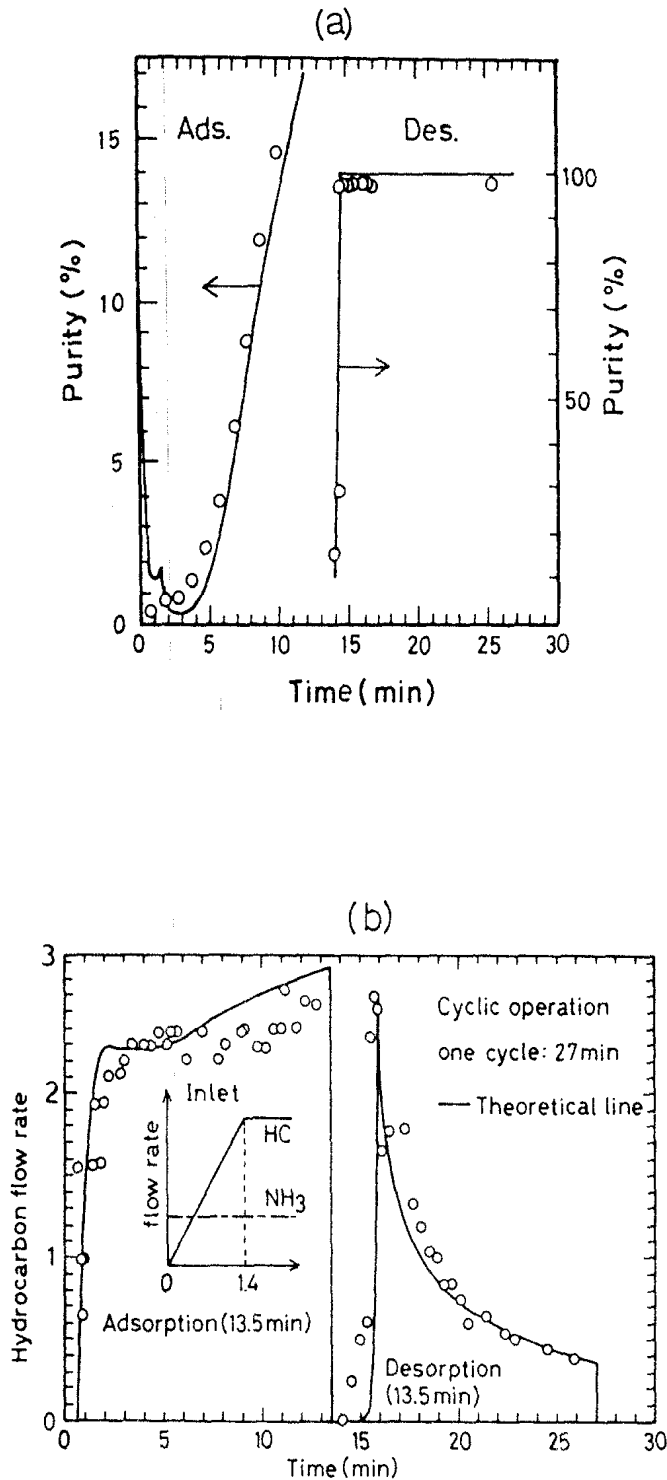
FIGURE 11.32. (a) Purity (% normal paraffins) and (b) flow rate of the hydrocarbon stream leaving the sieve bed during steady-state cyclic operation of the Ensorb linear paraffins unit at Baytown refinery (arbitrary units). The lines are theoretical curves calculated from a detailed numerical simulation of the system, points are plant data. (Courtesy of Aromatics Technology, Exxon Chemicals Corporation. Plant data were provided by Miss Ann Lucas and the numerical simulation was carried out by Dr. H. Yoshida.)

the basis of molecular weight. Because of the very great difference in volatility between ammonia and the linear paraffins the ancillary separation of desorbent from desorbate is easily achieved by flash distillation. This gives ammonia a significant advantage over most of the other desorbents such as light paraffins or amines.

The $C_{10}-C_{18}$ linear paraffins are adsorbed more strongly than ammonia so to achieve desorption a very high ammonia flow rate (about four times the hydrocarbon feed rate) is required. The desorption cycle is therefore operated under downflow conditions. Pressure drop across the bed is relatively high, necessitating the use of a relatively shallow bed and an oversquare configuration but, even so, the power costs associated with the ammonia circulation system make a significant contribution to overall process costs.

A small amount of ammonia is also added to the feed during the adsorption cycle since this has been found to reduce coking and improve product purity, presumably by suppressing the adsorption of polynuclear aromatics on the external surfaces of the zeolite crystals. To avoid possible lifting of the bed the flow is ramped at the start of the adsorption cycle. During the first few seconds of the desorption cycle, impurities are removed from the interstices of the bed and the surface of the adsorbent, and this fraction is recycled to the feed in order to maintain high purity of the linear paraffin product.

The variation of effluent flow rate and composition through the cycle is indicated in Figure 11.32. A detailed numerical simulation of this process has been made by treating the adsorbable n-paraffins as a single species. The competitive adsorption of the paraffins and ammonia was represented by a simple binary Langmuir isotherm. Diffusion of ammonia was assumed to be sufficiently rapid to ensure that equilibrium is always maintained while the adsorption–desorption kinetics of the n-paraffin were represented by a linear rate expression. The simulation has been shown to provide a good representation of the dynamic behavior of the real process and shows clearly that the aging of the adsorbent involves a decline in both equilibrium capacity and adsorption rate constant.

REFERENCES

1. W. R. Grace Inc., Data sheets for Davison 4A Molecular sieve.
2. G. J. Griesmer, R. A. Jones, and A. Lautensuch, *Chem. Eng. Prog. Symp. Ser.* **55**(24), 45 (1959).
3. G. Bunke and D. Gelbin, *Chem. Eng. Sci.* **33**, 101 (1978).
4. D. Gelbin and G. Bunke, *Chem. Eng. J.* **17**, 191 (1979).
5. J. W. J. Wunder, "Design of a Natural Gas Drier," paper presented at annual meeting of CIC, Edmonton, May 1962.
6. J. W. Carter, "The Adsorption Separation Process," in *Properties and Applications of Zeolites*, R. P. Townsend (ed.), Special publication No. 33. Chemical Society, London, 1979, p. 76.
7. J. W. Carter, *AIChE J.* **21**, 380 (1975).
8. C. Y. Pan and D. Basmadjian, *Chem. Eng. Sci.* **25**, 1653 (1970).

9. D. Basmadjian, K. D. Ha, and C. Y. Pan, *Ind. Eng. Chem. Process Design Develop.* **14**, 328 (1975).

10. D. Basmadjian, *Can. J. Chem. Eng.* **53**, 234 (1975)

11. K. S. Tan and I. H. Spinner, *Can. J. Chem. Eng.* **49**, 105 (1971).

12. K. S. Tan and I. H. Spinner, *Can. J. Chem. Eng.* **50**, 651 (1972).

13. J. Chao, Ph.D. thesis, University of New Brunswick, Fredericton, N. B., Canada, 1981.

14. J. P. Ausikaitis, in *Kirk and Othmer, Encyclopedia of Chemical Technology*, Vol. 8, 3rd ed. Wiley, New York, 1978, p. 126.

15. D. Basmadjian, "Adsorption Drying of Gases and Liquids," in *Advances in Drying*, Vol. 3. Hemisphere Publishing Co., Washington, D.C., 1983.

16. D. Basmadjian, *Ind. Eng. Chem. Process Design Develop.* **18**, 137–144 (1980).

17. D. Basmadjian, *J. Agricultural Eng. Research* **26**, 251–270 (1981).

18. D. K. Friday and M. D. LeVan, *AIChE J.* **28**, 86 (1982).

19. D. K. Friday and M. D. LeVan, *AIChE J.* (in press).

20. N. K. Hiester and T. Vermeulen, *Chem. Eng. Progress* **48**, 505 (1952).

21. C. W. Chi, *AIChE Symp. Ser.* **74**(179), 42 (1978).

22. C. W. Chi and W. P. Cummings, in *Kirk and Othmer, Encyclopedia of Chemical Technology*, Vol. 1, 3rd ed. Wiley, New York, 1978, p. 563.

23. C. W. Chi and H. Lee, *AIChE Symp. Ser.* **69**(134), 95 (1973).

24. C. W. Skarstrom, U.S. Patent No. 2,944,627 (July 12, 1960), to Exxon Research and Engineering.

25. C. W. Skarstrom, *Recent Developments in Separation Science*, Vol. 2, p. 95, N. N. Li (ed.). CRC Press, Cleveland, Ohio, 1975.

26. L. H. Shendalman and J. E. Mitchell, *Chem. Eng. Sci.* **27**, 1449 (1972).

27. Y. N. I. Chan, F. B. Hill, and Y. W. Wong, *Chem. Eng. Sci.* **36**, 243 (1981).

28. R. S. Knaebel and F. B. Hill, AIChE Annual Meeting, Los Angeles, Paper 91d, November (1982).

29. J. E. Mitchell and L. H. Shendalman, *AIChE Symp. Ser.* **69**(134), 25 (1973).

30. K. Chihara, and M. Suzuki, *J. Chem. Eng. Japan* **16**, 53 (1983).

31. N. S. Raghavan, M. M. Hassan, and D. M. Ruthven, *AIChE J.* (to be published).

32. H. Lee and D. E. Stahl, *AIChE Symp. Ser.* **69** (134), 1, (1973).

33. G. A. Sorial, W. H. Granville, and W. O. Daly, *Chem. Eng. Sci.*, **38**, 1517 (1983).

34. N. H. Berlin, U.S. Patent No. 3,280,536 (Oct. 25, 1966), to Exxon Research and Engineering.

35. J. C. Davis, *Chem. Eng.* Oct. 16 (1972), p. 88.

36. H. Jüntgen, *Carbon* **15**, 273 (1977).

37. K. Knoblauch, *Chem. Eng.* **85**(25), 87 (1978).

38. K. Knoblauch, J. Reichenberger, and H. Jüntgen, *Gas Erdgas* **116**, 382 (1975).

39. H. A. Stewart and J. L. Heck, *Chem. Eng. Prog.* **65**(9), 78 (1968).

40. J. L. Heck and T. Johansen, *Hydrocarbon Processing* **57**(1), 175 (1978).

41. R. T. Cassidy, in A.C.S. Symp. Ser. **135**, *Adsorption and Ion Exchange with Synthetic Zeolites*, W. H. Flank (ed.). American Chemical Society, Washington, D.C., 1980, p. 247.

42. G. E. Keller and R. L. Jones, in *Adsorption and Ion Exchange with Synthetic Zeolites*, W. H. Flank (ed.) American Chemical Society, Washington, D.C., 1980, p. 275.

43. P. H. Turnock and R. H. Kadlec, *AIChE J.* **17**, 335 (1971).

44. W. J. Asher, M. L. Campbell, W. R. Epperly, and J. L. Robertson, *Hydrocarbon Processing* **48**(1), 134 (1969).

45. W. J. Asher et al., U.S. Patent No. 3,070,542 (1962), to Exxon Research and Engineering.

12

ADSORPTION SEPARATION PROCESSES
II. Continuous Countercurrent Systems

The possibility of operating an adsorption separation process as a continuous countercurrent system, rather than in the traditional cyclic batch mode, was alluded to in the previous chapter. Countercurrent contact maximizes the driving force for mass transfer and therefore provides, in principle, more efficient utilization of the adsorbent capacity than is possible in a simple batch-contacting system. However, for countercurrent contact it is necessary to either circulate the adsorbent, as illustrated in Figure 11.1, or, by appropriate design of the fluid flow system, to simulate adsorbent circulation. This makes the design of countercurrent processes more complex and reduces operational flexibility. It is evident that for relatively easy separations (high separation factor and adequate mass transfer rates) the balance of advantage will lie with a simple batch system; but for difficult separations in which selectivity is limited or mass transfer is slow, the advantage of a continuous countercurrent system in reducing the required inventory of adsorbent must eventually outweigh the disadvantages of the more complex engineering. Beyond this general statement of principle no detailed guidance can be given without reference to specific systems since the economics are strongly influenced by factors such as the cost and durability of the adsorbent as well as by the fundamental kinetics and equilibria and the scale of the proposed operation. Continuous countercurrent adsorption processes are, however, widely used on an industrial scale for several important separations and it seems probable that such processes will become increasingly common in the future.

The general subject of continuous countercurrent adsorption processes has been well reviewed by Tondeur[1] and by de Rosset, Neuzil, and Broughton.[2] Much of the discussion of the present chapter is based on these papers.

12.1. THEORETICAL ANALYSIS: DILUTE SYSTEMS WITH ONE ADSORBABLE COMPONENT

There is complete formal analogy between continuous countercurrent adsorption and other continuous countercurrent operations such as distillation or gas absorption. Such processes are normally operated at steady state and, for an isothermal system containing only a single adsorbable species, the analysis is straightforward.

The system considered is shown diagrammatically in Figure 12.1. Assuming plug flow of solid and axially dispersed plug flow of fluid, the basic differential equation describing the system dynamics is

$$D_L \frac{\partial^2 c}{\partial z^2} - v\frac{\partial c}{\partial z} + \left(\frac{1-\epsilon}{\epsilon}\right)u\frac{\partial q}{\partial z} = \frac{\partial c}{\partial t} + \left(\frac{1-\epsilon}{\epsilon}\right)\frac{\partial q}{\partial t} \qquad (12.1)$$

Assuming a linear rate expression and a linear equilibrium relationship, we have, at steady state,

$$\frac{dq}{dt} = k(q^* - q) = k(Kc - q) = -u\frac{dq}{dz} \qquad (12.2)$$

so that Eq. (12.1) becomes

$$D_L \frac{d^2 c}{dz^2} - v\frac{dc}{dz} - \left(\frac{1-\epsilon}{\epsilon}\right)k(Kc - q) = 0 \qquad (12.3)$$

The adsorbed and fluid phase concentrations at the column outlet are related by an overall mass balance:

$$(q_L - q_0)\left(\frac{1-\epsilon}{\epsilon}\right) = \frac{v}{u}(c_L - c_0) \qquad (12.4)$$

while the appropriate (Danckwerts) boundary conditions are

$$z = 0, \qquad c_0 = c_0' - \frac{D_L}{v}\frac{dc}{dz}\bigg|_{z=0}, \qquad z = L, \qquad \frac{dc}{dz}\bigg|_{z=L} = 0 \qquad (12.5)$$
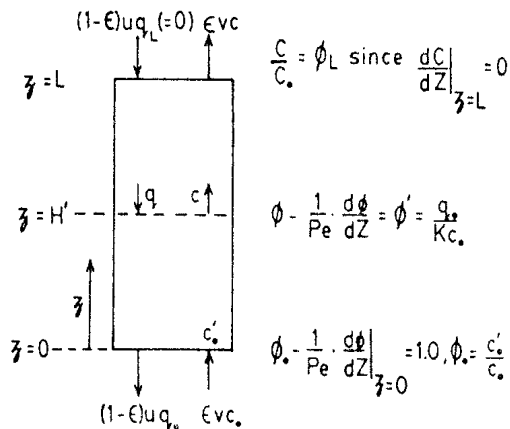
FIGURE 12.1. Schematic diagram of element of a countercurrent adsorption column.

These equations may be expressed in dimensionless form:

$$\frac{d^2\phi}{dZ^2} - (\text{Pe} + \text{St})\frac{d\phi}{dZ} + \text{PeSt}(1 - \gamma) = \text{PeSt}\left(1 - \frac{\gamma q_0}{Kc_0}\right) \quad (12.6)$$

$$\phi_0 = 1 + \frac{1}{\text{Pe}}\frac{d\phi}{dZ}\bigg|_{z=0}, \qquad \frac{d\phi}{dZ}\bigg|_{z=L} = 0 \quad (12.7)$$

The solution is

$$\frac{\phi(1 - 1/\gamma) + 1/\gamma - q_0/Kc_0}{1 - q_0/Kc_0} = \frac{m_1 e^{m_1 + m_2 Z} - m_2 e^{m_2 + m_1 Z}}{m_1 e^{m_1}(1 - m_2/\text{Pe}) - m_2 e^{m_2}(1 - m_1/\text{Pe})} \quad (12.8)$$

If we consider an adsorption process ($\gamma > 1.0$, $q_L = 0$) then, from Eq. (12.4)

$$\frac{q_0}{Kc_0} = \frac{1 - \phi_L}{\gamma} \quad (12.9)$$

$$\frac{\phi(\gamma - 1) + \phi_L}{\gamma - 1 + \phi_L} = \frac{m_1 e^{m_1 + m_2 Z} - m_2 e^{m_2 + m_1 Z}}{m_1 e^{m_1}(1 - m_2/\text{Pe}) - m_2 e^{m_2}(1 - m_1/\text{Pe})} \quad (12.10)$$

where m_1 (+) and m_2 (−) are given by the roots of the auxiliary equation:

$$m = \tfrac{1}{2}\left\{(\text{Pe} + \text{St}) \pm \left[(\text{Pe} + \text{St})^2 + 4\text{PeSt}(\gamma - 1)\right]^{1/2}\right\} \quad (12.11)$$

and the outlet concentration (ϕ_L) is given by:

$$\phi_L = \frac{\gamma - 1}{\gamma/A - 1}$$

$$A = \frac{m_1 - m_2}{m_1 e^{-m_2}(1 - m_2/\text{Pe}) - m_2 e^{-m_1}(1 - m_1/\text{Pe})} \quad (12.12)$$

The corresponding expressions for desorption ($\gamma < 1.0$) are similar except that the profile is reversed. If $\gamma = 1.0$, we have $m_2 = 0$, $m_1 = \text{Pe} + \text{St}$. This corresponds to the special case in which the entering fluid and solid are at equilibrium. Under these conditions there is a uniform concentration through the column with no mass transfer.

Somewhat simpler expressions are obtainable if any of the following conditions are fulfilled:

$$\text{St} \gg 1.0, \qquad \text{Pe} \gg 1.0, \qquad \gamma \to 1.0 \qquad (\gamma > 1.0) \quad (12.13)$$

Then $m_1 \approx \text{Pe} \gg m_2$ and Eq. (12.12) reduces to

$$A = \frac{1/m_2 - 1/m_1}{1/m_2 - 1/\text{Pe}} e^{m_2} \approx e^{m_2}$$

$$m_2 = \frac{-(\gamma - 1)}{1/\text{Pe} + 1/\text{St}} \quad (12.14)$$

and in the plug flow limit (Pe → ∞)

$$A = e^{-St(\gamma - 1)}$$

$$\phi_L = \frac{\gamma - 1}{\gamma e^{St(\gamma - 1)} - 1}$$

(12.15)

If the column is sufficiently long that $\phi_L \to 0$, then $q_0/Kc_0 \approx 1/\gamma$ and the profile is given by

$$\phi = \frac{m_1 e^{m_1 + m_2 Z} - m_2 e^{m_2 + m_1 Z}}{m_1 e^{m_1}(1 - m_2/\text{Pe}) - m_2 e^{m_2}(1 - m_1/\text{Pe})}$$

(12.16)

It is common practice in the design and analysis of countercurrent systems to represent the column as a sequence of ideal equilibrium stages. To obtain an expression for the HETP (H') we must consider a section in the interior of the column, as sketched in Figure 12.1. When $z = H'$ the hypothetical concentration c' leaving this section is at equilibrium with the solid leaving the bottom of the section

$$\phi\Big|_{H'/L} = \frac{c'}{c_0} + \frac{1}{\text{Pe}}\frac{d\phi}{dZ} = \frac{q_0}{Kc_0} + \frac{1}{\text{Pe}}\frac{d\phi}{dZ}\Big|_{H'/L} \approx \frac{1}{\gamma} + \frac{1}{\text{Pe}}\frac{d\phi}{dZ}\Big|_{H'/L}$$

(12.17)

and the HETP is seen to be given by

$$\frac{1}{\gamma} = \frac{m_1 e^{m_1 + m_2 H'/L}(1 - m_2/\text{Pe}) - m_2 e^{m_2 + m_1 H'/L}(1 - m_1/\text{Pe})}{m_1 e^{m_1}(1 - m_2/\text{Pe}) - m_2 e^{m_2}(1 - m_1/\text{Pe})}$$

(12.18)

If any of the inequalities of Eq. (12.13) are satisfied, this expression simplifies to

$$e^{m_2 H'/L} = \frac{1}{\gamma}, \qquad m_2 = -\frac{\gamma - 1}{\text{Pe}^{-1} + \text{St}^{-1}}$$

$$\frac{1}{N'} = \frac{H'}{L} = \frac{\ln\gamma}{(\gamma - 1)}(\text{Pe}^{-1} + \text{St}^{-1}) = \frac{\ln\gamma}{(\gamma - 1)}\left(\frac{D_L}{vL} + \frac{\gamma\epsilon v}{(1 - \epsilon)kKL}\right)$$

(12.19)

This may be compared with the corresponding expression for a chromatographic column [Eq. (8.49)] which, for $K \gg 1.0$ reduces to

$$\frac{1}{N} = \frac{H}{L} = \frac{\sigma^2}{\mu^2} = 2\left(\frac{D_L}{vL} + \frac{\epsilon v}{(1 - \epsilon)kKL}\right)$$

(12.20)

Comparison of Eqs. (12.19) and (12.20) shows clearly that H and H' are not identical, although both are related to the sum of the axial dispersion and mass transfer resistances. The comparison is summarized in Table 12.1. It is evident that for $\gamma \sim 1.0$, $H'/H \approx \frac{1}{2}$ but in general the relationship depends on

TABLE 12.1. Comparison of HETP for Chromatographic and Countercurrent Systems

		Plug Flow	Dispersed Plug Flow
Chromatographic	$\dfrac{H}{L}$	$\dfrac{2v}{kKL}\left(\dfrac{\epsilon}{1-\epsilon}\right) = \dfrac{2}{\gamma St}$	$2\dfrac{D_L}{vL} + \dfrac{2v}{kKL}\left(\dfrac{\epsilon}{1-\epsilon}\right) = 2[Pe^{-1} + (\gamma St)^{-1}]$
Countercurrent	$\dfrac{H'}{L}$	$\dfrac{\ln\gamma}{(\gamma-1)}\dfrac{1}{St}$	$\dfrac{\ln\gamma}{(\gamma-1)}\left(\dfrac{D_L}{vL} + \dfrac{\gamma ev}{kKL(1-\epsilon)}\right) = \dfrac{\ln\gamma}{(\gamma-1)}[Pe^{-1} + St^{-1}]$
H'/H		$\dfrac{\gamma\ln\gamma}{2(\gamma-1)}$	$(Pe\to\infty)\dfrac{\gamma\ln\gamma}{2(\gamma-1)}; \quad (Pe\to 0)\dfrac{\ln\gamma}{2(\gamma-1)}$

the flow ratio γ. Thus, in order to estimate the HETP for a countercurrent system from chromatographic data, it is necessary to know the relative importance of axial dispersion and mass transfer resistance as well as the overall value of H.

It is of interest to compare the predictions of the dispersed plug flow model with those of the discrete equilibrium stage model for a countercurrent system. For a linear equilibrium the dimensionless effluent concentration ($\phi_L = c_L/c_0$) for a system of N' countercurrent equilibrium stages is given by the familiar Kremser equation:*

$$\phi_L = \frac{\gamma - 1}{\gamma^{N'+1} - 1} \qquad (12.21)$$

Values of ϕ_L calculated from this expression with N' from Eq. (12.19) are compared in Table 12.2 with the corresponding values derived from the dispersed plug flow model [Eq. (12.12)] for several different values of the parameters Pe, St, and γ. Under most conditions the predictions from the two models are essentially the same, although deviations become pronounced when $\phi_L \to 0$. Thus, although the discrete model provides a useful engineering approximation which has the advantage of being readily extended to more complex nonlinear and multicomponent systems, it must be treated with caution when highly purified product streams are involved. The present analysis is, however, based on simple linear theory and it seems likely that in real systems the effects of isotherm nonlinearity and flow variation will

TABLE 12.2. Comparison of Predictions of Dispersed Plug Flow and Staged Models

	γ	Dispersed Plug Flow			Staged	
		A	ϕ_L		N'	ϕ_L
Pe = St = 2	1.2	0.79	0.385		1.1	0.429
	1.6	0.52	0.289		1.28	0.313
	2.0	0.36	0.221		1.44	0.225
	3.0	0.17	0.120		1.82	0.095
Pe = St = 10	1.2	0.368	0.088		5.5	0.088
	1.6	0.062	0.024		6.4	0.019
	2.0	0.013	0.007		7.2	0.003
	3.0	4.9×10^{-4}	3×10^{-4}		9.1	3×10^{-5}
Pe = St = 50	1.2	0.008	0.0014		27.4	0.0011
	1.6	1.5×10^{-6}	5.8×10^{-7}		32	1.2×10^{-7}

*See A. Kremser, *Natl. Petroleum News*, **22**, (21), 42 (1950); *also* M. Souders and G. C. Brown, *Ind. Eng. Chem.* **24**, 519 (1932).

probably be more important than the relatively small differences between the discrete and continuous models.

Expressions for the steady-state concentration profile have also been derived for some more complex countercurrent systems. The extension to a (plug flow) system in which the equilibrium relationship is of Langmuir rather than linear form (constant separation factor) is given by Pratt.[3] The solution for a linear plug flow system in which the mass transfer rate is controlled by intraparticle diffusion rather than by the linear rate law has been derived by Amundson and Kasten[4] while the asymptotic behavior of a dispersed plug flow Langmuir system has been investigated by Rhee and Amundson.[5]

The transient behavior of a continuous countercurrent multicomponent ·system has been considered in detail by Rhee, Aris, and Amundson[6] from the perspective of equilibrium theory. The final steady state predicted by equilibrium theory is simply a uniform concentration throughout the column with a transition at one end or the other, and the equilibrium theory analysis is therefore of less practical value for a countercurrent system, which is normally operated at steady state, than for a fixed-bed system which normally operates under transient conditions. The equilibrium theory analysis does, however, reveal the possibility of multiple steady states in a countercurrent system and shows how the evolution of the profiles may be predicted in order to determine which state is in fact obtained.

In general, as expected from equilibrium theory, the mass transfer zone in a countercurrent system occurs at one end of the column, and in a long column at a sufficient distance from this zone equilibrium is approached. The location of the mass transfer zone depends only on the fluid and solid phase concentration of the feed streams and the flow ratio γ; it is independent of the initial state of the column. In certain circumstances it is, however, possible to have a stable asymptotic solution in which the mass transfer zone has no tendency to migrate in either direction. Under these conditions the mass transfer zone may occur at any point in the column, depending on the precise initial conditions and the start-up procedure, with equilibrium states being approached both upstream and downstream of the mass transfer zone. When this isotherm is favorable such behavior is possible only for desorption at the correct value of γ determined by the feed concentrations. A full discussion is given by Rhee and Amundson.[5]

12.2. McCABE–THIELE ANALYSIS

Steady-state operation of a continuous countercurrent adsorption system may be conveniently discussed in terms of the simple McCabe–Thiele analysis. The simplest type of continuous countercurrent process is illustrated in Figure 12.2, and it is evident that any of the separation processes discussed in Chapter 11 could, in principle, be carried out in such a system, rather than in a cyclic batch process.
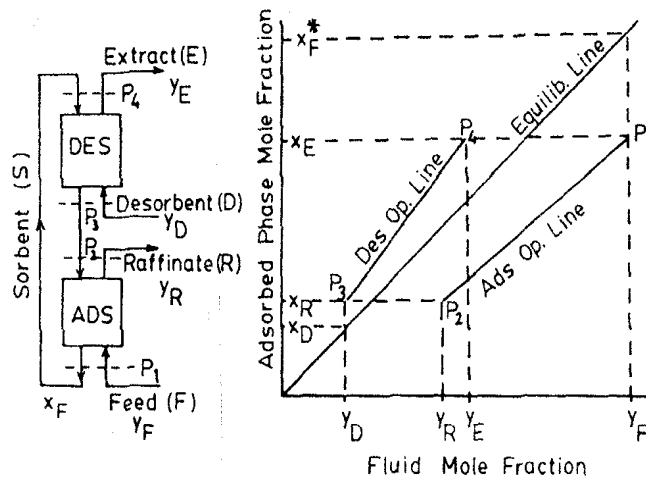
FIGURE 12.2. McCabe–Thiele diagram for steady-state operation of a countercurrent adsorber without equilibrium shift. (From ref. 1, reprinted with permission of Martinus Nijhoff Publishers.)

The operating lines, sketched in Figure 12.2, are determined by simple steady-state mass balances:

$$x - x_F = \left(\frac{F}{S}\right)(y - y_F) \quad \text{(adsorption)}$$

$$x - x_D = \left(\frac{D}{S}\right)(y - y_D) \quad \text{(desorption)}$$

(12.22)

The slopes of the operating lines F/S and D/S are fixed by the ratios of the flow rates in the adsorbed and fluid phases. If both adsorption and desorption sections operate under the same thermodynamic conditions (i.e., at the same pressure and temperature), the same equilibrium line will apply and it is evident that for an operable process we must have $D/S > F/S$, which implies that the flow rate of the purge or desorbent must be greater than that of the feed. Since $y_D < y_E$ and $y_E < y_F$ the concentration of the adsorbable component in the purge must be lower than in the raffinate product, and the concentration in the extract product must be lower than in the feed. This is the continuous countercurrent analog of an isothermal purge gas stripping process in which the volume of purge always exceeds the volume of feed. Such a process is seldom economic except for removal of an undesirable impurity, without recovery, when a plentiful and cheap supply of purge is available.

Stripping and Enriching Units

The operating diagram for a continuous countercurrent analog of a thermal swing or pressure swing batch process is illustrated in Figure 12.3. If the regeneration step is run at higher temperature or lower pressure, the equilibrium line for regeneration will lie below the equilibrium line for saturation, and the requirement that $D > F$ is removed. The system can then be operated
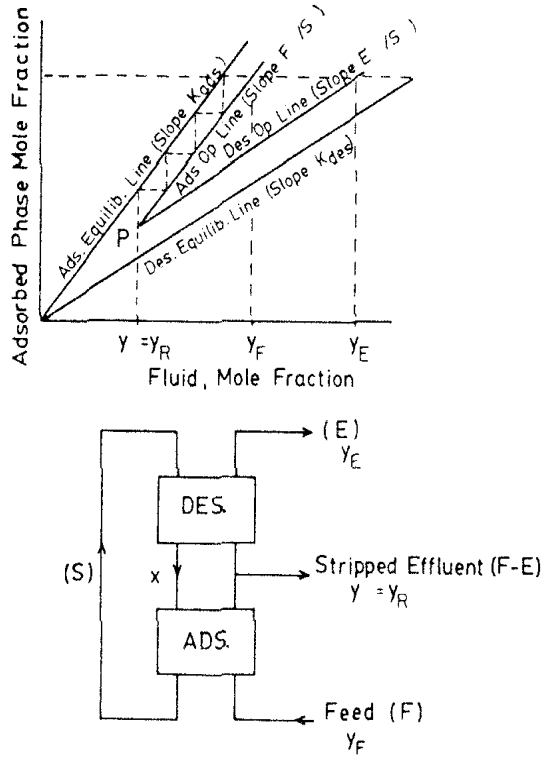
FIGURE 12.3. McCabe–Thiele diagram for steady-state operation of a stripping unit with equilibrium shift. Note that enrichment is limited but stripping is unlimited. (From ref. 1, reprinted with permission of Martinus Nijhoff Publishers.)

with a lower desorbent flow rate and since y_F is now less than y_E one may use a fraction of the raffinate product stream for regeneration, as is common practice in cyclic pressure or thermal swing systems. In the choice of operating conditions for such a system there is evidently a trade-off between raffinate product purity, regenerant flow rate (or the ratio D/F), and the quantity of adsorbent, which is approximately proportional to the number of stages.

Point P_2 may be moved close to the origin by bringing the slopes of the operating and equilibrium lines towards each other, that is, by decreasing the product rate $F - E$ and increasing the reflux $E/(F - E)$. In the limit, by increasing the reflux, the raffinate concentration may be reduced to any desired level. The same is not true of y_E which has an upper limit corresponding to an infinite number of stages on the rich side of the saturation and regeneration column, that is, operating and equilibrium lines intersect. Because stripping is unlimited while enrichment is limited such a system is commonly called a stripping unit.

By interchanging the flow conditions of the adsorption and desorption sections, one obtains an enriching unit, as sketched in Figure 12.4. In an enriching unit the extent of enrichment is unlimited but stripping is limited.

For a system with straight operating and equilibrium lines of defined slopes ($K_{ads}, K_{des}, F/S$, and R/S or E/S fixed) the maximum enrichment possible in a stripping unit and the maximum stripping possible in an enriching unit
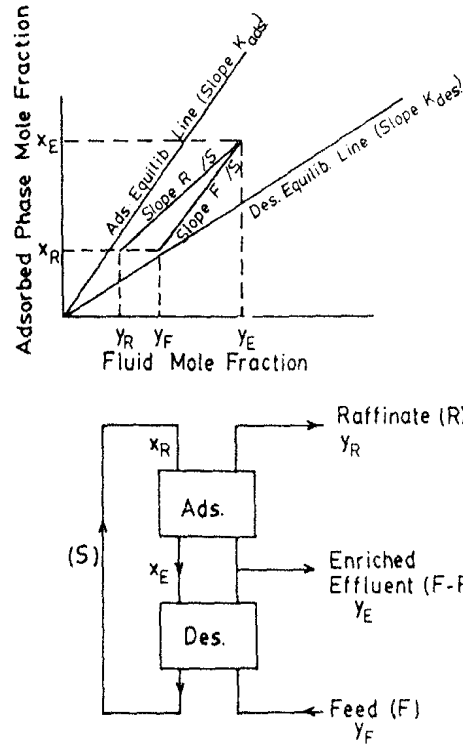
FIGURE 12.4. McCabe–Thiele diagram for steady-state operation of an enriching unit with equilibrium shift. Note that stripping is limited but enrichment is unlimited. (From ref. 1, reprinted with permission of Martinus Nijhoff Publishers.)

may be shown by simple geometry to be given by:

Enriching section

$$\left(\frac{y_E}{y_F}\right)_{max} - 1 = \left[\frac{K_{ads}}{K_{des}} - 1\right]\left(\frac{K_{des}S/E}{K_{des}S/E - 1}\right) \qquad (12.23a)$$

Stripping section

$$\left(\frac{y_F}{y_R}\right)_{max} - 1 = \left[\frac{K_{des}}{K_{ads}} - 1\right]\left(\frac{K_{des}S/R}{K_{des}S/R - 1}\right) \qquad (12.23b)$$

For infinite reflux ($K_{des}S/R$ or $K_{des}S/E \gg 1.0$) these expressions reduce to

$$\left(\frac{y_E}{y_F}\right)_{max} = \frac{K_{ads}}{K_{des}}, \qquad \left(\frac{y_F}{y_R}\right)_{max} = \frac{K_{des}}{K_{ads}} \qquad (12.24)$$

This defines the maximum possible enrichment or stripping for the specified equilibrium.

Complete Fractionation Process

A complete fractionation process to obtain a purified raffinate product and a concentrated extract product may be obtained by coupling together a
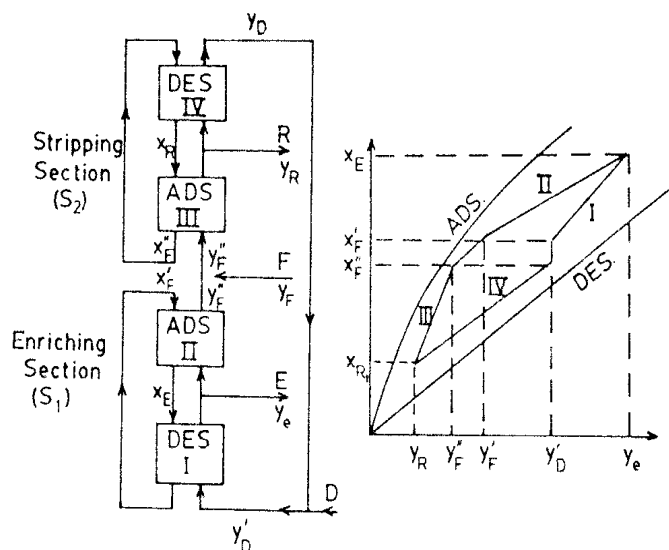
FIGURE 12.5. McCabe–Thiele diagram for complete fractionation process made up of stripping and enrichment sections. (From ref. 1, reprinted with permission of Martinus Nijhoff Publishers.)

stripping section and an enriching section as in a distillation column. Such a system together with its operating diagram is sketched in Figure 12.5. With such a system the slope of each segment (i.e., the ratio of flow rates in the corresponding section of the vessel) may be adjusted independently since we can adjust independently the adsorbent circulation rate in each section as well as the feed and product rates. In the limiting case of total reflux (no feed and no product), the operating lines in each section become coincident. The area enclosed by the polygon formed by the operating lines can be considered as a measure of the production rate which is zero at total reflux and increases as the operating lines converge towards the bounding equilibrium lines. It is evident that the production rate and product composition can be adjusted by changing the flow rates in the different sections which control the slopes of the corresponding operating lines. With the system sketched in Figure 12.5 there is an additional degree of freedom since the two sections may be operated under different thermodynamic conditions and the equilibrium lines for the stripping and enriching sections may therefore be adjusted independently.

A somewhat simpler process may be obtained at the cost of some loss in flexibility by combining the two adsorbent circuits, as indicated in Figure 12.6.

As in distillation, a given separation with defined feed, top, and bottom products may be achieved in different ways; a reduction in the number of theoretical stages may be compensated for by increased reflux and vice versa. In any section of the column there is, however, a minimum reflux, defined by Eq. (12.23), below which the required separation cannot be achieved. At this minimum reflux condition, an infinite number of stages would be required. This condition corresponds to the intersection or tangency of equilibrium and
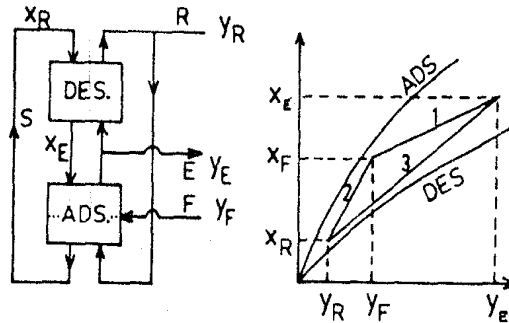
FIGURE 12.6. McCabe–Thiele diagram for simplified fractionation process. (From ref. 2, reprinted by permission of Martinus Nijhoff Publishers.)

operating lines on the McCabe–Thiele diagram. To ensure an operable process such "pinch points" must be avoided, and in a close separation this requirement can impose rather stringent restrictions on the permissible ranges of adsorbent and fluid flow rates in the various sections of the column. Some examples showing the occurrence of "pinch points" as well as how they may sometimes be avoided by inclusion of recycle between different sections have been given by Tondeur.[1]

Multicomponent Systems

As with distillation, the McCabe–Thiele analysis is strictly valid only for a binary system. To analyze the behavior of a multicomponent system it is, in principle, necessary to make plate-to-plate calculations. However, it is commonly found that only two components are present at significant concentrations within each individual section of the column. A preliminary analysis in which each section is considered as a pseudo binary McCabe–Thiele system can therefore provide useful guidance in the design of a multicomponent adsorption system.

12.3. THE HYPERSORPTION PROCESS

The hypersorption process[7,8] for the recovery of ethylene from a light gas stream containing mainly methane and hydrogen which was developed by the Union Oil Co. in 1947 appears to be the earliest full-scale commercial countercurrent adsorption process. The first hypersorption unit was built for the Dow Chemical Co. at Midland, Michigan, and was commissioned in May 1947.[7] The essential features of the process are shown schematically in Figure 12.7, and a somewhat more detailed sketch of the actual unit is given in Figure 12.8. The operation is essentially similar to that of the hypothetical system shown in Figure 12.5.

420°F

H₂O Des.
C Cooler

Cooling
Water 135 gal/min

120°F

Ads. of
C₂,C₃

150°F

Des of CH₄
Ads of C₂,C₃

210°F

365°F

Steam
Stripping
C Heater

510°F

Gas Lift
18000 lb/hr
480° F

Purge and
Lift Gas

14,900 SCFH
H₂ :64
CH₄:31.4
Other:4.6

Discharge
Gas

47,400 SCFH
H₂:32.3
CH₄:65.2
Other:2.5

Feed

66,800 SCFH
H₂ :37.2
CH₄:53.2
C₂H₄:6.4
Other:3.2

Make Gas

4500 SCFH
C₂H₄:93
Other : 7

Hot
Dowtherm

Steam 400 lb/Hr, 510°F,
75 psig

Lift Gas

Carbon Inventory :15,000 lb.
Total Column Height :85 ft.
Column Diameter :4.5 ft.

FIGURE 12.7.   Schematic diagram of hypersorption process showing test mass balance, temperatures, and other operating data.

The feed gas enters near the center of the Hypersorber column into a slowly downward moving bed of activated carbon adsorbent which preferentially adsorbs the heavier hydrocarbon gases. There are four main sections in the bed. In the section above the feed the heavier hydrocarbons are adsorbed, leaving a methane–hydrogen mixture which is discharged at the top of the adsorption section. A fraction of this gas passes on through the top section of the bed (the cooler) where it serves to desorb residual moisture from the adsorbent. Methane is preferentially adsorbed in the cooler region towards the bottom of this section so that the purge gas leaving the top of the unit contains a higher proportion of hydrogen and a lower proportion of methane than the discharge gas.

In the rectification section, below the feed point, the lighter components are stripped from the adsorbed phase while the heavier components are concentrated in the adsorbed phase. Desorption of the heavier components is accomplished by steam stripping in the bottom section of the column in which the temperature is raised to 510°F by a dowtherm heat exchanger and live
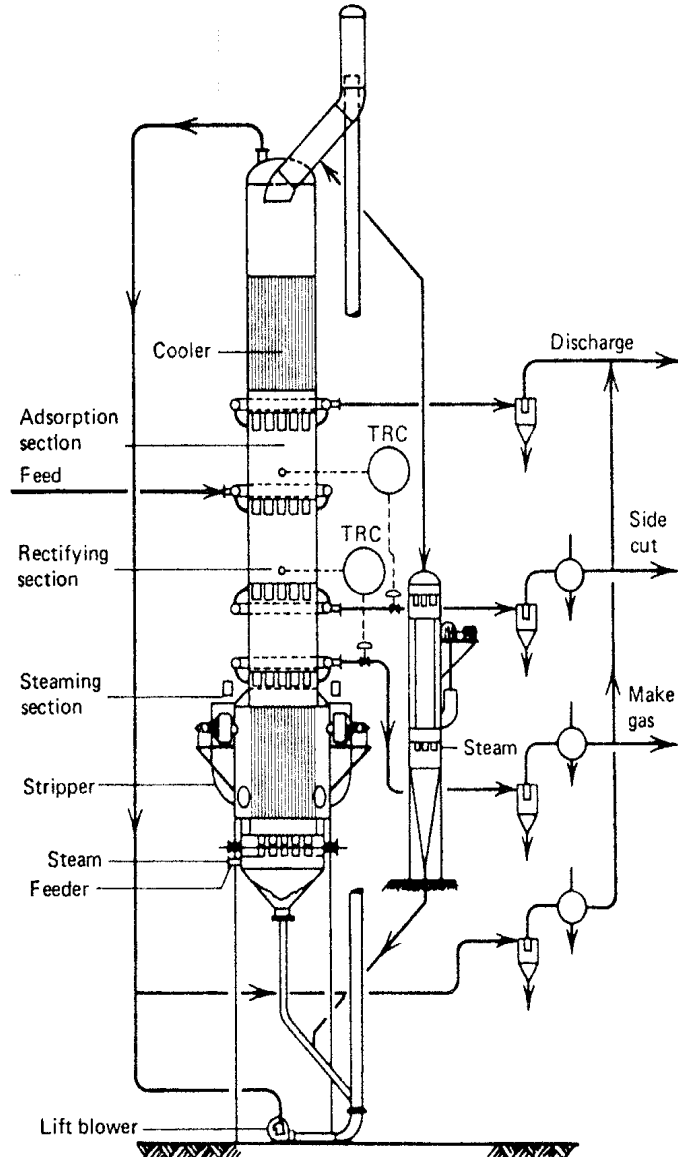
FIGURE 12.8. Simplified engineering diagram of a hypersorption column. (From ref. 8, reprinted with permission.)

steam, which is introduced at the bottom of the bed. The hot adsorbent is returned to the top of the column by a gas lift system, and it is then cooled and dehydrated in the top section by heat exchange and contact with the purge gas stream. The process can thus be considered as a combined thermal swing–displacement desorption cycle.

Complex mechanical arrangements are required to ensure a uniform and controlled plug flow of solids through the bed as well as in the solid heat exchangers. The gas lift system for returning the adsorbent to the top of the column adds further to the mechanical complexity of the system. Full descriptions of the mechanical details as well as performance data from an operating unit have been given by Kehde et al.[7] and Berg.[8]

Apart from the complexity of the mechanical design, attrition of the adsorbent is obviously a potential problem with this type of system. However, the results of attrition studies quoted by Berg[8] suggest that these problems had in fact been largely overcome since the attrition losses were as low as 0.001%/cycle, amounting to a loss of no more than about 7 lb/day for a full-scale unit.

In the literature of the period the hypersorption process was hailed as a technological breakthrough, and such processes were developed for a wide variety of separations, including hydrogen recovery, natural gas purification, and the separation of hydrogen chloride from light hydrocarbon gases. However, the process proved less economic than cryogenic distillation and is no longer operated commercially. The process might have enjoyed greater commercial success if it had been applied to a more "difficult" separation, but at that time the applications were constrained by the limited range of available adsorbents.

12.4. PERIODIC COUNTERCURRENT SORPTION IN MULTIPLE-COLUMN SYSTEMS

The benefits of countercurrent operation can be achieved without the problems associated with a moving-bed system by using a multiple-column fixed-bed system, with an appropriate sequence of column switching designed to simulate a counterflow system. The general scheme is illustrated in Figure 12.9. At the end of the first cycle, bed 1 is essentially saturated while the concentration front is just about to break through at the exit of bed 4. At this
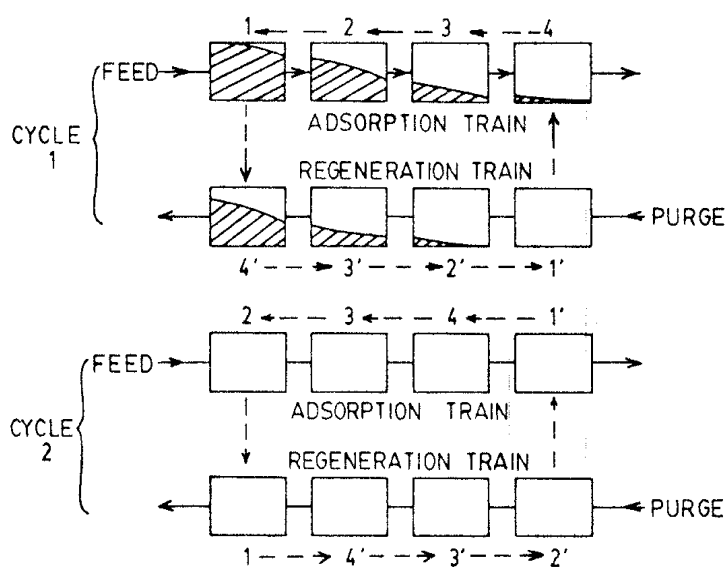
FIGURE 12.9. Schematic diagram showing the sequence of column interchange in a periodic countercurrent adsorption system. Shading indicates concentration profile at the end of the adsorption cycle.

point bed 1 is switched to the position of bed 4' in the regeneration train while a fully regenerated bed (bed 1') is added at the outlet of the adsorption train. The switch is repeated when bed 2 is fully saturated and the concentration front is about to reach the outlet of bed 1'. In this way the adsorbent is, in effect, flowing countercurrent to the fluid in both the adsorption and regeneration trains. With a sufficiently large number of beds one may achieve the equivalent of a true countercurrent system.

For simplicity the regeneration train is shown simply as a once-through flow system, such as might be employed in a thermal swing or purge gas stripping cycle, but the system may be easily adapted to more complex regeneration procedures. For example, beds 4' and 3' might be steam stripped while beds 2' and 1' are being purged.

Periodic countercurrent systems are widely used in ion exchange and water purification systems for the removal of trace concentrations of organic components with beds of activated carbon.[9,10] At low sorbate concentrations the adsorption isotherms for many organic pollutants are linear or only slightly favorable so that the mass transfer zone is wide, and in a simple two-bed cyclic batch system the LUB would therefore be uneconomically large. For such systems, in order to obtain an economic process, some form of countercurrent operation is necessary in order to reduce the adsorbent inventory.

The performance of a multiple-column periodic countercurrent system has been analyzed theoretically by Svedberg,[11] Neretnieks,[12] Rhee,[13] Rippin,[14,15] and others. The variation of adsorbent utilization with bed length is shown in Figure 12.10 for a single fixed bed, an ideal continuous countercurrent system, and a periodic countercurrent system containing 2, 4, and 6 beds.
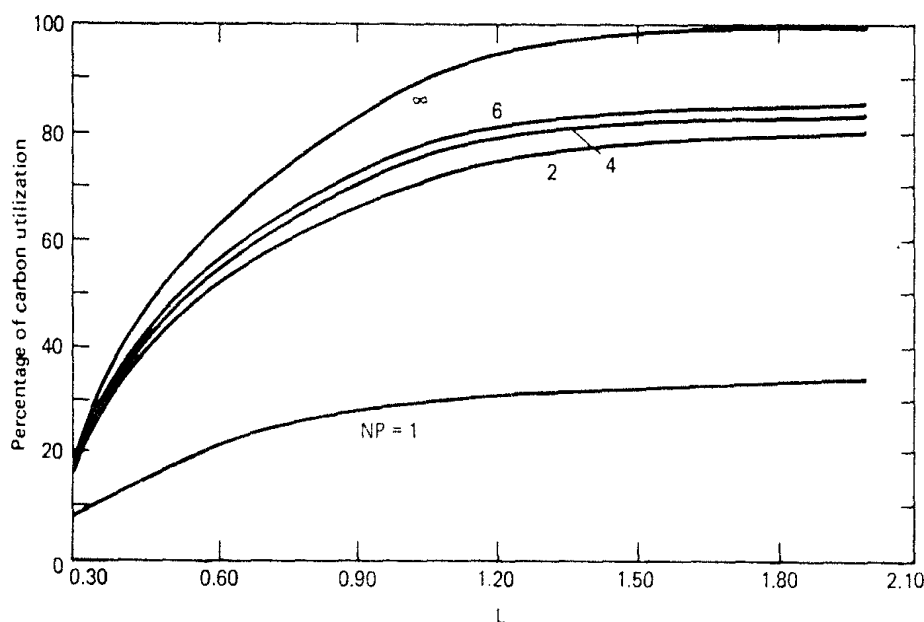
FIGURE 12.10. Comparison of continuous countercurrent, periodic countercurrent, and cyclic batch adsorption systems showing effectiveness of adsorbent utilization as a function of bed length. (From ref. 15, reprinted with permission.)

It is evident that in going from a single-column to a two-column system the utilization of the adsorbent increases dramatically from about 33% to 78%. Further subdivision gives a less dramatic improvement to about 85% utilization with a six-column system while in a true countercurrent system with a sufficiently long column the utilization approaches 100%.

In the above analyses attention is focused only on the adsorption cycle, and it is assumed that a fully regenerated bed is always available when required. This perspective is appropriate for water purification systems in which regeneration is generally carried out by draining the bed and then stripping with steam or a hot purge gas. In order to compare the periodic countercurrent system with other modes of operation it is, however, necessary to consider both adsorption and desorption cycles, as was done in chapter 11 for a simple two-bed cyclic system. Such an analysis has been carried out by Ortlieb and Gelbin[16] for an isothermal purge stripping system. They consider the average effluent purity, rather than the volume of the bed as the criterion of performance, and on this basis they show that the periodic countercurrent system gives only a modest advantage over a well-designed dual-bed cyclic system with reverse-flow regeneration.

It thus appears that the main advantage of the periodic countercurrent system, or indeed of a true countercurrent system, is the reduction in adsorbent inventory. Most of the gain is achieved by dividing the bed into two, and further subdivision beyond four sections would appear not to be justified except in unusual circumstances. There is also a reduction in the purge requirement for regeneration in a countercurrent system but, on the basis of Gelbin's analysis, this appears to be less significant than the reduction in adsorbent bed volume.

12.5. THE SORBEX PROCESS

Principle of Operation

"Sorbex" is the generic name used by UOP for their simulated countercurrent sorption process which has been successfully developed for a variety of large-scale commercial separations.[2,17] All Sorbex processes in current operation operate in the liquid phase, but in principle the process could also be applied to a vapor phase system. In order to understand the Sorbex process it is simplest to consider a true isothermal countercurrent displacement desorption system, as sketched in Figure 12.11. Such a system is similar in its essential features to the Hypersorption system but without the additional complexity of the thermal swing.

We consider the separation of a hypothetical two-component feed containing components A and B, with A being the more strongly adsorbed species. The desorbent (C) should have an adsorption affinity intermediate between that of A and B. The process splits the original mixture into two streams, one (the extract) containing A and C with very little B and the other (the raffinate)
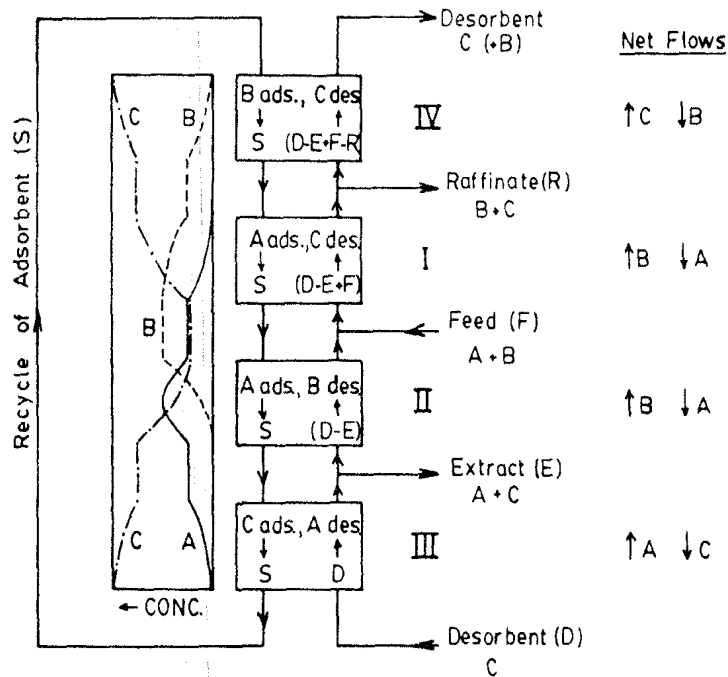
FIGURE 12.11. Schematic diagram showing the roles played by the four sections of a Sorbex countercurrent displacement desorption process.

containing $B + C$ with very little A. To recover A and B as pure products these streams must then be separated by conventional methods, usually distillation. It is therefore essential that the properties of the desorbent should be such that these ancillary separations can be easily accomplished. The Sorbex process then replaces one difficult separation $(A - B)$ by two easy separations $(A - C$ and $B - C)$.

As with the hypersorption system, there are four distinct sections in the bed. These sections are not necessarily physically separated, but they are distinct in the sense that, due to injection of feed or withdrawal of product, the liquid flow rate changes abruptly between sections while remaining essentially constant through an individual section. The roles played by each section, the liquid flow rates, and the concentration profile through the bed are indicated in Figure 12.11.

Zone I. In this section the more strongly adsorbed species (A) is adsorbed. The solid entering this zone contains mainly desorbent C with some of Component B which is displaced by the adsorption of A. The liquid at the top of this zone contains only B and C, and a portion of this liquid is removed as the raffinate product.

Zone II. The solid entering this zone has just been in contact with the feed and therefore contains both components A and B as well as desorbent C. The weakly adsorbed B is stripped from the solid by the more strongly adsorbed A. The concentration of A reaches a maximum at some point within this zone and the concentration of B falls essentially to zero at the bottom of this zone.

Zone III. The solid leaving zone II still contains an appreciable concentration of A as well as C. A is desorbed in zone III by countercurrent contact with a pure desorbent stream which enters at the bottom of the column. The extract product containing $A + C$, with essentially no B, is removed between zones II and III.

Zone IV. The adsorbent recycled to the top of the column is loaded with essentially pure desorbent. To reduce the load on the ancillary separation unit some of this desorbent is displaced, in the top section of the column, by the weakly adsorbed component B. The flow rates are adjusted so that the concentration of B falls almost to zero at the top of this zone, and essentially pure desorbent is withdrawn at the top and recycled to the bottom of the column. Since the top and bottom of the column are connected, one may consider the bed as an annulus. The concentration profile then has the appearance of an incompletely resolved stationary chromatogram.

In order for such a process to operate, the flow rates in each section of the column must satisfy the mass balance constraints imposed by a McCabe–Thiele analysis of the system. This requires that within each section the operating line must lie either above or below the equilibrium line to allow mass transfer to occur in the appropriate direction to give either adsorption or desorption, as required. These constraints are summarized in Table 12.3, and the required direction of the net flows in each section of the column is indicated in Figure 12.11. There are four flow rate variables (S/F, D/F, E/F, and R/F) and four inequality constraints, one for each section of the bed. Once the equilibrium is fixed the only remaining degree of freedom is the margin by which the inequality constraints are fulfilled. Once that is decided the inequality constraints become four equations which define all the flow rate ratios for the system. Once the flow rates are fixed a preliminary estimate of the number of theoretical stages in each section may be obtained from the usual McCabe–Thiele construction. To complete the preliminary design the HETP is required. This may be obtained either from fundamental kinetic data

TABLE 12.3. Mass Balance Constraints For Continuous Countercurrent Systems

Section	Condition
IV	$S/(D + F - E - R) \geqslant \alpha_{CB}$
I	$S/(D + F - E) \geqslant \alpha_{BA}$
II	$S/(D - E) \leqslant \alpha_{AB}$
III	$S/D \leqslant \alpha_{CA}$

Note: α_{ij} is the binary separation factor defined by $X_i Y_j / X_j Y_i$. A is the more strongly adsorbed component, B is the less strongly adsorbed component, and C is the desorbent.

or, more commonly, directly from liquid chromatographic measurements carried out with the same adsorbent under similar hydrodynamic conditions (same particle size and relative velocity). The relevant expressions are given in Table 12.1. A more detailed design would require a plate-to-plate calculation, as in a multicomponent distillation column, in order to take account of such effects as variation in separation factors and flow rates with composition.

Operating System

The actual Sorbex process is shown schematically in Figure 12.12. The process operates with a fixed adsorbent bed rather than with a moving bed and the countercurrent process is simulated by moving the feed, desorbent, and product points continuously by means of a rotary valve. The column sketched is divided into 12 segments, each with appropriate flow distributors to allow the introduction of feed or removal of products. In the position indicated, lines 2 (desorbent), 5 (extract), 9 (feed), and 12 (raffinate) are operational and all other lines are closed. When the rotary valve is moved to its next position the desorbent enters at point 3, extract leaves at point 6, feed at point 10, and desorbent at point 1. Functionally the bed has no top or bottom and is equivalent to an annulus. The same distance is always maintained between adjacent streams, but this distance may be different for the different segments of the column.

The Sorbex system is in effect similar to a periodic countercurrent adsorption system with displacement desorption. The individual sections of the column function as separate beds so that moving the feed and product points
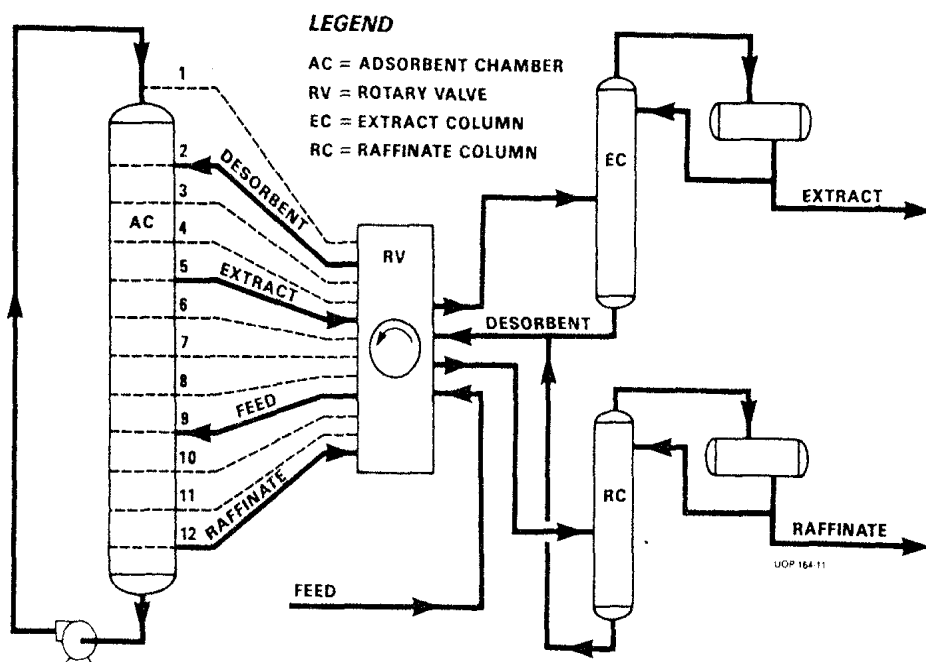
FIGURE 12.12. Schematic diagram of the UOP. Sorbex process showing simulated moving-bed system. (From ref. 2, reprinted by permission of UOP.)

makes the system equivalent to a moving-bed system in which the adsorbent moves countercurrent to the fluid. Provided that the problems of flow distribution and backmixing can be overcome, which requires good engineering design of the injection and draw-off system, it is possible with sufficient sections in the column to obtain a close approximation to ideal countercurrent flow. The flow rates in each of the four segments of the bed vary quite widely, and the circulating pump therefore must be controlled to circulate liquid at the correct rate corresponding to its position in the bed. For example, in the position sketched, the pump is located between raffinate and desorbent points; and the flow rate must therefore be the flow rate appropriate for zone IV $(D + F - E - R)$.

Parex and Ebex Processes

Sorbex processes have been developed for a number of industrially important separations, some of which are listed in Table 12.4. As of May 1983 there were 37 Sorbex units in operation with a further 23 units at the design stage.[*] The earliest and probably still the most important application is in the separation of the xylene isomers. The physical properties of the C_8 aromatic isomers are summarized in Table 12.5 from which it is apparent that only o-xylene can reasonably be separated by distillation. There has therefore been a considerable economic incentive to develop an efficient adsorption separation process for these isomers. The Parex process was the first such process to be commercialized, and this is now the generally accepted process for recovery of p-xylene. Installed capacity in the United States is about 600,000 tons/year (1982) and accounts for about one-quarter of the total market for paraxylene. The only acceptable alternative is the crystallization process which gives less efficient paraxylene recovery but at a significantly lower energy cost. The balance of economic advantage therefore depends largely on the relative importance of these factors, which varies greatly depending on the particular circumstances.

The Ebex process for ethylbenzene recovery was developed more recently and, although pilot scale operation has been demonstrated, no full-scale commercial unit has yet been built.

The adsorbents used in the Parex and Ebex processes are all various cationic forms of faujasite (Table 12.6). Due to the effect of liquid hold-up in the macropores, the effective separation factor for a pelleted zeolite adsorbent is appreciably lower than the separation factor for the same material in unaggregated form. The number of theoretical stages required for any specified product purity decreases as the separation factor increases, but the relationship is highly nonlinear. Simulation studies reveal that for an economic process the minimum acceptable intrinsic separation factor between the extract and raffinate products is about 3. With a separation factor of less than

*D. B. Broughton and S. A. Gembicki, Engineering Foundation Conference on Fundamentals of Adsorption, Schloss Elmau, Bavaria, May 1983.

TABLE 12.4. Commercial Sorbex Processes

Name	Feed	Extract	Raffinate	Process Details
Parex	Mixed C_8 aromatics	98–99% PX	OX, MX, EB	K-BaY + Toluene or $\left.\begin{array}{l}\text{Sr-BaX} \\ \text{K-BaX}\end{array}\right\}$ + PDEB
Ebex	Mixed C_8 aromatics	OX, MX, PX	99% EB	NaY or Sr-KX + Toluene
Molex	n-, branched and cyclo alkanes	n-paraffins	Branched and cyclic isomers	5A sieve + light paraffin desorbent
Olex	Olefins + paraffins	Olefins	Mixed paraffins	Probably CaX or SrX
Sarex	Corn syrup	Fructose	Other Sugars	Aqueous system CaY

2.0, it becomes difficult to design a satisfactory process while the economic impact of an increase in separation factor beyond 4.0 is relatively modest compared with the large improvement which is seen up to that point.

The separation factors for the C_8 aromatics are composition dependent and may be profoundly altered by the addition of other components to the system. It is therefore essential to consider the performance of adsorbent–desorbent combinations rather than the performance of individual adsorbents and desorbents. What is required is a suitable combination of adsorbent and desorbent which, within the appropriate concentration range, gives an adequate separation factor between the components which are to be separated and for which the ancillary separations of extract and raffinate products from the desorbent are easily accomplished. The total number of theoretical plates required for the separation process is minimized when the desorbent is

TABLE 12.5. Physical Properties of C_8 Aromatic Isomers

	Boiling Point (°C)	Relative Volatility at 138°C
Ethylbenzene	136.2	1.056
p-Xylene	138.4	1.00
m-Xylene	139.1	0.981
o-Xylene	144.4	0.855

TABLE 12.6. Separation Factors for C$_8$ Aromatics on Various Cationic Forms of X and Y Zeolites

Reference	Desorbent (D)	Adsorbent	Separation Factors (α)				Order of Affinity
			PX/D	EB/D	OX/D	MX/D	
Stine and Broughton[18]	Toluene	K-BaY	2.1	(1.0)	0.6	0.6	PX > EB~D > OX~MX
Neuzil[19]	PDEB	K-BaX	0.68	0.42	0.2	0.18	D > PX > EB > OX~MX
	PDEB	Sr-BaX	1.24	0.74	0.46	0.39	PX > D > EB > OX~MX
Broughton[20]	Toluene	NaY	1.0	0.44	1.0	1.8	MX > D~OX~PX > EB
Neuzil	Toluene	CaX	0.87	0.38	1.14	1.37	MX > OX > D > PX > EB
and Rosback[21]	Toluene	Sr-KX	1.27	0.55	1.29	1.26	MX > PX~OX > D > EB

PX = p-Xylene
OX = o-Xylene
MX = m-Xylene
EB = ethylbenzene
PDEB = paradiethylbenzene

Note: The separation factors quoted here are overall effective values which are lower than the intrinsic values as a result of the effect of hold-up in the macropores.

adsorbed more strongly than the raffinate product but less strongly than the extract product. This conclusion may be reached by simple qualitative reasoning based on the principle that the optimal situation will occur when the adsorption and desorption operations occur with comparable ease. If the desorbent is too strongly adsorbed, it cannot be easily displaced by the raffinate in section IV while if it is too weakly adsorbed it cannot itself displace the extract product in section III.

Representative separation factors, abstracted from the UOP patents, are summarized in Table 12.6. It has been found that the separation factor can sometimes be enhanced by pretreatment of the adsorbent with, for example, alkylamines.[22] Careful control of the moisture content of the sieve is also essential in order to maximize selectivity,[2] and it seems likely that a small amount of moisture is deliberately introduced with the feed in order to maintain the required moisture level. The earlier Parex units used toluene as the desorbent with K-BaY or K-BaX sieve as adsorbent. This proved to be a satisfactory combination for paraxylene recovery since toluene has the required adsorption affinity, being less strongly adsorbed than paraxylene but more strongly adsorbed than the other species. The use of toluene, however, suffers from two disadvantages. The Parex process is commonly used in conjunction with an isomerization unit which produces, as a by-product, small quantities of naphthenes which boil in the toluene range. These species are not separated in the ancillary distillation units and they therefore tend to accumulate and contaminate the toluene desorbent. The second disadvantage of toluene is that it is a "light desorbent," with a lower boiling point than the C_8 aromatics so, in the ancillary separation, it is distilled overhead. Since the desorbent is present in higher proportion than the C_8 species in both extract and raffinate streams a heavy desorbent would be more energy efficient.

In the more recent Parex units toluene has been replaced by paradiethyl-benzene as the desorbent. Being heavier than the C_8 aromatics, this species is not subject to naphthene contamination and it is separated as bottoms product thus reducing energy requirements. Although it is not clearly stated in the UOP literature, it seems likely that the adsorbent has also been changed to Sr-BaX sieve to satisfy the required order of affinities PX > PDEB > EB > MX~OX. With the K-BaY sieve and a PDEB desorbent the order of affinities is PDEB > PX > EB > MX~OX, which is less desirable for the reasons outlines above.

Typical feed and product compositions are given in Table 12.7 and a representative concentration profile as determined from pilot scale experiments is shown in Figure 12.13.

Whereas in the Parex process paraxylene is the most strongly adsorbed species and is removed in the extract, in the Ebex process ethylbenzene is the least strongly held species and is withdrawn as raffinate. Representative steady-state concentration profiles measured in a pilot scale Ebex unit are shown in Figure 12.13. It may be seen from Table 12.6 that the selectivity of the ethylbenzene adsorbents (NaY, CaX, and Sr-KX) is generally lower than

TABLE 12.7. Feed and Product Compositions for Full-Scale Parex Process with PDEB Desorbent (wt%)

	Feed	Extract	Raffinate
Nonaromatics	0.29	0	0.29
Toluene	0.45	1.54	0.28
EB	12.38	0.34	14.1
pX	11.76	97.94	0.53
mX	62.96	0.09	70.93
oX	12.16	0.09	13.87

Source: From ref. 2, reprinted with permission of Martinus Nijhoff Publishers.
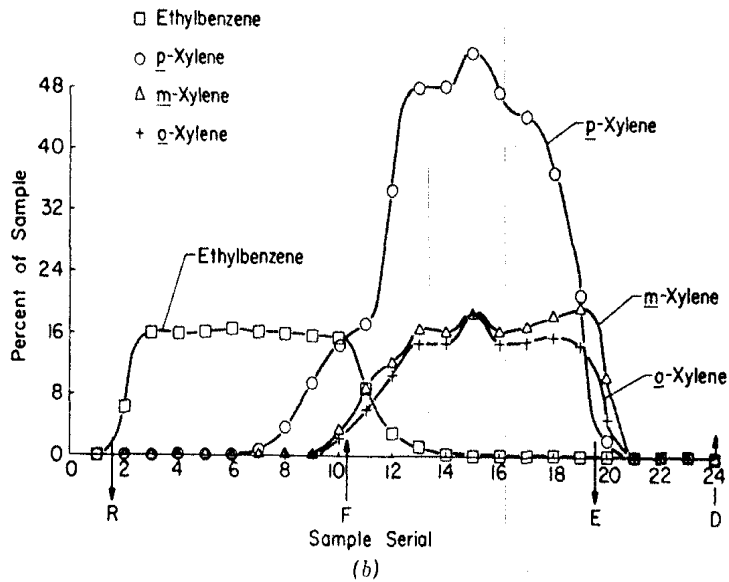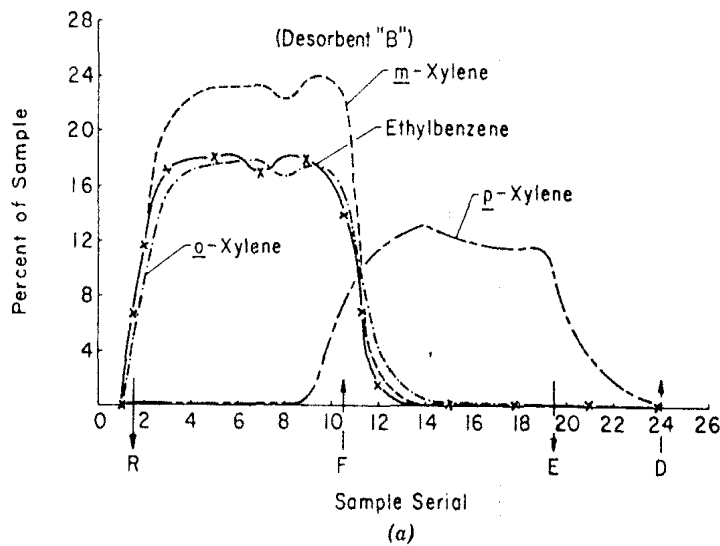
FIGURE 12.13. Experimental steady-state concentration profiles measured in pilot scale Sorbex systems: (*a*) Parex and (*b*) Ebex. (Reprinted with permission from ref. 23. Copyright 1978 American Chemical Society.)

that of the para selective adsorbents. This probably accounts for the difference in the commercial success of the Parex and Ebex processes.

Other Sorbex Processes

In the Molex process the Sorbex system is used for the separation of linear and branched hydrocarbons, using as adsorbent 5A molecular sieve. This is the same adsorbent as is used in the cyclic batch processes such as Ensorb and Isosiv. In contrast to the situation with the C_8 aromatics, the separation factor is very large and it seems unlikely that for such an "easy" separation the increased cost of a Sorbex unit is justified by the reduction in adsorbent inventory and/or desorbent circulation rate. Detailed cost comparisons do not appear to have been published, but it seems likely that any economic advantage which the Molex process may have arises more from the energy savings associated with liquid phase operation than from the intrinsic advantages of a countercurrent adsorption system.

The most recent Sorbex process to be developed is the Sarex process for separation of fructose from corn syrup. This process is unique in that it is the only Sorbex process which operates with an aqueous fluid phase. The separation depends on the well known ability of fructose to complex with Ca^{2+} ions and either cation exchange resins or zeolites (X or Y) in the Ca^{2+} form may be used as the adsorbent. Separation factors (fructose/glucose) are somewhat higher with the zeolite adsorbents making these materials preferable for commercial use. Fructose is the extract product and glucose the raffinate. The polysaccharides, which are commonly present in the feed, are not significantly adsorbed and are eluted in the raffinate. Futher details have been given by Bieser and deRosset[24] and Neuzil and Jensen[25] (see also Neuzil and Priegnitz[26]).

12.6. COMPARISON OF CHROMATOGRAPHIC AND CONTINUOUS COUNTERCURRENT PROCESSES

Chromatographic and continuous countercurrent processes are competitive in that both these types of process are applicable to "difficult" separations where the separation factor is small. In order to make clear the similarities and differences between these processes we introduce, following Valentin,[27] the idea of the number of equilibrations between fluid and solid phases. In a chromatographic column it follows from the definition of a theoretical plate that each sorbate molecule is equilibrated between fluid and solid on average just once for each plate. The number of equilibrations is therefore simply the number of theoretical plates to which the chromatographic column is equivalent. In a countercurrent system the situation is more complex because of the internal reflux. For simplicity we consider a system with linear equilibrium. At

any point in the countercurrent system:

$$\frac{\text{Net Upflow of Ads. Species}}{\text{Fluid Upflow of Ads. Species}} = 1 - \gamma \qquad (12.25)$$

where $\gamma = (1 - \epsilon)Ku/\epsilon v$ is the countercurrent flow ratio. The residence time in each stage is therefore increased by the factor $1/(1 - \gamma)$ compared with a chromatographic column operating at the same fluid flow rate with a stationary solid phase. This factor can also be thought of as the average number of times that each molecule is recycled or the average number of equilibrations/stage. The total number of equilibrations in a countercurrent column is therefore $N'/(1 - \gamma)$ where N' is the number of theoretical plates. In view of this essential difference between chromatographic and countercurrent processes it is logical to make comparisons on the basis of the number of equilibrations rather than on the basis of the number of stages or theoretical plates.

To illustrate the comparison we consider the simple system sketched in Figure 12.14 in which a feed containing 50% A + 50% B is to be separated into two product streams containing 1% A in B and 1% B in A. The system is assumed linear with constant molar flow rates in both phases and the same number of stages (N') above and below the feed. The relationship between the extent of separation (difference in mole fractions of top on bottom products, in this case $0.99 - 0.01 = 0.98$) and the number of stages in a countercurrent system with no external reflux has been shown by Rony[28] to be given by

$$\xi = 0.98 = \left| \frac{1}{1 + \gamma^{N'}} - \frac{1}{1 + (\alpha\gamma)^{N'}} \right| \qquad (12.26)$$

Counter-Current System   Chromatographic System
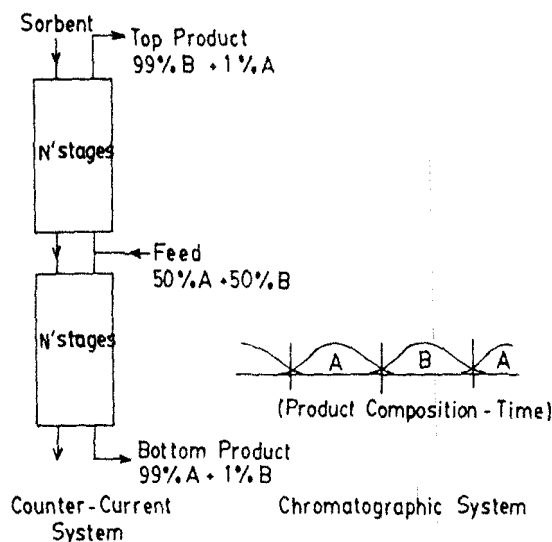
FIGURE 12.14. Sketch of hypothetical systems for comparison of continuous countercurrent and chromatographic system.
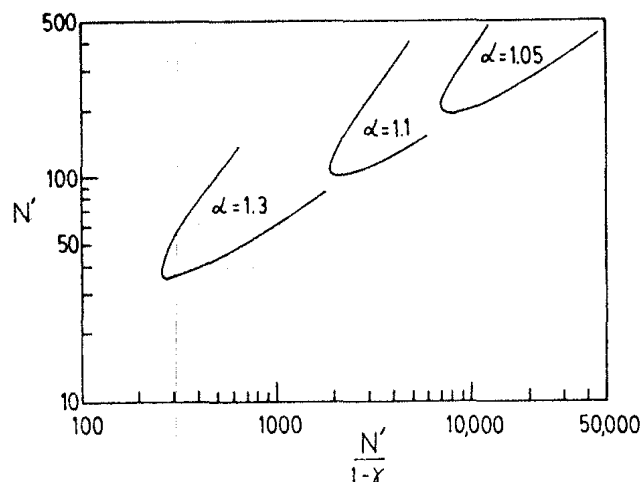
FIGURE 12.15. Results of calculation of number of stages required to achieve top and bottom products of 99% purity in a continuous countercurrent system.

where $\alpha = K_A / K_B$ is the separation factor. For any specified value of α Eq. (12.26) may be solved to obtain the locus (γ, N') which gives the required separation. The results of such a calculation are displayed in Figure 12.15 as a plot of N' versus $N'/(1 - \gamma)$, that is, the number of stages versus the number of equilibrations. The upper branches of these curves represent operation at low internal reflux with a large number of stages while the lower branches represent operation at high reflux with fewer stages. There are evidently minimum values for both N' and $N'/(1 - \gamma)$ below which the required separation cannot be achieved. The minima of $2N'/(1 - \gamma)$ and corresponding values of $2N'$ are summarized in Table 12.8. The values are quoted as $2N'$ since there are N' stages in both the rectification and stripping sections.

If the same separation is carried out in a chromatographic system the number of theoretical plates required is given by Eq. (10.13):

$$N = 4R_{AB}^2 \left(\frac{\alpha + 1}{\alpha - 1} \right)^2 (1 - 2\theta)^{-2} \qquad (12.27)$$

For maximum throughput we require $\theta = \frac{1}{6}$ (see Section 10.2) and for 1% overlap of the product peaks (i.e., to produce two cuts 99% A + 1% B and 99% B + 1% A) we should take $\bar{t}_A - \bar{t}_B \approx 3.2\sigma_{AB}$ or, from Eq. (10.8), $R_{AB} = 0.8$ which with Eq. (12.27) gives

$$N = 5.62 \left(\frac{\alpha + 1}{\alpha - 1} \right)^2 \qquad (12.28)$$

The values of N calculated from this expression are included in Table 12.8. It is evident that the number of chromatographic plates required to perform the specified separation is from 4 to 34 times as great as the number of stages required in a continuous countercurrent system with properly adjusted flow

TABLE 12.8.   Comparison of Chromatographic and Countercurrent Systems

Separation Factor	Countercurrent			Chromatographic	Ratio
(α)	γ	$2N'$	$2N'/(1-\gamma)$	N	$N/2N'$
1.3	0.854	76	520	330	4
1.1	0.941	220	3,700	2,473	11
1.05	0.972	400	14,000	9,470	34
Column section area $[\alpha(1-\gamma)^{-1}]$			16.8	1^b	
Number of sections/columns			4	6	
Plates/section^a			110	2,473	
HETP			0.5	1^b	
Adsorbent volume			0.25	1^b	

^{a} Figures in lower part of table are given for $\alpha = 1.1$ but relative volumes for other α values are almost the same.
^{b} Relative values.

rates and is of the same order as the number of countercurrent contacts $2N'/(1-\gamma)$.

In comparing the total adsorbent inventory required to achieve the same throughput in the chromatographic and countercurrent systems, it must be remembered that in the chromatographic system the feed is injected only for one-sixth of the total time, so for continuous flow six parallel columns (and therefore $6N$ theoretical plates) would be required. Similarly in the countercurrent system for a specified fluid velocity through the column the net flow rate is reduced by the factor $1/(1-\gamma)$ as a result of the internal reflux, and the regeneration of the adsorbent has also been ignored. For a close separation in a Sorbex system with a properly selected desorbent, a column with four sections is required (Figure 12.11) and each section of the column contains approximately the same number of stages. The total number of stages in the complete system is therefore approximately $4N'$. The ratio H'/H for the two systems may be estimated from the relations given in Table 12.1 and the relative volumes of the two systems may then be compared. On this basis it may be seen that in the example considered, for the same duty, the volume of adsorbent required in the countercurrent system is about one-quarter of that required for a production chromatograph. Although this is only a rough estimate, based on several rather severe idealizations, the final result is in reasonable agreement with estimates put forward by UOP[2] which are presumably derived from more detailed simulations.

REFERENCES

1. D. Tondeur, in *Percolation Processes: Theory and Applications*, A. E. Rodrigues and D. Tondeur (eds.), NATO ASI No. 33. Sijthoff and Noordhoff, Alphen van Rijn, Holland, 1981, p. 517.

2. A. J. de Rosset, R. W. Neuzil, and D. B. Broughton, in *Percolation Processes: Theory and Applications*, A. E. Rodrigues and D. Tondeur (eds.), NATO ASI No. 33. Sitjhoff and Noordhoff, Alphen van Rijn, Holland, 1981, p. 249. *See also* D. B. Broughton, R. W. Neuzil, J. M. Pharis, and C. S. Brearly *Chem. Eng. Prog.* **66**, (9) (1970).

3. H. R. C. Pratt, *Counter-Current Separation Processes*. Elsevier, Holland, 1967.

4. N. R. Amundson and P. R. Kasten, *Ind. Eng. Chem.* **44**, 1704 (1952).

5. H. K. Rhee and N. R. Amundson, *Chem. Eng. Sci.* **28**, 55 (1973).

6. H. K. Rhee, R. Aris, and N. R. Amundson, *Phil. Trans. Roy. Soc. (London)* **269**, 187 (1971).

7. H. Kehde, R. G. Fairfield, J. C. Frank, and L. W. Zahnstecher, *Chem. Eng. Prog.* **44**(8), 575 (1948).

8. C. Berg, *Trans. AIChE* **42**, 665–80 (1946).

9. R. L. Culp and G. Culp, *Advanced Wastewater Treatment*. Van Nostrand, New York, 1971.

10. C. I. Lawson and S. A. Fisher, *AIChE Symp. Ser.* **70**(136), 577 (1973).

11. V. G. Svedberg, *Chem. Eng. Sci.* **31**, 345 (1976).

12. I. Neretnieks, *Chem. Ing. Technik* **47**, 773 (1975).

13. E. Sung, C. D. Han, and H. K. Rhee, *AIChE J.* **25**, 87 (1979).

14. R. Klaus, R. C. Aiken, and D. W. T. Rippin, *AIChE J.* **23**, 579 (1977).

15. A. I. Liapis and D. W. T. Rippin, *AIChE J.* **25**, 455 (1979).

16. H. J. Ortlieb, G. Bunke, and D. Gelbin, *Chem. Eng. Sci.* **36**, 1009 (1981).

17. A. J. de Rossett, R. W. Neuzil, D. G. Tajbl, and J. M. Braland, *Sep. Sci. and Technol.* **15**, 637 (1980).

18. L. O. Stine and D. B. Broughton, U.S. Patent No. 3,636,121 (Nov. 7, 1969), to UOP.

19. R. W. Neuzil, U.S. Patent No. 3,997,620 (Oct. 28, 1975), to UOP.

20. D. B. Broughton, U.S. Patent No. 4,306,107 (Apr. 28, 1980), to UOP.

21. R. W. Neuzil and D. H. Rosback, U.S. Patent No. 3,998,901 (July 14, 1975), to UOP.

22. D. H. Rosback, U.S. Patent No. 4,283,587 (Aug. 11, 1981), to UOP.

23. A. J. de Rossett, R. W. Neuzil, and D. J. Korous, *Ind. Eng. Chem. Process Design Develop.* **15**, 261 (1978).

24. H. J. Bieser and A. J. deRosset "Continuous Countercurrent Separation of Saccharides with Inorganic Adsorbents," 28th Starch Convention, Detmold, West Germany, April 1977.

25. R. W. Neuzil and R. A. Jensen "Development of the Sarex Process for Separation of Saccharides," 85th National Meeting of AIChE, Philadelphia, June 1978.

26. R. W. Neuzil and J. W. Priegnitz, U.S. Patent No. 4,024,331 (May 1977), to UOP.

27. P. Valentin, "Separation of Components by Gas-Liquid Chromatography," paper presented at 166th Annual Meeting of American Chemical Society, 1974.

28. P. R. Rony, *Sep. Sci.* **5**(1), 1 (1970).

APPENDIX A

ELEMENTARY STATISTICAL THERMODYNAMICS

ENSEMBLES AND AVERAGE PROPERTIES

Statistical thermodynamics is based on the following postulates:

1. The time average of a mechanical variable in a thermodynamic system is equal to the ensemble average of that property in the limit corresponding to an infinitely large number of systems in the ensemble, provided that the systems of the ensemble conform to the thermodynamic state and environment of the actual system.

2. In an infinitely large ensemble representing an isolated thermodynamic system the systems of the ensemble are distributed with equal probability over all allowable quantum states consistent with the specified values of N, V, and U.

The correspondence between the types of system and ensemble may be summarized as follows:

Type of System	Independent Variables	Type of Ensemble	Partition Function
Isolated (no exchange of heat or matter)	N, V, U	Microcanonical	f
Closed, Isothermal (exchange of heat, no exchange of matter)	N, V, T	Canonical	$\mathscr{F}$
Open, Isothermal (exchange of both heat and matter)	μ, V, T	Grand Canonical	Ξ

The partition function, which is simply the sum of all Boltzmann factors for each allowable state of the system, provides the bridge between classical and statistical thermodynamics. To derive the relationships between the partition function and the classical thermodynamic properties we consider a closed system and a canonical ensemble.

THE PARTITION FUNCTION

Consider a system containing N molecules of which N_1 are in state 1, which is characterized by energy ϵ_1; N_2 are in state 2, characterized by energy ϵ_2; etc.

$$N = N_1 + N_2 + \cdots + = \sum N_i \tag{A1}$$

The internal energy U is given by

$$U = N_1 \epsilon_1 + N_2 \epsilon_2 + \cdots + = \sum N_i g_i \epsilon_i \tag{A2}$$

where a degeneracy factor g_i has been included to allow for the possibility that several physically distinguishable states may have the same energy. The partition function f for a single molecule in this system is defined by

$$f \equiv g_1 e^{-\epsilon_1/kT} + g_2 e^{-\epsilon_2/kT} + \cdots + = \sum g_i e^{-\epsilon_i/kT} \tag{A3}$$

where k is the Boltzmann constant.

For a particular system one may express the Boltzmann distribution law in the form

$$N_1 = K g_1 e^{-\epsilon_1/kT}, \qquad N_2 = K g_2 e^{-\epsilon_2/kT} \cdots \tag{A4}$$

where K is a constant; and by simple addition we obtain

$$N = Kf \quad \text{or} \quad \frac{N_i}{N} = \frac{e^{-\epsilon_i/kT}}{f} \tag{A5}$$

For a system containing N distinguishable molecules such as an ideal crystal, the system partition function $\mathscr{F}$ for all N molecules is given by

$$\mathscr{F} = f^N \tag{A6}$$

However, if the molecules are identical and indistinguishable, as in the gas phase,

$$\mathscr{F} = \frac{f^N}{N!} \tag{A7}$$

RELATIONSHIP TO THERMODYNAMIC PROPERTIES— CLOSED SYSTEMS

Internal Energy

From Eq. (A3) we obtain

$$\frac{\partial f}{\partial T} = \sum_i g_i \left(\frac{\epsilon_i}{kT^2} \right) e^{-\epsilon_i/kT} \tag{A8}$$

and from Eqs. (A2), (A5), and (A8)

$$U = \frac{NkT^2}{f} \frac{\partial f}{\partial T} = NkT^2 \left(\frac{\partial \ln f}{\partial T} \right)_V = kT^2 \left(\frac{\partial \ln \mathscr{F}}{\partial T} \right)_V \tag{A9}$$

Entropy

From Boltzmann's equation

$$S = k \ln W \tag{A10}$$

where W is the probability of the state,

$$\left. \begin{aligned} W &= \frac{N_i!}{\prod_i N_i!} \\ \ln W &= \ln(N!) - \sum_i \ln N_i \end{aligned} \right\} \tag{A11}$$

Using Stirling's approximation $[\ln(N!) = N \ln N - N]$

$$\ln W = \frac{S}{k} = N \ln N - \sum_i N_i \ln N_i \tag{A12}$$

Substituting for N_i from Eq. (A5)

$$\frac{S}{k} = N \ln N - \sum_i \left(N_i \ln N_i - N_i \ln f - \frac{N_i \epsilon_i}{kT} \right) = \frac{U}{kT} + N \ln f \tag{A13}$$

$$S = Nk \left[\ln f + T \left(\frac{\partial \ln f}{\partial T} \right)_v \right] = k \ln \mathscr{F} + kT \left(\frac{\partial \ln \mathscr{F}}{\partial T} \right)_v \tag{A14}$$

Helmholtz Free Energy

$$A \equiv U - TS = -NkT \ln f = -kT \ln \mathscr{F} \tag{A15}$$

Pressure

$$p \equiv -\left(\frac{\partial A}{\partial V} \right)_T = NkT \left(\frac{\partial \ln f}{\partial V} \right)_T = kT \left(\frac{\partial \ln \mathscr{F}}{\partial V} \right)_T \tag{A16}$$

Chemical Potential

$$\mu \equiv \left(\frac{\partial A}{\partial N}\right)_{T,V} = -kT\left[\ln f + \left(\frac{\partial \ln f}{\partial \ln N}\right)_{T,V}\right] = -kT\left(\frac{\partial \ln \mathscr{F}}{\partial N}\right)_{V,T} \quad (A17)$$

OPEN SYSTEMS

To calculate the concentration or the number of molecules present in an open system at defined μ, V, T we must consider the grand canonical ensemble which is simply an ensemble in which each subsystem is itself a canonical ensemble. The grand partition function Ξ is simply the sum of the Boltzmann factors for each of the j canonical ensembles, weighted according to $e^{N\mu/kT}$

$$\Xi(V, T, \mu) = \sum_{N,j}\left[e^{N\mu/kT}e^{-E_j(N,V)/kT}\right] = \sum_{N}\left[e^{N\mu/kT}\sum_{j}e^{-E_j(N,V)/kT}\right]$$

$$= \sum_{N}\mathscr{F}(N, V, T)e^{N\mu/kT} \quad (A18)$$

The probability that the system contains N molecules irrespective of energy state is given by

$$W(N) = \frac{\mathscr{F}(N, V, T)e^{N\mu/kT}}{\Xi} \quad (A19)$$

The average number of molecules per subsystem is therefore given by

$$\overline{N} = \sum_{N}\frac{N\mathscr{F}e^{N\mu/kT}}{\Xi} \quad (A20)$$

From Eq. (A18)

$$\left(\frac{\partial \Xi}{\partial \mu}\right)_{V,T} = \sum\left(\frac{N}{kT}\right)\mathscr{F}e^{N\mu/kT} \quad (A21)$$

$$\overline{N} = kT\left(\frac{\partial \ln \Xi}{\partial \mu}\right)_{V,T} = \lambda\frac{\partial \ln \Xi}{\partial \lambda} \quad (A22)$$

where $\lambda = e^{\mu/kT}$.

PARTITION FUNCTIONS FOR SIMPLE SYSTEMS

Free Linear Motion

The solution of the Schrödinger equation for free linear motion over a distance l gives, for the permissible energy levels,

$$\epsilon = \frac{n^2h^2}{8ml^2} \quad (A23)$$

whence

$$f_{lin} = \sum_{n=1}^{\infty} \exp\left(\frac{-n^2 h^2}{8 m l^2 k T} \right) \tag{A24}$$

Provided that $h^2/8 m l^2 k T \ll 1.0$, the summation may be replaced by the equivalent integral:

$$f_{lin} \approx \int_{n=0}^{\infty} \exp\left(-\frac{n^2 h^2}{8 m l^2 k T} \right) dn = \frac{(2 \pi m k T)^{1/2} l}{h} \tag{A25}$$

Free Motion on a Surface or Within a Limited Volume

The same argument may be extended to free superficial motion with the result

$$f_{trans} \approx \frac{(2 \pi m k T)}{h^2} \mathscr{A} \tag{A26}$$

and for free motion in three dimensions

$$f_{trans} \approx \left(\frac{2 \pi m k T}{h^2} \right)^{3/2} V \tag{A27}$$

Harmonic Oscillation

The energy levels for an harmonic oscillator are given by

$$\epsilon = \left(n + \tfrac{1}{2} \right) h \nu \qquad (n = 0, 1, 2, \ldots) \tag{A28}$$

The partition function is therefore

$$f_{vib} = \sum_{v=0}^{\infty} \exp\left[-\left(v + \frac{1}{2} \right) \frac{h \nu}{k T} \right] = \frac{e^{-h\nu/2kT}}{1 - e^{-h\nu/2kT}} \tag{A29}$$

In the classical limit $(kT \gg h\nu)$

$$f_{vib} \approx \frac{kT}{h\nu} \tag{A30}$$

For a three-dimensional oscillator

$$f_{vib} \approx \left(\frac{kT}{h\nu} \right)^3 \tag{A31}$$

Free Rotation

The allowable energy levels for free rotation of a rigid diatomic molecule with moment of inertia I are given by

$$\epsilon = \frac{J(J + 1)h^2}{8\pi^2 I} \qquad (J = 1, 2, \ldots) \tag{A32}$$

and the partition function is therefore

$$f_{\text{rot}} = \sum_{1}^{\infty} (2J + 1) \exp\left[\frac{-J(J + 1)h^2}{8\pi^2 I k T} \right] \tag{A33}$$

In the classical limit the summation may again be replaced by an integral to yield

$$f_{\text{rot}} = \frac{8\pi^2 I k T}{h^2} \tag{A34}$$

If the rotator is symmetrical this partition function must be reduced by the appropriate symmetry factor (σ) to eliminate permutations which are indistinguishable. For a symmetric diatomic molecule such as N_2 or O_2, $\sigma = 2$ while for unsymmetric molecules such as CO or NO, $\sigma = 1.0$. The corresponding expression for a polyatomic molecule with moments of inertia about the three principal axes I_x, I_y, I_z is

$$f_{\text{rot}} = \frac{\sqrt{\pi}}{\sigma} \left(\frac{8\pi^2 k T}{h^2} \right)^{3/2} (I_x I_y I_z)^{1/2} \tag{A35}$$

For molecules such as CH_4 or CF_4, $\sigma = 12$, corresponding to the number of identical positions of the molecule which may be achieved by rotation.

COMPLEX PARTITION FUNCTIONS

Provided that the different modes of motion can be considered to make independent contributions to the total energy, the partition function for a complex system is simply the product of the separate partition functions for each mode of motion; for example,

$$f = f_{\text{rot}} f_{\text{vib}} f_{\text{trans}} f_{\text{int}} \cdots \tag{A36}$$

This is a most useful property since in considering adsorption phenomena it is often permissible to assume that internal and rotational freedom is not greatly affected by sorption.

COMMUNAL ENTROPY

The translational partition function for a molecular confined within volume v is given by Eq. (A27). If we assume this to be the partition function for an ideal gas molecule with $v = V/N$ we derive the correct values for many of the thermodynamic properties with the notable exception of the entropy. The entropy, however, is lower by k per molecule. This discrepancy arises because the gas is not really a system in which the molecules can properly be

considered as localized but rather each molecule moves in a shared space. The system partition function is proportional to the number of distinguishable ways in which the system can be formed, so

$$\mathscr{F} = \left[\left(\frac{2\pi mkT}{h^2} \right)^{3/2} Nv \right]^N \Big/ N!$$

(A37)

For large values of N, we may use Stirlings approximation $(N^N/N! \approx e^N)$:

$$f = \mathscr{F}^{1/N} = \left(\frac{2\pi mkT}{h^2} \right)^{3/2} ev$$

(A38)

We thus see that the molecular partition function is increased by the factor e in comparison with a system in which the molecules occupy the same total space but with each one confined to its own box. From Eq. (A14) it is evident that the entropy will be increased by $R = Nk$ compared with a similar system of captive molecules. This quantity is often referred to as the communal entropy.

A more complete discussion of these relationships is to be found in most standard textbooks of physical chemistry; for example E. A. Moelwyn-Hughes, *Physical Chemistry*, 2nd ed, Chapter VIII, Pergamon Press (1961) as well as in Hill's book (see Appendix B).

Notation

A Helmholtz free energy

f partition function for molecule or subsystem

$\mathscr{F}$ partition function of canonical ensemble

g degeneracy factor

h Planck's constant

I moment of inertia

J integer (rotational quantum number)

k Boltzmann's constant

l length

m mass of molecule

n integer

N number of molecules or subsystems

p pressure

S entropy

T absolute temperature

U internal energy

V volume of system

v V/N (volume of subsystem). Also vibrational quantum number

W probability of state

μ chemical potential

ϵ energy levels

ν vibration frequency

Ξ grand partition function

σ symmetry factor

APPENDIX B

BIBLIOGRAPHY

A list of some of the major sources of more detailed information on various aspects of adsorption and adsorption separation processes is given below. This list is not intended as a complete bibliography but rather as an initial guide to the available literature.

GENERAL REFERENCE TEXTS (ZEOLITES)

Breck, D. W. *Zeolite Molecular Sieves*. Wiley: New York, 1974.

Barrer, R. M. *Zeolites and Clay Minerals as Adsorbents and Catalysts*. Academic Press: London, 1978.

Rabo, J. (ed.). *Zeolite Chemistry and Catalysis*. ACS Monograph No. 171, American Chemical Society, 1976.

Kokotailo, G. T. *Zeolites*. Springer-Verlag: New York, 1984.

PHYSICAL CHEMISTRY AND THERMODYNAMICS OF ADSORPTION

Hill, T. L. *Introduction to Statistical Thermodynamics*. Addison Wesley: Reading, Mass., 1960.

Young, D. M., and Crowell, A. D. *Physical Adsorption of Gases*. Butterworths: London, 1962.

Ross, S., and Olivier, J. P. *On Physical Adsorption*. Wiley: New York, 1964.

Clark, A. *Theory of Adsorption and Catalysis*. Academic: New York, 1970.

Ponec, V., Knor, Z. and Cerny, S. *Adsorption on Solids*. Butterworths: London, 1974.

ADSORPTION COLUMN DYNAMICS AND ADSORPTION PROCESSES

Rodrigues, A. E., and Tondeur, D. (eds.). *Percolation Processes*. NATO ASI No. 33, Sijthoff and Noordhoff, 1981.

Smisek, M., and Cerny, S. *Active Carbon*. Elsevier: Amsterdam, 1970.

Vermeulen, T. "Adsorption and Ion Exchange," Section 16. In *Chemical Engineer's Handbook*. R. H. Perry and C. H. Chilton (eds.). Fifth ed. McGraw Hill: New York, 1973.

Basmadjian, D. "Adsorption Drying of Gases and Liquids." In *Advances in Drying*, Vol. 3, Hemisphere Publishing Company: Washington, D.C., 1983.

Helfferich, F., and Klein, G. *Multicomponent Chromatography*. Marcel Dekker: New York, 1970.

Whyte, T. E., Yon, C. M., and Wagener, E. A. (eds.). "Industrial Gas Separations," *A.C.S. Symp. Ser.* **223**, American Chem. Soc., Washington, D.C. (1983).

MATHEMATICAL METHODS

Holland, C. D., and Liapis, A. I. *Computer Methods for Solving Dynamic Separation Problems*. McGraw-Hill: New York 1983.

CONFERENCE PROCEEDINGS

Proceedings of International Conferences on Molecular Sieves

1st: London (1967). Published as *Molecular Sieves*, Soc. Chem. Industry, London (1968).

2nd: Worcester, Mass. (1970). Published as *Adv. in Chem.*, **101** and **102**, American Chemical Society (1971).

3rd: Zurich (1973). Published as *Adv. in Chem.*, **121**, American Chem. Soc. (1973).

4th: Chicago (1977). Published as *A.C.S. Symp. Ser.*, **40**, American Chem. Soc. (1977).

5th: Naples (1980). Proceedings, Heyden, London (1980).

6th: Reno (1983). Proceedings, Butterworths, Guildford (1984).

Other Conferences on Molecular Sieves

Zeolite 76, A Conference on Natural Zeolites, Occurrence, Properties and Use, Tucson, Arizona, June (1976). Proceedings published by Pergamon Press (1978).

Symposium on Zeolites, Szeged, Hungary, September 11–14 (1978). Proceedings published as *Acta Phys. Chem.*, **24**, (1978).

Properties and Applications of Zeolites, April 18–20 (1979). Proceedings published as Special Publication No. 33, Chemical Society, London (1980).

Adsorption of Hydrocarbons in Zeolites. A workshop held at the Akademie Wissenschaften der DDR, Berlin, November 19–22 (1979). Preprints published by M. Bülow, Akademie der Wissenschaften der DDR, Berlin.

Adsorption of Hydrocarbons in Microporous Adsorbents—II. A workshop held at Eberswalde, DDR, November 22–26 (1982). Preprints published by W. Schirmer and H. Stach, Akademie der Wissenschaften der DDR, Berlin.

Adsorption and Ion Exchange with Synthetic Zeolites. Symposium held at San Francisco August 25–26 (1980). Proceedings published by American Chemical Society as *A.C.S. Symp. Ser.* No. 135.

Intrazeolite Chemistry. American Chemistry Society Symposium held at Kansas City, Missouri, September 1982. Proceedings published by American Chemical Society as *A.C.S. Symp. Ser.* No. 218.

NATO ASI "Zeolites." Sintra-Estoril, Portugal, May 1983. Proceedings to be published by Martinus Nijhoff, The Hague, Holland (1984).

Other Conferences on all Aspects of Adsorption

Engineering Foundation Conference "Fundamentals of Adsorption," Schloss Elmau, Bavaria, May 1983. Proceedings to be published by the Engineering Foundation (1984).

CEP and AIChE Symposia on Adsorption and Adsorption Processes

"Physical Adsorption Processes and Principles," *Chem. Eng. Prog. Symp. Ser.* (74), **63** (1967).

"Developments in Physical Adsorption," *Chem. Eng. Prog. Symp. Ser.* (96), **65** (1969).

"Adsorption Technology," *AIChE Symp. Ser.* (117), **67** (1971).

"Gas Purification by Adsorption," *AIChE Symp. Ser.* (134), **69**, (1973).

"Adsorption and Ion Exchange," *AIChE Symp. Ser.* (152), **71**, (1975).

"Adsorption and Ion Exchange Separation," *AIChE Symp. Ser.* (179), **74**, (1978).

"Recent Advances in Adsorption and Ion Exchange," *AIChE Symp Ser.* (219), **78**, (1982).

AUTHOR INDEX

SUBJECT INDEX